



Raihan, Sheikh Zahir (2017) Desensitisation of the human long chain fatty acid receptors FFA1 and FFA4. PhD thesis.

<http://theses.gla.ac.uk/8144/>

Copyright and moral rights for this work are retained by the author

A copy can be downloaded for personal non-commercial research or study, without prior permission or charge

This work cannot be reproduced or quoted extensively from without first obtaining permission in writing from the author

The content must not be changed in any way or sold commercially in any format or medium without the formal permission of the author

When referring to this work, full bibliographic details including the author, title, awarding institution and date of the thesis must be given

Enlighten:Theses
<http://theses.gla.ac.uk/>
theses@ gla.ac.uk

Desensitisation of the human long chain fatty acid receptors FFA1 and FFA4

Sheikh Zahir Raihan

M.Pharm, B.Pharm (Hons)

A thesis submitted
in fulfilment of the requirements for the Degree of
Doctor of Philosophy



**University
of Glasgow**

**Institute of Molecular,
Cells & System Biology**

February 2017

Abstract

G protein-coupled receptors (GPCRs) constitute the largest, most ubiquitous and most versatile family of membrane proteins encoded by the human genome. Due to diverse ligands and multiple physiological activities, this set of receptors has frequently been explored as potential drug targets. Deorphanisation of GPCRs successfully identified FFA1 and FFA4 (previously named GPR40 and GPR120) as long chain free fatty acid receptors. With diverse expression patterns and close association to pathophysiology of metabolic diseases, both receptors are being studied to understand both receptor pharmacology and their potential for drug development. Due to the overlap in the activation of FFA1 and FFA4 by endogenous fatty acid ligands, selective synthetic ligands have been developed for these receptors. Using a number of biochemical and biophysical assays, I have characterised TUG-770, TUG-905 and GW-1100 as FFA1 ligands and TUG-891, TUG-1197 and TUG-1275 as FFA4 ligands. TUG-905 was found to be most potent and selective FFA1 agonist and GW-1100 showed insurmountable antagonism at FFA1. At FFA4, TUG-1197 was found to be a highly potent and selective agonist. TUG-1275 showed insurmountable antagonism at FFA4 in β -arrestin2 recruitment, receptor internalisation and inositol monophosphate accumulation studies and showed complete selectivity for hFFA4. Agonist exposure rapidly phosphorylated FFA4 in an agonist-concentration-dependent fashion which was totally blocked by TUG-1275. The protein kinase C activator PMA was also noted to phosphorylate FFA4 in a concentration-dependent manner. Thus both homologous and heterologous phosphorylation is involved in FFA4 regulation. The FFA4-agonist TUG-891 produced robust internalisation of FFA4 as detected by each of confocal microscopy, and both cell surface ELISA and biotinylation. PMA was able to internalise FFA4 although it was unable to recruit β -arrestin2 to FFA4 suggesting that this internalisation might not be β -arrestin2-dependent. Constitutive internalisation was seen for FFA1, where the selective FFA1 antagonist GW-1100 had no effect. Repeated agonist-exposure desensitised both FFA1 and FFA4 as revealed in single-cell calcium imaging studies. Although there was a small reduction of FFA4-internalisation and a slight elevation of total calcium levels from a single-chronic exposure of agonist, elimination of β -arrestin1/2 from HEK293 cells by genome editing did not significantly change the desensitisation of FFA4 to repeated exposure of agonist.

and did not prevent agonist-promoted internalisation. These studies indicate that β -arrestins are not the sole factors in desensitisation of human FFA4. $G\alpha_{q/11}$ elimination by genome editing completely blocked intracellular calcium mobilisation and accumulation of inositol monophosphates mediated by both FFA1 and FFA4 indicating that $G\alpha_{q/11}$ coupling to agonist-activated receptors is essential for this functional signalling outcome via both receptors. FFA4 expressed in $G\alpha_{q/11}$ -null cells was found to be phosphorylated by agonist, indicating that phosphorylation-mediated desensitisation of this receptor is not dependent on $G\alpha_{q/11}$ proteins. FRET and BRET experiments revealed for the first time homo and hetero-oligomerisation of both FFA1 and FFA4. Although ligand regulation of oligomerisation was not investigated these preliminary observations of oligomerisation may help in the future to answer many questions of regulation and desensitisation of these receptors. The selective FFA1 and FFA4 ligands characterised here in this project might be used as tool compounds to further explore the physiology and pharmacology of these therapeutically important receptors.

Contents

Abstract.....	ii
Contents	iv
List of Tables	viii
List of Figures.....	ix
Acknowledgement	xiii
Author's Declaration	xiv
Abbreviations	xv
1 Introduction	1
1.1 G protein-coupled receptors	1
1.1.1 Structural feature of GPCRs.....	1
1.1.2 GPCR activation	4
1.1.3 GPCR signalling	4
1.1.4 Classification of GPCRs.....	8
1.1.5 Heterotrimeric G proteins and their effectors.....	8
1.1.6 GPCR biased signalling	9
1.1.7 GPCR oligomerisation	12
1.1.8 GPCR deorphanisation.....	17
1.2 Free fatty acid receptors	18
1.3 Short chain fatty acid receptors.....	20
1.4 Long chain fatty acid receptors	23
1.4.1 Free fatty acid receptor 1 (FFA1)	23
1.4.2 Free fatty acid receptor 4	31
1.5 Receptor desensitisation.....	44
1.5.1 Receptor phosphorylation	48
1.5.2 Receptor internalisation	49
1.5.3 Receptor recycling and resensitisation.....	51
1.5.4 Receptor down regulation	51
1.5.5 β -arrestin and GPCR trafficking	52
1.6 Aims of the project	53
2 Materials and Methodology	55
2.1 Materials	55
2.1.1 General Reagents, Enzymes and Kits	55
2.1.2 Antibodies and antisera	58
2.1.3 Tissue culture.....	58
2.1.4 Buffers and solutions	60
2.1.5 Pharmacological test compounds	62
2.2 Molecular Biology Protocols	63
2.2.1 Preparation of Luria Bertani broth.....	63
2.2.2 Preparation of LB plates	63
2.2.3 Preparation of competent bacterial cells	63

2.2.4	Transformation of competent bacterial cells	64
2.2.5	Preparation of plasmid DNA	65
2.2.6	Quantification of DNA	66
2.2.7	Polymerase chain reaction	66
2.2.8	PCR purification	67
2.2.9	Digestion of DNA with restriction endonucleases	68
2.2.10	DNA gel electrophoresis	68
2.2.11	DNA purification from agarose gels	69
2.2.12	Ligation of DNA	70
2.2.13	DNA sequencing	70
2.3	Construction of expression vectors to study hFFA1 and hFFA4	70
2.3.1	Construction of pcDNA5 for inducible expression of hFFA1	71
2.3.2	Construction of pcDNA3 for constitutive expression of hFFA1	72
2.3.3	Construction of pcDNA5 for inducible expression of hFFA4	73
2.3.4	Construction of pcDNA3 for constitutive expression of hFFA4	74
2.3.5	Construction of CD86-mVenus	75
2.4	Cell Culture and Transfections	76
2.4.1	Cell maintenance	76
2.4.2	Transfection and generation of stable cell lines	78
2.5	Biochemical and biophysical assays	81
2.5.1	Preparation of cell lysates	81
2.5.2	Preparation of cell membranes and cytosolic fractions	81
2.5.3	Estimation of protein concentration by BCA method	82
2.5.4	SDS-PAGE	82
2.5.5	Western blot	83
2.5.6	Quantification of Western blot	84
2.5.7	Visualisation of receptor expression by epifluorescence microscopy	85
2.5.8	Visualisation of receptor internalisation by confocal microscopy	85
2.5.9	FRET microscopy to investigate receptor oligomerisation	86
2.5.10	Analysis of FRET images	89
2.5.11	Imaging studies to investigate cell localisation	90
2.5.12	ArrayScan™ to quantify receptor internalisation	90
2.5.13	BRET based recruitment of β -arrestin2	93
2.5.14	BRET saturation experiments to detect receptor oligomerisation	94
2.5.15	Myo-Inositol 1 Phosphate accumulation assay	97
2.5.16	Single-cell calcium imaging	100
2.5.17	Calcium mobilisation assay using cell populations	101
2.5.18	Biotinylation	102
2.5.19	Cell surface ELISA	104
2.5.20	Fluorescence intensity	106
2.5.21	Data Analysis	106
3	Generation and characterisation of cell lines	110

3.1	Generation and characterisation of cell lines expressing hFFA1	110
3.1.1	Flp-In TM T-REx TM 293 cells able to express hFFA1-mVenus-HA	111
3.1.2	Flp-In TM T-REx TM 293 cells able to express hFFA1-GFP2-HA	115
3.1.3	A HEK293 cell line expressing hFFA1-mVenus-HA	118
3.1.4	A β -arrestin1/2-null HEK293 cell line expressing hFFA1-mVenus-HA	120
3.1.5	A $G\alpha_{q/11}$ knockout HEK293 cell line expressing hFFA1-mVenus-HA	122
3.2	Generation and characterisation of cell lines expressing hFFA4	124
3.2.1	Flp-In TM T-REx TM 293 cells able to express FLAG-hFFA4-mVenus	124
3.2.2	Flp-In TM T-REx TM HEK293 cells able to express FLAG-hFFA4-GFP2	128
3.2.3	HEK293 cell line expressing FLAG-hFFA4-mVenus	131
3.2.4	β -arrestin1/2 knockout HEK293 cell line expressing FLAG-hFFA4-mVenus	133
3.2.5	A $G\alpha_{q/11}$ knockout cell line expressing FLAG-hFFA4-mVenus	135
3.3	Generation and characterisation of double stable cell lines	137
3.3.1	Flp-In TM T-REx TM HEK293 cell lines expressing both hFFA1-mVenus and hFFA1-GFP2	137
3.3.2	Flp-In TM T-REx TM HEK293 cell lines expressing hFFA4-mVenus and hFFA4-GFP2	141
3.3.3	Flp-In TM T-REx TM HEK293 cell lines expressing both hFFA4-GFP2 and hFFA1-mVenus	145
3.3.4	A cell-based model for FFA4-ligand screening	150
3.4	Discussion	154
4	Characterisation of pharmacological ligands	156
4.1	Ligands acting at FFA4	156
4.1.1	Intracellular calcium level	157
4.1.2	β -arrestin2 recruitment	160
4.2	TUG-1275 is a FFA4 antagonist	162
4.2.1	TUG-1275 blocks agonist-promoted phosphorylation of hFFA4	162
4.2.2	TUG-1275 inhibits agonist-induced β -arrestin2 recruitment to hFFA4	164
4.2.3	TUG-1275 inhibits agonist-promoted internalisation of hFFA4 in quantitative internalisation assays	166
4.2.4	TUG-1275 inhibits agonist promoted internalisation of hFFA4 visualised via confocal microscopy	168
4.2.5	TUG-1275 inhibits agonist-promoted elevation of intracellular calcium	171
4.2.6	TUG-1275 inhibits TUG-891 mediated accumulation of IP ₁	173
4.3	Ligands acting at hFFA1	175
4.3.1	Regulation of intracellular calcium levels by hFFA1	175
4.3.2	β -arrestin2 recruitment at hFFA1	178
4.4	GW-1100 is a FFA1 antagonist	180
4.4.1	GW-1100 inhibits β -arrestin2 recruitment at hFFA1	180
4.4.2	GW-1100 inhibits the elevation of intracellular calcium levels via FFA1	182
4.5	Discussion	184
4.5.1	Ligands for hFFA1	184
4.5.2	Ligands for hFFA4	186
5	Desensitisation of hFFA1 and hFFA4	190
5.1	Desensitisation of hFFA1	190
5.1.1	Repeated exposure of agonist desensitises hFFA1	190

5.1.2	Internalisation of hFFA1	193
5.2	Desensitisation of hFFA4.....	197
5.2.1	Repeated exposure of agonist desensitises hFFA4	197
5.2.2	Phosphorylation of hFFA4.....	199
5.2.3	Internalisation of hFFA4	204
5.3	Role of β -arrestins in the desensitisation process.....	216
5.3.1	β -arrestin1/2 in the desensitisation of hFFA1	216
5.3.2	Role of β -arrestin1/2 in the desensitisation of hFFA4.....	220
5.4	Role of $G_{q/11}$ in the regulation of hFFA1 and hFFA4	230
5.4.1	Role of $G_{q/11}$ in the regulation of hFFA1	230
5.4.2	Role of $G_{q/11}$ in the regulation of hFFA4.....	233
5.5	Discussion.....	243
6	Oligomerisation of hFFA1 and hFFA4	247
6.1	Homo-oligomerisation of hFFA1	247
6.1.1	FRET microscopy reveals homo-oligomerisation in hFFA1	247
6.1.2	Cell localisation of hFFA1 oligomers.....	250
6.2	Homo-oligomerisation of hFFA4	252
6.2.1	FRET microscopy reveals homo-oligomerisation of hFFA4	252
6.2.2	Cell localisation of hFFA4 homo-oligomers	254
6.2.3	BRET saturation reveals homo-oligomerisation of hFFA4	256
6.3	Hetero-oligomerisation of hFFA1 and hFFA4	259
6.3.1	FRET microscopy reveals hetero-oligomerisation between hFFA1 and hFFA4.....	259
6.3.2	Cell localisation of hFFA1/hFFA4 hetero-oligomers	262
6.3.3	Hetero-oligomerisation of hFFA1 and hFFA4 detected by BRET	264
6.4	Discussion.....	266
7	Final discussion	270
	References	277

List of Tables

Table 1-1. G_{α} subunits and their effectors	5
Table 1-2. $G_{\beta\gamma}$ subunits and their effectors	5
Table 1-3. Classification of GPCRs	8
Table 1-4. G protein family and their expression	9
Table 1-5. FFA1 ligands	30
Table 1-6. Tissue expression and physiological function of FFA4	41
Table 1-7. FFA4 ligands	44
Table 2-1. Pharmacological test compounds.....	62
Table 2-2. Polymerase chain reaction mixture	66
Table 2-3. Restriction digestion mixture	68
Table 2-4. Ligation reaction mixture.....	70
Table 2-5. Plasmids and primers used in cloning.....	71

List of Figures

Figure 1-1. Structural organisation of a cartoon GPCR.	3
Figure 1-2. Illustration of GPCR signalling.	7
Figure 1-3. G protein biased signalling.	11
Figure 1-4. Biased signalling.	12
Figure 1-5. Potential roles of GPCR oligomerisation during the GPCR life cycle.	14
Figure 1-6. Signaling pathways and their associated biological outcomes for the FFA2 and FFA3 receptors.	21
Figure 1-7. Expression and function of FFA1.	24
Figure 1-8. Signalling pathways and their associated biological outcomes for the FFA1 receptor.	26
Figure 1-9. Snake plot of hFFA1 receptor.	27
Figure 1-10. FFA4 expression and functions.	32
Figure 1-11. Splice variation of FFA4.	34
Figure 1-12. Signalling pathways and their associated biological outcomes for FFA4.	35
Figure 1-13. Anti-inflammatory activity mediated through FFA4 biased signalling.	37
Figure 1-14. Desensitisation processes for GPCRs.	47
Figure 2-1. Preparation of competent XL-1 blue.	64
Figure 2-2. Schematic diagram of the PCR process.	67
Figure 2-3. Construction of pcDNA5/FRT/TO for the expression of hFFA1-mVenus-HA and hFFA1-GFP2-HA.	72
Figure 2-4. Construction of pcDNA3 incorporating hFFA1-mVenus-HA or hFFA1-GFP2-HA.	73
Figure 2-5. Construction of pcDNA5/FRT/TO incorporating FLAG-hFFA4-mVenus or FLAG-hFFA4-GFP2.	74
Figure 2-6. Construction of pcDNA3 incorporating FLAG-hFFA4-mVenus or FLAG-hFFA4-GFP2.	75
Figure 2-7. Construction of plasmid incorporating CD86-mVenus.	76
Figure 2-8. Basis of FRET microscopy.	88
Figure 2-9. High content screen of ligand induced receptor internalisation by ArrayScan™ II High Content Analyser.	92
Figure 2-10. BRET based recruitment of β -arrestin2.	94
Figure 2-11. BRET saturation for detection of receptor oligomerisation.	96
Figure 2-12. Myo-Inositol 1 phosphate (IP1) accumulation assay.	99
Figure 2-13. Biotinylation to investigate receptor internalisation.	103
Figure 2-14. Enzyme-linked immunosorbent assay.	105
Figure 3-1. Characterisation of a Flp-In™ T-REx™ 293 cell line able to express inducibly hFFA1-mVenus-HA.	112
Figure 3-2. Functional characterisation of a Flp-In™ T-REx™ 293 cell line able to express inducibly hFFA1-mVenus-HA.	114

Figure 3-3. Characterisation of a Flp-In TM T-REx TM 293 cell line able to express inducibly hFFA1-GFP2-HA.	116
Figure 3-4. Functional characterisation of a Flp-In TM T-REx TM 293 cell line able to express inducibly hFFA1-GFP2-HA.....	117
Figure 3-5. Characterisation of constitutive expression of hFFA1-mVenus-HA in HEK293 cells...	119
Figure 3-6. Characterisation of β -arrestin1/2-null HEK293 cells constitutively expressing hFFA1-mVenus-HA.	121
Figure 3-7. Characterisation of $G\alpha_{q/11}$ -null HEK293 cells constitutively expressing hFFA1-mVenus-HA.....	123
Figure 3-8. Characterisation of a Flp-In TM T-REx TM 293 cell line able to express inducibly FLAG-hFFA4-mVenus.	125
Figure 3-9. Functional characterisation of the expression of FLAG-hFFA4-mVenus.	127
Figure 3-10. Characterisation of a Flp-In TM T-REx TM 293 cell line able to express inducibly FLAG-hFFA4-GFP2.	129
Figure 3-11. Functional characterisation of the expression of FLAG-hFFA4-GFP2.	130
Figure 3-12. Characterisation of the constitutive expression of FLAG-hFFA4-mVenus in HEK293 parental cells.	132
Figure 3-13. Characterisation of β -arrestin1/2 knockout HEK293 cells constitutively expressing FLAG-hFFA4-mVenus.	134
Figure 3-14. Characterisation of $G\alpha_{q/11}$ -knockout HEK293 cells constitutively expressing FLAG-hFFA4-mVenus.	136
Figure 3-15. Immunoblotting clones expressing both hFFA1-mVenus-HA and hFFA1-GFP2-HA. ..	138
Figure 3-16. Characterisation of a Flp-In TM T-REx TM 233 cell line inducibly expressing hFFA1-mVenus-HA and constitutively expressing hFFA1-GFP2-HA.....	139
Figure 3-17. Relative expression of hFFA1-mVenus and hFFA1-GFP2 in a Flp-In TM T-REx TM 293 cell line.	140
Figure 3-18. Selection of clones inducibly expressing FLAG-hFFA4-mVenus and constitutively expressing FLAG-hFFA4-GFP2.....	141
Figure 3-19. Characterisation of a Flp-In TM T-REx TM 233 cell line inducibly expressing FLAG-hFFA4-mVenus and constitutively expressing FLAG-hFFA4-GFP2.	143
Figure 3-20. Relative expression of FLAG-hFFA4-mVenus and FLAG-hFFA4-GFP2 in a Flp-In TM T-REx TM 293 cell line.	144
Figure 3-21. Selection of clones inducibly expressing FLAG-hFFA4-GFP2 and constitutively expressing hFFA1-mVenus-HA.....	145
Figure 3-22. Characterisation of a Flp-In TM T-REx TM 233 cell line inducibly expressing FLAG-hFFA4-GFP2 and constitutively expressing hFFA1-mVenus-HA.	146
Figure 3-23. Relative expression of FLAG-hFFA4-GFP2 and hFFA1-mVenus-HA in a Flp-In TM T-REx TM 293 cell line.....	148
Figure 3-24. Effect of doxycycline on the constitutive expression of hFFA1.....	149
Figure 3-25. Characterisation of expression of FLAG-hFFA4-eYFP and β -arrestin2- <i>Renilla</i> luciferase in Flp-In TM T-REx TM 293 double stable cells.....	151
Figure 3-26. Functional characterisation of a cell-based model for FFA4-ligand screening.	153
Figure 4-1. TUG-891 and TUG-1197 produce elevation of intracellular calcium via hFFA4.	158
Figure 4-2. TUG-891 but not TUG-1197 displays low potency mediated activation of hFFA1.....	159

Figure 4-3. β -arrestin2 recruitment to hFFA4 induced by agonists.	161
Figure 4-4. TUG-1275 prevents agonist-promoted phosphorylation of hFFA4.	163
Figure 4-5. TUG-1275 inhibits TUG-891 promoted β -arrestin2 recruitment to hFFA4.	165
Figure 4-6. TUG-1275 inhibits TUG-891 promoted internalisation of hFFA4.	167
Figure 4-7. TUG-891 promoted internalisation of hFFA4 as visualized by confocal microscopy. .	169
Figure 4-8. TUG-1275 inhibits TUG-891 promoted internalisation of hFFA4 as visualized by confocal microscopy.	170
Figure 4-9. TUG-1275 inhibits hFFA4 but not hFFA1 agonist promoted intracellular calcium levels.	172
Figure 4-10. TUG-1275 inhibits TUG-891 promoted accumulation of IP_1 via hFFA4.	174
Figure 4-11. TUG-770 and TUG-905 cause elevation of intracellular calcium via hFFA1.	176
Figure 4-12. TUG-770 but not TUG-905 displays low potency mediated activation of hFFA4.	177
Figure 4-13. TUG-770 and TUG-905 induce β -arrestin2 recruitment to hFFA1.	179
Figure 4-14. GW-1100 inhibits TUG-905 promoted β -arrestin2 recruitment to hFFA1.	181
Figure 4-15. GW-1100 inhibits TUG-905 mediated elevation of intracellular calcium via hFFA1.	183
Figure 5-1. Repeated exposure hFFA1 to agonist desensitises the receptor.	192
Figure 5-2. Visualisation of agonist promoted internalisation of hFFA1.	194
Figure 5-3. hFFA1 undergoes constitutive internalisation.	196
Figure 5-4. Agonist promoted desensitisation of hFFA4 signalling.	198
Figure 5-5. Homologous phosphorylation of hFFA4.	200
Figure 5-6. Protein kinase C mediates heterologous phosphorylation of hFFA4.	202
Figure 5-7. PKC contributes to agonist-promoted phosphorylation of hFFA4.	203
Figure 5-8. TUG-891 promotes internalisation of hFFA4.	205
Figure 5-9. PMA induces internalisation of hFFA4.	207
Figure 5-10. Role of PKC in the internalisation of hFFA4.	209
Figure 5-11. Quantification of hFFA4 internalisation.	211
Figure 5-12. Ligand regulation of cell surface hFFA4.	213
Figure 5-13. Quantification of hFFA4 internalisation by biotinylation.	215
Figure 5-14. Visualisation of agonist promoted internalisation of hFFA1.	217
Figure 5-15. Repeated treatment of agonist desensitises hFFA1.	219
Figure 5-16. Recruitment of β -arrestin2 to hFFA4.	220
Figure 5-17. Internalisation of mVenus tagged form of hFFA4.	222
Figure 5-18. Quantification of hFFA4 internalisation with cell surface ELISA.	224
Figure 5-19. Agonist promoted mobilisation of intracellular calcium via hFFA4.	225
Figure 5-20. Repeated treatment with TUG-891 desensitises hFFA4.	227
Figure 5-21. Desensitisation of hFFA4.	229
Figure 5-22. $G_{q/11}$ coupling to intracellular calcium mobilisation via hFFA1.	231

Figure 5-23. $G\alpha_{q/11}$ coupling to inositol phosphate signalling via hFFA1.	232
Figure 5-24. $G\alpha_{q/11}$ coupling to intracellular calcium mobilisation via hFFA4.	234
Figure 5-25. $G\alpha_{q/11}$ coupling to inositol phosphate signalling via hFFA4.	235
Figure 5-26. Agonist promoted phosphorylation of hFFA4 in $G\alpha_{q/11}$ -null cells.	237
Figure 5-27. Internalisation of hFFA4 is not dependent on $G\alpha_{q/11}$	239
Figure 5-28. Internalisation of hFFA4 is not dependent on $G\alpha_{q/11}$	240
Figure 5-29. PKC mediated internalisation of hFFA4 in $G\alpha_{q/11}$ -null cells.	242
Figure 6-1. FRET analysis of interactions between hFFA1-mVenus-HA and hFFA1-GFP2-HA.	249
Figure 6-2. RFRET analysis of interactions between hFFA1-mVenus-HA and hFFA1-GFP2-HA.	250
Figure 6-3. Co-localisation of the energy donor and acceptor fluorophores attached to hFFA1.	251
Figure 6-4. FRET analysis of interactions between FLAG-hFFA4-mVenus and FLAG-hFFA4-GFP2.	253
Figure 6-5. Co-localisation of the energy donor and acceptor forms of hFFA4.	255
Figure 6-6. Homo-oligomerisation of hFFA4 revealed in BRET saturation studies.	258
Figure 6-7. FRET analysis of interactions between FLAG-hFFA4-GFP2 and hFFA1-mVenus-HA.	260
Figure 6-8. RFRET analysis of interactions between FLAG-hFFA4-GFP2 and hFFA1-mVenus-HA.	261
Figure 6-9. Co-localisation of hFFA4 and hFFA1.	263
Figure 6-10. Hetero-oligomerisation of hFFA1 and hFFA4 in BRET saturation studies.	265

Acknowledgement

I would like to thank my supervisor, Professor Graeme Milligan, for giving me the opportunity to complete my PhD in his state-of-the-art molecular pharmacology laboratory. I especially appreciate that he supported my research with his dynamic guidance and encouragement throughout the work and during my write-up. Professor Graeme has created a competent research group that helped me to boost up my research experience.

I would like to thank my co-supervisor Dr. Brian Hudson for his help and input into this project. I owe a special debt of gratitude to Laura Jenkins who supported me all times. Without her help it would never been easy to settle in the new environment. Her constant support and encouragement helped me to learn a number of molecular techniques and experiments. Many thanks to Dr. John Padiani for his continuous support in making me understand many microscopic experiments specifically confocal and FRET microscopy. Thanks to Dr. Elisa Alvarez-Curto for her invaluable suggestions during my work. I am very grateful to Dr. Kenneth Watterson for his valuable opinion during my work. I really appreciate the encouragement from Dr. Sara Marsango, Dr. Amanda Mackenzie, Dr. Daniele Bolognini, Dr. Richard Ward. Thanks to my fellow PhD students Nina Divorty and Eugenia Sergeev; we started work together. Thanks to Zobaer Al Mahmud, Frederike Muskens and Davide Capoferri who made the lab enjoyable.

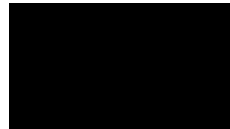
I am very grateful to have incredibly supportive friends and family. I specially thank to my mother Jobeyda Begum and my father Tofazzal Hossain for always keeping me in their prayers. Thanks to my brothers and sisters for their constant encouragement. Heartiest thanks to my wife Meherun Nahar, my daughter Jemin Raihan and my son Zabid Raihan for their support and sacrifice during my studies.

Finally, I would like to thank the Commonwealth Scholarship Commission for funding my research and the University of Glasgow for giving me the opportunity to work in an excellent academic environment.

Author's Declaration

I declare that, except where explicit reference is made to the contribution of others, that this thesis is the result of my own work and has not previously been submitted for a degree or diploma at the University of Glasgow or at any other institution.

Signature



Name: Sheikh Zahir Raihan

Date: 28.04.2017

Abbreviations

[Ca ²⁺] _i	Intracellular calcium concentration
ADME	Absorption, Distribution, Metabolism and Excretion
AP-2	Adaptor Protein-2
ATP	Adenosine Triphosphate
BCA	Bicinchoninic acid
BIM-1	Bisindolylmaleimide-1
BRET	Bioluminescence Resonance Energy Transfer
BSA	Bovine Serum Albumin
Ca ²⁺	Calcium
cAMP	Cyclic Adenosine Monophosphate
Cas-9	CRISPR associated protein 9
CCK	Dholecystokinin
CCPs	Clathrin-Coated Pits
CD-86	Cluster of Differentiation 86
cDNA	Complementary deoxyribonucleic acid
cGMP	Cyclic Guanosine Monophosphate
CHO	Chinese Hamster Ovary
COX-2	Cyclooxygenase-2
CRISPR	Clustered Regularly Interspaced Short Palindromic Repeats
DAG	Diacylglycerol
DIO	Diet Induced Obesity
DMEM	Dulbecco's Modified Eagle's Medium
DMSO	Dimethyl Sulfoxide
DNA	Deoxyribonucleic acid
dNTP	Deoxynucleoside Triphosphate
ECL	Enhanced Chemiluminescent
EDTA	Ethylene Diamine Tetra Acetic acid
EGFP	Enhanced Green Fluorescent Protein
ELISA	Enzyme-Linked Immunosorbent Assay
ER	Endoplasmic Reticulum
eYFP	Enhanced Yellow Fluorescent Protein
FBS	Foetal Bovine Serum
FFA	Free Fatty Acid receptor
FFA1	Free Fatty Acid receptor 1
FFA2	Free Fatty Acid receptor 2
FFA3	Free Fatty Acid receptor 3
FFA4	Free Fatty Acid receptor 4
FRET	Fluorescence Resonance Energy Transfer
G protein	Guanine nucleotide binding protein
GABA	γ-Aminobutyric Acid
GDP	Guanosine Diphosphate
GFP	Green Fluorescent Protein
GFP2	Green Fluorescent Protein 2
GIP	Gastric Inhibitory Peptide
GLP-1	Glucagon-Like Peptide-1
GLUT4	Glucose Transporter Type 4

GOI	Gene of Interest
GPCR	G Protein-Coupled Receptor
GRKs	G protein Receptor Kinases
GSIS	Glucose-Stimulated Insulin Secretion
GTP	Guanosine Triphosphate
HBSS	Hank's Balanced Salt Solution
HEK	Human Embryonic Kidney
HFD	High Fat Diet
HRP	Horseradish Peroxidase
HTRF	Homogenous Time Resolved Fluorescence
IL	Interleukin
INS-1E	Insulin secreting cell line-1E
IP1	Inositol 1 Phosphate
IP3	Inositol 1,4,5 Trisphosphate
LB	Luria-Bertani
LPS	Lipopolysaccharide
MAP	Mitogen-Activated Protein Kinases
MCFAs	Medium Chain Fatty Acids
MIN6	Mouse Insulinoma cell line
mRNA	messenger Ribonucleic Acid
MUFA	Monounsaturated Fatty Acid
PAGE	Polyacrylamide Gel Electrophoresis
PAR1	Protease Activated Receptor 1
PBS	Phosphate Buffered Solutions
PCR	Polymerase Chain Reaction
PEI	Polyethyleneimine
PKA	Protein Kinase A
PKC	Protein Kinase C
PLC	Phospholipase C
PMA	Phorbol Myristate Acetate
PPAR γ	Peroxisome Proliferator Activated Receptor γ
PTX	Pertussis Toxin
PUFA	Poly Unsaturated Fatty Acid
PYY	Peptide YY
RET	Resonance Energy Transfer
RFRET	Ratiometric Fluorescence Resonance Energy Transfer
RIPA	Radioimmune Precipitation Assay
RLuc	Renilla Luciferase
ROI	Region of Interest
SCFAs	Short Chain Fatty Acids
SDS	Sodium Dodecyl Sulphate
siRNA	Small Interfering Ribonucleic Acid
TBE	Tris/Borate/EDTA
TMB	Tetramethylbenzidine
VEGF	Vascular Endothelial Growth Factor

1 Introduction

1.1 G protein-coupled receptors

G protein-coupled receptors (GPCRs, also termed 7-transmembrane or heptahelical receptors) constitute the largest, most ubiquitous and most versatile family of membrane proteins (Syrovatkina et al., 2016) encoded by the human genome (Lagerstrom and Schioth, 2008). These receptors are key molecular targets of drug discovery (Milligan et al., 2015; Kenakin, 2015; Tautermann, 2014; Holliday et al., 2012). In human cells, over 800 GPCRs have been identified (Fredriksson et al., 2003). These receptors are activated by a wide spectrum of extracellular stimuli, including hormones, chemokines, neurotransmitters, ions, photons, and lipids (Bockaert and Pin, 1999). Coupling with heterotrimeric guanine-nucleotide-binding regulatory proteins (G-proteins) these receptors initiate downstream signalling networks resulting in a broad range of physiological and pathological processes (Venkatakrisnan et al., 2013; Lefkowitz, 2000). Numerous drugs acting on GPCRs have been developed targeting asthma, migraines, cardiac malfunctions, neurological disorders, inflammatory diseases, cancer and recently metabolic disorders (Blad et al., 2012; Rask-Andersen et al., 2011). Owing to their diverse ligands and multiple physiological activities, this set of receptors has frequently been explored as potential drug targets, which is evident from the fact that about 20% of the currently exploited drug targets are based on GPCRs (Rask-Andersen et al., 2011; Klabunde and Hessler, 2002). Moreover, 5 of the top 15 generic drugs and 7 of the top 15 prescription drugs target GPCRs (Salon et al., 2011).

1.1.1 Structural feature of GPCRs

GPCR structures are very important for understanding the molecular mechanisms in signal transduction as well as for developing new therapeutics for the treatment of human diseases. Palczewski et al (2000) first discovered the crystal structure of a GPCR, bovine rhodopsin. Later on a high-resolution structure of the human β_2 -adrenergic receptor bound to a diffusible ligand was elucidated (Cherezov et al., 2007). Then, the first active-state GPCR structure (of ligand free rhodopsin, opsin) followed in 2008 (Scheerer et al., 2008). With the development of membrane protein engineering and crystallography, over 100

structures of GPCRs have been described (Caffrey, 2011; Rosenbaum et al., 2007). These structures have enabled understanding of the structural similarity and diversity of the GPCR family as well as the molecular basis of GPCR-ligand pharmacology. The solved GPCR structures reveal some common structural features among the receptors (Venkatakrishnan et al., 2013).

GPCRs share a common structural architecture of seven TM helical bundles connected by three extracellular loops (ECL1-3) and three intracellular loops (ICL1-3). The N-terminus of a GPCR is at the extracellular side, and the C-terminus is located intracellularly. ECL2 is the longest extracellular loop and exhibits distinct conformations in different GPCR structures. In most of the known GPCR structures, ECL2 is anchored to the extracellular tip of helix, which limits the movement of ECL2 and stabilizes the conformation of the extracellular region (Lu and Wu, 2016; Venkatakrishnan et al., 2013). The N-terminus and the extracellular loops are responsible for recognizing ligands and modulating ligand access. The 7TM bundle region forms the structural core, binding ligands and transducing extracellular signals to the intracellular region through conformational changes (Zhang et al., 2015; Rosenbaum et al., 2009). The intracellular (IC) parts interact with cytosolic G-proteins, arrestins, G protein-coupled receptor kinases (GRKs) and other downstream signalling effectors (Figure 1-1).

Principally the TM region forms the structural core of the receptor. A unique feature of the extracellular region is the presence of disulphide bridges that contribute to receptor stability. Disulphide bridges between TM3 and ECL2 seem to be highly conserved in most GPCR structures (Venkatakrishnan et al., 2013). The TM helix bundle serves as the communication link between the ligand-binding pocket and the downstream signalling effectors (Katritch et al., 2012). In addition to the ICLs, a short amphipathic helix VIII (H8) running parallel to the membrane surface was observed in most of the GPCR structures. This helix VIII has also been reported to be involved in receptor activation and interaction with multiple signalling effectors (Lu and Wu, 2016; Unal and Karnik, 2012).

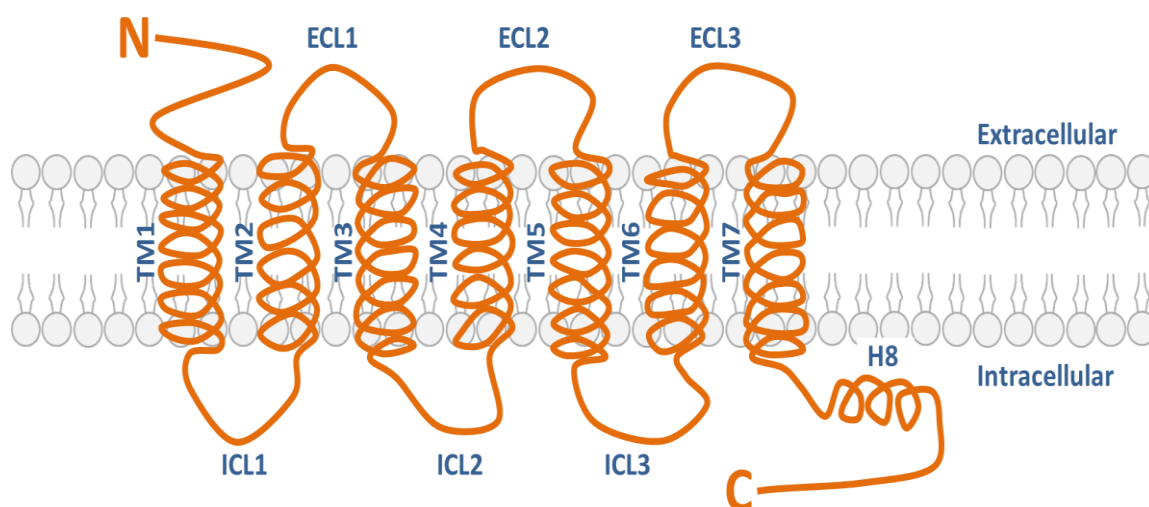


Figure 1-1. Structural organisation of a cartoon GPCR. Membrane spanning transmembrane (TM) helices (TM1–TM7) are shown. N and C termini and the segments containing defined secondary structure in the extracellular (EC) and intracellular (IC) region are shown. The N-terminus of a GPCR is at the extracellular side, and the C-terminus locates intracellularly. The 7TM helical bundle connected by three extracellular loops (ECL1-3) and three intracellular loops (ICL1-3). A short amphipathic helix VIII (H8) runs parallel to the membrane surface in many family members.

1.1.2 GPCR activation

In spite of the remarkable diversity of ligands and ligand-binding sites of GPCRs, the receptors share similar activation mechanisms. However, size, shape and electro-static properties of the ligand-binding pockets are distinct between different receptors (Zhang et al., 2015). Although all ligands have been observed to bind in a pocket in the extracellular side of the TM bundle, different ligands penetrate to different depths within this pocket.

During GPCR activation, both the intracellular parts and the extracellular parts of GPCRs play critical roles. In most of the GPCR structures, there is a large extracellular vestibule as part of an extended hydrophilic channel to the orthosteric binding pocket where the ligands gain access into the binding pockets (Hanson et al., 2012; Srivastava et al., 2014). The organisation of the extracellular loops, particularly the ECL2 connecting transmembrane domains IV and V, is more variable and appears to play a role in ligand binding and entry to the classical ligand binding pocket (Venkatakrishnan et al., 2013; Wheatley et al., 2012). Ligand binding ultimately causes structural rearrangements in the ICLs, facilitating the binding of intracellular effectors (Nygaard et al., 2009; Kobilka, 2007; Samama et al., 1993). Various studies have suggested that ICL2 and ICL3 are G-protein-interacting sites on GPCRs (Wess, 1997). Both GPCRs and G-proteins diffuse freely within the plasma membrane and only agonist-activated GPCRs couple to and activate G-proteins (Strange, 2008). Based on types of G proteins, signal is transduced (Lefkowitz, 2000).

1.1.3 GPCR signalling

GPCRs can be activated by a large number of extracellular stimuli and initiate signalling pathways to transduce a diverse range of cellular activities (Masuho et al., 2015; Civelli et al., 2013). G proteins are inactive when bound to guanosine diphosphate (GDP) and activated with the binding with guanosine triphosphate (GTP). In the inactive form, GDP-bound $G\alpha$ subunits bind tightly to the obligate heterodimer of $G\beta\gamma$. Activation of GPCRs causes conformational changes allowing association with heterotrimeric G proteins. Receptor activation promotes the exchange of GDP for GTP to the G protein (Figure 1-2). GTP binding causes dissociation of $G\alpha$ subunit from $G\beta\gamma$ dimer, resulting in two

functional subunits ($G\alpha$ and $G\beta\gamma$). $G\alpha$ subunit signalling is terminated by the intrinsic GTPase activity of $G\alpha$, which hydrolyses the bound GTP to GDP. GTPase-activating proteins bind to $G\alpha$ to accelerate the intrinsically low GTPase activity of the $G\alpha$ subunit. $G\beta\gamma$ signalling is terminated by re-association with $G\alpha$ -GDP (Syrovatkina et al., 2016). Both $G\alpha$ and $G\beta\gamma$ subunits signal to various cellular pathways (Syrovatkina et al., 2016; Wettschureck and Offermanns, 2005; Gether, 2000). Signal transduction mediated by $G\alpha$ subunit has been summarised below (Table 1-1; Syrovatkina et al., 2016).

Table 1-1. $G\alpha$ subunits and their effectors

$G\alpha$ subunit	Well-defined G-protein effectors	Other G-protein-interacting proteins
$G\alpha_s$, $G\alpha_{olf}$	Adenylate cyclase (+)	Tubulin, Src tyrosine kinase, axin
$G\alpha_o$, $G\alpha_{i1-3}$, $G\alpha_{t1,2}$, $G\alpha_g$, $G\alpha_z$	Adenylate cyclase (-), cGMP phosphodiesterase (+)	Rap1GapII, Src tyrosine kinase, nucleobindin 2, Tubulin, Pins, Pcp1, LGN, GRIN1, Eya2, Pcp2
$G\alpha_q$, $G\alpha_{11}$, $G\alpha_{14}$, $G\alpha_{15/16}$	Phospholipase C- β (+), p63RhoGEF	GRK2, actin, tubulin, PI3K, TPR1, Btk tyrosine kinase, Phospholipase C- ϵ , TRPM8
$G\alpha_{12}$, $G\alpha_{13}$	p115RhoGEF, leukemia-associated RhoGEF, and PDZ-RhoGEF	Gap1, rasGap, Btk tyrosine kinase, Radixin, Hax-1, Cadherins, α -SNAP, p120caterin, Integrin α IIb β 3

(+) indicates stimulation. (-) represents inhibition. Table adapted from Syrovatkina et al. (2016)

In addition to $G\alpha$ proteins, $G\beta\gamma$ can also signal to downstream effectors (Table 1-2; Syrovatkina et al., 2016; Khan et al., 2013). $G\beta\gamma$ can regulate adenyllyl cyclases, phospholipase C β , the inwardly rectifying potassium channel and voltage-gated calcium channels.

Table 1-2. $G\beta\gamma$ subunits and their effectors

Well-defined $G\beta\gamma$ effectors	Other $G\beta\gamma$ -interacting proteins
Adenylate cyclase (+)	Btk-family tyrosine kinase, IP $_3$ receptors, Raf
Phospholipase C- β (+)	kinase, Protein kinase D, Histone
Phosphoinositide 3 Kinases	deacetylase 5 (HDAC5), Tubulin, F-actin,
G protein-coupled receptor kinases	Vinculin, ElmoE, Rab11, mitofusin1, Radil,
K $^+$ and Ca $^{2+}$ channels	activator protein 1, TFE3, TRPM1

(+) indicates stimulation. Table adapted from Syrovatkina et al. (2016)

$G\alpha_s$ and $G\alpha_i$ families of G-proteins regulate adenylyl cyclases. $G\alpha_s$ stimulates adenylyl cyclase to convert ATP into cAMP. Elevated cAMP results in the activation of cAMP-regulated proteins, such as protein kinase A (Figure 1-2). $G\alpha_i$ proteins, on the other hand, inhibit certain isotypes of adenylyl cyclases, leading to reduced intracellular cAMP levels (Wettschureck and Offermanns, 2005). The $G\alpha_q$ family of G-proteins activates the β -isoforms of phospholipase C, which cleaves phosphatidylinositol 4,5-bisphosphate into inositol trisphosphate (IP3) and membrane-bound diacylglycerol (DAG) (Figure 1-2). IP3 binding with IP3 receptors on the membrane of the endoplasmic reticulum causes release of intracellular calcium. On the other hand, DAG activates protein kinase C (Rhee, 2001). Due to the relatively higher amounts of $G\alpha_i$ families of G-proteins in cells, $G\alpha_i$ activation is thought to be the primary source for $G\beta\gamma$ -mediated signalling processes.

Recent studies have revealed that some internalised GPCRs not only remain active but also exhibit sustained signalling (Thomsen et al., 2016; Irannejad et al., 2013; Feinstein et al., 2013). In these case receptors interact strongly with β -arrestins via a C-terminal tail containing clusters of serine/threonine phosphorylation sites. The functional consequences in some instances include biased responses, where the cell-surface signal elicits one set of actions while the signal from internalised receptors exhibits different effects. The vasopressin type 2 receptor continues to generate cAMP and promote PKA activation for prolonged periods after ligand washout and receptor internalization in endosomes (Feinstein et al., 2013). It has been shown that the adrenergic agonist isoprenaline promoted receptor and G protein activation in the plasma membrane as expected, but also in the early endosome membrane, and that internalized receptors contributed to the overall cellular cyclic AMP response within several minutes after agonist application (Irannejad et al., 2013).

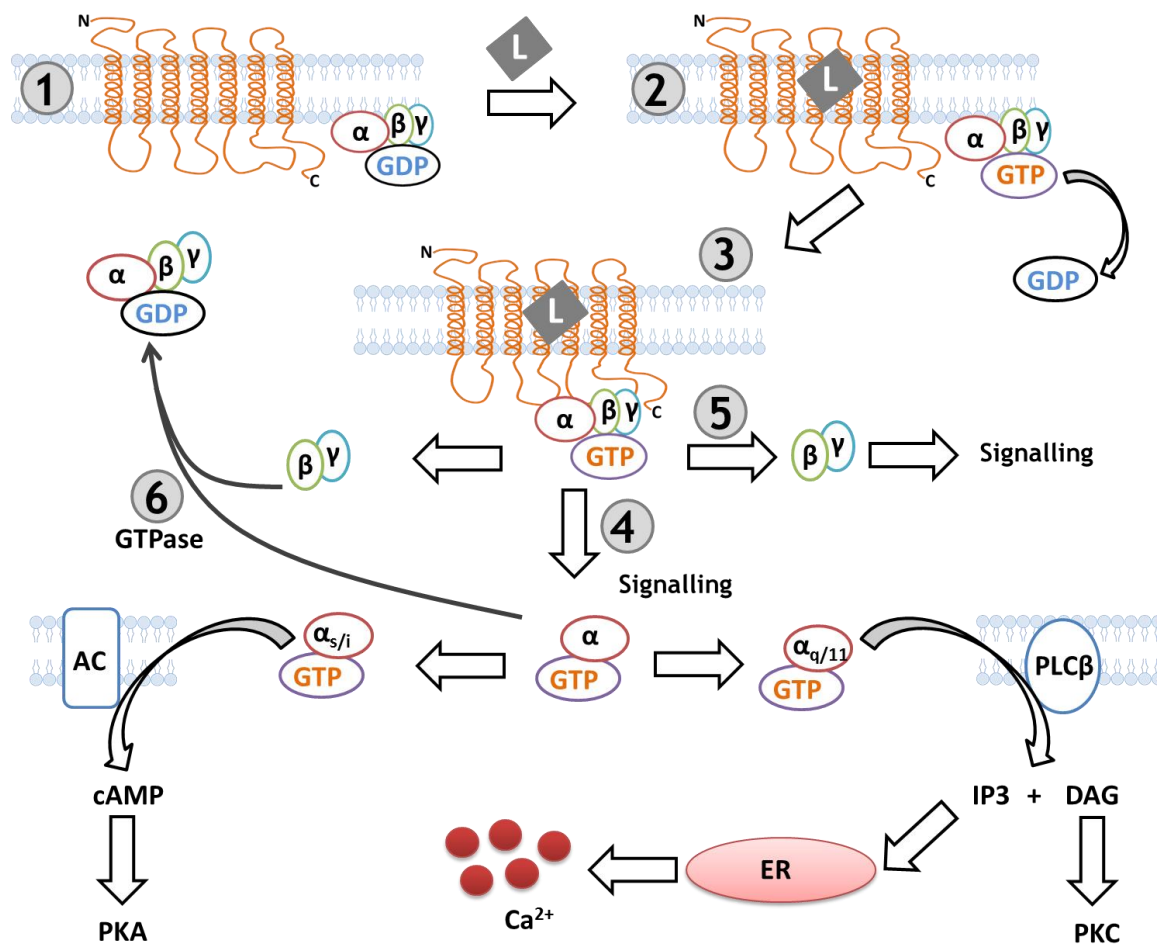


Figure 1-2. Illustration of GPCR signalling. (1) GPCR in the inactive form, GDP-bound $G\alpha$ subunits tightly bound to the heterodimer of $G\beta\gamma$. (2) Receptor activation by extracellular ligands. (3) GPCR binds with heterotrimeric GTP-binding proteins, with the release of GDP from the $G\alpha$ subunit. Exchange of GTP causes dissociation of the GTP-bound $G\alpha$ -subunit and $G\beta\gamma$ -dimer from the GPCR. (4) Dissociated $G\alpha$ subunits can couple with an effector and commence functional signal transduction. Activation of $Gq/11$ activates phospholipase C which promotes release of inositol trisphosphate (IP3) and diacylglycerol (DAG). IP3 binding with IP3 receptors causes release of intracellular calcium from endoplasmic reticulum. On the other hand, DAG activates protein kinase C. Activation of $G\alpha_s$ and $G\alpha_i$ families of G-proteins regulate adenylyl cyclases to convert ATP into cAMP. Elevated cAMP results in the activation of cAMP-regulated proteins, such as protein kinase A. (5) The dissociated $G\beta\gamma$ subunits can also initiate signalling by stimulating adenylyl cyclases, phospholipase C β , inwardly rectifying K^+ channel and voltage-gated Ca^{2+} channels (not shown). (6) G protein signalling is terminated by the intrinsic GTPase activity of $G\alpha$, which hydrolyses the bound GTP to GDP and association with $G\beta\gamma$ subunits to form GDP- $G\alpha\beta\gamma$ complex.

1.1.4 Classification of GPCRs

According to the GPCR data bank GPCRs are classified into six group of families (Table 1-3; Munk et al., 2016)) based on sequence homology and phylogenetic analysis: Class A (Rhodopsin family), class B1 (Secretin family), class B2 (Adhesion family), class C (Glutamate family), class F (Frizzled family) and class T (Taste 2 family). Two more classes of GPCRs exist in non-vertebrates: classes D and class E. It has been suggested that the receptors can be more appropriately classified based on ligand type (Pawson et al., 2014) and can be grouped into receptor families by pharmacological classification of their endogenous ligands that span ions, neurotransmitters, lipids, carbohydrates, nucleotides, amino acids, peptides and proteins.

Table 1-3. Classification of GPCRs

Class	Name/Receptors	No. in Human
A	Rhodopsin	689
B1	Secretin	15
B2	Adhesin	33
C	Glutamate	22
F	Frizzled	11
T	Taste 2	25
D	Fungal mating pheromone receptors	0
E	cAMP receptors	0

Table adapted from Munk et al. (2016)

1.1.5 Heterotrimeric G proteins and their effectors

G-proteins function as molecular binary switches with their biological activity determined by the bound nucleotide (Syrovatkina et al., 2016). Heterotrimeric G-proteins directly relay the signals from activated-GPCRs. These G-proteins are composed of α , β , and γ subunits. There are different isoforms of $G\alpha$ subunits (Table 1-4; Syrovatkina et al., 2016).

Table 1-4. G protein family and their expression

Gα Family	Isoforms	Expression
Gα _s	Gα _s	Ubiquitous
	Gα _{olf}	Olfactory neurons
Gα _i	Gα _{i1}	Widely distributed
	Gα _{i2}	Widely distributed
	Gα _{i3}	Ubiquitous
	Gα _{0A}	Neurons
	Gα _{0B}	Neuroendocrine
	Gα _{t1}	Retinal rods, taste cells
	Gα _{t2}	Retinal cones
	Gα _g	Taste and brash cells
	Gα _z	Neurons, platelets
Gα _q	Gα _q	Ubiquitous
	Gα ₁₁	Ubiquitous
	Gα ₁₄	Kidney, lung, liver
	Gα ₁₅	Hematopoietic cells
Gα ₁₂	Gα ₁₆	Hematopoietic cells
	Gα ₁₂	Ubiquitous
	Gα ₁₃	Ubiquitous

Table adapted from Syrovatkina et al. (2016)

The β and γ subunits are tightly associated and can be regarded as one functional unit. Gβ has five isoforms: Gβ₁, Gβ₂, Gβ₃, Gβ₄ and Gβ₅. While Gβ₅ is mainly found in the brain, other Gβ subunits are widely distributed. Gγ subunits are more diverse. There are 11 isoforms of Gγ: Gγ₁- Gγ₅ and Gγ₇- Gγ₁₂ (Syrovatkina et al., 2016).

1.1.6 GPCR biased signalling

Heterotrimeric G proteins are the main propagators of GPCR-mediated signalling. A specific cellular response is often attributed to the result of a specific G protein activation (Kobilka, 2007; Wettschureck and Offermanns, 2005; Gether, 2000). However, different ligands may activate the same GPCR resulting

coupling with different signalling proteins, thus promoting different signalling cascades. Biased agonism or functional selectivity refers to the ability of GPCR ligands to trigger a subset of responses among all those that can be controlled by a receptor (Benredjem et al., 2016; Mancini et al., 2015b; Wisler et al., 2014). However, system bias is an important issue during investigation of biased agonism. System bias reflects the differences in measurements of biochemical amplification at the cellular level between the assays used (Gundry et al., 2017).

Kenakin et al. (1995) first noted biased agonism as a reversal of the order of potencies for different ligands between alternative G protein signalling pathways. Ligands causing biased signalling are termed biased ligands. Ligand bias is thought to be due to the stabilization of distinct receptor conformational states that differentially activate these alternative signalling pathways (Gundry et al., 2017). Biased agonists have the promise to act as more selective drugs by specifically targeting pathogenic or therapeutic signalling pathways while avoiding others that could lead to side effects. The simplest biased signalling in GPCRs is seen when ligands are able to selectively promote interactions of GPCRs with a specific G protein over other G proteins (Figure 1-3). Biased signalling in GPCRs may allow development of ligands which specifically modulate effectors supporting desired actions (Benredjem et al., 2016; Rajagopal et al., 2010; Kenakin, 2007). Biased agonists have different functional and physiological consequences from conventional balanced agonists and they activate only a selective portion of a cascade (Benredjem et al., 2016; Whalen et al., 2011).

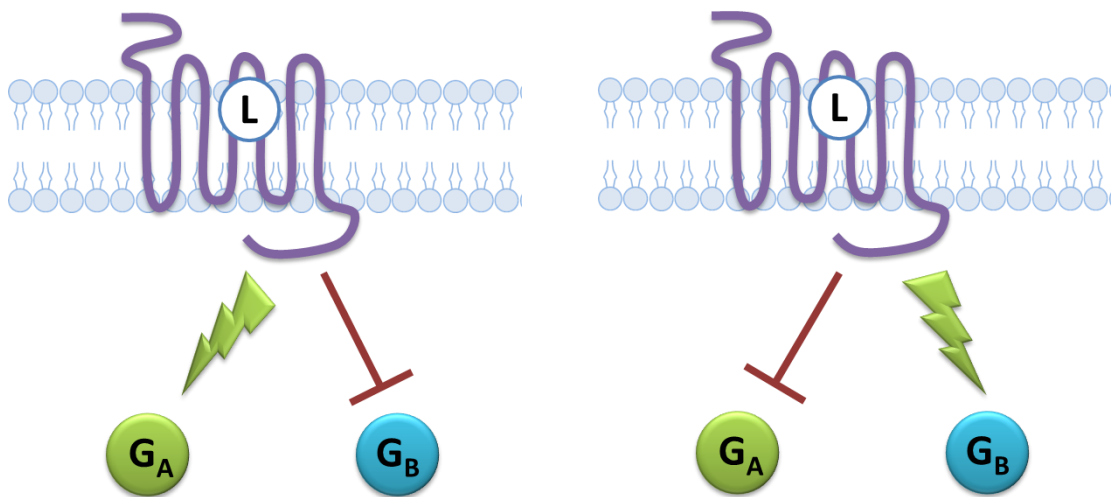


Figure 1-3. G protein biased signalling. GPCR bias agonism may manifest as bias signalling through one specific G protein subunit over another.

Although GPCRs primarily operate by coupling to G proteins, GPCRs can also promote signals that occur independently of G protein activation (Benredjem et al., 2016; Wisler et al., 2014). Typically in GPCR signalling, G proteins and β -arrestins activate distinct signalling pathways, G proteins activate second messengers and β -arrestins regulate receptor desensitization, internalization and activation of MAP kinases (Smith and Rajgopal., 2016; DeWire et al., 2007). Some ligands can selectively promote interactions of GPCRs with heterotrimeric G proteins over β -arrestins or vice versa (Figure 1-4) (Milligan et al., 2017; Shukla et al., 2011). The anti-inflammatory activities mediated through the free fatty acid receptor FFA4 is believed to be responsible via β -arrestin biased signalling (Alvarez-Curto and Milligan, 2016a).

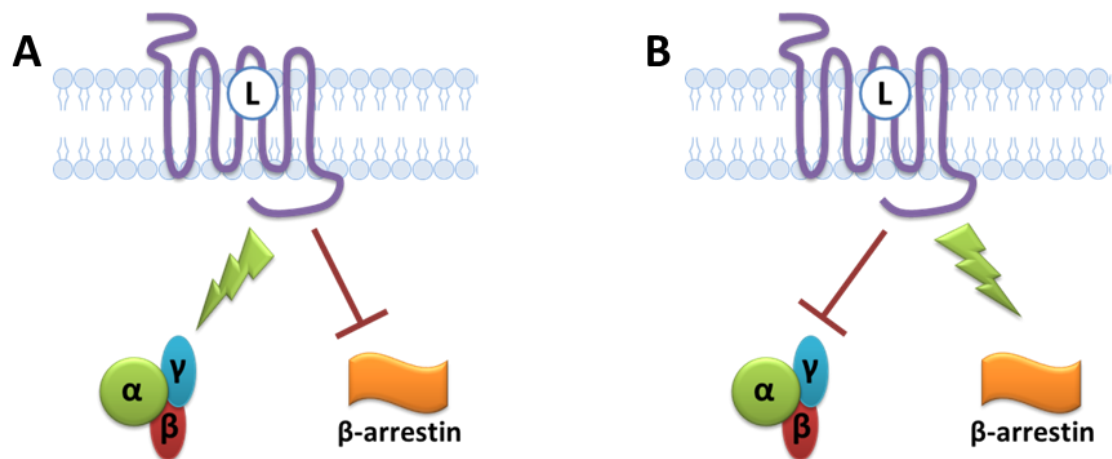


Figure 1-4. Biased signalling. GPCR bias agonism may manifest as bias signalling through (A) G protein subunit over β -arrestin or (B) β -arrestin over G protein subunit.

1.1.7 GPCR oligomerisation

Class A GPCRs represent the largest family of integral membrane proteins and major pharmacological targets which have traditionally been considered to exist and function as monomers (Milligan et al., 2015; Kenakin, 2015; Tautermann, 2014). However, evidence has accumulated over a few years that these receptors can form homo-or hetero-oligomers (Ferre et al., 2014; Milligan, 2013; Pin et al., 2009; Milligan and Bouvier, 2005; Bouvier, 2001). Potential dimeric forms of rhodopsin were identified via a crystal structure. Crystal structures of the class A GPCRs suggests potentially conserved interaction interfaces (Milligan, 2013). Although the observed interfaces may reflect artifacts from the the conditions of crystallisation or during crystal formation, the possibilities of the existence of oligomerisation has gained attention (Ferre et al., 2014). Oligomers of adenosine A₁, dopamine D₂ and metabotropic GABA_B have been observed *in situ* in brain tissue, indicating that the phenomenon is not simply an artefact due to anomalously high levels of expression (Bouvier, 2001). Studies of oligomerisation using traditional biochemical techniques such as immunoblotting, co-immunoprecipitation and cross-linking are very laborious and has lots of limitations including the paucity of selective pharmacological tools and immunological reagents to identify and modulate the function of oligomers. However, with the development of sophisticated biochemical and

biophysical methods over few years, the evidence of GPCRs oligomerisation accumulated steadily to be assemble as homodimers, heterodimers or higher-order oligomers (Milligan, 2007; Milligan, 2008; Milligan, 2009).

GPCR oligomerisation may provide added value in signalling versatility and diversity. However, it's functional significance including maturation, ligand pharmacology, signalling and trafficking are yet to be fully elucidated (Marsango et al., 2015; Ferre et al., 2014; Milligan, 2013). Receptor oligomerisation may go some way toward answering the question, fundamental to GPCR biology, of how a single ligand, acting at a specific receptor, can induce a set of signalling responses, which in turn lead to a range of physiological outcomes (Milligan, 2013; Milligan, 2007). Various experiments revealed that GPCR oligomerisation is generated at an early stage of biosynthesis. In fact, it has been suggested that early-stage oligomerisation may be required for effective folding and maturation of the receptor (Milligan, 2010, 2013; Bulenger et al., 2005). Terrillon and Bouvier (2004) suggested that the entire GPCR life cycle may be controlled by oligomerisation (Figure 1-5). GPCR biosynthesis, transport along the secretory pathway, mechanisms of receptor activation, signal transduction and regulation are greatly influenced by receptor oligomerisation (Terrillon and Bouvier, 2004).

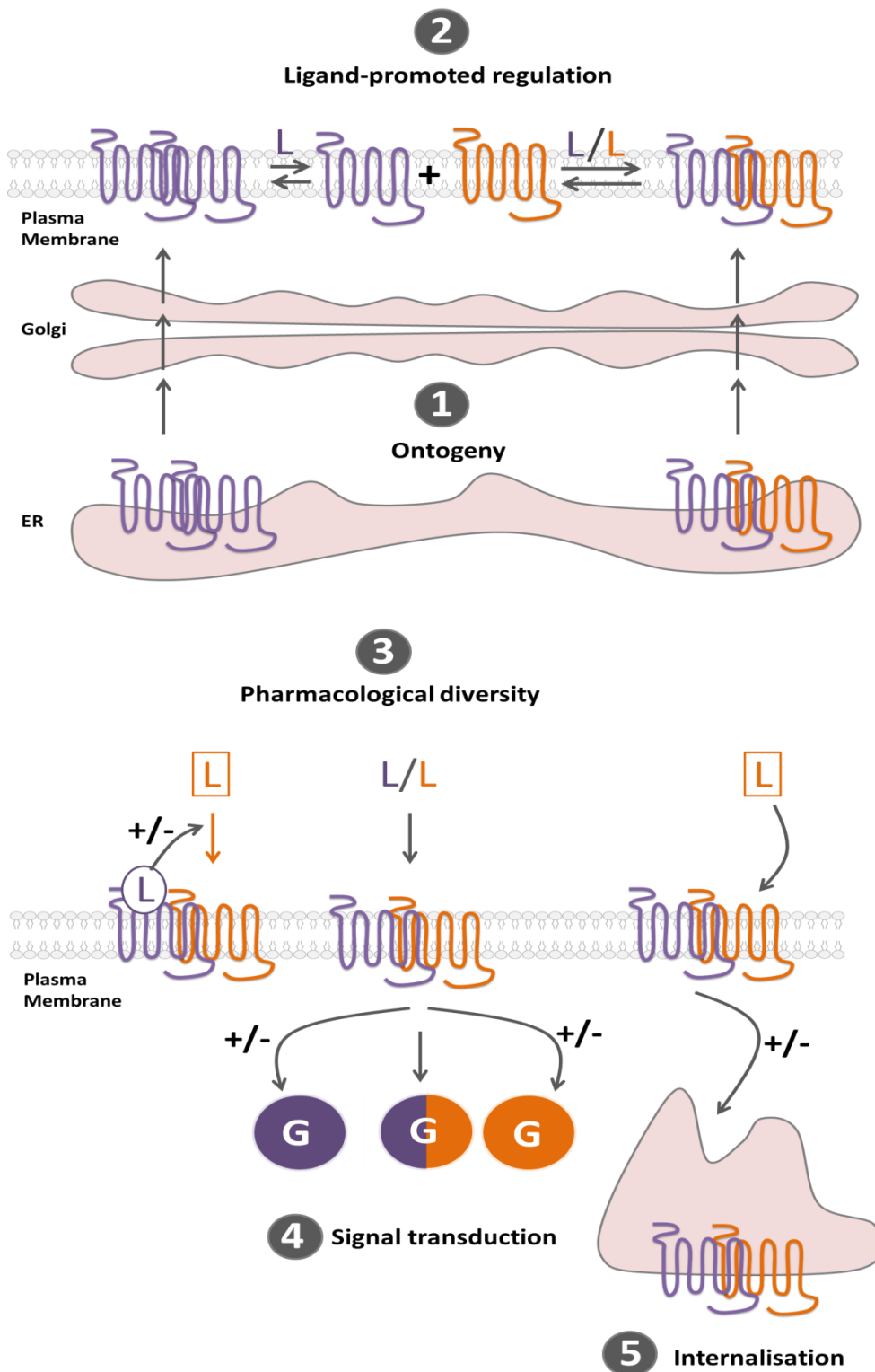


Figure 1-5. Potential roles of GPCR oligomerisation during the GPCR life cycle. (1) Oligomerisation might have a primary role in receptor maturation and allows the correct transport of GPCRs from the ER to the cell surface. (2) Once at the plasma membrane, oligomers might become the target for dynamic regulation by ligand binding. (3) Hetero-oligomerisation might lead to both positive (+) and negative (-) ligand binding cooperativity, as well as (4) potentiating (+)/attenuating (-) signalling or changing G-protein selectivity. (5) Hetero-oligomerisation might promote co-internalisation of two receptors after the stimulation of only one protomer. Alternatively, the presence of a protomer that is resistant to agonist-promoted endocytosis, within a hetero-oligomer, can inhibit the internalisation of the complex. (ER, endoplasmic reticulum; G, G protein; L, ligand). Figure adapted from Terrillon and Bouvier, (2004).

Oligomerisation was previously reported in class C GPCRs, particularly in GABA_B receptors which were reported to form hetero-oligomer between GABA_{R1} and GABA_{R2} necessary for the function of GABA (Kniazeff et al., 2011; Pin et al., 2009). GABA_B receptors display mostly as dimeric and tetrameric species at lower densities, however, higher-order species also appeared with increased expression levels (Calebiro et al., 2013). The cell surface delivery of the GABA_B receptor depends on the heteromeric interaction between GABA_BR₁ and GABA_BR₂ polypeptides. When expressed only alone, the GABA_BR₁ polypeptide is retained in the endoplasmic reticulum. However, co-expression with the GABA_BR₂ polypeptide generates hetero-oligomerisation that results in delivery of the receptor-complex to cell surface. Similar results were reported for the β_2 -adrenoceptor when the C-terminal tail was replaced with the equivalent region of GABA_BR₁ (Salahpour et al., 2004). Oligomerisation is essential for perception of different tastes and flavours. Hetero-oligomerisation between TAS1R₁ and TAS1R₃ taste receptors is necessary for the perception of savoury or umami flavours (Chandrashekar et al., 2006).

Rising evidence indicates that class A GPCRs can form oligomers when expressed in heterologous cell systems (Ferre et al., 2014; Milligan, 2013). Both D₂ and D₃ dopamine receptors form homo- and hetero-oligomers that influence dopaminergic neurotransmission (Pou et al., 2012; Perreault et al., 2011). Monomeric forms of dopamine D₁ or D₂ receptors are coupled Gs or Gi proteins respectively. However, D₁-D₂ hetero-oligomer couples with G α_q protein for signal transduction (Rashid et al., 2007). Aslanoglou et al. (2015) reported both M₂-M₂ and M₃-M₃ homo-oligomers of muscarinic receptors alongside M₂-M₃ hetero-oligomers when both receptors were stably expressed in Flp-InTM T-RExTM 293 cells. These authors showed that selective agonist occupancy of the M₂ receptor resulted in enhanced M₂-M₂ homomer interactions but decreased M₂-M₃ heteromer interactions. Spatial intensity distribution analysis of the serotonin 5-hydroxytryptamine 2C (5-HT_{2C}) receptor revealed that this receptor forms oligomers at the basolateral plasma membrane of cells and that antagonists can reduce their complexity to favour monomeric and dimeric forms of the receptor (Ward et al., 2015). Adenosine A₁-A_{2A} hetero-oligomers can sense the adenosine concentration and respond via G α_i at low concentrations and via G α_s at high concentrations (Cristovao-Ferreira et al., 2013). Signalling by β_2 -adrenergic

receptor can occur through monomeric forms (Whorton et al., 2007), but in crystal structures this receptor has been observed in dimeric configurations (Gahbauer and Bockmann, 2016; Cherezov et al., 2007). β_1 - and β_2 -adrenoceptors form dimers and higher-order oligomers in proportions dependent on the subtype of receptor and on receptor density (Calebiro et al., 2013). At low densities, monomeric species were predominant for the β_1 -adrenoceptor, whereas a higher proportion of dimers were seen for β_2 -adrenoceptors. At densities comparable to receptor expression in native tissue, dimers and higher-order oligomers were the predominant species for both β_1 - and β_2 -adrenoceptors, and agonists did not modify the oligomerisation status.

No universal mechanism of oligomerisation in GPCRs has been identified. Possible membrane-driven mechanisms that influence the oligomerization of GPCRs are potentially dependent on the membrane environment around the receptors (Gahbauer and Bockmann, 2016). A membrane nanodomain known as lipid rafts has been reported to be important in a number of studies (Goddard et al., 2013; Fallahi-Sichani and Linderman, 2009). Disruption of functional oligomers of purinergic P2Y₁₂ receptors into non-functional dimers or monomers leads to partitioning of the receptors out of lipid rafts (Savi et al., 2006). Oligomerization may thus be required for correct localization in membrane nanodomains that are also important for proper signalling (Gahbauer and Bockmann, 2016). However, little is known about the dynamics and regulation of GPCR oligomer formation (Milligan, 2013). Two specific types of intermolecular association have been identified in GPCR homo-oligomers: disulphide bonds and TM-domain interactions. It was observed that TM1, TM4, and TM5 were most frequently involved in oligomeric interactions in β_1 - and β_2 -adrenergic receptors (Mondal et al., 2013).

The development of resonance energy transfer (RET) based-techniques such as fluorescence and bioluminescence resonance transfer (FRET and BRET) have played an important role in the discovery and characterisation of homo- and hetero-oligomers in living cells (Alvarez-Curto et al., 2010; Bouvier et al., 2007; Milligan and Bouvier, 2005; Bouvier, 2001). Using fusion constructs between a GPCR and bioluminescent and/or fluorescent proteins, BRET and FRET are effective techniques to investigate oligomerisation (Ward and Milligan, 2014; Milligan and Bouvier, 2005). Detection of BRET and FRET, even in the absence of

added agonist, suggests that many GPCRs can form constitutive homodimers in intact living cells and that GPCR oligomerisation is not just a biochemical artefact (Bouvier, 2001).

Oligomerisation may modulate various GPCR functions such as cell surface targeting, cooperativity, activation, G-protein coupling and signalling (Milligan, 2010; Palczewski, 2010; Bouvier, 2001). Where the capacity of a selective ligand of one of the receptors to co-internalise two co-expressed receptors have also been used as evidence for hetero-oligomerisation (Milligan, 2010, 2013; Ward et al., 2011b). Altered hetero-oligomerisation has also been reported to lead to clinical disorder (Dalrymple et al., 2008; AbdAlla et al., 2000).

Although promising, there are lots of debates on over interpretation of results or artefacts due to the systems used to explore oligomerisation (Kuszak et al., 2009 and Whorton et al., 2007). One of the most debated issues remains whether ligands promote association or dissociation of oligomers, or whether they bind to pre-formed oligomers and change the oligomeric receptor conformation (George et al., 2002). More structural evidence and studies are needed to explore if there are common underlying mechanisms for GPCR oligomerisation and how such oligomers function in physiological states.

1.1.8 GPCR deorphanisation

GPCRs are encoded by more than 800 genes in the human genome and related GPCRs were quickly recognized and sorted by phylogeny (Fredriksson et al., 2003; Bjarnadottir et al., 2006). From these, approximately 350 GPCRs have been characterized as non-olfactory receptors (Lagerstrom and Schioth, 2008). Approximately 260 of these GPCRs have already been characterized as by identifying their endogenous ligands (Civelli et al., 2013). According to the International Union of Basic and Clinical Pharmacology (IUPHAR), there currently remain over 70 orphan GPCRs with unknown function or ligands (Pawson et al., 2014). This set of GPCRs might be a great therapeutic candidates for the development of future drugs (Ngo et al., 2016; Stockert and Devi, 2015; Hudson et al., 2011).

A common deorphanisation strategy is to consider sequence homology with GPCRs that have known ligands and to identify likely ligands on this basis (Civelli et al., 2006 and Wise et al., 2004). Reverse pharmacology (Mills and Duggan, 1994) has been extensively used to identify ligands for orphan GPCRs. This approach employs expression of an orphan GPCR in a heterologous cell system and then investigation of signalling outcome with potential ligands. This process utilises readouts of receptor internalisation, β -arrestin recruitment or intracellular calcium mobilisation promoted by promiscuous or chimeric G proteins (Milligan, 2002; Hudson et al., 2011). A high throughput technology is frequently employed where a large number of known or potential ligands are screened to identify cellular activities via the orphan GPCR (Civelli et al., 2013; Wise et al., 2004). Reverse pharmacology has proved successful for matching many orphan GPCRs with their cognate ligands (Civelli et al., 2013; Wise et al., 2004), but newer strategies are needed as the success rate of this deorphanisation approach has waned in the last few years. Elucidation of an increasing number of GPCR X-ray crystal structures has facilitated precious structural information of many GPCRs. This structural information has allowed design of novel ligands for potential binding with orphan receptors (Hudson et al., 2011; Mobarec et al., 2009).

However, it is not clear that every orphan GPCR necessarily requires an endogenous ligand, as some of them instead may rely upon constitutive activity or hetero-oligomerise to achieve activation (Civelli et al., 2013). Regardless of their endogenous means of stimulation, identification of surrogate ligands that can modulate the activity of orphan GPCRs will be invaluable for unlocking both their pharmacology and function. However, the pairing of GPCRs with their respective endogenous agonists remains a challenge for pharmacologists.

1.2 Free fatty acid receptors

Free fatty acids were previously known to act as a critical source of energy in our body. They are obtained from food sources and metabolites produced during digestion and from triglyceride stores by lipase-mediated degradation (Hara et al., 2014b). In these decades, it has been reported that free fatty acids can function as signalling molecules in the regulation of various cellular and physiological processes (Milligan et al., 2006b; Stinkens et al., 2015). During

deorphanisation, orphan GPCRs including GPR40, GPR43, GPR41 and GPR120 have been shown to recognise and to be activated by a number of endogenous and dietary free fatty acids (Hara et al., 2014a; Milligan et al., 2006b). The International Union of Basic and Clinical Pharmacology has renamed these previously orphan GPCRs as FFA1, FFA2, FFA3, and FFA4, respectively (Davenport et al., 2013). Among these, FFA1, FFA2 and FFA3 are structurally related (Sawzdargo et al., 1997) but FFA4 is structurally distant (Hirasawa et al., 2005, 2008). These receptors regulate metabolic activity by sensing the level of energy substrate. Many of them control the secretion of metabolic hormones, thus helping to maintain energy homeostasis. It is broadly understood that the pathophysiology of various metabolic diseases like obesity, diabetes and inflammatory disorders are closely associated with FFA signalling (Blad et al., 2012; Reimann et al., 2012).

The physiological significance of individual free fatty acids varies on the carbon chain length (Offermanns, 2014). Based on the number of carbons, these molecules have been classified as short chain fatty acids (SCFAs; $C \leq 6$), medium chain fatty acids (MCFAs; $C=6-12$) and long chain fatty acids (LCFAs; $C \geq 13$). In addition to chain length, fatty acids also vary in the number and positions of unsaturations, and are often broadly classified into the saturated, monounsaturated (MUFAs), and polyunsaturated fatty acids (PUFAs).

Nutrient acquisition and energy regulation are closely related with the gut microbial fermentation of non-digestible carbohydrates. Our gut microbiota produce SCFAs including acetate, propionate and butyrate. These SCFAs have been identified to play vital roles in the prevention and treatment of metabolic disorders and inflammatory conditions (Bolognini et al., 2016a; Milligan et al., 2014; Kuwahara, 2014; Karlsson et al., 2013). Increasing uptake of dietary fibre has been found to reduce the development of these pathophysiological conditions. For example, insulin sensitivity and energy expenditure increase with the increase of fibre-intake (Gao et al., 2009).

The MCFAs and LCFAs are derived either from dietary fat or through de novo synthesis primarily in the liver (Ulven and Christiansen, 2015). Humans are able to synthesise SFAs and MUFAs, however, we are unable to synthesise PUFAs due to the lack of enzymes required for incorporating unsaturation at the n-3 and n-6

positions (Yates et al., 2014). The MCFAs and LCFAs have received significant attention for their effects on enteroendocrine cells in the gut, pancreatic β -cells and adipose tissues (Milligan et al., 2017; Watterson et al., 2014). The well-characterized FFA receptors can be classified into two groups, SCFA receptors, FFA2 and FFA3 and LCFA receptors, FFA1 and FFA4.

1.3 Short chain fatty acid receptors

FFA2 and FFA3 were orphanised in 2003, which was reported by three separate groups (Brown et al., 2003; Le Poul et al., 2003; Nilsson et al., 2003) and are activated by SCFAs. Brown et al. (2003) and Le Poul et al. (2003) demonstrated that FFA2 and FFA3 show a high level of sequence homology which makes them poorly ligand selective (Bolognini et al., 2016b). Although FFA2 and FFA3 share common endogenous ligands and tissue distribution, their G protein signalling is quite different (Milligan et al., 2017). FFA2 can interact with both $G_{\alpha_{i/0}}$ and $G_{\alpha_{q/11}}$ family of G proteins, whereas FFA3 couples predominantly with $G_{i/0}$ G proteins (Figure 1-6). FFA2- $G_{\alpha_{q/11}}$ coupling enhances intracellular Ca^{2+} and PLC, while G_{α_i} coupling inhibits cAMP production (Milligan et al., 2017). Hudson et al. (2013a and 2012) showed that FFA2 recruits β -arrestin2 in an agonist-concentration dependent fashion. Lee et al. (2013) described that β -arrestin recruitment might be linked to anti-inflammatory actions of FFA2.

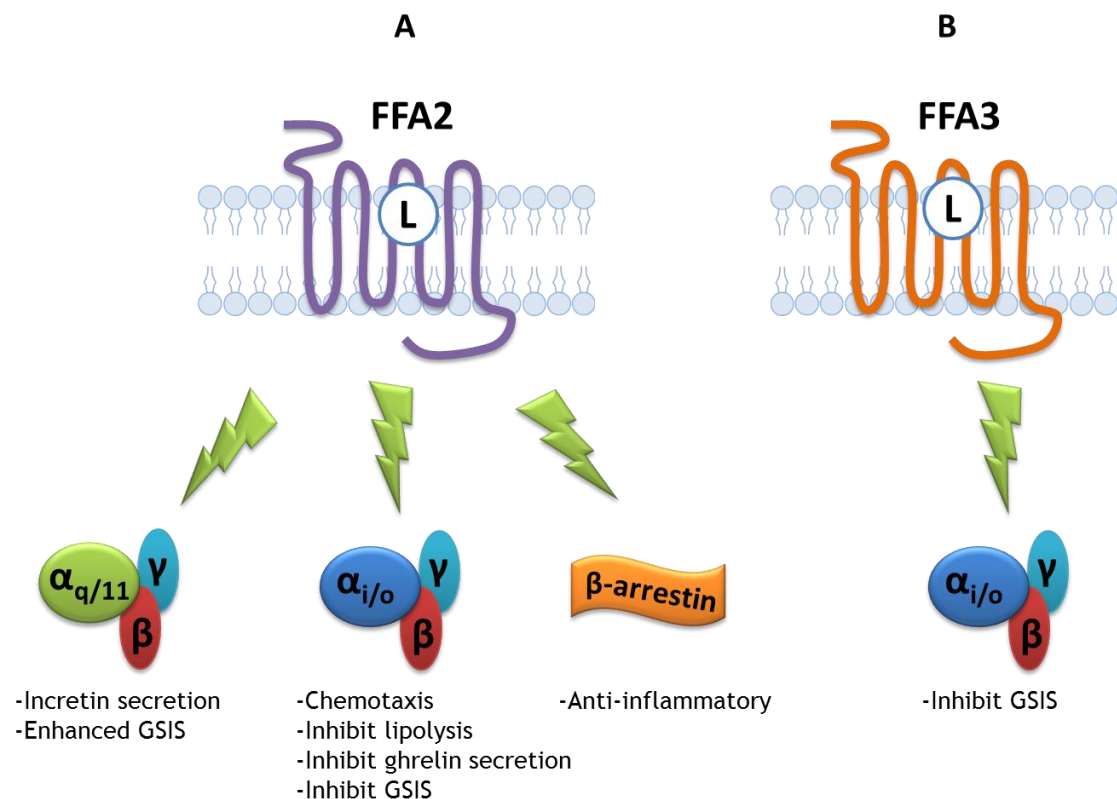


Figure 1-6. Signaling pathways and their associated biological outcomes for the FFA2 and FFA3 receptors. (A) FFA2 signals through $G\alpha_{i/o}$ and $G\alpha_{q/11}$ families of G proteins. $G\alpha_{q/11}$ signalling results increased incretin secretion and enhanced GSIS. $G\alpha_{i/o}$ signalling results in chemotaxis, inhibition of lipolysis, inhibition of ghrelin secretion and inhibition of GSIS. β -arrestin mediated signalling results in anti-inflammatory action. (B) FFA3 activation causes signalling through $G\alpha_{i/o}$ G proteins resulting inhibition of GSIS. (FFA2, Free fatty acid receptor 2; FFA3, Free fatty acid receptor 3; GSIS, Glucose stimulated insulin secretion). Figure was adapted from Milligan et al., (2017).

FFA2 mRNA was found to be expressed in a variety of tissues but highest expression was found in immune cells including neutrophils and monocytes, peripheral blood mononuclear cells, B-lymphocytes and polymorphonuclear cells (Brown et al., 2003; Le Poul et al., 2003; Nilsson et al., 2003). FFA2 expression was also found in pancreas, spleen, skeletal muscle and enteroendocrine cells (Kaji et al., 2014). FFA2 activation has been found to release GLP-1 release from primary L cell line (Tolhurst et al., 2012). Tolhurst et al. (2012) demonstrated that knockout of FFA2 in a mouse model causes significant reduction in GLP-1 and insulin secretion. In adipocytes, FFA2 activation causes attenuation of insulin signalling and decrease fat accumulation (Kimura et al., 2013). Bjursell et al. (2011) showed that FFA2 deficiency protects from high fat diet-induced obesity and dyslipidemia. The knockout mouse models highlighted the

importance of FFA2 in glucose homeostasis and lipid metabolism, which may have therapeutic potential for type 2 diabetes and obesity (Talukdar et al., 2011).

FFA3 (GPR41) is a short chain fatty acid receptor activated by similar ligands of FFA2 (Brown et al., 2003; Le Poul et al., 2003). SCFA Butyrate reported to be highly selective agonist for FFA3 (Kaji et al., 2014). Expression of FFA3 has been reported in adipose tissue, pancreas, placenta, spleen, lung, intestine and the peripheral nervous system (Miyamoto et al., 2016). Expression of FFA3 in human ascending colon has been reported by Tazoe et al. (2009) and the expression levels were higher in the mucosa than in the submucosa and muscle layer. Increase number of scientific reports indicates that FFA3 signalling is important in energy homeostasis and immune functions (Milligan et al., 2017; Bolognini et al., 2016a; Ulven, 2012). FFA3 has also been implicated in acute inflammatory responses (Alvarez-Curto and Milligan, 2016a; Kim et al., 2013a). The morphological studies indicated that PYY- and GLP-1- containing L cells expressing FFA3 are chemosensory cells and that activation of FFA3 by luminal SCFAs may regulate PYY and/or GLP-1 secretion (Kaji et al., 2014). On pancreatic beta cells, FFA3 action was found to inhibit insulin release (Kebede et al., 2009). However, FFA3 agonism enhances insulin sensitivity (De Vadder et al., 2014). In a mouse model, FFA3 activation by propionate resulted in augmentation of plasma leptin concentrations (Xiong et al., 2004). FFA3 activation has been reported to increase gastric emptying and decrease in energy metabolism (Talukdar et al., 2011). FFA3-mediated sympathetic activation demonstrated a good control of energy balance (Kimura et al., 2011). Propionate activated FFA3 was reported to attenuate appetite, hepatic glucose production and improvement of glucose tolerance in mice deficient of intestinal gluconeogenesis (De Vadder et al., 2014). FFA3 contributes to the suppression of energy expenditure under fasting conditions in cultured sympathetic neurons and in mice *in vivo* (Kimura et al., 2011). In FFA3 knockout mice, reduction of SCFAs showed to modulate blood pressure (Pluznick et al., 2013).

FFA3 and GPR42 are two closely related genes localized on human chromosome 19 (Liaw and Connolly, 2009). In primates, FFA3 is segmentally duplicated resulting in GPR42, a gene currently classified as a suspected pseudogene (Puhl et al., 2015). The identity of the cognate physiological ligands for GPR42 is not

clear, although propionate is known to occur *in vivo* at high concentrations under certain pathophysiological conditions (Brown et al., 2003).

1.4 Long chain fatty acid receptors

1.4.1 Free fatty acid receptor 1 (FFA1)

1.4.1.1 Deorphanisation of FFA1

In 2003, three groups independently deorphanised FFA1 (Briscoe et al., 2003; Itoh et al., 2003; Kotarsky et al., 2003). It was the first GPCR discovered to be activated by free fatty acids. Briscoe et al. (2003) used a large library of more than 1500 known and putative natural GPCR agonists and tested these in HEK293 cells expressing FFA1. They demonstrated that a range of medium to long chain saturated and unsaturated fatty acids were capable of increasing intracellular calcium levels in a concentration-dependent manner. Itoh et al. (2003) used CHO cells stably expressing human, mouse or rat FFA1 and used over 1,000 chemical compounds for screening. They reported that LCFAs were able to mobilise intracellular calcium. Kotarsky et al. (2003) used HeLa, CHO, and MIN6 cells for the expression of FFA1 and demonstrated that linolenic acid potently activates FFA1.

1.4.1.2 Expression of FFA1

Expression analysis of messenger RNA in human tissues by real-time quantitative reverse transcription-PCR demonstrated specific expression of FFA1 in pancreas and brain (Briscoe et al., 2003; Itoh et al., 2003). Highest levels of expression were seen in pancreatic β -cell lines and MIN6 cells (Briscoe et al., 2003). Northern blot analysis of selected human tissues also showed detectable expression of the corresponding mRNA mainly in the liver, heart, and the skeletal muscle (Kotarsky et al., 2003). FFA1 expression has also been identified in immune cells, taste buds and cells of the central nervous system (Miyamoto et al., 2016). FFA1 is also expressed by various enteroendocrine cell types, including the L cells that secrete GLP-1 and PYY (Edfalk et al., 2008), K cells that secrete gastric inhibitory peptide (GIP) (Parker et al., 2009) and I cells that secrete cholecystokinin (CCK) (Liou et al., 2011).

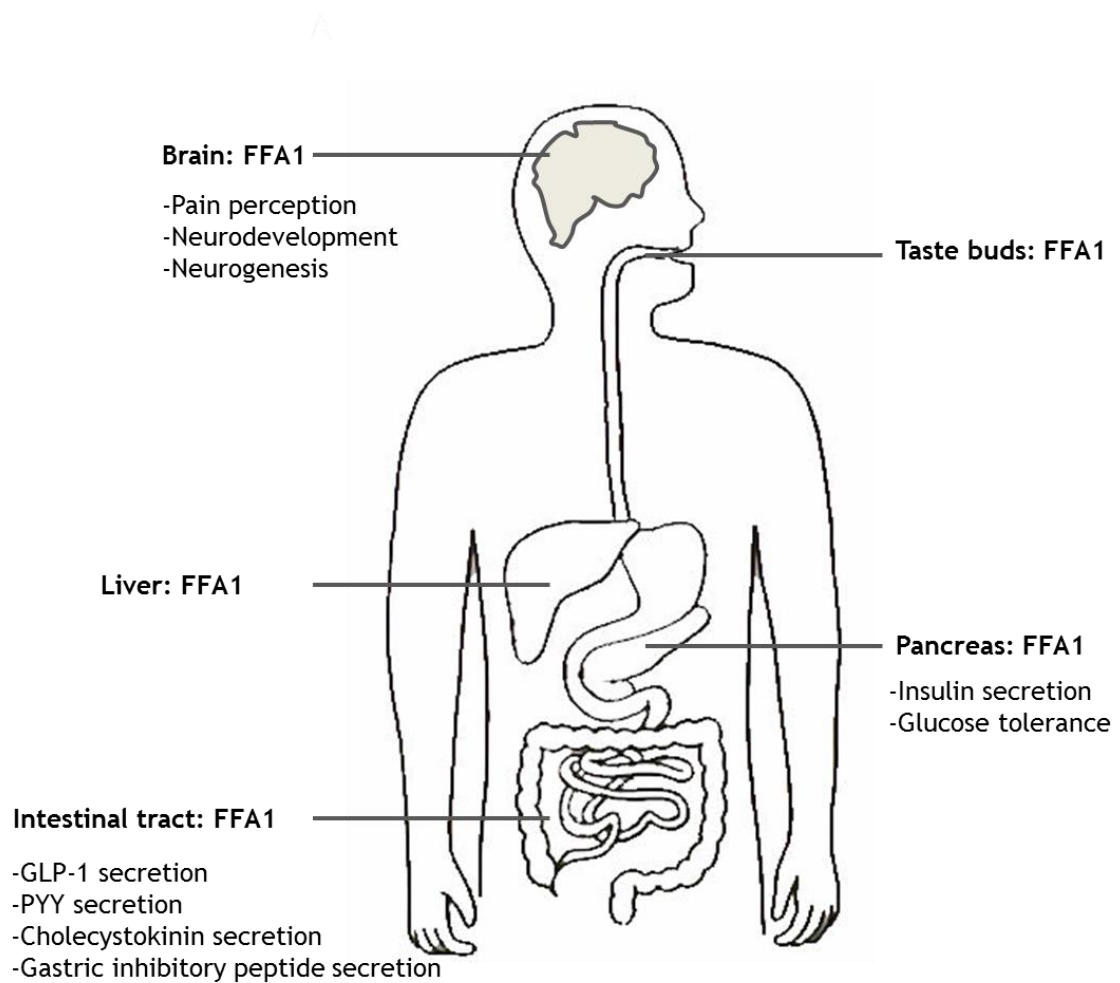


Figure 1-7. Expression and function of FFA1. Reported expression and functions of FFA1 in different cells. FFA1 is highly expressed in the pancreas where FFA1 activity is linked with insulin secretion and helps in glucose tolerance. In the intestinal tract, FFA1 agonism causes releases of GLP-1, PYY, CCK and GIP. In brain, FFA1 found to signal in pain perception, neurodevelopment and neurogenesis. FFA1 expression is also reported in liver and taste buds. (GLP-1, glucagon like peptide 1; PYY, peptide hormone YY; CCK, cholecystokinin; GIP, gastric inhibitory peptide).

1.4.1.3 FFA1 signalling

The initial studies on FFA1 signalling suggested that the receptor coupled to the Ca^{2+} -mobilizing G proteins, $\text{G}\alpha_q$ and $\text{G}\alpha_{11}$ (Briscoe et al., 2003; Kotarsky et al., 2003). Partial sensitivity to pertussis toxin indicated some level of $\text{G}\alpha_i$ mediated signalling for this receptor (Itoh et al., 2003; Kotarsky et al., 2003). However, $\text{G}\alpha_{i/o}$ signalling is less important for FFA1. Coupling with $\text{G}\alpha_{i/o}$ and $\text{G}\alpha_q$ G protein families has been seen in breast cancer cell lines indicating that $\text{G}\alpha_i$ mediated signalling might be tissue specific (Yonezawa et al., 2004). Hauge et al. (2014) reported $\text{G}\alpha_s$ coupling when the receptor was stimulated with certain FFA1 agonists. Recruitment of β -arrestin1/2 to agonist-activated FFA1 has been reported, which indicates a potential signalling bias at this receptor (Figure 1-8). Mancini et al. (2015a) showed that pharmacological blockade of $\text{G}\alpha_q$ activity decreases FFA1-induced insulin secretion. Moreover, knockdown or genetic ablation of β -arrestin2 in insulin-secreting cell lines and mouse pancreatic islets, respectively, uniquely demonstrated β -arrestin2-mediated insulinotropic signalling (Mancini et al., 2015a). Activation of $\text{G}\alpha_{q/11}$ signalling can mobilise intracellular calcium and activation of the extracellular signal-regulated kinase signalling cascades. On the other hand, $\text{G}\alpha_s$ coupling increases cyclic AMP levels which is opposed by $\text{G}\alpha_{i/o}$ coupling.

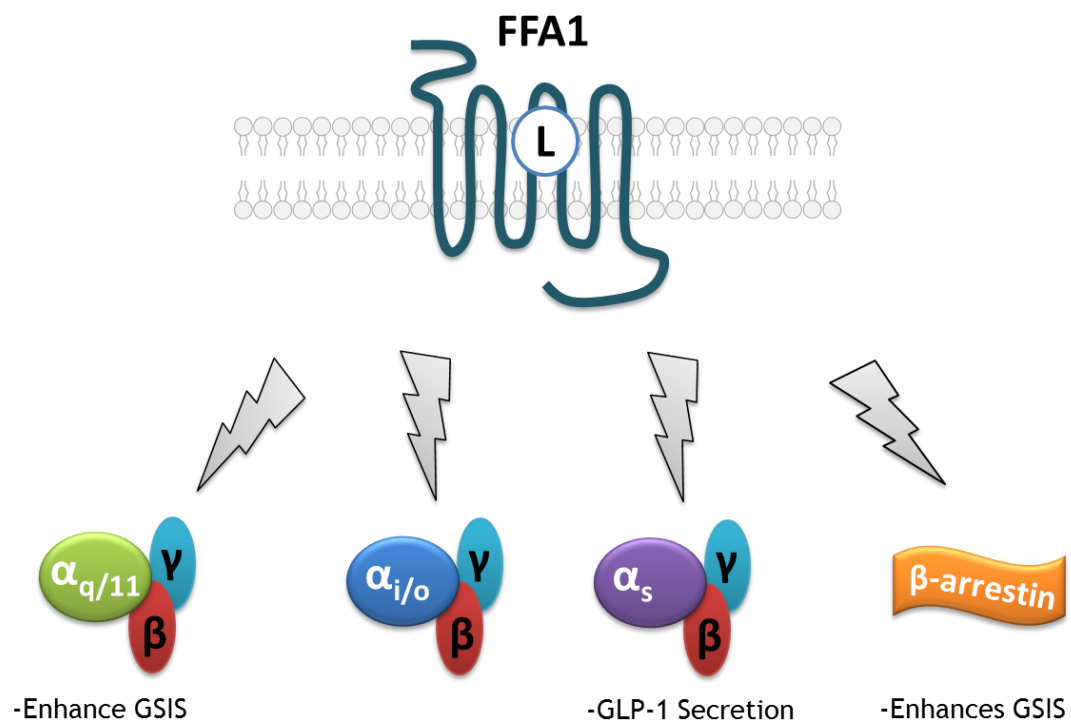


Figure 1-8. Signalling pathways and their associated biological outcomes for the FFA1 receptor. FFA1 predominantly signals through $G\alpha_{q/11}$ proteins resulting enhanced glucose stimulated insulin secretion. $G\alpha_s$ signalling causes release of glucagon like peptide 1 secretion from enteroendocrine cells. β -arrestin biased signalling associated with enhanced glucose stimulated insulin secretion. (GLP-1, glucagon like peptide 1; GSIS, glucose stimulated insulin secretion). Figure has been adapted from Milligan et al. (2017).

1.4.1.4 Physiological functions associated with FFA1

Due to FFA1 expression in a number of tissues and diversity of G protein and arrestin signalling, important physiological roles associated with FFA1 have been demonstrated in various studies. FFA1 agonism results in enhanced glucose stimulated insulin secretion (GSIS) (Mancini and Poitout, 2013). In a glucagon-secreting cell line overexpression of FFA1 demonstrated FFA-induced glucagon production (Flodgren et al., 2007). Overexpression of human FFA1 in the pancreatic β -cells of transgenic mice prevented the development of hyperglycemia feeding high fat administration. In a genetically diabetic mouse model, overexpression of FFA1 showed enhanced insulin secretion and produced improvement in glucose tolerance (Nagasumi et al., 2009). However, glucolipotoxicity associated with β -cell dysfunction has been reported following chronic FFA1 stimulation (Mancini and Poitout, 2013). Takahashi et al. (2017)

reported that FFA1 inhibits cell motility of highly migratory osteosarcoma cells. FFA1 is expressed in intestinal enteroendocrine cells and possibly also in glucagon-producing cells, which are associated with glucose homeostasis. Physiological functions of FFA1 are therefore linked to its pattern of expression. FFA1 agonism causes secretion of glucagon like peptide-1 (GLP-1) and peptide hormone YY (PYY) from L cells, secretion of cholecystikinin (CCK) from I cells and secretion of gastric inhibitory peptide (GIP) from K cells (Hara et al., 2014b). All of these incretins produce effects related to energy homeostasis.

1.4.1.5 Structure of FFA1

The key structural features of FFA1 are exemplified in Figure 1-9 described by Stoddart et al. (2008). The receptor contains cysteine residues in the first and second extracellular loops that are likely to contribute to structure via the formation of intramolecular disulfide bonds, proline residues in TM domains 5, 6, and 7, an asparagine in TM1, and an aspartate in TM2. They also contain an arginine at the bottom of TM3, which is within the highly conserved Asp-(Glu)-Arg-Tyr motif. Two N-glycosylation consensus sequences (Asn-x-Ser/Thr) can be identified in extracellular loop 2 (Stoddart et al., 2008).

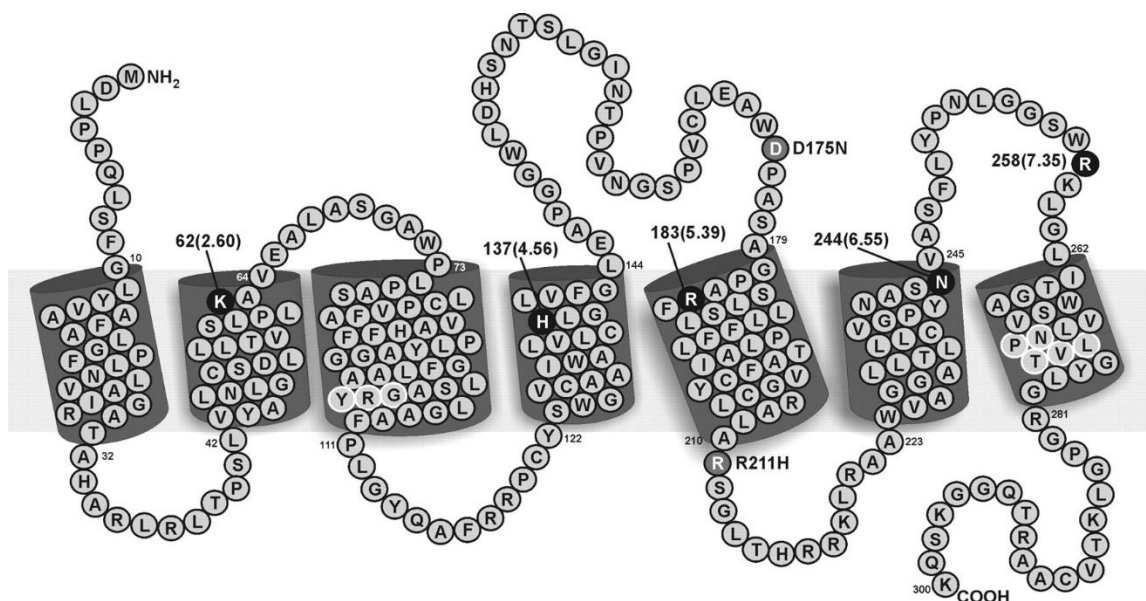


Figure 1-9. Snake plot of hFFA1 receptor. Key structural features of hFFA1 have been illustrated. Conserved motifs are shown in dark gray (white lettering) as are the two known human polymorphisms, Arg²¹¹His and Asp¹⁷⁵Asn. The hFFA1 receptor has two putative N-glycosylation sites (Asn¹⁵⁵ and Asn¹⁶⁵; motif: Asn-x-Ser/Thr) and two potential protein kinase C phosphorylation sites (Thr²¹⁵ and Ser²⁹⁸, Ser/Thr-x-Arg/Lys). Basic residues conserved across the hFFA1 are indicated in black (white lettering). Figure taken from Stoddart et al. (2008).

1.4.1.6 Ligands of FFA1

Deorphanisation studies revealed activation of FFA1 by both saturated (C12-C16) and unsaturated (C18-C22) free fatty acids, including lauric acid, palmitic acid, eicosatrienoic acid, linolenic acid, linoleic acid, oleic acid, palmitoleic acid, undecanoic acid, myristic acid, docosahexaenoic acid (DHA) and arachidonic acid (Briscoe et al., 2003; Itoh et al., 2003; Kotarsky et al., 2003). Only modest variation in potency was observed within this group of ligands. These ligands also have overlapping activity with other free fatty acid receptors. Due to potential insulin releasing effects associated with FFA1 agonism, a lot of effort has been given to the development of synthetic ligands (Milligan et al., 2015). GW9508 was the first reported synthetic ligand, characterized by Briscoe et al. (2006). However, GW9508 was reported to also activate FFA4 with lower potency (Briscoe et al., 2006; Hudson et al., 2013b). Briscoe et al. (2006) also introduced GW1100 as the first FFA1 antagonist. They demonstrated that GW9508 promoted GSIS from rodent MIN6 insulinoma cells, and this effect was blocked by GW1100 (Briscoe et al., 2006).

The thiazolidinedione drugs e.g. rosiglitazone and netoglitazone are also able to activate the FFA1 as reported by Kotarsky et al. (2003). However, later studies demonstrated that the beneficial results might not reflect direct activation of FFA1, rather via PPAR γ -mediated alterations in FFA1 expression (Kim et al., 2013b). After the discovery of GW1100 as a potent FFA1 antagonist, other antagonist series have also been described. Hu et al. (2009) developed DC260126, a sulphonamide derivative which showed improved insulin sensitivity and β -cell protection in diabetic mice. Palmitate-mediated potentiation of GSIS was significantly prevented with the pyrimidinylhydrazone-based FFA1 antagonist ANT-203 (Kristinsson et al., 2013). Negoro et al. (2010) developed TAK-875 as a potent, selective, and orally bioavailable FFA1 agonist. In type 2 diabetic rats, TAK-875 produced increased insulin secretion, reduction of plasma glucose excursion and has promising pharmacokinetic profiles (Negoro et al., 2012). Subsequently, TAK-875 (fasiglifam) progressed into clinical trials but unfortunately, these trials were terminated because of potential liver toxicity (Mancini and Poitout, 2015b). AMG-837, a partial agonist of FFA1 developed by Amgen Inc. showed enhanced insulin secretion with lowering of glucose levels in rodents (Lin et al., 2011). This molecule reached phase I clinical trials, but no

further development has been reported (Li et al., 2016). Amgen further developed AM-3189 (Ma et al., 2016) and AM-4668 (Liu et al., 2014) with superior pharmacokinetic properties and *in vivo* efficacy. AM 1638 and AM 5262 were also reported to be full agonists, with superior *in vivo* efficacy and the significant advantage of also stimulating incretin secretion (Chen et al., 2016).

Eli Lilly developed LY2881835, LY292208 and LY2922470 which are potent FFA1 agonists and demonstrated a dose-dependent reduction in glucose levels along with significant increase in insulin and GLP-1 secretion during preclinical testing (Hamdouchi et al., 2016). LY2881835 significantly increased GSIS in mouse MIN6 cells and in rat, human, and mouse primary pancreatic cells. This compound was progressed to phase I clinical trials, but further development was discontinued due to significant side effects (Chen et al., 2016). Hengrui (Li et al., 2016) reported that SHR0534, a structural analogue of TAK-875, is currently recruiting participants in phase I clinical trials (China). However, the chemical structure of SHR0534 is not published. P11187 developed by Piramal Phytocare has entered phase I clinical trials in US, but the chemical structure has also not been disclosed (Li et al., 2016). JTT-851, a clinical candidate developed by Japan Tobacco, completed a phase II clinical trials in 2013, but no further development has been reported (Li et al., 2016).

Christiansen et al. (2008) reported a phenoxyacetic acid compound TUG-424 to be a potent and selective FFA1 agonist, however, this compound showed lower than ideal *in vitro* metabolic stability and short plasma half-life. With further structural modification and optimisation, they developed TUG-469 as a potent FFA1 agonist with the ability to enhance insulin secretion in a glucose concentration-dependent fashion (Christiansen et al., 2010). Christiansen et al. (2012) also modified the structure of TUG-469 by incorporation of a hydrophilic 3-mesylpropoxy appendage akin to TAK-875 and developed TUG-905. This compound showed high potency on both human and murine FFA1 orthologs. The authors used the rat β -cell line INS-1E endogenously expressing FFA1 and found that TUG-905 was able to induce a concentration-dependent response in insulin secretion. Moreover, the compound was rapidly absorbed and there was a reduced first-pass metabolism. In their ongoing ligand development, TUG-770 was identified as a potent FFA1 agonist with excellent physicochemical and pharmacokinetic properties (Christiansen et al., 2013a). Authors initially

evaluated this compound *in vitro* in the rat INS-1E cell line, where the compound showed increased insulin secretion. Further, the compound showed improved glucose tolerance in diet induced obese mice, a situation that was sustained after 29 days of chronic dosing. Christiansen et al. (2013b) also developed compound 40 with excellent *in vitro* ADME properties. The same research recently identified compound 24 as a potent FFA1 agonist with low lipophilicity and very high ligand efficiency that exhibited a robust glucose lowering effect (Hansen et al., 2016).

I have used TUG-905 and TUG-770 (Table 1-5) in my project for further characterisation as well as tool compounds for studying FFA1 pharmacology and desensitisation studies. These compounds appear as promising candidate for development of improved therapeutics in the treatment of type 2 diabetes.

Table 1-5. FFA1 ligands

Natural ligands	Linolenic acid, linoleic acid, oleic acid, lauric acid, palmitic acid, eicosatrienoic acid, palmitoleic acid, undecanoic acid, myristic acid, docosahexaenoic acid and arachidonic acid
Synthetic ligands	GW9508, TAK-875 (fasiglifam) AMG-837, AM-3189, AM-4668, AM 1638, AM 5262 LY2881835, LY292208, LY2922470 SHR0534 JTT-851 DC260126, pyrimidinylhydrazones ANT-203 TUG-424, TUG-469, TUG-905*, TUG-770* GW1100*
Ligands entered into clinical trials	AMG-837 LY2881835 SHR0534 JTT-851 TAK-875 (fasiglifam)
* Ligands used in this project	

1.4.2 Free fatty acid receptor 4

1.4.2.1 Deorphanisation of FFA4

FFA4 was deorphanised by Hirasawa et al. (2005) and they reported this receptor to be activated by polyunsaturated LCFAs. They tested over 1000 chemical compounds on HEK293 cells stably expressing FFA4. In these studies, α -linolenic acid was the most potent natural agonist of FFA4 identified. Although the fatty acid profiles are similar to those for FFA1, there is only 10% homology in amino acids between these two receptors (Hirasawa et al., 2008).

1.4.2.2 Expression of FFA4

During deorphanisation of FFA4, Hirasawa et al. (2005) demonstrated abundant expression of mRNA in mouse and human including in intestine, lung, spleen, adrenal glands and thymus. Gotoh et al. (2007) confirmed that FFA4 is also highly expressed in human and mouse adipose tissues. The level of mRNA of FFA4 increased during adipocyte differentiation. Matsumura et al. (2007) analysed the mRNA expression and immunoreactivity of FFA4 in rat taste buds. FFA4 is also expressed on multiple immune cell types specifically in monocytes and macrophages (Oh et al., 2010). Detailed examination of FFA4 expression in the intestine indicated that FFA4 is expressed by cells on each of the L, K, and I cells of intestine (Iwasaki et al., 2015). Taneera et al. (2012) analysed global gene expression in human islets and identified gene coexpression and protein-protein interaction networks that were strongly associated with islet insulin secretion and glycosylated haemoglobin. FFA4 expression has also been reported in α (Suckow et al., 2017), β (Moran et al., 2014), and δ (Stone et al., 2014) cell types of pancreatic islets.

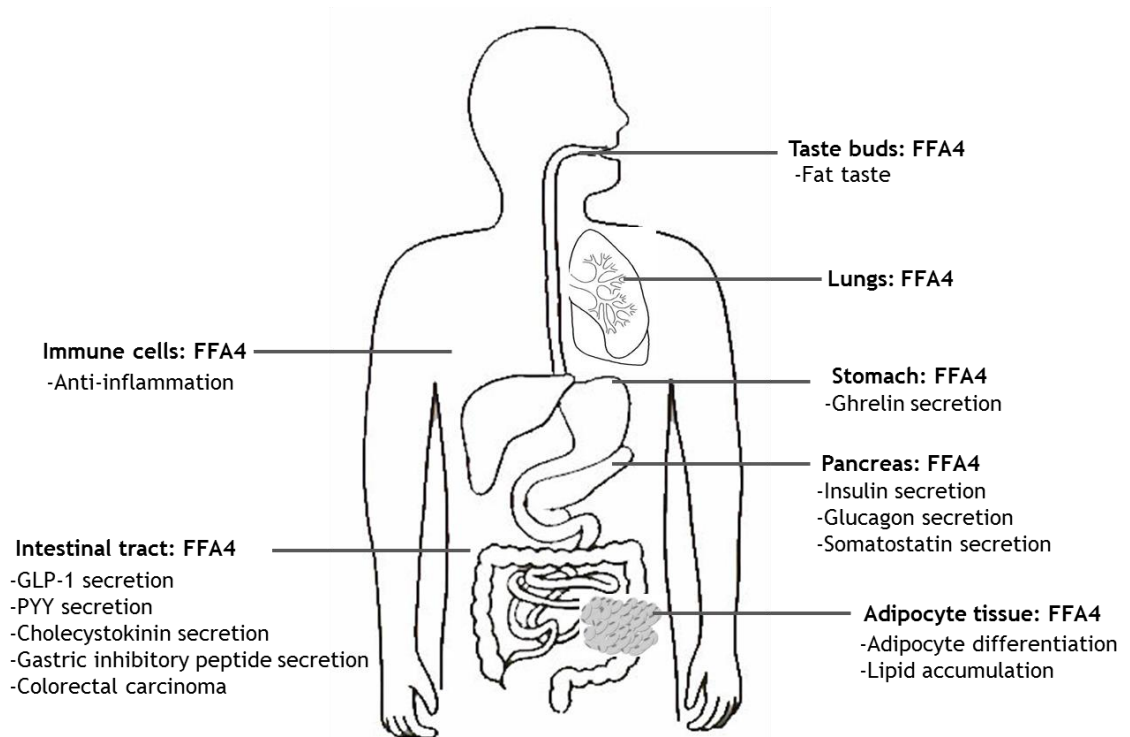


Figure 1-10. FFA4 expression and functions. Reported expression and functions of FFA4. High expression of FFA4 is seen in the intestinal tract where the receptor is associated with GLP-1 secretion, PYY secretion, CCK secretion, GIP secretion. FFA4 expression in the intestine also has been suggested to be linked with colorectal carcinoma. FFA4 causes adipocyte differentiation and lipid accumulation. In the pancreas, FFA4 expression has been shown to have effects on insulin secretion, glucagon secretion and somatostatin secretion. Expression in the immune cells particularly in monocytes and macrophages has been associated with anti-inflammatory activity. Expression in stomach has been associated with the release of ghrelin. In the taste buds FFA4 has been shown to be associated with fat taste sensing. FFA4 is also expressed in the lung.

1.4.2.3 FFA4 splice variation

Human express two splice variants of FFA4, long (L) and short (S) that differ by a 16 amino acid insertion in the third intracellular loop of the long form (Figure 1-11) (Moore et al., 2009). No splice variants have been seen in the cynomolgus monkey or rodents (Moore et al., 2009) indicating that splice variation is species dependent. Watson et al. (2012) demonstrated that the long isoform was unable to elevate intracellular calcium, therefore, presumably is unable to interact effectively with $G_{\alpha_{q/11}}$ G proteins. However, the L isoform was able to recruit β -arrestin, providing one of the first examples of a native β -arrestin-biased receptor (Watson et al., 2012). Burns and Moniri (2010) expressed both L and S isoform of FFA4 in HEK293 cells and studied agonist-promoted phosphorylation. Interestingly, they found both isoforms undergo rapid phosphorylation but there was no significant difference in the degree or rate of phosphorylation. Despite such studies, the functional and physiological importance of the long isoform remains uncertain (Milligan et al., 2017).

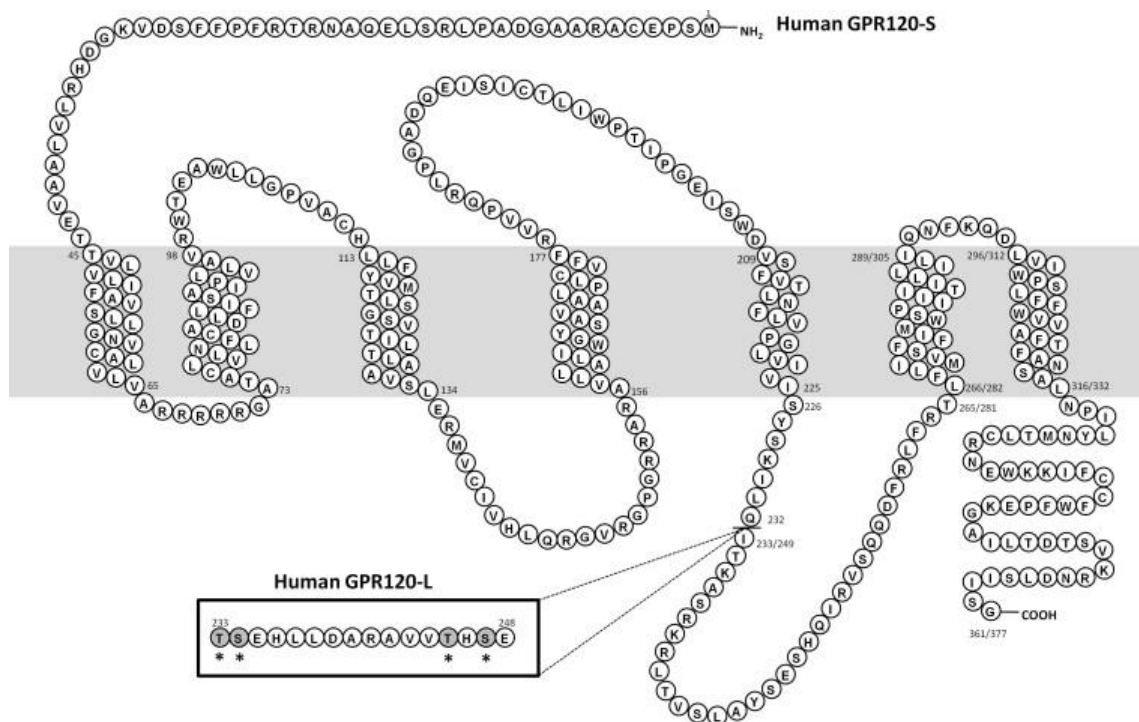


Figure 1-11. Splice variation of FFA4. The amino acid sequence of human FFA4. Numbers signify amino acid residues relative to indicator methionine. The insert shows the additional 16 amino acid gap introduced to GPR120-L and the four identified phospho-labile Ser/Thr sites are shaded and asterisked. Figure taken from Burns and Moniri (2010).

1.4.2.4 FFA4 signalling

During deorphanisation LCFAs induced mobilisation of intracellular calcium which indicates $G\alpha_{q/11}$ coupling to FFA4 receptors (Hirasawa et al., 2005). Analysis of anti-apoptotic effects through FFA4 activation also showed that this receptor coupled through pertussis toxin-insensitive $G\alpha_q$ families (Hirasawa et al., 2008). Hudson et al. (2013b) confirmed this by showing that use of the $G\alpha_{q/11}$ -selective inhibitor YM-254890 could block agonist promoted elevation of intracellular calcium levels. Furthermore, Alvarez-Curto et al. (2016b) expressed human and mouse forms of FFA4 in $G\alpha_q/G\alpha_{11}$ -null cells and demonstrated that FFA4 in these backgrounds could not produce any intracellular calcium mobilisation or accumulation of inositol monophosphates upon agonist exposure. This study confirmed $G\alpha_{q/11}$ -mediated signalling at FFA4. FFA4 activation also causes robust β -arrestin2 recruitment (Shimpukade et al., 2012; Hudson et al., 2013b). A G-protein independent, β -arrestin-2 mediated pathway has been proposed by Oh et al. (2010) from the findings that FFA4-activation produces

anti-inflammatory actions. Engelstoft et al. (2013) reported a pertussis toxin-sensitive $G\alpha_{i/o}$ pathway for ghrelin and somatostatin secretion during signalling through FFA4. Stone et al. (2014) also reported $G\alpha_{i/o}$ signalling when FFA4 activation caused a marked inhibition of glucose-induced somatostatin secretion from delta cells. As such it is clear that FFA4 can couple a range of signalling pathway in different cells and tissues (Figure 1-12).

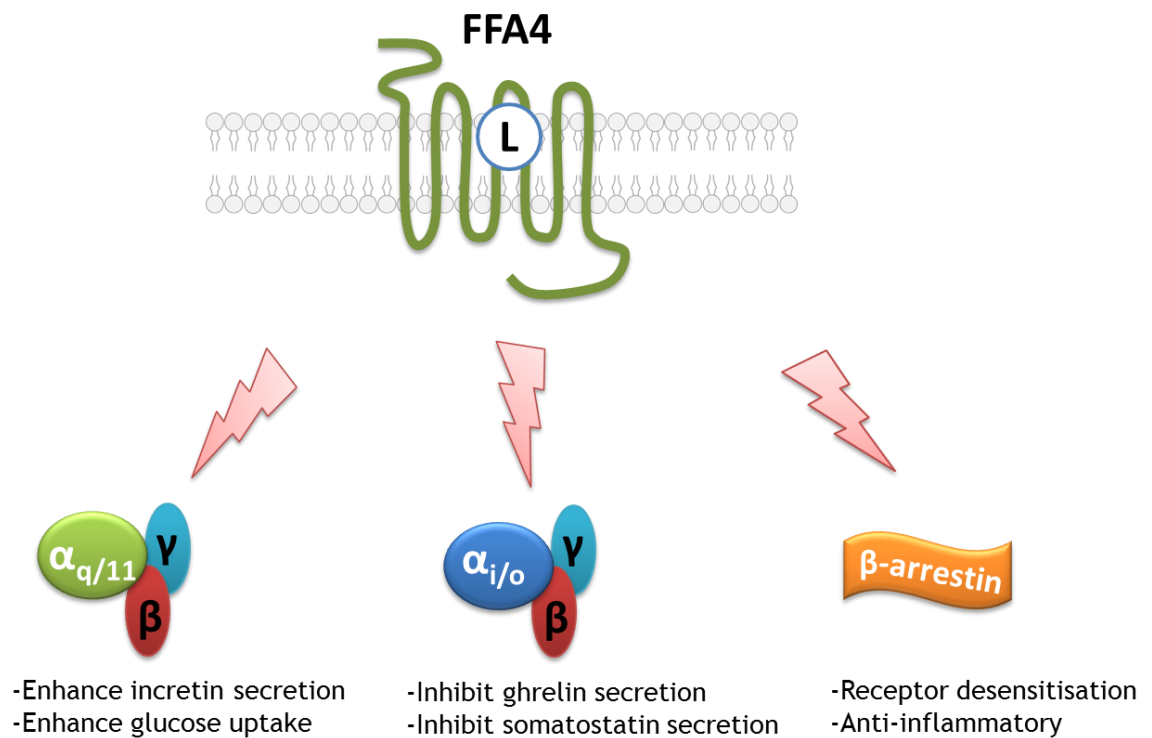


Figure 1-12. Signalling pathways and their associated biological outcomes for FFA4. FFA4 predominantly signals through $G\alpha_{q/11}$ proteins resulting in enhanced incretin secretion and enhanced glucose uptake. Signalling via $G\alpha_{i/o}$ causes inhibition of ghrelin and somatostatin secretion. β -arrestin mediated signalling is associated with receptor desensitisation and anti-inflammatory activity. Figure has been adapted from Milligan et al. (2017).

Growing evidence suggests that FFA4 mediated anti-inflammatory activity might be due to β -arrestin mediated biased signalling (Oh et al., 2010). Alvarez-Curto and Milligan (2016a) described the probable mechanism (Figure 1-13). FFA4 activation and concomitant recruitment of β -arrestin2 promotes further interactions between β -arrestin-2 and TAB-1, the transforming growth factor kinase protein (TAK-1) binding protein, which acts as an activator of TAK-1. This receptor mediated β -arrestin-2-TAB-1 interaction, which is suggested to prevent the formation of a TAB-1/TAK-1 complex halts the subsequent relay of signalling that results in the inflammatory response (Alvarez-Curto and Milligan, 2016a; Oh et al., 2010).

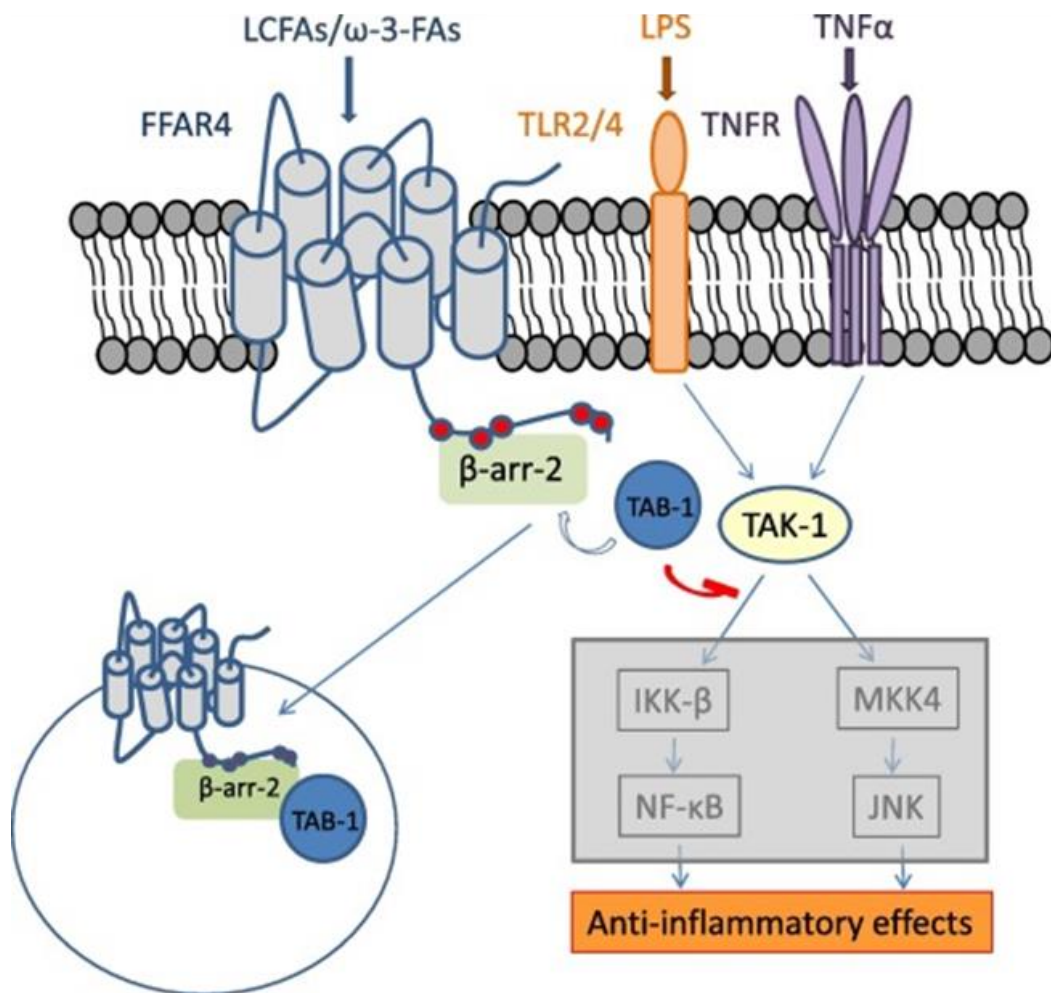


Figure 1-13. Anti-inflammatory activity mediated through FFA4 biased signalling.

Macrophages expressing FFA4 respond to omega-3 fatty acids that activate the receptor eliciting phosphorylation of the carboxyl-terminal tail (represented by red dots), subsequent β-arrestin2 recruitment and receptor internalisation. At this point the receptor-β-arrestin2 complex interacts with the TAB-1 protein, that is taken into the endocytic vesicle, making it unavailable to activate the TAK-1 protein responsible for the transduction downstream of signalling coming from activated Toll-like and TNFα receptors. This further blocks the NF-κB/JNK cascades, therefore inhibiting inflammatory responses in these cells. (LCFA, long chain fatty acid; ω-3-FAs, omega-3 fatty acids, TLR2/4, Toll-like receptors 2 and 4, TNFR, TNFα receptor). Figure taken from Alvarez-Curto and Milligan (2016a).

1.4.2.5 Physiological functions associated with FFA4

A number of initial studies on the physiological significance of FFA4 were focused on the role of FFA4 on incretin release from enteroendocrine cells. In particular, Hirasawa et al. (2005) reported that LCFAs stimulate secretion of the incretin GLP-1 from the STC-1 mouse enteroendocrine cell line and Tanaka et al. (2008a) showed that administration of α -linolenic acid increases plasma GLP-1 levels in a rat model. The proliferation of pancreatic β -cells was upregulated upon long term administration of LCFAs (Tanaka et al., 2008a). Agonist-mediated secretion of CCK from STC-1 cells has also been reported (Tanaka et al., 2008b). However, there are some mixed results of the role of FFA4 on incretin secretions. Xiong et al. (2013) used a knockout mouse model and demonstrated that GLP-1 secretion was via stimulation of FFA1 not FFA4. Liou et al. (2011) used a population of I cells from duodenal mucosa in transgenic mice and also found that secretion of CCK was mediated via FFA1 not FFA4. Iwasaki et al. (2015) used purified K cells from mouse intestine and found that GIP secretion was reduced to 75% in FFA4-deficient mice compared to wild-type. So, the variation of the roles of FFA4 in mouse and human enteroendocrine cells might be due to different outcomes in pharmacological intervention and genetic knockdown.

A number of studies supports that FFA4 might be an adipogenic receptor which has important roles in adipocyte differentiation and maturation. Gotoh et al. (2007) found a high expression of FFA4 mRNA in subcutaneous, epididymal and mesenteric adipose tissue in HFD-fed mice. Moreover, FFA4-deficient mice fed a HFD were found to develop obesity, glucose intolerance, and fatty liver. There was also decreased adipocyte differentiation, lipogenesis and enhanced hepatic lipogenesis in HFD-fed FFA4-deficient mice (Ichimura et al., 2012). Studies with humans showed higher expression of FFA4 in adipose tissue of obese individuals than in lean controls. Oh et al. (2010) reported that FFA4 induces a translocation of glucose transporter 4 in 3T3-L1 adipocytes and directly increased glucose uptake. Taken together, these data demonstrated that FFA4 acts as a lipid sensor *in vivo* and plays a critical role in sensing dietary fat to regulate glucose and lipid metabolism.

FFA4-mediated anti-inflammatory activity has been investigated extensively. Oh et al. (2010) demonstrated that FFA4 activation by DHA significantly reduced LPS-stimulated secretion of the cytokines TNF- α and IL-6 from RAW264.7 cells. The effect was prevented by FFA4 knockdown, demonstrating that the anti-inflammatory effect was mediated through FFA4 (Oh et al., 2010). These authors demonstrated that β -arrestin2 knockdown extinguished the DHA-mediated anti-inflammatory activity, while β -arrestin1 and $G\alpha_{q/11}$ knockdown were without effect. Li et al. (2013) demonstrated that knockdown of FFA4 abrogate the DHA effects on cyclooxygenase-2 induction, prostaglandin E_2 production, and IL-6 gene expression. Moreover, β -arrestin2 recruitment to DHA-activated FFA4 was found to repress Toll-like receptor 4 signalling via Akt/JNK phosphorylation which was reversed by FFA4 knockdown (Li et al., 2013). A detailed mechanism has been proposed by Alvarez-Curto and Milligan (2016a) (Figure 1-13).

FFA4 agonism has been associated with energy homeostasis. Oh et al. (2010) assessed the effects of FFA4 stimulation on insulin sensitivity in primary adipose tissue cultures and in 3T3-L1 adipocytes. These authors found that DHA-stimulation of FFA4 led to an increase in glucose transport and translocation of GLUT4 to the plasma membrane in adipocytes, the effect was blocked with knockdown of FFA4 or $G\alpha_{q/11}$. Interestingly, $G\alpha_{q/11}$ knockdown was found to attenuate insulin stimulatory effects. As $G\alpha_q$ is important for insulin-induced glucose transport (Imamura et al., 1999), the studies of Oh et al. (2010) indicated that FFA4-mediated $G\alpha_{q/11}$ signalling might be linked with insulin signaling and glucose transport in adipocytes. Ichimura et al. (2012) showed that HFD fed FFA4-deficient mice develop obesity-associated insulin resistance. These authors found a marked reduction of peripheral insulin sensitivity in FFA4 knockout mice. In later studies, Ichimura et al. (2014) demonstrated that GLP-1 and CCK are involved in the regulation of feeding behaviors, energy metabolism and bodyweight. Paulsen et al. (2014) found that FFA4 is upregulated in obesity susceptible DIO rats when compared to diet-resistant rats. The broad expression of FFA4 in the gut epithelium supports reports indicating a putative role of FFA4 as a sensor of dietary fat. FFA4 activation has been reported to inhibit secretion of the hunger regulating gastric hormone, Ghrelin (Lu et al., 2012). Taken together, these studies demonstrated that FFA4 has a great role in energy metabolism.

Recent studies described a role of FFA4 in bone metabolism. Ahn et al. (2016) showed that FFA4 was abundantly expressed in both mature osteoclasts and osteoblasts. FFA4 worked as a dual-acting factor that increased osteoblastic bone formation and decreased osteoclastic bone resorption. Kim et al. (2016) reported that FFA4 negatively regulates osteoclast differentiation, survival, and function. FFA4 knockdown has been found to inhibit osteoclastogenesis and also to suppress osteoclast survival (Kim et al., 2016). Adipocyte differentiation from bone marrow mesenchymal stem cells has also been suggested to be promoted by FFA4 (Gao et al., 2015). Gao et al. (2016) use murine bone marrow-derived mesenchymal stem cells and observed that ecosapentanoic acid-induced autophagy was modulated by FFA4, but not FFA1. Thus, FFA4 works as important target for modulating bone production and degradation.

Increasing evidence shows that FFA4 also play a role in tumorigenesis, migration, and metastasis. Wu et al. (2013) reported a potential of FFA4 receptor agonists to promote angiogenesis in colorectal carcinoma cells. This report suggests that FFA4 receptor activation promotes angiogenesis by stimulating release of VEGF, IL-8 and COX-2-derived PGE2. FFA4 can also regulate tumor growth and migration of various cancer types, including melanoma and prostate cancers (Hopkins et al., 2017; Houthuijzen, 2016). Houthuijzen et al. (2017) showed that FFA4 activation results in a signalling cascade that ultimately induces chemoresistance and showed that antagonism FFA4 can limit the development of chemotherapy resistance.

Thus, it is clear that the expression pattern of FFA4 and the diversified physiological and pathological roles (Table 1-6) have made this receptor a potential target for therapeutic interventions.

Table 1-6. Tissue expression and physiological function of FFA4

Tissue	Cell type or cell line	Physiological or cellular function
Intestinal	L-cells	Secretion of GLP-1
	L-cells	Inhibition of GLP-2 secretion
	K-cells	Secretion of GIP
	Murine STC1, GLUTag	Secretion of GLP-1
	HCT116, HT-29, Caco-2 human colon epithelial cancer cells	Increase cytosolic Ca^{+2} Increase phosphorylation of ERK1/2
Gastric	Ghrelin secreting	Inhibition of ghrelin secretion
tongue	Circumvallate papillae epithelia	Fat sensing, GLP-1 secretion
	Type II taste cells	Taste perception
Adipose	SQ, PR, Mes, Epi fat 3T3-L1 cells	Adipocyte differentiation, GLUT4 translocation, glucose uptake VEGF-A induced angiogenesis
	M2 and M1 macrophages	Anti-inflammatory effects, insulin sensitization
Macrophages	M2 and M1 macrophages, murine Raw264.7 cells, human THP-1 cells	Anti-inflammatory effects, reduced inflammasome assembly and activity, insulin sensitization
Pancreatic Islets	Islet cells	Protection from lipotoxicity
	Human and mouse α -cells	Glucagon synthesis and secretion Downstream hepatic glucagon sensitivity
	Mouse delta-cells	Inhibition of somatostatin secretion
	Murine α TC1-6 cells	
Skeletal muscle	Rat and murine gastrocnemius and soleus skeletal muscle	Reduced inflammation, improved insulin sensitivity
	Rat L6 and murine C2C12 myoblasts	GLUT4 translocation and increased glucose uptake
Liver	Murine macrophage-like Kupffer cells	Reduced inflammation
	Human hepatocytes, hepatic stem/progenitor cells, and hepatic Kupffer cells	Reduced inflammation, macrophage polarization
	Rat liver WB-F344 cells	Cell migration
Bone	Osteoclasts	Reduced inflammation, inhibition of osteoclast development and bone resorption
	Murine ST2 and MC3T3-E1 preosteoblasts	
Table taken from Moniri, 2016		

1.4.2.6 Ligands of FFA4

Although FFA1 and FFA4 have only 10% homology in amino acid sequence, they share common endogenous ligand profiles (Hara et al., 2014b). During deorphanisation of FFA4, Hirasawa et al. (2005) reported saturated FFAs with chain length of C14 to C18 and unsaturated FFAs with chain length of C16 to C22 to activate this receptor. The natural product grifolic acid was also reported to act as a selective partial agonist of FFA4 (Hara et al., 2009). Because of the marked overlap in activation of FFA1 and FFA4 receptors by fatty acid ligands

there has been a need to identify and develop selective FFA4 receptor agonists to elucidate receptor pharmacology and therapeutic interventions.

Briscoe et al. (2006) reported GW9508 as more selective agonist for FFA1 over FFA4, however, due to lack of better alternatives, GW9508 has been used in many studies of FFA4 mediated functions where the expression levels of FFA1 were absent or significantly lower than FFA4 (Hansen and Ulven, 2017; Milligan et al., 2015). Suzuki et al. (2008) synthesised a series of compounds containing carboxylic acids, based on the structure of the PPAR- γ activating thiazolidinediones. They reported NCG21 as the most potent and selective analogue acting on FFA4, 16-fold selective over FFA1. Shimpukade and co-workers (2012) developed a series of ortho-biphenyl compounds, and developed TUG-891 reported as the first potent FFA4 agonist. The compound showed 100-fold selectivity over FFA1 receptors (Shimpukade et al., 2012). These authors used a FFA4- β -arrestin-2 interaction assay during optimization of TUG-891 which might have resulted in ligand bias towards this end point. Hudson et al. (2013b) further characterised this compound and found that the compound shows limited selectivity over mouse FFA1 which has limited its use in preclinical *in vivo* studies in mice. TUG-891 was later used in a mass spectrometry-based proteomics study of FFA4 in an effort to map the sites of phosphorylation and residues interacting with β -arrestin2, it was found that activation of the receptor with this agonist leads to phosphorylation of Thr³⁴⁷, Thr³⁴⁹, Ser³⁵⁰, Ser³⁵⁷ and Ser³⁶⁰ (Butcher et al. 2014). Mutagenesis and modelling studies have confirmed that TUG-891 is an orthosteric ligand that binds to essentially the same pocket as aLA (Hudson et al. 2014). Despite the less pronounced selectivity between FFA4 and FFA1 at the mouse orthologues, the compound still represents a useful tool compound for both *in vitro* and *in vivo* studies of the biology of FFA4. In my project, I have used TUG-891 as a tool compound to study pharmacology and desensitisation of FFA4.

Stone et al. (2014) reported that Metabolex 36 (Cymabay Therapeutics, California, USA) and two AstraZeneca compounds AZ-423 and AZ-670 work as selective agonists of FFA4. These compounds were able to lower both basal and glucose-induced somatostatin secretion from murine pancreatic islets. Engelstoft et al. (2013) tested compound B (Cymabay Therapeutics) and found it to inhibit ghrelin secretion in a dose-dependent manner. This compound also showed a

dose-dependent inhibition of somatostatin release (Egerod et al. 2015). Oh et al. (2014) used the Merck compound cpdA which demonstrated potent anti-inflammatory effects on macrophages. This compound was also shown to improve systemic and hepatic insulin sensitivity and beneficial effects were also seen on hepatic lipid metabolism (Oh et al., 2014). Adams et al. (2016) discovered the chromane propionic acid, compound 18 as a selective FFA4 agonist over FFA1 and demonstrated suitable pharmacokinetic properties in oral glucose tolerance test studies in wild-type and FFA4-knockout mice. Cox et al. (2016) described the design, synthesis, and evaluation of a novel spirocyclic agonist series, including agonist 14. This compound was evaluated *in vivo* and demonstrated acute glucose lowering effects in oral glucose tolerance tests, as well as improvements of insulin resistance in diet-induced obese mice (Cox et al., 2016). Compounds from LG Life Sciences including LC540449 and LGLS-120-A, demonstrated significant improvement in insulin resistance and body weight of the type 2 diabetic DIO mice (Li et al., 2016). Although having therapeutic potential, no ligands of FFA4 have yet entered into clinical trials.

GlaxoSmithKline developed a distinct class of diarylsulfonamide-based FFA4 ligands and among them GSK137647A was reported to be a potent and selective FFA4 agonist (Sparks et al., 2014). Unfortunately, poor solubility limits its usefulness for *in vivo* studies. GlaxoSmithKline, however, recently reported a phenylpropanoic acid derivative, compound 29, as a FFA4 agonist capable of lowering plasma glucose in preclinical models of type-2 diabetes (Sparks et al., 2017). Sparks et al. (2014) identified the sulfonamide compound 39 (AH 7614) and reported it as a potent FFA4 antagonist. The antagonist counteracted effects of GSK137647A on insulin and GLP-1 secretion in MIN6 and NCI-H716 cells (Sparks et al., 2014). However, the nature of antagonism of this compound is yet to be elucidated. Our medicinal chemistry team synthesised this compound and have designated it TUG-1275. In my project, I have used this antagonist as a tool compound.

Banyu Pharmaceutical disclosed a series of cyclic sulfonamide FFA4 agonists structurally distinct from other known FFA4 agonists (Azevedo et al., 2016). They reported cpd 2 as a potent FFA4 agonist. The scaffold in this series contains no acidic group and cannot be negatively charged under physiological conditions (Hansen and Ulven, 2017). Explorations of the structure-activity of cpd 2 allowed

Azevedo et al. (2016) to identify TUG-1197 as a very potent and highly selective FFA4 agonist. The compound was found to be active in an acute oral tolerance test in normal mice and significantly lowered the glucose level in wild-type but not in FFA4-knockout mice (Azevedo et al., 2016). The compound was investigated further in a chronic study in DIO mice where it caused significant insulin sensitization and a moderate but significant bodyweight loss, effects that were not observed in FFA4-knockout mice (Azevedo et al., 2016). This compound is a promising drug candidate for therapeutic intervention. In my project, I have used TUG-1197 for further characterisation.

Table 1-7. FFA4 ligands

Natural ligands	Myristic acid, palmitic acid, palmitoleic acid, stearic acid, elaidic acid, oleic acid, α -Linolenic acid, γ -Linolenic acid, eicosatrienoic acid, eicosapentaenoic acid, docosatetraenoic acid, docosahexaenoic acid, grifolic acid.
Synthetic ligands	NCG21, Metabolex 36 AZ-423 and AZ-670 compound B, propionic acid 18 , Spirocyclic agonist 14 cpbA, LC540449 and LGLS-120-A GSK137647A, compound 29, cpd 2 AH 7614 (compound 39, TUG-1275*) TUG-891* TUG-1197*
Ligands entered into clinical trials	None
<i>*Ligands used in this project.</i>	

1.5 Receptor desensitisation

Because GPCR signalling potentiates many important cellular functions, it is essential that activation is initiated then terminated rapidly, specifically and precisely even when agonist stimulation is continued. Signalling is attenuated by GPCR desensitisation, which is an adaptive response of the cell to arrest G protein signalling (Kohout and Lefkowitz, 2003). Desensitisation prevents potential harmful effects from chronic over stimulation of GPCR signal transduction cascades. However functional desensitisation is a potential problem in therapeutic effectiveness of agonist drugs especially chronic medication

(Rosethorne et al., 2015; Elzein and Zablocki, 2008). The IUPHAR guide states that desensitisation and tachyphylaxis are overlapping terms that refer to a spontaneous decline in the response to a continuous application of an agonist. Tachyphylaxis is a term commonly used to describe loss of response *in vivo* or clinical settings where as desensitisation is used when observed in *in vitro* experiments using cell culture or isolated tissues (Neubig et al., 2003).

Almost every GPCR that has been studied can undergo desensitisation. A universal mechanism for desensitising GPCRs has been reported (Figure 1-14). Desensitisation involves the coordinated actions of two families of proteins, the G protein-coupled receptor kinases (GRKs) and the arrestins (Drake et al., 2006; Reiter and Lefkowitz, 2006; Lefkowitz and Shenoy, 2005; Krasel et al., 2005) and also host of proteins that are recruited from the endocytic and ubiquitination pathways (Rajagopal and Shenoy, 2017). GRK-mediated phosphorylation is not sufficient to inhibit receptor-G protein interactions. For termination of G protein coupling to the activated receptor, β -arrestin recruitment is necessary. β -arrestin sterically hinders further coupling of the receptor the heterotrimeric G protein, and this interruption of signalling generates receptor desensitisation. Both GRKs and arrestins are involved in removal of ligand-activated GPCRs from the plasma membrane.

The regulation of desensitisation varies depend on the isoforms of GRKs and arrestins and their modulation by other accessory proteins. The GRK family consists of seven different genes. GRK1 and GRK7 are expressed in retinal rods and cones respectively, whereas GRK4 has very limited expression in the cerebellum, testis and kidney. GRKs 2, 3, 5, and 6 are quite ubiquitously expressed (Lefkowitz, 2013). Translocation and membrane localisation of GRK 2 and 3 are mediated in part by their binding to heterotrimeric G protein $\beta\gamma$ subunits whereas GRK 5 and 6 are constitutively localized to the plasma membrane. Palmitoylation of GRK6 is essential for membrane association (Drake et al., 2006). The arrestins constitute a four-member family. Arrestin1 and arrestin4 (α -arrestin) are referred to as visual arrestins, expressed in retinal rods and cones respectively. Arrestin2 (β -arrestin1) and arrestin3 (β -arrestin2) are expressed ubiquitously and play key roles in the function and regulation of non-visual GPCRs (Srivastava et al., 2015; Lefkowitz, 2013; Shenoy and Lefkowitz, 2011; Lefkowitz, 2004).

Desensitisation can be separated into individual processes in the pathway including receptor phosphorylation, β -arrestin recruitment, receptor internalisation, receptor recycling and downregulation (Figure 1-14). All of these may contribute to an overall loss in the ability of the cells to respond to agonists (Shenoy and Lefkowitz, 2011; Drake et al., 2006; Reiter and Lefkowitz, 2006; Lefkowitz, 2004). Recent studies suggest that these processes do not necessarily shut down receptor-mediated signalling. Indeed, it has been shown that some internalised receptors are still capable of signalling from endosomes (Thomsen et al., 2016; Wisler et al., 2014; Irannejad et al., 2013; Reiter and Lefkowitz, 2006). Moreover, β -arrestin recruitment to receptors can initiate sets of non-G protein-mediated signalling pathways (Smith and Rajagopal, 2016; Thomsen et al., 2016).

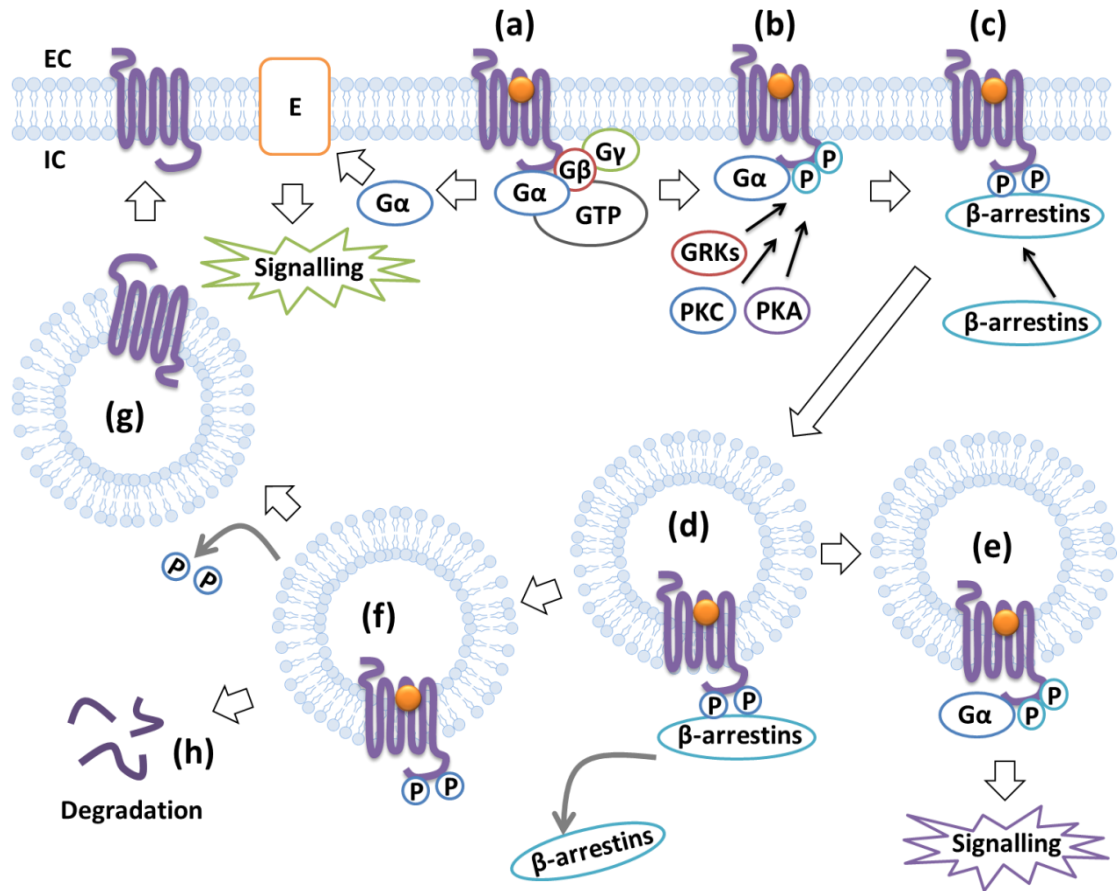


Figure 1-14. Desensitisation processes for GPCRs. (a) The binding of agonist to a GPCR induces signalling to heterotrimeric G proteins. Activated G proteins regulate effectors (E) for cellular activity specific to the type of G protein. (b) Agonist binding also induces receptor phosphorylation by GRKs as well as second messenger-activated kinases including PKA and PKC. (c) Cytosolic β -arrestins interact with the phosphorylated receptor, leading to uncoupling of the GPCR from G proteins. (d) β -arrestin recruitment facilitates subsequent recruitment of several proteins of the endocytotic machinery (not shown) to form clathrin-coated pits which are internalised into cytoplasmic compartments. (e) endocytosed GPCRs may be capable of further G protein signalling. (f) the ligand is dissociated and the receptor is dephosphorylated. (g) dephosphorylated GPCR recycles back to the plasma membrane or is (h) down regulated by lysosomal degradation.

Traditionally, receptor desensitisation has been classified as homologous (agonist-dependent) or heterologous (agonist-independent) processes (Rajagopal and Shenoy, 2017; Kohout and Lefkowitz, 2003). Homologous desensitisation is usually thought to involve versatile changes at the level of the GPCR itself, whereas heterologous desensitisation may involve changes in signalling components downstream of the GPCR. The GRK- β -arrestin mechanism is a major mediator of homologous desensitisation. Phosphorylation of the receptor by second messenger kinases such as PKA and PKC is a major mechanism of heterologous desensitisation of receptors. In heterologous desensitisation, second messenger-dependent protein kinases including protein kinase A (PKA) and protein kinase C (PKC) indiscriminately phosphorylate and desensitise receptors that have not been exposed to agonist. Thus, receptors that have not bound to agonist, including receptors for other ligands can be desensitised by these heterologous processes.

1.5.1 Receptor phosphorylation

After binding to an agonist a GPCR assumes a conformation that allows it to bind with GRKs and/or second messenger-dependent kinases including PKA and PKC. In doing so receptors become phosphorylated at residues on its intracellular surfaces (Reiter and Lefkowitz, 2006; Shenoy and Lefkowitz, 2003). Protein kinases are phosphotransferases that transfer the γ phosphate group from ATP onto serine, threonine or tyrosine amino acid residues (Gavi et al., 2006). Multiple phosphorylation sites exist in most GPCRs and these are mainly located at the carboxyl termini and third intracellular loops (Alfonzo-Mendez et al., 2016). Phosphorylation is the initial step in receptor desensitisation. For example, overexpression of GRKs has been found to markedly inhibit protease activated receptor 1 (PAR1) signalling (Paing et al., 2002). Phosphorylation of the receptor promotes high-affinity binding of arrestin family protein to the receptor, which physically interdicts further coupling to G proteins. This hindrance of coupling can result in as much as an 80% diminution of receptor signalling (Kohout and Lefkowitz, 2003).

Experimental evidence has shown that different phosphorylation patterns exist on GPCRs, depending on which ligand activates them and the cell in which they are expressed. On the other hand, the effects of a specific phosphorylation

event are determined by what site(s) becomes phosphorylated and the identity of the phosphorylating kinases (Kohout and Lefkowitz, 2003). These phosphorylation sites work as ‘phosphorylation barcodes’ which can help define signalling outcomes from receptor activation (Prihandoko et al., 2016; Butcher et al., 2014; Butcher et al., 2011; Tobin, 2008). Different ligands may cause different patterns of GPCR phosphorylation in a cell-specific manner (Alfonzo-Mendez et al., 2016). Receptor mutations that impair agonist-induced GPCR phosphorylation limit β -arrestin recruitment and lead to poor receptor internalisation (Rajagopal and Shenoy, 2017; Kohout and Lefkowitz, 2003; Luttrell and Lefkowitz, 2002). For example, mutation of the phosphorylation sites of mFFA4 has been found to significantly compromise arrestin3 recruitment and receptor internalisation (Prihandoko et al., 2016).

1.5.2 Receptor internalisation

Both agonist-dependent and -independent internalisation has been observed for many GPCRs (Smith and Rajagopal, 2016). Internalisation plays a key role in the regulation of GPCR signalling and desensitisation (Ferguson, 2001).

Internalisation result in a fall in the number of GPCRs at the plasma membrane, often causing a reduction in the cellular response to agonist. However, internalisation does not necessarily cause desensitisation because the loss of receptors from the surface might be too limited to alter overall function. Indeed, there are cases where the drop in surface receptor number occurs without desensitisation and vice versa (Koenig and Edwardson, 1997).

It is now well established that GPCRs can use more than one internalisation pathway. They may use one of the many backup mechanisms which differ with cell type or with different functional states of the same cell. Many GPCRs have recognisable internalisation motifs in their sequence. The internalisation pathway depends on the relative strength of these motifs, as well as arrestin expression levels (Gurevich and Gurevich, 2006; Fan et al., 2001).

1.5.2.1 Agonist-dependent internalisation

Receptor internalisation following agonist exposure is a well-characterised response for a wide variety of GPCRs. Receptor internalisation occurs within

minutes of agonist exposure follows receptor phosphorylation and subsequent β -arrestin recruitment (Kohout and Lefkowitz, 2003). β -arrestin1/2 recruitment at GPCRs causes the release of the C-tail of an arrestin which increases the accessibility of clathrin, the adaptor protein complex-2 (AP-2) and components of the endocytic machinery (Zhuo et al., 2014). The heterotetrameric AP-2 protein complex is involved in the formation of clathrin-coated pits (CCPs) and functions as an adaptor by linking receptors directly to the clathrin lattice which then undergoes endocytosis (internalisation) (Figure 1-14).

A least in simple cellular systems most GPCRs use CCP pathway during internalisation, however, additional pathways has been reported. Nichols and Lippincott-Schwartz (2001) described endocytosis by non-clathrin endocytic mechanisms, including uptake through caveolae based pathways. Caveolae are non-coated plasma membrane invaginations characterised by their association with a family of cholesterol-binding proteins called caveolins. GPCRs that have been identified in caveolae include the bradykinin, endothelin, M_2 -muscarinic, adenosine- A_1 , cholecystokinin receptors and β_2 -adrenergic (Marchese et al., 2003).

1.5.2.2 Agonist-independent internalisation

Agonist-independent or constitutive internalisation has been seen for many GPCRs including α_{1a} adrenergic receptor, angiotensin AT_{1A} receptor, type 1 cannabinoid receptor, chemokine CXCR4 receptor, metabotropic glutamate receptor 1, metabotropic glutamate receptor 5, M_2 muscarinic receptor and thyrotropin receptor (Xu et al., 2007). Constitutive internalisation is in general substantially slower compared to the cognate agonist-mediated internalisation. For example, the β_2 -adrenoceptor undergoes internalisation with a half-life of approximately 10 minutes in the presence of agonist but remains on the cell surface for greater than 1 hour in the absence of agonist (Drake et al., 2006). Although most of constitutive internalisation is also through clathrin dependent pathways, however, some GPCRs, including mGluR5, has been demonstrated to be endocytosed by clathrin-independent pathway (Fourgeaud et al., 2003).

1.5.3 Receptor recycling and resensitisation

In the endosomes, most GPCRs are dephosphorylated and return to the plasma membrane as resensitised receptors to undergo another round of signal transduction (Krupnick and Benovic, 1998). Receptor resensitisation requires dissociation of ligands and β -arrestin before the receptors can be dephosphorylated. Luttrell and Lefkowitz (2002) showed that dephosphorylation of the receptor occurs in an acidified vesicle compartment. Treatment of cells with ammonium chloride has been found to block association of the receptor with the phosphatase and prevent receptor dephosphorylation. It has been demonstrated that endocytosis is required for resensitisation of many GPCRs. Using mutant receptors that can signal and become desensitized, but exhibit defective endocytosis has demonstrated that internalisation is required for resensitisation (Luttrell and Lefkowitz, 2002).

1.5.4 Receptor down regulation

Down-regulation is a desensitisation process in which receptors undergo proteolysis and leads to a decrease in the total number of GPCRs available for signalling. It is also a part of long-term signalling attenuation. Downregulation is a longer term process that is associated with destruction of receptors in the lysosomes and often also decreased mRNA levels of the receptor. Receptor ubiquitination and β -arrestin recruitment play regulatory roles in receptor downregulation (Drake et al., 2006). Ubiquitin, a polypeptide of 76 amino acids, when attached to GPCRs, promotes receptor sorting into degradative pathways, typically on early to late endosomes or maturing vesicular bodies (Kennedy and Marchese, 2015; Zhuo et al., 2014). Many GPCRs seem to be degraded by metallo-proteinases present in lysosomes. However, before this takes place, the ubiquitin moieties are removed by ubiquitin-specific peptidases. Interestingly, removal of the GPCR ubiquitin moiety by peptidases is also involved in recycling GPCRs to the cell-surface for resensitisation (Alfonzo-Mendez et al., 2016). Kohout et al. (2001) showed that downregulation of β_2 adrenergic receptors does not occur in β -arrestin-1 and β -arrestin-2 double-knockout cells. GPCRs that display strong and persistent β -arrestin binding and co-internalise with a β -arrestin are more likely to be transported to the lysosomes for receptor degradation. In contrast, GPCRs that bind β -arrestin transiently and dissociate

from β -arrestin shortly after movement of the receptor into the clathrin-coated vesicles recycle rapidly (Oakley et al., 2000; Shenoy and Lefkowitz, 2003).

1.5.5 β -arrestin and GPCR trafficking

A role for β -arrestins in agonist-promoted internalisation of GPCRs was first discovered in 1996 (Ferguson et al. 1996; Goodman et al. 1996). The mechanism whereby β -arrestin participates in GPCR internalisation is fairly well established (Tian et al., 2014). In addition, arrestins appear to recruit ubiquitin ligases to promote ubiquitination of GPCRs which plays a role in receptor trafficking. Knockout, antisense and siRNA strategies have provided definitive evidence of a direct role for arrestins in the internalisation of many GPCRs (Smith and Rajgopal, 2016). The simple mechanism is that β -arrestin binding directly compete with G protein for overlapping sites. β -arrestins contribute to desensitisation and internalisation in both A and B classes of rhodopsin family GPCRs. Class A GPCRs show higher affinity for β -arrestin2 over β -arrestin1 and are associated with transient β -arrestin induced ubiquitination. However, class B GPCRs show approximately equal affinities between β -arrestin1 and β -arrestin2 and are associated with stable β -arrestin induced ubiquitination (Smith and Rajgopal., 2016). It has been found that class A patterns can be switched to class B by covalently linking ubiquitin to β -arrestin or by switching the C terminus of the receptor to that of a class B receptor (Smith and Rajgopal, 2016).

The role of β -arrestin in GPCR trafficking has developed new dimensions with the discovery that these proteins can bind with trafficking proteins including clathrin and AP-2 (Kang et al., 2009; Kang et al., 2014). The discovery that arrestins are ubiquitinated upon receptor binding and regulate ubiquitination of GPCRs revealed another mechanism in the regulation of GPCRs trafficking (Smith and Rajgopal, 2016). Interactions with the phosphorylated GPCR promotes β -arrestin ubiquitination and subsequent GPCR ubiquitination (Kang et al., 2014).

1.6 Aims of the project

In recent years, both FFA1 and FFA4 have earned tremendous interest in the scientific community for their potential of being novel therapeutic targets for treating metabolic disorders, specifically type-2 diabetes, and inflammatory conditions (Milligan et al., 2017; Milligan et al., 2015). Activation of these receptors can trigger intracellular events, for example the mobilisation of intracellular calcium (Milligan et al., 2017). Since GPCRs are often desensitised rapidly, which not only provides a means for terminating relevant acute signalling but also provides a mean for signalling bias, it is worth studying these aspects for these fatty acid receptors, given their promise as important therapeutic targets. Although the pharmacology of long chain free fatty acid receptors has been documented, the desensitisation, trafficking and oligomerisation have remained elusive.

The first aim of my project was to generate and characterise a number of cell lines expressing either hFFA1 or hFFA4 or both and to optimise their expression. The second aim was to characterise a range of pharmacological ligands able to activate or block these receptors. The third aim was to investigate the nature of desensitisation of these receptors in heterologous cell systems. The question of whether desensitisation of these fatty acid receptors is β -arrestin-independent or -independent was answered after analysis of receptor function when expressed in cells deficient in both common forms of arrestin. Because knock-down strategies cannot completely abolish the expression of proteins of interest, knockout strategy is best suited system to investigate GPCR signalling and desensitisation (Alvarez-Curto et al., 2016b). In this project CRISPR/Cas9-mediated, genome-edited, HEK293 cells lacking β -arrestins (β -arrestin1/2) and G proteins ($G\alpha_{q/11}$) were used with expression of the receptor of interest. In an attempt to more accurately understand the pharmacology of various receptor ligands, I used a number of biochemical and biophysical techniques including phosphorylation studies, BRET, ArrayScan II, intracellular calcium mobilisation in single cell and cell populations, inositol monophosphate accumulation, biotinylation, cell surface ELISA, confocal microscopy and FRET microscopy. The development of these assays allowed exploration of the activation, desensitisation and trafficking of hFFA1 and hFFA4. Understanding the desensitisation of FFA1 and FFA4 might aid in the development of agonist-based

therapies and importantly, might also help illuminate best therapeutic approaches for future treatment paradigms with agonist-based therapies of other GPCRs.

There is growing evidences that class A GPCRs can assemble as homodimers, heterodimers or higher-order oligomers (Milligan, 2007; Milligan, 2008; Milligan, 2009). Even though GPCRs are capable of functioning as monomers, they may exist as dimers or higher oligomers and receptor internalisation and trafficking might be modulated by such oligomerisation (Milligan, 2013). So, the last aim of these studies was to investigate possible oligomerisation of hFFA1 and hFFA4 using FRET microscopy and BRET saturation experiments. With this end in mind, I in this dissertation, describe the regulation and desensitisation of these therapeutically important free fatty acid receptors (especially hFFA4) using heterologous cell systems.

2 Materials and Methodology

2.1 Materials

2.1.1 General Reagents, Enzymes and Kits

Fisher Scientific UK Ltd., Loughborough, Leicestershire, UK

Sodium hydroxide (NaOH), potassium di-hydrogen orthophosphate (KH_2PO_4), Tris base, Ethylene diamine tetra acetic acid (EDTA), calcium chloride (CaCl_2), D-glucose, DTT ($\text{C}_4\text{H}_{10}\text{O}_2\text{S}_2$), urea, glacial acetic acid, sucrose, potassium acetate ($\text{C}_2\text{H}_3\text{O}_2\text{K}$), manganese chloride (MnCl_2), glycerol, glycine, MOPS, ethylene glycol, ethanol

Sigma-Aldrich Company Ltd., Poole, Dorset, UK

Tween-20, ampicillin, kanamycin, paraformaldehyde (PFA), dimethyl sulfoxide (DMSO), Hoechst 33342, ethylene glycol, Triton X-100, Na-deoxycholate, magnesium chloride (MgCl_2), bromophenol blue, BCA solution A, copper sulphate (CuSO_4), Poly-D-Lysine

VWR International Ltd., Leicestershire, England, UK

AnalaR Normapur HEPES, SDS, di-sodium hydrogen phosphate (Na_2HPO_4), sodium chloride (NaCl), potassium chloride (KCl), di-potassium hydrogen phosphate (K_2HPO_4), methanol, isopropanol, 30 mm coverslips, 22 mm coverslips, microscope slides

Life Technologies Limited, Paisley, Glasgow, UK

NuPAGE® Novex® 4-12% Bis-Tris gels (10, 12, 15 wells), MOPS SDS running buffer (20X), XCell SureLock™ mini-cell electrophoresis gel tank system, XCell II™ Blot module, Countess™ automated cell counter, All oligonucleotides used for PCR reactions, X-Rhod-1 AM, Hoechst 33342, Fura-2 AM, SYBR® Safe DNA gel stain.

Carestream Health, Inc. Rochester, NY

Carestream® KODAK® BioMax® Light film/ Medical X-Ray film

Amersham Protran, GE Healthcare, UK

Nitrocellulose blotting membrane

Pierce, Perbio Science UK Ltd., Tattenhall, Cheshire, UK

EZ-Link® Sulfo-NHS-SS Biotin, immobilised streptavidin beads

Thermo Fisher Scientific, Waltham, MA

SuperSignal™ West Pico Chemiluminescent Substrate kit, Enhanced Luminol Reagent and Oxidising Reagent

KPL, Inc., Maryland, USA

SureBlue® TMB substrate

Nanolight Technologies, Pinetop, AN, USA

Coelenterazine *h* or 2-Deoxycoelenterazine

New England Biolabs, MA, USA

Restriction endonucleases

Promega UK Ltd., Southampton, UK

Pfu DNA polymerase, restriction endonucleases, T4 DNA ligase

Qiagen, Crawley, West Sussex, UK

QIAfilter maxiprep kit, QIAprep Spin miniprep kit, QIAQuick gel extraction kit, QIAQuick PCR purification kit

Roche Applied Science, Lewes, East Sussex, UK

Complete™ EDTA-free protease inhibitor tablet, deoxyribonucleotide triphosphates (dNTPs), DNA molecular weight marker X, bovine serum albumin (BSA), fatty acid free (BSA)

Tocris Bioscience, Bristol, UK

Phorbol 12-myristate 13-acetate (PMA), Go 6976 (5,6,7,13-Tetrahydro-13-methyl-5-oxo-12H-indolo[2,3-a]pyrrolo[3,4-c]carbazole-12-propanenitrile), Bisindolylmaleimide-1 (3-[1-[3-(dimethylamino)propyl]-1H-indol-3-yl]-4-(1H-indol-3-yl)-1H-pyrrole-2,5-dione)

LI-COR Biosciences Ltd., Cambridge, UK

Odyssey® Blocking Buffer (TBS), Odyssey® Blocking Buffer (PBS). Chameleon® Protein Ladders

GE Healthcare Life Sciences, Buckinghamshire, UK

Full range Rainbow™ molecular weight marker

Bio-RAD Ltd., Hercules, California, USA

Agarose

Bioline Reagents Limited, London, UK

Hyperladder™ 1Kb

Formedia Ltd., Hunstanton, England, UK

Agar, Trypton, Yeast extract powder

Cisbio Bioassays, Codolet, France

Cellular signalling assay kits (IP-One)

2.1.2 Antibodies and antisera

In house made antisera

Rabbit $G\alpha_q/G\alpha_{11}$, sheep GFP antisera were produced in-house. The anti-phospho FFA4 rabbit antiserum was raised to a doublyphosphorylated peptide containing phosphates on residues corresponding to Thr³⁴⁷ and Ser³⁵⁰ of FFA4.

Sigma-Aldrich Company Ltd., Poole, Dorset, UK

Anti- α -tubulin (mouse) primary antibody, anti-FLAG monoclonal (mouse) primary antibody, horseradish peroxidase conjugated anti-goat (rabbit) secondary antibody

GE Healthcare Life Sciences, Buckinghamshire, UK

Secondary horseradish peroxidase conjugated anti-rat (goat) antibody, horseradish peroxidase conjugated anti-mouse (sheep) secondary antibody

Cell Signaling Technology, Inc., Danvers, MA, USA

β -arrestin1 and β -arrestin2 monoclonal antibody (rabbit)

LI-COR Biotechnology-UK Ltd., Cambridge, UK

IRDye[®] 800CW Donkey anti-Rabbit IgG secondary antibody, IRDye[®] 680RD Donkey anti-Goat IgG secondary antibody, IRDye[®] 680RD Donkey anti-Mouse IgG secondary antibody

2.1.3 Tissue culture

Invitrogen Life Technologies, Paisley, UK

Dulbecco's Modified Eagle Media (DMEM), Foetal bovine serum (FBS), Hygromycin B, Blasticidin S HCl, Versene-EDTA, GIBCO[®] Hank's Balanced Salt Solution (HBSS), sodium bicarbonate 7.5% solution

Sigma-Aldrich Company Ltd., Poole, Dorset, UK

Dulbecco's Modified Eagle Media (DMEM), Penicillin/Sterptomycin, Glutamine, Poly-D-Lysine, Trypsin-EDTA solution 0.25%

Promega UK Ltd., Southampton, UK

G-418 sulfate (Geneticin)

Polysciences, Inc. Warrington, PA

Polyethyleneimine (PEI)

Corning Incorporated, Corning, NY, USA

Corning® 96 well clear flat bottom polystyrene high bind microplate, Corning graduated pipette (5/10/25 ml), Corning TC centrifuge tube (15/50 ml), Corning® TC flask (25/75/150 cm²), Corning® 100 mm tissue-culture dishes, Corning® TC plates (6/12/24/96 well)

Greiner Bio-One GmbH, Kremsmünster, Austria

Cell culture microplate 96 well F-Bottom (clear/opaque, black/white) plate

PerkinElmer, Waltham, MA

OptiPlate™ 384-well, ProxiPlate™ 384-well plate

Molecular Devices, Sunnyvale, CA

96-well FlexStation™ Pipet Tips (Black)

Alpha Laboratories, Parham Drive, Hampshire, United Kingdom

Vial Cryogenic (1.2ml Graduated) sterile tube

Eppendorf, Hauppauge, NY

Eppendorf Repeater® manual handheld dispenser

Perkin-Elmer, Norwalk, CT

Disposable plate seal

2.1.4 Buffers and solutions

2.1.4.1 Phosphate buffered solutions (PBS)

10X PBS buffer was prepared with this formula: 137 mM NaCl, 2.7 mM KCl, 1.8 mM KH_2PO_4 , 10 mM Na_2HPO_4 , pH adjusted to 7.4. Before use, 10X was diluted with distilled water to 1X, sterilized and stored at room temperature.

2.1.4.2 Tris Buffered Saline (TBS)

10X of TBS buffer was prepared with this formula: 20 mM Tris-base, 150 mM NaCl, pH adjusted to 7.4. Prior use diluted to 1X with distilled water, sterilized and stored at room temperature.

2.1.4.3 Radioimmune precipitation assay (RIPA) Buffer (2X)

250 mM HEPES (pH 7.4), 300 mM NaCl, 2 % (v/v) Triton X-100, 1% (w/v) Na-deoxycholate, 0.2% (w/v) SDS, pH adjusted to 7.4 and stored at 4 °C.

2.1.4.4 Radioimmune precipitation assay (RIPA) Buffer (1X)

2X RIPA buffer was diluted to 1X with 10 mM NaF, 5 mM EDTA 0.5 M, 10 mM NaH_2PO_4 0.5M, 5% Ethylene glycol and distilled water, pH adjusted to 7.4. Before use complete EDTA free protease inhibitor tablets were added and stored at 4°C.

2.1.4.5 Transfer buffer

Glycine (0.2 M), Tris (25 mM), Methanol (20% v/v)

2.1.4.6 Tris-EDTA (TE) Buffer

10 mM Tris, 0.1 mM EDTA, pH adjusted to 7.4. Before use Complete™ EDTA free protease inhibitor tablets were added and stored at 4 °C.

2.1.4.7 Microscope Buffer

130 mM NaCl, 5 mM KCl, 20 mM HEPES, 10 mM Glucose, 1 mM MgCl₂, 1 mM CaCl₂, pH adjusted to 7.4, stored at 4 °C.

2.1.4.8 Glycine Buffer

192 mM Glycine, 25 mM Tris, pH adjusted to 8.3, stored at 4 °C.

2.1.4.9 Borate Buffer

10 mM Boric acid, 154 mM NaCl, 7.2 mM KCl, 1.8 mM CaCl₂, pH adjusted to 9.0, stored at 4 °C.

2.1.4.10 Laemmli Buffer (2X)

0.4 M DTT, 0.17 M SDS, 50 mM Tris, 50% (v/v) glycerol, 0.01% (w/v) bromophenol blue, stored in -20 °C.

2.1.4.11 Competent Bacteria Buffers

Competent Bacteria Buffer 1: 1 M KAc, 1 M RbCl₂, 1 M CaCl₂, 1 M MnCl₂, 80% glycerol, pH adjusted to 5.8 with acetic acid, filter sterilised and stored at 4 °C.

Competent Bacteria Buffer 2: 100 mM MOPS (pH 6.5), 1 M CaCl₂, 1 M RbCl₂, 80% glycerol, pH adjusted to 6.5 with concentrated HCl, filter sterilised and stored at 4 °C.

2.1.4.12 Luria-Bertani (LB) Media

1% (w/v) bactotryptone, 0.5% (w/v) yeast extract, 1% NaCl (w/v), pH adjusted to 7.4, sterilised by autoclaving at 126 °C.

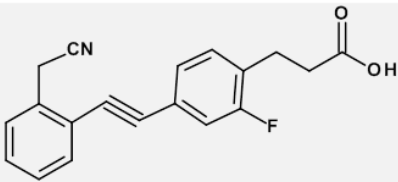
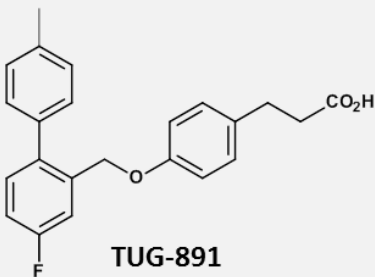
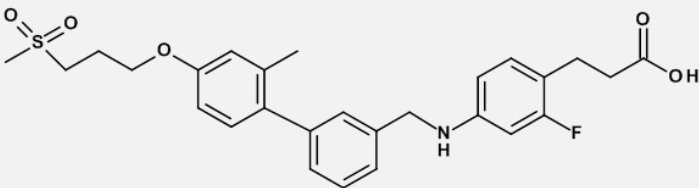
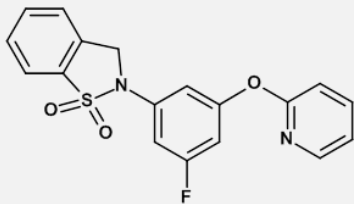
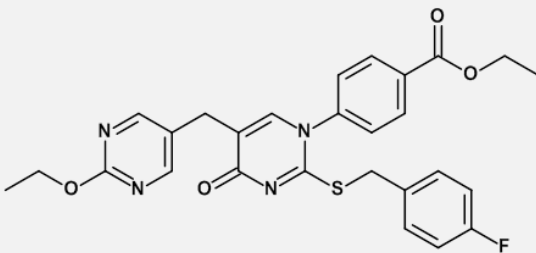
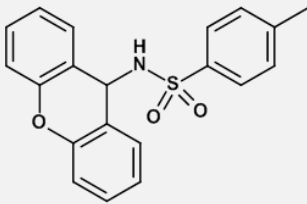
2.1.4.13 LB Media containing agar

1% (w/v) bactotryptone, 0.5% (w/v) yeast extract, 1% NaCl (w/v), 1.5% (w/v) agar, pH adjusted to 7.4, sterilised by autoclaving at 126 °C.

2.1.5 Pharmacological test compounds

TUG-891, 3-((4-((4-fluoro-4'-methyl-[1,1'-biphenyl]-2-yl)methoxy)phenyl)propanoic acid) (Shimpukade et al., 2012); TUG-1197, 2-(3-Fluoro-5-(pyridin-2-yloxy)phenyl)-2,3-dihydrobenzo[d]isothiazole-1,1-dioxide (Azevedo et al., 2016); TUG-770, 4-[2-[2-(cyanomethyl)phenyl]ethynyl]-2-fluorobenzenepropanoic acid (Christiansen et al., 2013a); TUG-905, 3-(2-fluoro 4-(((2'-methyl-4'-(3-(methylsulfonyl)propoxy)-[1,1'-biphenyl]-3-yl)methyl)amino)phenyl) propanoic acid (Christiansen et al., 2012); TUG-1275 (4-methyl-N-9H-xanthen-9-yl-benzenesulfonamide); GW-1100 (4-[5-[(2-ethoxy-5-pyrimidinyl)methyl]-2-[[4-(4-fluorophenyl)methyl]thio]-4-oxo-1(4H)-pyrimidinyl]-benzoic acid, ethyl ester) (Briscoe et al., 2006). Due to poor water solubility, all of these powdered test compounds were dissolved in dimethyl sulfoxide (DMSO) to a 10 μ M working stock solution. Except GW-1100, all other compounds were synthesised by our medicinal chemistry team (Table 2-1).

Table 2-1. Pharmacological test compounds

FFA1 Ligands	FFA4 Ligands
 <p>TUG-770</p>	 <p>TUG-891</p>
 <p>TUG-905</p>	 <p>TUG-1197</p>
 <p>GW-1100</p>	 <p>TUG-1275</p>

2.2 Molecular Biology Protocols

2.2.1 Preparation of Luria Bertani broth

Luria-Bertani (LB) broth is the most widely used media for the growth of bacteria. Bacteria grow faster in LB because the tryptone and yeast supply essential growth factors that they would otherwise have to synthesise. LB broth also contains essential electrolytes for transport and osmotic balance, due to the NaCl component. To make one litre of LB Broth 10 g tryptone, 5 g yeast extract and 5 g NaCl were added into distilled water. The mixture was stirred adequately and autoclaved at 126 °C. The solution was allowed to cool and stored at room temperature.

2.2.2 Preparation of LB plates

LB was prepared as detailed in section 2.2.1 and to this 1.5% (w/v) bacto-agar was added. This was autoclaved and allowed to cool to 50 °C prior to the addition of antibiotics. The media was mixed to ensure equal distribution of antibiotic (100 µg/ml) and was poured to 10-cm-petri dish. LB agar was allowed to cool at room temperature before being stored at 4 °C. Before use for bacterial culture, plates were warmed up to 37° in dry air oven.

2.2.3 Preparation of competent bacterial cells

Escherichia coli laboratory strain XL-1 blue was made competent chemically. XL-1 blue stock stored at -80 °C was thawed on ice and streaked onto an agar plate in the absence of antibiotics and incubated overnight at 37 °C. A single colony was inoculated into a 30 ml universal containing 5 ml of freshly prepared LB broth (section 2.1.4.12) and grown in a shaking incubator overnight (≈16 hours). This culture was used to inoculate 100 ml of LB broth that was grown with aeration at 37 °C until the optical density at 600 nm reached ≈0.48. The culture was chilled on ice for 20 minutes and then centrifuged at 2000 x g for 10 minutes at 4 °C. All traces of LB broth were removed and the pellet was gently re-suspended in 20 ml of competent bacteria buffer 1 (section 2.1.4.11). The suspension was incubated on ice for 20 minutes prior to centrifugation at 2000 x g for 10 minutes at 4 °C. Following removal of supernatant, cell pellets were re-suspended in 2 ml of competent bacteria buffer 2 (section 2.1.4.11). After

incubation on ice for 20 minutes the competent bacteria were aliquoted into pre-chilled sterile 1.5 microcentrifuge tubes at a volume of 220 μ l and stored immediately at -80°C until required. The process has been described diagrammatically in Figure 2-1.

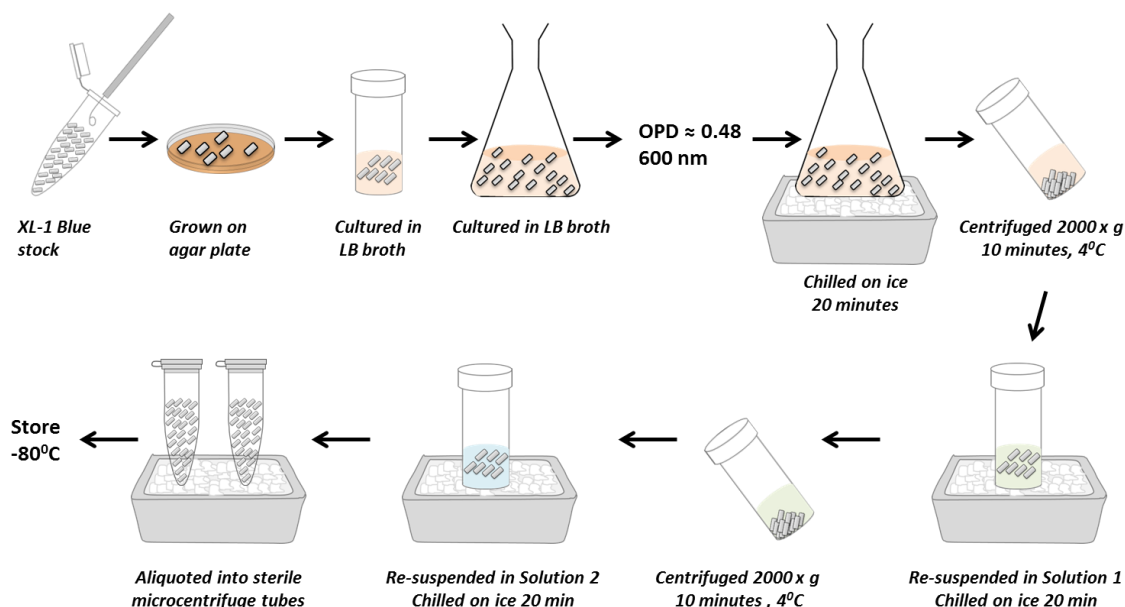


Figure 2-1. Preparation of competent XL-1 blue. Schematic diagram of preparation of XL-1 blue bacteria. XL-1 blue was streaked aseptically onto an agar plate and incubated overnight at 37°C . A single colony was inoculated into 5 ml LB broth and grown in a shaking incubator for 16 hours. This culture was used to inoculate 100 ml of LB broth and grown until the optical density at 600 nm reached ≈ 0.48 . The culture was chilled on ice for 20 minutes and centrifuged at $2000 \times g$ for 10 minutes at 4°C . The pellets were gently re-suspended in 20 ml of buffer 1 (section 2.1.4.11) and chilled on ice for 20 minutes prior to centrifugation at $2000 \times g$ for 10 minutes at 4°C . Following removal of supernatant, cell pellets were re-suspended in 2 ml of buffer 2 (section 2.1.4.11). After incubation on ice for 20 minutes the competent bacteria were aliquoted into pre-chilled, sterile 1.5 microcentrifuge tubes at a volume of 220 μ l and stored immediately at -80°C until required.

2.2.4 Transformation of competent bacterial cells

An aliquot of competent bacteria was allowed to thaw on ice. To 50 μ l of competent bacteria between 1 and 10 ng of DNA was added and incubated on ice for 15 minutes. The cells were subjected to a heat shock at 42°C for 90 seconds in a water bath and incubated immediately on ice for 2 minutes. To the cells, 500 μ l of LB broth (section 2.1.4.12) was added and incubated at 37°C for 1 hour in a shaking incubator. 100 μ l of the reaction was spread onto a LB plate (section 2.1.4.13) containing the appropriate antibiotic and incubated inverted overnight at 37°C . After 16 hours incubation colonies were seen in the plate. Individual colonies were selected for the preparation of plasmid DNA (section 2.2.5).

2.2.5 Preparation of plasmid DNA

2.2.5.1 Miniprep

The Wizard® Plus SV Minipreps DNA purification system (Promega) was used for making miniprep of DNA. Briefly, bacterial cells were pelleted by centrifugation at 13,200x g for 5 minutes at 4 °C and re-suspended by pipetting in 250 µl of re-suspension buffer (50 mM Tris-HCl, 10 mM EDTA, pH 8.0 containing 100 µg/ml RNase A). Cells were treated with 250 µl of lysis buffer (200 mM NaOH, 1% (w/v) SDS), inverted 4 times to mix. 10 µl of alkaline protease solution was added and inverted 4 times to mix. The mixture was incubated for 5 minutes at room temperature. Lysis was terminated by the addition of 350 µl of neutralisation buffer (3 mM potassium acetate, pH 5.5). The cell lysates were centrifuged for 10 minutes at 13,200x g at room temperature and the supernatant was loaded onto miniprep columns. The columns were centrifuged for 1 minute at 13,200x g and washed twice with 750 µl wash buffer (1.0 mM NaCl, 50 mM Tris-HCl, pH 7.0, 15% (v/v) isopropanol). After washing, bound DNA was eluted into a clean 1.5 ml Eppendorf tube with 100 µl sterile H₂O.

2.2.5.2 Maxiprep

QIAfilter® maxiprep kit (Qiagen) was used to produce larger scale DNA samples. Purification of DNA was carried out as per manufacturer's instructions. Briefly, a 100 ml culture of transformed bacteria was pelleted by centrifugation 4000x g at 4 °C for 30 minutes. All traces of media were removed and the pellet re-suspended in 10 ml of chilled buffer P1 (50 mM Tris-HCl pH 8.0, 10 mM EDTA, 100 µg/µl Rnase A). Cell lysis was achieved by the addition of 10 ml buffer P2 (200 mM NaOH, 1% (w/v) SDS) and incubated for 10 minutes at room temperature. 10 ml of buffer P3 (3.0 M potassium acetate pH 5.5) was added to neutralise the reaction and the solution was immediately applied to a QIAfilter® cartridge and left for 10 minutes at room temperature to settle. Meanwhile, a Qiagen tip 500 was equilibrated by the addition of buffer QBT (750 mM NaCl, 50 mM MOPS pH 7.0, 15% (v/v) isopropanol). After 10 minutes, the lysed cells were added onto the equilibrated tip and allowed to filter through. The column was washed with 60 ml of buffer QC (1.0 M NaCl, 50 mM MOPS pH 7.0, 15% (v/v) isopropanol). The DNA was eluted by the addition of 15 ml of buffer QF (1.25 M NaCl, 50 mM Tris-HCl pH 8.5, 15% (v/v) isopropanol) to the tip. The DNA was

precipitated by the addition of 10.5 ml isopropanol and pelleted by centrifugation at 12,000x g for 30 minutes at 4 °C. The DNA pellet was washed with 5 ml of 70% (v/v) ethanol and then centrifuged for 15 minutes at 12,000x g at 4 °C. The supernatant was carefully removed and the pellet allowed to air dry prior to resuspension in 1 ml of sterile water.

2.2.6 Quantification of DNA

Quantification of DNA samples was performed by examining the absorbance of a 1:100 dilution of the sample at 260 nm. An A_{260} value of 1 unit was taken to correspond to 50 µg/ml of double stranded DNA. The A_{280} value of sample was also measured to assess the purity of the DNA solution. A DNA solution with A_{260}/A_{280} ratio of between 1.7 and 2.0 was considered pure enough for use.

2.2.7 Polymerase chain reaction

Polymerase chain reaction (PCR) was carried out to amplify specific sections of DNA. Pfu DNA polymerase was used due to its high fidelity and its ability to withstand higher temperatures. This method was used to introduce tags and to introduce new restriction sites to construct fusion proteins (Table 2-1). All reactions were performed using sterile materials. A typical PCR reaction mixture has been described below in Table 2-2.

Table 2-2. Polymerase chain reaction mixture

Reagents	Amounts (vol.)
Pfu polymerase buffer (10x)	5 µl
Deoxynucleotide tri-phosphates (dNTPs): (0.2mM of each dATP, dCTP, dGTP, dTTP)	1 µl
Primer mix (10 µM each)	1.5 µl
DNA template (50 ng/µl)	0.5 µl
Pfu polymerase enzyme (3u/µl)	0.5 µl
dH ₂ O to a final volume of	50 µl

Reactions were carried out on an Eppendorf gradient Thermocycler. The annealing temperatures were dependent on the T_m of primers used. I have used the following PCR cycles (Figure 2-2).

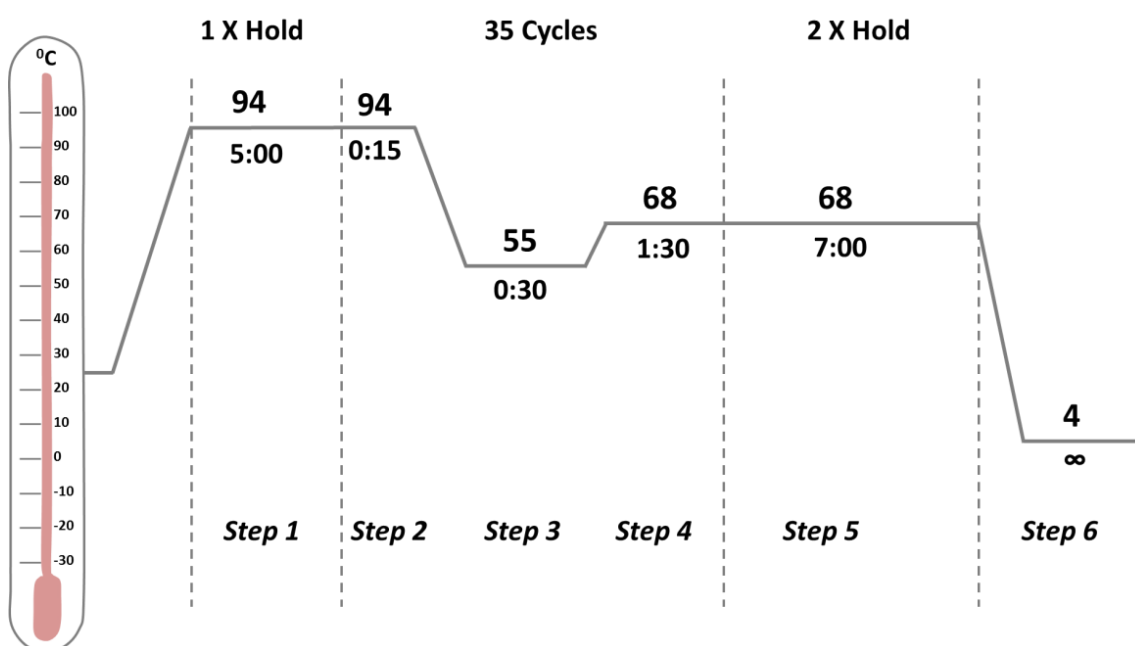


Figure 2-2. Schematic diagram of the PCR process. *Step 1 (94 °C):* This step causes activation of polymerase enzyme. *Step 2 (94 °C):* Denaturation step, high temperature separates the two strands of the DNA, allowing the other agents in the PCR cocktail to access the genetic information. *Step 3 (55 °C):* The annealing step, the primers binds to the regions next to the target gene to amplify. *Step 4 (68 °C):* The synthesis step, this is the optimum temperature for the enzyme to work, allowing efficient incorporation of the dNTPs by the polymerase to extend the primers into full-length copies of the target region. Steps 2, 3 and 4 are repeated 35 times to allow more copies to be made. The number of copies of the target region increase exponentially, as with each cycle the number of total copies is double. *Step 5 (68 °C):* This step follows the repetition of steps 2-5 and makes sure that strand synthesis has been completed before the reaction is stopped. *Step 6 (4 °C):* This cools the reaction to a temperature at which the reaction stops.

2.2.8 PCR purification

QIAquick® PCR purification kits (Qiagen) were used for the purification of PCR products. Briefly, 5 volumes of Buffer PB was added to 1 volume of the PCR sample and mixed properly. QIAquick® spin column was placed in a 2 ml collection tube and centrifugation at 13,200 x g for 1 minute. The flow-through was discarded and the QIAquick® column was placed back into the same tube. 750 µl of wash Buffer PE was added and centrifugation at 13,200 x g for 1 minute at room temperature. The flow-through was discarded and the QIAquick® column was again placed back into the same tube. The column was additionally centrifugation at 13,200 x g for 1 minute. The column was placed in a clean 1.5

ml microcentrifuge tube and 30 μ l of pure distilled water was added into the column and centrifugation at 13,200 x g for 1 minute. The eluent is the pure PCR product.

2.2.9 Digestion of DNA with restriction endonucleases

Digests were prepared using the appropriate restriction enzyme (1-2 units), buffer as specified by the manufacturer, and 1 μ g of DNA, in a final volume of 50 μ l (Table 2-3). Reactions were incubated at 37 $^{\circ}$ C for a minimum of 2 hours to overnight.

Table 2-3. Restriction digestion mixture

Reagents	Amounts (vol.)
CutSmart buffer (10x)	5 μ l
Restriction enzyme 1	1 μ l
Restriction enzyme 2	1 μ l
Plasmid/pcr product	10 μ l (2 μ g)
dH ₂ O to a final volume of	up to 50 μ l

2.2.10 DNA gel electrophoresis

Digested DNA samples or PCR reactions were examined using agarose gel electrophoresis. Agarose gel was prepared by adding 1 g multi-purpose agarose to 30 ml 1X TBE buffer. To dissolve, the mixture was heated in a microwave for 1 minute, swirled, and this process continued for approximately 2 minutes until the solution was homogenous. The solution was cooled to 50 $^{\circ}$ C in a temperature-controlled incubator before SYBR[®] Safe DNA gel stain was added (3 μ l) and swirled gently to mix properly. The mixture was poured carefully into the centre of a UVT (ultra violet transmission) tray sealed with dams at either end, placed within a horizontal HORIZON[®] gel tank (Life Technologies) containing a 1 mm thick DELRIN[®] comb with the desired well size. Once the agarose gel had set, the dams were removed. 1X TBE buffer was added to fill the tank covering the gel to a depth of 1 to 2 mm and the comb was removed gently. A 1 kb HyperLadder[™] (Bioline Reagents) was added to 5X DNA gel loading buffer

and loaded into the first well. DNA samples loaded with 5X DNA loading buffer were loaded into the bottom of each well. The volume was dependent on the size of the comb used to set the gel. The safety lock lid containing power cables was secured over the gel tank, which was connected to a 250 volts DC power supply. The gels were run at 125 mA for 30 minutes. The DNA fragments were visualised using ultraviolet light using a Gel Doc UV transilluminator (Bio-Rad Laboratories) fitted with Quantity One[®] software to document and image of gels.

2.2.11 DNA purification from agarose gels

The QIAquick[®] gel extraction kit was used for the purification of DNA from agarose gels. Briefly, the DNA fragment from the agarose gel was excised with a clean, sharp scalpel. The gel slice was weighed in a colourless tube. 3 volumes of buffer QG was added into to 1 volume of excised gel and incubated at 50^o C for 10 min (or until the gel slice was completely dissolved). The tube was vortexed every 2-3 min to help dissolve gel. After the gel slice was dissolved completely, the colour of the mixture was checked as yellow (similar to Buffer QG without dissolved agarose). If the colour of the mixture was orange or violet, 10 µl of 1 M sodium acetate (pH 5.0) was added and mixed and the colour turned yellow. 3 gel volume of isopropanol was added into the sample and mixed. The QIAquick[®] spin column was placed in the provided 2 ml collection tube and centrifugation at 13,200 x g for 1 minute. The flow-through was discarded and the column was placed back into the same tube. The process was repeated if the sample volumes were >800 µl. Buffer QG (500 µl) was added in to the column and centrifugation at 13,200 x g for 1 minute. The flow-through was discarded and was placed back into the same tube. To wash, 750 µl buffer PE was added in to the column and centrifugation at 13,200 x g for 1 minute. The flow-through was discarded and was placed back into the same tube and centrifugation again at 13,200 x g for 1 minute to remove residual wash buffer. The column was placed into a clean 1.5 ml microcentrifuge tube. To elute DNA, 30 µl of pure water was added in to the centre of the The QIAquick[®] membrane and centrifuged at 13,200 x g for 1 minute.

2.2.12 Ligation of DNA

Digested DNA constructs were ligated into plasmid vector using T4 DNA ligase. A ratio of 1:3 and 1:6 vector:PCR product was used in a volume of 20 µl containing 1 unit of ligase and the supplied buffer (Table 2-4). The reaction was incubated at room temperature for 4 hours. The ligation reactions were transformed as described in section 2.2.4.

Table 2-4. Ligation reaction mixture

Reagents	Amounts
Digested vector (pcDNA5 ~6000bp)	50 ng
Digested insert (pcr product, i.e. mVenus)	25 ng
T4 DNA buffer (10X)	2 µl
T4 DNA Ligase	1 µl
dH ₂ O to a final volume of	up to 20 µl

2.2.13 DNA sequencing

DNA sequencing was performed by the DNA Sequencing and Service (School of Life Sciences, University of Dundee, Scotland) using an automated ABI PRISM® capillary DNA sequencer and Big-Dye® terminator cycle sequence kit (Applied Biosystems®, Life Technologies Ltd., Paisely, UK) to analyse fluorescently labelled DNA fragments by capillary electrophoresis.

2.3 Construction of expression vectors to study hFFA1 and hFFA4

The pcDNA5 FRT/TO expression vector for human FFA1 and FFA4 in the form of hFFA1-eYFP and FLAG-hFFA4-Nluc were a gift from Dr. Brian Hudson. Using these vectors and amplifying new fluorescent proteins (mVenus/GFP2), I have made several fluorophore labelled receptor constructs (Table 2-5). I also received pEGFP-N1 plasmid containing CD86 from Dr. Richard Ward. Using these vectors and amplifying new fluorescent proteins (mVenus/GFP2), I have made several fluorophore labelled receptor constructs (Table 2-5). All constructs were verified by sequencing.

Table 2-5. Plasmids and primers used in cloning

Construct	Plasmids	PCR product	Rest. Sites	Primers
FLAG-hFFA4-mVenus	pcDNA3 and pcDNA5/FRT/TO	mVenus	KpnI XhoI	5'-AAAAAGGTACCATGGTGAGCAAG-3' 5'-AAAAACTCGAGTTAGAAGTACAGCTCGTCAT-3'
hFFA1-mVenus-HA	pcDNA3 and pcDNA5/FRT/TO	mVenus-HA	EcoRV XhoI	5'-AAAAAGATATCATGGTGAGCAAGGGC GAG-3' 5'-AAAAACTCGAGTTAAGCGTAATCTGGAACATCGTATGGGTACTTGTACAGCTCGTC CATGCC-3'.
FLAG-hFFA4-GFP2	pcDNA3 and pcDNA5/FRT/TO	GFP2	KpnI XhoI	5'-AAAAAGGTACCATGGTGAGCAAG-3' 5'-AAAAACTCGAGTTAGAAGTACAGCTCGTCAT-3'
hFFA1-GFP2-HA	pcDNA3 and pcDNA5/FRT/TO	GFP2-HA	EcoRV XhoI	5'-AAAAAGATATCATGGTGAGCAAGGGC GAG-3' 5'-AAAAACTCGAGTTAAGCGTAATCTGGAACATCGTATGGGTACTTGTACAGCTCGTC CATGCC-3'
CD86-mVenus	pEGFP-N1	mVenus	KpnI NotI	5'-ATATCACATGAGGTACCGGTGAGCAAG GCGAGGAGCTGTTC-3' 5'-ACGTACACAAGCGGCCGCTTACTTGTA CAGCTCGTCCATGCC-3'

2.3.1 Construction of pcDNA5 for inducible expression of hFFA1

pcDNA5/FRT/TO is an expression plasmid containing a FRT site linked to the hygromycin resistance gene for Flp recombinase-mediated integration and selection of a stable cell line expressing the gene of interest under the control of a tetracycline-regulated CMV/TetO₂ promoter (Ward et al., 2011a). Amongst other features, it carries an ampicillin antibiotic resistance gene for selection in *E. coli* bacteria and a Hygromycin antibiotic resistance gene for selection of stable transfects in mammalian cells. HA epitope-tagged mVenus or GFP2 were generated by PCR (section 2.2.7) using EcoRV forward and XhoI reverse primers (Table 2-5). The vector pcDNA/FRT/TO/hFFA1-eYFP and PCR-products were digested by EcoRV and XhoI restriction endonucleases. The restriction fragments were ligated to construct pcDNA/FRT/TO/hFFA1-mVenus-HA and pcDNA/FRT/TO/hFFA1-GFP2-HA (Figure 2-3). Constructs were verified by sequencing.

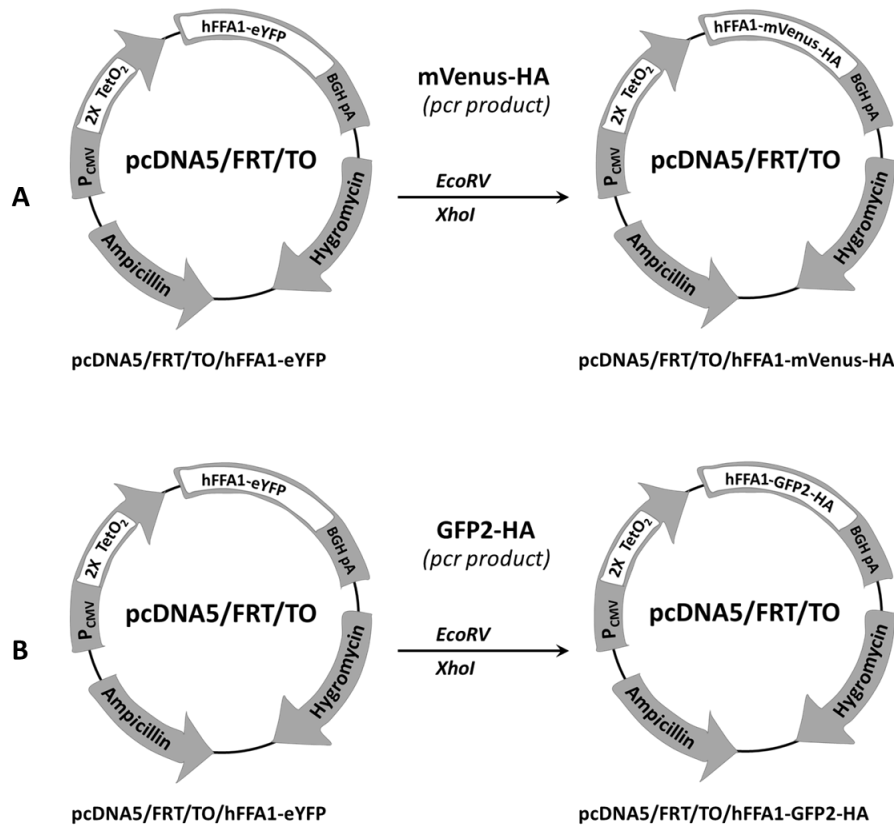


Figure 2-3. Construction of pcDNA5/FRT/TO for the expression of hFFA1-mVenus-HA and hFFA1-GFP2-HA. A pcDNA5/FRT/TO containing hFFA1-eYFP construct was digested by EcoRV and XhoI restriction enzymes. The construct mVenus-HA or GFP2-HA was cloned by a PCR thermocycler using EcoRV forward and XhoI reverse primers (Table 2-5). These constructs were digested by EcoRV and XhoI restriction enzymes and sub-cloned into pcDNA5/FRT/TO/hFFA1-eYFP vector to generate (A) pcDNA5/FRT/TO/hFFA1-mVenus-HA and (B) pcDNA5/FRT/TO/hFFA1-GFP2-HA.

2.3.2 Construction of pcDNA3 for constitutive expression of hFFA1

To construct vectors for constitutive expression of hFFA1-mVenus-HA or hFFA1-GFP2-HA an empty vector pcDNA3 was utilized. This plasmid carries an ampicillin antibiotic resistance gene for selection in *E. coli* bacteria and a Neomycin antibiotic resistance gene (for instance, G418 or geneticin) for selection of stable transfects in mammalian cells (Ward et al., 2013). pcDNA5/FRT/TO vectors containing hFFA1-mVenus-HA or hFFA1-GFP2-HA were digested by HindIII and XhoI restriction endonucleases to generate fragments of hFFA1-mVenus-HA or hFFA1-GFP2-HA. These fragments were ligated into an empty pcDNA3 (Figure 2-4). Constructs were verified by sequencing (section 2.2.13).

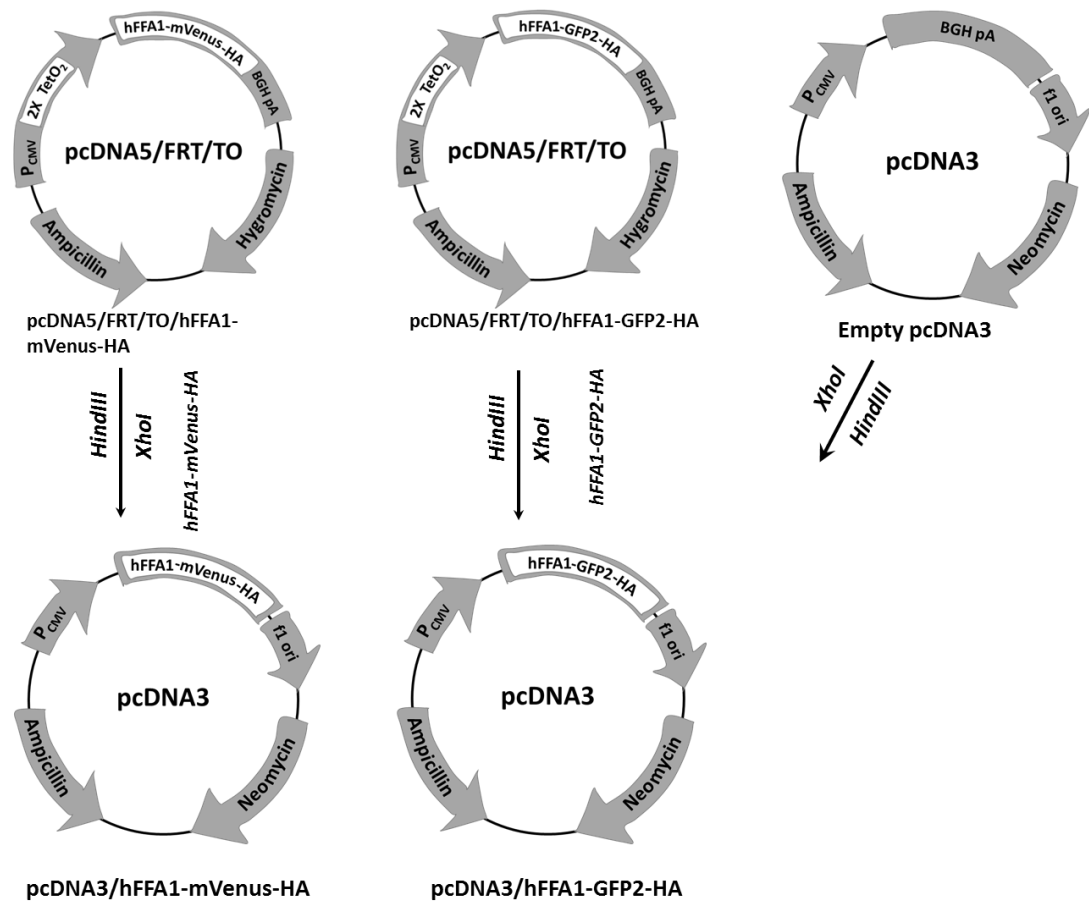


Figure 2-4. Construction of pcDNA3 incorporating hFFA1-mVenus-HA or hFFA1-GFP2-HA. A pcDNA5/FRT/TO containing hFFA1-mVenus-HA or hFFA1-GFP2-HA construct were digested by HindIII and XhoI to generate fragments of hFFA1-mVenus-HA or hFFA1-GFP2-HA. These fragments were sub-cloned into an empty pcDNA to generate pcDNA3/hFFA1-mVenus-HA and pcDNA3/hFFA1-GFP2-HA.

2.3.3 Construction of pcDNA5 for inducible expression of hFFA4

mVenus or GFP2 constructs were generated by PCR (section 2.2.7) using KpnI forward and XhoI reverse primers (Table 2-5). The pcDNA5/FRT/TO/FLAG-hFFA4-eYFP and PCR-products were digested by KpnI and XhoI restriction enzymes. Subsequent ligations generated pcDNA5/FRT/TO/FLAG-hFFA4-mVenus and pcDNA5/FRT/TO/FLAG-hFFA4-GFP2 (Figure 2-5). Constructs were verified by sequencing.

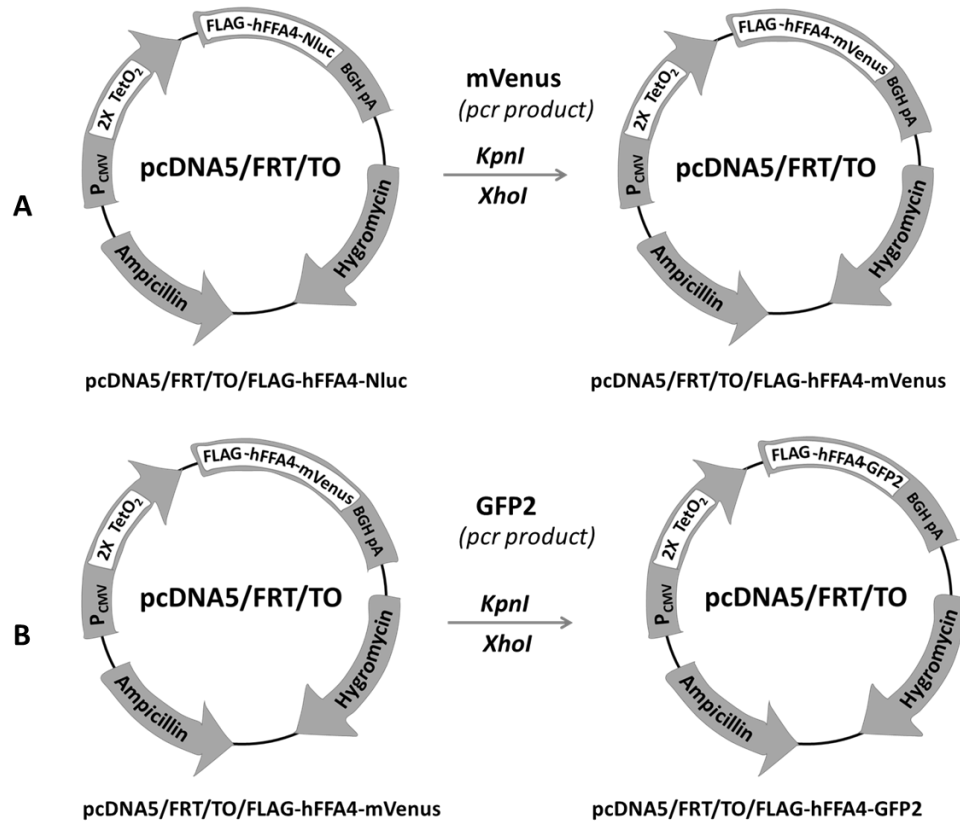


Figure 2-5. Construction of pcDNA5/FRT/TO incorporating FLAG-hFFA4-mVenus or FLAG-hFFA4-GFP2. A pcDNA5/FRT/TO containing FLAG-hFFA4-eYFP construct was digested by KpnI and XhoI. mVenus or GFP2 constructs were cloned by PCR using KpnI forward and XhoI reverse primers. These constructs were digested by KpnI and XhoI enzymes and sub-cloned into pcDNA5/FRT/TO/ to generate (A) pcDNA5/FRT/TO/FLAG-hFFA4-mVenus and (B) pcDNA5/FRT/TO/FLAG-hFFA4-GFP2.

2.3.4 Construction of pcDAN3 for constitutive expression of hFFA4

To construct vectors for constitutive expression of FLAG-hFFA4-mVenus or FLAG-hFFA4-GFP2 an empty pcDNA3 was utilized. The pcDNA5/FRT/TO vector containing FLAG-hFFA4-mVenus or FLAG-hFFA4-GFP2 was digested by HindIII and XhoI to generate fragments of FLAG-hFFA4-mVenus or FLAG-hFFA4-GFP2. These fragments were ligated into an empty pcDNA3 (Figure 2-6). Constructs were verified by sequencing.

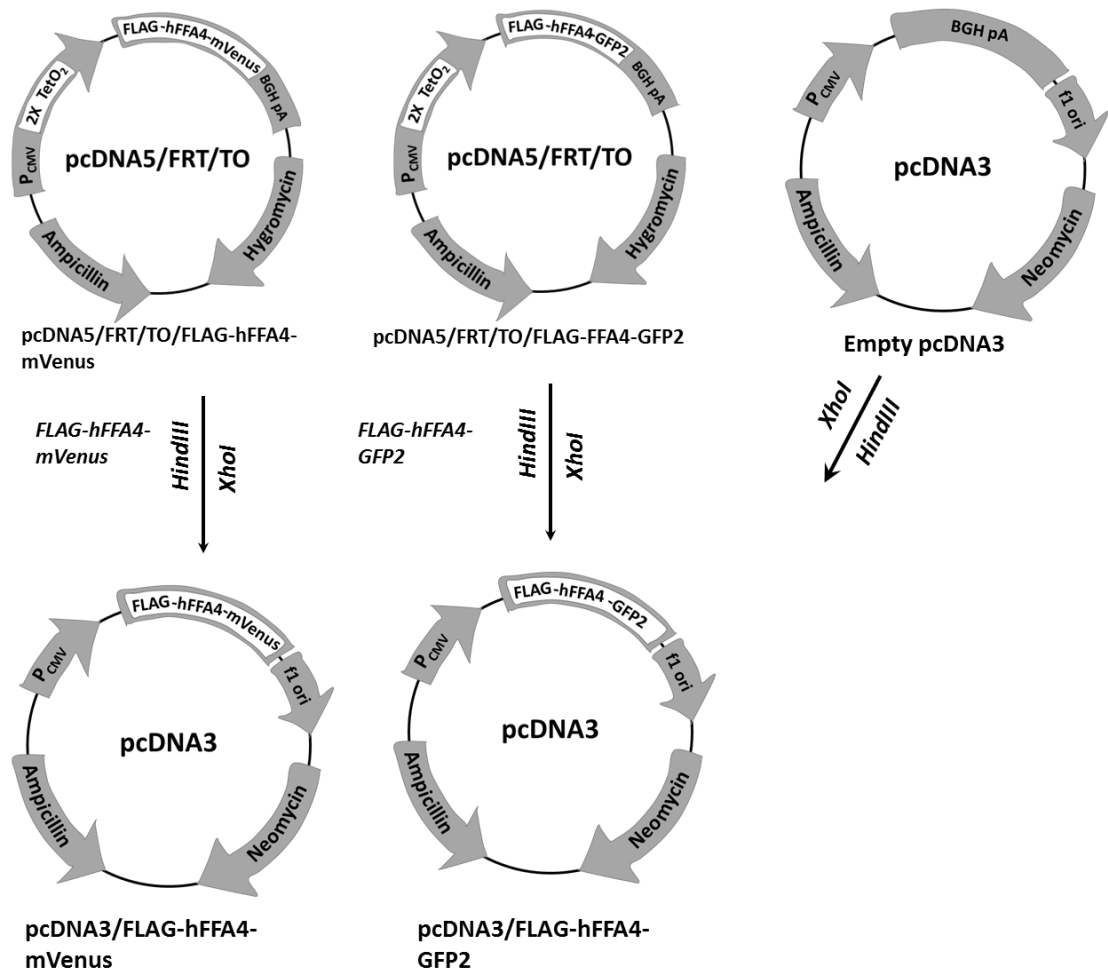


Figure 2-6. Construction of pcDNA3 incorporating FLAG-hFFA4-mVenus or FLAG-hFFA4-GFP2. A pcDNA5/FRT/TO containing FLAG-hFFA4-mVenus or FLAG-hFFA4-GFP2 was digested by HindIII and XhoI to generate fragments FLAG-hFFA4-mVenus and FLAG-hFFA4-GFP2. These fragments were sub-cloned into an empty pcDNA3 to generate pcDNA3/FLAG-hFFA4-mVenus and pcDNA3/FLAG-hFFA4-GFP2.

2.3.5 Construction of CD86-mVenus

CD86-EGFP N1 plasmid carries Kanamycin/Neomycin antibiotic resistance gene for selection in *E.coli* bacteria. A PCR-product of mVenus was cloned by KpnI forward and NotI reverse primers. CD86-EGFP vector and PCR guided mVenus were digested by KpnI and NotI enzymes. DNA fragments were ligated to generate CD86-mVenus plasmid (Figure 2-7). The Construct was verified by sequencing.

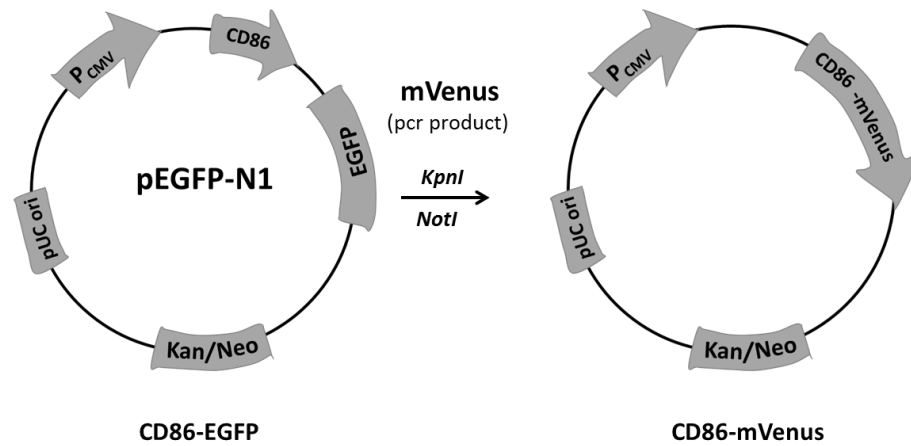


Figure 2-7. Construction of plasmid incorporating CD86-mVenus. CD86-EGFP N1 plasmid was digested with KpnI and NotI. mVenus construct was cloned by PCR using KpnI forward and NotI reverse primers. This construct was digested by KpnI and NotI restriction enzymes and sub-cloned into the CD86-EGFP N1 plasmid to generate CD86-mVenus expression vector.

2.4 Cell Culture and Transfections

All cell cultures and transfection were performed under sterile conditions in a Faster Ultrasafe class II laminar flow biosafety cabinet. Cells were incubated in a designated cell culture facility in an inCu saFe® SANYO humidified incubator supplied with 5% CO₂ and maintained at 37 °C. Cell culture was maintained in vented T75² flasks with canted necks containing 10-15 ml media with phenol red and heat-inactivated foetal bovine serum (FBS).

2.4.1 Cell maintenance

2.4.1.1 HEK293T, HEK293 and genome-edited HEK293 cells

Human embryonic kidney cells stably expressing the SV40 large T-antigen (HEK293T), HEK293 parental cells and CRISPR/Cas9 genome-edited HEK293 cells lacking Gα_q/Gα₁₁ or β-arrestin1/2 proteins (Alvarez-Curto et al., 2016b; Scharge et al., 2015) were grown in Dulbecco's modified Eagle's media (DMEM) supplemented with 10% (v/v) FBS, L-glutamine (0.292 g/L), penicillin (100 units/mL) and streptomycin (100 µg/mL). Cells were grown in a humidified incubator supplied with 5% CO₂ and maintained at 37 °C.

2.4.1.2 Cells able to constitutively express hFFA1 or hFFA4

HEK293 parental and genome-edited HEK293 cells constitutively expressing either hFFA1 or hFFA4 were generated (section 2.4.2.4). Stable cell lines were maintained in DMEM supplemented with 10% (v/v) FBS, L-glutamine (0.292 mg/mL), penicillin (100 units/mL), streptomycin (100 µg/mL) and G418 (1 mg/mL) antibiotics. Cells were grown in a humidified incubator supplied with 5% CO₂ and maintained at 37 °C.

2.4.1.3 Flp-In™ T-REx™ -293 cells

Flp-In™ T-REx™ HEK293 parental cells were maintained in DMEM media (4500 mg/L glucose + L-glutamine, – pyruvate) supplemented with 10% FBS (v/v), blasticidin (5 µg/mL), Zeocin (100 µg/mL), penicillin (100 units/mL) and streptomycin (100 µg/mL). Cells were grown in a humidified incubator supplied with 5% CO₂ and maintained at 37 °C.

2.4.1.4 Flp-In™ T-REx™ -293 cells able to inducibly express hFFA1 or hFFA4

Flp-In™ T-REx™ HEK293 cells inducibly expressing hFFA1 or hFFA4 were cultured in single stable DMEM media (4500 mg/L glucose + L-glutamine, – pyruvate) supplemented with 10% FBS (v/v), blasticidin (5 µg/mL), penicillin (100 units/mL), streptomycin (100 µg/mL) and hygromycin B (200 µg/mL). Cells were grown in a humidified incubator supplied with 5% CO₂ and maintained at 37 °C.

2.4.1.5 Flp-In™ T-REx™ -293 double stable cells

Flp-In™ T-REx™ HEK293 double stable cells inducibly expressing either hFFA1 or hFFA4 and constitutively expressing another form of receptors were cultured in double stable DMEM media containing 10% (v/v) FBS, penicillin (100 units/mL), streptomycin (100 µg/mL), hygromycin B (200 µg/mL) and G-418 (1 mg/mL). Cells were grown in a humidified incubator supplied with 5% CO₂ and maintained at 37 °C.

2.4.1.6 Passage of cells

Cell passaging or splitting technique was applied to keep cells alive and growing under cultured conditions for extended periods of time. Upon reaching the

desired confluence, media was aspirated by sterile pipette. Cells were first washed with sterile 1X PBS before addition of pre-warmed 0.25% trypsin-EDTA and incubation for few minutes to allow detachment of cells from the bottom of flask. Flasks were tapped gently to ensure complete dissociation from the plastic ware. Pre-warmed DMEM was added to make a cell suspension. Cells (1:10 or 1:20 ratio) were transferred to a new sterile flask with fresh culture media.

2.4.1.7 Cryopreservation of mammalian cells

Early passages of all cell lines were cryopreserved to avoid loss by contamination, to minimize genetic change in continuous cell lines, and to avoid aging and transformation in finite cell lines. Before cryopreservation, cells were characterised and checked for contamination. Upon reaching 70% confluence in a T75² flask, cells were trypsinised as gently as possible to minimise damage to the cells and suspended in 10 ml complete growth media. Cell suspension was centrifuged at 1200 x g for 3 minutes to pellet cells. Using a sterile pipette, the supernatant was withdrawn without disturbing the cells. Cells were re-suspended in 1 ml of DMEM and 1 ml FBS (10% DMSO). Cells were preserved at -80 °C in a sterile cryogenic vial (1 ml/ vial) and then transferred to liquid nitrogen storage.

2.4.2 Transfection and generation of stable cell lines

Heterologous cell systems able to express GPCRs considered an appropriate way to investigate molecular mechanism of cell signalling and pharmacology (Chakraborty et al., 2015; Andrell and Tate, 2013). In this process, transfection is an important tool for studying the effects of altered gene expression on cellular physiology. Successful transfection expresses the gene of interest without harming the cells to be transfected. The main challenge of transfection is to insert the negatively charged nucleic acid molecules against negatively charged plasma membranes. Hence, chemical methods were utilized with the use of positively charged transfection reagents forming a layer around the negatively charged nucleic acids to neutralize their charge.

2.4.2.1 Transient transfection

For short-term experiments, transient transfection was employed. However, as the gene was not incorporated into the genome, cells were discarded after single experiment. HEK293T cells were seeded on to 10 cm² dish to a volume of 10 ml media. Transfection of cells was performed when the cells had reached 60-70% confluency. Cells were transfected by the use of cationic DNA complexing agent polyethyleneimine (Longo et al., 2013). A mixture of 5 µg DNA was prepared in 250 µl NaCl (150 mM). PEI (1 mg/mL) was diluted as 1:6 ratio in 250 µl NaCl (150 mM). Two mixtures were added together, vortexed and incubated for 10 minutes at room temperature. Cell media was replaced by fresh media and the DNA/PEI mixture was added drop-wise into the media. Transfected plates were incubated in a humidified incubator supplied with 5% CO₂ and maintained at 37 °C. Assays with these cells 48 hours post transfection.

2.4.2.2 Generation of Flp-In™ T-Rex™ HEK293 inducible cell line

Flp-In™ T-REx™ HEK293 cells inducibly expressing hFFA1 or hFFA4 were generated. The Flp-In™ T-REx™ HEK293 cell line facilitates rapid and homogenous expression of cDNA constructs when expressed from a Flp-In™ vector such as pcDNA5/FRT/TO, which contains the hygromycin resistance gene and a flippase recognition target (FRT) site that enables selection of transformants that are inserted via DNA recombination by Flp recombinase at the FRT-site (Ward et al., 2011a). Before transfection, Flp-In™ T-Rex™ 293 cells were seeded into 10-cm dishes in DMEM media and cells were grown until 65% confluent. Using PEI transfection protocol (section 2.4.2.1) cells were co-transfected with the gene of interest (GOI) sub cloned into pcDNA5/FRT/TO and the plasmid pOG44, which encoded the Flp recombinase (which then catalysed integration). A plasmid ratio of 9:1, 7.2 µg pOG44 and 0.8 µg GOI containing pcDNA5/FRT/TO was used (Ward et al., 2013). After 24 hours of transfection, the media was replaced with fresh media. 48 hours after transfection, cells were split into 10-cm dishes at densities lower than 25%. 72 hours after transfection, selection was begun by changing the media containing hygromycin B (200 µg/mL), but not zeocin (as the zeocin resistance was destroyed by the integration process). Cells began to die off due to the presence of hygromycin B. The media was changed in every 2-3 days. Approximately 2 weeks after

transfection, visible foci appeared. The cells were then be pooled, expanded, and tested for tetracycline-regulated expression of the GOI. Early passages of cells were cryopreserved (section 2.4.1.7).

2.4.2.3 Generation of Flp-In™ T-REx™ HEK293 double stable cell line

To investigate the possible oligomerisation in hFFA1 and hFFA4, I have generated Flp-In™ T-REx™ 293 double stable cell lines inducibly expressing either hFFA1 or hFFA4 and constitutively expressing another FRET pair-tagged receptor. Once a stable Flp-In™ T-Rex™ 293 cell line inducibly expressing hFFA1 or hFFA4 was established (section 2.4.2.2), a second and different fluorophore-tagged hFFA1 or hFFA4 was introduced. The second insertion constitutively expressed the receptor of interest. The second receptor construct was sub cloned into an appropriate mammalian expression vector, the pcDNA3, incorporating geneticin selectable resistance gene.

Flp-In™ T-Rex™ 293 single stable cells was cultured into 10-cm dishes with the single stable DMEM media (section 2.4.1.4) and maintain the cells until they were 60-70% confluent. Using PEI protocol (section 2.4.2.1), cells were transfected with 5 µg of the second cDNA. After 24 hours of transfection, the medium was changed for fresh DMEM. After 48 hours, cells were split into 10-cm dishes at various densities below 20%. Following day, the media was replaced with selection media containing G418 (1 mg/mL). Cells began to die off. In every 2-3 days, media was changed for fresh double stable media. The process continued until visible foci appeared. Individual clones were identified and expanded. The second cDNA was not integrated at a defined site, and as such, individual clones were selected and analysed for appropriate levels of expression (section 3).

2.4.2.4 Generation of cell lines for constitutive expression

HEK293 parental cells and CRISPR/Cas9 genome-edited HEK293 cells lacking $G\alpha_q/G\alpha_{11}$ or β -arrestin1/2 proteins (Alvarez-Curto et al., 2016b) were used for constitutive expression of either hFFA1-mVenus-HA or FLAG-hFFA4-mVenus. Cells were cultured in DMEM supplemented with 10% (v/v) FBS, L-glutamine (0.292 mg/mL), penicillin (100 units/mL) and streptomycin (100 µg/mL). Cells were seeded into 10-cm dishes and were grown until 65% confluent. Using PEI protocol

(section 2.4.2.1), cells were transfected with 5 µg of pcDNA3/GOI. 24 hours following transfection, the media was replaced by fresh media. 48 hours post-transfection, cells were splitted into 10-cm dishes at densities lower than 25%. 72 hours after transfection, selection was begun by changing the media containing G418 (1 mg/mL). In every 2-3 days, media was changed for fresh double stable media. Cells began to die off. The process continued until visible foci appeared. Individual clones were identified and expanded. As in this transfection, the cDNA was not integrated at a defined site. So individual clones were selected and analysed for appropriate levels of expression (section 3).

2.5 Biochemical and biophysical assays

2.5.1 Preparation of cell lysates

Cell lysates were obtained by harvesting the cells with ice-cold radioimmuno-precipitation assay (RIPA) buffer (section 2.1.4.4). The cell pellet was disrupted as above and placed on a rotating wheel for 1 hour at 4 °C. Cell extracts were then centrifuged for 30 minutes at 14 000× g. The supernatant was transferred to a fresh tube and the protein concentration of the supernatant was determined (section 2.5.3).

2.5.2 Preparation of cell membranes and cytosolic fractions

Cells treated with or without doxycycline, were harvested after 24 h, in ice-cold 1X PBS (section 2.1.4.1) and centrifuged at 4000x g for 10 minutes at 4 °C. Cell pellets were collected and frozen at -80 °C for a minimum of 1 hour. Pellets were thawed and re-suspended in ice-cold TE buffer (section 2.1.4.6) supplemented with Complete™ protease inhibitor mixture (Roche Diagnostics). Cells were homogenized using 50 strokes of a glass on Teflon homogenizer and passed through a 25-gauge needle (5-10 times). Samples were then centrifuged at 1000x g for 10 min at 4 °C to remove unbroken cells and nuclei. The supernatant fraction was removed and transferred to ultracentrifuge tubes and subjected to centrifugation at 50,000x g for 30 minutes at 4 °C. The supernatant was collected as the cytoplasmic fraction of the cells. The pellet was the membrane fraction and was re-suspended in TE buffer. Protein concentration was assessed (section 2.5.3) and all samples were stored at -80 °C until required.

2.5.3 Estimation of protein concentration by BCA method

The bicinchoninic acid (BCA) method was employed to estimate protein concentrations in cell lysates, cytosolic and membrane preparations. This assay utilises BCA and copper sulphate solutions, in which proteins reduce the Cu(II) ions to Cu(I) ions in a concentration dependent manner and the reduced Cu(I) can be bound by BCA. When BCA binds Cu(I) a colour change from green to purple occurs which has an absorption maximum of 562 nm. First, bovine serum albumin standards of known concentrations (0-2 mg/ml) were prepared with TE buffer. Both standards and samples were added to a clear 96-well ELISA plate in triplicate (10 µl/well). BCA reagent in a 50:1 ratio with copper sulphate was mixed and immediately added (200 µl) using an Eppendorf Repeater® manual handheld dispenser to each sample. The test plate was covered using a disposable plate seal and incubated at 37 °C for 10 minutes. Absorbance values generated at 562 nm for each BCA standard were determined using a POLARstar Omega microplate reader (BMG Labtech, Germany) and used to plot a standard curve. By linear regression analysis the protein concentration of each test sample was calculated.

2.5.4 SDS-PAGE

Sodium dodecyl sulphate (SDS) polyacrylamide gel electrophoresis (PAGE) is a very common method for separating proteins by electrophoresis which uses a discontinuous polyacrylamide gel as a support medium and sodium dodecyl sulphate to denature the proteins. Polyacrylamide gels restrain larger molecules from migrating as fast as smaller molecules. Using the property of electrophoretic mobility, samples of protein mixture were separated by SDS-PAGE and used in conjunction with Western blotting to identify and resolve protein of interest. NuPAGE® Novex® 4-12% Bis-Tris gels was inserted into an XCell SureLock™ mini-cell electrophoresis gel tank system. NuPAGE® Novex® SDS running buffer (20X) was diluted in distilled water to 1X and poured into the gel tank. For denaturation, proteins samples were diluted with Laemmli buffer (2X) to a final 1X concentration. To allow estimation of protein size, a standard protein marker was added to the first well, followed by each sample to be analysed. Chameleon® protein ladder (LI-COR® Biosciences Ltd., Cambridge, UK) was used LI-COR® based analysis and Rainbow™ marker (GE Healthcare, UK) was

used for chemiluminescence method. If there was any empty well, 1X Laemmli buffer was used for filling up the well. MOPS buffer was added to top-up the buffer core and the gel tank lid was replaced. An electrophoresis current at 175 volts DC was applied until the dye front reached the foot of the gel.

2.5.5 Western blot

Following separation of cellular proteins using SDS-PAGE, samples were transferred from the Bis-Tris gel to a nitrocellulose blotting membrane using an XCell II™ Blot module. The nitrocellulose membrane and sponges were soaked in 1X transfer buffer (section 2.1.4.5) and the cassette was locked in place filled with 1X transfer buffer. A fixed voltage of 35 volts was applied for 1 hour to allow protein transfer into the nitrocellulose membrane. After the blotting, the membrane was blocked with 5% fat-free milk in PBS-T buffer (PBS containing 0.1% Tween 20) or with LI-COR® PBS blocking buffer (LI-COR Biosciences) at room temperature on a rotating shaker for 1 hour. Primary antibody/antiserum diluted with PBST was added to the membrane and incubated overnight at 4 °C on a benchtop shaker. After incubation, membrane was washed four times for 5 minutes in PBST under gentle agitation at room temperature. The secondary antibody was diluted with PBST and added to the membrane. The membrane was placed on a shaking incubator at room temperature for 1 hour. Based on the detection technique to be used, secondary antibody was chosen. For using chemiluminescence Western blot detection, the secondary antibody was conjugated with horseradish peroxidase (HRP) enzyme. For fluorescence detection method in LI-COR®, IRDye® secondary antibody (LI-COR Biosciences) was used. After completion of incubation with secondary antibody, the membrane was washed four times for 5 minutes using PBST under gentle agitation at room temperature.

For the use of chemiluminescence detection of Western blot, the membrane was placed on Saran wrap to which a working solution of Enhanced Chemiluminescent (ECL) HRP substrate was added by mixing a 1:1 ratio of Enhanced Luminol Reagent and Oxidising Reagent, components of the SuperSignal™ West Pico Chemiluminescent Substrate kit (Thermo Fisher Scientific). Luminol was oxidised by the HRP-conjugated secondary antibody and thus light was emitted which was proportional to the amount of protein bound to

the nitrocellulose membrane. Using the SuperSignal™ kit, this signal was stable for 6-8 hours. Once the membrane was coated for approximately 5 minutes, excess ECL reagent was removed and the membrane placed within a plastic coating inside a developing cassette. All air pockets were smoothed out and the plastic coating taped in place. Once inside a dark room, under red light, a sheet of Carestream® KODAK® BioMax® Light film was placed inside the developing cassette, removed after the desired exposure time and processed through a KODAK® X-OMAT® Film developer.

For fluorescence detection method in LI-COR®, membrane incubated with a IRDye® secondary antibody was air-dried and scanned using an LI-COR® Odyssey CLx Imager with Image Studio™ software of Odyssey® Fc Dual-Mode Imaging System. The membrane was placed on the Odyssey® Fc imaging tray and inserted in the imaging drawer. The desired channel(s) (600, 700, 800) indicating the channel(s) for image acquisition were selected. The integration time for each of the selected channels was setup. For typical acquisitions, the exposure time was set to the default value of 2 minutes. Finally the image was acquired. After acquiring an image, the best display was determined from the Choose Display dialog window. The adjust display dialog was open which further allowed adjustments as needed. The best display was selected.

2.5.6 Quantification of Western blot

Quantitative analysis of specific bands was performed with the use of Image Studio Lite v5.2 (LI-COR, Cambridge, UK) or ImageJ/Fiji software previously described by Schindelin et al. (2012). In LI-COR® method, for analysis of one channel, other channel was deselected. Rectangle shape was selected from the 'Add Rectangle' to add a rectangle to the image. Alternatively, shape was drawn for manual selection of the blot. The shape could be moved with cursor for proper positioning of the shape to be quantified. To move the shape, drag the four-pointed cursor within the selection shape. For background subtraction, a median value of pixels in the background segment was selected. The border width was set to 3 in the background dialog. Clicking the shapes tab found above the table and then clicking the report button showed the signal value which is the quantification of densitometry of the Western blot.

2.5.7 Visualisation of receptor expression by epifluorescence microscopy

Epifluorescence microscopy uses fluorescence to generate an image. If cells are illuminated with a specific wavelength of light, a fluorophore-tagged protein absorbs that light with the emission of a longer wavelength light creating an image of a different colour than the absorbed light. Fluorescent images were acquired using a Nikon TE2000-E inverted microscope (Nikon Instruments, Melville, NY) equipped with a 40x (numerical aperture-1.3) oil immersion Plan Fluor lens and a cooled digital CoolSNAPHQ charge-coupled device camera (Photometrics, Tucson AZ, USA). In this arrangement, both the illuminated and emitted light travelled through the same objective lens and hence referred to as epifluorescence microscopy. This microscopy was used to characterise the expression of fluorescence-tagged hFFA1 or hFFA4 (section 3). mVenus or eYFP was excited using an argon laser at 488 nm and detected with a band-pass filter at 505 to 530 nm. For GFP2 detection, excitation was done by a laser line of 405 nm and emission was detected at 490-510 nm.

Glass coverslips (22 mm) were sterilised in 100% ethanol and air-dried under sterile conditions in a category II laminar flow cabinet. Each coverslip was placed in a 6-well plate and coated with poly-*D*-lysine hydrobromide (1 mg/mL) and air-dried. Cells were added to the centre of each coverslip and were grown in a humidified cell culture incubator for few hours at 37 °C with 5% CO₂. To induce receptor expression, media was replaced with doxycycline-added media and incubated for 18-24 hours. During the day of the experiment, cells on the coverslips were washed with pre-warmed (37 °C) HBSS (supplemented with 10 mM glucose). The coverslips were then placed into a microscope chamber containing HBSS buffer. Using MetaMorph and MetaFluor imaging software (Universal Imaging Corporation, Downing, PA, USA) images were collected and processed.

2.5.8 Visualisation of receptor internalisation by confocal microscopy

Confocal microscopy is a fluorescence microscopy where better resolution of the fluorescent image can be obtained by optical sectioning. This microscopy enables the reconstruction of three-dimensional structures from sets of images

obtained at different depths within a thick object. It is an optical imaging technique for increasing optical resolution and contrast of a micrograph by means of adding a spatial pinhole placed at the confocal plane of the lens to eliminate out-of-focus light. A Zeiss VivaTome spinning disk confocal microscopy system (Carl Zeiss GmbH, Oberkochen, Germany) was used to investigate mVenus-tagged receptors. This microscope was equipped with a 63x oil-immersion Plan Fluor Apochromat objective lens with a numerical aperture of 1.4. A pinhole of 20 and an electronic zoom of 1 or 2.5 were used. mVenus was excited using an argon laser at 488 nm and detected with a band-pass filter at 505 to 530 nm.

Cells expressing recombinant receptors were plated onto sterile poly-D-lysine coated coverslips (30 mm) and allowed to attach overnight. For inducible expression, cells were treated with doxycycline and incubated for 18-24 hours for receptor expression. On the day of the experiment, cells were washed with pre-warmed (37 °C) HBSS (supplemented with 10 mM glucose). The coverslips were then placed into the microscope chamber containing known volume of HBSS. Vehicle treated cells were imaged first. Ligands were added in the microscope chamber in a volume that the final concentration remained 1X. Images were taken after addition of ligand and every specified time after ligand addition for a total 45 or 60 minutes. The images were manipulated using MetaMorph® imaging software.

2.5.9 FRET microscopy to investigate receptor oligomerisation

Receptor oligomerisation was detected using confocal intermolecular FRET microscopy performed on a Zeiss 880 laser scanning microscope equipped with the laser lines 405 nm & 514 nm and two spectral PMT detectors set to collect light emitted between 490-510 nm, (PMT spectral detector 1), or 520-540 nm, (PMT spectral detector 2). A Zeiss 63x, Plan Apochromat oil immersion objective lens (NA =1.4) was used to illuminate and excite the fluorophore tags and 512 x 512 images were recorded in 16 bit format using a fast scan speed. Gain on each detector was set to 800 volts and the pinhole was set to 1 airy unit.

Cells expressing recombinant receptors were plated onto sterile poly-D-lysine coated coverslips (30 mm) and allowed to attach overnight. For inducible

expression, cells were treated with doxycycline and incubated for 18-24 hours for receptor expression. On the day of the experiment, cells were washed with pre-warmed (37 °C) HBSS (supplemented with 10 mM glucose). The coverslips were then placed into the microscope chamber containing known volume of HBSS. The coverslips were then placed into the microscope chamber containing known volume of HBSS. Excitation light was generated from the 405 nm and 514 nm for the sequential excitation of the mVenus- and GFP2-tagged constructs respectively. The acceptor channel image was sequentially acquired first before simultaneous acquisition of the donor and FRET channel images. The filter sets were the following: mVenus (excitation, 514 nm; emission, 518/29 nm); GFP2 (excitation, 405 nm; emission, 486/507 nm); and FRET (excitation, 405 nm; emission, 518/529 nm). The basis of FRET microscopy have been described in Figure 2-8.

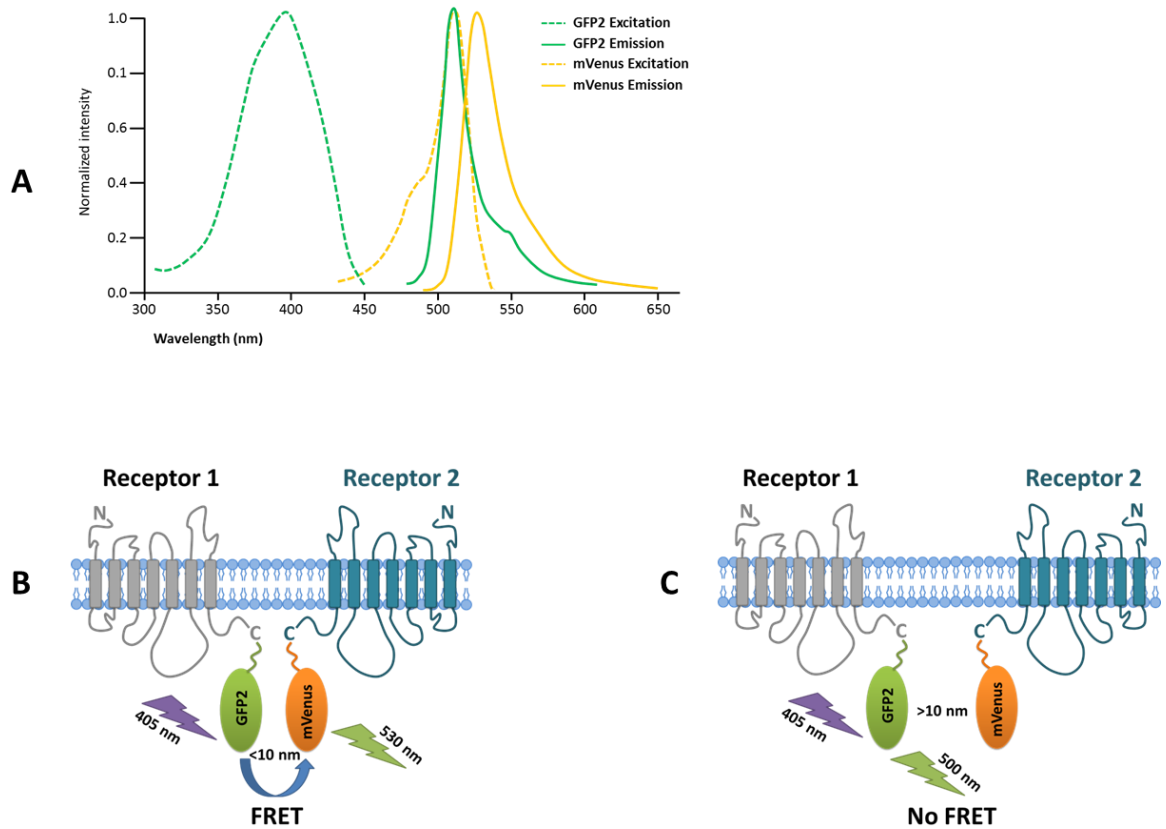


Figure 2-8. Basis of FRET microscopy. (A) Normalized spectra of the excitation (dashed line) and the emission (solid line) of GFP2 (green) and mVenus (yellow) fluorophores. GFP2 emission has perfect overlap with mVenus excitation which makes them best FRET pairs. (B) Basis of FRET. If GFP2 and mVenus-tagged receptors are in close proximity (<10 nm), excitation of GFP2 with 405 nm light causes emission at 500 nm which in turn can excite nearby mVenus with emission at 530 nm light. (C) No FRET occurs when GFP2 and mVenus-tagged receptors are far apart (>10 nm). Excitation of GFP2 with 405 nm light causes emission only at 500 nm without exciting mVenus.

2.5.10 Analysis of FRET images

Saved acceptor and donor/FRET channel images were background-subtracted by drawing a ROI on the image where no cell fluorescence was detected and running an image J background fluorescent intensity macro to remove the mean fluorescence intensity quantified within the defined background ROI from the channel image. Each background-subtracted channel image was then corrected for potential sources of acceptor or donor cross contamination bleedthrough, (e.g. proportion of donor or acceptor contamination signal crossing over into the FRET channel, proportion of donor or acceptor contamination signal spilling over into the acceptor and donor channel, respectively). The degree of spillover was quantified by preparing control cell lines which only expressed receptors tagged with the donor or acceptor fluorescent protein. Spillover contamination free corrected FRET images were created using Youvan's fully specified bleed through algorithm (Youvan et al., 1997) as follows:

$$\begin{aligned} \text{Net corrected FRET image} = & \text{raw FRET image} \\ & - (\text{acceptor image} - (B_{DA} \times \text{donor image})) \times (B_{AF}) \\ & - (\text{donor image} - (B_{AD} \times \text{acceptor image})) \times (B_{DF}) \end{aligned}$$

where B_{DA} and B_{AD} represent the proportion of donor or acceptor bleed through into the acceptor and donor channel, respectively. B_{AF} and B_{DF} represent the amount of acceptor and donor contamination in the raw FRET signal channel. All bleed through coefficients were calculated from control cells expressing receptors tagged with GFP2 or mVenus alone.

Net corrected FRET values were ratiometrically normalized to the amount of donor and acceptor fluorophore expressed to generate a final ratiometric value (RFRET) using following equation:

$$\text{RFRET} = \frac{\text{raw FRET}}{(\text{acceptor} - (B_{DA} \times \text{donor})) \times (B_{AF}) + (\text{donor} - (B_{AD} \times \text{acceptor})) \times (B_{DF})}$$

Knowing the expected bleed through of the donor and acceptor into the FRET channel, therefore in the absence of energy transfer, RFRET, will have a predicted value of 1. Values greater than 1 reflect the occurrence of FRET

(Alvarez-Curto et al., 2010). Quantified RFRET values provided markedly better data quality compared with other ratiometric FRET metric algorithms.

2.5.11 Imaging studies to investigate cell localisation

Cell localisation studies were performed in cells co-expressing GFP2 and mVenus-tagged receptors. Cells were grown on poly-D-lysine coated coverslips (22 nm) and expression of receptors was induced by doxycycline for 18-24 hours. Images were taken using epifluorescence microscopy (section 2.5.7).

MetaMorph® imaging software was used for image analysis. A region of no fluorescence adjacent to the cell was used to determine the background level of fluorescence in the GFP2 and mVenus channels. The background amount was then subtracted from each pixel in each channel. Pearson's correlation coefficients were measured by comparing the amounts of fluorescence measured in each matched pixel of the two different channels using the Metamorph "correlation plot" application. The degree of co-localisation was quantified by plotting the amount of background-subtracted mVenus from the pixels against the amount of background GFP2 fluorescence in the corresponding pixels of the mVenus image. Correlation coefficients were quantified that described the degree by which GFP2 and mVenus fluorescence at each pixel within the region varied from a perfect correlation of 1.00.

2.5.12 ArrayScan™ to quantify receptor internalisation

Using the automated cell-based imaging and analysis system ArrayScan™ High Content Screening (Cellomics, Pittsburgh, PA), the pharmacology of receptor internalisation was examined by monitoring the accumulation of fluorophore-tagged receptors within centralized intracellular locations (Conway et al., 1999; Giuliano et al., 1997). The ArrayScan™ is an ideal screening format consisting of a high resolution imaging system capable of quantitatively monitoring small changes in cellular localisation of molecule of interest. This system includes optics that permit subcellular resolution of fluorescence signals from many cells in a field within a well of a microplate. In addition, the system contains microtiter plate scanning hardware, fluorescence excitation, and emission optics, a solid-state camera, a computer with powerful processing, analyses, and database management capabilities. The ArrayScan™ System automatically scans

a microplate acquiring multicolour fluorescence image datasets of fields of cells at a pre-selected spatial resolution. Data can be presented on a cell-by-cell basis, as averages of wells or simply as 'spot' reports. An algorithm has been adopted with the system (Figure 2-9). The algorithm detects and quantifies the formation of receptor-fluorophore aggregates within the intracellular compartment. The algorithm collects information about these spots including size, area, intensity, and number.

Under sterile conditions, black with clear bottom 96-well plates were coated with poly-D-lysine. 40 µl mixture of poly-D-lysine and DMEM (1: 20 dilution) was added in each well. Flp-In™ T-REx™ 293 cells were seeded at a density of 70,000 cells/well in DMEM (100 µl/well). The plate was incubated few hours in a humidified atmosphere at 37 °C with 5% CO₂, to allow cells to adhere sufficiently. For inducible cell lines, doxycycline was prepared as 10x with the complete media and was added in each well (15 µl/well) and incubated for 18-24 hours for receptor expression. During the day of the experiment, media was completely aspirated and washed twice with pre-warmed HBSS (supplemented with 10 mM glucose) and finally addition of 90 µl HBSS per well. The plate was incubated for 30 minutes in the incubator before addition of ligands. Ligands were prepared as 10x concentrations with HBSS and were added to the plate at 10 µl per well using a multichannel pipette. The plate was then incubated at 37°C in the cell culture incubator for the time of interest (usually 45 minutes). After ligand treatment, media was completely aspirated and cells were fixed with 4% paraformaldehyde in 1X PBS (50 µl/well) and subsequently incubated for 1 hour at room temperature. Paraformaldehyde was removed by aspiration and cells were washed 3 times with 100 µl 1X PBS. Plates were then used for further experiment or were wrapped in Saran wrap and store at 4 °C for next day experiment.

The fixed cells were incubated with Hoechst 33342 trihydrochloride nuclear stain, diluted to 500 nM in 1X PBS (100 µl/well) and incubated for 30 minutes at room temperature protected from light. Hoechst 33342 was removed by aspiration and cells were washed 3 times with 100 µl 1X PBS before assessment of receptor internalisation using the ArrayScan™ High Content Analyser. Cell nuclei identified by Hoechst staining were detected as a surrogate measure of cell number, while fluorescence intensity measured as internalised receptors.

Using an internalisation vesicle inclusion form factor of 1.0 and a TopHat transformed algorithm to remove background interference, four images/well were taken simultaneously. Images were then normalized to cell number to obtain a quantitative measure of receptor internalisation.

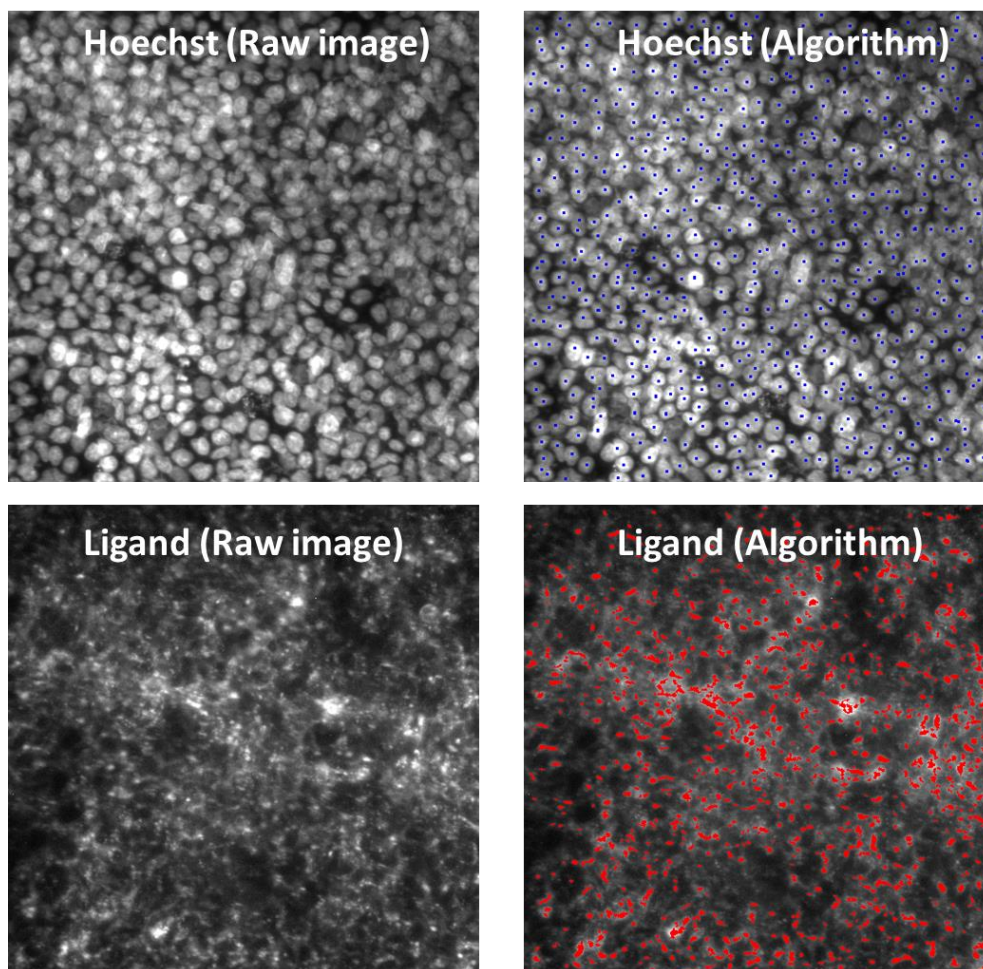


Figure 2-9. High content screen of ligand induced receptor internalisation by ArrayScan™ II High Content Analyser. The system automatically scans a microplate acquiring multicolour fluorescence image datasets of fields of cells at a pre-selected spatial resolution. Hoechst 33342 fluorescence quantifies nuclei (upper panel) and ligand induced receptor internalisation are identified by algorithm adopted with the system. The algorithm detects and quantifies the formation of receptor-fluorophore aggregates within the intracellular compartment. The algorithm collects information about these spots including size, area, intensity, and number. Images can be normalized to cell number to obtain a quantitative measure of receptor internalisation.

2.5.13 BRET based recruitment of β -arrestin2

Bioluminescence resonance energy transfer (BRET) allows monitoring of protein-protein interactions in real time in living cells. This technology is based on the principle of non-radiative energy transfer occurring between the electromagnetic dipoles of a luminescent energy donor (e.g. *Renilla luciferase*) and a fluorescent energy acceptor (e.g. eYFP) (Milligan, 2004). Given close proximity occurring between these polypeptides and oxidation of the luciferase substrate coelenterazine h, energy is emitted and is transferred from donor to acceptor and subsequently re-emitted at a characteristic wavelength, which can be quantified as BRET signal (Figure 2-10). BRET does not occur if the two proteins are separated by more than 10 nm, making the technique ideal for monitoring protein-protein interactions in biological systems.

BRET¹ method (Hamdan et al., 2005) was employed for ligand screening and desensitisation studies in hFFA1 and hFFA4. The β -arrestin2 protein was fused to luminescent energy donor, such as *Renilla luciferase* and the receptor to a fluorescent energy acceptor, such eYFP or mVenus and the two were then co-expressed in the same cells. A Flp-InTM T-RExTM 293 cells constitutively expressing β -arrestin2-Rluc and inducibly expressing hFFA4-eYFP were used for FFA4 ligand screening (section 4). However, transient transfection (Hudson et al., 2014) was employed for hFFA1 ligand screening. HEK293T cells were seeded into 10-cm dishes and were grown until 70% confluent. Transfections were carried out with polyethyleneimine (section 2.4.2.1) using a previously described protocol (Hudson et al., 2014). Briefly, HEK293T cells were co-transfected with mVenus-tagged receptor and β -arrestin2-Rluc plasmids in a ratio of 4:1. An additional transfection was performed with only the *Renilla luciferase* construct and empty expression vector. 24 hours post-transfection, cells (70,000/well) were subcultured into poly-D-lysine-coated white 96-well opaque plates and maintained for a further 24 hours prior to the experiment. To conduct the experiments, cells were first washed and then incubated at 37 °C for 30 min in HBSS. The Rluc substrate coelenterazine h was added to a final concentration of 2.5 μ M before a further incubation in dark for 10 min at 37 °C. Test compounds were then added at the specified concentration, and cells were incubated for a final 5-min period prior to measuring luminescent emission at 535 and 475 nm using a PHERAstar FS plate reader (BMG-Labtech, Germany) fitted with a BRET¹

optic module. Net BRET was defined as the 535 nm/475 nm ratio of cells co-expressing Renilla luciferase and mVenus minus the BRET ratio of cells expressing only the Renilla luciferase construct in the same experiment. This value was multiplied by 1000 to obtain mBRET units.

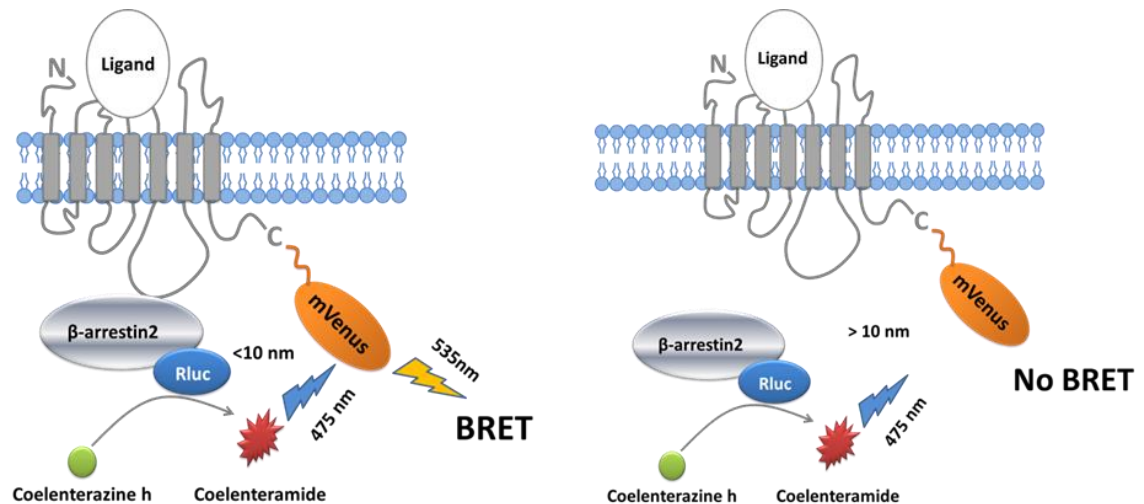


Figure 2-10. BRET based recruitment of β -arrestin2. The BRET is based on the principle of non-radiative energy transfer occurring between a luminescent energy donor (e.g. *Renilla* luciferase) and a fluorescent energy acceptor (e.g. mVenus). If ligand addition causes recruitment of β -arrestin2 to the receptor, oxidation of the luciferase substrate coelenterazine h causes energy emission at 475 nm which can be transferred from donor to acceptor with a re-emission of 535 nm light. This is the BRET signal. If ligand activation cannot recruit β -arrestin2 or there is a distance >10 nm between them, no energy will be transferred to the fluorophore and there will be no BRET.

2.5.14 BRET saturation experiments to detect receptor oligomerisation

BRET saturation is a popular approach to study receptor oligomerisation (Ward and Milligan, 2014; Alvarez-Curto et al., 2010; Ayoub and Pflieger, 2010; Milligan and Bouvier, 2005). In this study I have used a new version of the traditional BRET assay using a small (19 kDa) monomeric luciferase derived from deep-sea shrimp (Nanoluciferase or Nluc) as a donor and the well-characterized monomeric fluorescent protein mVenus as an acceptor (Mo and Fu, 2016). It is hypothesised that mVenus- and Nluc-tagged receptors might allow BRET upon addition of a luciferase-substrate if interactions between the partner proteins bring the luciferase and the mVenus into proximity. If Nluc and Venus-tagged receptor are in close proximity (<10 nm), oxidation of luciferase-substrate

coelenterazine h can emit light at 475 nm which can excite the nearby Venus-tagged receptor with subsequent emission 535 nm light (Figure 2-11) using the PHERAstar FS plate reader (BMG-Labtech, Germany). By varying the ratio of energy acceptor (i.e. mVenus) and energy donor (i.e. Nluc), BRET saturation curves (Figure 2-11, B) can be generated in which half-maximal signal provides a measure of the relative affinity of receptor interactions (Milligan and Bouvier, 2005).

HEK293T cells were seeded into 6-well plates and were grown until 70% confluent. Transfections were carried out with polyethyleneimine (section 2.4.2.1). In this experiment, cells were transfected with constant amount of Nluc-tagged receptor (donor), and increasing amount of mVenus-tagged receptor (acceptor). To maintain equal transfection efficacy, total transfected plasmid amount was kept constant, with the addition of a non-coding plasmid. The measured BRET ratio was plotted as a function of acceptor/donor expression ratio. In this plotting, specific interactions resulted in a saturation curve, while non-specific interactions lead to a linear relationship (Figure 2-11, B). The BRET₅₀ value (half-maximal BRET value) was used to determine the presence of dimerisation. Pairs with low BRET₅₀ value thought to form oligomers, while high BRET₅₀ values indicated weak interaction or the absence of interaction between the investigated receptors (bystander plot, Figure 2-11).

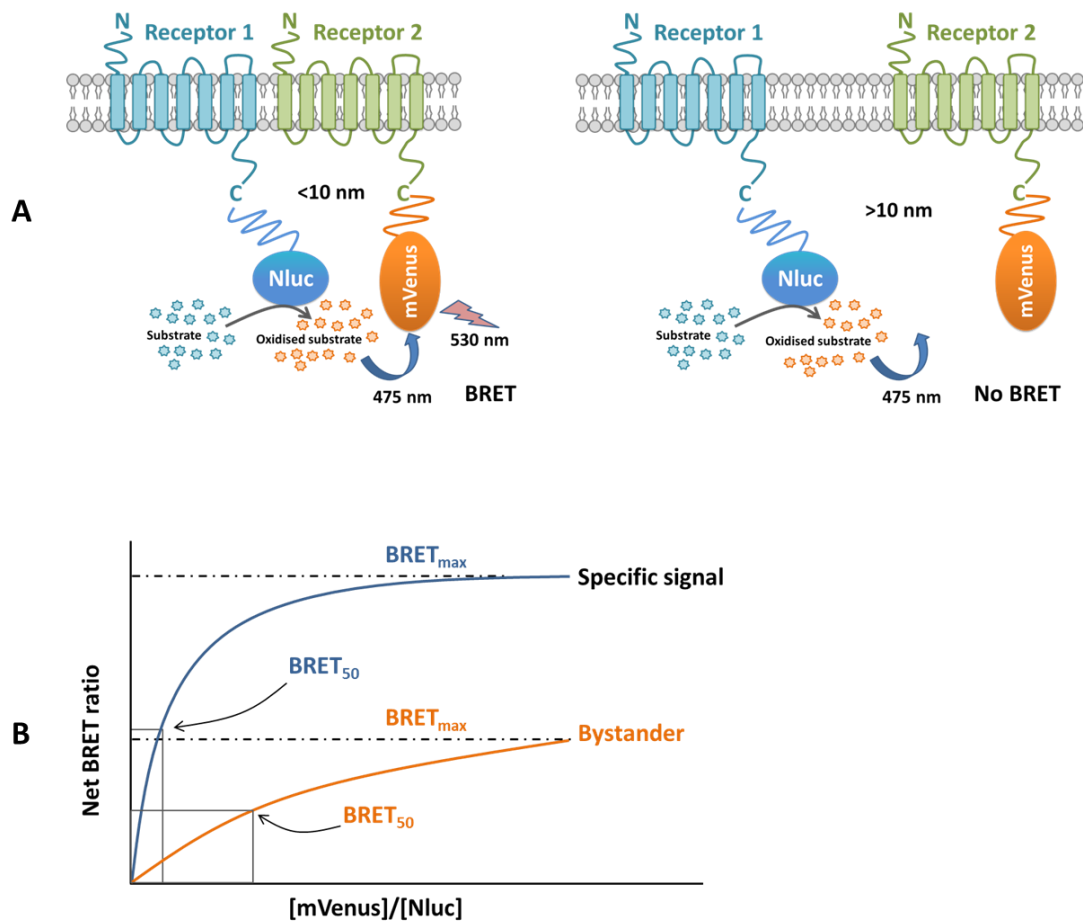


Figure 2-11. BRET saturation for detection of receptor oligomerisation. The basis of BRET saturation experiments BRET signals are plotted as a function of increasing values of acceptor-associated fluorescence over donor-associated luminescence ($mVenus/Nluc$). Curves are plotted using the equation for hyperbolic one-binding-site isotherm. The maximal BRET value ($BRET_{max}$) depends on multiple parameters such as the distance and relative orientation of donor and acceptor molecules. This value is not informative of the interaction specificity. The $BRET_{50}$, which corresponds to the $mVenus/Nluc$ value at half-maximal BRET, reflects the association propensity of the interacting partners. In experiments conducted with one donor and various acceptors of comparable structure and distribution (e.g. mutants of the same protein), $BRET_{50}$ values might reflect differences in the relative affinity of the two partners. Bystander BRET results in a pseudolinear curve that might saturate at sufficiently high $mVenus/Nluc$ values.

2.5.15 Myo-Inositol 1 Phosphate accumulation assay

Levels of myo-Inositol 1 phosphate (IP1) in lysates of cultured cell are measured using an Homogeneous, Time-Resolved-Fluorescence (HTRF) assay kit from Cisbio (Cisbio Bioassays, Codolet, France). IP1 is a metabolite in the $G\alpha_q/PLC/IP_3/[Ca^{2+}]_i/PKC$ signalling cascade (Alvarez-Curto et al., 2016b) and is stable in the presence of LiCl (present in the kit lysate buffer). Measured levels of IP1 thus reflect the activation status of this pathway. The Cisbio IP-One Tb assay is based on a FRET response between a labelled (d2) IP1 analog and a labelled (Lumi4TM-Tb-cryptate) monoclonal antibody specific for IP1. The unlabelled IP1 in the lysate inhibits this response by competing for the antibody binding site (Figure 2-12). The ratio of the fluorescence signals (665 nm/620 nm) from the acceptor (d2) and donor (Lumi4TM-Tb-cryptate) moieties provides the signal readout. Use of a fluorescence ratio minimizes possible photophysical interference from buffer conditions and coloured compounds.

IP1 assays (Cisbio Bioassays) were performed according to the manufacturer's instructions. Cells were seeded into 10-cm dishes and were grown until 80% confluent. By the use of versene-EDTA solution cells were splitted in DMEM media. Cell numbers were counted via the addition of trypan blue to cell suspension (1:1 ratio) using a plastic chamber and a CountessTM automated cell counter (Life Technologies Ltd.). Cell suspension was centrifuged at 1200x g, 3 minutes at room temperature to collect cell pellets. Cell pellets were re-suspended in 1 mL sterile PBS (1X) and re-centrifuged at 1200x g, 3 minutes at room temperature. Upon aspiration of supernatant, cells were re-suspended in IP-One Stimulation Buffer (1X) to make 1.07×10^6 cells/mL. Ligands were prepared with IP-One stimulation buffer. Using a 384-well OptiPlateTM (Perkin-Elmer) ligand solution was added at 7 μ L per well. A series of IP-1 standards were prepared in IP-One Stimulation Buffer and added at 14 μ L per well. This included a positive control, a negative control and a standard curve that was used to calibrate the assay. Upon addition of test compound and control, the microplate was centrifuged briefly at 800x g for 30 seconds at room temperature. This ensured settlement of compound at the bottom of each well. Cells (7 μ L/well) were added using an Eppendorf Repeater[®] manual handheld dispenser to wells containing test compound only. The plate was covered using a TopSealTM to prevent evaporation and centrifuged at 800x g, 30 seconds at room temperature.

The plate was then incubated for 2 hours at 37 °C. IP1-d2 and anti-IP1 Lumi4™-Tb cryptate were diluted (1:20 ratio) in Cell Lysis Buffer. IP1-d2 was added (3 µl per well) to all wells except the negative control wells. The anti-IP1 Lumi4™-Tb cryptate was added in the same fashion at 3 µl per well to all wells including the negative control. Plates were centrifuged at 800x g, 30 seconds at room temperature. The plate was covered with a fresh TopSeal™ and incubated for 1 hour at 37 °C. After the incubation the 665 nm and 620 nm reads were measured simultaneously using a PHERAstar FS plate reader (BMG-Labtech, Germany). IP1 accumulation (nM) was generated by calculation of the fluorescence ratio, which was calibrated by plotting a standard curve.

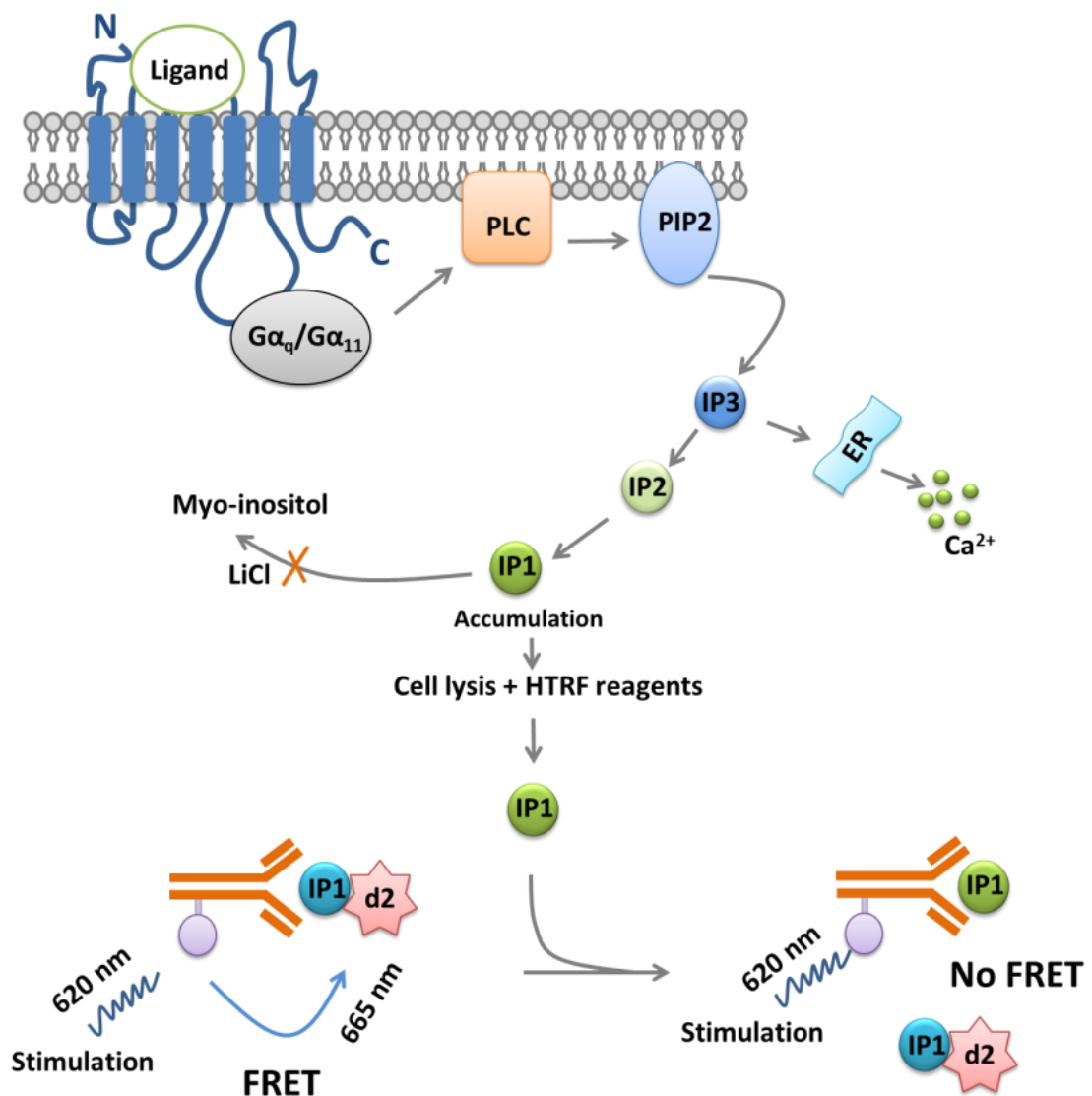


Figure 2-12. Myo-Inositol 1 phosphate (IP1) accumulation assay. Schematic diagram of IP1 accumulation assay: $G_{\alpha_q}/G_{\alpha_{11}}$ coupled GPCR activation induces IP₃ release catalysed by PLC. IP₃ promotes mobilisation of intracellular calcium. However, IP₃ degradation occurs rapidly and leads ultimately to the production of IP₁. Processing of IP₁ into myo-inositol can be prevented by the addition of LiCl. The HTRF® technology is based on a FRET response between a labelled (d2) IP₁ analog and a labelled (Lumi4™-Tb-cryptate) monoclonal antibody specific for IP₁. The unlabelled IP₁ in the lysate inhibits this response by competing for the antibody binding site. The ratio of the fluorescence signals (665 nm/620 nm) from the acceptor (d2) and donor (Lumi4™-Tb-cryptate) moieties provides the signal readout.

2.5.16 Single-cell calcium imaging

Imaging calcium signals is a powerful tool in physiology and pharmacology (Russell, 2011). By combining appropriate Ca^{2+} indicators with appropriate optical imaging techniques, cellular Ca^{2+} signals can be monitored with a high degree of spatial and temporal resolution. Cells expressing mVenus-tagged hFFA1 or hFFA4 were grown on poly-D-lysine-coated coverslips. For Flp-In™ T-REx™ HEK293 cells, these were treated with doxycycline for 18-24 hours to induce receptor expression. Cells were loaded with the Ca^{2+} -sensitive dye Fura-2 AM (1.5 μM) in DMEM growth media and incubated for 45 minutes at 37 °C. After loading of the dye, cells were washed with pre-warmed microscope buffer (section 2.1.4.7) and incubated in dark for 15 minutes at room temperature. Ligand induced mobilisation of intracellular calcium in single cell was performed as described elsewhere (Stoddart et al., 2008).

After loading of the dye, coverslips were placed into a microscope chamber containing microscope buffer solution and illuminated with an ultrahigh point intensity 75-W xenon arc lamp (Optosource, Cairn Research, Faversham, Kent, UK) and imaged using a Nikon Diaphot inverted microscope equipped with a Nikon (Tokyo, Japan) 40× oil immersion Fluor objective lens (numerical aperture = 1.3) and a monochromator (Optoscan, Cairn Research), which was used to alternate the excitation wavelength between 340/380 nm and to control the excitation band pass (340 nm band pass = 10 nm; 380 nm band pass = 8 nm). Fura-2 fluorescence emission at 510 nm was monitored using a high-resolution interline-transfer cooled digital charge-coupled device camera (Cool Snap-HQ, Roper Scientific/Photometrics, Tucson, AZ). MetaFluor® imaging software (Universal Imaging Corp., Downing, PA) was used for control of the monochromator, charge-coupled device camera, and for processing of the cell image data. Sequential images (2 × 2 binning) were collected every 2 s, and exposure to excitation light was 100 ms/image. Agonist was added after 60 seconds (after 30 images) for 60 seconds using a perfusion system.

Ratio images were presented in MetaFluor® intensity-modulated display mode, which associates the colour hue with the excitation ratio value and the intensity of each hue with the source image brightness. Briefly, background subtracted images acquired at 340 and 380 nm excitation were first used for calculating the

340/380 nm ratio of each pixel. After determination of the upper and lower thresholds, the ratio value of each pixel was associated with one of the 24 hues from blue (low $[Ca^{2+}]_i$) to red (high $[Ca^{2+}]_i$). Pooled average intensity-modulated display ratio intensity values measured from single cells were expressed as the mean \pm SEM of at least 20 cells.

2.5.17 Calcium mobilisation assay using cell populations

Mobilisation of intracellular calcium was measured by using a FlexStation™ II benchtop scanning fluorometer (Molecular Devices, Sunnyvale, CA) that can measure the change of intracellular Ca^{2+} concentration using both single-wavelength and dual-wavelength fluorescent probes. The system incorporates a fluid transfer system for addition of test compounds from a source plate to the cell plate during data acquisition. Both plates are contained within a temperature-controlled unit that can be controlled accurately between room temperature and 45 °C. Compounds are added to the cell plate one column at a time and responses are monitored for the duration of the experiment in each column. The instrument is controlled by an external personal computer running the SOFTmax® PRO software, which provides integrated instrument control, data display, and statistical data analysis

Fura-2 AM (Life Technologies), developed by Roger Tsien and collaborators (Grynkiewicz et al., 1985) has two excitation peaks at 340 nm and 380 nm with the emission at 510 nm. This calcium indicator was used to investigate the mobilisation of intracellular Ca^{2+} in mVenus/eYFP-tagged receptors (section 4). When binds to free Ca^{2+} , the excitation peak of Fura-2 shifts to shorter wavelengths, but the 510-nm emission peak does not change. The dual excitation wavelength capability of the FlexStation™ II permits ratiometric measurements of Fura-2 peak emissions after excitations at 340 and 380 nm, and changes in the 340/380 ratio reflects changes in intracellular-free Ca^{2+} concentrations. X-Rhod-1 AM (Life Technologies), a long-wavelength calcium indicator (Micu et al., 2007) was also used to investigate the ligand-promoted intracellular Ca^{2+} mobilisation (section 3). X-Rhod-1 AM has excitation/emission maxima of ~580/602 nm which allows simultaneous detection Ca^{2+} transients and green-fluorescent protein (GFP) with minimal crosstalk (Bolsover et al., 2001). For this reason, this dye was used in the case of GFP2-tagged hFFA1 or hFFA4.

Cells (70,000/well) were grown in poly-D-lysine coated clear-bottom black 96-well plates (Greiner Bio-One). For Flp-In™ T-REx™ HEK293 cells, these were treated with doxycycline for 18-24 hours to induce receptor expression. Cells were loaded with the Ca²⁺-sensitive dye Fura-2 AM (1.5 µM) or X-Rhod-1 AM (3 µM) in DMEM growth media and incubated for 45 minutes at 37 °C. After loading of the dye, cells were washed with pre-warmed (37 °C) HBSS and incubated in dark for 15 minutes at 37 °C. 2X ligand solution was made with HBSS (150 µl/well) in a 96-well ELISA plate. The plate was then read in the FlexStation™ II at 37 °C. Baseline fluorescence was measured for 16 seconds; test compounds were then added, and fluorescence was measured for an additional 74 seconds.

2.5.18 Biotinylation

Incorporation of a biotin label is an effective way to assess cell surface proteins and their subsequent trafficking in cell populations (Ward and Milligan, 2013). To quantify agonist-promoted internalisation of hFFA4, this cell surface biotin labelling technique was employed (section 5). Cell surface expression of receptors and their subsequent internalisation can be detected with the incorporation of a biotin label. This process is based upon the use of a thiol-cleavable, amine-reactive biotinylation reagent EZ-Link® Sulfo-NHS-SS-Biotin. Upon treatment of cells with this reagent the N-hydrosulphosuccinimide (NHS) group can potentially react with the lysine residues found in cell surface proteins. Biotin can bind to immobilised streptavidin to allow the isolation of labelled cell surface receptors and these interactions can be used to isolate biotinylated receptors. Treatment of the biotinylated receptors with a reducing agent such as 2-mercaptoethanol causes the release of reduced receptors which can then be analysed by SDS-PAGE and Western blotting with an appropriate antiserum. The extent of removal of receptors in response to agonists can be monitored from the band intensity in the Western blot. The process has been described schematically in the Figure 2-13.

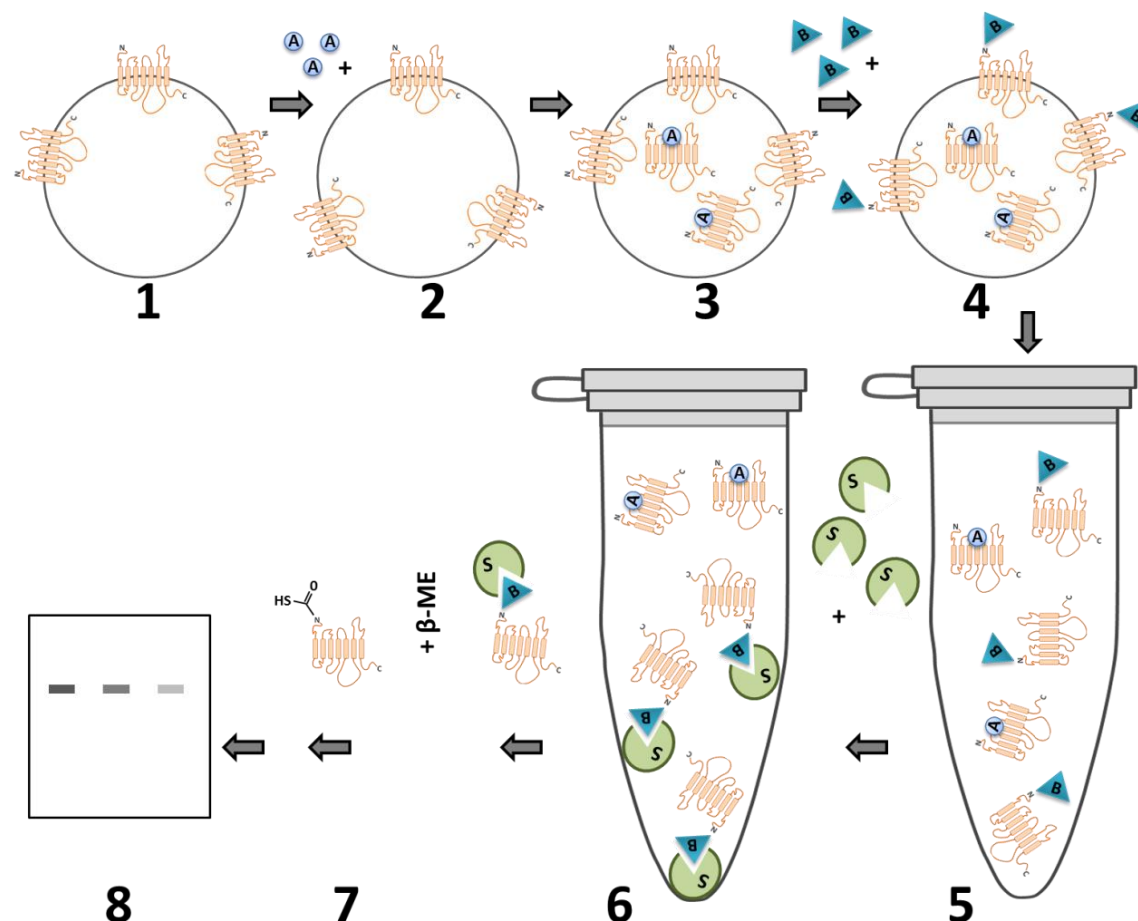


Figure 2-13. Biotinylation to investigate receptor internalisation. Schematic diagram of the steps in biotinylation process: (1) Cells expressing a receptor of interest at the cell surface, (2) Treatment of cell with agonists for the desired time period, (3) Agonist promotes internalisation of the corresponding receptors, (4) Addition of EZ-Link® Sulfo-NHS-SS-Biotin (B) cause biotinylation of the surface expressed receptors, (5) Lysis of cells makes a mixture of both biotinylated and unbound receptors, which is treated as total lysates, (6) The lysate of cells were treated with immobilised streptavidin (S) beads which upon centrifugation separates only biotinylated receptors in beads, (7) Treatment of the biotinylated-receptor-streptavidin complex with the reducing agent β -mercaptoethanol (β -ME) releases the biotinylated receptors, (8) Finally, biotinylated and reduced receptor lysates were analysed by SDS-PAGE and Western blotting.

Cells were grown in 6-well plates coated with poly-D-lysine and waited until 80% confluence. If inducible expression of receptors were needed, the corresponding Flp-In™ T-REx™ HEK293 cells were treated with doxycycline for 18-24 hours. On the day of the experiment, cells were washed with pre-warmed (37 °C) HBSS two times and incubated for 15 minutes in a humidified incubator at 37 °C. Agonist solution was prepared in HBSS. Cells were treated with agonists for different time points. The agonist effect was terminated by placing cells on ice and washing twice with 2 ml/well of ice-cold borate buffer. All subsequent procedures were performed on ice. Biotin was freshly prepared in ice-chilled

borate buffer as 0.8 mM EZ-Link Sulfo-NHS-SS Biotin. Cells were treated with this biotin solution and incubated for 15 minutes in the dark. Cells were then quenched by rinsing twice with 2 ml/well of glycine buffer and the second wash was left on ice for 5 minutes. Cells were then lysed with 1X RIPA buffer as described in the section 2.5.1. To remove insoluble material, cell lysates was centrifugation at 14000x g, 4 °C for 30 minutes. Supernatants were collected into clean 1.5 ml microcentrifuge tubes. Protein content in the soluble extracts was measured by BCA (section 2.5.3) and the concentrations were equalised for all samples. This lysates represented as the total extract. Samples were saved for Western blotting. To isolate biotinylated receptors from this lysate, ImmunoPure® (Pierce) immobilised streptavidin beads (100 µl/tube) were added. To avoid damaging the beads, the 200 µl pipette tips was cut and then used to dispense the streptavidin beads. For proper mixing with beads, samples were placed on a rotating wheel for 1 hour at 4 °C. The samples were centrifuged at 1200x g, 4 °C for 2 minutes. The supernatant was collected as the unbound proteins (cytosolic receptors). The beads were re-suspended in 1X RIPA buffer and centrifuged at 1200x g, 4 °C for 2 minutes. Supernatant was discarded. The process was repeated two times. The streptavidin beads contained only the biotinylated proteins. The biotinylated proteins were eluted from the beads with 200 µl of 2x Laemmli buffer containing 5% β-mercaptoethanol for 1 hour at 37 °C. To pellet the beads, the samples were then centrifuged at 1200x g, 4 °C for 2 minutes. The supernatant was saved for analysis by SDS-PAGE (section 2.5.4) and Western blot (2.5.5).

2.5.19 Cell surface ELISA

Cell surface enzyme-linked immunosorbent assay (ELISA) is an immunoenzymatic technique for the quantitative detection of cell-surface molecules (Gan and Patel, 2013; Lourenco and Roque-Barreira, 2010). Analysis of receptor internalisation by this method was based herein on the presence of an N-terminal epitope tag, FLAG on hFFA4 receptor, which can no longer be recognized by the cognate antibody once the receptor is internalised. So, it has been hypothesised that removal of N-terminal FLAG-epitope tag from the cell surface would define the extent of internalisation of the FLAG-hFFA4-mVenus receptor construct after exposure to agonists (Figure 2-14).

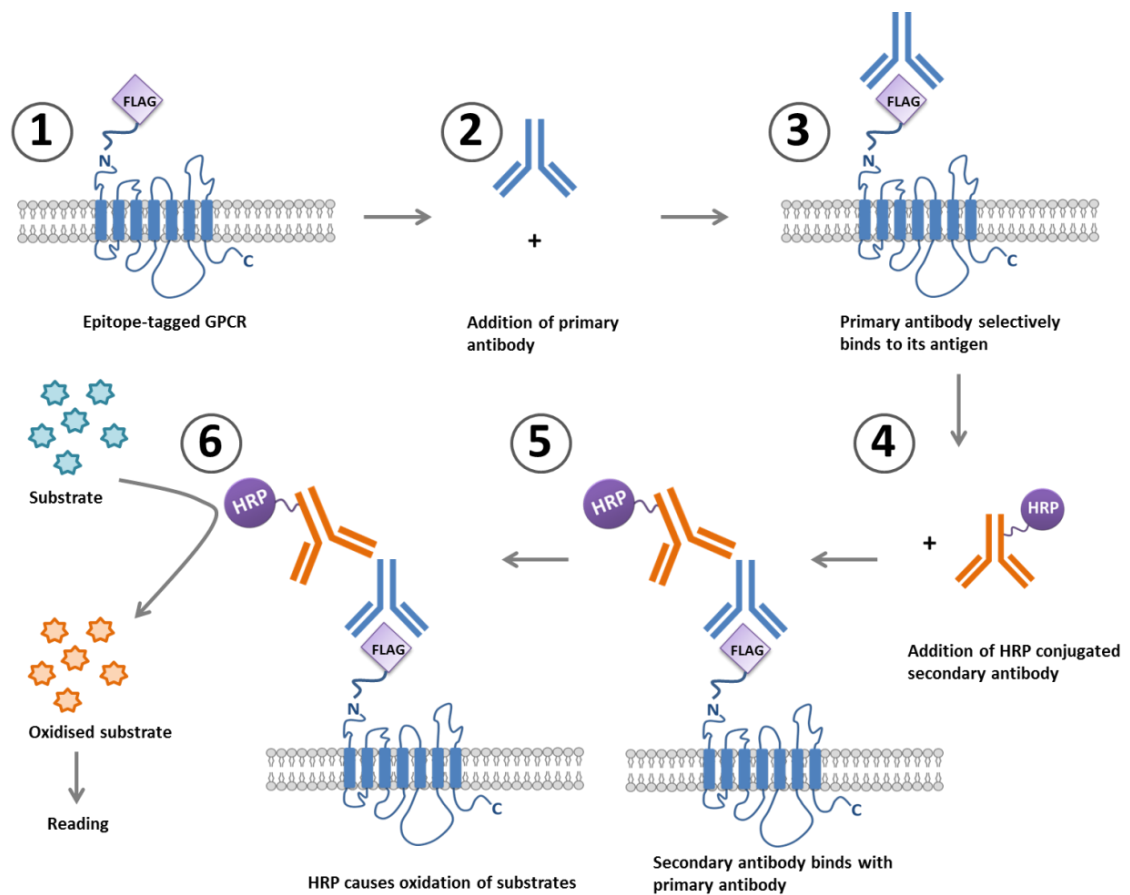


Figure 2-14. Enzyme-linked immunosorbent assay. Schematic diagram of steps in ELISA assays: (1) Cell surface expression of FLAG-tagged receptors in a heterologous cell system, (2) Cells were incubated with anti-FLAG monoclonal primary antibody, (3) Anti-FLAG antibody binds with the FLAG-epitope, (4) Addition of a horseradish peroxidase-conjugated secondary antibody, (5) Secondary antibody selectively binds with the primary antibody, (6) Upon addition 3,3',5,5'-tetramethylbenzidine, RHP oxidises the substrate and emits light 650 nm. The signal is read with PolarStar® Omega plate reader (BMG-Labtech, Germany).

Cells (70,000/well) were grown in poly-D-lysine coated flat-bottom 96-well ELISA plates (Greiner Bio-One). For Flp-In™ T-REX™ HEK293 cells, these were treated with doxycycline for 18-24 hours to induce receptor expression. On the day of the assay, medium was aspirated and replaced with 100 µl pre-warmed (37 °C) HBSS and incubated for 15 minutes in the humidified incubator. Ligands were prepared as 10X in a 96-well ELISA plate. Cells were treated with ligands for desired concentrations or desired time points. After ligand treatment, cells were washed with PBS 1X containing 5% bovine serum albumin and incubated for 30 minutes at room temperature followed by washing of cells with PBS 1X buffer. Cells were treated with anti-FLAG mouse monoclonal primary antibody prepared (1:1000 dilution) with PBS 1X buffer and incubated for 30 minutes at room

temperature. Finally anti-mouse horseradish peroxidase-conjugated secondary antibody (1:10,000 dilution) mixed with Hoechst 33342 (1:10,000 dilution) prepared with PBS was added (100 μ l/well). The plate was incubated in the dark at room temperature for 30 minutes. Cells were washed three times with PBS before measuring Hoechst fluorescence (355/460 nm) using a PolarStar® Omega plate reader (BMG-Labtech, Germany). After washing a final time with PBS and incubating with 3,3',5,5'-tetramethylbenzidine horseradish peroxidase substrate (Thermo Fisher) in the dark at room temperature, the absorbance at 620 nm was measured on a PolarStar Omega plate reader. To calculate surface expression, the 620-nm absorbance was corrected for cell number based on Hoechst fluorescence.

2.5.20 Fluorescence intensity

Fluorescence intensity of mVenus or GFP2 expression was frequently measured during characterisation of cell lines as well as in various experiments. Cells (70,000/well) were grown in poly-D-lysine coated clear-bottom black 96-well plates (Greiner Bio-One). For Flp-In™ T-REx™ HEK293 cells, these were treated with doxycycline for 18-24 hours to induce receptor expression. For the measurement of mVenus expression, PHERAstar® FS microplate reader (BMG LABTECH GmbH, Ortenberg, Germany) was used applying 485 nm excitation and 520 nm emission protocol. For GFP2 expression only, I used CLARIOstar® microplate reader (BMG LABTECH GmbH, Ortenberg, Germany) applying 415-20 nm excitation and 510-20 nm of emission protocol. For the measure of dual expression, i.e. mVenus and GFP2, the protocol was setup as: mVenus (497-15/540-20 nm) and GFP2 (405-20/510-20). In all experiments gain adjustment was done using the well with highest expression (wells treated with highest concentration of doxycycline).

2.5.21 Data Analysis

All data analysis and curve fitting were carried out using the GraphPad Prism software package (GraphPad Software Inc. San Diego, CA).

2.5.21.1 Analysis of agonist functional data

A series of eight-point agonist concentration responses were fit to the (agonist) versus response (variable slope) three parameter nonlinear regression analysis in GraphPad Prism. The last point was a vehicle-only control and was plotted one log unit lower than the lowest concentration of test ligand assessed. The three-parameter curve fit assumed that the concentration response had a standard slope, equal to a Hill slope of 1.0, with a formula:

$$Response = Bottom \frac{(Top - Bottom)}{1 + 10^{LogEC_{50} - X}}$$

In which Top is the maximum asymptote of the curve, or the E_{max}; Bottom is the vehicle only control response; LogEC₅₀ is the negative logarithm of the agonist's EC₅₀ (the concentration of ligand that generates the half maximum response); X is the agonist concentration.

The pEC₅₀ values were obtained individually for each experiment and pEC₅₀ from each experiment were then used to calculate the mean ± standard error of the mean (SEM). This gave a grouped pEC₅₀ ± SEM value for each ligand's response.

2.5.21.2 Analysis of functional antagonist competition experiments

To determine antagonist activity, agonist responses were measured at a fixed EC₈₀ concentration of the reference agonist in the presence of a series of concentrations of antagonist. An agonist-only response was also performed. Analysis was performed using the equation (section 2.5.21.1), except that the IC₅₀ (the concentration whereby 50% of the agonist response was inhibited) was calculated rather than the EC₅₀. The equation for antagonism is as follows:

$$Response = Bottom \frac{(Top - Bottom)}{1 + 10^{LogIC_{50} - X}}$$

The pIC₅₀ values were obtained from the 'best fit' curve-fit from each individual experiment, which was performed a minimum of three times and each value was

used to calculate the $pIC_{50} \pm SEM$ in the same was as described in section 2.5.21.1.

2.5.21.3 Schild EC₅₀ analysis

To determine if the interaction between agonist and antagonist was competitive, Schild analysis was carried out based on the model described by Arunlakshana and Schild (1959). The Schild analysis performed herein used the GraphPad Prism global non-linear regression curve fit. For BRET, intracellular calcium response and quantitative internalisation, eight-point concentration responses of agonist (where the last point is a vehicle-only control) were assessed in triplicate against various concentrations of antagonist in a 96-well plate, respectively. An agonist only concentration-response curve was also performed. To obtain the Top and Bottom values of the agonist-only control a three-parameter curve fit analysis (section 2.5.21.1) was performed. Antagonist competition data was then fit to the Gaddum/Schild EC₅₀ shift global fit analysis using GraphPad Prism with the formula below:

$$Response = Bottom + \frac{(Top - bottom)}{1 + \left(\frac{10^{LogEC_{50}} [1 + ([B]/10^{-pA_2})^S]}{[A]} \right)^{Hillslope}}$$

Where A is the agonist concentration; B is the antagonist concentration; EC₅₀ or the negative logarithm of the EC₅₀ is the concentration of agonist that generates a half maximal response in the absence of inhibitor; pA₂ is the negative logarithm of the concentration of antagonist needed to shift the agonist concentration response curve by a factor of 2; the Hill Slope is the steepness of the family of curves (with a Hill Slope of 1.0 being standard); the Schild Slope (S) quantifies if the shift in the agonist's response with increasing antagonist concentration that corresponds to the prediction of competitive interaction; Top is the maximal asymptote of the curve; Bottom is the basal response.

2.5.21.4 Statistical analysis

Statistical analysis was performed using a one-way analysis of variance (ANOVA) when comparing the means of multiple treatment groups. Tukey's post-hoc

analysis was used to determine significance between treatment groups versus the control group, with a p value <0.05 deemed statistically significant.

3 Generation and characterisation of cell lines

The biochemical analysis of cellular processes in mammalian cells is often facilitated by the creation of cell lines expressing a protein of interest (Spitzer et al., 2013). The increased amount of sequence information available from the human genome has placed greater emphasis upon heterologous cell expression systems as targets for high throughput structure-function evaluation of novel drug targets and disease markers (Thomas and Smart, 2005). Use of heterologous cell systems expressing G-protein-coupled receptors (GPCRs) is an appropriate way for understanding the molecular basis of their activation, downstream signalling, regulation and pharmacology (Chakraborty et al., 2015; Andrell and Tate, 2013).

In this chapter, I have characterised cell lines stably expressing hFFA1 or hFFA4 or both of these receptors in an inducible or constitutive manner. Stable expression allows consistent expression levels of receptors and therefore also consistency between experiments. For inducible and controlled expression of the receptor of interest, the Flp-InTM T-RExTM-293 cell line (Invitrogen Life Technologies) was utilised. In other cell lines, receptors were expressed constitutively. It is possible that in successfully transfected cells the cDNA of the receptor might not be integrated in a transcriptionally active locus. So, it was necessary to characterise these cell lines to optimise the expression level as well as validate assay conditions.

3.1 Generation and characterisation of cell lines expressing hFFA1

The hFFA1 receptor was fused at its C terminus to monomeric Venus fluorescent protein (mVenus) or a monomeric green fluorescent protein (GFP2) followed by incorporation of the HA epitope tag. A number of expression vectors were constructed including pcDNA5/FRT/TO/hFFA1 and pcDNA3/hFFA1 (section 2.3). These plasmids were used to express hFFA1 in a constitutive or inducible manner in different cell lines.

3.1.1 Flp-In™ T-REx™ 293 cells able to express hFFA1-mVenus-HA

hFFA1-mVenus-HA was cloned into the doxycycline-inducible locus of Flp-In™ T-REx™ 293 cells (Ward et al., 2011a). After the initial transfection cells were cultured with DMEM containing hygromycin and blasticidin to allow selection for positive clones (section 2.4.2.2). Cells from these clones were then isolated and expanded for characterisation. Early passages of cells were cryopreserved.

3.1.1.1 Characterisation of the expression of hFFA1-mVenus-HA

Preliminary characterisation involved detection of receptor-expression by epifluorescence microscopy (section 2.5.7). Cells were treated with or without doxycycline for 18-24 hours and maintained at 37 °C and 5% CO₂ to allow receptor expression. Microscopic images of doxycycline-treated cells revealed expression of mVenus-tagged hFFA1 mostly at the cell surface (Figure 3-1, A). However, some intracellular signal was also noted in these cells (Figure 3-1, A). The overlay of fluorescence images (Figure 3-1, A) with bright field images (Figure 3-1, B) confirmed homogenous expression (Figure 3-1, C) of the receptor upon induction with doxycycline. No visible expression of the receptor was observed in cells grown in the absence of doxycycline (Figure 3-1, D).

Doxycycline-induced expression of hFFA1 was next investigated by immunoblotting (section 2.5.5). Cells were treated with varying concentrations of doxycycline for 18-24 hours. Lysates of these cells were resolved by SDS-PAGE and immunoblotted using an anti-green fluorescent protein (GFP) sheep polyclonal antiserum. Expression of the receptor in such lysates was detected as a smear bands (~50-70 kDa) in the immunoblot (Figure 3-1, E). No expression of hFFA1 was detected in lysates of doxycycline-untreated cells (Figure 3-1, E). Quantitative densitometry (section 2.5.6) of such immunoblots indicated a doxycycline-concentration dependent expression of the receptor (Figure 3-1, F). The fluorescence emission (section 2.5.20) of cells was also dependent on the concentration of doxycycline used to induce cells for receptor expression (Figure 3-1, G).

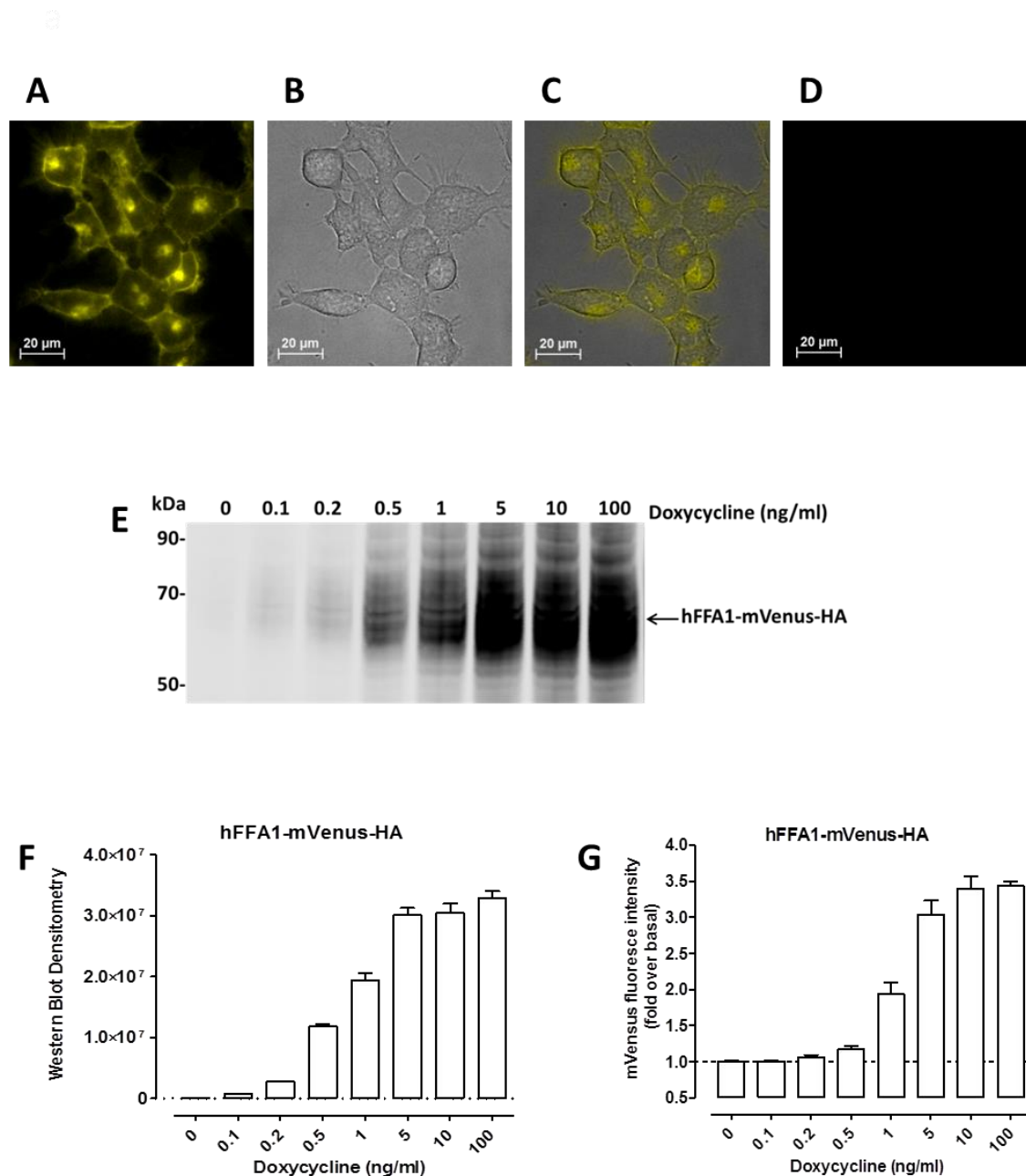


Figure 3-1. Characterisation of a Flp-In™ T-REx™ 293 cell line able to express inducibly hFFA1-mVenus-HA. Flp-In™ T-REx™ 293 cells harbouring hFFA1-mVenus-HA at the Flp-In locus were generated. Epifluorescence microscopy (section 2.5.7) was used to visualise receptor expression: **(A)** Epifluorescence images of cells treated with doxycycline; **(B)** Bright field image of doxycycline-treated cells; **(C)** Overlayed image of A+B; **(D)** Epifluorescence image of cells cultured in the absence of doxycycline. All images shown are representative of three independent experiments. **(E)** Receptor expression was induced by varying concentrations of doxycycline and lysates of cells were immunoblotted using an anti-GFP antiserum. **(F)** Densitometry of such immunoblots. **(G)** Fluorescence intensity (section 2.5.20) of mVenus in cells treated with varying concentrations of doxycycline. Data represent the mean \pm SEM of three independent experiments.

3.1.1.2 Functional characterisation of the expression of hFFA1-mVenus-HA

Agonist-promoted elevation of intracellular calcium was measured to investigate the functional expression of hFFA1. In single-cell calcium imaging (section 2.5.16), cells treated with doxycycline (100 ng/ml) for 24 hours were challenged with the selective FFA1 agonist TUG-905 (3 μ M) for 60 seconds. A transient increase in the level of intracellular calcium was observed which returned to baseline upon ligand removal and washout (Figure 3-2, A). The TUG-905-promoted $[Ca^{2+}]_i$ response was also investigated in cell populations (section 2.5.17). Receptor expression was induced by varying concentrations of doxycycline and these cells then challenged with varying concentrations of TUG-905. The agonist-response was dependent on the concentration of doxycycline used to induce the expression of hFFA1 (Figure 3-2, B). Cells grown in the absence of doxycycline did not show any $[Ca^{2+}]_i$ response to TUG-905 (Figure 3-2, B).

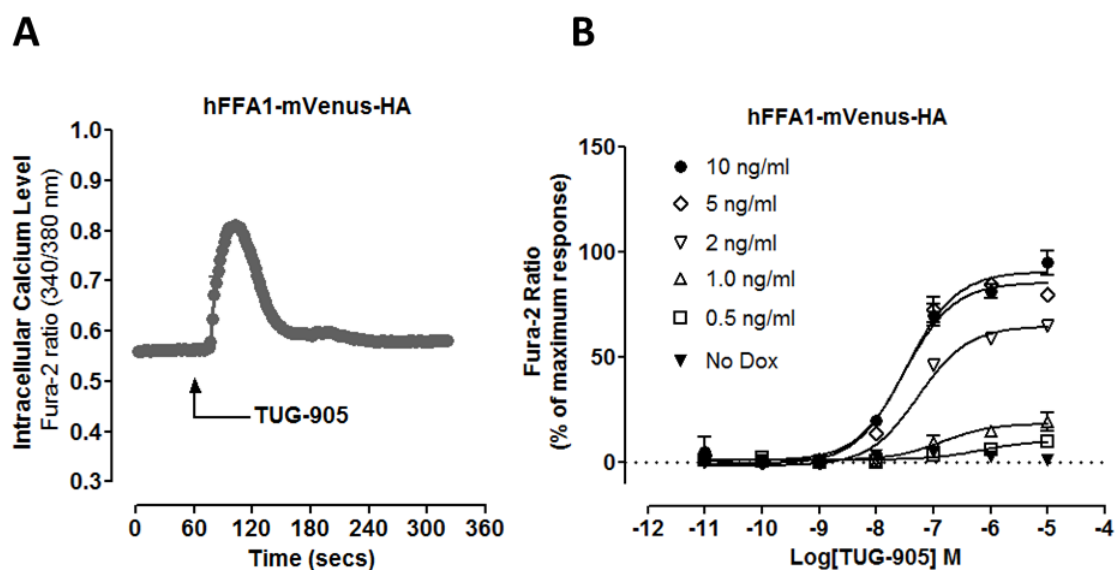


Figure 3-2. Functional characterisation of a Flp-In™ T-REx™ 293 cell line able to express inducibly hFFA1-mVenus-HA. Flp-In™ T-REx™ 293 cells able to express hFFA1-mVenus-HA were investigated for the function of the receptor. **(A)** Cells were plated onto poly-*D*-lysine-coated 22 mm glass coverslips and receptor expression was induced by doxycycline (100 ng/ml) for 18-28 hours. The capacity of 3 μ M TUG-905 to modulate intracellular calcium level was assessed in single-cell calcium imaging (section 2.5.16). Data represent mean \pm SEM from three separate experiments of at least 20 individual cells. **(B)** Cells were seeded (75,000 cells/well) into poly-*D*-lysine coated black clear-bottom 96-well plates. Receptor expression was induced by addition of varying concentrations of doxycycline for 18-24 hours. Cells were labelled with Fura-2 AM for 45 minutes and then challenged with varying concentrations of TUG-905. Mobilisation of intracellular calcium was recorded in a FlexStation plate reader (section 2.5.17). Efficacy was normalised to percentage of maximum response. Data represent the mean \pm SEM of three independent experiments.

3.1.2 Flp-InTM T-RExTM 293 cells able to express hFFA1-GFP2-HA

A pcDNA5/FRT/TO/hFFA1-GFP2-HA plasmid was constructed (section 2.3) for inducible expression of hFFA1. This vector was inserted into the Flp-In locus of Flp-InTM T-RExTM-293 cells and pools of positive cells were selected. This cell line allows inducible expression of hFFA1-GFP2-HA under the control of the tetracycline/doxycycline (Ward et al., 2011a).

3.1.2.1 Characterisation of the expression of hFFA1-GFP2-HA

The expression of hFFA1-GFP2-HA was initially characterised using epifluorescence microscopy (section 2.5.7). Cells were plated on glass coverslips and the expression of hFFA1-GFP2-HA was induced with or without doxycycline. Epifluorescence microscopic images revealed that doxycycline-treated cells expressed the receptor predominantly at the cell surface with fewer in intracellular spaces (Figure 3-3, A). Homogenous expression of the receptor was seen when fluorescent images (Figure 3-3, A) and bright field images (Figure 3-3, B) were overlaid (Figure 3-3, C). No expression of the receptor was noted in cells cultured in the absence of doxycycline (Figure 3-3, D).

The inducible expression of hFFA1-GFP2-HA was next assessed by immunoblotting (section 2.5.5). Cells were treated with varying concentrations of doxycycline and incubated 18-24 hours for induction of the receptor expression. SDS-PAGE of lysates from these cells and immunoblotting using an anti-GFP antiserum revealed expression of the polypeptide at 50-70 kDa in the immunoblot (Figure 3-3, E). No expression was detected in lysates of doxycycline-untreated cells (Figure 3-3, E). The densitometry (section 2.5.6) of such immunoblots showed a doxycycline-concentration dependency in the expression of the receptor construct (Figure 3-3, F). The result was also in the case of GFP2 fluorescence intensity measurements (Figure 3-3, G).

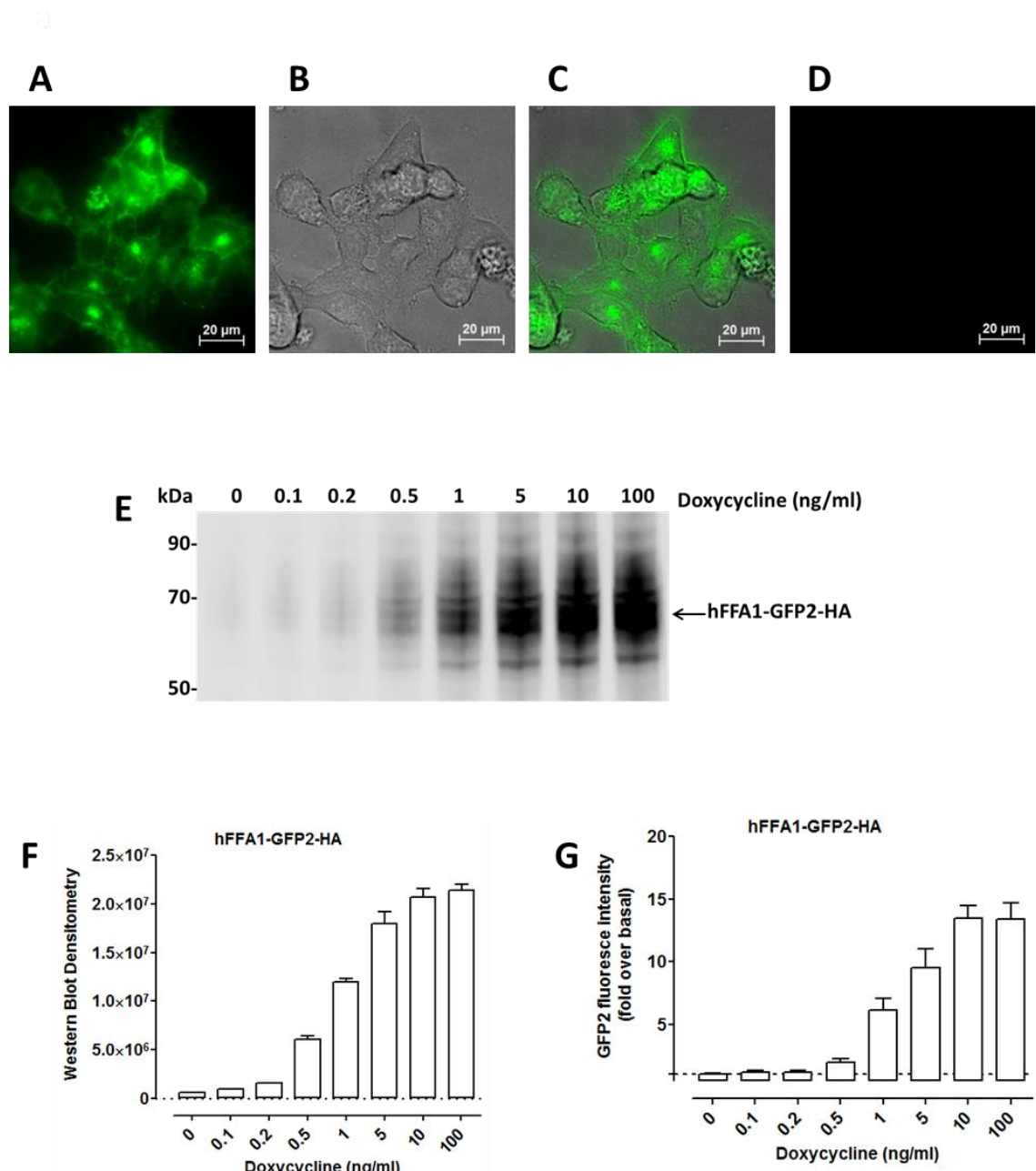


Figure 3-3. Characterisation of a Flp-In™ T-REx™ 293 cell line able to express inducibly hFFA1-GFP2-HA. Flp-In™ T-REx™-293 cells harbouring hFFA1-GFP2-HA were characterised for receptor expression. Cells were treated with or without doxycycline for 18-24 hours and then visualised using an epifluorescence microscope: **(A)** Fluorescence image of doxycycline-treated cells; **(B)** Bright field image of the doxycycline-treated cells; **(C)** Overlay of fluorescence and bright field images; **(D)** Fluorescence image of cells grown in the absence of doxycycline. All microscopic images shown are representative of two independent experiments. **(E)** Anti-GFP-immunoblots of cell lysates treated with varying concentrations of doxycycline. **(F)** Densitometry (section 2.5.6) of the immunoblot. **(G)** Fluorescence intensity (section 2.5.20) of GFP2 in cells treated with varying concentrations of doxycycline. Data represent the mean ± SEM of three independent experiments.

3.1.2.2 Functional characterisation of the expression of hFFA1-GFP2-HA

Agonist promoted activation of FFA1 promotes elevation of intracellular calcium levels (Briscoe et al., 2003; Christiansen et al., 2012). To investigate the functional expression of hFFA1-GFP2-HA in this cell line, cells induced with different concentrations of doxycycline were challenged with varying concentrations of TUG-770. The elevation of intracellular calcium level was measured using a FlexStation plate reader (section 2.5.17). In doxycycline-treated cells the mobilisation of intracellular calcium was dependent on the concentration of agonist (Figure 3-4). The efficacy of the calcium response was dependent on the concentration of doxycycline used to induce expression of receptors. No response was noted in cells grown in the absence of doxycycline (Figure 3-4).

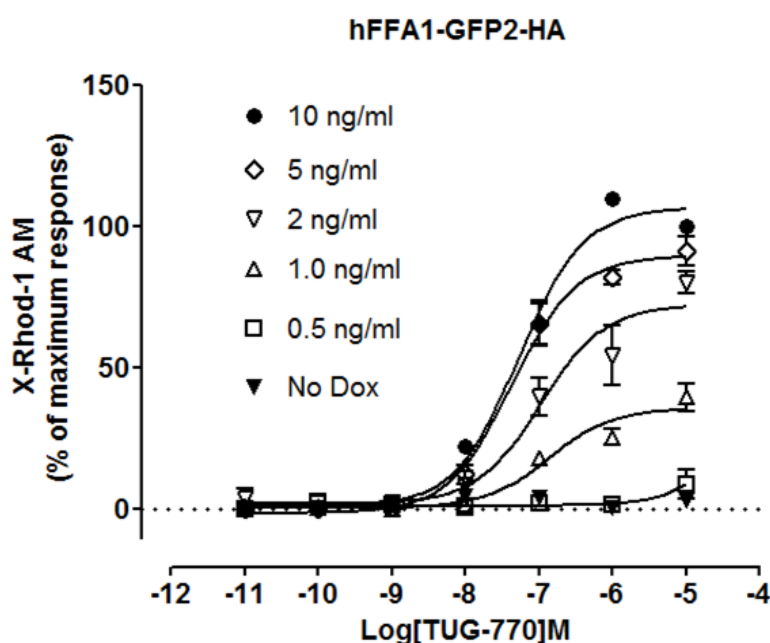


Figure 3-4. Functional characterisation of a Flp-In™ T-REx™ 293 cell line able to express inducibly hFFA1-GFP2-HA. Flp-In™ T-REx™-293 cells able to inducibly express hFFA1-GFP2-HA were seeded (75,000 cells/well) into poly-*D*-lysine coated black clear-bottom 96-well plates. Receptor expression was induced by addition of varying concentrations of doxycycline for 18-24 hours. Cells were labelled with X-Rhod-1 AM for 45 minutes and then challenged with varying concentrations of TUG-770. Data represent the mean \pm SEM of three independent experiments.

3.1.3 A HEK293 cell line expressing hFFA1-mVenus-HA

An HA-epitope and mVenus fluorescent protein-tagged version of hFFA1 in pcDNA3/hFFA1-mVenus-HA was transfected into HEK293 parental cells using PEI. Positive clones, i.e. those resistant to antibiotic G-418 were individually collected and expanded. Following clonal selection, 15 clones were initially tested by fluorescence microscopy (section 2.5.7) for construct expression. Clones lacking mVenus fluorescence were disregarded. Clone-1 was selected and characterised as a stable cell line constitutively expressing hFFA1-mVenus-HA. Epifluorescence microscope images revealed constitutive expression of the receptor (Figure 3-5, A). Overlay of fluorescence (Figure 3-5, A) and bright field images (Figure 3-5, B) indicated homogenous expression of the receptor (Figure 3-5, C).

The function of expressed receptors was investigated by measuring the capacity of cells to mobilise intracellular calcium upon agonist exposure. Cells labelled with Fura-2 AM for 45 minutes were challenged with varying concentrations of TUG-905. Cells were able to elevate the calcium level in an agonist-concentration dependent manner (Figure 3-5, D).

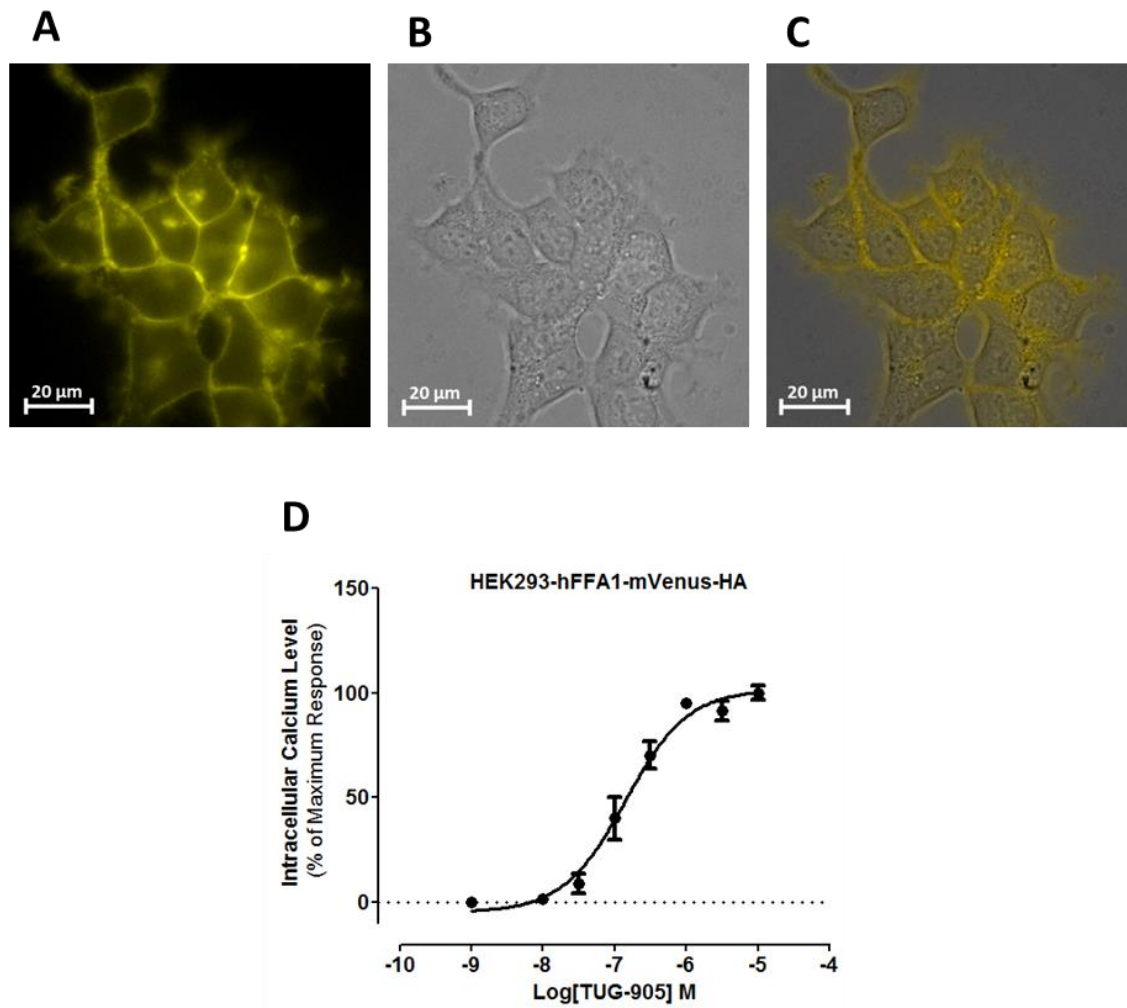


Figure 3-5. Characterisation of constitutive expression of hFFA1-mVenus-HA in HEK293 cells. HEK293 parental cells were transfected with pcDNA3/hFFA1-mVenus-HA and clone 1 was selected for characterisation. Epifluorescence microscopy was employed to visualise receptor expression: **(A)** Fluorescence image of hFFA1-mVenus-HA; **(B)** Bright field image of cells; **(C)** Fluorescence image was overlaid on bright field image. All microscopic images shown are representative of two independent experiments. **(D)** Functional characterisation of the expression of hFFA1. Cells were seeded (70,000 cells /well) into poly-*D*-lysine coated black clear-bottom 96-well plates. Fura-2 AM-labelled cells were challenged with varying concentrations of TUG-905. Efficacy was normalised as percentage of maximum response. Data represent the mean \pm SEM of three independent experiments.

3.1.4 A β -arrestin1/2-null HEK293 cell line expressing hFFA1-mVenus-HA

β -arrestin1/2-null cells (Alvarez-Curto et al., 2016b; Schrage et al., 2015) were transfected with pcDNA3/hFFA1-mVenus-HA to generate a stable cell line constitutively expressing hFFA1-mVenus-HA. Subsequently positive cells were collected and screened using epifluorescence microscopy (section 2.5.7) to select a suitable clone for further characterisation.

Cells plated onto poly-*D*-lysine coated glass coverslips were visualised mVenus fluorescence in these cells (Figure 3-6, A). An overlay image (Figure 3-6, C) generated from fluorescent image (Figure 3-6, A) and corresponding bright field image (Figure 3-6, B) revealed homogenous expression of the receptor in this β -arrestin1/2 knockout cell line. The elimination of β -arrestin1/2 in this genome-edited cell line was investigated by immunoblotting (section 2.5.5). Cytosolic preparations from parental HEK293 cells and β -arrestin1/2-null cells were immunoblotted using anti- β -arrestin1 rabbit monoclonal antibodies. HEK293 parental cells but not β -arrestin1/2-null cells expressed β -arrestin1 (\approx 50 kDa; Figure 3-6, D).

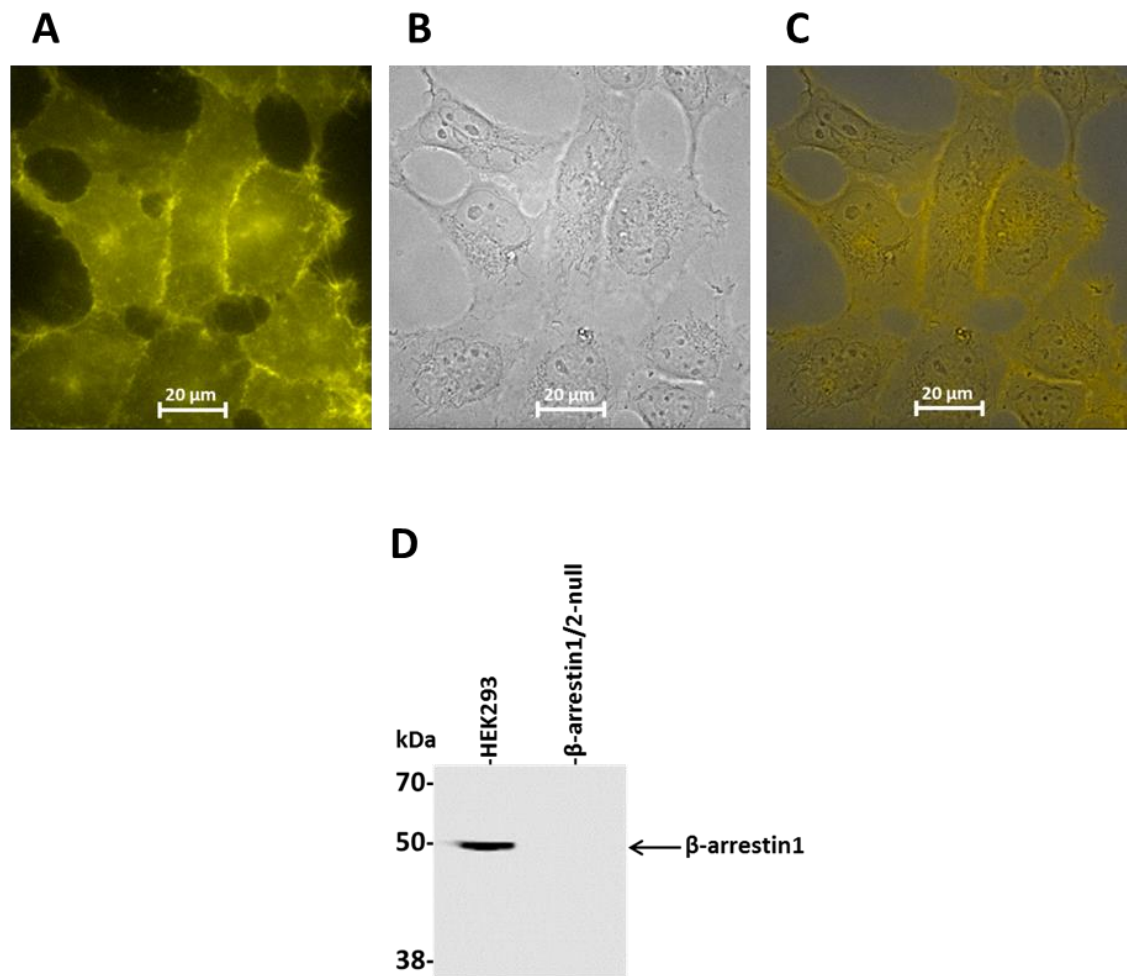


Figure 3-6. Characterisation of β -arrestin1/2-null HEK293 cells constitutively expressing hFFA1-mVenus-HA.

β -arrestin1/2-null cells expressing hFFA1-mVenus-HA were generated and characterised. Cells were plated onto poly-*D*-lysine-coated 22 mm glass coverslips and the expression of mVenus tagged hFFA1 was visualised by epifluorescence microscopy: (A) Fluorescence image; (B) Bright field image; (C) Overlay image. All images shown are representative of two independent experiments. (D) Cytosolic preparations of HEK293 parental cells and β -arrestin1/2-null cells were resolved by SDS-PAGE (section 2.5.4) and immunoblotted using anti- β -arrestin1 rabbit monoclonal antibodies. Expression of β -arrestin1 (\approx 50 kDa) was seen in HEK293 parental cells but was absent in β -arrestin1/2 knockout cells.

3.1.5 A $G\alpha_{q/11}$ knockout HEK293 cell line expressing hFFA1-mVenus-HA

hFFA1-mVenus-HA was constitutively expressed in CRISPR/Cas9 genome-edited $G\alpha_q/G\alpha_{11}$ -null cells (Alvarez-Curto et al., 2016b; Schrage et al., 2015). After successful transfection, positive clones were collected and screened via epifluorescence microscopy. Clones unable to express the receptor were disregarded. Clones with homogenous expression of hFFA1 were selected. Epifluorescence microscopic images showed constitutive expression of hFFA1-mVenus-HA (Figure 3-7, A). The overlaid image of cells (Figure 3-7, C) generated from combined fluorescent images (Figure 3-7, A) and bright field images (Figure 3-7, B) indicated homogenous expression of the receptor in this cell line.

The elimination of $G\alpha_q/G\alpha_{11}$ proteins in this knockout cell line was investigated by immunoblotting. Membrane preparations of HEK293 parental cells and $G\alpha_q/G\alpha_{11}$ -null cells were resolved by SDS-PAGE (section 2.5.4). Immunoblotting (section 2.5.5) with an anti- $G\alpha_{q/11}$ antiserum showed the expression of $G\alpha_q/G\alpha_{11}$ proteins (≈ 40 kDa) in HEK293 cells which was absent in the $G\alpha_q/G\alpha_{11}$ -null HEK293 cells (Figure 3-7, D).

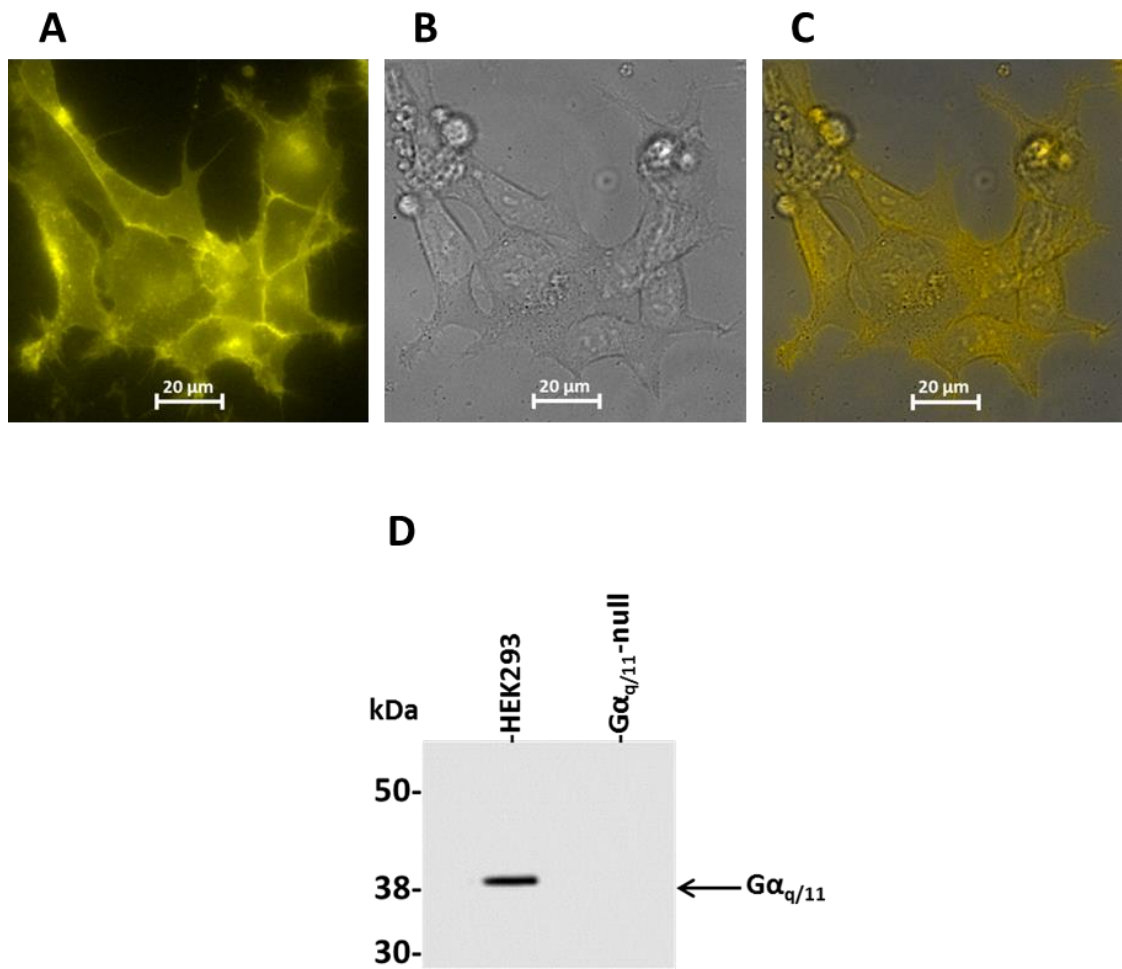


Figure 3-7. Characterisation of $G\alpha_{q/11}$ -null HEK293 cells constitutively expressing hFFA1-mVenus-HA. $G\alpha_q/G\alpha_{11}$ -null cells expressing hFFA1-mVenus-HA were generated and characterised. Cells were plated onto poly-*D*-lysine-coated 22 mm glass coverslips and visualised by epifluorescence microscopy: (A) Fluorescence image; (B) Bright field image; (C) Overlay image. (D) Membrane preparations of HEK293 parental cells and $G\alpha_q/G\alpha_{11}$ -null cells were resolved by SDS-PAGE and immunoblotted using an anti- $G\alpha_{q/11}$ antiserum. Expression of $G\alpha_{q/11}$ was detected in the immunoblot (≈ 40 kDa) of HEK293 parental cell preparations but this was absent in $G\alpha_q/G\alpha_{11}$ knockout cells. All pictures shown are representative of three independent experiments.

3.2 Generation and characterisation of cell lines expressing hFFA4

pcDNA3 and pcDNA5/FRT/TO plasmids were constructed incorporating hFFA4 with the FLAG-epitope at the N-terminus and monomeric Venus or monomeric GFP2 at the C-terminus. These forms of plasmids were used to generate different cell lines able to express hFFA4 in a constitutive or inducible manner.

3.2.1 Flp-InTM T-RExTM 293 cells able to express FLAG-hFFA4-mVenus

For inducible expression of FLAG-hFFA4-mVenus, pcDNA5/FRT/TO/FLAG-hFFA4-mVenus was transfected into the Flp-In locus of Flp-InTM T-RExTM 293 cells. After initial transfection cells were cultured with DMEM containing the selection antibiotics hygromycin and blasticidin. Approximately 2 weeks after transfection, visible foci appeared. The cells were then pooled, expanded, and tested for doxycycline-regulated expression of the receptor.

3.2.1.1 Characterisation of the expression of FLAG-hFFA4-mVenus

Preliminary characterisation involved detection of mVenus expression. Cells were treated with or without doxycycline for 18-24 hours and visualised by epifluorescence microscopy (section 2.5.7). Epifluorescence images of cells treated with doxycycline were found to express the mVenus-tagged hFFA4 largely at the cell surface (Figure 3-8, A). Fluorescence images (Figure 3-8, A) were overlaid on bright field images (Figure 3-8, B) to confirm the homogeneity of receptor expression (Figure 3-8, C). No expression of the receptor was seen in cells grown in the absence of doxycycline (Figure 3-8, D). Regulated expression of FLAG-hFFA4-mVenus was assessed by immunoblotting (section 2.5.5) cell lysates prepared from cells treated with varying concentrations of doxycycline. Immunoblotting using an anti-GFP antiserum revealed expression of the receptor as a smear of polypeptides (~52-76 kDa; Figure 3-8, E). No expression was detected in lysates prepared from doxycycline-untreated cells (Figure 3-8, E). Densitometric analysis (section 2.5.6) of Western blots (Figure 3-8, F) showed a doxycycline concentration-dependent expression of the receptor. The mVenus fluorescence intensity was also dependent on the concentration of doxycycline use to induce receptors in this cell line (Figure 3-8, G).

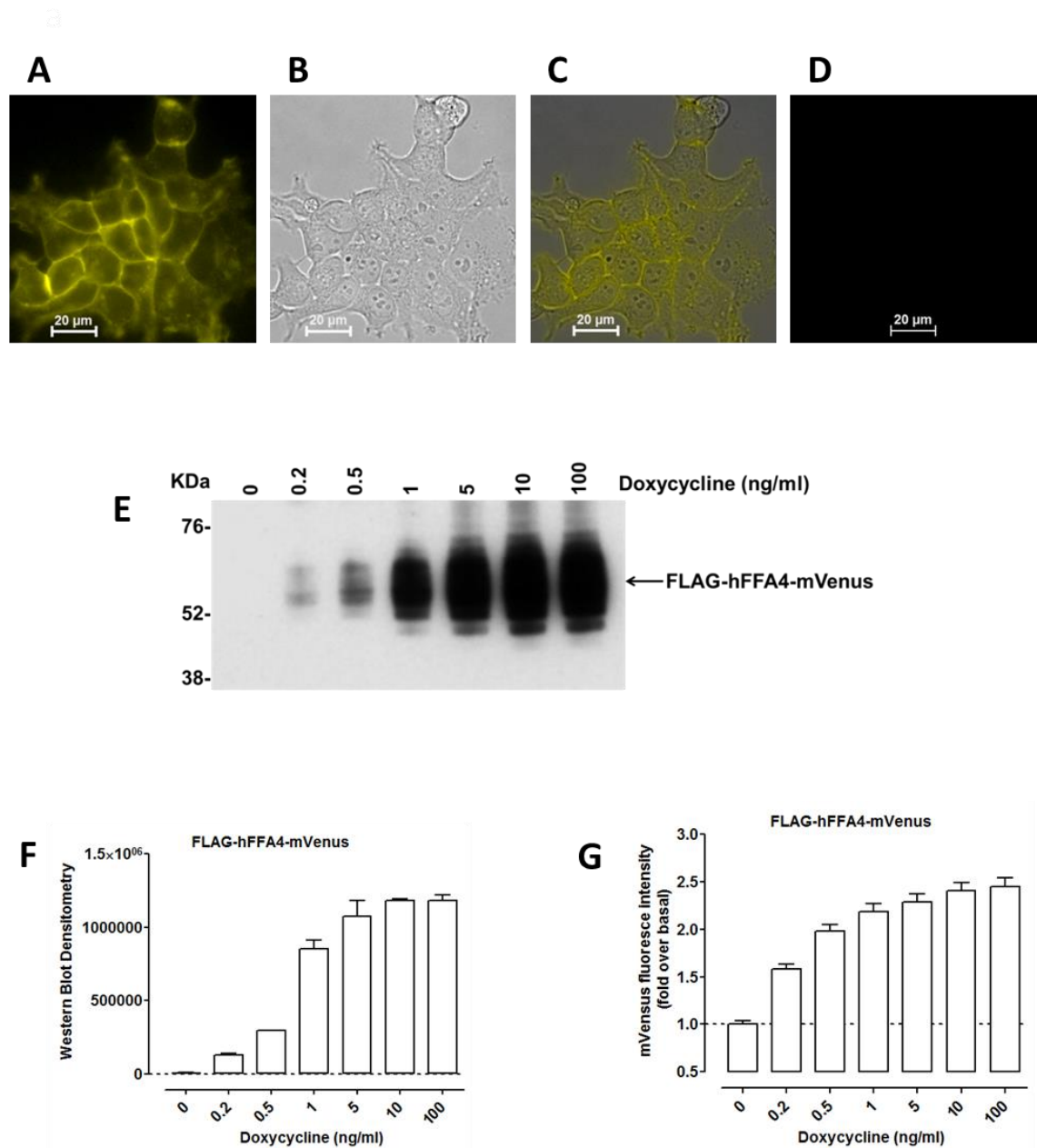


Figure 3-8. Characterisation of a Flp-In™ T-REx™ 293 cell line able to express inducibly FLAG-hFFA4-mVenus. Flp-In™ T-REx™ 293 cells harbouring FLAG-hFFA4-mVenus at the Flp-In locus were generated and characterised. Expression of mVenus-tagged receptor was visualised in cells treated with or without doxycycline: **(A)** Epifluorescence image cells treated with doxycycline; **(B)** Bright field image of doxycycline-treated cells; **(C)** Images were overlaid; **(D)** Epifluorescence image of cells cultured in the absence of doxycycline. All images shown are representative of three independent experiments. **(E)** Cells were plated on 6-well plates and receptor expression induced by varying concentrations of doxycycline. Lysates from these cells were immunoblotted (section 2.5.5) using an anti-GFP antiserum. **(F)** Densitometry (section 2.5.6) of western blots. **(G)** Fluorescence intensity (section 2.5.20) of mVenus in cells treated with varying concentrations of doxycycline. Data represent the mean \pm SEM of three independent experiments.

3.2.1.2 Functional characterisation of the expression of hFFA4-mVenus

The function of FLAG-hFFA1-mVenus expressed in this cell line was investigated via agonist-promoted elevation of intracellular calcium. In single-cell calcium imaging studies, 60 seconds exposure to TUG-891 (3 μ M) of doxycycline-treated cells produced a transient elevation of intracellular calcium which returned to baseline after ligand removal and washout (Figure 3-9, A). To investigate calcium mobilisation in cell populations, cells were treated with varying concentrations of doxycycline for 18-24 hours. Fura-2 AM labelled cells were challenged with varying concentrations of TUG-891. Elevation of intracellular calcium levels occurred in an agonist-concentration dependent fashion (Figure 3-9, B). The efficacy of the calcium response was dependent on the concentration of doxycycline used to induce these cells. Cells grown in the absence of doxycycline did not show any response (Figure 3-9, B).

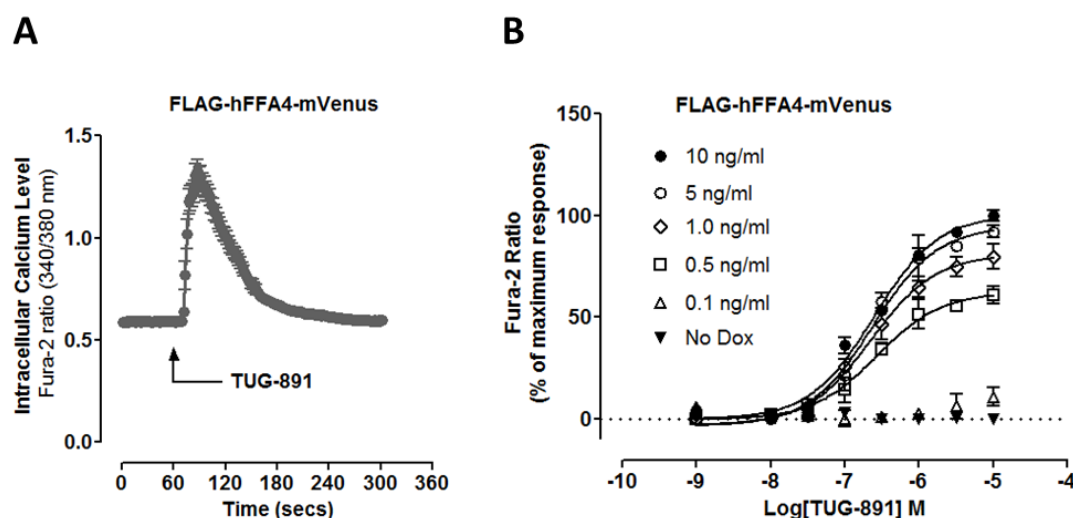


Figure 3-9. Functional characterisation of the expression of FLAG-hFFA4-mVenus.

Flp-In™ T-REx™ 293 cells able to inducibly express FLAG-hFFA4-mVenus were investigated for their function. **(A)** Cells were plated onto poly-*D*-lysine-coated 22 mm glass coverslips and receptor expression was induced by doxycycline (100 ng/ml) for 18-28 hours. The capacity of 3 μ M TUG-891 to modulate intracellular calcium level was assessed in single-cell calcium imaging (section 2.5.16). Data represent mean \pm SEM from three separate experiments of at least 20 individual cells. **(B)** Cells were seeded (75,000 cells/well) into poly-*D*-lysine coated black clear-bottom 96-well plates. Receptor expression was induced by varying concentrations of doxycycline. Cells were labelled with Fura-2 AM for 45 minutes and then challenged with varying concentrations of TUG-891. Mobilisation of intracellular calcium was recorded in a FlexStation plate reader (section 2.5.17). Efficacy was normalised to percentage of maximum response. Data represent the mean \pm SEM of three independent experiments.

3.2.2 Flp-InTM T-RExTM HEK293 cells able to express FLAG-hFFA4-GFP2

A pcDNA5/FRT/TO/FLAG-hFFA4-GFP2 plasmid was constructed (section 2.3) for inducible expression of FLAG-hFFA4-GFP2 in Flp-InTM T-RExTM-293 cells. This plasmid was cloned into the Flp-In locus of these cells to generate an inducible cell line. The expression of the receptor construct from the locus is controlled by addition of doxycycline (Ward et al., 2011a).

3.2.2.1 Characterisation of the expression of FLAG-hFFA4-GFP2

The expression of FLAG-hFFA4-GFP2 was initially characterised using an epifluorescence microscope (section 2.5.7). Cells were treated with doxycycline and incubated for 18-24 hours to allow receptor expression. Epifluorescence microscopic images showed that doxycycline-treated cells expressed the receptor (Figure 3-10, A) predominantly at the cell surface. An overlay image (Figure 3-10, C) generated from fluorescence images (Figure 3-10, A) and bright field images (Figure 3-10, B) revealed homogenous expression of the receptor. No expression of GFP2 was seen in cells cultured in the absence of doxycycline (Figure 3-10, D).

Expression of FLAG-hFFA4-GFP2 was also investigated by immunoblotting (section 2.5.5) of lysates prepared from cells treated with different concentrations of doxycycline. Anti-GFP antiserum immunoblots showed doxycycline-concentration dependent expression of receptors (52-76 kDa; Figure 3-10, E). Cells grown in the absence of doxycycline did not express the receptor construct (Figure 3-10, E). Densitometry of such immunoblots (Figure 3-10, F) indicated the expression of hFFA4 in a doxycycline-concentration dependent manner. Cells treated with varying concentrations of doxycycline also showed a doxycycline-concentration dependent increase in the intensity of GFP2 fluorescence (Figure 3-10, G).

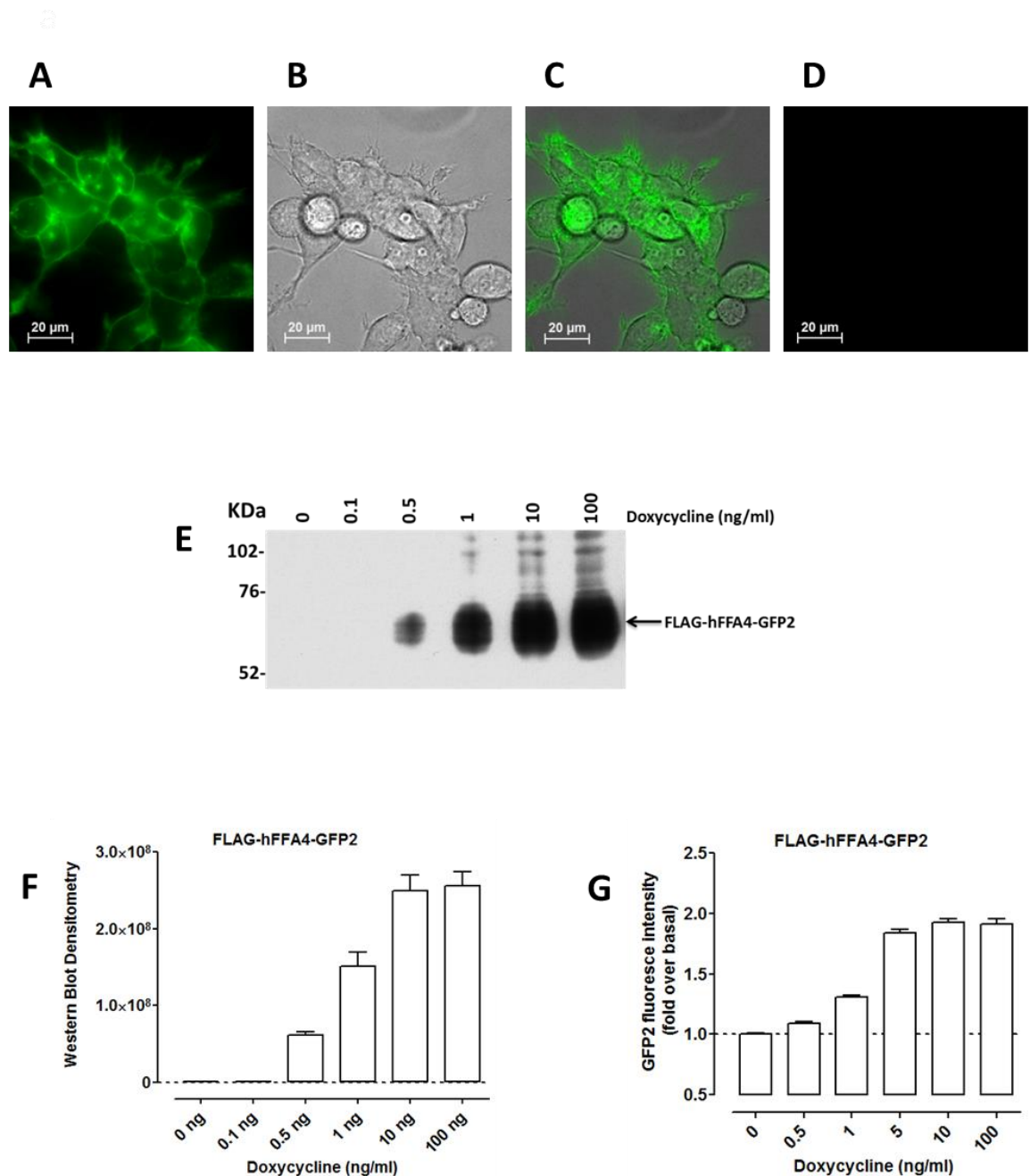


Figure 3-10. Characterisation of a Flp-In™ T-REx™ 293 cell line able to express inducibly FLAG-hFFA4-GFP2. Flp-In™ T-REx™ 293 cells harbouring FLAG-hFFA4-GFP2 at the Flp-In locus were generated. Epifluorescence microscopy (section 2.5.7) of cells treated with or without doxycycline: **(A)** Fluorescence image of cells treated with doxycycline; **(B)** Bright field image of doxycycline-treated cells; **(C)** Overlay image; **(D)** Fluorescence image of cells grown in the absence of doxycycline. All microscopic images shown are representative of three independent experiments. **(E)** Cells were plated on 6-well plates and receptor expression was induced by varying concentrations of doxycycline. Lysates from these cells were immunoblotted (section 2.5.5) using an anti-GFP antiserum. **(F)** Densitometry (section 2.5.6) of western blots. **(G)** Fluorescence intensity (section 2.5.20) of GFP2 in cells treated with varying concentrations of doxycycline. Data represent the mean \pm SEM of three independent experiments.

3.2.2.2 Functional characterisation of the expression of FLAG-hFFA4-GFP2

Agonist promoted activation of FFA4 promotes elevation of intracellular calcium levels (Hudson et al., 2013b; Hirasawa et al., 2005). The functional expression of FLAG-hFFA4-GFP2 in this cell line was investigated by the capacity to elevate intracellular calcium levels upon agonist stimulation. Receptor expression was induced by varying concentrations of doxycycline for 18-24 hours. Cells were labelled with the calcium sensitive dye X-Rhod-1 AM for 45 minutes and then challenged with varying concentrations of TUG-891. An agonist-concentration dependent increase of intracellular calcium levels was observed (Figure 3-11). The efficacy of the calcium response was dependent on the concentration of doxycycline used to induce cells for receptor expression (Figure 3-11). Cells cultured without doxycycline did not show any calcium response.

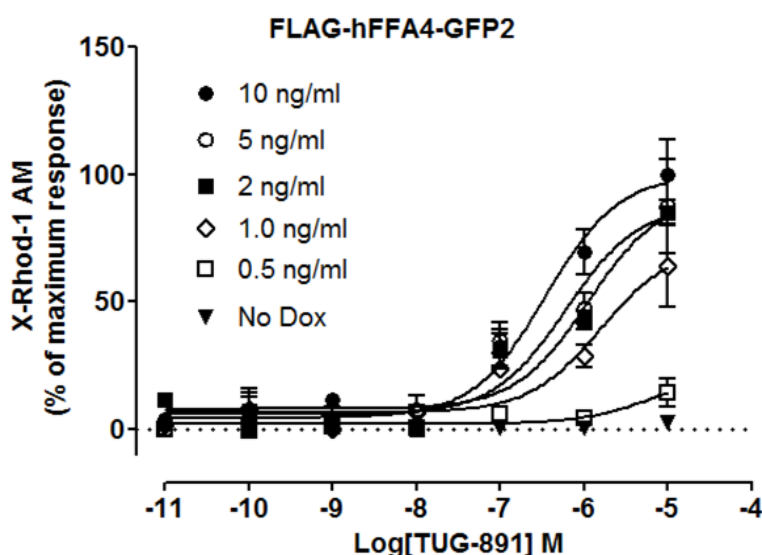


Figure 3-11. Functional characterisation of the expression of FLAG-hFFA4-GFP2.

Flp-In™ T-REx™-293 cells able to express FLAG-hFFA4-GFP2 were seeded (75,000 cells/well) into poly-*D*-lysine coated black clear-bottom 96-well plates. Receptor expression was induced by addition of varying concentrations of doxycycline for 18-24 hours. Cells were labelled with X-Rhod-1 AM for 45 minutes and the challenged with varying concentrations of TUG-891. Mobilisation of intracellular calcium was recorded in a FlexStation plate reader (section 2.5.17). Data represent the mean \pm SEM of three independent experiments.

3.2.3 HEK293 cell line expressing FLAG-hFFA4-mVenus

For constitutive expression of FLAG-hFFA4-mVenus, a pcDNA3/FLAG-hFFA4-mVenus plasmid was permanently transfected into HEK293 parental cells. G-418 resistant clones were collected and visualised by fluorescent microscopy to identify GFP2 expressing cells. Clones having homogenous expression were identified and characterised for the generation of a stable cell line.

Epifluorescence microscopic images revealed cell surface expression of FLAG-hFFA4-mVenus (Figure 3-12, A). The overlay image (Figure 3-12, C) generated from fluorescence images (Figure 3-12, A) and bright field images (Figure 3-12, B) indicated a homogenous expression of the receptor. The cell line was also fully functional in the agonist promoted elevation of intracellular calcium levels. The mobilisation of intracellular calcium was dependent on the concentration of agonist used to activate hFFA4 (Figure 3-12, D).

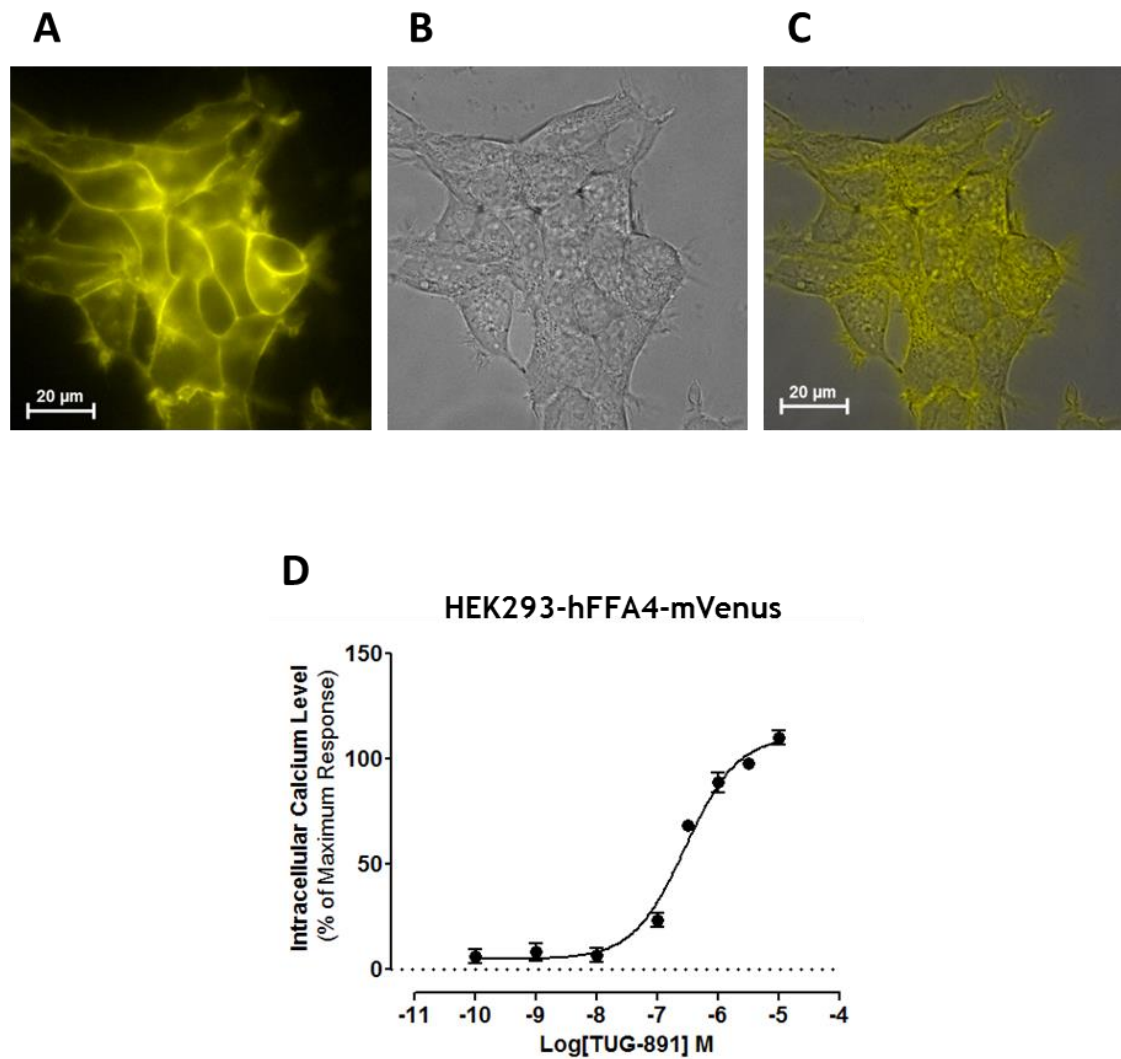


Figure 3-12. Characterisation of the constitutive expression of FLAG-hFFA4-mVenus in HEK293 parental cells. HEK293 parental cells were transfected with pcDNA3/FLAG-hFFA4-mVenus. Epifluorescence microscopy (section 2.5.7) was employed to visualise the expression of mVenus tagged hFFA4: (A) Fluorescence image of FLAG-hFFA4-mVenus; (B) Bright field image of cells; (C) Overlaid image. All microscopic images shown are representative of three independent experiments. (D) Functional characterisation of the expression of hFFA4. Cells were seeded (70,000 cells /well) into poly-*D*-lysine coated black clear-bottom 96-well plates. Fura-2 AM labelled cells were challenged with varying concentrations of TUG-891. Mobilisation of intracellular calcium was recorded in a FlexStation plate reader (section 2.5.17). Efficacy was normalised as percentage of maximum response. Data represent the mean \pm SEM of three independent experiments.

3.2.4 β -arrestin1/2 knockout HEK293 cell line expressing FLAG-hFFA4-mVenus

pcDNA3/FLAG-hFFA4-mVenus was stably transfected into β -arrestin1/2-null HEK293 cells (Alvarez-Curto et al., 2016b; Schrage et al., 2015). Subsequently positive cells resistant to medium containing G-418 were collected and screened for mVenus expression using an epifluorescence microscope (section 2.5.7).

Fluorescence images indicated a constitutive expression of hFFA4 in this cell lines (Figure 3-13, A). The expression was (Figure 3-13, C). The elimination of β -arrestin1/2 was confirmed by immunoblotting (section 2.5.5) of cytosolic preparations of HEK293 parental cells and β -arrestin1/2 knockout cells. Immunoblots with an anti- β -arrestin1 or anti- β -arrestin2 rabbit monoclonal antibodies revealed the presence of both β -arrestin1 and β -arrestin2 (≈ 50 kDa) in HEK293 parental cells (Figure 3-13, D). However, β -arrestin1 and β -arrestin2 proteins were totally eliminated in the knockout cells (Figure 3-13, D).

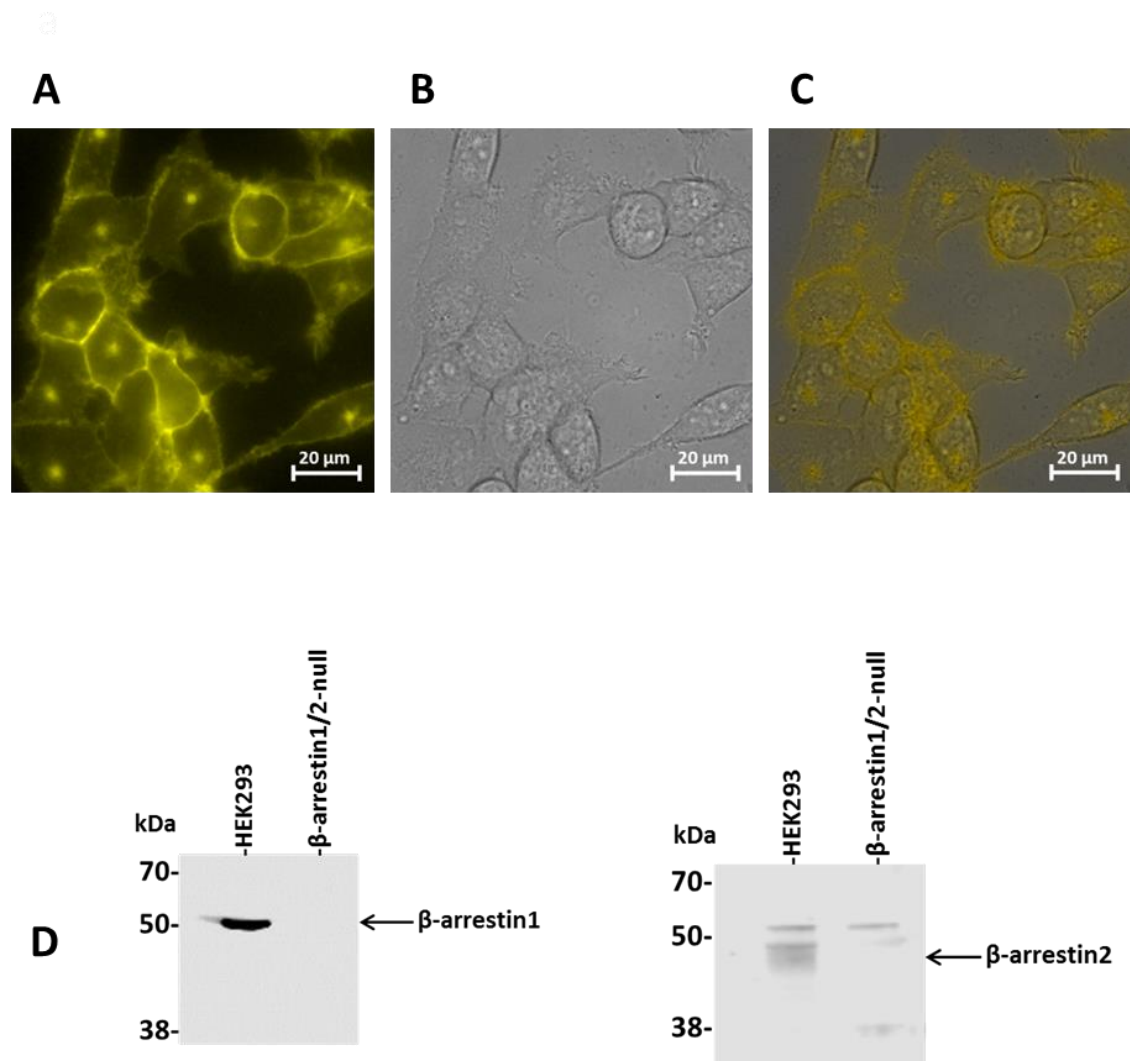


Figure 3-13. Characterisation of β -arrestin1/2 knockout HEK293 cells constitutively expressing FLAG-hFFA4-mVenus. β -arrestin1/2-null HEK293 cells stably transfected with FLAG-hFFA4-mVenus were generated and characterised. Cells were plated onto poly-*D*-lysine-coated 22 mm glass coverslips and the expression of mVenus tagged hFFA4 was visualised by epifluorescence microscopy: (A) Fluorescence image; (B) Bright field image; (C) Overlay image. All microscopic images shown are representative of three independent experiments. (D) Cytosolic preparations of HEK293 parental cells and β -arrestin1/2-null cells were immunoblotted (section 2.5.5) using anti- β -arrestin1 and anti- β -arrestin2 rabbit monoclonal antibodies. Expression of β -arrestin1/2 (\approx 50 kDa) was seen in HEK293 parental cells whilst these were absent in β -arrestin1/2 knockout cells.

3.2.5 A $G\alpha_{q/11}$ knockout cell line expressing FLAG-hFFA4-mVenus

CRISPR/Cas9-mediated genome-edited $G\alpha_q/G\alpha_{11}$ -null cells (Alvarez-Curto et al., 2016b; Schrage et al., 2015) were stably transfected with pcDNA3/FLAG-hFFA4-mVenus for constitutive expression of FLAG-hFFA4-mVenus. Epifluorescence images revealed the expression of FLAG-hFFA4-mVenus (Figure 3-14, A). Overlay images revealed homogenous expression of the receptor (Figure 3-14, C). Membrane preparations of HEK293 parental cells and $G\alpha_q/G\alpha_{11}$ knockout cells were immunoblotted (section 2.5.5) with an anti $G\alpha_{q/11}$ antiserum to investigate the presence of $G\alpha_q/G\alpha_{11}$ proteins in these cells. $G\alpha_q/G\alpha_{11}$ proteins were expressed in the HEK293 parental cells, however, they were abolished in the $G\alpha_{q/11}$ -null cells (Figure 3-14, D). The expression of hFFA4 was also investigated by immunoblotting of cell lysates using an anti-GFP antiserum. Both HEK293 parental and $G\alpha_{q/11}$ -null cells expressed the receptor (≈ 50 -70 kDa). However immunoblots from equal amount of lysates indicated somewhat higher level of hFFA4 expressed in the parental cells (Figure 3-14, E).

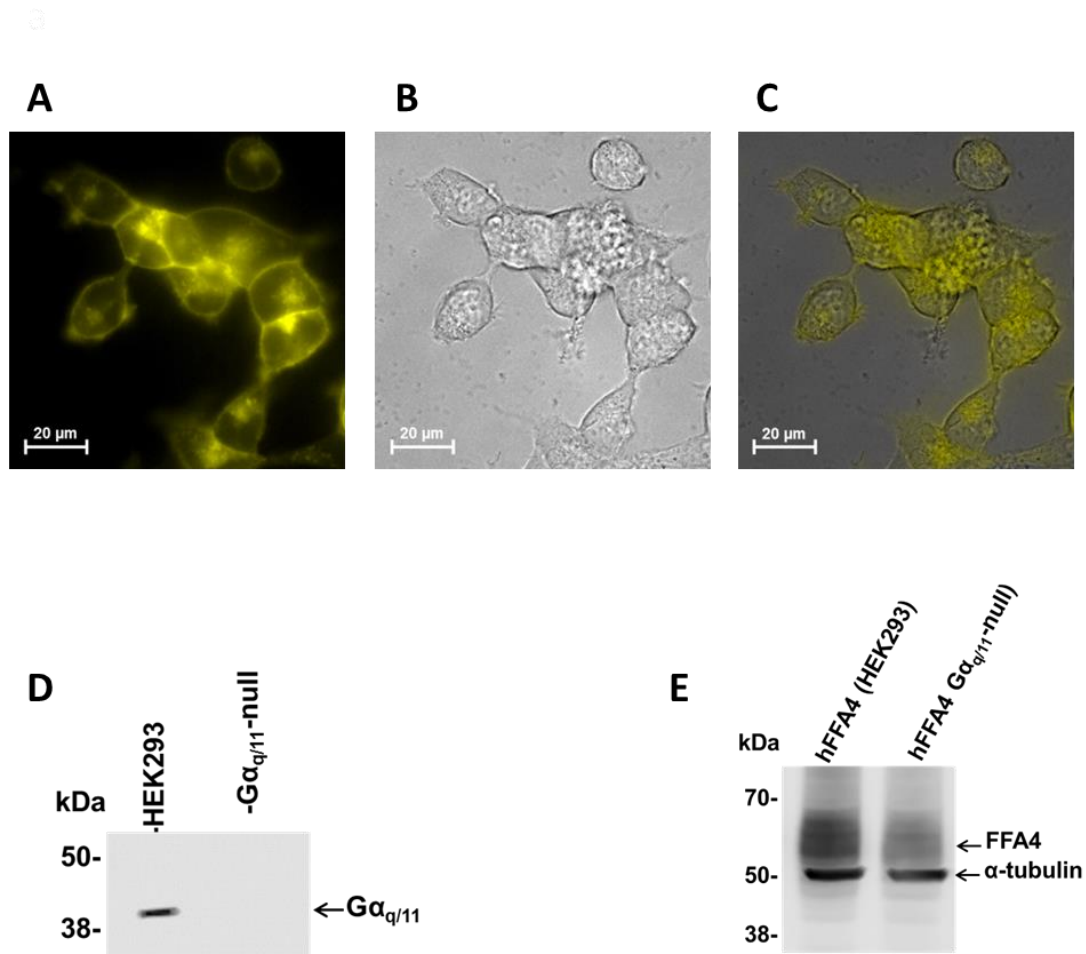


Figure 3-14. Characterisation of $G\alpha_{q/11}$ -knockout HEK293 cells constitutively expressing FLAG-hFFA4-mVenus. CRISPR/Cas9-mediated $G\alpha_q/G\alpha_{11}$ -null cells expressing FLAG-hFFA4-mVenus were generated and characterised. Cells were visualised by epifluorescence microscopy: **(A)** Fluorescence image; **(B)** Bright field image; **(C)** Overlay image. **(D)** Membrane preparations of HEK293 parental cells and $G\alpha_q/G\alpha_{11}$ -null cells were immunoblotted using an anti- $G\alpha_{q/11}$ antiserum. Expression of $G\alpha_{q/11}$ was detected in the immunoblot (≈ 40 kDa) of HEK293 parental cells but was absent in $G\alpha_q/G\alpha_{11}$ knockout cells. **(E)** Cell lysates of HEK293 parental and $G\alpha_{q/11}$ -null cells constitutively expressing FLAG-hFFA4-mVenus were immunoblotted (section 2.5.5) using an anti-GFP antiserum. Antibodies to α -tubulin were co-added with the anti-GFP antiserum and provided a control for equal loading of the lanes of the SDS-PAGE. All pictures shown are representative of three independent experiments.

3.3 Generation and characterisation of double stable cell lines

To investigate the possible oligomerisation in hFFA1 and hFFA4, I have generated Flp-InTM T-RExTM-293 double stable cell line inducibly expressing hFFA1 or hFFA4 and constitutively expressing another FRET pair. This process is based on the Flp-InTM system to express one receptor constitutively while the expression of other receptor, delivered to the Flp-InTM locus, is controlled by the experimenter (Ward et al., 2013). Moreover, a cell-based model for FFA4-ligand screening was also developed by generating a double stable cell line inducibly expressing hFFA4 and constitutively expressing β -arrestin2-*Renilla* luciferase.

3.3.1 Flp-InTM T-RExTM HEK293 cell lines expressing both hFFA1-mVenus and hFFA1-GFP2

Flp-InTM T-RExTM 293 single stable cells inducibly expressing hFFA1-mVenus-HA was further transfected with pcDNA3/hFFA1-GFP2-HA. G-418 resistant clones were isolated and expanded. Following clonal selection, 12 clones were initially tested by fluorescence microscopy. Constitutive expression of the hFFA1-GFP2-HA expression was visualised, whereas treatment with doxycycline was required for turn-on of expression of hFFA1-mVenus-HA in these cells. Clones lacking the expression of hFFA1-GFP2-HA were disregarded (images are not shown). Clone 1, clone 3 and clone 8 were selected for characterisation by immunoblotting (section 2.5.5). Cells from these clones were treated with or without doxycycline and lysates prepared from these cells were immunoblotted with an anti-GFP antiserum. Anti-GFP antiserum could detect both forms of receptors (Figure 3-15). Among three clones, clone 1 was selected for further characterisation.

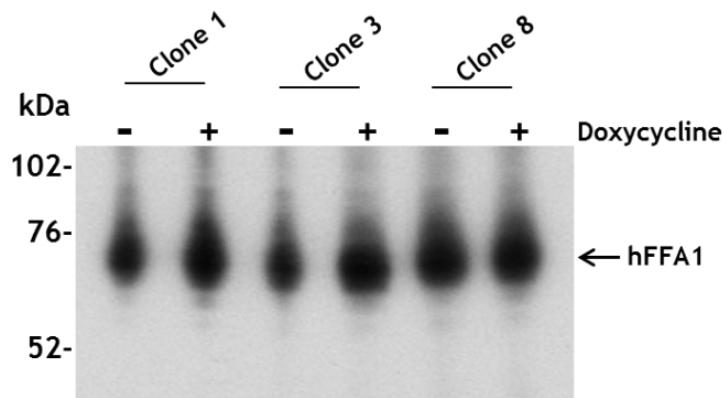


Figure 3-15. Immunoblotting clones expressing both hFFA1-mVenus-HA and hFFA1-GFP2-HA. Flp-In™ T-REx™ double stable cells inducibly expressing hFFA1-mVenus-HA and constitutively expressing hFFA1-GFP2-HA were plated on 6-well plates and treated with (+) or without (-) doxycycline for 18-24 hours. Lysates from these cells were immunoblotted (section 2.5.5) with an anti-GFP antiserum.

Cells of clone 1 were treated with or without doxycycline and visualised by epifluorescence microscopy (section 2.5.7). In doxycycline-treated cells inducible expression of hFFA1-mVenus-HA (Figure 3-16, A-i) and constitutive expression of hFFA1-GFP2-HA (Figure 3-16, A-ii) was seen. Overlay images showed homogenous expression of mVenus (Figure 3-16, A-iv) and GFP2 (Figure 3-16, A-v) tagged-hFFA1. Cells grown in the absence of doxycycline did not show expression of the hFFA1-mVenus-HA (Figure 3-16, B-i).

Regulated expression of hFFA1-mVenus-HA was assessed by immunoblotting (section 2.5.5) cell lysates prepared from cells treated with different concentration of doxycycline. Immunoblotting with an anti-GFP antiserum revealed expression of receptors as smear of polypeptides (\approx 50-70; Figure 3-16, C). The expression of hFFA1-mVenus-HA was dependent on the concentration of doxycycline used to induce expression of hFFA1-mVenus-HA (Figure 3-16, C). Immunoblots of the doxycycline-untreated cells was due to the constitutive expression of the hFFA1-GFP2-HA (Figure 3-16, C).

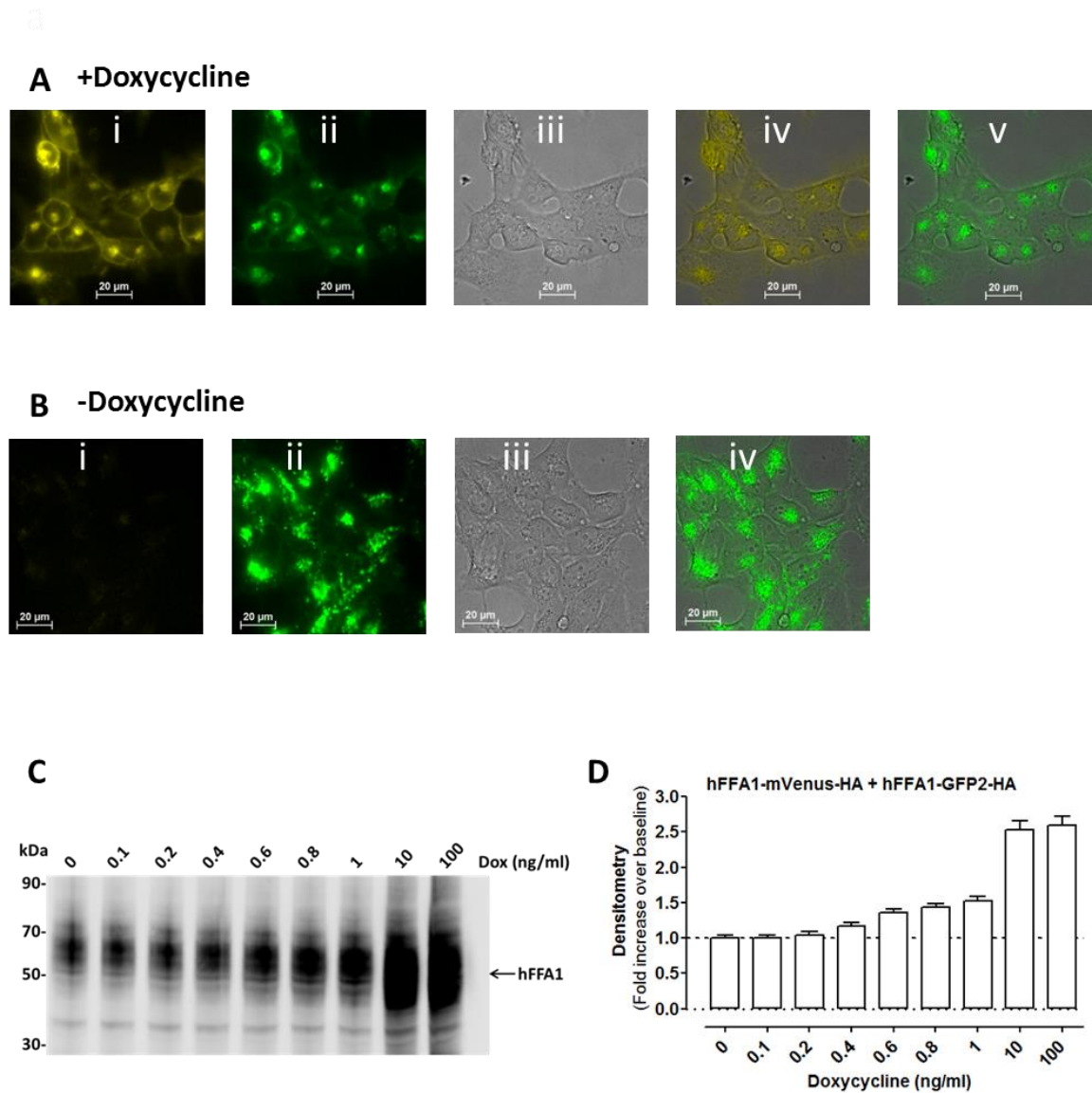


Figure 3-16. Characterisation of a Flp-In™ T-REx™ 233 cell line inducibly expressing hFFA1-mVenus-HA and constitutively expressing hFFA1-GFP2-HA. Flp-In™ T-REx™ 293 double stable cells inducibly expressing hFFA1-mVenus-HA and constitutively expressing hFFA1-GFP2-HA were generated and characterised. **(A)** Cells were treated with doxycycline and visualised by epifluorescence microscopy: (i) fluorescence images of mVenus; (ii) fluorescence images of GFP2; (iii) bright field images of cells; (iv) overlay image of mVenus; (v) overlay image of GFP2. **(B)** Cells were grown in the absence of doxycycline and visualised by microscopy: (i) fluorescence image of mVenus (no visible expression); (ii) fluorescence image of GFP2; (iii) bright field image of cells; (iv) overlay image of GFP2. All images shown are representative of three independent experiments. **(C)** Cells were treated with varying concentrations of doxycycline and lysates of cells were immunoblotted using an anti-GFP antiserum. **(D)** Densitometry of immunoblots. Data represent the mean \pm SEM of three independent experiments.

To examine the relative expression mVenus and GFP2-tagged forms hFFA1, fluorescence intensity was measured (section 2.5.20) with cells treated with varying concentrations of doxycycline. The mVenus fluorescence intensity was dependent on the concentration of doxycycline used to induce the expression of hFFA1-mVenus-HA (Figure 3-17, A). However, GFP2 fluorescence did not changed with doxycycline treatment (Figure 3-17, B).

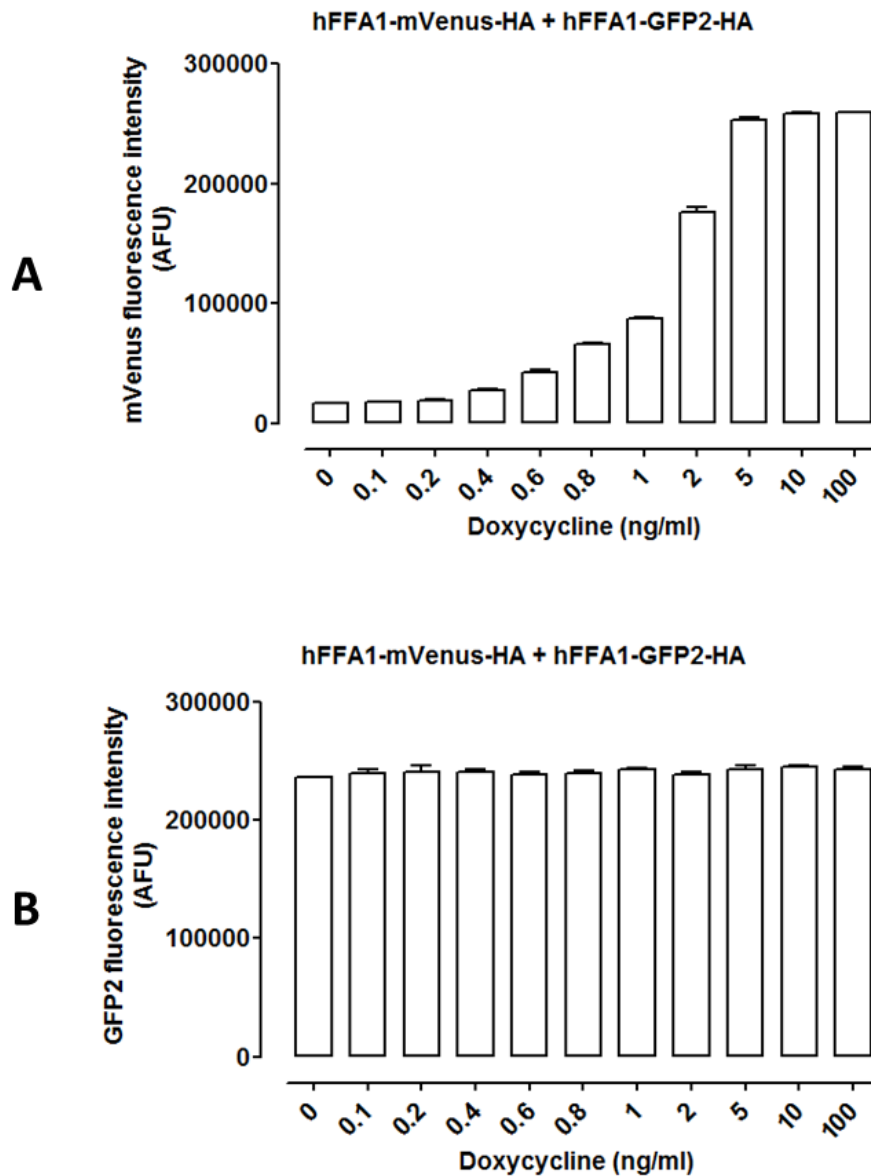


Figure 3-17. Relative expression of hFFA1-mVenus and hFFA1-GFP2 in a Flp-In™ T-REx™ 293 cell line. Flp-In™ T-REx™ 293 double stable cells inducibly expressing hFFA1-mVenus-HA and constitutively hFFA1-GFP2-HA were seeded into poly-*D*-lysine coated black 96-well plates. Cells were treated with varying concentrations of doxycycline for 18-24 hours. Fluorescence intensity (section 2.5.20) was measured for (A) mVenus (B) GFP2. Data represent the mean \pm SEM of three independent experiments.

3.3.2 Flp-In™ T-Rex™ HEK293 cell lines expressing hFFA4-mVenus and hFFA4-GFP2

Once a stable Flp-In™ T-Rex™ FLAG-hFFA4-mVenus cell line was established, a second plasmid pcDNA3/FLAG-hFFA4-GFP2 was introduced for the constitutive expression of FLAG-hFFA4-GFP2. Individual clone resistant to G-418 were collected and analysed for appropriate level of the receptor expression.

Preliminarily 20 clones were collected and characterised by epifluorescence microscopy (images are not shown). Clones unable to express FLAG-hFFA4-GFP2 were disregarded and 7 successful clones were identified for further characterisation. Cells were treated with or without doxycycline to induce receptor expression. Lysates from these cells were immunoblotted with an anti-GFP antiserum. The immunoblots revealed expression of receptors as a smear of polypeptides (≈ 52 -76 kDa; Figure 3-18). Clone 8 was selected for further characterisation.

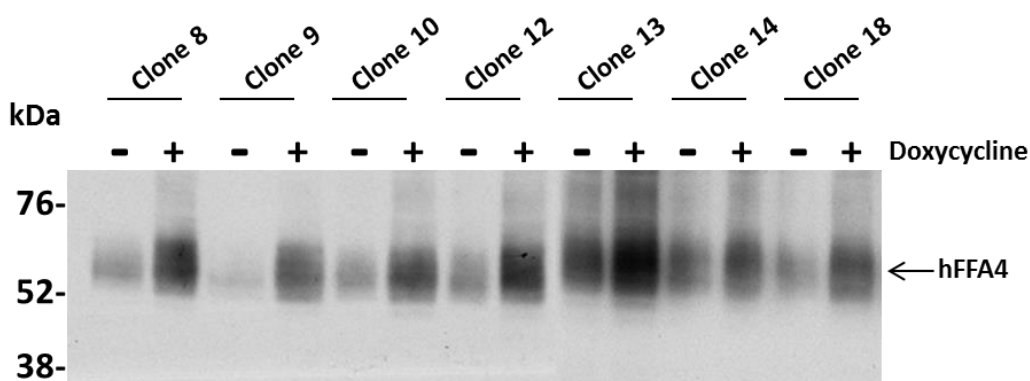


Figure 3-18. Selection of clones inducibly expressing FLAG-hFFA4-mVenus and constitutively expressing FLAG-hFFA4-GFP2. Selected clones of Flp-In™ T-Rex™ double stable cells inducibly expressing FLAG-hFFA4-mVenus and constitutively expressing FLAG-hFFA4-GFP2 were plated on 6-well plates and treated with (+) or without (-) doxycycline for 18-24 hours. Lysates from these cells were immunoblotted (section 2.5.5) using an anti-GFP antiserum.

Cells of clone 8 were treated with or without doxycycline and visualised by epifluorescence microscopy (section 2.5.7). Expression of mVenus and GFP2-tagged form of hFFA4 were detected (Figure 3-19, A-i-ii). Expression of receptors was largely at the cell surface; however, some intracellular signal was also noticed. Overlay images confirmed homogenous expression of FLAG-hFFA4-

mVenus (Figure 3-19, A-iv) and FLAG-hFFA4-GFP2 (Figure 3-19, A-v). No visible expression of mVenus was observed in cells grown in the absence of doxycycline (Figure 3-19, B-i). The expression of FLAG-hFFA4-GFP2 was not dependent on doxycycline treatment (Figure 3-19, B-ii) and the expression was homogenous (Figure 3-19, B-vi).

The regulated expression of FLAG-hFFA4-mVenus was investigated in cells treated with varying concentrations of doxycycline. Lysates of these cells were immunoblotted with an anti-GFP antiserum. Expression of receptors was detected as smear of proteins (≈ 52 -76 kDa) in the immunoblots (Figure 3-19, C). Anti-GFP2 antiserum could identify both mVenus and GFP2 tagged receptors. The expression of FLAG-hFFA4-mVenus increased with the increase of concentration of doxycycline (Figure 3-19, C-D).

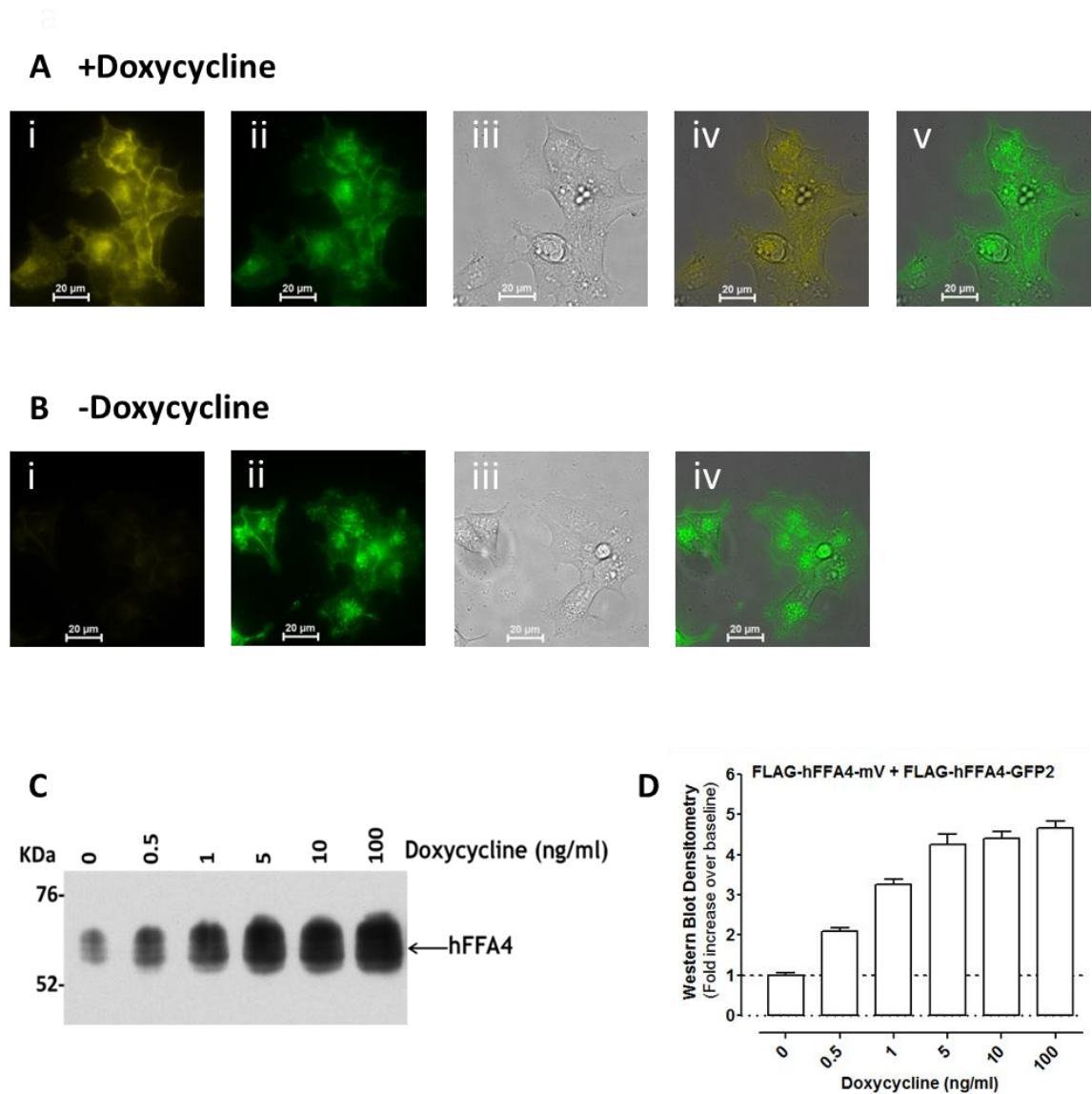


Figure 3-19. Characterisation of a Flp-In™ T-REx™ 233 cell line inducibly expressing FLAG-hFFA4-mVenus and constitutively expressing FLAG-hFFA4-GFP2. Flp-In™ T-REx™ 293 double stable cells inducibly expressing FLAG-hFFA4-mVenus and constitutively expressing FLAG-hFFA4-GFP2 were characterised. **(A)** Cells were treated with doxycycline and visualised by microscopy: **(i)** fluorescence images of mVenus; **(ii)** fluorescence images of GFP2; **(iii)** bright field images of cells; **(iv)** overlay images of mVenus; **(v)** overlay image of GFP2. **(B)** Cells grown in the absence of doxycycline and visualised by microscopy: **(i)** fluorescence images of mVenus (no visible expression); **(ii)** fluorescence images of GFP2; **(iii)** bright field images of cells; **(iv)** overlay images of GFP2. All microscopic images shown are representative of three independent experiments. **(C)** Cells were treated with varying concentrations of doxycycline and lysates of cells were immunoblotted (section 2.5.5) using an anti-GFP antiserum. **(D)** Densitometry (section 2.5.6) of immunoblots. Data represent the mean \pm SEM of three independent experiments.

Fluorescence of mVenus and GFP2 were measured to assess the relative expression of FLAG-hFFA4-mVenus and FLAG-hFFA4-GFP2. Cells were treated with varying concentrations of doxycycline for 18-24 hours to allow expression of FLAG-hFFA4-mVenus. A doxycycline-concentration dependent increase of mVenus fluorescence was seen in these cells (Figure 3-20, A). However doxycycline-treatment did not have any effect on the fluorescence of GFP2 (Figure 3-20, B).

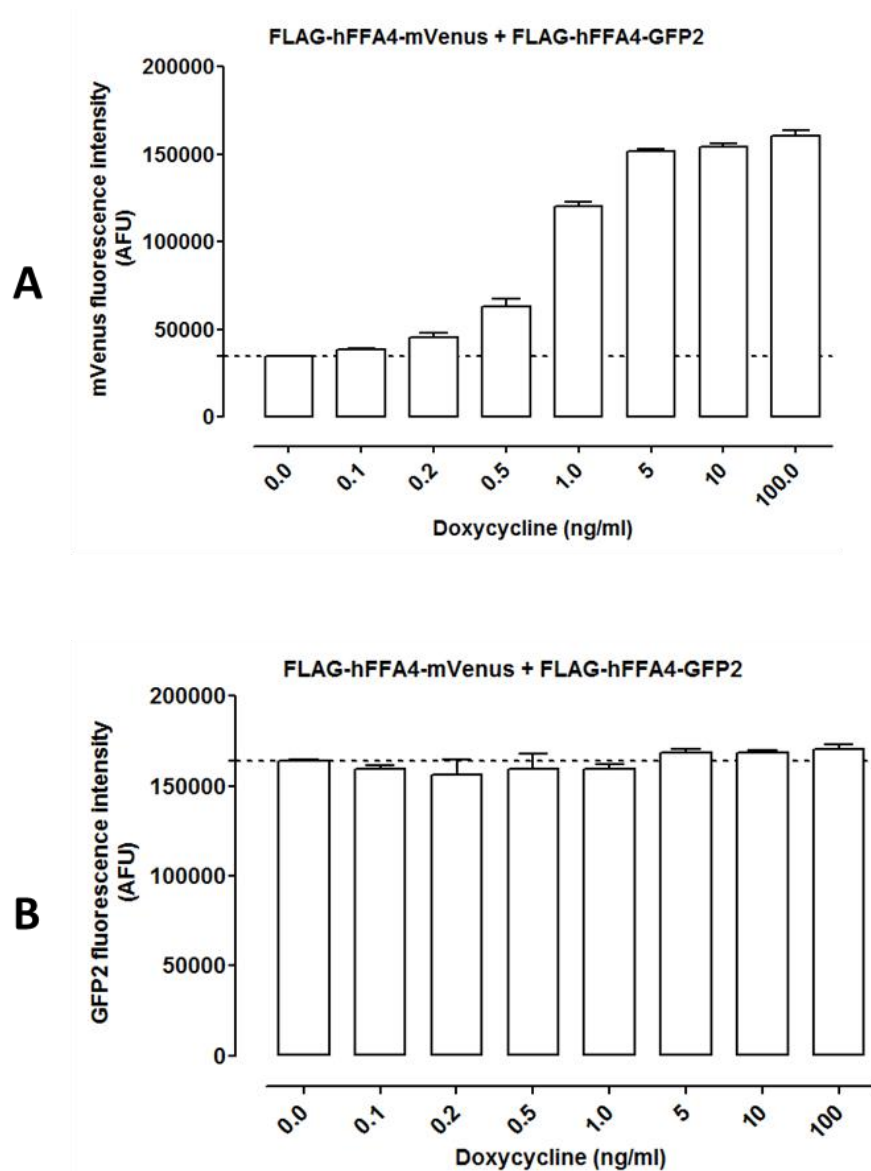


Figure 3-20. Relative expression of FLAG-hFFA4-mVenus and FLAG-hFFA4-GFP2 in a Flp-In™ T-REx™ 293 cell line. Flp-In™ T-REx™ 293 double stable cells able to express inducibly FLAG-hFFA4-mVenus and constitutively FLAG-hFFA4-GFP2 were seeded into poly-*D*-lysine coated black 96-well plates. Cells were treated with varying concentrations of doxycycline and fluorescence intensities (section 2.5.20) were measured for (A) mVenus and (B) GFP2. Data represent the mean \pm SEM of three independent experiments.

3.3.3 Flp-In™ T-Rex™ HEK293 cell lines expressing both hFFA4-GFP2 and hFFA1-mVenus

Flp-In™ T-Rex™ 293 single stable cells able to express inducibly FLAG-hFFA4-GFP2 was further transfected with a pcDNA3/hFFA1-mVenus-HA. Positive clones, i.e., those resistant to the antibiotic G-418 were individually collected and expanded. Following clonal selection, 12 clones were initially tested by epifluorescence microscopy for construct expression (images are not shown). Four clones were identified and further characterised by immunoblotting with an anti-GFP antiserum. The immunoblots revealed expression of receptors as a smear of polypeptides (\approx 52-76 kDa; Figure 3-21). Anti-GFP antiserum identified both mVenus and GFP2-tagged receptors (Figure 3-21). Clone 1 was selected for further characterisation.

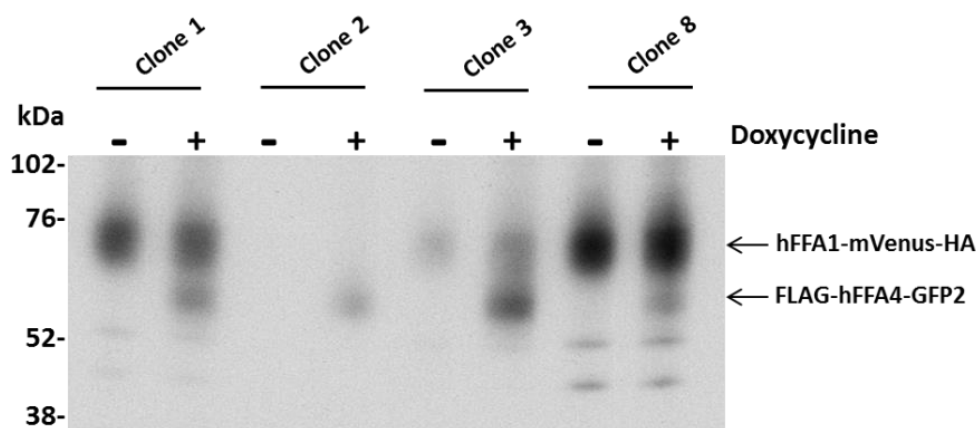


Figure 3-21. Selection of clones inducibly expressing FLAG-hFFA4-GFP2 and constitutively expressing hFFA1-mVenus-HA. Clones of Flp-In™ T-Rex™ 293 double stable cells inducibly expressing FLAG-hFFA4-GFP2 and constitutively expressing hFFA1-mVenus-HA were treated with or without doxycycline for 18-24 hours. Lysates of these cells were immunoblotted (section 2.5.5) with an anti-GFP antiserum.

Cells of clone 1 were treated with or without doxycycline and visualised by epifluorescence microscopy. Homogenous expression of both FLAG-hFFA4-GFP2 and hFFA1-mVenus-HA were revealed in the doxycycline-treated cells (Figure 3-22, A). No visible expression was noticed in cells cultured without doxycycline (Figure 3-22, B). However constitutive expression of hFFA1-mVenus-HA was noticed in the doxycycline-untreated cells (Figure 3-22, B).

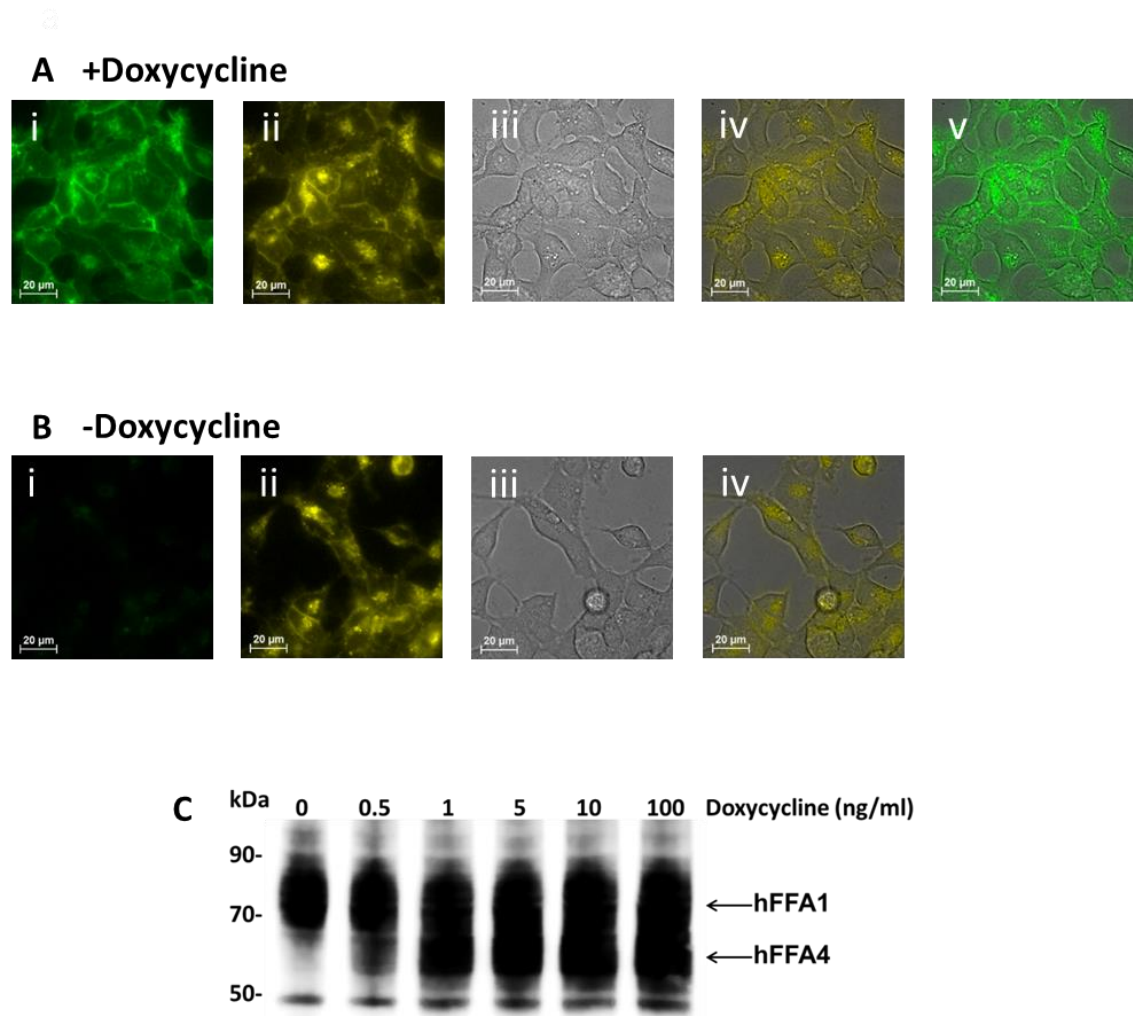


Figure 3-22. Characterisation of a Flp-In™ T-REx™ 233 cell line inducibly expressing FLAG-hFFA4-GFP2 and constitutively expressing hFFA1-mVenus-HA.

Flp-In™ T-REx™ 293 double stable cells inducibly expressing FLAG-hFFA4-GFP2 and constitutively expressing hFFA1-mVenus-HA were characterised. **(A)** Cells were treated with (+) or without (-) doxycycline and visualised by epifluorescence microscopy: **(i)** fluorescence images of GFP2, **(ii)** fluorescence images of mVenus, **(iii)** bright field images of cells, **(iv)** overlay image of mVenus, **(v)** overlay images of GFP2. **(B)** Epifluorescence images in cells cultured in the absence of doxycycline: **(i)** fluorescence images of GFP2 (no visible expression), **(ii)** fluorescence images of mVenus, **(iii)** bright field images of cells, **(iv)** overlay image of mVenus. All images shown are representative of three independent experiments. **(C)** Cells were treated with varying concentrations of doxycycline and lysates from these cells were immunoblotted (section 2.5.5) using an anti-GFP antiserum.

The regulated expression of FLAG-hFFA4-GFP2 was assessed in cells treated with varying concentrations of doxycycline. Immunoblotting of lysates from these cells with an anti-GFP antiserum revealed expression of both receptors as smear of polypeptides (\approx 52-76 kDa) in the immunoblots (Figure 3-22, C). The expression of FLAG-hFFA4-mVenus increased with the increase of concentration of doxycycline (Figure 3-22, C). Both mVenus and GFP2-tagged receptors were identified by anti-GFP antiserum.

Fluorescence measurement of GFP2 and mVenus was performed to investigate the relative expression receptors. GFP2 fluorescence was dependent on the concentration of doxycycline used to induce cells (Figure 3-23, A). Surprisingly the mVenus fluorescence decreased in a doxycycline-concentration dependent manner (Figure 3-23, B).

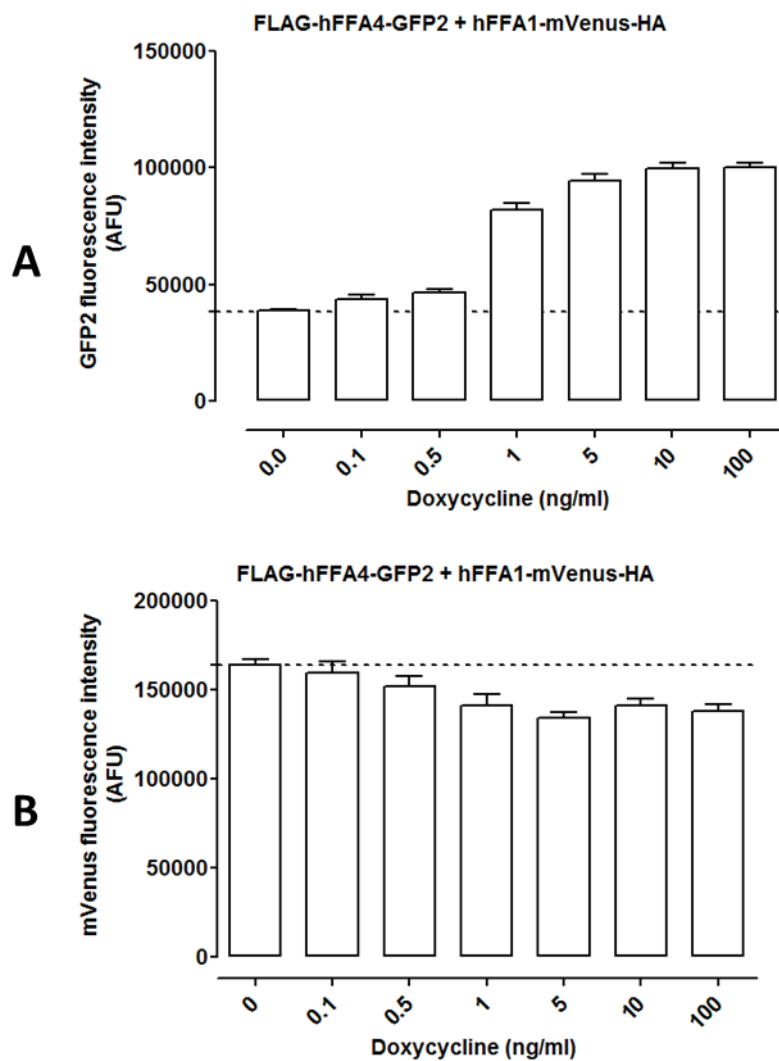


Figure 3-23. Relative expression of FLAG-hFFA4-GFP2 and hFFA1-mVenus-HA in a Flp-In™ T-REx™ 293 cell line. Flp-In™ T-REx™ 293 double stable cells inducibly expressing FLAG-hFFA4-GFP2 and constitutively expressing hFFA1-mVenus-HA were seeded into poly-*D*-lysine coated black 96-well plates. Expression of FLAG-hFFA4-GFP2 was induced by varying concentrations of doxycycline for 18-24 hours. Fluorescence intensity (section 2.5.20) was measured for (A) GFP2 and (B) mVenus. Data represent the mean \pm SEM of three independent experiments.

The effect of doxycycline on the constitutive expression of hFFA1 was investigated by immunoblotting cells treated with varying concentrations of doxycycline. Immunoblotting with an anti-HA antibody selectively identified the expression of hFFA1-mVenus-HA as a smear of proteins (≈ 70 ; Figure 3-24, A). The reduction of the expression of hFFA1-mVenus-HA was doxycycline-concentration dependent manner (Figure 3-24, A-B).

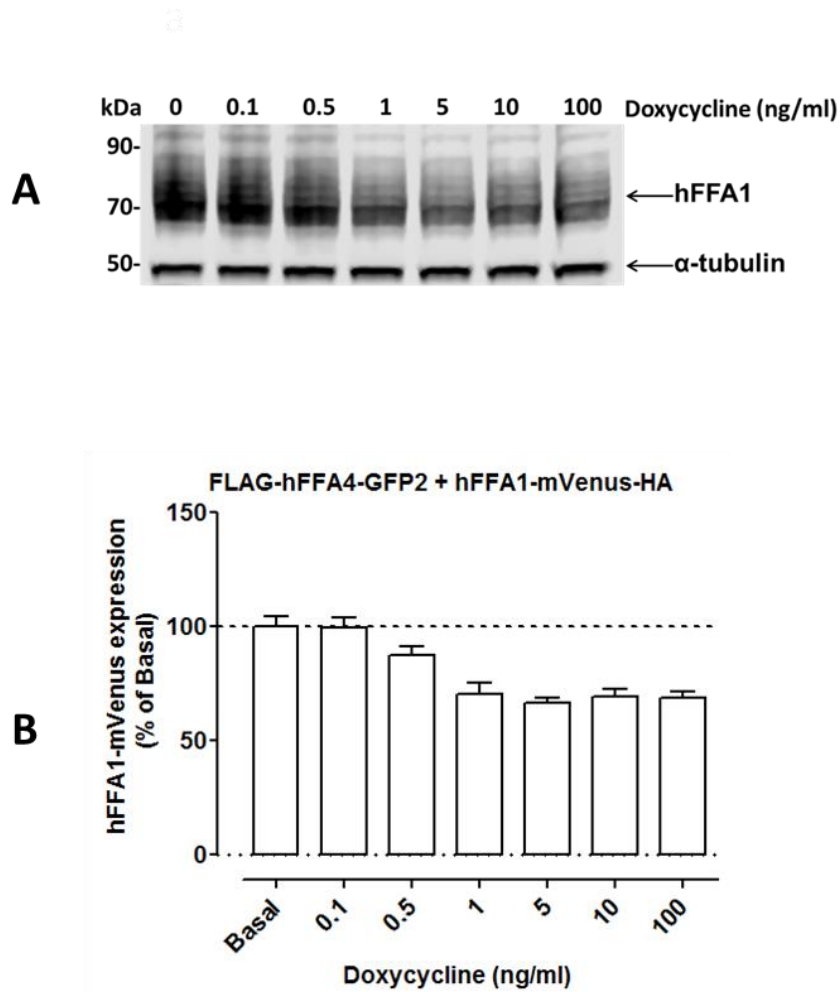


Figure 3-24. Effect of doxycycline on the constitutive expression of hFFA1. Flp-In™ T-REx™ 293 double stable cells inducibly expressing FLAG-hFFA4-GFP2 and constitutively expressing hFFA1-mVenus-HA were treated with varying concentrations of doxycycline. Cells grown in the absence of doxycycline were taken as control (basal expression of hFFA1). **(A)** Lysates of cells were immunoblotted using an anti-HA antibodies. **(B)** Densitometry (section 2.5.6) of immunoblots. Data represent the mean \pm SEM of three independent experiments.

3.3.4 A cell-based model for FFA4-ligand screening

Ligand binding to FFA4 activates G proteins and arrestins, which are involved in differential signalling pathways (Milligan et al., 2017). Because functionally selective or biased ligands activate one of these two pathways more effectively than the other, they may be useful for drug development for certain disease states (Violin et al., 2014). The identification of such ligands requires robust drug screening assays for both G protein and arrestin activity. A Flp-In™ T-Rex™ 293 double stable cell line able to express inducibly FLAG-hFFA4-eYFP and constitutively expressing β -arrestin2-*Renilla* luciferase was generated by Dr. Elisa Alvarez-Curto. I characterised this cell line with the aim to develop a cell-based model that allows sensitive detection of ligand-mediated activation of FFA4 via the recruitment of β -arrestin2 to the receptor.

The inducible expression of FLAG-hFFA4-eYFP was characterised using epifluorescence microscopy (section 2.5.7) in cells treated with or without doxycycline. Fluorescence images indicated expression of eYFP-tagged hFFA4 predominantly at the cell surface (Figure 3-25, A-i). Overlay images (Figure 3-25, A-iii) showed homogenous expression of receptors. Cells cultured in the absence of doxycycline did not show any visible expression of hFFA4-eYFP (Figure 3-25, A-iv).

The expression of hFFA4-eYFP and β -arrestin2-*Renilla* luciferase was detected by immunoblotting (section 2.5.5). Lysates prepared from cells treated with varying concentrations of doxycycline were immunoblotted with an anti-GFP antiserum. The expression of FLAG-hFFA4-eYFP was dependent on the concentration of doxycycline used to induce cells (Figure 3-25, B). Cells lysates treated with anti- β -arrestin2 antibodies revealed expression of β -arrestin2-*Renilla* luciferase no-matter the treatment of doxycycline (Figure 3-25, C).

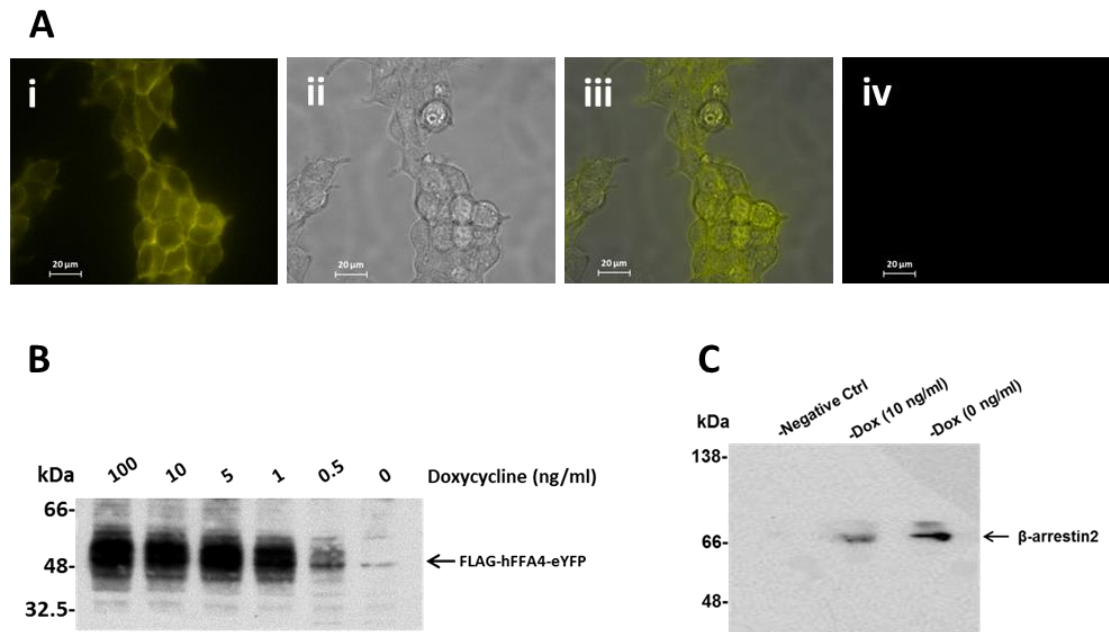


Figure 3-25. Characterisation of expression of FLAG-hFFA4-eYFP and β -arrestin2-*Renilla* luciferase in Flp-In™ T-Rex™ 293 double stable cells. Flp-In™ T-Rex™ 293 double stable cells were characterised to investigate the inducible expression of FLAG-hFFA4-eYFP and constitutive expression of β -arrestin2-*Renilla* luciferase. **(A)** Cells were treated with or without doxycycline and visualised by epifluorescence microscopy: **(i)** fluorescence image of the expression of FLAG-hFFA4-eYFP; **(ii)** bright field image of doxycycline-treated cells; **(iii)** overlay image of eYFP; **(iv)** fluorescence image of cells grown in the absence of doxycycline. All microscopic images shown are representative of three independent experiments. **(B)** Receptor expression was induced by varying concentrations of doxycycline and lysates of cells were immunoblotted using an anti-GFP antiserum. **(C)** Cells were treated with or without doxycycline and immunoblotted with an anti- β -arrestin2 goat polyclonal antiserum. Flp-In™ T-Rex™ 293 single stable cells inducibly expressing FLAG-hFFA4-eYFP were treated with doxycycline and used as negative control.

The FFA4-agonist TUG-891 produced recruitment of β -arrestin-2-*Renilla* luciferase. BRET measurements revealed this to be rapid and ligand concentration-dependent (Figure 3-26, A). The BRET efficacy was dependent on the concentration of doxycycline use to induce cells for the expression of FLAG-hFFA4-eYFP (Figure 3-26, A). No BRET was seen in cells grown in the absence of doxycycline. This cell line was fully functional in the elevation of intracellular calcium levels upon agonist treatment. Cells were treated with varying concentrations of doxycycline and challenged with varying concentrations of TUG-891. There was an agonist-concentration dependent increase of intracellular calcium (Figure 3-26, B). However, doxycycline-untreated cells did not show any response.

Agonist promoted internalisation of hFFA4 was assessed in this cell line. Expression of FLAG-hFFA4-eYFP was induced by doxycycline. Cells were challenged with varying concentrations of TUG-891 for 45 minutes and internalisation of eYFP spots were measured using a Cellomics ArrayScan II (section 2.5.12). FFA4 internalised in an agonist-concentration dependent fashion (Figure 3-26, C).

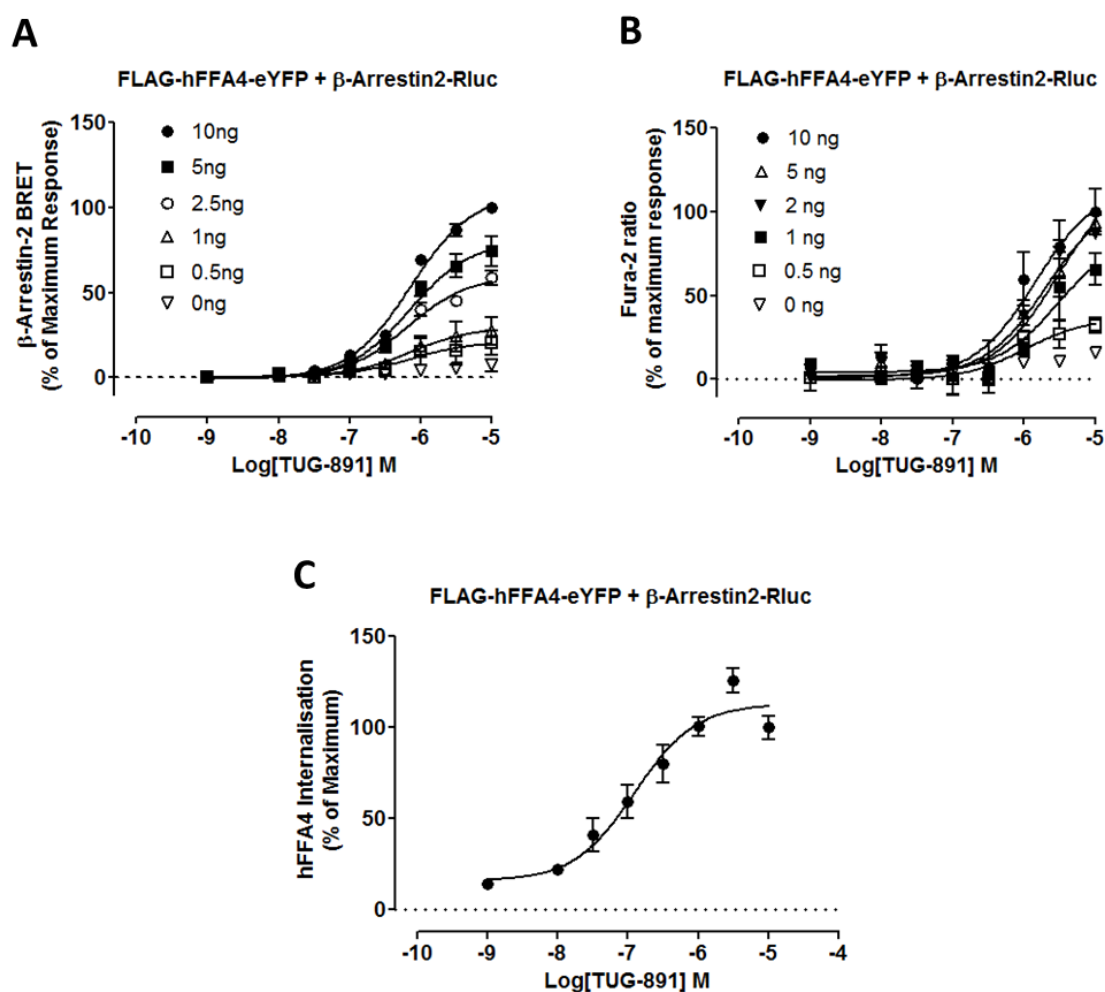


Figure 3-26. Functional characterisation of a cell-based model for FFA4-ligand screening. Flp-In™ T-Rex™ 293 double stable cells able to express inducibly FLAG-hFFA4-eYFP and constitutively β -arrestin2-*Renilla* luciferase were characterised for their functional signalling upon agonist treatment. **(A)** Cells were seeded (80,000 cells /well) into poly-*D*-lysine coated white 96-well plates and receptor expression was induced by varying concentrations of doxycycline. BRET measurement in cells treated with varying concentrations of TUG-891. Cells were seeded (70,000 cells/well) into poly-*D*-lysine coated black clear-bottom 96-well plates. **(A)** Cells were treated with varying concentrations of doxycycline and challenged with varying concentrations of TUG-891. **(C)** Cells were treated with varying concentrations of TUG-891 for 45 minutes and internalisation of hFFA4-eYFP was measured using an ArrayScan II plate reader (section 2.6.8). Data represent the mean \pm SEM of three independent experiments.

3.4 Discussion

Creation of cell lines expressing a receptor-protein facilitates the investigation of receptor pharmacology as well as drug discovery (Chakraborty et al., 2015). Establishing stable cell lines requires substantial time and effort in comparison to transient transfection processes. Although a transient expression system allows protein production within a few days after introduction of the expression plasmid, a stable cell allows expression of the target protein uniformly and potentially indefinitely. Moreover cell production is reproducible and can be scaled up easily (Ward et al., 2011b; Andrell and Tate, 2013). The present experiments have characterised the expression and function of hFFA1 and hFFA4 in different cell lines. All cell lines were characterised utilising well characterised approaches, including epifluorescence microscopy, fluorescence intensity measurements, immunoblotting and functional signalling.

Flp-In™ T-Rex™ 293 is a human embryonic kidney cell line that contains a single integrated FRT site and is able to stably express the tetracycline repressor protein. Addition of tetracycline or doxycycline to the tissue culture medium releases the tetracycline repressor protein and enables the translation of the receptor of interest (Ward et al., 2011a; Koener and Hermans, 2011). The inducible expression of either hFFA1 or hFFA4 in Flp-In™ T-Rex™ 293 cells was homogeneous and doxycycline-concentration dependent manner (Figure 3-1; Figure 3-3; Figure 3-8; Figure 3-10). Epitope tags and/or fluorophore tags allow characterisation of the expression of receptors and minimises the need for generating protein-specific antibodies at the early stages of analysis (Ward et al., 2011a). Epifluorescence microscopic images of mVenus or GFP2 fluorescence effectively identified the expression of the desired receptor constructs in these cell lines. Moreover, immunoblotting with an anti-GFP antiserum also successfully identified either mVenus or GFP2 tagged receptors.

Making cell lines constitutively expressing hFFA1 or hFFA4 required a lengthy process of characterisation. As integration of pcDNA3 into the host cell genome is a random process, the expression levels from these are dependent on where the cDNA is integrated (Ward et al., 2013; Longo et al., 2013). Selection of clones was required to identify cells homogeneously expressing receptors under prolonged culture. The constitutive expression of hFFA1 or hFFA4 was

homogenous in HEK293 parental (Figure 3-5; Figure 3-12), β -arrestin1/2-null (Figure 3-6; Figure 3-13) and $G\alpha_{q/11}$ -null cells (Figure 3-7; Figure 3-14).

In the recent past, a considerable body of evidence has accumulated to indicate that GPCRs can exist as dimeric or oligomeric species (Milligan, 2013; Milligan, 2009; Milligan, 2006a). Co-expression of receptors with differentially epitope-tagged forms or attachment of fluorescence resonance energy transfer (FRET)-competent pairs to the receptor allows investigation of possible oligomerisation (Ward et al., 2013). The co-expression of mVenus and GFP2 tagged hFFA1 or hFFA4 or both receptors characterised in this chapter showed effective and regulated co-expression of potential FRET pairs.

Moreover, I have characterised a cell-based model that will allow inducible expression of FLAG-hFFA4-eYFP and constitutive expression of β -arrestin2-*Renilla* luciferase. This cell line is currently being used to screen libraries of compounds to identify novel agonists, and also antagonists, of FFA4 to assess the importance and potential therapeutic utility in targeting this receptor in conditions including metabolic disease, obesity and inflammation.

4 Characterisation of pharmacological ligands

Since the deorphanisation of fatty acid receptors, there has been a continuing effort to develop ligands to explore the pharmacology and therapeutic potential of these receptors. Although FFA1 and FFA4 receptors are not structurally related, they share activity with the same group of free fatty acids (Milligan et al., 2015). Due to the physiological relevance of FFA1 and FFA4 in modulating a number of metabolic processes, there have been significant efforts toward development of synthetic molecules (Moniri, 2016). In an academic context, the University of Southern Denmark has developed a number of synthetic ligands reported to have moderate to high potency and selectivity to FFA1 or FFA4 (Christiansen et al., 2012, 2013a; Hudson et al., 2013b; Azevedo et al., 2016). To explore the pharmacology and desensitisation of these receptors, I have examined a number of these pharmacological ligands (section 2.1.5) using different molecular techniques.

4.1 Ligands acting at FFA4

Following deorphanisation of the fatty acid receptors, a marked overlap in activation of FFA1 and FFA4 receptors by fatty acid ligands has been reported. For receptor pharmacology and drug discovery, there is a need to identify and develop selective ligands for these fatty acid receptors (Milligan et al., 2015).

When I started my project in late 2013, few ligands were available for exploring the pharmacology of FFA4. NCG21 was reported to be a potent agonist of FFA4 (Suzuki et al., 2008), however in other studies from our group this compound displayed modest potency and very limited selectivity (Shimpukade et al., 2012; Hudson et al., 2013b). Shimpukade et al. (2012) initially reported TUG-891 as a 100-fold selective agonist for FFA4 over FFA1. Hudson et al (2013b) characterised TUG-891 in a number of model cell systems and reported it to be a potent and selective agonist for hFFA4. However, TUG-891 showed only limited selectivity over mouse FFA1 which has limited its use *in vivo* in this species. Recently, Azevedo et al. (2016) have reported TUG-1197 as a full agonist of FFA4 and that it is completely selective for FFA4 over FFA1. Sparks et al (2014) initially reported compound 39 (commercially available as AH-7614, Torcis Bioscience) as a potent and selective antagonist of FFA4, however they did not

characterise the nature of antagonism produced by this compound. Our medicinal chemistry team synthesised this compound and have designated it TUG-1275 (section 2.1.5). I began this work by characterizing these ligands in heterologous cell systems able to express hFFA1 or hFFA4.

4.1.1 Intracellular calcium level

Flp-InTM T-RExTM 293 inducible cells stably harbouring the relevant mVenus-tagged receptor at the T-RExTM genomic locus were employed to explore the capacity of FFA4-ligands to elevate intracellular calcium in cell populations (section 2.5.17).

Expression of the receptor was induced by addition of the antibiotic doxycycline (100 ng/ml) for 18-24 hours. Cells were then incubated for 45 minutes with the calcium-sensitive dye Fura-2 AM and then challenged with varying concentrations of agonists. Both TUG-891 and TUG-1197 produced a concentration-dependent increase in intracellular calcium (Figure 4-1). TUG-891 and TUG-1197 displayed similar potency ($pEC_{50} = 6.47 \pm 0.22$ for TUG-891 and 6.59 ± 0.24 for TUG-1197). However, TUG-1197 showed significantly ($p < 0.05$) higher efficacy compared to TUG-891.

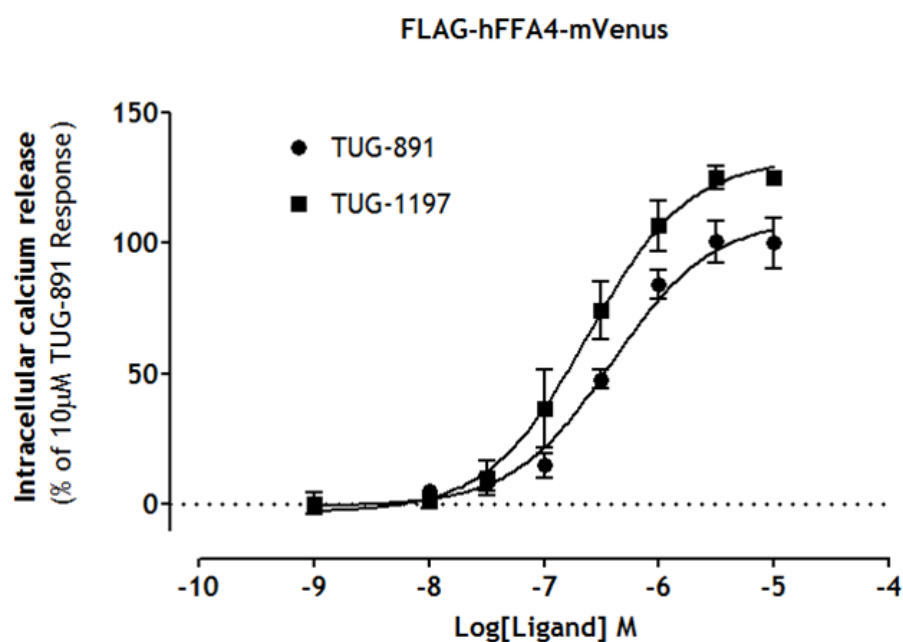


Figure 4-1. TUG-891 and TUG-1197 produce elevation of intracellular calcium via hFFA4. Flp-In™ T-REx™ 293 cells able to express FLAG-hFFA4-mVenus were seeded (75,000 cells /well) into poly-D-lysine coated black clear-bottom 96-well plates. Expression of hFFA4 was induced by the antibiotic doxycycline (100 ng/ml) for 18-24 hours. Cells were labelled for 45 minutes with the calcium-sensitive dye Fura-2 AM and cells were then exposed to varying concentrations of TUG-891 or TUG-1197. Mobilisation of intracellular calcium was recorded in a FlexStation plate reader (section 2.5.17). Efficacy was normalized as percentage of 10 μ M TUG-891 maximum response. Data represent the mean \pm SEM of three independent experiments.

Due to the marked overlap in the activation of FFA1 and FFA4 by both endogenous fatty acids and a number of synthetic ligands, it was of interest to see if either TUG-891 or TUG-1197 could also promote elevation of intracellular calcium through activation of hFFA1. A selective and potent ligand of hFFA1 (TUG-905) (Christiansen et al., 2012) was also employed in these experiments. Flp-In™ T-REx™ 293 cells able to express hFFA1-mVenus-HA upon addition of doxycycline was employed. TUG-1197 showed no activity at hFFA1 up to 10 μ M whilst TUG-891 produced a limited effect at 10 μ M (Figure 4-2). By contrast, TUG-905 potently activated hFFA1 ($pEC_{50} = 7.41 \pm 0.13$). TUG-1197 showed full selectivity for hFFA4 over hFFA1 in capacity to elevate intracellular calcium levels (Figure 4-2).

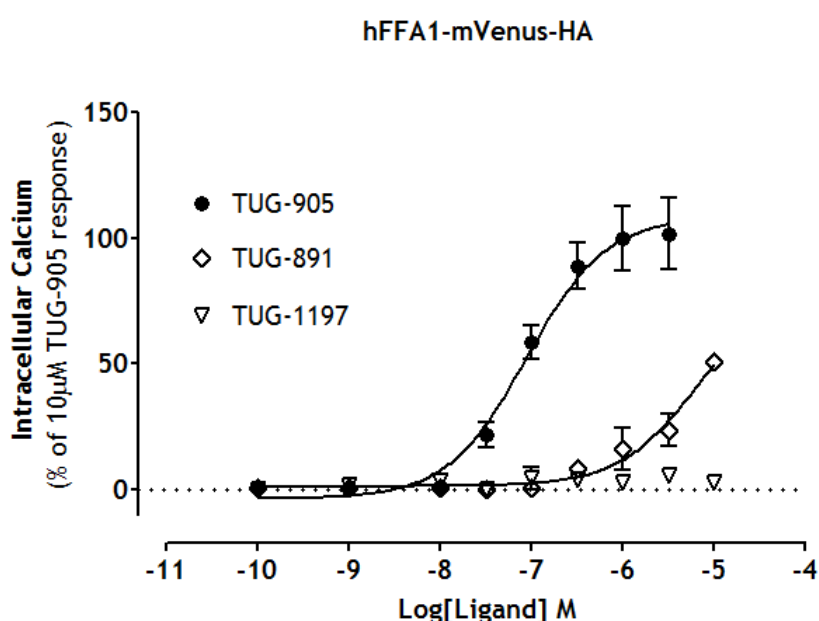


Figure 4-2. TUG-891 but not TUG-1197 displays low potency mediated activation of hFFA1. Flp-In™ T-REx™ 293 cells able to express hFFA1-mVenus-HA were seeded (75,000 cells /well) into poly-D-lysine coated black clear-bottom 96-well plates. Expression of hFFA1 was induced by the antibiotic doxycycline (100 ng/ml) for 18-24 hours. Cells were labelled with the calcium-sensitive dye Fura-2 AM and then challenged with varying concentrations of a FFA1 selective agonist (TUG-905) and either TUG-891 or TUG-1197. Mobilisation of intracellular calcium was recorded in a FlexStation plate reader (section 2.5.17). Efficacy was normalized as percentage of maximum response of the control ligand TUG-905. Data represent the mean \pm SEM of three independent experiments.

4.1.2 β -arrestin2 recruitment

Apart from activation of G-proteins, agonist promoted association of β -arrestin2 with receptors has been shown to promote novel signalling pathways (Luttrell and Lefkowitz, 2002) as well as receptor desensitisation (Thomsen et al., 2016). Measurement of β -arrestin2 recruitment to FFA4 employing bioluminescence resonance energy transfer (BRET) is a popular way of screening for FFA4 active ligands (Milligan et al., 2015). This technology is based on the principle of non-radiative energy transfer occurring between the electromagnetic dipoles of a luminescent energy donor (e.g. *Renilla* luciferase) and a fluorescent energy acceptor (e.g. eYFP) (Milligan, 2004). Given close proximity occurring between these polypeptides and oxidation of the luciferase substrate coelenterazine h, energy is emitted and is transferred from donor to acceptor and subsequently re-emitted at a characteristic wavelength, which can be quantified (section 2.5.13).

The BRET-based β -arrestin2 recruitment assay employed herein has previously been utilized for FFA4 (Hudson et al., 2013b). Flp-InTM T-RExTM 293 cell line able to inducibly express FLAG-hFFA4-eYFP and constitutively expressing β -arrestin2-*Renilla* luciferase (section 3.3.4) was used. Agonist-induced β -arrestin2 recruitment to the receptor was quantified following incubation with varying concentrations of agonist in 96-well plate format. Prior to commencement of the BRET assay, receptor expression assessed as eYFP fluorescence was measured to check doxycycline-induced expression of eYFP-tagged hFFA4. Subsequently, agonist-induced β -arrestin2 BRET was measured following a 5-minute agonist incubation at 37 °C (Shimpukade et al., 2012; Hudson et al., 2013b). Both TUG-891 and TUG-1197 produced β -arrestin2 recruitment in a concentration-dependent manner (Figure 4-3). TUG-891 and TUG-1197 displayed similar potency (pEC_{50} 6.55 ± 0.12 for TUG-891 and 6.74 ± 0.10 for TUG-1197) in this assay. TUG-1197 showed higher efficacy compared to TUG-891. However, the efficacy difference was not statistically significant ($p > 0.05$).

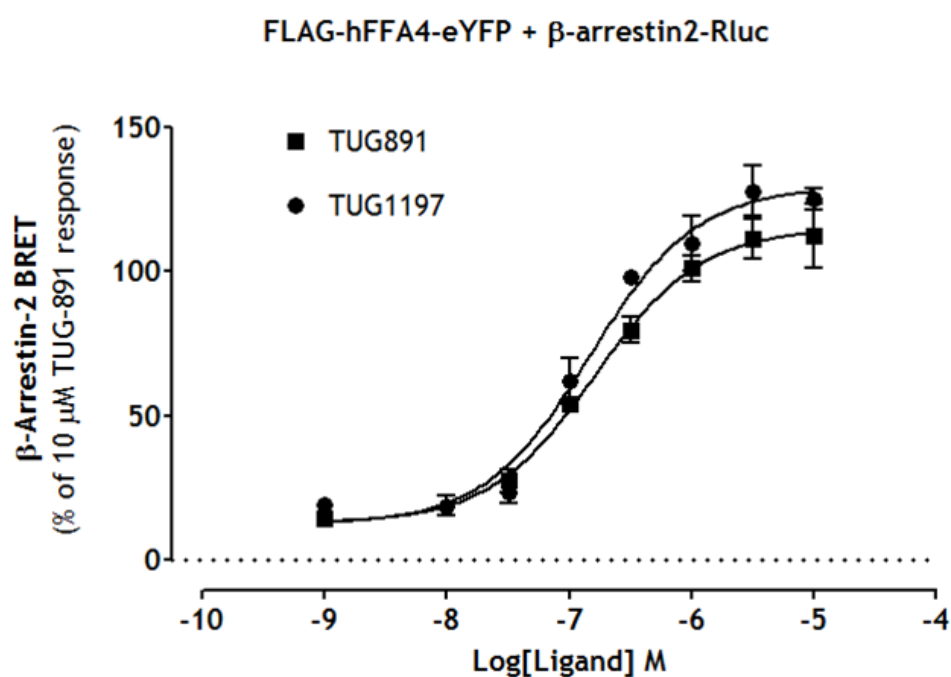


Figure 4-3. β -arrestin2 recruitment to hFFA4 induced by agonists. Flp-In™ T-REx™ 293 cells able to express inducibly FLAG-hFFA4-eYFP and constitutively expressing β -arrestin2-*Renilla* luciferase were seeded (80,000 cells /well) into poly-D-lysine coated white 96-well plates. Receptor expression was induced by the antibiotic doxycycline (100 ng/ml) for 18-24 hours. BRET in response to TUG-891 and TUG-1197 was measured. Data represent the mean \pm SEM of three independent experiments.

4.2 TUG-1275 is a FFA4 antagonist

Flp-InTM T-RExTM 293 cells able to express FLAG-hFFA4-mVenus or hFFA1-mVenus-HA were also used to characterise the pharmacology of TUG-1275.

4.2.1 TUG-1275 blocks agonist-promoted phosphorylation of hFFA4

Receptor phosphorylation is a rapidly induced covalent modification regulating GPCR signalling (Luttrell and Lefkowitz, 2002). It has been previously reported that agonists promote rapid phosphorylation of hFFA4 (Hudson et al., 2013b; Burns and Moniri, 2010), so it was of interest to see whether TUG-1275, which as ‘compound 39’ (Sparks et al., 2014) has been reported as the first FFA4 antagonist, could block such agonist-induced phosphorylation.

Flp-InTM T-RExTM 293 cells able to express FLAG-hFFA4-mVenus were challenged with either TUG-891 or TUG-1197. Within 10 minutes both agonists caused robust phosphorylation of the receptor which was detected in immunoblots (Figure 4-4) using a phosphorylation-state specific antiserum, raised against a peptide of hFFA4-containing phospho-Thr³⁴⁷ and phospho-Ser³⁵⁰ (Butcher et al., 2014). TUG-1275 was able to abolish phosphorylation induced by either agonist.

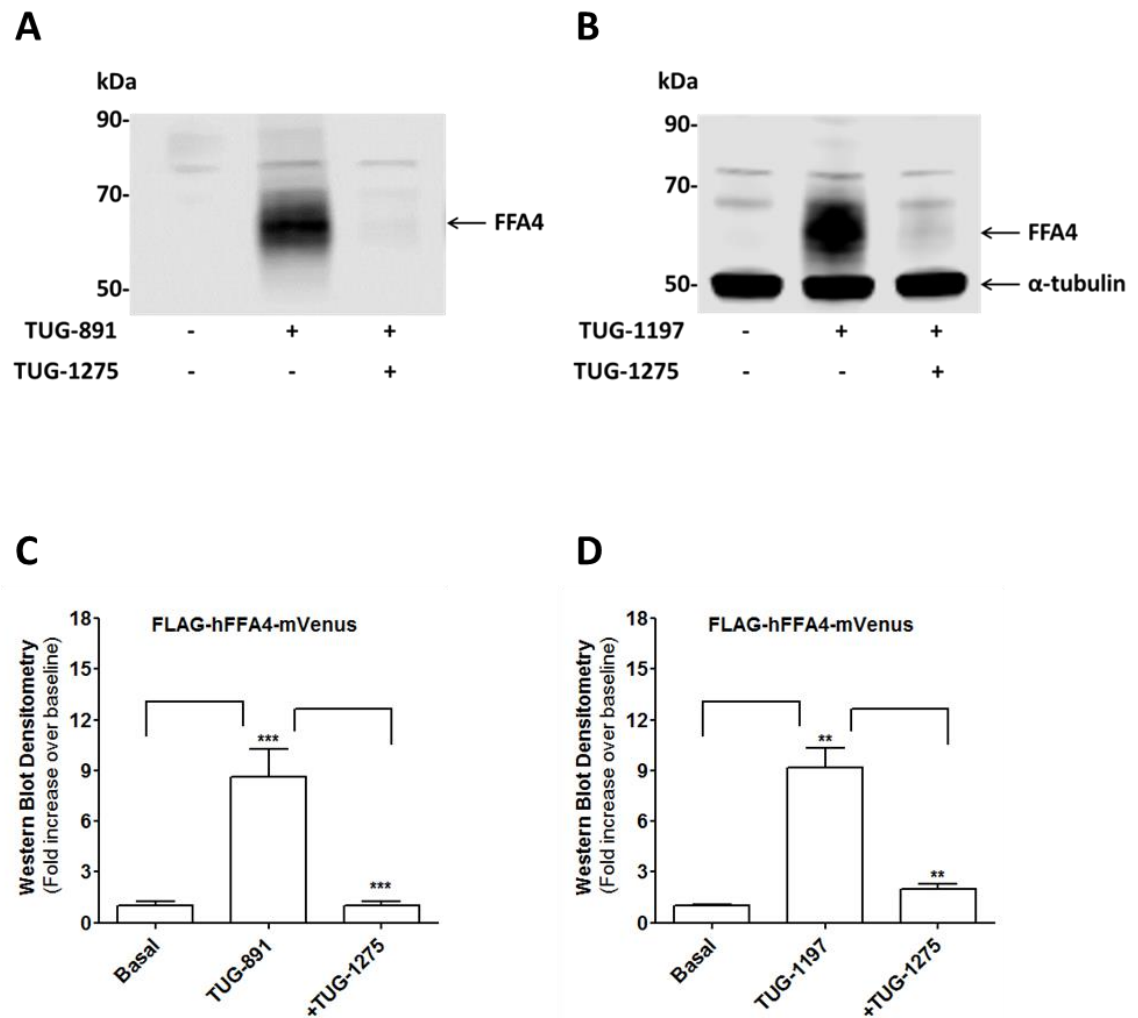


Figure 4-4. TUG-1275 prevents agonist-promoted phosphorylation of hFFA4. Flp-In™ T-REx™ 293 cells able to express FLAG-hFFA4-mVenus were seeded in a 6-well plate and receptor expression was induced by the antibiotic doxycycline (100 ng/ml) for 18-24 hours. Cells were then challenged for 10 minutes in the absence (baseline) or presence of 10 μ M **(A)** TUG-891 or **(B)** TUG-1197. To assess function of TUG-1275 cells were pre-treated for 15 minutes with 10 μ M TUG-1275 followed by incubation with agonist ligands for a further 15 minutes. Lysates of cells were resolved by SDS-PAGE and phosphorylated receptors were detected by immunoblotting with a phospho-Thr³⁴⁷/Ser³⁵⁰ hFFA4 antiserum. Antibodies to α -tubulin were co-added with the phospho-Thr³⁴⁷/Ser³⁵⁰ hFFA4 antiserum and provided a control for equal loading of the lanes of the SDS-PAGE. Densitometry of immunoblots shown in **(C)** (** p <0.001) and **D** (** p <0.01). Data represent the mean \pm SEM of three independent experiments.

4.2.2 TUG-1275 inhibits agonist-induced β -arrestin2 recruitment to hFFA4

Agonist-promoted activation of GPCRs can cause recruitment of β -arrestin2 to the receptor (Thomsen et al., 2016). Many of the ligands discovered as agonists of FFA4 have been identified via the use of FFA4- β -arrestin2 interaction assays (Milligan et al., 2015). I therefore assessed the effect of TUG-1275 on agonist promoted recruitment of β -arrestin2 to hFFA4. Flp-InTM T-RExTM 293 cells able to express inducibly FLAG-hFFA4-eYFP and constitutively expressing β -arrestin2-*Renilla* luciferase were used for these experiments. In the presence of an EC₈₀ concentration of TUG-891 (3 μ M), TUG-1275 completely reversed the TUG-891 response with pIC₅₀ = 8.27 ± 0.17 (Figure 4-5 A). Cells pre-incubated with TUG-1275 followed by co-addition of 0.1% DMSO (vehicle) did not show any response (Figure 4-5 A). TUG-1275 alone had no effect in this system.

Consecutive concentration-response curves of TUG-891 were generated in the presence of increasing concentrations of TUG-1275 (Figure 4-5 B). Cells pre-treated with TUG-1275 (0.001, 0.01, 0.1 and 1 μ M) caused a concentration-dependent decrease in β -arrestin2 recruitment. TUG-1275 at a concentration of 0.01 μ M produced a significant rightward shift in the concentration-response curve of TUG-891 (pEC₅₀= 6.69 ± 0.04 in the absence and pIC₅₀= 6.45 ± 0.03 in the presence of 0.01 μ M TUG-1275; $p < 0.05$; $n = 3$). However, at concentrations of 0.1 μ M and 1 μ M, TUG-1275 caused significant reduction ($p < 0.05$) of the maximal response with a continuing rightward shift and a decrease in efficacy. These data are consistent with insurmountable antagonism.

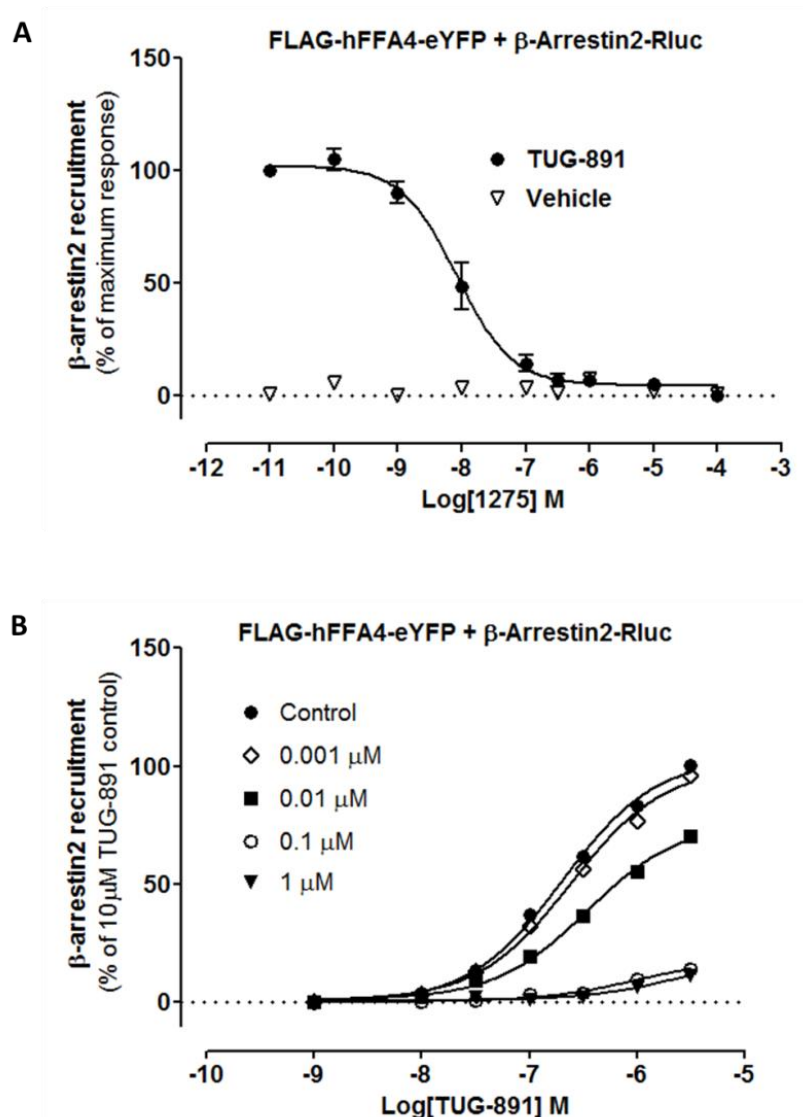


Figure 4-5. TUG-1275 inhibits TUG-891 promoted β -arrestin2 recruitment to hFFA4.

Flp-In™ T-REx™ 293 cells able to inducibly express FLAG-hFFA4-eYFP and constitutively expressing β -arrestin2-*Renilla* luciferase were seeded (80,000 cells/well) into poly-D-lysine coated white 96-well plates. Receptor expression was induced by the antibiotic doxycycline (100 ng/ml) for 18-24 hours. **(A)** BRET measurement in cells pre-treated for 15 minutes with varying concentrations of TUG-1275 followed by treatment with vehicle (0.1% DMSO) or TUG-891 (3 μ M). **(B)** BRET measurement in cells pre-treated for 15 minutes with 0.1% DMSO (vehicle control) or TUG-1275 (0.001, 0.01, 0.1 and 1 μ M) followed by addition of varying concentration of TUG-891. Data represent the mean \pm SEM of three independent experiments.

4.2.3 TUG-1275 inhibits agonist-promoted internalisation of hFFA4 in quantitative internalisation assays

Initial de-orphanisation of FFA4 employed an assay based on ligand-induced receptor internalisation (Hirasawa et al., 2005). Therefore, receptor internalisation experiments were conducted in which the ability of defined concentrations of pre-added TUG-1275 to block internalisation in response to various concentrations of TUG-891 was assessed. Herein, ligand-mediated internalisation of FFA4 was assessed in Flp-In™ T-REx™ 293 inducible cells able to express the human form of FFA4 (hFFA4) tagged with mVenus fluorescent protein. Ligand-induced changes in the amount of internalisation of FLAG-hFFA4-mVenus into endocytic compartments were calculated using an ArrayScan II high content imager (Conway et al., 1999) with associated quantitative algorithms. Images were processed to identify internalised 'spots' of mVenus fluorescence, which were then normalized to cell number based on nuclei identified by Hoechst 33342. This method has previously been described by Hudson et al (2013b).

To probe the mechanism of TUG-1275-mediated blockade of hFFA4 I used 30 minutes end point after addition of TUG-891 to facilitate achievement of ligand equilibrium. Cells were pre-treated for 15 minutes with varying concentrations of TUG-1275 followed by addition of 3 μ M of TUG-891 (an approximate EC₈₀ concentration of this agonist) for 45 minutes. TUG-1275 produced a concentration-dependent inhibition of TUG-891 promoted internalisation of the receptor (Figure 4-6 A). TUG-1275 completely reversed the TUG-891 response with pIC₅₀ 7.70 \pm 0.10. Cells pre-incubated with TUG-1275 followed by co-addition of 0.1% DMSO (vehicle) did not show any response (Figure 4-6 A).

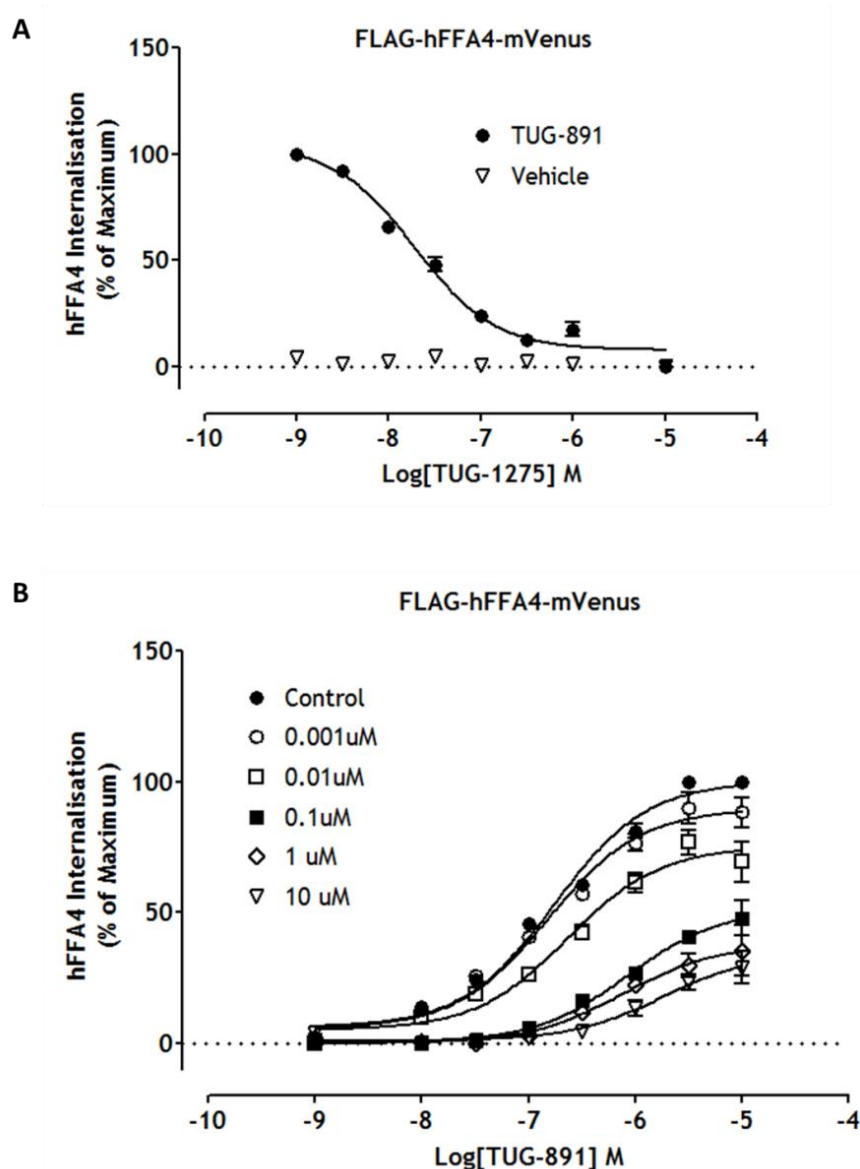


Figure 4-6. TUG-1275 inhibits TUG-891 promoted internalisation of hFFA4. Flp-In™ T-REx™ 293 cells able to express FLAG-hFFA4-mVenus were seeded (75,000 cells /well) into poly-D-lysine coated black clear-bottom 96-well plates and receptor expression was induced by the antibiotic doxycycline (100 ng/ml) for 18-24 hours. **(A)** Quantification of internalised hFFA4 in cells pre-treated for 15 minutes with vehicle (0.1% DMSO) or varying concentrations of TUG-1275 followed by addition of 3 μ M of TUG-891 for 45 minutes incubation. **(B)** Quantification of internalised hFFA4 in cells pre-treated for 5 minutes with vehicle 0.1% DMSO (control) or TUG-1275 (0.001, 0.01, 0.1, 1 and 10 μ M) followed by addition of varying concentrations of TUG-891. Data represent the mean \pm SEM of at least three independent experiments.

Concentration-response curves for TUG-891 in the presence of increasing concentrations of TUG-1275 were generated. Cells pre-treated with TUG-1275 (0.001, 0.01, 0.1, 1 and 10 μM) caused a concentration-dependent decrease in the internalisation of the receptor (Figure 4-6 A and 4-6 B). TUG-1275 at a concentration of 0.01 μM produced a non-significant rightward shift in the concentration-response curve of TUG-891 ($\text{pEC}_{50} = 6.64 \pm 0.03$ in the absence and $\text{pIC}_{50} = 6.42 \pm 0.15$ in the presence of 0.01 μM TUG-1275; $p > 0.05$; $n = 3$). However, at concentrations of 0.1, 1 and 10 μM , TUG-1275 showed significant ($p < 0.05$) decreases in the maximal response to TUG-891 linked to reduction in measured potency ($\text{pIC}_{50} = 5.91 \pm 0.09$, 5.66 ± 0.31 and 5.72 ± 0.11 respectively). In these experiments it was clear that the primary inhibitory effect of TUG-1275 was to produce a decrease in the maximal response to TUG-891. Interestingly, even at highest concentration of TUG-1275 tested a residual response to TUG-891 remained. This response to TUG-891 was similar in the presence of 1 and 10 μM TUG-1275 and, as such, the effect of TUG-1275 appeared to saturate. Such an outcome is consistent with TUG-1275 functioning as a non allosteric modulator of FFA4.

4.2.4 TUG-1275 inhibits agonist promoted internalisation of hFFA4 visualised via confocal microscopy

Internalisation of mVenus-tagged hFFA4 in live cells was visualized using a Zeiss VivaTome spinning disk confocal microscopy system (section 2.5.8). Flp-In™ T-REx™ 293 cells able to express the FLAG-hFFA4-mVenus construct inducibly were used to visualize the effect of TUG-1275 on TUG-891 promoted internalisation of the receptor. Cells cultured on glass coverslips were pre-treated for 15 minutes with TUG-1275 (10 μM) followed by co-addition of TUG-891 (10 μM) for the next 45 minutes (Figure 4-8). As a control cells were challenged only with TUG-891 (Figure 4-7). Cells were imaged before the addition of ligand, and every 15 minutes after ligand addition for a total of 45 minutes.

At zero time, prior to the addition of TUG-891, the bulk of mVenus-tagged receptors was located primarily at the cell surface (Figure 4-7). Within 15 minutes of the addition the agonist, the intensity of mVenus became less distinct at the cell surface and there was then observed punctate clusters of receptors in intracellular vesicles. The internalised mVenus 'spots' increased over time and

within 45 minutes of incubation with agonist most of the receptors were inside the cell (Figure 4-7).

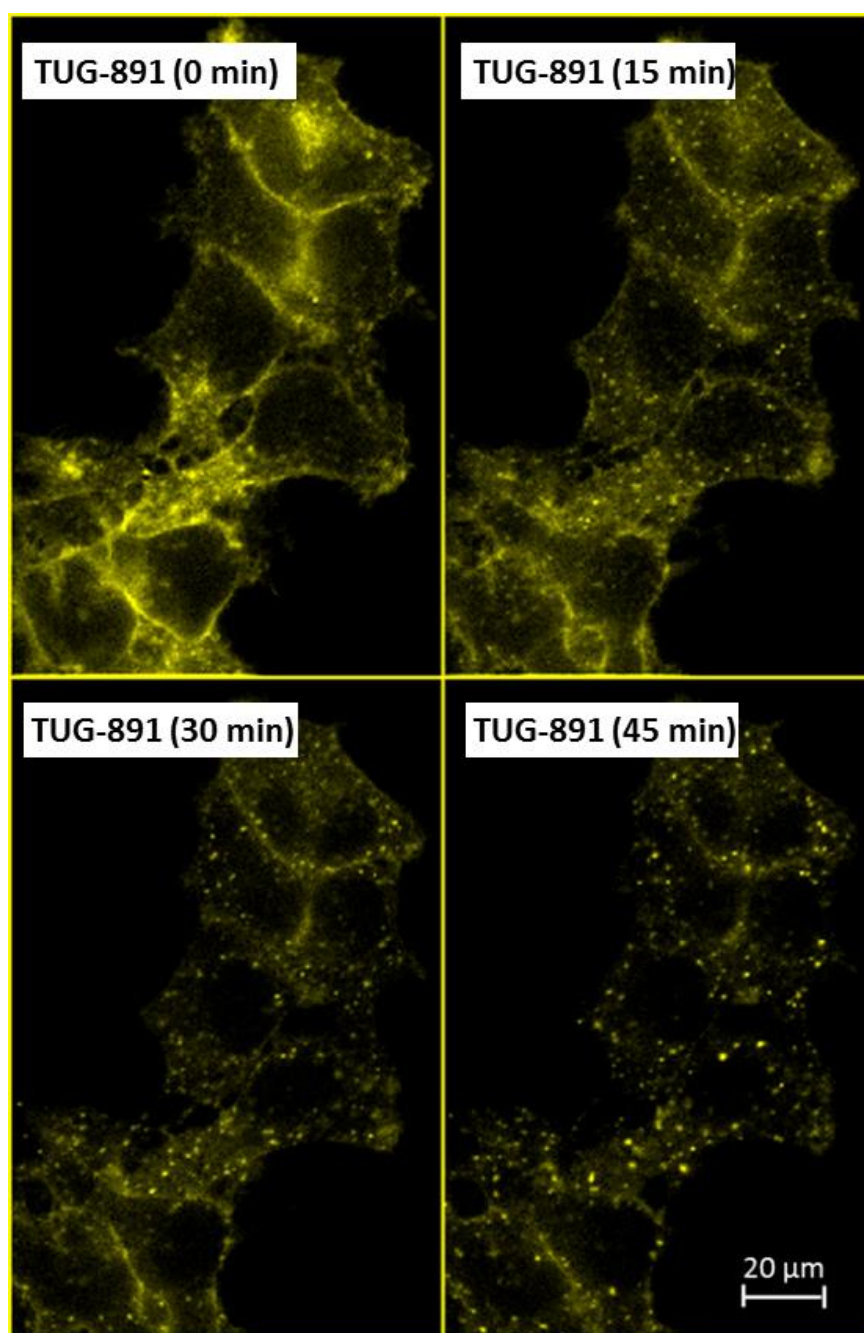


Figure 4-7. TUG-891 promoted internalisation of hFFA4 as visualized by confocal microscopy. Flp-In™ T-REx™ 293 cells able to express FLAG-hFFA4-mVenus were plated down onto poly-*D*-lysine-coated 30 mm glass coverslips and receptor expression was induced using doxycycline (100 ng/ml). The internalisation of hFFA4 in these cells was then imaged using a Zeiss VivaTome spinning disk confocal microscopy system. TUG-891 (10 μM) promoted internalisation of FLAG-hFFA4-mVenus. Images were taken before the addition of TUG-891, and every 15 minutes after ligand addition for a total of 45 minutes.

To assess the effect of TUG-1275, cells were pre-treated 15 minutes with TUG-1275 followed by addition of TUG-891 (Figure 4-8). Cells were imaged at 15 minutes after incubation with TUG-1275 (10 μ M) and then every 15 minutes following addition of TUG-891. In this case, TUG-1275 did not fully abolish TUG-891 promoted internalisation of hFFA4-mVenus (Figure 4-8). Compared to control (Figure 4-7), apparent reduction of hFFA4 internalisation was visualised upon treatment of cells with TUG-1275 (Figure 4-8). However, quantification was not done in these experiments.

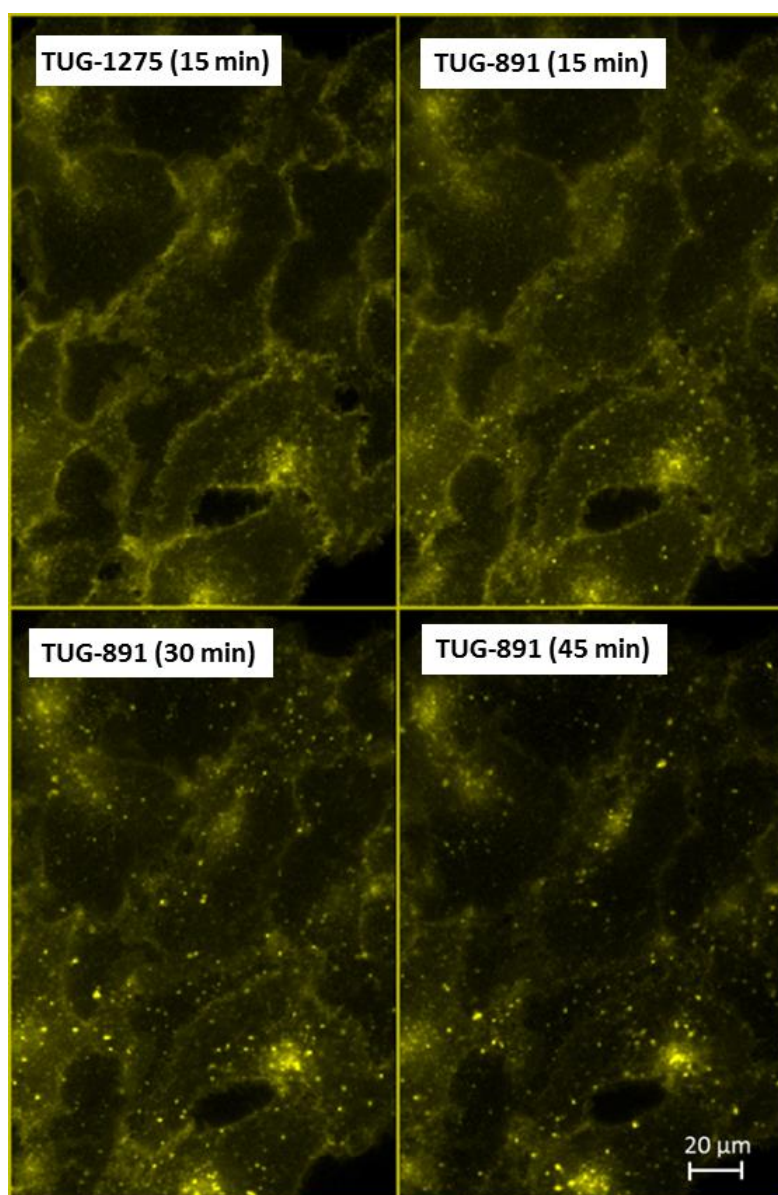


Figure 4-8. TUG-1275 inhibits TUG-891 promoted internalisation of hFFA4 as visualized by confocal microscopy. FFA4 Flp-In™ T-REx™ 293 cells able to express FLAG-hFFA4-mVenus were plated down onto poly-*D*-lysine-coated 30 mm glass coverslips and receptor expression was induced using doxycycline (100 ng/ml). The internalisation of hFFA4 in these cells was then imaged using a Zeiss VivaTome spinning disk confocal microscopy system. TUG-891 (10 μ M) mediated internalisation was reduced in the presence of TUG-1275 (10 μ M). Images were

taken after pre-incubation for 15 minutes with TUG-1275, and every 15 minutes after the addition of TUG-891 for a total 45 minutes of agonist exposure.

4.2.5 TUG-1275 inhibits agonist-promoted elevation of intracellular calcium

Long-chain fatty acids were initially found to evoke a specific rise in intracellular calcium level in cells transfected to express FFA4 (Hirasawa et al., 2005), which reflects activation of the $G_{\alpha q/11}$ family of heterotrimeric G-proteins. Pharmacological profiling of TUG-1275 for capacity to inhibit the functional output from $G_{\alpha q/11}$ signalling via FFA4 was explored in Flp-In™ T-REx™ 293 cell line able to inducibly express either FLAG-hFFA4-mVenus or hFFA1-mVenus-HA. Fura-2 AM labelled cells were challenged with ligands and changes in Ca^{2+} levels assessed using a FlexStation™ plate reader (section 2.5.17).

Concentration-response curves for TUG-891 and TUG-1197 were generated in the presence of increasing concentrations of TUG-1275 (Figure 4-9 A). Cells were pre-treated for 15 minutes with varying concentration of TUG-1275 and then challenged with 3 μ M of TUG-891 or TUG-1197. TUG-1275 completely reversed the responses of both TUG-891 and TUG-1197 ($pIC_{50} = 7.59 \pm 0.05$ for TUG-891 and 7.35 ± 0.12 for TUG-1197).

Concentration-response curves for TUG-891 in the presence of increasing concentrations of TUG-1275 showed the antagonist to inhibit in a non-competitive manner (Figure 4-9 B). TUG-1275 at a concentration of 0.03 μ M produced a significant rightward shift in the concentration-response curve of TUG-891 ($pEC_{50} = 6.41 \pm 0.09$ in the absence and $pIC_{50} = 5.77 \pm 0.08$ in the presence of 0.03 μ M TUG-1275; $p < 0.05$; $n = 3$). However, TUG-1275 at concentrations of 0.1 and 1 μ M caused also significant decreases in the maximal response ($pIC_{50} = 5.55 \pm 0.22$ and 5.65 ± 0.20 respectively) whilst 10 μ M showed complete inhibition of the response (Figure 4-9 B). The concentration-dependent rightward shift in the TUG-891 curve followed by a reduction of the efficacy indicated a non-competitive mode of antagonism of this compound.

To explore the selectivity of TUG-1275 Flp-In™ T-REx™ 293 cells able to inducibly express hFFA1-mVenus-HA were used. Cells were pre-treated for 15 minutes with varying concentration of TUG-1275 followed by co-addition of the

FFA1 agonists TUG-770 or TUG-905. Here, however, TUG-1275 was not able to inhibit intracellular calcium elevation produced via these ligands at this receptor FFA1 (Figure 4-9 C) indication a high selectivity of TUG-1275 for hFFA4 over hFFA1.

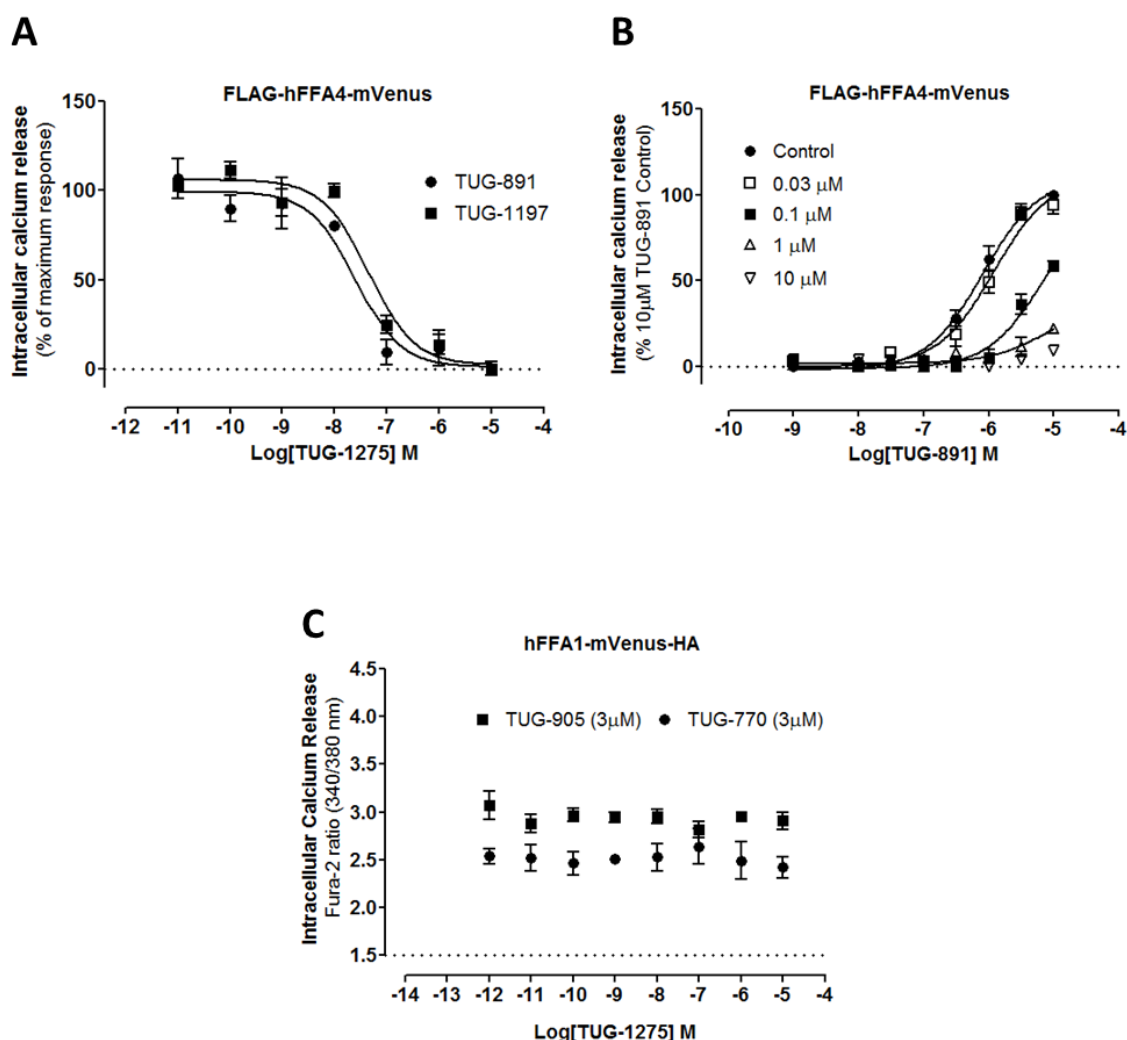


Figure 4-9. TUG-1275 inhibits hFFA4 but not hFFA1 agonist promoted intracellular calcium levels. Flp-In™ T-REx™ 293 cells able to express either FLAG-hFFA4-mVenus or hFFA1-mVenus-HA were seeded (75,000 cells /well) into poly-D-lysine coated black clear-bottom 96-well plates and expression of receptors was induced by the antibiotic doxycycline (100 ng/ml). Cells were labelled with the calcium-sensitive dye Fura-2 AM and then challenged with ligands. **(A)** Cells expressing FLAG-hFFA4-mVenus were pre-treated for 15 minutes with varying concentrations of TUG-1275 followed by treatment with 3 μ M TUG-891 or TUG-1197. **(B)** Cells expressing FLAG-hFFA4-mVenus were pre-treated with 0.1% DMSO (control) or TUG-1275 (0.03, 0.1, 1 and 10 μ M) followed by addition of varying concentrations of TUG-891. **(C)** Cells expressing hFFA1-mVenus-HA were pre-treated for 15 minutes with varying concentration of TUG-1275 followed by addition of 3 μ M TUG-770 or TUG-905 (approximate EC₈₀ concentrations). Efficacy was normalized as percentage of maximum response. Data represent the mean \pm SEM of three independent experiments.

4.2.6 TUG-1275 inhibits TUG-891 mediated accumulation of IP₁

The G $\alpha_{q/11}$ subunits activate phospholipase C, which in turn hydrolyses phosphatidylinositol-4,5-bisphosphate to produce inositol-1,4,5-trisphosphate (IP₃) and diacylglycerol. IP₃ binds to the IP₃ receptor on the endoplasmic reticulum, which allows Ca²⁺ release into the cytoplasm and cytosolic calcium accumulation. IP₃ is degraded rapidly and challenging to quantify directly. However, in the presence of lithium chloride, inositol monophosphate (IP₁) metabolites of IP₃ are maintained and can be quantified (Trinquet et al., 2006). Thus, agonist stimulation of the G $\alpha_{q/11}$ pathway can be measured through accumulation of IP₁. To monitor this process I employed a commercially available IP-One assay kit in 384-well plate format (section 2.5.15).

Flp-In™ T-REx™ 293 cells able to inducibly express FLAG-hFFA4-mVenus were pre-treated for 15 minutes with varying concentration of TUG-1275 followed by addition of 3 μ M TUG-891. This pre-treatment completely reversed the TUG-891 promoted accumulation of IP₁ (pIC₅₀ 6.82 \pm 0.05) (Figure 4-10 A).

Concentration-response curves for IP₁ accumulation were generated for the agonist TUG-891 in the absence and presence of 10 μ M of TUG-1275 (Figure 4-10 B). Cells pre-treated for 15 minutes with TUG-1275 followed by co-addition of varying concentration of TUG-891 produced a significant rightward shift in the concentration-response curve of the agonist (pEC₅₀ = 6.79 \pm 0.03 in the absence and pIC₅₀ = 5.57 \pm 0.03 in the presence of TUG-1275 (p < 0.005; n = 3). Using this single concentration of TUG-1275 did not allow conclusions to be drawn as to the mode of antagonism. Interestingly, TUG-1275 also reduced the basal IP₁ accumulation via hFFA4 in these cells, suggesting both that FFA4 displays constitutive activity and that TUG-1275 might function as an inverse agonist or there might be possibilities of the presence of an endogenously released agonist.

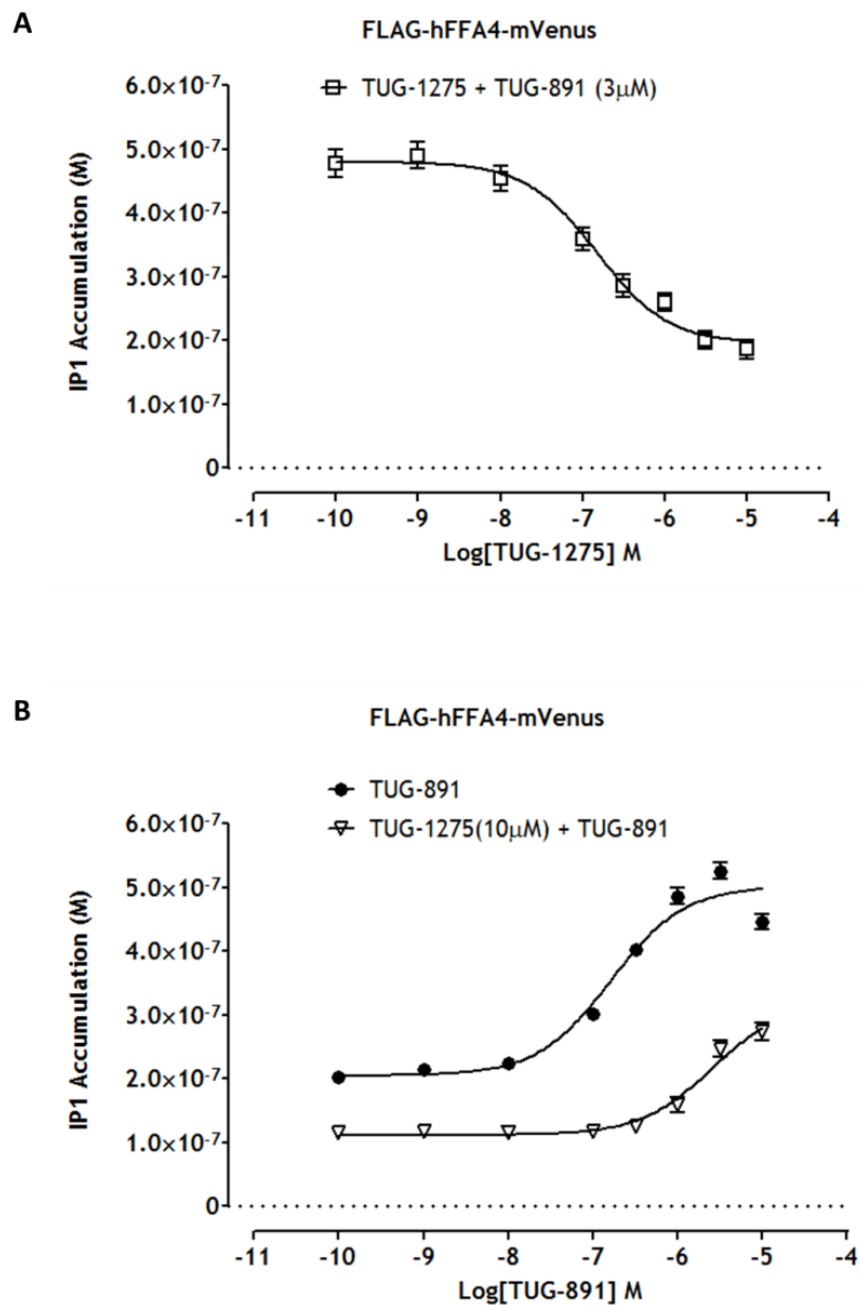


Figure 4-10. TUG-1275 inhibits TUG-891 promoted accumulation of IP₁ via hFFA4.

Flp-In™ T-REx™ 293 cells were induced for the expression of FLAG-hFFA4-mVenus and were seeded (7,500 cell/well) in white solid-bottom 384-well plates. **(A)** A concentration-inhibition response for TUG-1275 was generated for cells pre-treated for 15 minutes with different concentrations of TUG-1275 followed by addition of 3 μ M TUG-891. **(B)** Cells were pre-treated for 15 minutes with TUG-1275 (10 μ M) or vehicle (0.01% DMSO) followed by co-incubation with varying concentration of TUG-891. Data represent the mean \pm SEM of three independent experiments.

4.3 Ligands acting at hFFA1

Since discovery that FFA1 acts as a receptor for medium- and longer-chain saturated and unsaturated fatty acids (Briscoe et al., 2003) a number of synthetic ligands of this receptor have been reported in the scientific literature (Milligan et al., 2015). The physiological functions of FFA1 have validated this receptor as an attractive drug target for type-2 diabetes and other metabolic disorders (Hara, 2017). Few drugs have entered into clinical trials however (Li et al., 2016). Despite this there has been a continuing effort to develop novel FFA1 ligands to explore understanding of the physiological and pathophysiological functions of this receptor as well to promote potential drug discovery for the treatment of metabolic disorders.

Our medicinal chemistry group at the University of Southern Denmark have developed a wide range of novel FFA1 agonists including TUG-770 (Cristiansen et al., 2013) and TUG-905 (Cristiansen et al., 2012). Briscoe et al (2006) reported the small molecule GW-1100 as a non-competitive antagonist of FFA1. For target validation, antagonists can act as valuable pharmacological tool compounds (Milligan et al., 2015). To explore the pharmacology of hFFA1, each of the above compounds were characterised in heterologous cell systems able to express hFFA1 or hFFA4.

4.3.1 Regulation of intracellular calcium levels by hFFA1

Activation of FFA1 by fatty acids (Briscoe et al., 2003) or synthetic ligands (Hudson et al., 2014) has been shown to result in an increase in intracellular calcium levels. Flp-In™ T-REx™ 293 inducible cell lines stably harbouring the mVenus-tagged FFA1 receptor at the T-REx™ genomic locus were employed to explore the capacity of FFA1-ligands to promote elevation of intracellular calcium levels in cell populations. Cells were labelled for 45 minutes with the calcium-sensitive dye Fura-2 AM (section 2.5.17) and then challenged with varying concentrations of the FFA1-agonists TUG-770 and TUG-905.

Both TUG-770 and TUG-905 produced a concentration-dependent increase in intracellular calcium levels ($pEC_{50} = 7.39 \pm 0.10$ for TUG-770 and 7.41 ± 0.13 for TUG-905) (Figure 4-11).

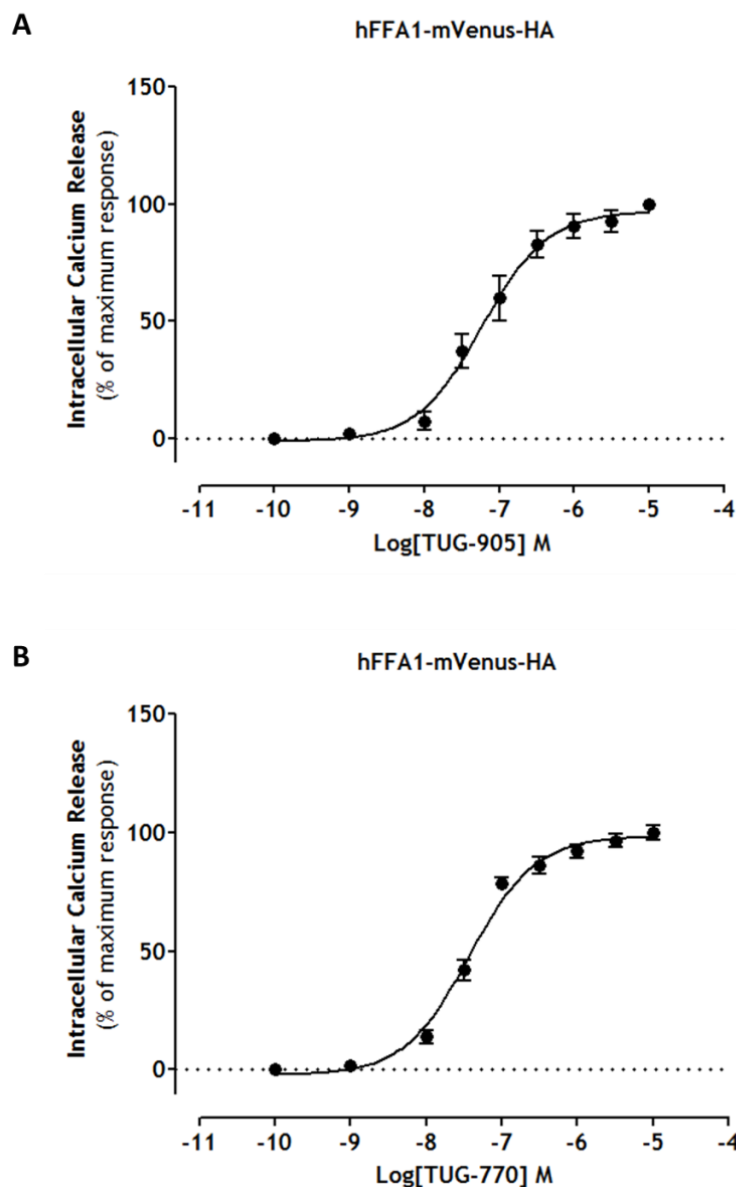


Figure 4-11. TUG-770 and TUG-905 cause elevation of intracellular calcium via hFFA1. Flp-In™ T-REx™ 293 cells able to express hFFA1-mVenus-HA were seeded (75,000 cells /well) into poly-D-lysine coated black clear-bottom 96-well plates and expression of the receptor construct was induced by the antibiotic doxycycline (100 ng/ml). Cells were labelled for 45 minutes with the calcium-sensitive dye Fura-2 AM and then exposed to varying concentration of **(A)** TUG-770 or **(B)** TUG-905. Efficacy was normalized as percentage of maximum response. Data represent the mean \pm SEM of three independent experiments.

Due to the marked overlap in the activation of FFA1 and FFA4 by both endogenous fatty acids and a number of synthetic ligands, it was of interest to examine if either TUG-770 or TUG-905 could also promote elevation of intracellular calcium levels through activation of hFFA4. A potent and selective FFA4-agonist TUG-1197 (Azevedo et al., 2016) was also employed in these experiments. Flp-In™ T-REx™ 293 cells able to inducibly express FLAG-hFFA4-mVenus upon addition of doxycycline were employed. TUG-905 showed no activity at hFFA4 at concentrations up to 10 μ M whilst TUG-770 showed responses at higher concentrations ($pEC_{50} = 5.23 \pm 0.04$) (Figure 4-12). By contrast, TUG-1197 potently activated hFFA4 ($pEC_{50} = 6.59 \pm 0.24$).

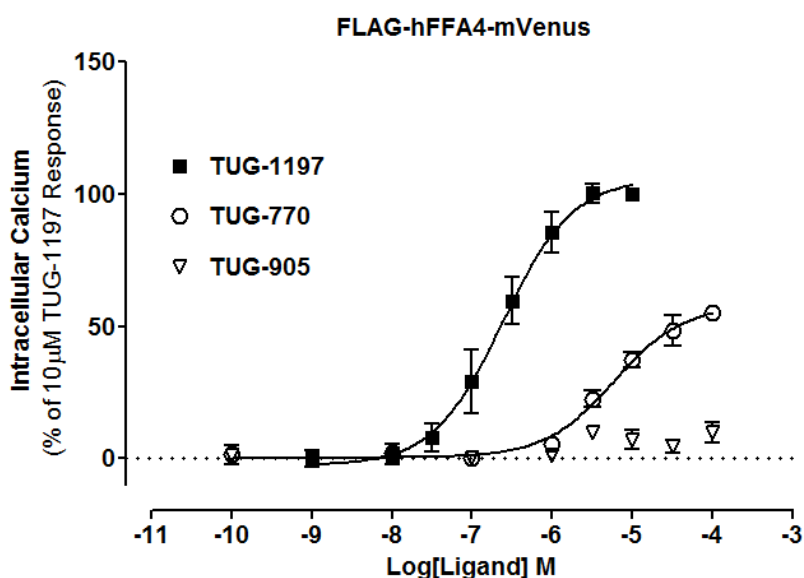


Figure 4-12. TUG-770 but not TUG-905 displays low potency mediated activation of hFFA4. Flp-In™ T-REx™ 293 cells able to express FLAG-hFFA4-mVenus were seeded (75,000 cells /well) into poly-D-lysine coated black clear-bottom 96-well plates and expression of hFFA4 was induced by the antibiotic doxycycline (100 ng/ml). Cells were labelled for 45 minutes with the calcium-sensitive dye Fura-2 AM and then challenged with varying concentrations of the FFA4 selective agonist TUG-1197 or either TUG-770 or TUG-905. Efficacy was normalized as percentage of maximum response of TUG-1197. Data represent the mean \pm SEM of three independent experiments.

4.3.2 β -arrestin2 recruitment at hFFA1

As noted earlier BRET-based β -arrestin2 interaction (section 2.5.13) screening is a very popular method to identify ligands for many GPCRs (Stoddart et al., 2015; Milligan, 2004). HEK-293T cells were transiently co-transfected with mVenus-tagged hFFA1 and a β -arrestin2 *Renilla* luciferase construct as described by Hudson et al (2014). 24 hours post-transfection, expression of hFFA1-mVenus was assessed by microscopy as well as by the measurement of fluorescence intensity of mVenus. Subsequently, agonist-induced β -arrestin2 BRET was measured following a 15-minute agonist incubation at 37 °C (Christiansen et al., 2015). Both TUG-770 and TUG-905 produced β -arrestin2 recruitment in a concentration-dependent manner (pEC_{50} 7.51 ± 0.15 for TUG-770 and 8.03 ± 0.11 for TUG-905) (Figure 4-13).

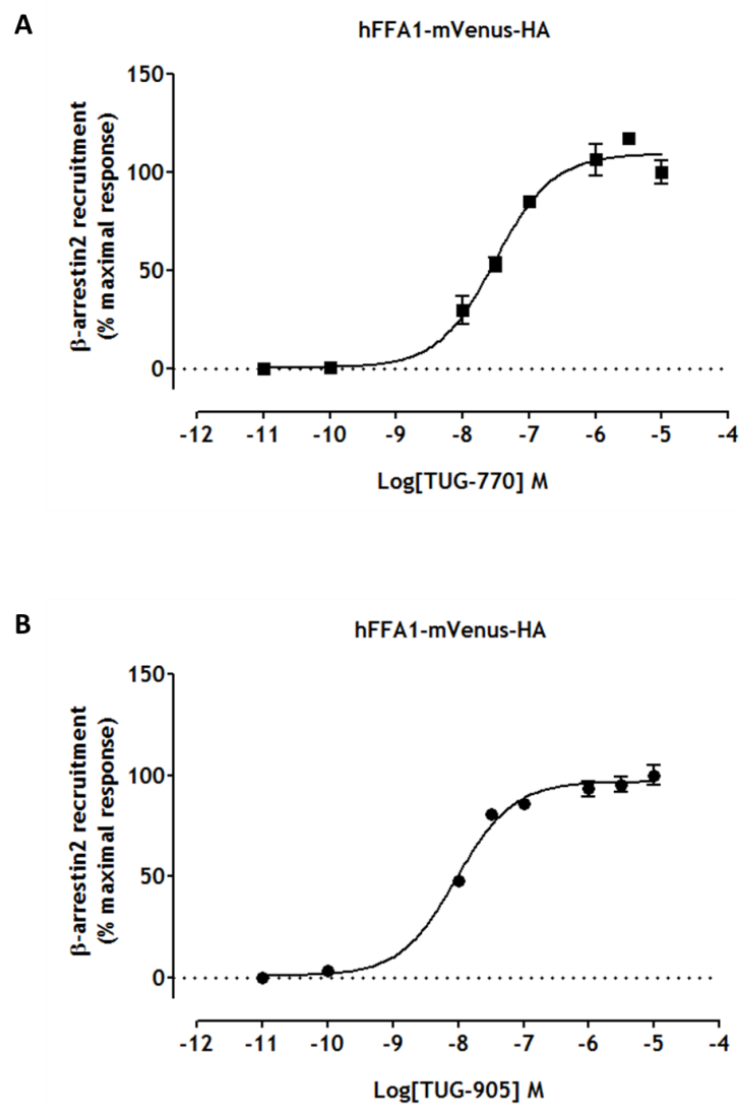


Figure 4-13. TUG-770 and TUG-905 induce β -arrestin2 recruitment to hFFA1. HEK-293T cells were co-transfected with a mVenus fluorescent protein-tagged form of hFFA1 and a β -arrestin2 *Renilla* luciferase plasmid. Cells were seeded (80,000 cells /well) into poly-D-lysine coated white 96-well plates. BRET in response to **(A)** TUG-770 or **(B)** TUG-905 was subsequently measured. Efficacy was normalized as percentage of maximum BRET response. Data represent the mean \pm SEM of three independent experiments.

4.4 GW-1100 is a FFA1 antagonist

Briscoe et al (2006) reported the small molecule GW-1100 as a non-competitive antagonist of the receptor FFA1. To explore the pharmacology of GW-1100 further this compound was characterised in heterologous cell systems able to express either hFFA1 or hFFA4.

4.4.1 GW-1100 inhibits β -arrestin2 recruitment at hFFA1

Ligand-induced β -arrestin2 interactions with FFA1 have also been reported in a number of ligand discovery projects (Mancini et al. 2015a). I therefore assessed the effect of GW-1100 on agonist-promoted recruitment of β -arrestin2 to hFFA1.

HEK-293T cells were co-transfected with mVenus-tagged hFFA1 and a β -arrestin2 *Renilla* luciferase as described previously by Hudson et al (2014). Concentration-response curves were generated for the hFFA1 agonist TUG-905 in the presence of increasing concentrations of GW-1100 (Figure 4-14 A). Cells were pre-treated for 15 minutes with GW-1100 (0.3, 1 and 3 μ M) followed by co-addition of varying concentration of the FFA1-agonist TUG-905. Cells pre-treated for 15 minutes with 0.1% DMSO followed by treatment of varying concentration of TUG-905 were taken as control. GW-1100 produced concentration-dependent inhibition of β -arrestin2 recruitment to hFFA1 (Figure 4-14 A). GW-1100 at a concentration of 1 μ M produced a non-significant rightward shift in the concentration-response curve to TUG-905 ($pEC_{50} = 8.04 \pm 0.05$ in the absence and $pIC_{50} = 7.75 \pm 0.10$ in the presence of 1 μ M GW-100; $P > 0.05$). However, at a concentration of 3 μ M, GW-1100 showed a significant reduction in the maximal BRET response alongside a rightward shift in agonist potency ($pIC_{50} = 7.22 \pm 0.11$). This is consistent with non-competitive antagonism of the receptor.

Potential antagonism of GW-1100 in the recruitment of β -arrestin2 to hFFA4 was examined in Flp-InTM T-RExTM 293 cells able to inducibly express FLAG-hFFA4-eYFP and that constitutively express β -arrestin2-*Renilla* luciferase. Cells were pre-treated for 15 minutes with 0.1% DMSO (control) or GW-1100 (10 μ M) followed by co-addition of varying concentration of TUG-891. GW-1100 did alter β -arrestin2 recruitment to hFFA4 (Figure 4-14 B), confirming its high selectivity for FFA1.

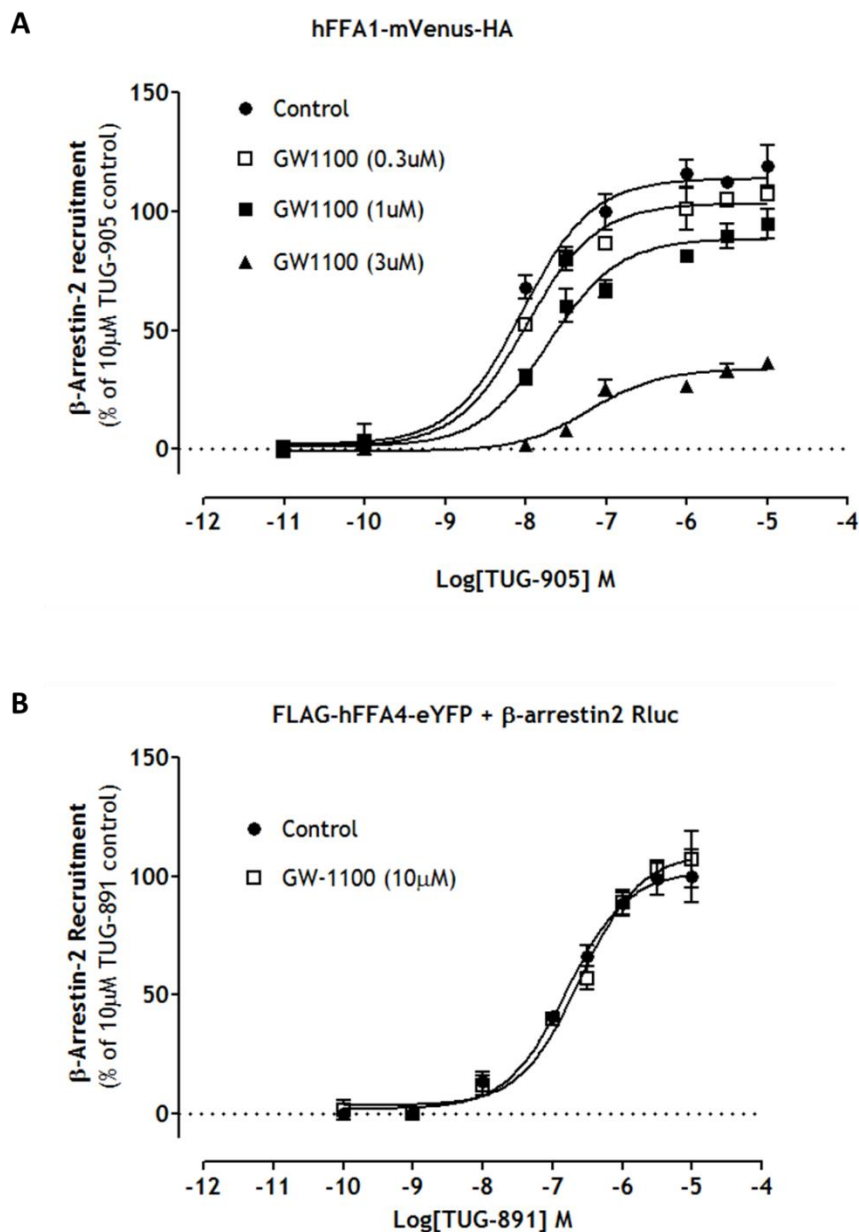


Figure 4-14. GW-1100 inhibits TUG-905 promoted β -arrestin2 recruitment to hFFA1.

BRET was employed to measure the interaction of hFFA1 and β -arrestin2 in 96-well BRET plate format. **(A)** HEK-293T cells were co-transfected with a mVenus fluorescent protein-tagged form of hFFA1 with a β -arrestin2 *Renilla* luciferase plasmid. BRET measurements were performed in cells pre-treated for 15 minutes with 0.1% DMSO (control) or GW-1100 (0.3, 1 and 3 μ M) followed by co-addition of varying concentrations of TUG-905 for 15 minutes. **(B)** Flp-InTM T-RExTM 293 cells able to inducibly express FLAG-hFFA4-eYFP and constitutively expressing β -arrestin2-*Renilla* luciferase were used to examine the selectivity of GW-1100. Cells were pre-incubated for 15 minutes with 10 μ M GW-1100 or 0.1% DMSO (control) followed by 5 minutes co-addition of varying concentration of the FFA4-agonist TUG-891. Data represent the mean \pm SEM of three independent experiments.

4.4.2 GW-1100 inhibits the elevation of intracellular calcium levels via FFA1

The pharmacological profiling of GW-1100 was explored further in Flp-In™ T-REx™ 293 cells able to inducibly express hFFA1-mVenus-HA using the potent and selective FFA1 agonist TUG-905 (Christiansen et al., 2012).

The cells were pre-treated 15 minutes with varying concentration of GW-1100 followed by co-addition of 3 μ M TUG-905. GW-1100 completely reversed TUG-905 mediated increases in intracellular calcium levels with pIC_{50} 6.81 ± 0.06 (Figure 4-15 A).

Increasing concentrations of GW-1100 altered the concentration-response curves to TUG-905 (Figure 4-15 B). At 3 μ M GW-1100 produced a significant rightward shift ($p < 0.05$) in the concentration-response curve of TUG-905 ($pEC_{50} = 7.15 \pm 0.02$ in the absence and $pIC_{50} = 6.63 \pm 0.09$ in the presence of 3 μ M GW-1100). At a concentration of 10 μ M, GW-1100 also produced a rightward shift ($pIC_{50} = 6.31 \pm 0.13$) but now linked to a significant reduction ($p < 0.05$) in the maximal TUG-905-response.

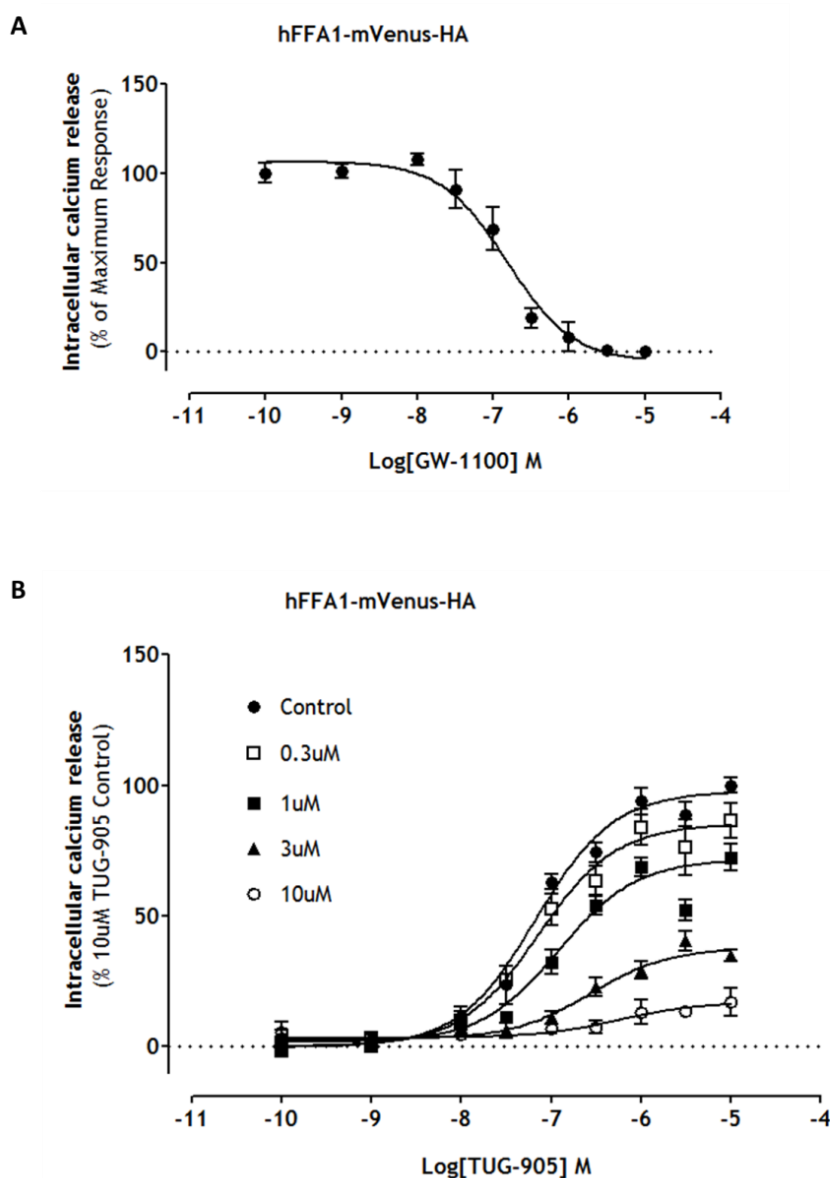


Figure 4-15. GW-1100 inhibits TUG-905 mediated elevation of intracellular calcium via hFFA1. Flp-In™ T-REx™ 293 cells able to express hFFA1-mVenus-HA were seeded (75,000 cells /well) into poly-D-lysine coated black clear-bottom 96-well plates and expression of receptors was induced by the antibiotic doxycycline (100 ng/ml). Cells were labelled with the calcium-sensitive dye Fura-2 AM and then challenged with ligands. **(A)** Cells were pre-treated for 15 minutes with varying concentration of GW-1100 followed by treatment with 3 μ M TUG-905. **(B)** Cells were pre-treated with 0.1% DMSO (control) or GW-1100 (0.3, 1, 3 and 10 μ M) followed by co-addition of varying concentration of TUG-905. Data represent the mean \pm SEM of three independent experiments.

4.5 Discussion

4.5.1 Ligands for hFFA1

It is well established that long chain free fatty acid receptors are closely associated with many metabolic diseases, particularly with type-2 diabetes, and activation of these receptors plays a key role in increasing glucose-stimulated insulin secretion (Li et al., 2016; Milligan et al., 2015). Due to the physiological relevance of FFA1 and FFA4 in modulating a myriad of metabolic processes, they have received increasing attention as attractive drug targets for diabetes and related diseases (Milligan et al., 2015; Milligan et al., 2006b; Hirasawa et al., 2008; Suzuki et al., 2008). Although FFA1 and FFA4 are structurally distant, they share common natural ligands (Milligan et al., 2015). This has limited the exploration of physiological functions as well as the elucidation of receptor pharmacology. Identification and characterisation of selective ligands will enable target validation and enhance development of drugs targeting these therapeutically important receptors. In this effort, there is now more emphasis on developing synthetic ligands (Milligan et al., 2017; Moniri, 2016; Dranse et al., 2013).

Christiansen et al. (2012) previously showed that the FFA1 agonist TUG-905 induces a concentration-dependent increase in insulin secretion in the rat INS-1E β -cell line. TUG-905 also showed a concentration-dependent increase in elevation of intracellular Ca^{2+} levels (Figure 4-11) which might be responsible for the release of insulin. TUG-905 also recruited β -arrestin2 to hFFA1 in a concentration-dependent fashion (Figure 4-13) which might contribute to receptor desensitisation. Christiansen et al (2012) reported TUG-905 as 4800-fold selective agonist over hFFA4. However, these authors compared the potency of this compound in the elevation of intracellular calcium levels via FFA1 with that in the recruitment of β -arrestin2 to FFA4. In my experiments, TUG-905 mediated intracellular calcium levels were examined in both FFA1 and FFA4 and found to be complete selective over hFFA1 (Figure 4-12).

TUG-770 showed similar efficacy and potency to TUG-905 in both calcium mobilisation (Figure 4-11) and β -arrestin2 recruitment (Figure 4-13). During identification and characterisation, Christiansen et al (2013b) reported TUG-770 as a potent agonist of hFFA1 having 150-fold selectivity for FFA1. These authors

again calculated selectivity of TUG-770 in calcium assays via FFA1 with that in β -arrestin2 recruitment to hFFA4. In the elevation of intracellular calcium levels, TUG-770 found to be 157-fold selective over hFFA4 (Figure 4-12). Again, the relative expression levels of the receptors were not taken into consideration during calculation of selectivity values. This selectivity pattern is consistent with the published report of Christiansen et al (2013b). These authors also showed that TUG-770 was able to release insulin and improve glucose tolerance in diet-induced obese mice. This effect might be mediated through both FFA1 and FFA4 as at higher concentrations. TUG-770 was found to increase intracellular calcium via hFFA4 activation (Figure 4-12). Elevation of intracellular calcium level via FFA1 is linked to the secretion of many hormones including insulin release from pancreas (Schmidt et al., 2011). TUG-770 and TUG-905 promoted elevation of intracellular calcium might be related to the improved insulin secretion and also glucose tolerance as reported previously (Christiansen et al., 2012; Christiansen et al., 2013b). Moreover, calcium signalling indicates that hFFA1 signalling is mediated through G α q/11 G proteins. Agonist-promoted recruitment of β -arrestin2 to GPCRs is related to receptor desensitisation as well the regulation of vast array of cellular functions (Smith and Rajagopal, 2016). From these studies, it might be concluded that TUG-905 is a good candidate for further agonist-based drug discovery at FFA1 and can also be considered a useful tool compound to further unravel the contributions of this receptor.

Briscoe et al. (2006) introduced GW-1100 as the first FFA1 antagonist. These authors showed that this compound can block the FFA1-agonist GW-9508 in promoting release of insulin in a glucose-dependent fashion from rodent MIN6 insulinoma cells. This small molecule has been by far the most widely used FFA1 antagonist for both *in vitro* and preclinical studies (Milligan et al., 2017; Manosalva et al., 2015). In my study, I have described the pharmacology of GW-1100 in Flp-InTM T-RExTM 293 cells able to express hFFA1 or hFFA4. GW-1100 inhibited agonist-promoted intracellular calcium mobilisation in a concentration-dependent manner (Figure 4-15). GW-1100 also inhibited the recruitment of β -arrestin2 to hFFA1 in a concentration-dependent fashion and showed complete selectivity over hFFA4 (Figure 4-14), confirming that GW-1100 is a selective antagonist of the hFFA1 receptor. The inhibitory nature was consistent with insurmountable antagonism of hFFA1.

4.5.2 Ligands for hFFA4

After the deorphanisation of FFA4, it has been difficult to identify ligands that are highly selective for FFA4 over FFA1. Shimpukade et al. (2012) described the ortho-biphenyl compound, TUG-891 as the first potent FFA4 agonist, which has identified by a FFA4- β -arrestin2 interaction assay to show 1000 fold selectivity over FFA1. Unfortunately, the compound shows more potency on the murine orthologue of FFA1, and therefore its selectivity over FFA1 in this species is reported as only 3-fold and 50-fold selective in calcium mobilisation and β -arrestin2 recruitment assays, respectively (Hudson et al., 2013b). TUG-891 is commercially available and is widely used as a tool compound in both *in vitro* and *in vivo* studies. In this project, TUG-891 was used as a tool compound to study the pharmacology and desensitisation of hFFA4. Exposure of Flp-In™ T-REx™ 293 cells able to express hFFA4 to TUG-891 was found to elevate intracellular calcium levels (Figure 4-1), recruit β -arrestin2 (Figure 4-3) and internalise the receptor (Figure 5-11) in a concentration-dependent manner. In the calcium response, TUG-891 was found to be 75 fold selective over hFFA1, although the relative expression levels of the receptors was not taken into consideration. On the other hand, another FFA4-ligand TUG-1197 (Azevedo et al., 2016) was also used in this project. This compound also produced a concentration-dependent increase in intracellular calcium level (Figure 4-1) and β -arrestin2 recruitment (Figure 4-3). Compared to TUG-891, TUG-1197 showed significantly ($p < 0.05$) higher efficacy in the elevation of intracellular calcium (Figure 4-1). However, the efficacy difference was assay dependent as the efficacy difference was not significant in β -arrestin2 recruitment assay (Figure 4-3). The efficacy and potency of TUG-891 and TUG-1197 were not compared with any endogenous ligand in these experiments. However, Hudson et al. (2013b) compared the actions of TUG-891 with the endogenous fatty acid agonist α -linolenic acid (aLA) and reported TUG-891 as 50 fold more potent than aLA. In calcium signalling this compound showed complete selectivity for hFFA4 over hFFA1 (Figure 4-2). The selectivity of TUG-TUG-1197 on the murine orthologue of FFA1 has yet to be tested. Interestingly, TUG-1197 is distinctly different in structure from most other FFA4 agonists, lacking any acidic group (Azevedo et al., 2016). Azevedo et al. (2016) reported that this compound is inactive at other fatty acid receptors including both FFA2 and FFA3 at concentrations up to 30 μ M and showed improved glucose homeostasis in acute and chronic studies in

mice. The complete selectivity profile of this compound has made it an important pre-clinical candidate for the treatment of type-2 diabetes.

Burns and Moniri (2010) reported that fatty acid ligands promote rapid and transient phosphorylation of FFA4. Ligand promoted phosphorylation of GPCRs is a common phenomenon in process within receptor desensitisation (Thomsen et al., 2016). In Flp-InTM T-RExTM 293 cell lines, both TUG-891 and TUG-1197 caused robust phosphorylation (Figure 4-4) of hFFA4 detected by immunoblotting using an antiserum that identifies hFFA4 in which both Thr³⁴⁷ and Ser³⁵⁰ are phosphorylated (Butcher et al. 2015).

Sparks et al. (2014) identified the sulphonamide compound 39 (AH 7614) as a potent FFA4 antagonist, able to inhibit agonist-promoted insulin release from MIN6 and NCI-H716 cells. Due to the closely related chemical nature of the agonist 'compound 8' developed by these authors, they predicted competitive antagonism for 'compound 39'. However, further characterisation was required needed. Our medicinal chemistry team synthesised the same compound and designated it as TUG-1275. In Flp-InTM T-RExTM 293 cells able to express hFFA4, this compound showed non-competitive antagonism in a number of assays including agonist-promoted recruitment of β -arrestin2, receptor internalisation, regulation of intracellular calcium, IP1 accumulation and receptor phosphorylation.

Agonist-promoted recruitment of β -arrestins not only functions in receptor desensitisation but also in distinct G protein-independent signalling (Smith and Rajgopal, 2016). TUG-1275 was able to inhibit TUG-891-promoted recruitment of β -arrestin2 in a concentration-dependent manner (Figure 4-5). Hirasawa et al (2005) first deorphanised FFA4 using internalisation of FFA4 in high content assays. During internalisation, many GPCRs undergo endocytosis to cytoplasmic endosomal compartments or vesicles for further intracellular sorting or recycling back to the cell surface (Zheng et al., 2016). I applied the high-content screening platform 'ArrayScan II' and found that TUG-1275 significantly inhibited TUG-891-promoted internalisation of hFFA4. The inhibition was antagonist-concentration dependent (Figure 4-6). The reduction of agonist-promoted internalisation was also visualised by confocal microscopy (Figure 4-7 and Figure 4-8) although the internalisation was not completely abolished by this

antagonist. Sparks et al. (2014) reported compound 39 (TUG-1275) to block effects of both a fatty acid and a synthetic FFA4 agonist in FFA4-transfected U2OS human osteosarcoma cells and to antagonize both FFA4-mediated insulin secretion from mouse insulinoma MIN6 cells and the secretion of GLP-1 from the human intestinal cell line. These authors suggested that this compound would likely act as a competitive antagonist for FFA4, the limited data presented in their report did not actually suggest such a mode of action, which appeared to be insurmountable in assays measuring intracellular calcium levels (Figure 4-9), recruitment of β -arrestin2 (Figure 4-5) and FFA4 internalisation (Figure 4-6). In these experiments it was clear that the primary inhibitory effect of TUG-1275 was to produce a decrease in the maximal response to TUG-891. Although this is consistent with outcomes reported by Sparks et al. (2014) using intracellular Ca^{2+} assays, the longer time course of the internalization studies largely eliminates potential issues of ligand hemi-equilibrium that can greatly influence outcomes and mechanistic interpretation in assays, such as those based on Ca^{2+} mobilization, that employ much shorter end points (Charlton and Vauquelin, 2010). These findings indicated that TUG-1275 is not a competitive antagonist of FFA4. Interestingly, even at the highest concentration of TUG-1275 tested a residual response to TUG-891 remained (Figure 4-6). This response to TUG-891 was similar in the presence of 1 and 10 μM TUG-1275 and, as such, the effect of TUG-1275 appeared to saturate. Such an outcome is consistent with TUG-1275 functioning as an insurmountable antagonist of FFA4. Watterson et al. (2017) recently reported this compound as allosteric ligand for the FFA4 receptor.

GPCR activated $\text{G}\alpha_{q/11}$ signalling triggers the release of calcium from the activation of the inositol phosphate cascade (Moran et al., 2016; Werry et al., 2003). TUG-1275 was found to inhibit agonist-activated elevation of intracellular calcium levels in a concentration-dependent manner (Figure 4-9). $\text{G}\alpha_{q/11}$ signalling promotes the production of inositol phosphates with IP_3 responsible for releasing intracellular calcium from the endoplasmic reticulum (Moran et al., 2016; Werry et al., 2003). A myo-inositol-1-phosphate (IP_1) accumulation assay was applied to study the antagonism of TUG-1275. Agonist promoted accumulation of IP_1 was significantly reduced with co-addition of the antagonist, and also indicated that TUG-1275 is a non-competitive inhibitor of hFFA4 (Figure 4-10). Agonist-mediated receptor phosphorylation is regulated by a number of

GRKs (Thomson et al., 2016). TUG-1275 showed complete blockage of TUG-891 and TUG-1197-promoted phosphorylation of hFFA4 (Figure 4-4). Overall, it can be concluded that TUG-1275 is a potent and insurmountable antagonist of hFFA4.

5 Desensitisation of hFFA1 and hFFA4

The desensitisation of a GPCR can be described as the loss of responses subsequent to prolonged or repeated administration of an agonist (Thomsen et al., 2016; Shenoy and Lefkowitz, 2011). Because GPCR signalling underlies a diverse array of cellular processes, it is essential that the mechanism of activation is initiated and terminated rapidly, specifically and precisely even when agonist stimulation is continued (Syrovatkina et al., 2016). Desensitisation of GPCRs is an adaptive response of the cell to control the magnitude and duration of GPCR signalling, thereby safeguarding against exaggerated cellular responses (Thomsen et al., 2016; Kelly et al., 2008). The process of GPCR desensitisation itself is a signalling event that involves multiple pathways, including receptor phosphorylation events, arrestin-mediated internalisation into endosomes, receptor recycling/resensitisation, and lysosomal degradation (Thomsen et al., 2016; Rosenbaum et al., 2009).

5.1 Desensitisation of hFFA1

Elevation of intracellular calcium following agonist stimulation of hFFA1 (Briscoe et al., 2003; Hudson et al., 2014) is indicative of the activation of classical $G\alpha_q$ -phospholipase C signalling pathways. In previous section (4.3.1) I have shown that a selective and potent FFA1 agonist TUG-905 (Christiansen et al., 2012) causes a concentration-dependent increase in $[Ca^{2+}]_i$ level. In this section single-cell calcium imaging (section 2.5.16) was employed to study the desensitisation of hFFA1 at the functional level. Single-cell measurements allow repeated ligand treatment and washout. This study utilises fluorescence microscopy combined with dynamic video imaging to examine the events associated with desensitisation.

5.1.1 Repeated exposure of agonist desensitises hFFA1

Flp-InTM T-RExTM-293 cells able to express inducibly hFFA1-mVenus-HA were cultured onto poly-D-lysine coated coverslips and single-cell imaging was performed using an epifluorescence microscope. Exposure of cells to a FFA1-selective agonist TUG-905 (3 μ M) for 60 seconds, caused a transient increase in the level of intracellular calcium (Figure 5-1, A). However, following washout of

drug from the cells (5 minutes) with microscope buffer, the calcium level returned to baseline (Figure 5-1, A). Subsequent exposure of cells to the agonist for 60 seconds pulse at various intervals ($t = 420, 780$ and 1140 s; Figure 5-1, A) failed to elicit full calcium responses. The second-treatment with the agonist resulted in a response that was only $23.75 \% \pm 3.85\%$ ($p < 0.001$) of the first signal. A third and fourth treatment with TUG-905 resulted in responses of $23.66 \% \pm 4.63\%$ ($p < 0.001$) and $14.05 \% \pm 2.77\%$ ($p < 0.001$) of the original response respectively (Figure 5-1, A & B). So, acute activation of hFFA1 occurs within seconds of application of the agonist and is followed by acute desensitisation of this receptor.

However, the above results did not reflect a simple rundown of capacity of cells to generate calcium signals (for example, irreversible depletion of internal Ca^{2+} stores) because when cells were stimulated subsequently with ATP ($100 \mu\text{M}$) they were still competent to produce a full calcium response (Figure 5-1, A). Thus agonist-promoted activation of hFFA1 can lead not only to mobilisation of $[\text{Ca}^{2+}]_i$, but also to desensitisation of the functional signalling of the receptor.

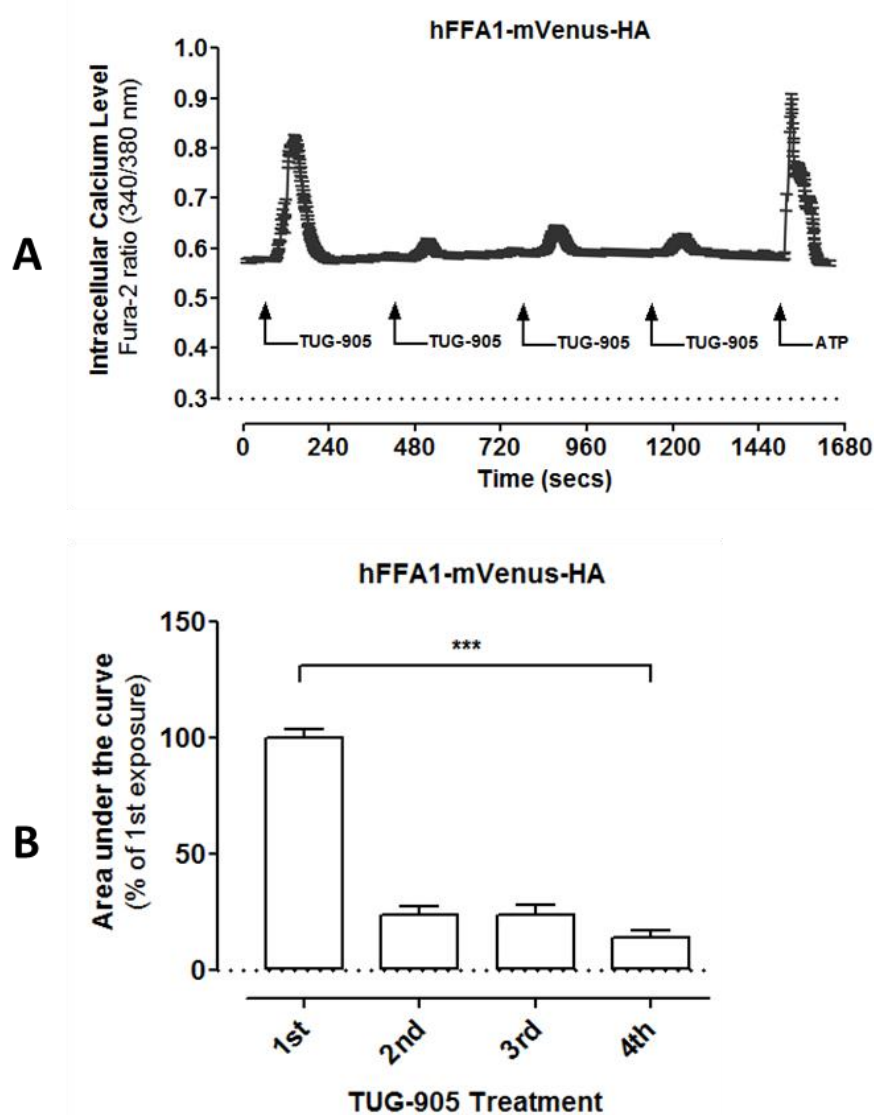


Figure 5-1. Repeated exposure hFFA1 to agonist desensitises the receptor. Flp-In™ T-REx™ 293 cells able to express hFFA1-mVenus-HA were plated down onto poly-*D*-lysine-coated 22 mm glass coverslips and receptor expression was induced using doxycycline (100 ng/ml). **(A)** Cells initially challenged for 60 seconds with TUG-905 (3 μ M) responded with an increase in $[Ca^{2+}]_i$ but failed to show full responses to subsequent agonist challenges ($t = 420, 780$ and 1140 s). ATP (100 μ M) treatment ($t = 1500$ s) showed full calcium response. **(B)** Mean of the area under the curve of calcium mobilisation were plotted (*** $p < 0.001$). Data represent mean \pm SEM from three separate experiments of at least 20 individual cells.

5.1.2 Internalisation of hFFA1

Agonist promoted internalisation of GPCRs is a common feature of desensitisation (Thomsen et al., 2016). Internalisation of mVenus-tagged hFFA1 in live cells was visualized using a Zeiss VivaTome spinning disk confocal microscopy system (section 2.5.8). Flp-InTM T-RExTM 293 cells able to inducibly express hFFA1-mVenus-HA were cultured on glass coverslips and challenged with 10 μ M of TUG-905 in a microscope chamber. Live cells were imaged before the addition of the agonist, and every 15 minutes after agonist addition for a total 45 minutes. A substantial proportion of hFFA1 was visualised inside the cell even before addition of TUG-905 (Figure 5-2). This might be due to a constitutive internalisation of the receptor. Exposure of the agonist beyond 45 minutes did not show any detectable change in the distribution pattern of hFFA1.

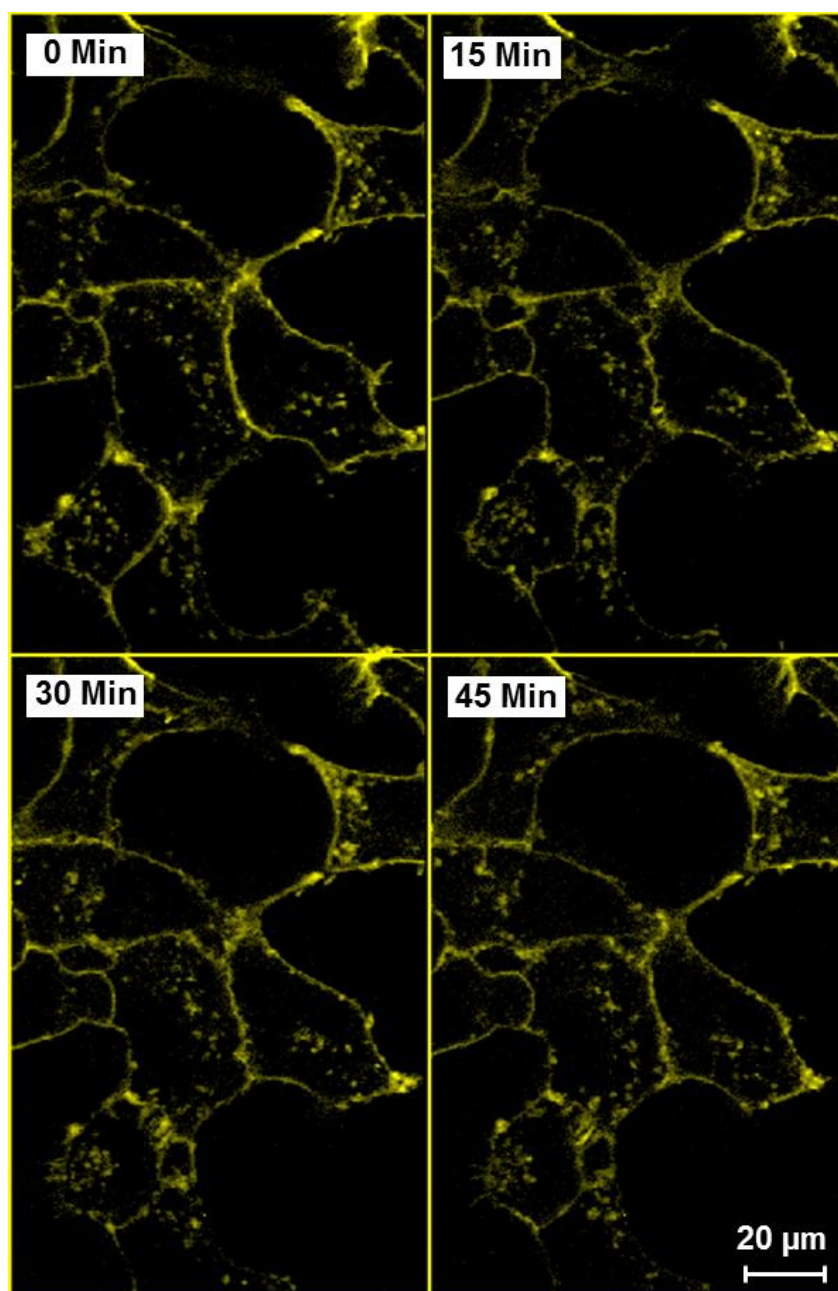


Figure 5-2. Visualisation of agonist promoted internalisation of hFFA1. Flp-In™ T-REx™ 293 cells able to express hFFA1-mVenus-HA were plated down onto poly-*D*-lysine-coated 30 mm glass coverslips and receptor expression was induced using doxycycline (100 ng/ml). The internalisation of hFFA1 in live cells was then imaged using a Zeiss VivaTome spinning disk confocal microscopy system (section 2.5.8). Images were taken before the addition of TUG-905 (10 μM), and every 15 minutes interval up to 45 minutes. All pictures shown are representative of two independent experiments.

To further investigate the hFFA1 internalisation, cells were incubated for 24 hours with a selective FFA1-antagonist GW-1100 (Briscoe et al., 2006) and imaged with a confocal microscope. Compared to the untreated (Figure 5-3, A) or vehicle treated (Figure 5-3, B) cells, GW-1100 did not make any apparent change to the distribution pattern of hFFA1 (Figure 5-3, C).

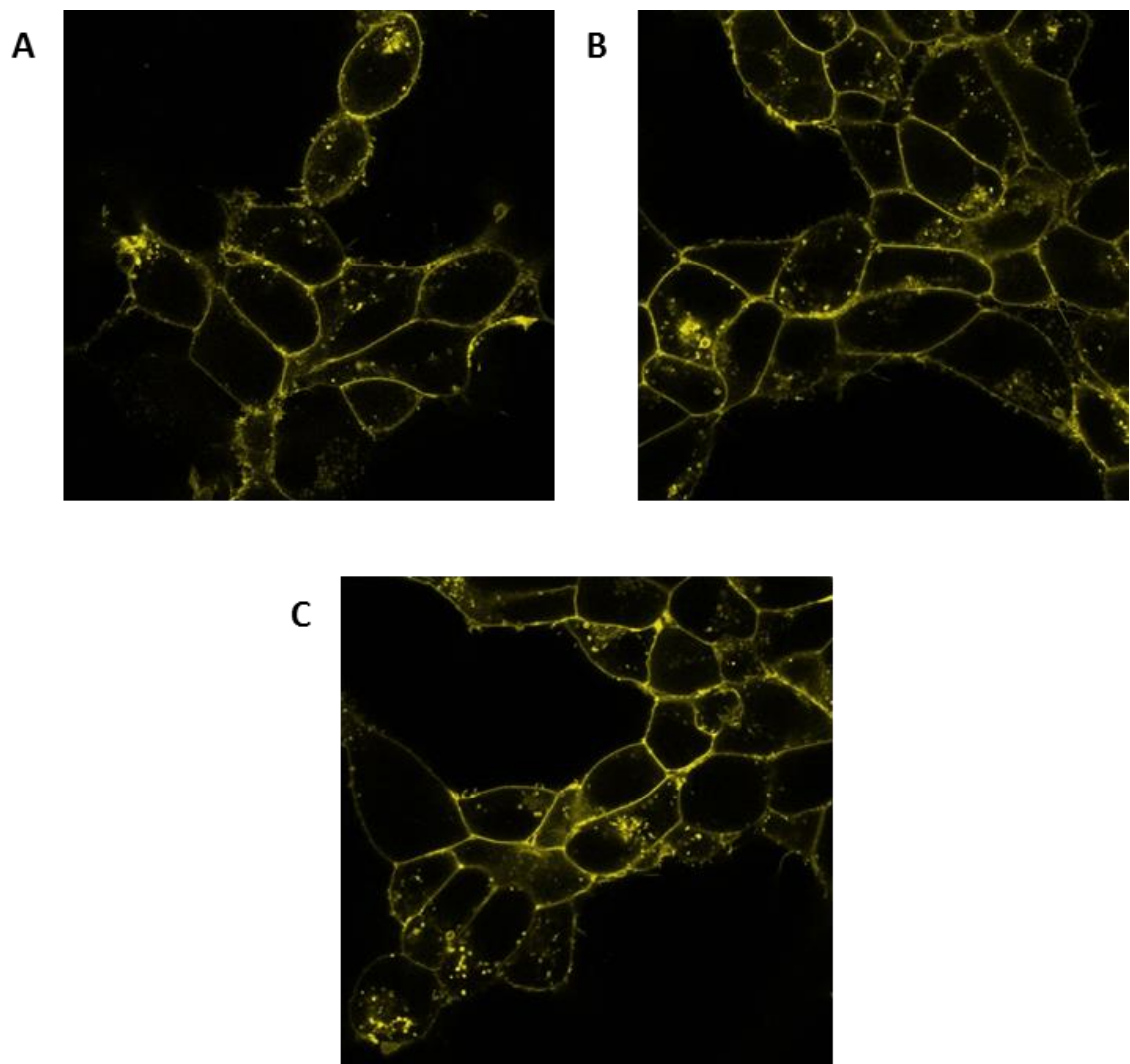


Figure 5-3. hFFA1 undergoes constitutive internalisation. Flp-In™ T-REx™ 293 cells able to express hFFA1-mVenus-HA were plated down onto poly-*D*-lysine-coated 30 mm glass coverslips and receptor expression was induced using doxycycline (100 ng/ml). Cells were incubated for 24 hours with **(A)** DMEM only (untreated) **(B)** vehicle (0.1% DMSO) and **(C)** GW-1100 (10 µM). Live cells were then imaged using a Zeiss VivaTome spinning disk confocal microscopy system (section 2.5.8). All pictures shown are representative of two independent experiments.

5.2 Desensitisation of hFFA4

Activation of FFA4 by long chain fatty acids (Hirasawa et al., 2005) or synthetic ligands (Hudson et al., 2013b) has been reported to result in an increase of intracellular calcium levels. Previously I have described that the FFA4 selective agonist TUG-891 (Shimpukade et al., 2012) evoked a specific rise of intracellular calcium level in a concentration-dependent fashion (section 4.1.1). These findings reflect the activation of $G_{q/11}$ signalling cascades for FFA4. Herein, I have described TUG-891 promoted functional desensitisation of hFFA4 employing single-cell calcium measurement.

5.2.1 Repeated exposure of agonist desensitises hFFA4

Flp-InTM T-RExTM-293 cells able to express inducibly FLAG-hFFA4-mVenus were loaded with Fura-2 AM and agonist-mediated change of fluorescence emission (340/380 nm) was monitored in a microscope chamber (section 2.5.16). A large transient rise in intracellular calcium level was recorded in response to the addition of TUG-891 (3 μ M) for 60 seconds (Figure 5-4, A). However, the level of calcium released returned to the baseline after ligand removal and washout (5 minutes). Following washout, a further 60 seconds treatment ($t = 420$ s) of cells with the agonist failed to elicit calcium response similar to the first treatment. The area under the curve of calcium level in the second treatment was only $66.19 \% \pm 6.42\%$ ($p < 0.01$) of the initial response (Figure 5-4, A & B). A third ($t = 780$ s) and fourth ($t = 1140$ s) treatments with TUG-891 resulted in further reduction to $51.96 \% \pm 5.50\%$ ($p < 0.001$) and $48.33 \% \pm 4.27\%$ ($p < 0.001$) respectively (Figure 5-4, A & B).

This reduction of response appeared not to be related to cell viability because cells were fully capable of eliciting calcium response when treated with ATP ($t = 1500$ s; Figure 5-4, A). Thus, repeated treatment of agonist to hFFA4 desensitises this receptor

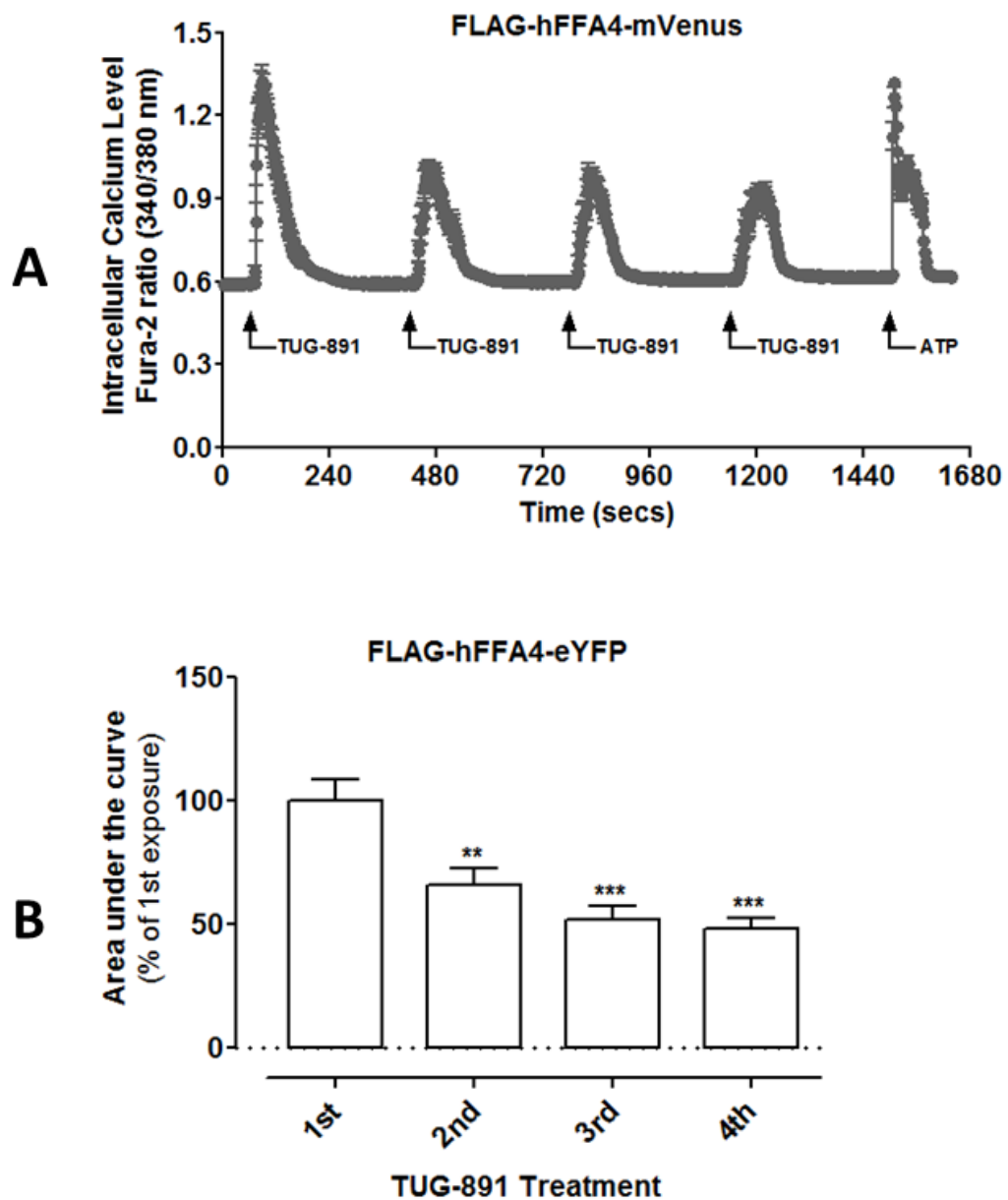


Figure 5-4. Agonist promoted desensitisation of hFFA4 signalling. Flp-In™ T-REx™ 293 cells able to express FLAG-hFFA4-mVenus were plated down onto poly-*D*-lysine-coated 22 mm glass coverslips and receptor expression was induced using doxycycline (100 ng/ml). **(A)** The capacity of 3 μ M TUG-891 to modulate intracellular calcium level was assessed in single-cell calcium imaging studies (section 2.5.16) of cells loaded with Fura-2 AM. **(B)** Mean of the area under the curve of calcium levels were plotted (** $p < 0.01$; *** $p < 0.001$ compared to initial signal). Data represent mean \pm SEM from three separate experiments of at least 20 individual cells.

5.2.2 Phosphorylation of hFFA4

The generally established paradigm for GPCR desensitisation involves receptor phosphorylation initiated by agonist (Gartner et al., 2013). This is the initial stage of desensitisation of receptors to promote interactions with β -arrestins and to initiate the uncoupling of G proteins from receptors (Moore et al., 2007). Homologous phosphorylation occurs by a number of G protein-coupled receptor kinases when agonist activates the GPCR (Kohout and Lefkowitz, 2003). However, GPCRs can be phosphorylated by downstream mediators of other GPCRs that employ the same G-protein effector pathways; this is termed heterologous phosphorylation (Lefkowitz and Shenoy, 2005). As phosphorylation of GPCRs can trigger β -arrestin recruitment (Thomsen et al., 2016), the ability of hFFA4 to be phosphorylated in an agonist-dependent or -independent manner was investigated in this section.

5.2.2.1 Homologous phosphorylation of hFFA4

Flp-InTM T-RExTM 293 cells inducibly expressing hFFA4 that incorporated a N-terminal FLAG-epitope tag and a C-terminal mVenus fluorophore (FLAG-hFFA4-mVenus) were employed to study agonist-promoted homologous phosphorylation. Cells were challenged for 10 minutes in the absence (baseline) or presence of varying concentrations of the agonist TUG-891 (Shimpukade et al., 2012) or TUG-1197 (Azevedo et al., 2016). Lysates of cells were resolved by SDS-PAGE (section 2.5.4) and phosphorylated receptors were identified by immunoblotting (\approx 50-70 kDa) using a phosphorylation-state specific antiserum, raised against a peptide of hFFA4-containing phospho-Thr³⁴⁷ and phospho-Ser³⁵⁰ (Butcher et al., 2014).

Both TUG-891 (Figure 5-5, A & B) and TUG-1197 (Figure 5-5, C & D) phosphorylated hFFA4 in a concentration-dependent fashion. Mean densitometry of the immunoblot from varying concentration of TUG-891 showed a plateau at 10 μ M ($EC_{50} \sim 1.6 \mu$ M; $p < 0.001$; Figure 5-5, B). TUG-1197 also produced maximal phosphorylation at 10 μ M ($EC_{50} \sim 4.2 \mu$ M; $p < 0.001$; Figure 5-5, D). Internal loading controls for such studies were provided by concurrent detection of levels of α -tubulin that migrates in SDS-PAGE at a position of a 50 kDa marker protein.

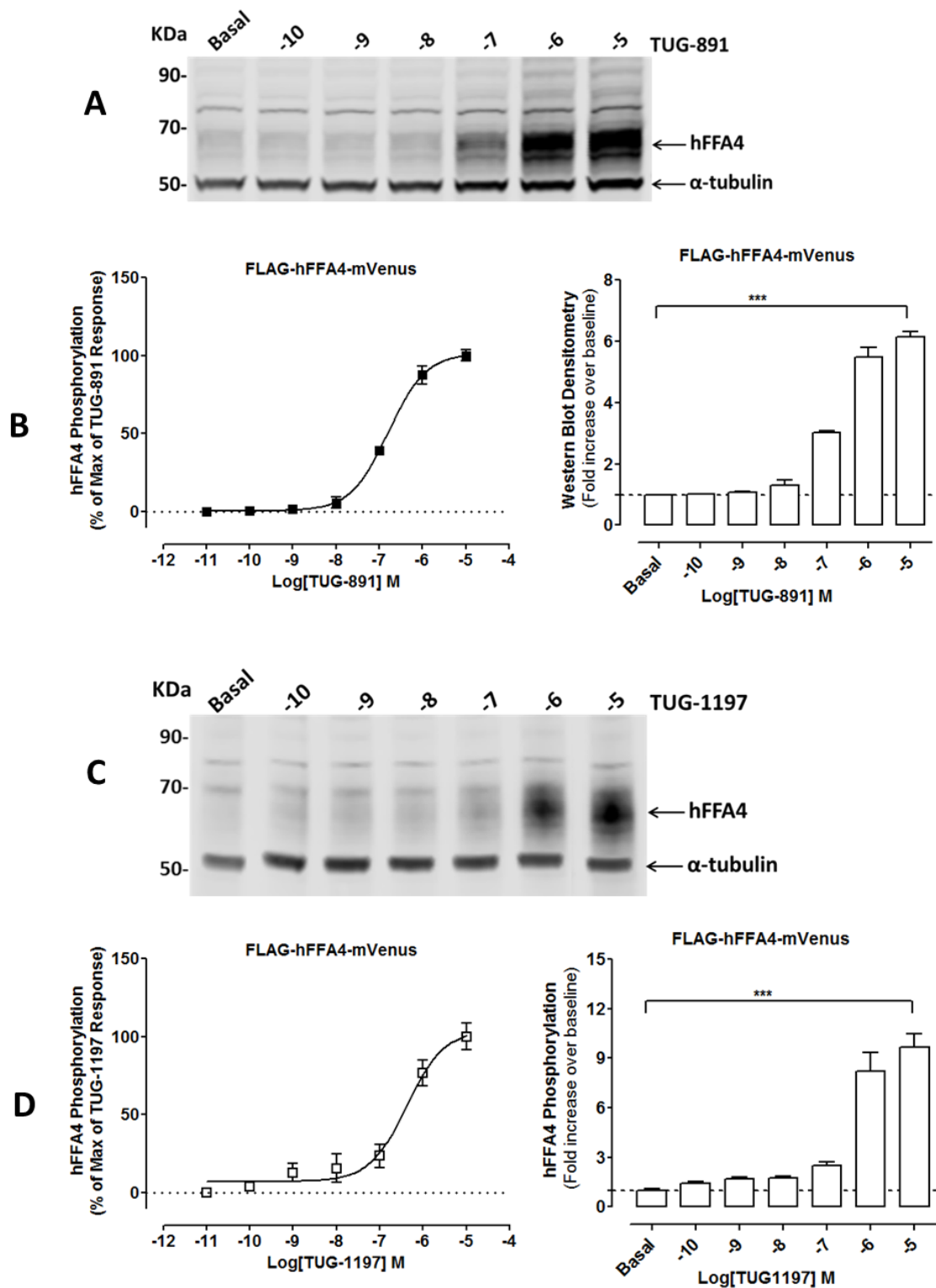


Figure 5-5. Homologous phosphorylation of hFFA4. Flp-In™ T-REx™ 293 cells able to express FLAG-hFFA4-mVenus were seeded in a 6-well plates and receptor expression was induced by the antibiotic doxycycline (100 ng/ml). Cells were challenged 10 minutes in the absence (baseline) or presence of varying concentrations of TUG-891 (**A-B**) or TUG-1197 (**C-D**). Lysates of cells were then resolved by SDS-PAGE (section 2.5.4) and phosphorylated receptors were detected by immunoblotting (section 2.5.5) with a phospho-Thr³⁴⁷/Ser³⁵⁰ hFFA4 antiserum. In (**A**) and (**C**) antibodies to α-tubulin were co-added with the phospho-Thr³⁴⁷/Ser³⁵⁰ hFFA4 antiserum and provided a control for equal loading of the lanes of the SDS-PAGE. Densitometry of immunoblots were plotted (***) $p < 0.001$; **B, D**). Data represent the mean \pm SEM of three independent experiments.

These data indicate that each agonist promoted homologous phosphorylation of hFFA4. With 10 μM concentration TUG-891 caused 6 fold increase of phosphorylation of hFFA4 which was 9 fold increase of TUG-1197. However, both TUG-891 and TUG-1197 showed phosphorylation plateau at 10 μM concentration (Figure 5-5, B & D).

5.2.2.2 Protein kinase C mediated heterologous phosphorylation of hFFA4

It is a common phenomenon that GPCRs can undergo heterologous phosphorylation by downstream mediators of other GPCRs (Burns et al., 2014; Lefkowitz and Shenoy, 2005). The heterologous process typically involves protein kinase A and protein kinase C (PKC), which are linked to adenylyl cyclase and phospholipase C cascades, respectively (Thomsen et al., 2016). A PKC activator phorbol myristate acetate (PMA) was used to examine potential heterologous phosphorylation of hFFA4.

Flp-InTM T-RExTM 293 cells able to inducibly express FLAG-hFFA4-mVenus were challenged with different concentrations of PMA. SDS-PAGE of the lysates and subsequent immunoblotting using FFA4-phospho-Thr³⁴⁷/Ser³⁵⁰ antibodies (Butcher et al., 2014) showed a concentration-dependent phosphorylation of hFFA4 (Figure 5-6, A & B). Maximal phosphorylation was produced 1 μM (EC_{50} ~35 nM; $p < 0.001$; Figure 5-6, B).

To confirm the involvement of PKC in this phosphorylation, two PKC inhibitors, bis-indolyl-maleimide-I (BIM-I) and Go-6976 (Sánchez-Reyes et al., 2014) were utilized. Cells were pre-treated for 15 minutes in absence (basal) or presence of 1 μM BIM-I or Go-6976 followed by 10 minutes incubation with PMA (1 μM). Both BIM I ($p < 0.01$) and Go 6976 ($p < 0.05$) significantly inhibited PMA induced phosphorylation of hFFA4 (Figure 5-6, C & D).

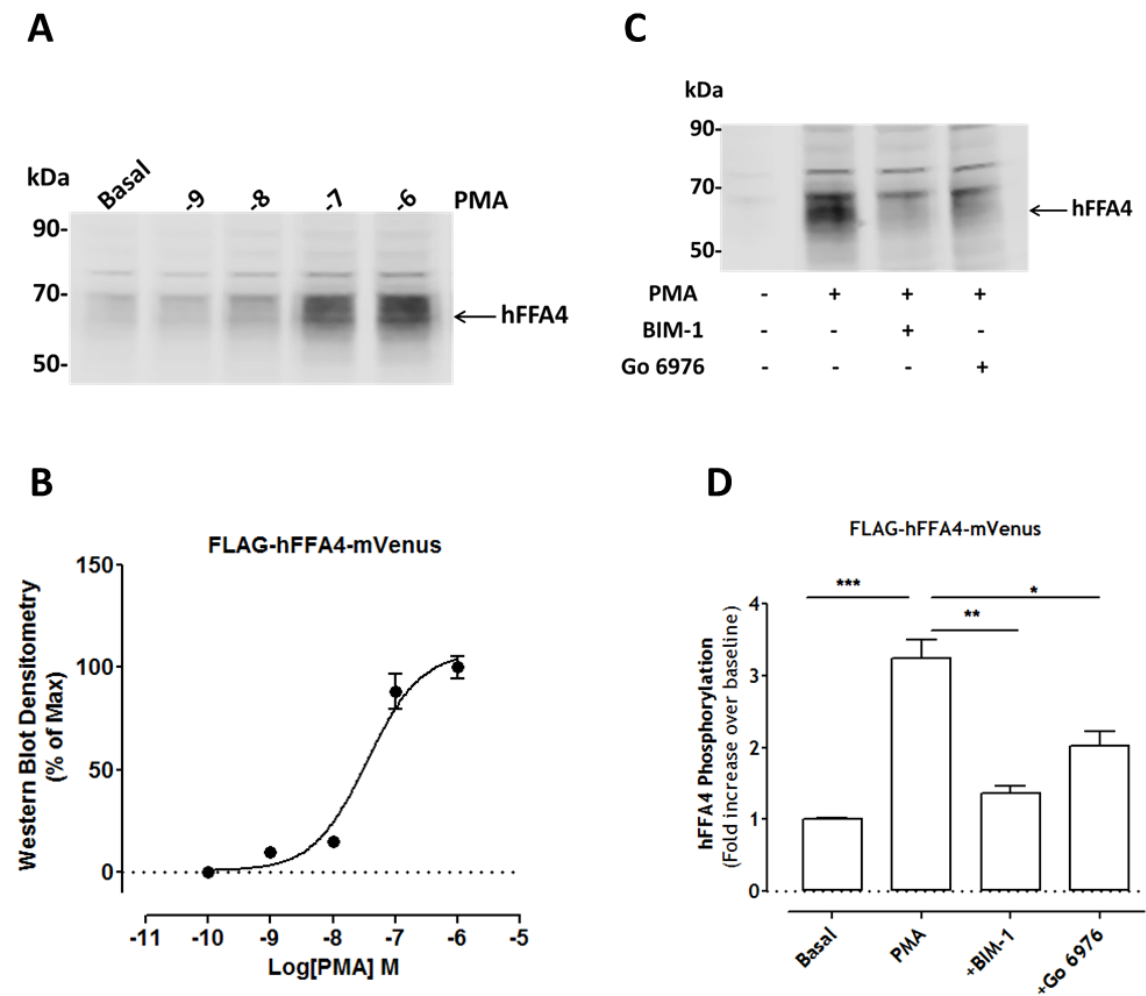


Figure 5-6. Protein kinase C mediates heterologous phosphorylation of hFFA4. (A) Flp-In™ T-REx™ 293 cells able to express FLAG-hFFA4-mVenus were challenged for 10 minutes in the absence (baseline) or presence of varying concentration of phorbol myristate acetate (PMA). (C) Cells were pre-treated 15 minutes in absence (basal) or presence of 1 μ M bis-indolyl-maleimide I (BIM I) or Go-6976 followed by 10 minutes co-treatment with PMA (1 μ M). Lysates of cells were resolved by SDS-PAGE and phosphorylated receptors were detected by immunoblotting with a phospho-Thr³⁴⁷/Ser³⁵⁰ hFFA4 antiserum. (B, D) Densitometry of immunoblots (* p <0.05; ** p <0.01; *** p <0.001). Data represent the mean \pm SEM of three independent experiments.

Next, I examined the contribution of PKC to agonist-promoted phosphorylation of hFFA4 in the absence (basal) or presence of BIM-I (1 μ M) or Go-6976 (1 μ M). The immunoblot indicated that BIM-I and Go-6976 were not able to abolish, but significantly ($p<0.05$) inhibited TUG-1197 promoted phosphorylation of hFFA4 (Figure 5-7).

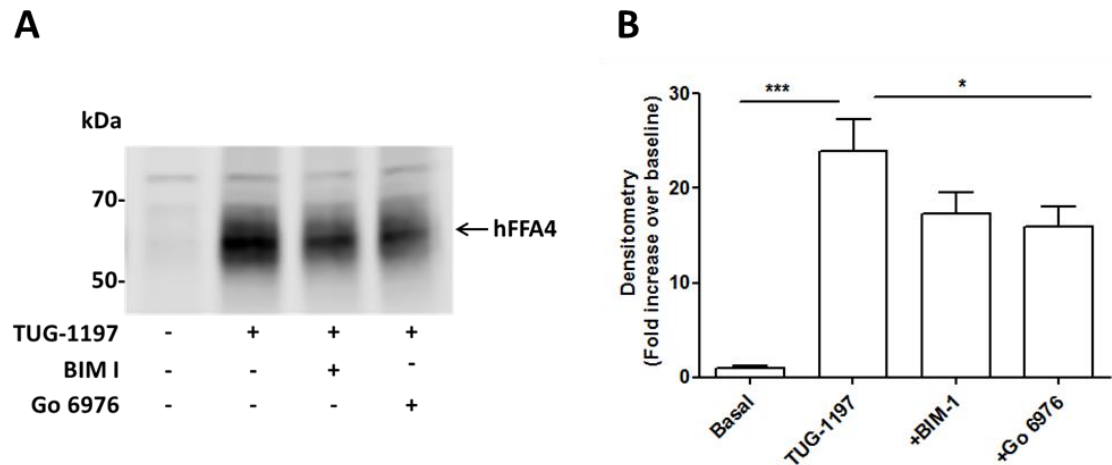


Figure 5-7. PKC contributes to agonist-promoted phosphorylation of hFFA4. (A) Flp-In™ T-REx™ 293 cells able to express FLAG-hFFA4-mVenus were pre-treated for 15 minutes in the absence (basal) or presence of BIM-I (1 μ M) or Go-6976 (1 μ M) followed by 10 minutes co-treatment with TUG-1197 (10 μ M). Lysates of cells were resolved by SDS-PAGE and phosphorylated receptors were detected by immunoblotting with a phospho-Thr³⁴⁷/Ser³⁵⁰ hFFA4 antiserum. (B) Densitometry of immunoblots (** $p<0.001$ compared to basal; * $p<0.05$ compared to TUG-1197). Data represent the mean \pm range.

5.2.3 Internalisation of hFFA4

In drug discovery using FFA4, many of the ligands have been identified using the process of ligand-induced receptor internalisation (Hirasawa et al., 2005; Hudson et al., 2013b). Rapid internalisation of the agonist-activated receptor into the intracellular compartments of target cells plays an important role in the regulation of GPCR signalling and desensitisation (Ferguson, 2001). Ligand-induced changes in the internalisation of FLAG-hFFA4-mVenus in to endocytic compartments can be visualised using confocal microscopy (section 2.5.8) and the internalised receptors can be quantified using a high content imager, e.g. the ArrayScan II (section 2.5.12). Cell surface ELISA (section 2.5.19) and biotinylation (section 2.5.18) are also important techniques to quantify cell surface receptors and hence receptor internalisation. Utilising all of these methods ligand-mediated internalisation of FFA4 was examined in Flp-In™ T-REx™ 293 cells able to inducibly express FLAG-hFFA4-mVenus (section 3.2.1).

5.2.3.1 Visualisation of agonist promoted internalisation of hFFA4

A Zeiss VivaTome spinning disk confocal microscopy system was used to visualise the internalisation of mVenus-tagged hFFA4 in live cells. Cells were challenged with TUG-891 (10 μ M) and ligand-promoted internalisation of hFFA4 was monitored every 15 minutes after ligand addition for a total 45 minutes.

Before the addition of the agonist TUG-891 the mVenus-tagged receptors were located primarily at the cell surface (Figure 5-8). Within 15 minutes of the addition the agonist, the intensity of mVenus became less distinct at the cell surface and punctate clusters of receptors were seen in intracellular vesicles. The internalised mVenus spots increased over time and within the 45 minutes of incubation most of the receptors were inside the cell (Figure 5-8).

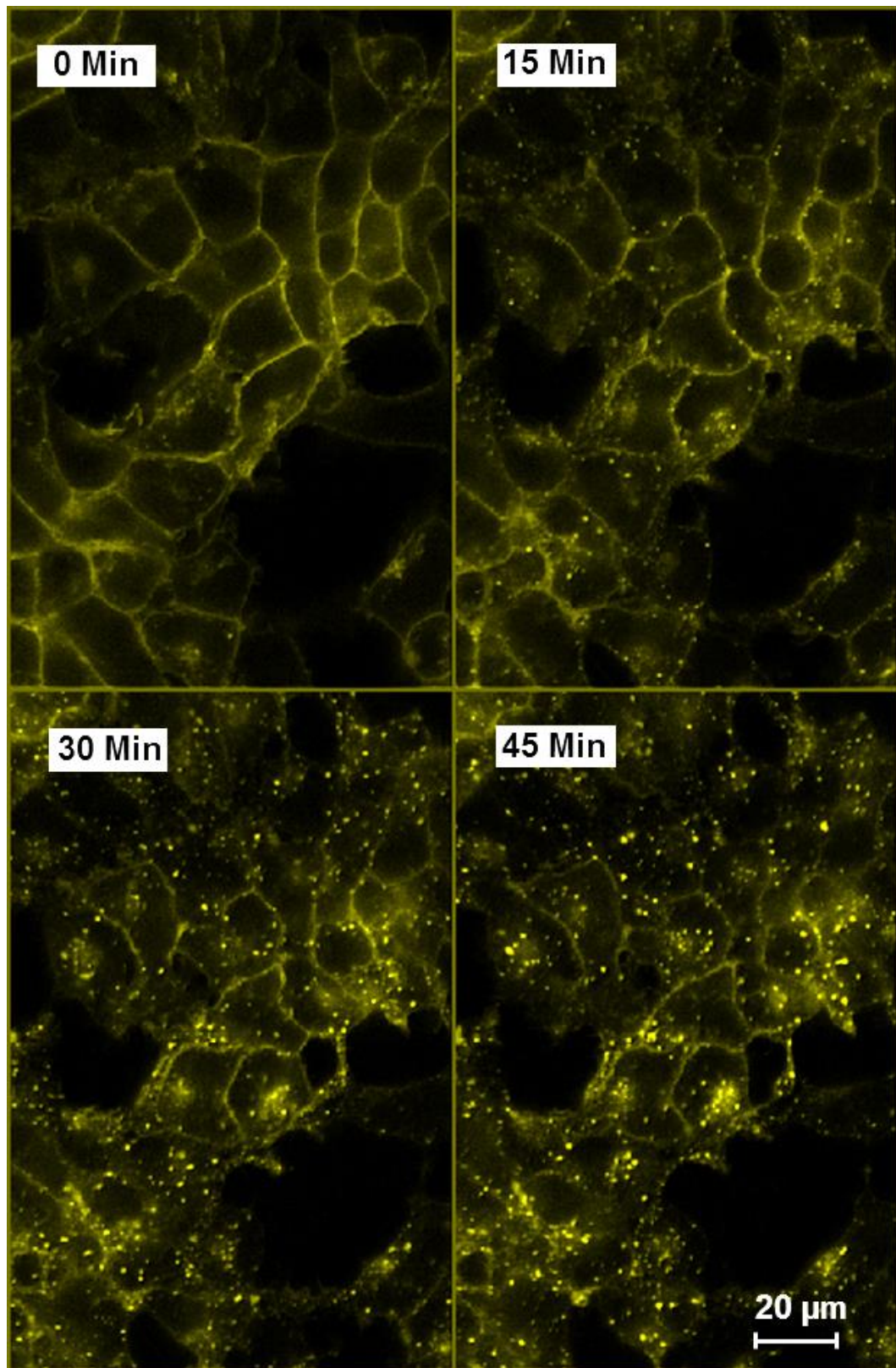


Figure 5-8. TUG-891 promotes internalisation of hFFA4. Flp-In™ T-REx™ 293 cells able to express FLAG-hFFA4-mVenus were plated down onto poly-*D*-lysine-coated 30 mm glass coverslips and receptor expression was induced using doxycycline (100 ng/ml). The internalisation of hFFA4 in live cells was then imaged using a Zeiss VivaTome spinning disk confocal microscopy system (section 2.5.8). Images were taken before the addition of TUG-891 (10 μM), and every 15 minutes after ligand addition for a total of 45 minutes. All pictures shown are representative of three independent experiments.

5.2.3.2 Visualisation of PMA-mediated internalisation of hFFA4

As PMA treatment caused phosphorylation of hFFA4 (Figure 5-6), it was of interest to investigate whether PMA could promote internalisation of the receptor. Cells cultured on glass coverslips were challenged with PMA (1 μ M) and receptor internalisation was imaged at 15 minute intervals for a total 45 minutes. Interestingly, within 15 minutes of PMA-treatment, a strong internalisation of hFFA4-mVenus into the intracellular vesicle was noted. The internalised spots increased over time and within 45 minutes most of the receptors were inside the cell (Figure 5-9).

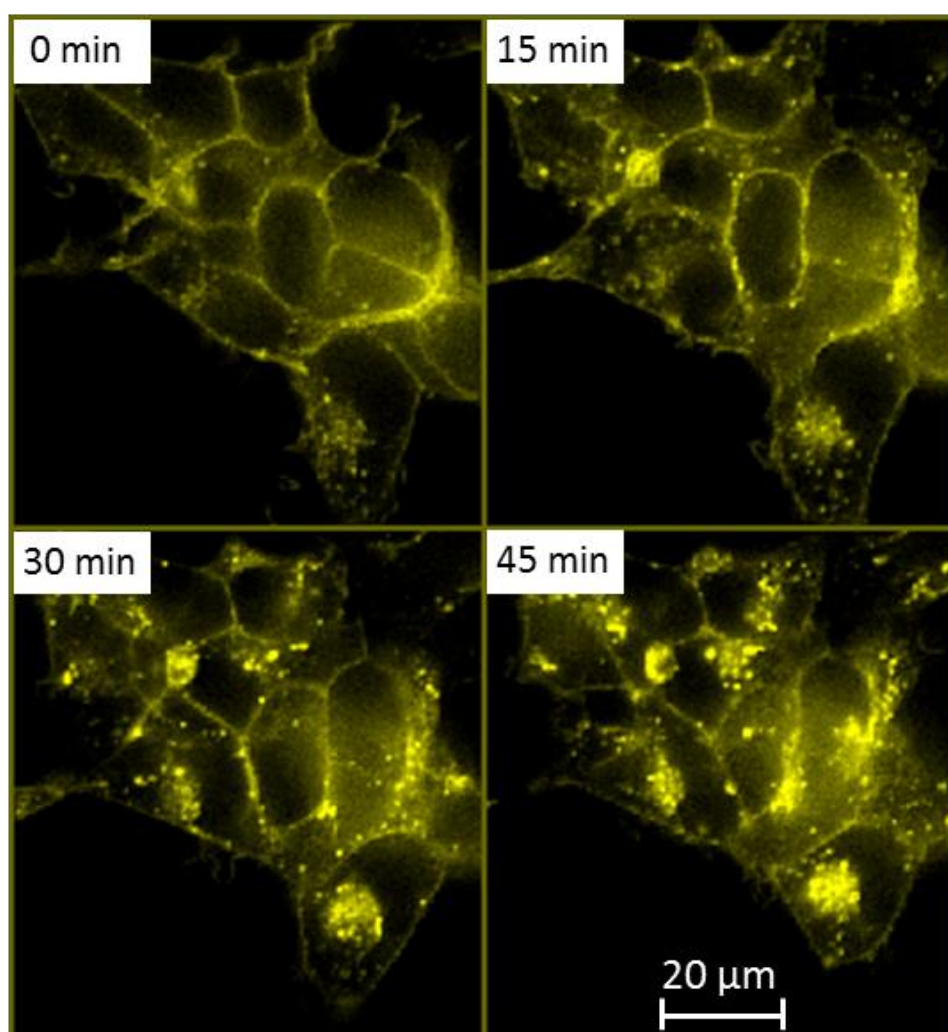


Figure 5-9. PMA induces internalisation of hFFA4. Flp-In™ T-REx™ 293 cells able to express FLAG-hFFA4-mVenus were plated down onto poly-*D*-lysine-coated 30 mm glass coverslips and receptor expression was induced using doxycycline (100 ng/ml). The internalisation of hFFA4 in live cells was then imaged using a Zeiss VivaTome spinning disk confocal microscopy system (section 2.5.8). Images were taken before the addition of PMA (1 μ M), and every 15 minutes after ligand addition for a total of 45 minutes. All pictures shown are representative of two independent experiments.

The role of PKC in PMA-mediated FFA4-internalisation was further investigated with the aid of the PKC inhibitor BIM-I. Cells were pre-treated with BIM-I (1 μ M) followed by co-addition of PMA (1 μ M) and then visualised under a confocal microscope. Before addition of BIM-1, mVenus-tagged hFFA4 were mostly detected at the cell membrane (Figure 5-10). Images from incubation of BIM-I at zero minute and 15 minutes did not show any apparent change in the internalisation. After 15 minutes of BIM-I addition, PMA was added in the microscope chamber and the change of internalisation was monitored in every 15 minutes for the next 60 minutes. In comparison to cells treated only with PMA (60 min; Figure 5-9), BIM-I treatment showed an apparent reduction of the internalisation of hFFA4 (Figure 5-10).

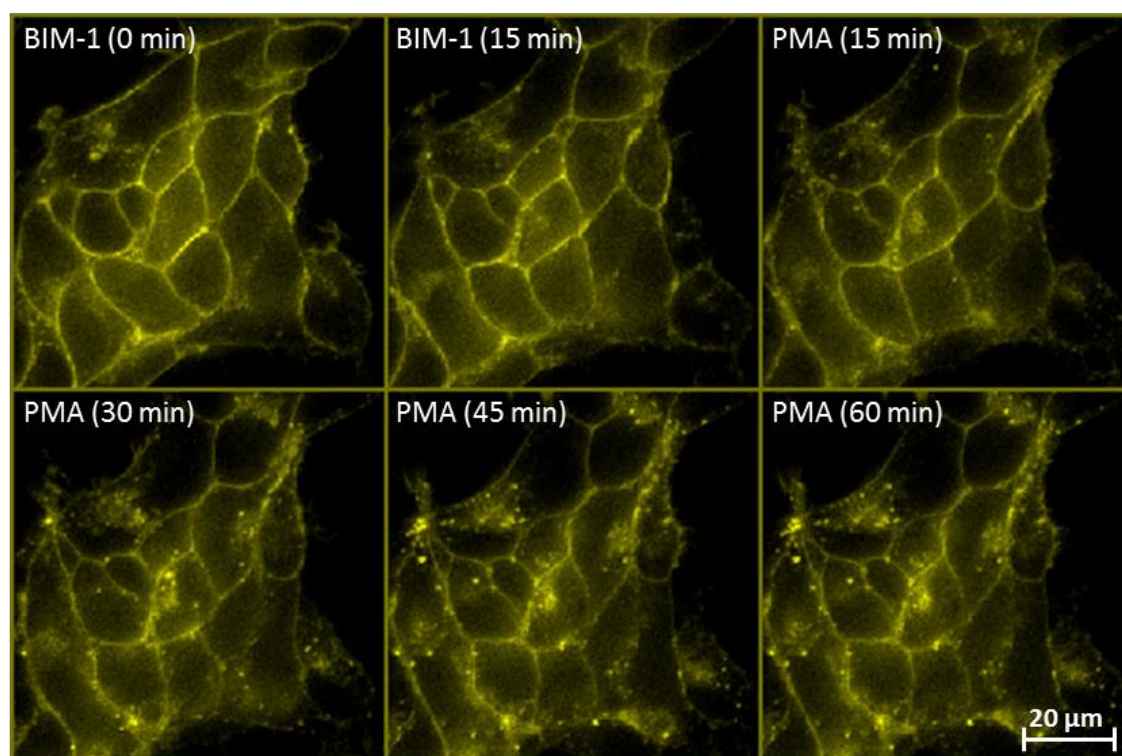


Figure 5-10. Role of PKC in the internalisation of hFFA4. Flp-In™ T-REx™ 293 cells able to express FLAG-hFFA4-mVenus were plated down onto poly-*D*-lysine-coated 30 mm glass coverslips and receptor expression was induced using doxycycline (100 ng/ml). The internalisation of hFFA4 in live cells was imaged using a Zeiss VivaTome spinning disk confocal microscopy system (section 2.5.8). Images were taken at zero minutes and after 15 minutes of BIM-I (1 µM); PMA (1 µM) was then added and cells were imaged every 15 minutes. Figure 5-9 was used as control. All pictures shown are representative of two independent experiments.

5.2.3.3 Quantification of hFFA4 internalisation

Ligand-induced changes in the amount of internalisation of FLAG-hFFA4-mVenus in to endocytic compartments were calculated using an automated cell-based imaging and analysis system ArrayScan™ II (Conway et al., 1999) (section 2.5.12). This quantitative cytometric high content imager counts in each well both the number of nuclei stained by Hoechst 33342 and the number of internalised fluorescent-tagged receptor spots, methods previously described by Hudson et al (2013b). The level of internalisation was expressed as % of maximum response.

Flp-In™ T-REx™ 293 cells able to express FLAG-hFFA4-mVenus were challenged with varying concentrations of TUG-891 and TUG-1197 and the internalised receptors were quantified in the ArrayScan II plate reader. Both of the agonists showed a concentration-dependent increase in internalisation of receptors (Figure 5-11, A & B). Both TUG-891 and TUG-1197 displayed similar potency ($pEC_{50} = 6.97 \pm 0.08$ for TUG-891 and 6.76 ± 0.20 for TUG-1197).

As the protein kinase C activator PMA also caused hFFA4 phosphorylation (Figure 5-6) and receptor internalisation (Figure 5-9), it was of interest to quantify the PMA induced internalisation of hFFA4. PMA treatment for 45 minutes was found to internalise hFFA4 in a concentration-dependent fashion (Figure 5-11, C) with $pEC_{50} 6.09 \pm 0.11$.

A time course of agonist promoted internalisation was also investigated. Cells were treated with TUG-891 (10 μ M) for varying time points up to 60 minutes. The internalisation plateau reached within 30 minutes of agonist exposure (Figure 5-11, D).

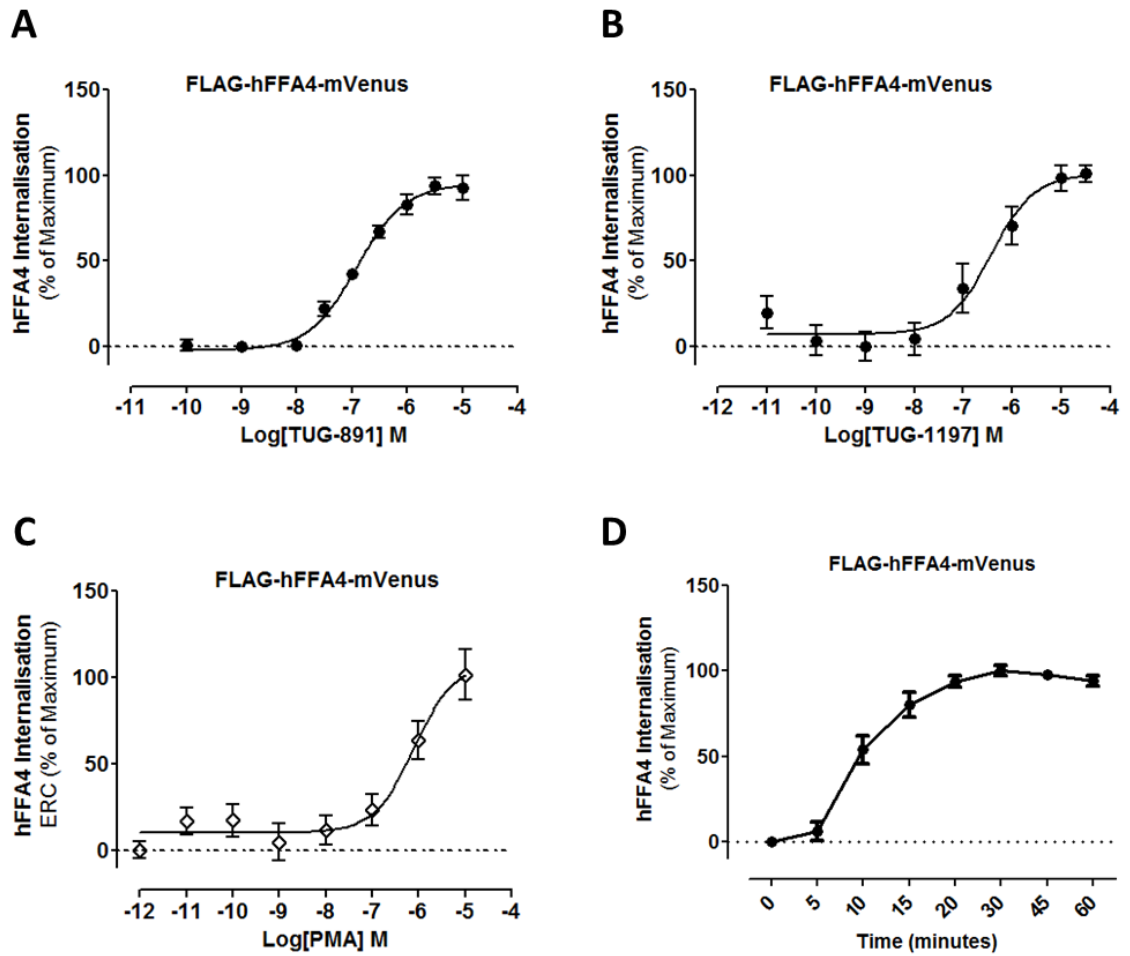


Figure 5-11. Quantification of hFFA4 internalisation. Flp-In™ T-REx™ 293 cells able to express FLAG-hFFA4-mVenus were seeded (70,000 cells /well) into poly-D-lysine coated black clear-bottom 96-well plates. Expression of hFFA4 was induced by the antibiotic doxycycline (100 ng/ml) for 18-24 hours. **(A)** TUG-891, **(B)** TUG-1197 and **(C)** PMA promoted internalisation of hFFA4 was measured using ArrayScan II (section 2.5.12). **(D)** A time course of internalisation was measured in cells treated with TUG-891 up to 60 minutes. Efficacy was normalized as percentage of maximum response. Data represent the mean \pm SEM of three independent experiments.

5.2.3.4 Internalisation of hFFA4 quantified by cell surface ELISA

Cell surface enzyme-linked immunosorbent assay (ELISA) is an immunoenzymatic technique (section 2.5.19) for the quantitative detection of cell-surface molecules (Gan and Patel, 2013; Lourenco and Roque-Barreira, 2010). Analysis of receptor internalisation by this method was based herein on the presence of an N-terminal epitope tag, FLAG on hFFA4 receptor, which can no longer be recognized by the cognate antibody once the receptor is internalised. So, it has been hypothesised that removal of N-terminal FLAG-epitope tag from the cell surface would define the extent of internalisation of the FLAG-hFFA4-mVenus receptor construct after exposure to agonists.

Flp-InTM T-RExTM 293 cells able to express FLAG-hFFA4-mVenus were treated for 45 minutes with varying concentrations of TUG-891 and cells were then treated with an anti-FLAG antibody to detect cell surface FLAG-tagged receptors. TUG-891 resulted a concentration-dependent decrease of the surface receptors ($pEC_{50} = 7.07 \pm 0.12$) (Figure 5-12, A). A time course of internalisation of hFFA4 was also investigated in this cell line treated with TUG-891 (10 μ M) for up to 60 minutes. Within 15 minutes of agonist exposure there was a significant reduction ($P < 0.05$) of surface FLAG-hFFA4-mVenus (Figure 5-12, B). About 40% reduction of cell surface hFFA4 was noted in these experiments (Figure 5-12, B).

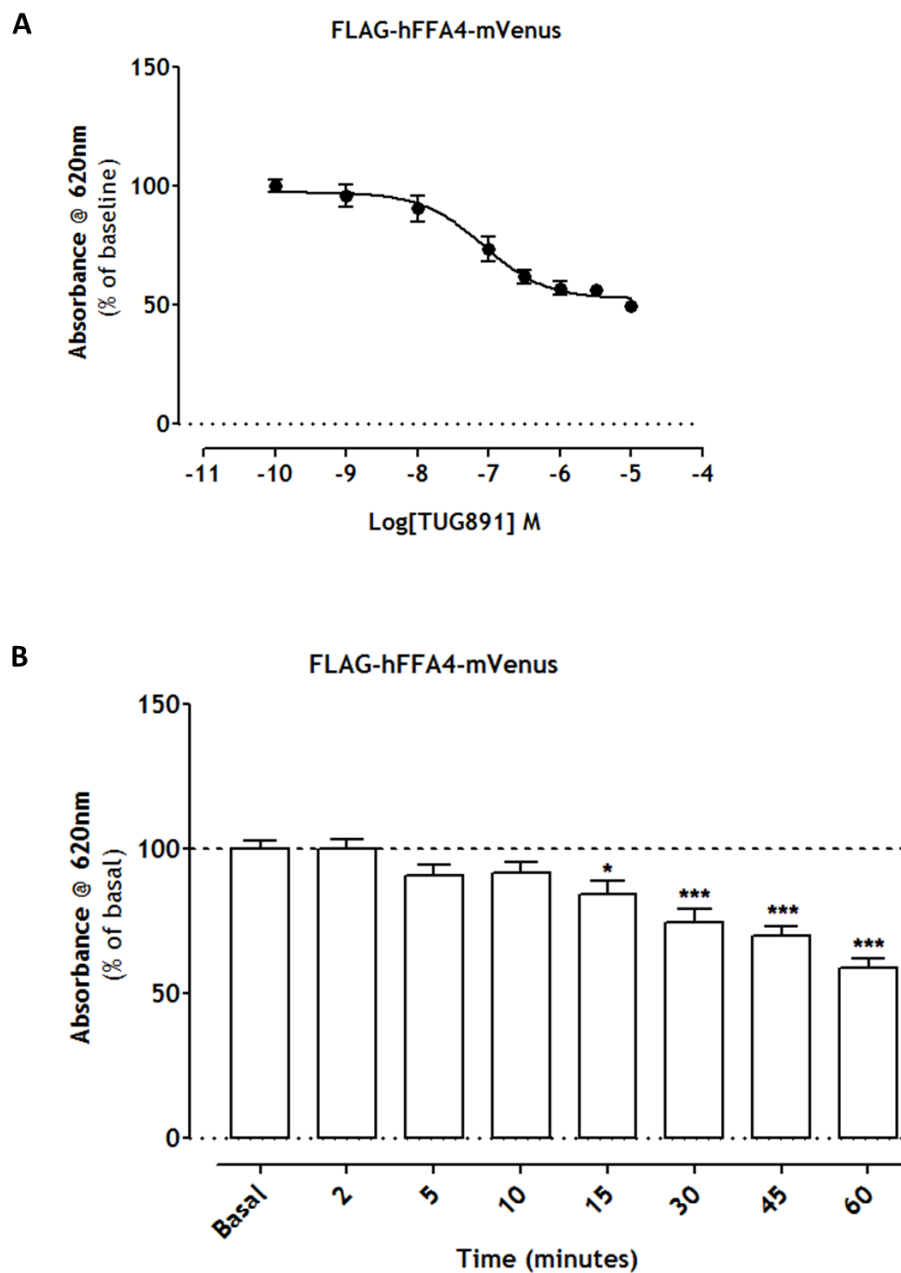


Figure 5-12. Ligand regulation of cell surface hFFA4. Flp-In™ T-REx™ 293 cells harbouring FLAG-hFFA4-mVenus were induced by doxycycline to express the receptor construct. **(A)** Cells were treated for 45 minutes with varying concentrations of TUG-891. **(B)** Cells were challenged with TUG-891 (10 μ M) for indicated times. Cell surface ELISA (section 2.5.19) was performed using an anti-FLAG monoclonal primary antibody and with an anti-mouse horseradish peroxidase-conjugated secondary antibody. Absorption at 620 nm was recorded after addition of the substrate 3,3',5,5'-tetramethylbenzidine. Such studies were quantified as 100% of cell surface hFFA4 in vehicle (0.1% DMSO) treated cells (basal). Data represent the mean \pm SEM of three independent experiments (* p <0.05, *** p <0.001 compared to basal).

5.2.3.5 Internalisation of hFFA4 quantified by biotinylation

Incorporation of a biotin label is an effective way to assess cell surface proteins and their subsequent trafficking in cell populations (Ward et al., 2013). To quantify agonist-promoted internalisation of hFFA4, a cell surface biotin labelling technique (section 2.5.18) was employed here.

Expression of FLAG-hFFA4-mVenus was induced with doxycycline in Flp-In™ T-REx™ 293 cells and these were treated with TUG-891 (10 μ M) for different periods of time. Cells were then subjected to biotinylation to identify cell surface receptor proteins. Biotinylated proteins were isolated and then resolved by SDS-PAGE (section 2.5.4). Detection of biotinylated anti-GFP immunoreactivity (section 2.5.5) in samples from both untreated and TUG-891-treated cells defined the presence of cell surface receptors (\approx 48-66 kDa). TUG-891 treatment showed a gradual decrease of hFFA4-mVenus at the cell surface with time (Figure 5-13, A). The cell surface receptors with 5 minutes and 10 minutes agonist exposure were $86.44\% \pm 8.62\%$ ($p>0.05$) and $83.76\% \pm 6.05\%$ ($p>0.05$) respectively. However, within 15 and 30 minutes only $64.01\% \pm 3.87\%$ ($p<0.01$) and $50.82\% \pm 7.84\%$ ($p<0.01$) receptor were on the cell surface (Figure 5-13, B). Immunoblot from total lysates showed no apparent change in the amount of total hFFA4 expression over this period (Figure 5-13, C).

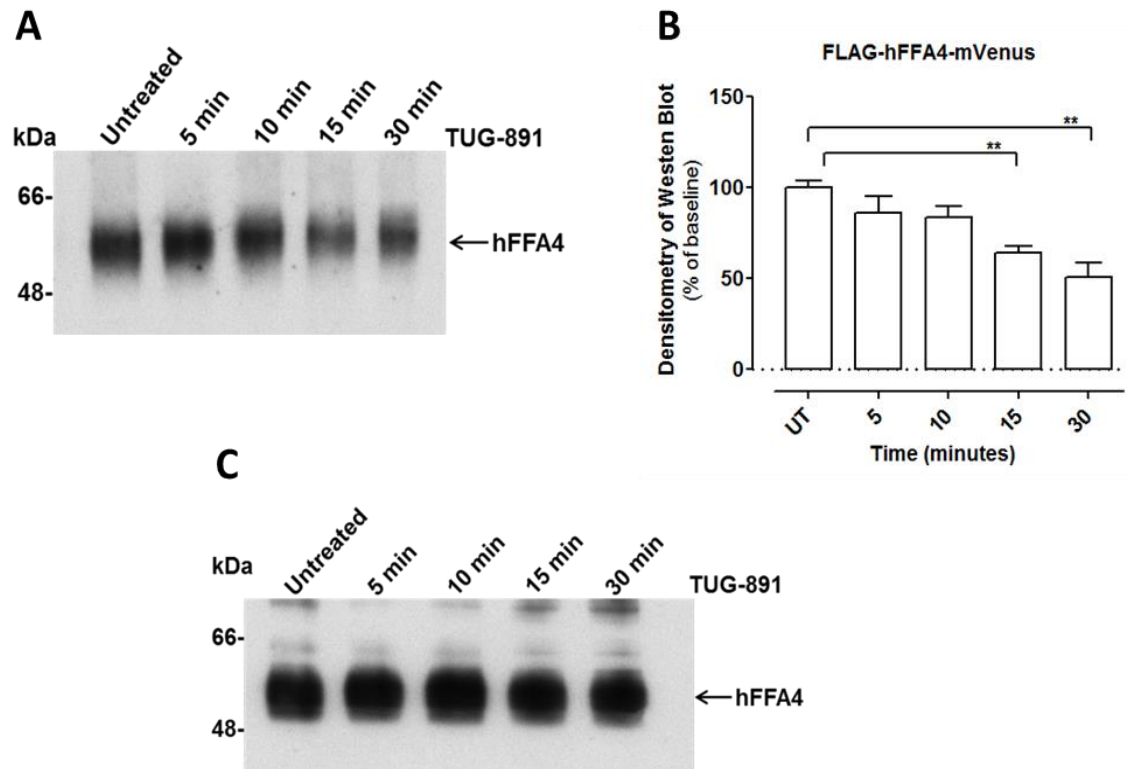


Figure 5-13. Quantification of hFFA4 internalisation by biotinylation. Flp-In™ T-REx™ 293 cells harbouring FLAG-hFFA4-mVenus were challenged with TUG-891 (10 μ M) for the indicated time period. Cell surface receptors were biotinylated (section 2.5.18) and isolated with streptavidin-agarose beads. **(A)** Precipitated samples and **(C)** total lysates were then resolved by SDS-PAGE and immunoblotted (section 2.5.5) with anti-GFP antiserum. **(B)** Densitometry (section 2.5.6) of the immunoblot A (** p <0.01). Data represent the mean \pm SEM of three independent experiments.

5.3 Role of β -arrestins in the desensitisation process

In the classical paradigm of desensitisation processes, activation of GPCRs with agonist leads to coupling of heterotrimeric G proteins, followed by phosphorylation of GPCRs which triggers the recruitment of β -arrestins, leading to receptor desensitisation and internalisation (Thomsen et al., 2016; Ranjan et al., 2016). In this section, I investigated the role of β -arrestin1/2 in the desensitisation of the long chain fatty acid receptors hFFA1 and hFFA4.

5.3.1 β -arrestin1/2 in the desensitisation of hFFA1

5.3.1.1 Agonist promotes recruitment of β -arrestin2 to hFFA1

Arrestins have been described to play an important role in the internalisation of most GPCRs (Thomsen et al., 2016). Therefore, the interaction of the hFFA1 receptor and β -arrestin2 was investigated. BRET method was applied in HEK293T cells transiently transfected with hFFA1-mVenus-HA and β -arrestin2-Renilla luciferase. I have described previously (section 4.3.2) that the agonists TUG-770 and TUG-905 promoted β -arrestin2 recruitment to hFFA1 in a concentration-dependent fashion (Figure 4-12).

5.3.1.2 β -arrestin1/2 and agonist promoted internalisation of hFFA1

To explore the consequences of elimination of β -arrestin1/2 for agonist promoted internalisation of hFFA1, HEK293 parental cells and CRISPR/Cas9 genome edited, β -arrestin1/2-null cells (Alvarez-Curto et al., 2016b; Schrage et al., 2015) constitutively expressing hFFA1-mVenus-HA were employed. The absence of β -arrestin1 in the knockout cells was confirmed by immunoblotting (section 3.1.4).

Cells were treated with the selective FFA1 agonist TUG-905 (10 μ M) and internalisation was imaged using confocal microscopy (section 2.5.8). Cells were imaged before agonist treatment and every 15 minutes after ligand addition for a total of 45 minutes. Surprisingly, no detectable change of internalisation was found in either of the cell lines (Figure 5-14).

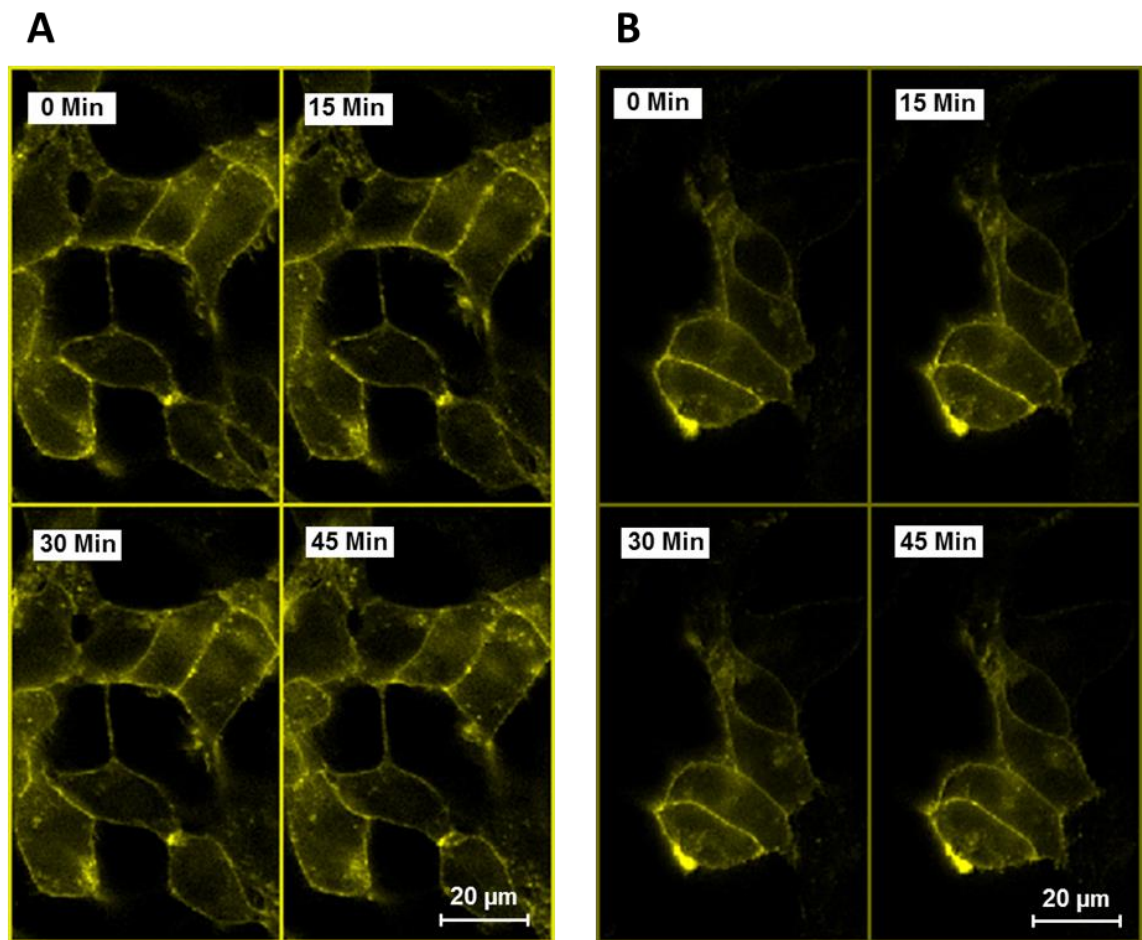


Figure 5-14. Visualisation of agonist promoted internalisation of hFFA1. hFFA1-mVenus-HA was constitutively expressed in (A) HEK293 parental cells and (B) β -arrestin1/2-null HEK293 cells. Cells were plated down onto poly-*D*-lysine-coated 30 mm glass coverslips and the internalisation of hFFA1 was then imaged using a Zeiss VivaTome spinning disk confocal microscopy system (section 2.5.8). Images were taken before the addition of TUG-905 (10 μ M), and every 15 minutes after ligand addition for a total of 45 minutes. All pictures shown are representative of two independent experiments.

5.3.1.3 β -arrestin1/2 has no effect on functional desensitisation of hFFA1

Functional desensitisation of hFFA1 was seen previously (Figure 5-1) in Flp-In™ T-REx™-293 cells inducibly expressing hFFA1-mVenus-HA. Hence, HEK293 cells and β -arrestin1/2-null cells constitutively expressing hFFA1 were employed to investigate the effect of elimination of β -arrestin1/2 on the desensitisation of hFFA1.

Single-cell calcium imaging (section 2.5.16) in both of the cell lines showed that a 60 second exposure to TUG-905 (3 μ M) resulted in a sharp increase of intracellular calcium level which gradually reduced with removal of agonist and subsequent washout of cells with buffer. Repeated treatment with agonist caused significant desensitisation ($p < 0.001$) of hFFA1 signalling in both of the cell lines (Figure 5-15, A & B). The area under the curve (AUC) of initial calcium response was taken as 100% response to compare the functional output of repeated agonist exposure. In the HEK293 parental cell line, repeated agonist treatment ($t = 420, 780$ and 1140 s) showed $19.22\% \pm 2.19\%$, $22.13\% \pm 2.92\%$ and $23.97\% \pm 1.53\%$ responses in second, third and fourth treatment of TUG-905 respectively (Figure 5-15, C). In β -arrestin1/2-null cells, the second, third and fourth treatment of agonist showed $21.63\% \pm 1.92\%$, $24.44\% \pm 2.39\%$ and $27.37\% \pm 5.27\%$ respectively (Figure 5-15, C). However, differences in the desensitisation pattern between HEK293 parental cells and genome edited β -arrestin1/2-null cells were not significant ($p > 0.05$).

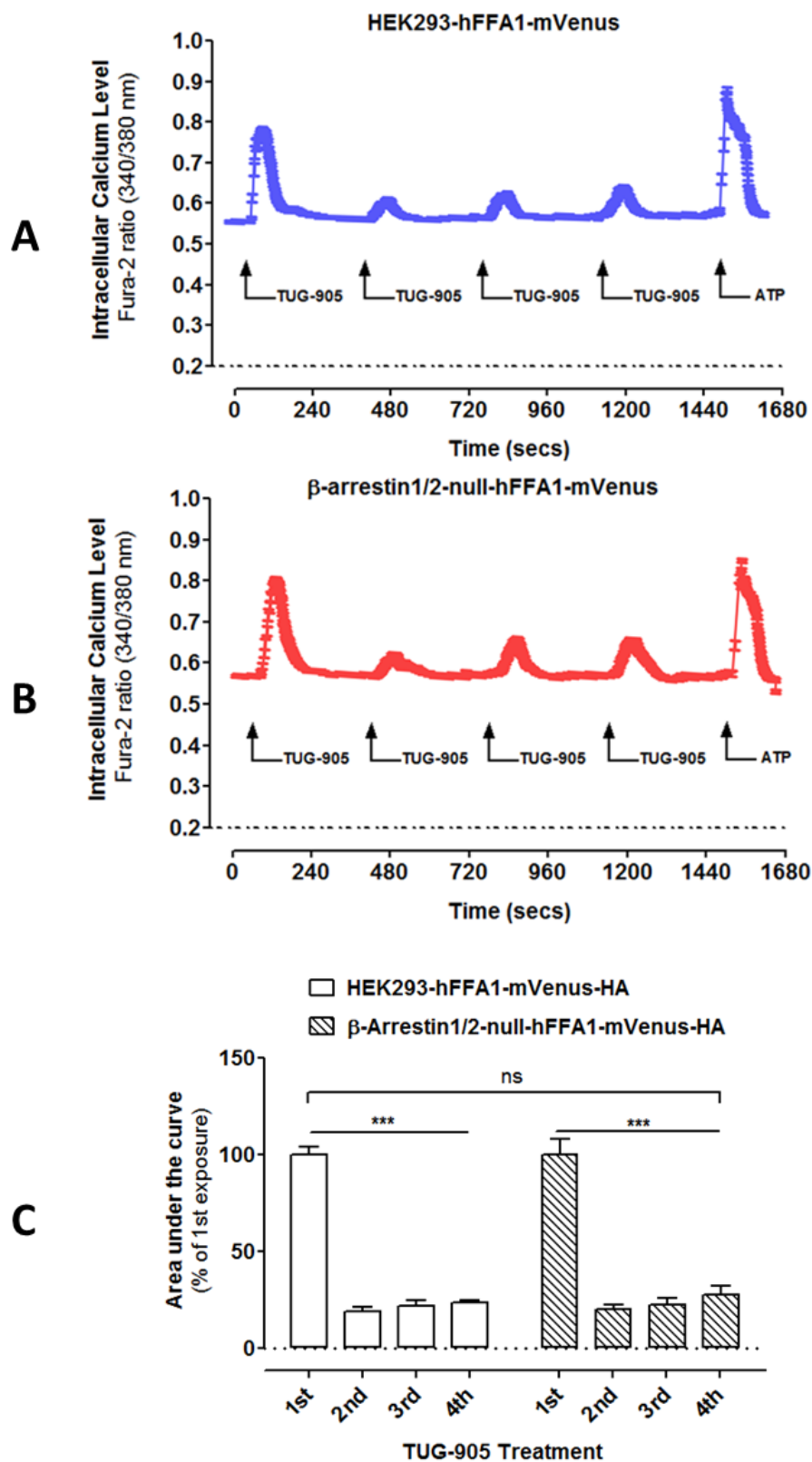


Figure 5-15. Repeated treatment of agonist desensitises hFFA1. (A) HEK293 cells and (B) CRISPR/Cas9 genome β -arrestin1/2-null cells able to express hFFA1-mVenus-HA were plated down onto poly-D-lysine-coated 22 mm glass coverslips. Single-cell calcium imaging (section 2.5.16) was performed in cells challenged for 60 second period with TUG-905 (3 μ M; t = 60, 420, 780 and 1140 s). ATP (100 μ M) was added at t = 1500 s. (C) Mean of the area under the curve of calcium mobilisation were plotted (** p < 0.001; ns = nonsignificant). Data represent mean \pm SEM from three separate experiments of at least 20 individual cells.

5.3.2 Role of β -arrestin1/2 in the desensitisation of hFFA4

5.3.2.1 Recruitment of β -arrestin2 to hFFA4

I have demonstrated previously (section 4.1.2) that β -arrestin2 was recruited to hFFA4 in response to addition of the agonists TUG-891 and TUG-1197. There was agonist-concentration-dependency in the β -arrestin2 recruitment to hFFA4 (Figure 4-3). Flp-In™ T-REx™ 293 double stable cells able to inducibly expressing FLAG-hFFA4-eYFP and constitutively expressing β -arrestin2-*Renilla* luciferase were treated for 5 minutes with varying concentrations of PMA or TUG-891. BRET (section 2.5.13) analysis showed that TUG-891 ($pEC_{50} = 6.85 \pm 0.12$) but not PMA was able to recruit β -arrestin2 to hFFA4 (Figure 5-16).

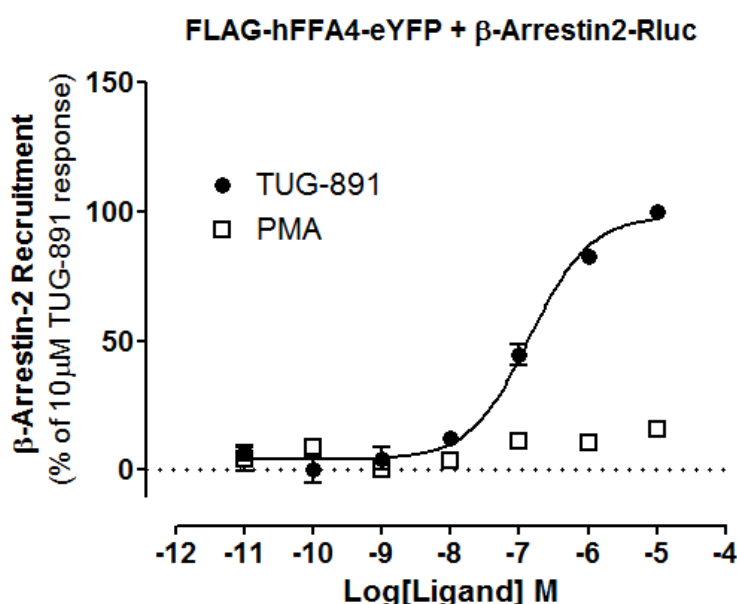


Figure 5-16. Recruitment of β -arrestin2 to hFFA4. Flp-In™ T-REx™ 293 cells able to express inducibly FLAG-hFFA4-eYFP and constitutively expressing β -arrestin2-*Renilla* luciferase were seeded (80,000 cells /well) into poly-D-lysine coated white 96-well plates. Receptor expression was induced by the antibiotic doxycycline (100 ng/ml) for 18-24 hours. BRET (section 2.5.13) in response to varying concentration of TUG-891 (●) and PMA (□) were measured. Data represent the mean \pm SEM of three independent experiments.

5.3.2.2 Visualisation of agonist-promoted internalisation of hFFA4 in β -arrestin1/2 knock out cells

Previously I have described the visualisation of hFFA4 internalisation upon treatment with TUG-891 in Flp-In™ T-REx™ 293 inducible cell lines (Figure 5-8). Hence HEK293 parental cells and β -arrestin1/2-null cells (Alvarez-Curto et al., 2016) constitutively expressing FLAG-hFFA4-mVenus were used to investigate agonist-promoted internalisation of the receptor. The absence of β -arrestin1/2 in the knockout cells was confirmed by immunoblotting (section 3.2.4; Figure 3-13). Cells were challenged with the FFA4 agonist TUG-891 (10 μ M) and the internalisation of the receptor was confocally imaged at every 15 minutes for a total 50 minutes. Interestingly, TUG-891 caused internalisation of hFFA4 in both of the cell lines (Figure 5-17).

Images of cells in HEK293 prior to addition of agonist showed that most of the mVenus-tagged hFFA4 was at the cell surface. However, within 20 minutes of agonist treatment a number of punctate clusters of receptors in the intracellular compartment were seen (Figure 5-17, A & B). In the HEK293 parental cell line, the internalised mVenus spots increased over time and within the 50 minutes of incubation most of the receptors were inside the cell (Figure 5-17, A). In β -arrestin1/2-null cells, there was no further change to the distribution pattern of hFFA4 within 50 minutes of incubation (Figure 5-17, B). Absence of β -arrestin1/2 showed an apparent reduction of the internalisation of hFFA4 (Figure 5-17, B).

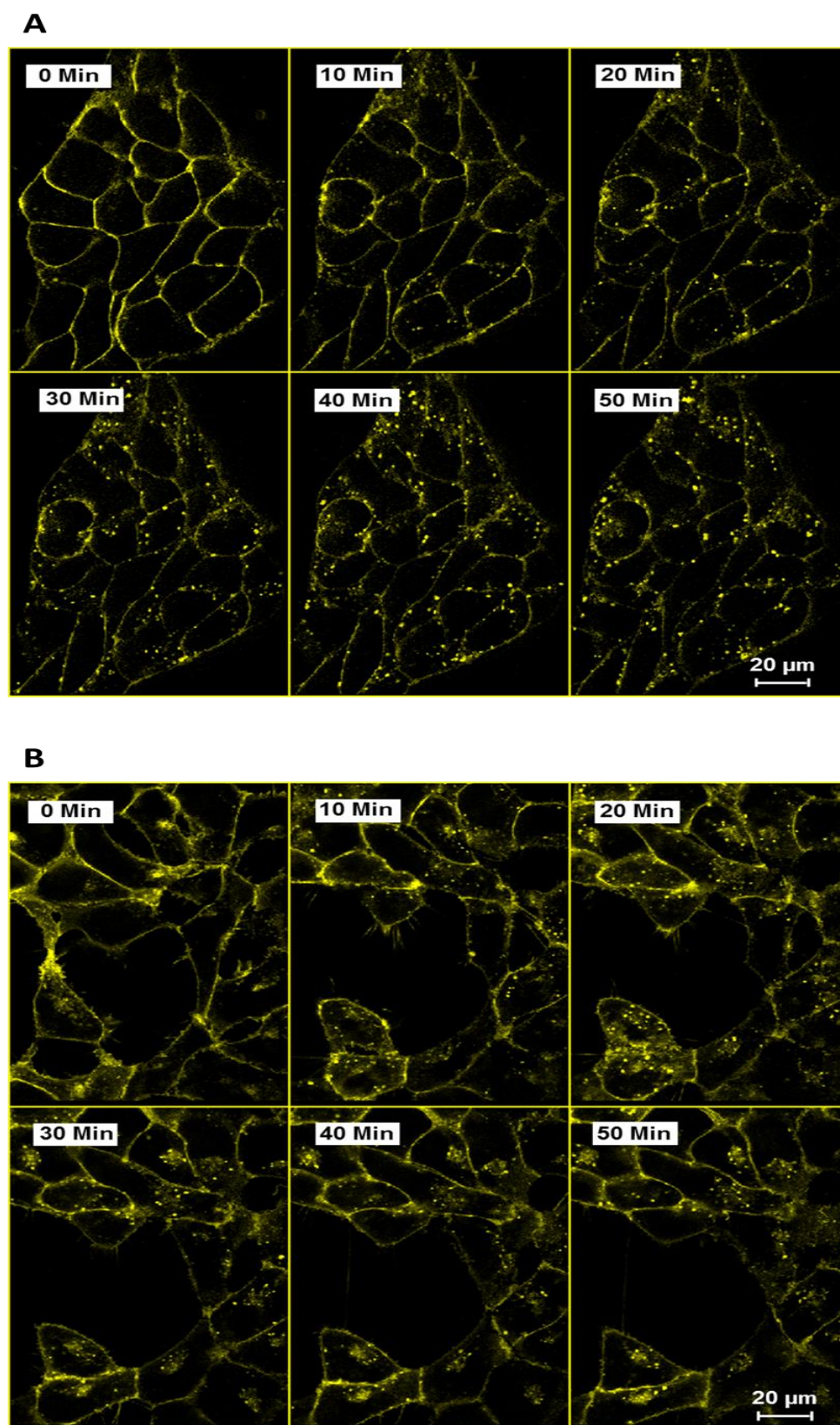


Figure 5-17. Internalisation of mVenus tagged form of hFFA4. FLAG-hFFA4-mVenus was stably expressed in HEK293 cells (**A**) and CRISPR/Cas9 genome edited HEK293 cells lacking β -arrestin1 and β -arrestin2 (**B**). Cells were plated down onto poly-*D*-lysine-coated 30 mm glass coverslips and the internalisation of hFFA4 was then imaged using a Zeiss VivaTome spinning disk confocal microscopy system (section 2.5.8). Images were taken before the addition of TUG-891, and every 10 minutes after ligand addition for a total of 50 minutes. All pictures shown are representative of three independent experiments.

5.3.2.3 Quantification of hFFA4 internalisation by cell surface ELISA

To quantify agonist-promoted receptor internalisation, cell surface ELISA (section 2.5.19) was used to measure the changes in FLAG-epitope-tagged cell surface hFFA4. Internalisation is detected as a decrease in cell surface receptor levels, compared with non-agonist-treated controls. FLAG-hFFA4-mVenus was constitutively expressed in β -arrestin1/2-null and HEK293 parental cells. Cells were stimulated with TUG-891 (10 μ M) for different times and the removal of the N-terminal FLAG-epitope tag from the surface of cells was quantified against anti-FLAG antibody.

Exposure of cells to TUG-891 for 30 minutes caused $17.12\% \pm 3.50\%$ internalisation in HEK293 parental cells, whereas in the β -arrestin1/2-null cells the internalisation was only $16.87\% \pm 6.79\%$ (Figure 5-18). The agonist-promoted internalisation of hFFA4 increased over time (5, 15, 30, 45 and 60 minutes). Within 45 and 60 minutes incubation with agonist, receptor internalisation in HEK293 parental cells and β -arrestin1/2-null cells were $23.50\% \pm 4.05\%$ ($p < 0.001$) and $37.07\% \pm 4.66\%$ ($p < 0.001$) respectively. However, the internalisation pattern was not significant ($p > 0.05$) between two cell lines at any time point (Figure 5-18).

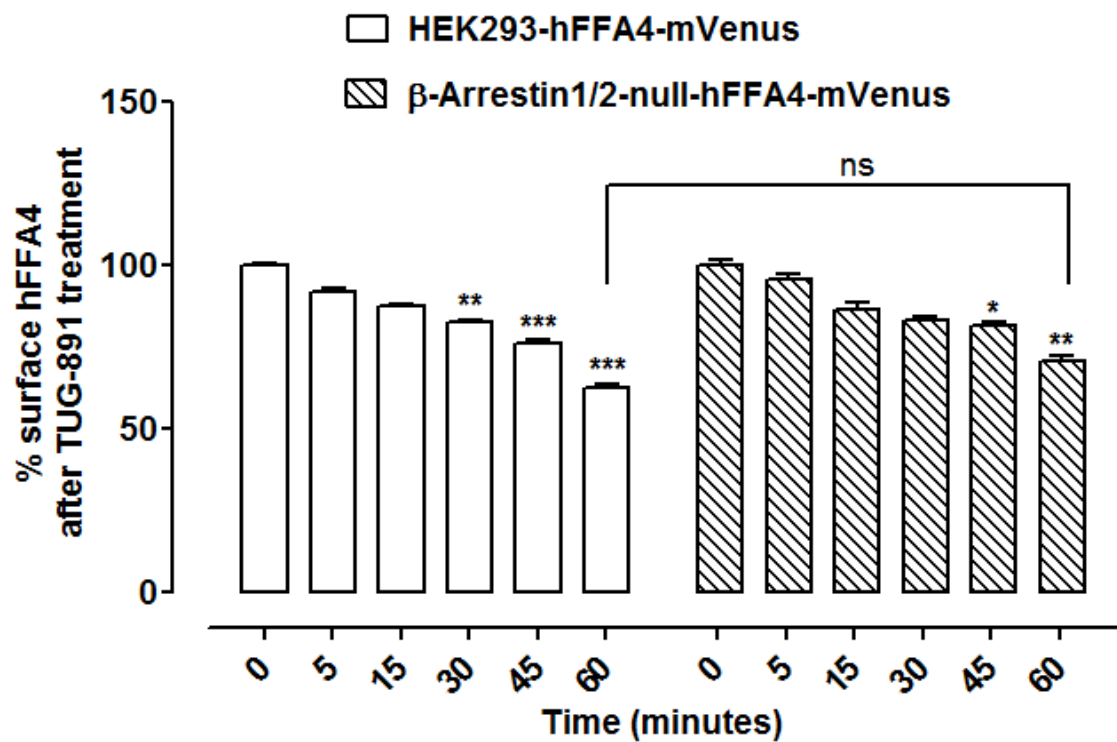


Figure 5-18. Quantification of hFFA4 internalisation with cell surface ELISA. FLAG-hFFA4-mVenus was stably expressed in HEK293 parental cells and in β -arrestin1/2-null cells. Cells were challenged with TUG-891 (10 μ M) for various time points. Cell surface ELISA (section 2.5.19) was performed using an anti-FLAG monoclonal primary antibody and with an anti-mouse horseradish peroxidase-conjugated secondary antibody. Absorption at 620 nm was recorded after addition of the substrate 3,3',5,5'-tetramethylbenzidine. Such studies were quantified as 100% of cell surface hFFA4 in vehicle (0.1% DMSO) treated cells (basal). Data represent the mean \pm SEM of three independent experiments (* p <0.05, ** p <0.01, *** p <0.001, ns= non-significant).

5.3.2.4 Agonist promoted elevation of intracellular calcium

The effect of elimination of β -arrestin1/2 on the signalling outcomes of hFFA4 was assessed in β -arrestin1/2-null cells constitutively expressing FLAG-hFFA4-mVenus. Cells were labelled for 45 minutes with Fura2-AM and then challenged with varying concentrations of TUG-891. The change in the fluorescence of Fura-2 AM was recorded using a FlexStation™ plate reader (section 2.5.17). HEK293 parental cells constitutively expressing FLAG-hFFA4-mVenus were used as control in this experiment. There were no differences in agonist-induced Ca^{2+} responses in the two cell lines (Figure 5-19).

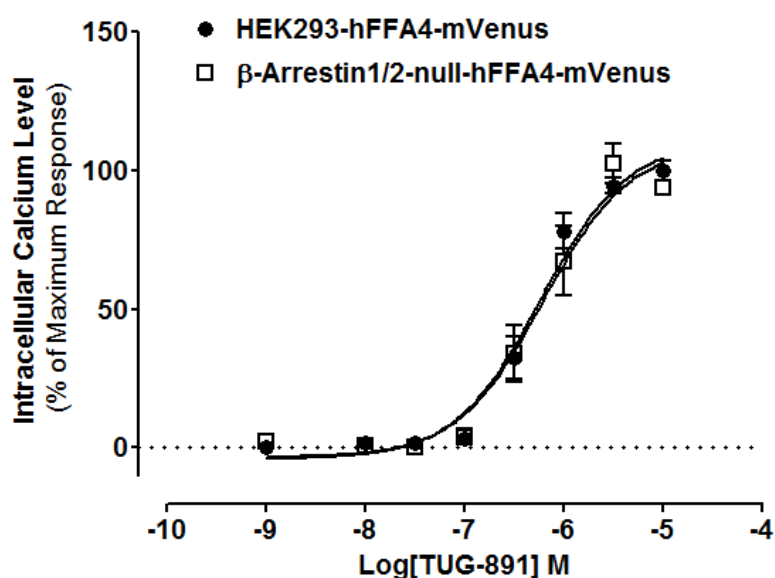


Figure 5-19. Agonist promoted mobilisation of intracellular calcium via hFFA4.

CRISPR/Cas9 mediated β -arrestin1/2-null cells (\square) and HEK293 parental cells (\bullet) able to express FLAG-hFFA4-mVenus were seeded (75,000 cells /well) into poly-D-lysine coated black clear-bottom 96-well plates. Cells were labelled 45 minutes with the calcium-sensitive dye Fura-2 AM and then challenged with varying concentration of TUG-891. Mobilisation of intracellular calcium was recorded in a FlexStation™ plate reader (section 2.5.17). Efficacy was normalised as percentage of maximum response. Data represent the mean \pm range of two independent experiments.

5.3.2.5 Desensitisation of functional signalling of hFFA4

hFFA4 expressed in Flp-InTM T-RExTM-293 cells desensitised upon repeated treatment of an agonist of the receptor (Figure 5-4). It was of interest to investigate the effect of elimination of β -arrestin1/2 on the functional desensitisation of hFFA4 signalling. FLAG-hFFA4-mVenus was constitutively expressed in β -arrestin1/2-null cells and HEK293 parental cells. Single-cell calcium imaging (section 2.5.16) was employed to assess responses to TUG-891 on repeated or a single prolonged agonist exposure.

A sixty second pulse with TUG-891 (3 μ M) in both of the cell lines resulted a rapid rise of the level of intracellular calcium, which returned to baseline after removal of the ligand and subsequent washout with microscope buffer (Figure 5-20, A & B). However, repeated exposure to TUG-891 ($t = 420, 780$ and 1140 s) caused significant desensitisation of the functional signalling in both of the cell lines (Figure 5-20, C). The desensitisation was calculated as area under the curve of calcium mobilisation upon agonist treatment. Initial response was taken as 100% response to compare responses of further treatments.

Compared to the initial response, repeated agonist treatment ($t = 420, 780$ and 1140 s) showed $62.98\% \pm 6.64\%$, $56.43\% \pm 4.67\%$ and $56.37\% \pm 5.06\%$ responses in second, third and fourth treatment in the HEK293 parental cells (Figure 5-20, C; $p < 0.001$). In the case of β -arrestin1/2-null cells, the second, third and fourth treatment of agonist showed $73.31\% \pm 6.17\%$, $66.75\% \pm 5.07\%$ and $66.22\% \pm 5.60\%$ respectively (Figure 5-20, C; $p < 0.05$; $p < 0.01$). However, there was no significant ($p > 0.05$) change in the desensitisation of signalling between the two cell lines.

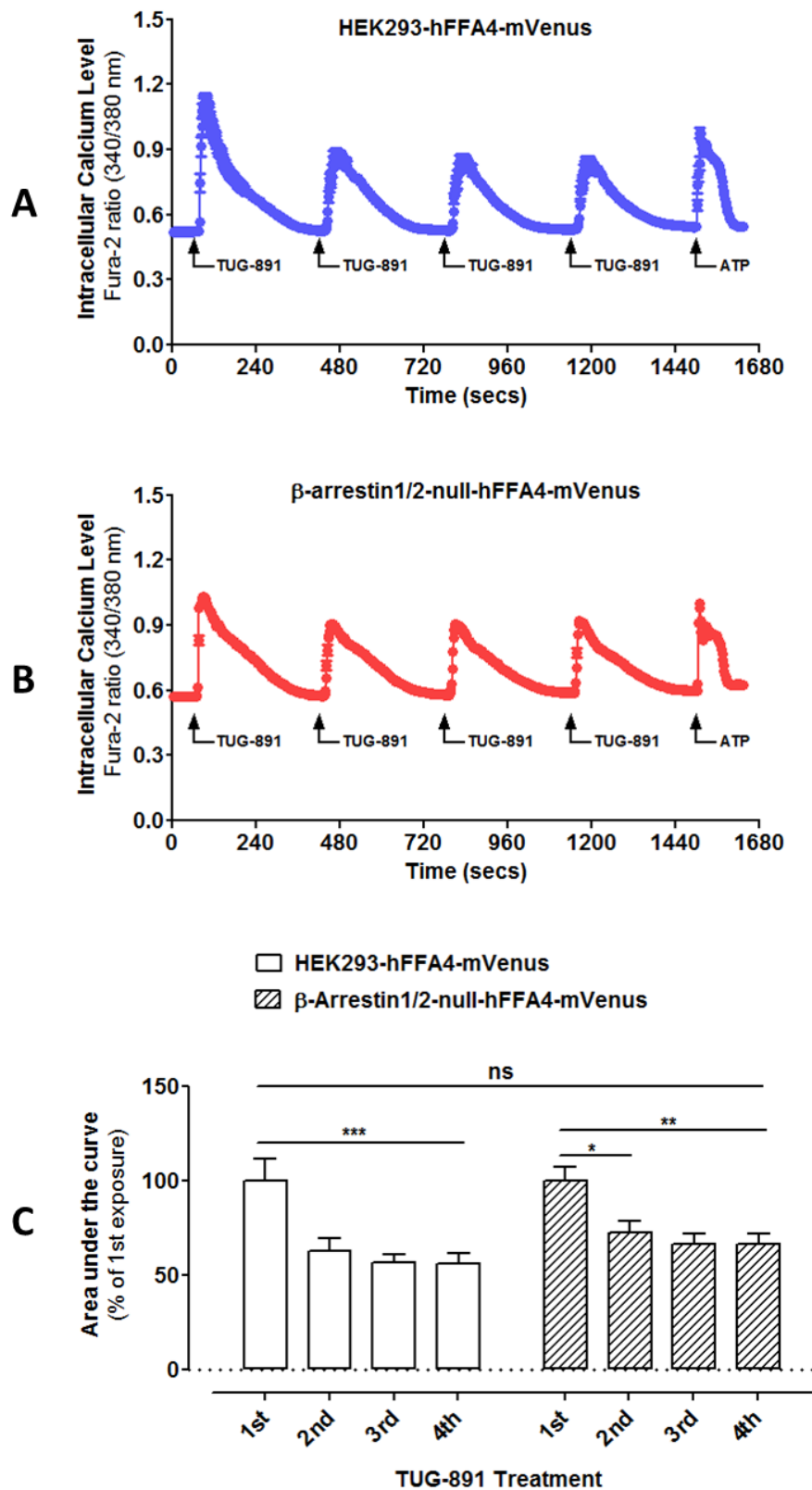


Figure 5-20. Repeated treatment with TUG-891 desensitises hFFA4. (A) HEK293 cells and (B) CRISPR/Cas9 genome β -arrestin1/2-null cells able to express FLAG-hFFA1-mVenus were plated down onto poly-D-lysine-coated 22 mm glass coverslips. Single cell calcium imaging (section 2.5.16) was done in cells challenged for 60 seconds with TUG-891 (3 μ M; t = 60, 420, 780 and 1140 s). ATP (100 μ M) was added at t = 1500 s. (C) Mean of the area under the curve of calcium mobilisation were plotted (* p <0.05; ** p <0.01; *** p <0.001; ns = nonsignificant). Data represent mean \pm SEM from three separate experiments of at least 20 individual cells.

The desensitisation from a prolonged exposure of TUG-891 (3 μ M) for up to 24 minutes was assessed in both of the lines. Following the single addition of TUG-891, there was a rapid increase in intracellular calcium, which decreased afterwards and maintained a steady calcium level above baseline (Figure 5-21, A & B). To confirm the functional capability of cells, ATP (100 μ M) was added (t = 1500 s) and showed that cells were competent to produce full calcium response. The area under the curve of calcium mobilisation showed a significant ($p < 0.05$) higher level of intracellular calcium response in β -arrestin1/2-null cells (Figure 5-21, C & D).

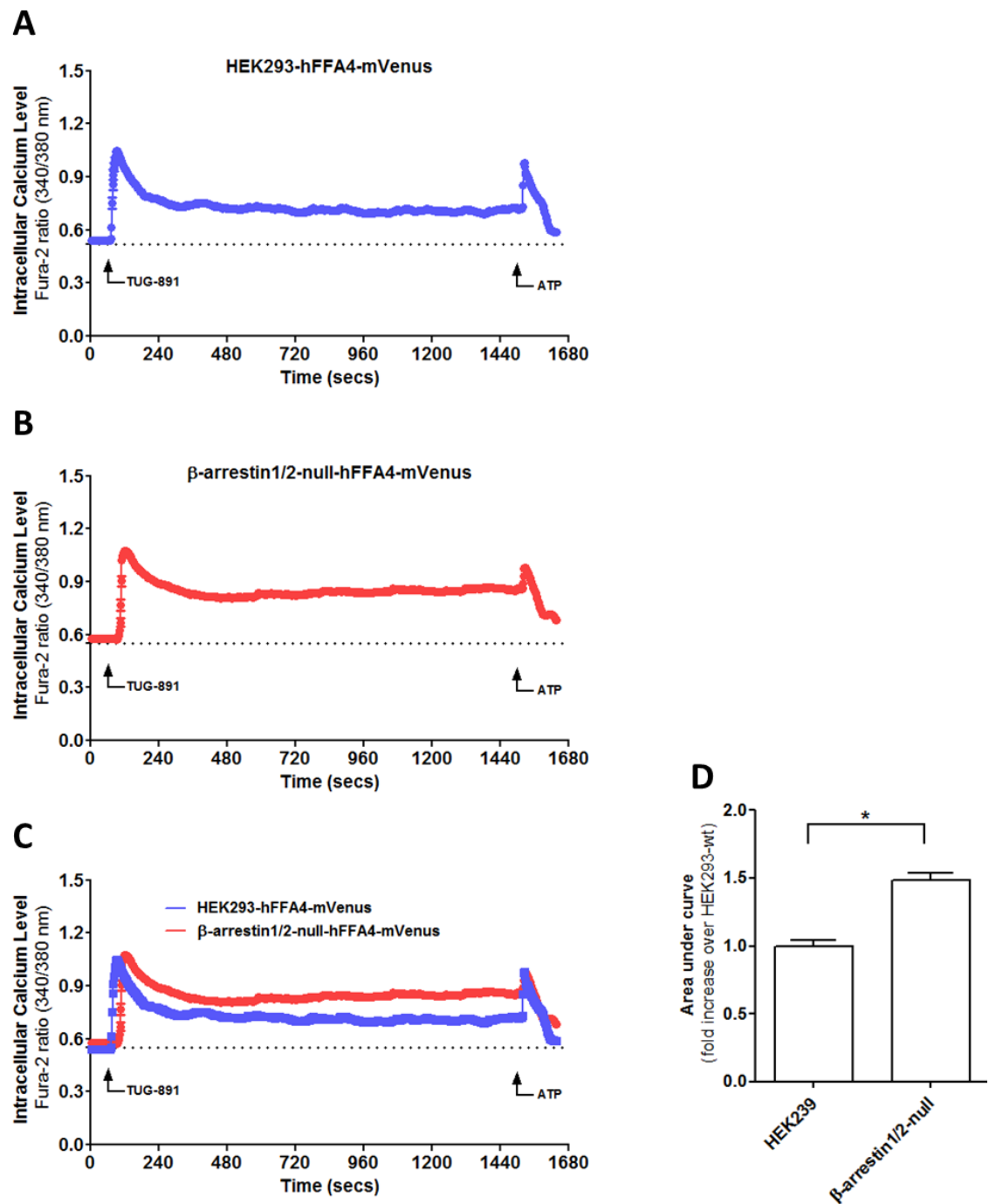


Figure 5-21. Desensitisation of hFFA4. (A) HEK293 cells and (B) CRISPR/Cas9 genome β -arrestin1/2-null cells able to express FLAG-hFFA4-mVenus were plated down onto poly-*D*-lysine-coated 22 mm glass coverslips. Single cell calcium imaging (section 2.5.16) was performed from a single addition of TUG-891 (3 μ M; t = 60 s) for up to 24 minutes. ATP (100 μ M) was added at t = 1500 s. (C) The calcium mobilisation in both of the cell line was overlaid (D) Mean of the area under the curves of calcium responses in both of the cell lines were plotted (* p < 0.05). Data represent mean \pm SEM from three separate experiments of at least 20 individual cells.

5.4 Role of $G\alpha_{q/11}$ in the regulation of hFFA1 and hFFA4

Agonist promoted increases in intracellular calcium mobilisation have been reported for both FFA1 (Briscoe et al., 2003) and FFA4 (Hirasawa et al., 2005). Signals from activation of FFA1 and FFA4 are transduced predominantly via $G\alpha_{q/11}$ -family G proteins (Fujiwara et al., 2005; Latour et al., 2007; Hirasawa et al., 2005; Hudson et al., 2013b), and the pharmacological $G\alpha_{q/11}$ inhibitor YM-254890 (Takasaki et al., 2004) has been used in several studies to confirm this observation (Stoddart et al., 2007; Hudson et al., 2013b). To validate the contribution of these G proteins in signalling as well as to explore the regulation and desensitisation of these long chain free fatty acid receptors I have employed CRISPR/Cas9 genome-edited HEK293 cells lacking $G\alpha_q$ and $G\alpha_{11}$ proteins (Alvarez-Curto et al., 2016b; Schrage et al., 2015). Each of these receptors was constitutively expressed in $G\alpha_{q/11}$ -null cells as well as in HEK293 parental cells. The absence of $G\alpha_{q/11}$ proteins was confirmed by immunoblotting against anti- $G\alpha_{q/11}$ antiserum (section 3.1.5; section 3.2.5).

5.4.1 Role of $G\alpha_{q/11}$ in the regulation of hFFA1

5.4.1.1 $G\alpha_{q/11}$ coupling to intracellular calcium mobilisation via hFFA1

$G\alpha_q/G\alpha_{11}$ -null cells able to express hFFA1-mVenus-HA were treated with the selective agonist TUG-905 (Christiansen et al., 2012) and the calcium mobilisation was assessed in both single cells and in cell populations. In single cell imaging studies, TUG-905 treatment of HEK293 parental cells showed a sharp raise of calcium level which was totally absent in $G\alpha_q/G\alpha_{11}$ -null cells (Figure 5-22, A). In cell population studies, HEK293 parental cells showed elevation of intracellular calcium level in a concentration-dependent fashion ($pEC_{50} = 6.85 \pm 0.08$) whereas $G\alpha_{q/11}$ -null cells were unable to respond (Figure 5-22, B). However, the calcium signalling was regained when $G\alpha_q$ protein was re-introduced into these $G\alpha_{q/11}$ -null cell lines (Figure 5-22, C).

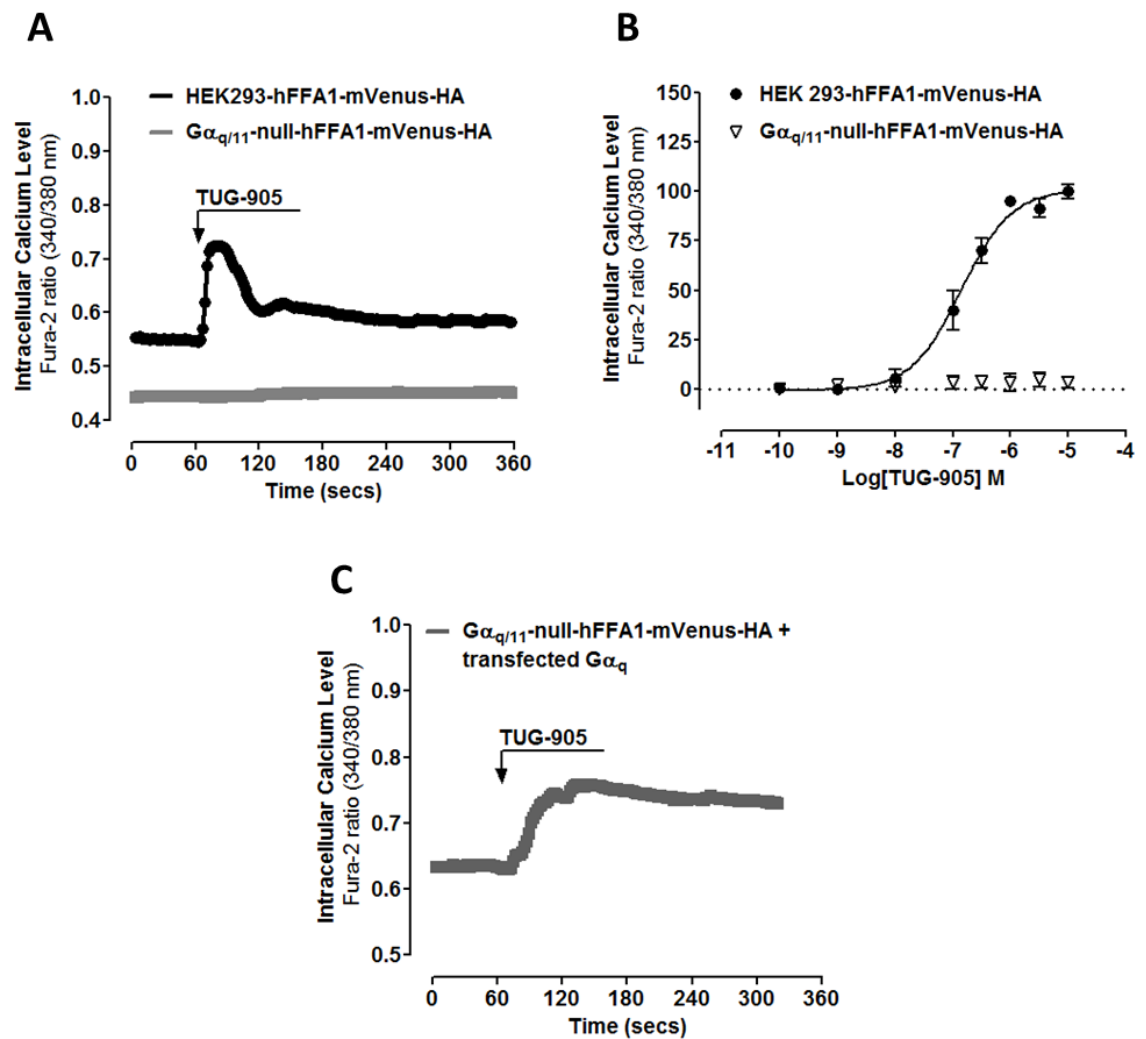


Figure 5-22. $G_{\alpha_{q/11}}$ coupling to intracellular calcium mobilisation via hFFA1. HEK293 parental and $G_{\alpha_{q/11}}$ -null cells were stably transfected to express human FFA1 in the form of hFFA1-mVenus-HA. **(A)** Single-cell calcium imaging (section 2.5.16) was done in cells challenged for 60 seconds with TUG-905 (3 μ M); **(B)** Mobilisation of intracellular calcium in cell populations (section 2.5.17) was investigated in both cell lines treated with varying concentrations of TUG-905. **(C)** TUG-905 (3 μ M) promoted mobilisation of intracellular calcium was monitored in single cell calcium imaging studies in $G_{\alpha_{q/11}}$ -null cells transfected with G_{α_q} protein. Data represent **(A & C)** mean \pm SEM from three separate experiments of at least 20 individual cells. Data represent **(B)** in the mean \pm SEM of three independent experiments.

5.4.1.2 $G\alpha_{q/11}$ coupling to inositol phosphate signalling via hFFA1

Accumulation of inositol monophosphates (IP1) (section 2.5.15) is a downstream indicator of $G\alpha_q/G\alpha_{11}$ activation (Moran et al., 2016; Werry et al., 2003). HEK293 parental cells and $G\alpha_q/G\alpha_{11}$ -null cells able to express hFFA1-mVenus-HA were challenged with the selective FFA1 agonist TUG-905. A concentration-dependent accumulation of IP1 was produced ($pEC_{50} = 6.86 \pm 0.12$) in HEK293 parental cells. However, this response was absent in $G\alpha_{q/11}$ -null cells (Figure 5-23). Interestingly, there was a significant ($p < 0.001$) increase in basal IP1 accumulation in HEK293 parental cells. This is potentially consistent with hFFA1 displaying a significant degree of constitutive activity.

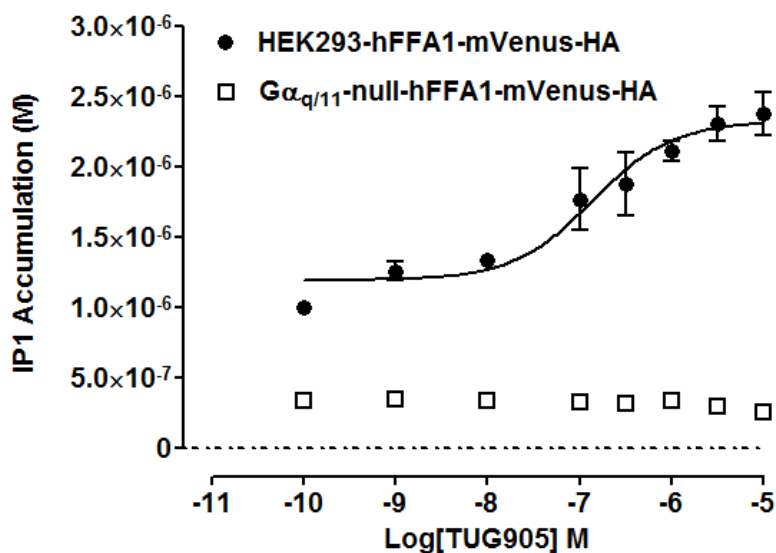


Figure 5-23. $G\alpha_{q/11}$ coupling to inositol phosphate signalling via hFFA1. HEK293 parental (●) and $G\alpha_{q/11}$ -null (□) cells were stably transfected to express human FFA1 in the form of hFFA1-mVenus-HA. Cells were seeded (7,500 cell/well) in a white solid-bottom 384-well plate and the accumulation of inositol mono phosphates (IP1) was assessed (section 2.5.15) after challenging cells with varying concentrations of TUG-905. Data represent the mean \pm SEM of three independent experiments.

5.4.2 Role of $G\alpha_{q/11}$ in the regulation of hFFA4

5.4.2.1 $G\alpha_{q/11}$ coupling to intracellular calcium mobilisation via hFFA4

CRISPR/Cas9-mediated genome edited $G\alpha_{q/11}$ -null cells and HEK293 parental cells constitutively expressing FLAG-hFFA4-mVenus were employed to investigate $G\alpha_{q/11}$ coupling to the mobilisation of intracellular calcium in single cell calcium imaging as well as in cell populations.

Single cell calcium imaging studies revealed that TUG-891 (3 μ M) treatment caused a rapid elevation of intracellular level in HEK293 parental cells. However, cells lacking $G\alpha_{q/11}$ proteins failed to produce the agonist-mediated response (Figure 5-24, A). In cell population studies, TUG-891 showed a concentration-dependent elevation of intracellular calcium level ($pEC_{50} = 6.54 \pm 0.07$) in HEK293 parental cells whereas the effect was absent in $G\alpha_{q/11}$ -null cells (Figure 5-24, B). However, insertion of $G\alpha_q$ protein in the $G\alpha_{q/11}$ -null cells regained the calcium mobilisation capacity (Figure 5-24, C).

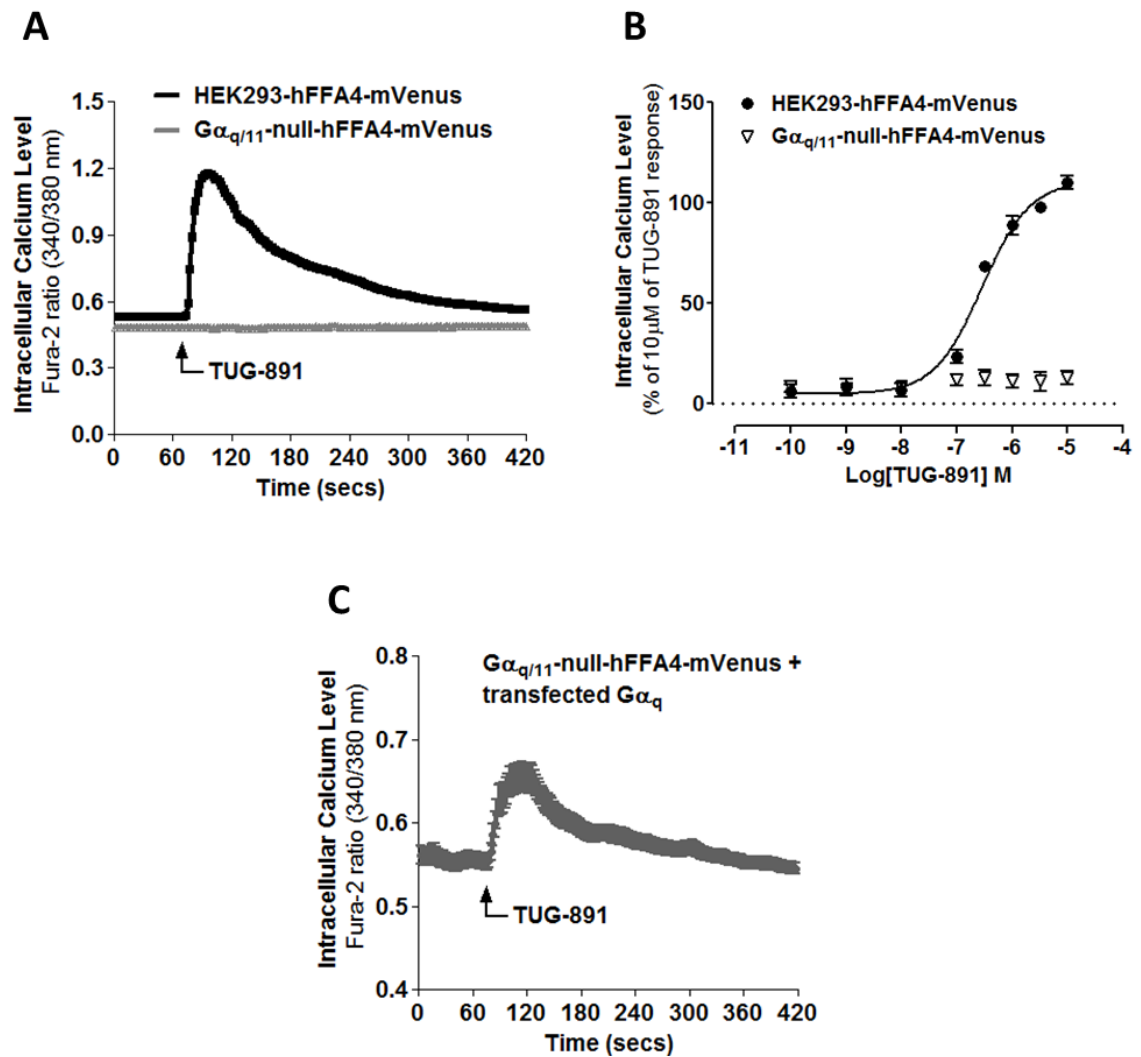


Figure 5-24. $G\alpha_{q/11}$ coupling to intracellular calcium mobilisation via hFFA4. HEK293 parental and $G\alpha_{q/11}$ -null cells were stably transfected to express human FFA4 in the form of FLAG-hFFA4-mVenus. **(A)** Single-cell calcium imaging (section 2.5.16) was done in cells challenged for 60 seconds with TUG-891 (3 μ M) **(B)** Mobilisation of intracellular calcium in cell population (section 2.5.17) was investigated in both cell line treated with varying concentrations of TUG-891. **(C)** TUG-891 (3 μ M) promoted mobilisation of intracellular calcium was monitored in single cell calcium imaging studies in $G\alpha_{q/11}$ -null cells co-transfected with $G\alpha_q$ protein. Data represent **(A & C)** mean \pm SEM from three separate experiments of at least 20 individual cells. Data represent **(B)** in the mean \pm SEM of three independent experiments.

5.4.2.2 $G_{\alpha q/11}$ coupling to inositol phosphate signalling via hFFA4

The signalling outcome of $G_{\alpha q/11}$ elimination was assessed in HEK293 parental cells and $G_{\alpha q/11}$ -null cells able to express FLAG-hFFA4-mVenus as the agonist stimulated accumulation of IP1. TUG-891 exposure to HEK293 parental cells caused a concentration-dependent accumulation of IP1 ($pEC_{50} = 6.60 \pm 0.11$) via hFFA4. The $G_{\alpha q/11}$ -null cells did not show any response in this end point (Figure 5-25).

A significant ($p < 0.001$) increase in basal IP1 accumulation (section 2.5.15) was noted in the HEK293 parental cell cells. hFFA4 showed constitutive activity in the $G_{\alpha q/11}$ signalling (Figure 5-25).

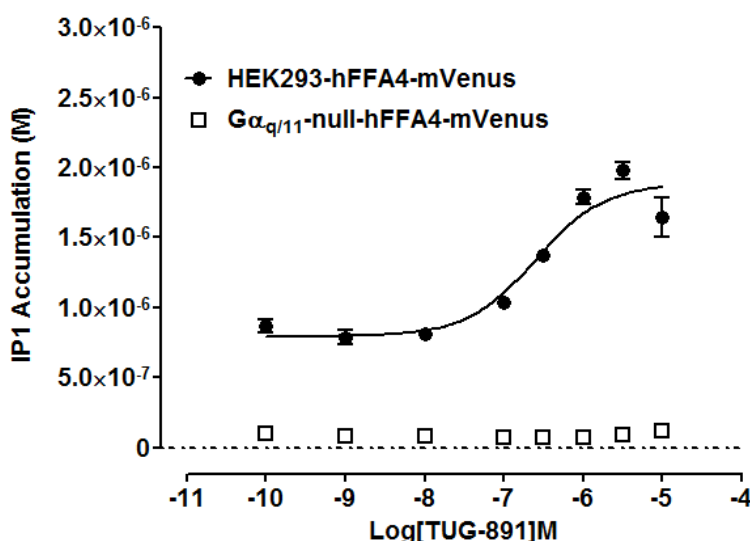


Figure 5-25. $G_{\alpha q/11}$ coupling to inositol phosphate signalling via hFFA4. HEK293 parental (●) and $G_{\alpha q/11}$ -null (□) cells were stably transfected to express human FFA4 in the form of FLAG-hFFA4-mVenus. Cells were seeded (7,500 cell/well) in a white solid-bottom 384-well plate and the accumulation of inositol mono phosphates (IP1) was assessed (section 2.5.15) after challenging cells with varying concentrations of TUG-891. Data represent the mean \pm SEM of three independent experiments.

5.4.2.3 Eliminating $G\alpha_{q/11}$ has no effect on hFFA4 phosphorylation

Phosphorylation status of a receptor following drug treatment can provide valuable information regarding receptor activation (Butcher et al., 2016). FFA4 phosphorylation indicates the activation of $G\alpha_{q/11}/IP_3/Ca^{2+}/PKC$ signalling cascade of this receptor (Burns et al., 2014). I examined agonist-promoted phosphorylation of hFFA4 expressed in cells lacking $G\alpha_q$ and $G\alpha_{11}$ proteins.

Cells were challenged for 10 minutes in the absence (baseline) or presence of TUG-891 (10 μ M) followed by preparation of cell lysates. SDS-PAGE (section 2.5.4) of the lysates and immunoblotting (section 2.5.5) with a phosphor-Thr³⁴⁷/Ser³⁵⁰ hFFA4 antiserum (Butcher et al., 2014) showed significant phosphorylation ($p<0.001$) of hFFA4 in both parental and genome-edited cell lines (Figure 5-26, A & B). Immunoblots of the same lysate using anti-GFP antiserum indicated somewhat higher level of hFFA4 expression in parental cells (Figure 5-26, C).

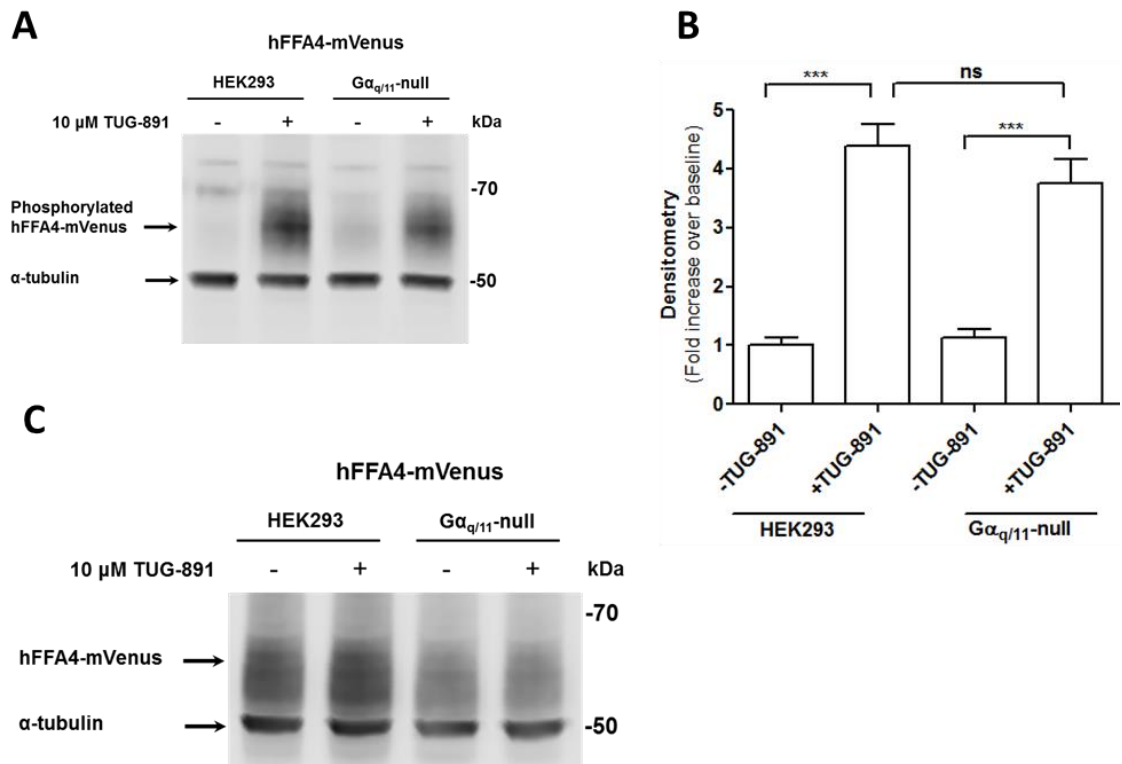


Figure 5-26. Agonist promoted phosphorylation of hFFA4 in $G\alpha_{q/11}$ -null cells. HEK293 parental cells and $G\alpha_{q/11}$ -null HEK293 cells constitutively expressing FLAG-hFFA4-mVenus were seeded in a 6-well plates. **(A)** Cells were challenged for 10 minutes with TUG-891 (10 μ M). Lysates of cells were then resolved by SDS-PAGE and phosphorylated receptors were detected by immunoblotting with a phospho-Thr³⁴⁷/Ser³⁵⁰ hFFA4 antiserum. **(B)** Densitometry of the immunoblot A (***) $p < 0.001$, ns= not significant). **(C)** Lysates of cells were also resolved by SDS-PAGE and immunoblotted with anti-GFP antiserum to detect the level of receptor expression. Data represent the mean \pm SEM of three independent experiments.

5.4.2.4 Elimination of $G\alpha_{q/11}$ protein does not compromise internalisation of hFFA4

As described previously (Figure 5-8), addition of the FFA4 agonist TUG-891 resulted in rapid internalisation of FLAG-hFFA4-mVenus in Flp-In™ T-REx™ 293 cell lines. In this section, hFFA4 internalisation was visualised using HEK293 parental and CRISPR/Cas9 genome edited $G\alpha_q/G\alpha_{11}$ -null cells. Addition of the FFA4 agonist TUG-891 (10 μ M) resulted robust internalisation of hFFA4-mVenus in both of the cell lines (Figure 5-27; Figure 5-28).

A Zeiss VivaTome spinning disk confocal microscopy system was used to visualise the internalisation of mVenus-tagged hFFA4 in live cells. Cells were challenged with TUG-891 (10 μ M) and ligand-promoted internalisation of hFFA4 was monitored every 15 minutes after ligand addition for a total 45 minutes.

Before the addition of the agonist TUG-891 the mVenus-tagged receptors were located primarily at the cell surface (Figure 5-27; Figure 5-28). Within 15 minutes of the addition the agonist, the intensity of mVenus became less distinct at the cell surface and punctate clusters of receptors were seen in intracellular vesicles. The internalised mVenus spots increased over time and within the 45 minutes of incubation most of the receptors were inside the cell (Figure 5-27; Figure 5-28). Elimination of $G\alpha_q/G\alpha_{11}$ proteins did not have any effect on agonist-promoted internalisation of hFFA4.

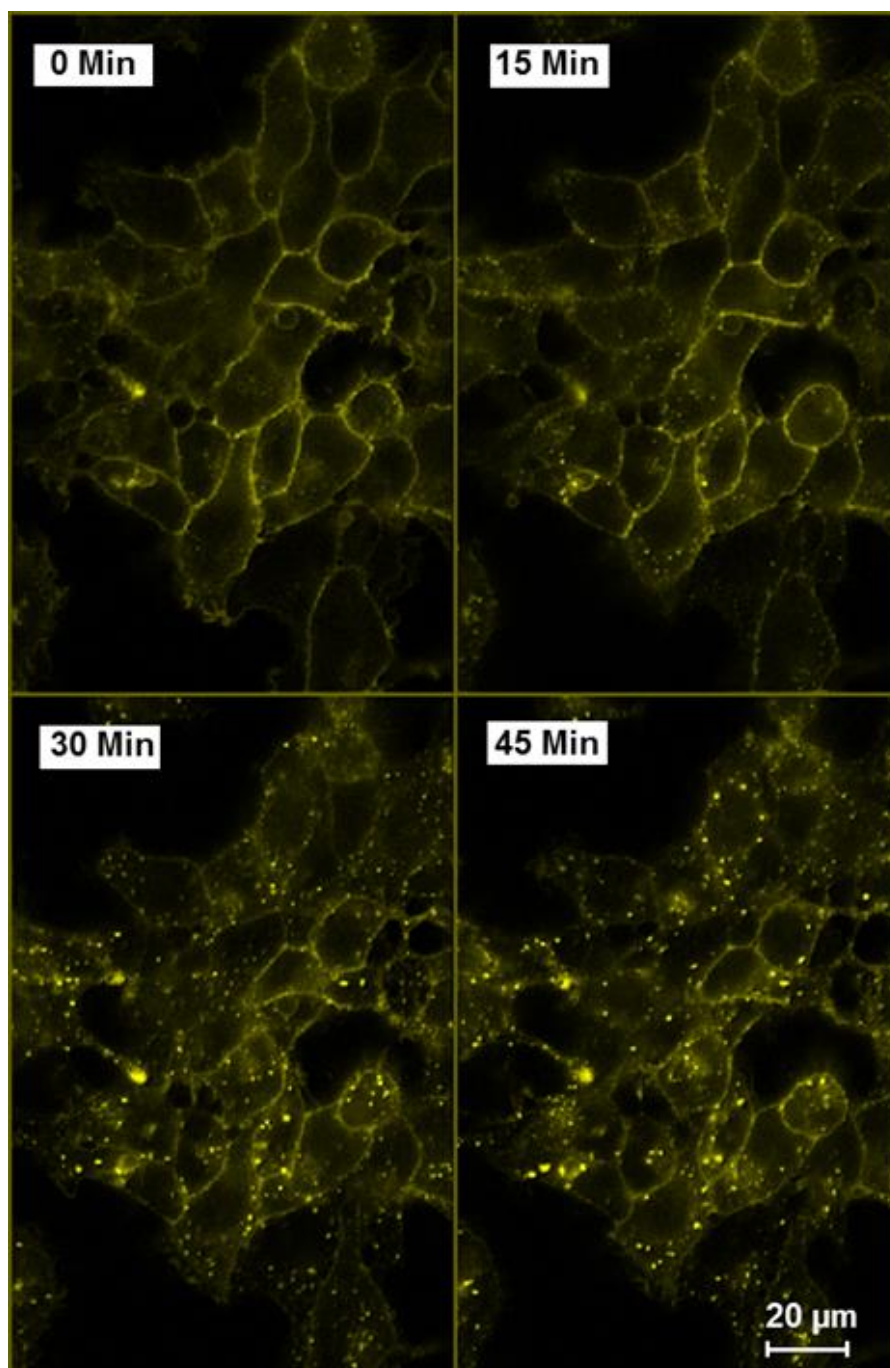


Figure 5-27. Internalisation of hFFA4 is not dependent on $G\alpha_{q/11}$. HEK293 parental cells able to constitutively express FLAG-hFFA4-mVenus were plated down onto poly-*D*-lysine-coated 30 mm glass coverslips. The internalisation of hFFA4 in live cells was then imaged using a Zeiss VivaTome spinning disk confocal microscopy system (described in the section 2.5.8). TUG-891 (10 μ M) caused internalisation of FLAG-hFFA4-mVenus in HEK293 parental cells. Images were taken before the addition of TUG-891, and every 15 minutes after ligand addition for a total of 45 minutes of agonist exposure. All pictures shown are representative of three independent experiments.

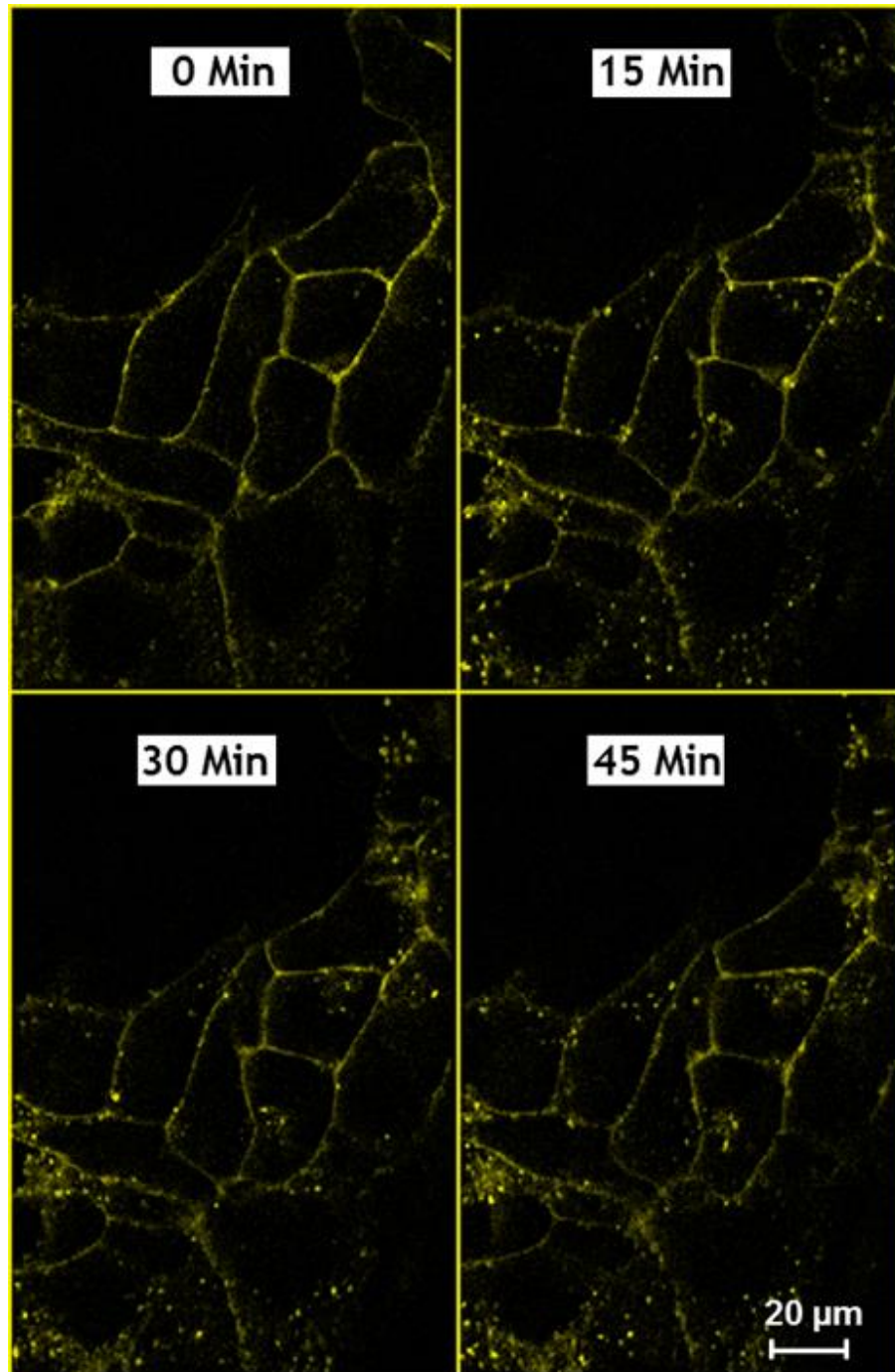


Figure 5-28. Internalisation of hFFA4 is not dependent on $G\alpha_{q/11}$. HEK293 parental cells and $G\alpha_{q/11}$ -null HEK293 cells able to constitutively express FLAG-hFFA4-mVenus were plated down onto poly-*D*-lysine-coated 30 mm glass coverslips. The internalisation of hFFA4 in live cells was then imaged using a Zeiss VivaTome spinning disk confocal microscopy system (described in the section 2.5.8). TUG-891 (10 μ M) caused internalisation of FLAG-hFFA4-mVenus in $G\alpha_{q/11}$ -null HEK293 cells. Images were taken before the addition of TUG-891, and every 15 minutes after ligand addition for a total of 45 minutes of agonist exposure. All pictures shown are representative of three independent experiments.

The role of protein kinase C in the internalisation in $G\alpha_{q/11}$ -null background was investigated. PMA induced hFFA4 internalisation was observed in this cell lines (Figure 5-29). Cells were challenged with PMA (1 μ M) and receptor internalisation was visualised at 15 minute intervals for a total 45 minutes. Within 15 minutes of PMA-treatment, few internalised mVenus spots were seen (Figure 5-29). Confocal images showed that internalised spots increased over time and within 45 minutes internalised mVenus spots were visualised inside the cell (Figure 5-29). However, quantification of the intensity of internalised mVenus is needed to quantify the extent of PMA-induced internalisation hFFA4 in $G\alpha_{q/11}$ -null cells.

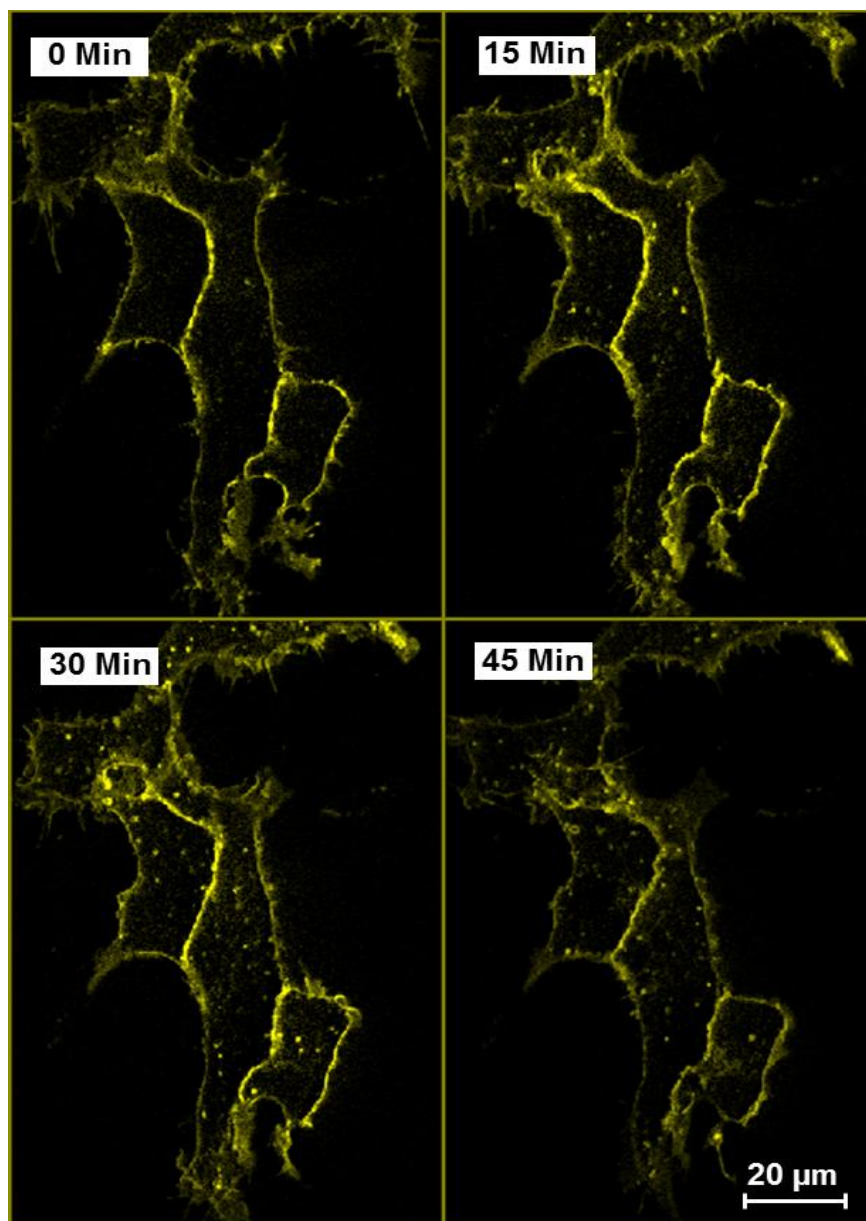


Figure 5-29. PKC mediated internalisation of hFFA4 in $G\alpha_{q/11}$ -null cells. CRISPR/Cas9 genome edited $G\alpha_{q/11}$ -null cells stably expressing FLAG-hFFA4-mVenus were plated down onto poly-*D*-lysine-coated 30 mm glass coverslips. The internalisation of hFFA4 in live cells was then visualised using a Zeiss VivaTome spinning disk confocal microscopy system (section 2.5.8). Images were taken before the addition of PMA (1 μ M), and every 15 minutes up to a total 45 minutes of ligand exposure. All pictures shown are representative of three independent experiments.

5.5 Discussion

Following agonist stimulation GPCRs undergo conformational changes that allow binding to heterotrimeric G proteins, leading to the activation of various signalling pathways and initiation of intracellular trafficking (Zhang and Kim, 2017; Thomsen et al., 2016). Agonist-promoted desensitisation is a common phenomenon regulating the signalling of many GPCRs (Rajagopal and Shenoy, 2017; Syrovatkina et al., 2016; Kohout and Lefkowitz, 2003). The canonical mechanism involves agonist-promoted phosphorylation of the receptor, recruitment of β -arrestins, association with various adaptor proteins, receptor internalisation and receptor resensitisation and/or down-regulation (Thomsen et al., 2016; Rosenbaum et al., 2009). Nowadays both FFA1 and FFA4 are considered as potential therapeutic targets for the control of metabolic diseases, particularly obesity, diabetes and inflammatory disorders (Milligan et al., 2017; Milligan et al., 2015). Most of the reported attempts are designed to produce agonist-based therapeutics (Milligan et al., 2017; Cornall et al., 2014, Hudson et al., 2013c). In this chapter I have focused my investigation predominantly on hFFA4 as there has been less effort to date in studying this GPCR compared to hFFA1.

As for many other GPCRs, repeated exposure of agonist desensitised both hFFA1 and hFF4 as revealed in single-cell calcium imaging studies, although these cells were functional as they still produced a full calcium signal treatment with ATP (Figure 5-1; Figure 5-4). Such agonist-mediated desensitisation may present a challenge to agonist-based drug development targeting hFFA1 and hFFA4. A typical desensitisation mechanism operates at the receptor level to prevent or block initiation of the signalling cascade in the presence of maintained agonist stimulation (Syrovatkina et al., 2016). Such phenomena prevent over-stimulation of the receptor to arrest G protein signalling (Kohout and Lefkowitz, 2003). Agonist-promoted homologous desensitisation involves a coordinated action of GRKs and arrestins (Smith and Rajagopal, 2016). hFFA4 was found to be phosphorylated in an agonist concentration-dependent fashion and this was totally blocked by the FFA4 antagonist TUG-1275 (Figure 5-5). Both FFA1 and FFA4 showed recruitment of β -arrestin2 upon stimulation with corresponding agonists (Figure 4-3 and Figure 4-12). Phosphorylation promotes the high-affinity binding of arrestins to a receptor, which physically interdicts further coupling to

G proteins (Smith and Rajagopal, 2016; Kohout and Lefkowitz, 2003). Phosphorylation is an important hallmark of GPCR attenuation. GRK phosphorylation of GPCRs is by itself insufficient to produce extensive desensitisation of many GPCRs and arrestins are also needed (Kelly et al., 2008). Elimination of receptor phosphorylation by mutagenic alteration of the relevant amino acids has been found to abolish β -arrestins recruitment, desensitisation and internalisation of mFFA4 (Prihandoko et al., 2016). Thus, a loss of G protein signal transduction in the single-cell calcium imaging studies (Figure 5-1; Figure 5-4) might be due to a loss of coupling efficiency between the receptor and $G\alpha_{q/11}$ leading to desensitisation.

GPCRs can also undergo heterologous phosphorylation, typically involving the second messenger-activated kinases PKA or PKC (Thomsen et al., 2016; Burns et al., 2014; Lefkowitz and Shenoy, 2005). PKC is able to phosphorylate many GPCRs and in the majority of cases, such receptor phosphorylation is associated with clear attenuation of function (Rajagopal and Shenoy, 2017). GPCRs phosphorylated by PKC or PKA can also be good substrates for the binding of arrestins (Kelly et al., 2008). Interestingly, robust phosphorylation of hFFA4 was found upon treatment with the PKC activator PMA in a concentration-dependent manner and this was significantly blocked by each of the PKC inhibitors BIM-I and Go-6979 (Figure 5-6). Moreover, PKC inhibitors were also able to inhibit partially agonist-promoted phosphorylation of hFFA4 (Figure 5-7). Again, PKC caused robust internalisation of hFFA4 (Figure 5-9). These results suggest that a PKC-linked signalling cascade is involved in the phosphorylation and internalisation of FFA4. PKC mediated desensitisation is not uncommon in many GPCRs. PKC mediated desensitisation has been seen in muscarinic acetylcholine receptor (Montiel et al., 2004). Glucagon receptor undergoes phosphorylation and desensitization mediated by $PKC\alpha$ (Krillov et al., 2011).

The β -arrestins are versatile, multifunctional adapter proteins that are best known for their ability to desensitise GPCRs, but also regulate a diverse array of cellular functions (Smith and Rajagopal., 2016). Phosphorylation of GPCRs is also linked to receptor internalisation. Mutation of phosphorylation sites on receptors was found to limit β -arrestin recruitment leading to poor receptor internalisation (Rajagopal and Shenoy, 2017; Prihandoko et al., 2016; Kohout and Lefkowitz, 2003; Luttrell and Lefkowitz, 2002). Internalisation plays a key

role in the regulation of GPCR signalling and desensitisation (Ferguson, 2001). In my experiments, agonist treatment caused robust internalisation of hFFA4 as revealed in confocal microscopy (Figure 5-6), ArrayScan II (Figure 5-11), cell surface ELISA (Figure 5-12) and biotinylation (Figure 5-13) studies. Immunoblots of total lysates from biotin labelling studies indicated that hFFA4 degradation is not a key aspect in the regulation of this receptor (Figure 5-13), at least in short term studies. Agonist-promoted internalisation in these assays demonstrated homologous internalisation of hFFA4. A heterologous internalisation was also seen for hFFA4. PMA treatment was also able to internalise hFFA4 (Figure 5-9) in a concentration-dependent manner (Figure 5-11). The PKC inhibitor BIM-1 seemed to reduce such PMA-mediated internalisation as revealed by confocal microscopy (Figure 5-10). Interestingly PMA had no effect on the recruitment of β -arrestin2 to hFFA4 (Figure 5-16) suggesting that this internalisation is not β -arrestin2 dependent. Accumulating evidence, however, has suggested that some GPCRs can be internalized even without agonist stimulation and/or activity by a process known as constitutive internalization (Xu et al., 2007). Constitutive internalisation was seen for FFA1, where the selective FFA1 antagonist GW-1100 had no effect (Figure 5-3) indicating a complex desensitisation mechanism for hFFA1. Blockage of agonist-mediated internalization of FFA1 by using hypertonic sucrose treatment (Li et al., 2010) which markedly reduces agonist-receptor complex internalization or by siRNA mediated depletion of the heavy chain of clathrin might be helpful to explore this type of internalisation of FFA1. Qian et al (2014) has reported FFA1 to undergo both constitutive and agonist-mediated internalisation which was believed to cause desensitisation of the receptor. Difficulty in detecting agonist promoted internalisation of hFFA1 might be due to the higher constitutive activity of this receptor, thereby favouring constitutive desensitisation of the receptor.

It was of interest to investigate the role of β -arrestins in this internalisation process. In β -arrestin1/2-knockout cells both hFFA1 and hFFA4 receptors were able to mobilise intracellular calcium. The calcium responses were similar to those seen in parental HEK293 cells (Figure 5-19). Surprisingly, lack of β -arrestin1/2 did not compromise agonist-promoted internalisation of hFFA4. Although an apparent reduction of internalisation was seen in confocal microscopy (Figure 5-17), the effect was not significant as assessed in cell

surface ELISA experiments (Figure 5-18). Moreover, elimination of β -arrestin1/2 did not result in any significant differences in the desensitisation of either hFFA1 or hFFA4 upon repeated agonist treatment (Figure 5-15 and Figure 5-20). A single chronic exposure to TUG-891 however, showed a significant reduction ($p < 0.05$) in total calcium levels (Figure 5-21) which might be due to a minor contribution of β -arrestin1/2 in the desensitisation of hFFA4. It has become increasingly clear that the canonical mechanism of β -arrestin-mediated desensitisation is by no means universal for all GPCRs (Reiter and Lefkowitz, 2006 ; van Koppen and Jakobs, 2004). β -arrestin-independent internalisation has been reported for many GPCRs for example (Premont and Gainetdinov, 2007; Mundell et al., 2006; Paing et al., 2002; Kohout et al., 2001; Lee et al., 1998).

To date, the predominant view is that hFFA1 and hFFA4 signals primarily via the heterotrimeric G proteins $G_{\alpha_{q/11}}$ and that its biological effects are mediated by downstream second messenger molecules produced from this activation, namely diacylglycerol and inositol 1,4,5-trisphosphate as well as subsequent Ca^{2+} mobilization (Milligan et al., 2017; Ferdaoussi et al., 2012; Hirasawa et al., 2005). When incubated in the presence of TUG-905, an increase in intracellular calcium level above basal was observed in parental HEK293 cells constitutively expressing hFFA1 (Figure 5-22). However, TUG-905-mediated calcium signalling and accumulation of IP1 were abolished in $G_{\alpha_{q/11}}$ -knockout cells. This was also the case for hFFA4 activated with TUG-891 (Figure 5-24; Figure 5-25). A reduction in basal inositol monophosphate levels in the $G_{\alpha_{q/11}}$ -null cells expressing hFFA4 indicates a level of $G_{\alpha_{q/11}}$ mediated constitutive activity of the receptor. On the other hand, agonist mediated hFFA4 phosphorylation in both parental and $G_{\alpha_q}/G_{\alpha_{11}}$ -null HEK293 cells (Figure 5-26) indicating that $G_{\alpha_{q/11}}$ proteins are not required for this to occur. Moreover, hFFA4 expressed in $G_{\alpha_q}/G_{\alpha_{11}}$ -null HEK293 cells found to internalise upon addition of TUG-891. However, quantitative measurement is needed to find any difference in the extent of internalisation compared to HEK293 parental cells. These results support that $G_{\alpha_{q/11}}$ coupling to agonist-activated receptors is essential for the functional signalling outcomes via both hFFA1 and hFFA4. Moreover, these findings validate the CRISPR/Cas9 engineered HEK293 cells lacking $G_{\alpha_{q/11}}$ as a useful model system for GPCR signalling research (Alvarez-Curto et al., 2016b).

6 Oligomerisation of hFFA1 and hFFA4

An emerging paradigm in GPCR research is the notion that receptors do not act exclusively as monomers, but also form functionally relevant dimers and oligomers (Gomes et al., 2016; Franco et al., 2016; Milligan, 2013; Milligan, 2009; Milligan, 2006a). Recently several biophysical methods based on resonance energy transfer (RET) between two molecules have been developed to examine the quaternary organisation of integral membrane proteins, including GPCRs, in intact cells (Gomes et al., 2016; Milligan, 2013; Ward et al., 2013; Milligan and Bouvier, 2005). These techniques are based upon energy transfer between either two autofluorescent proteins (in FRET studies) or an autofluorescent protein and an enzyme able to generate bioluminescence (in BRET studies). These probes are usually attached to the intracellular C-terminal tail of the GPCRs of interest (Ward and Milligan, 2014; Milligan and Bouvier, 2005).

As FFA1 and FFA4 undergo internalisation and desensitisation upon agonist exposure and they share some common affinity for many ligands, the pharmacology as well as cellular trafficking of these receptors might be modulated by receptor oligomerisation. Co-expression, co-internalisation, cross-desensitisation and oligomerisation of these receptors are yet to be explored. Despite these many questions regarding oligomerisation for FFA1/FFA4, there is also a challenge to work in transfected cell lines and relate the outcomes to physiologically relevant situations.

6.1 Homo-oligomerisation of hFFA1

6.1.1 FRET microscopy reveals homo-oligomerisation in hFFA1

I have generated previously Flp-In™ T-REx™-293 cells able to constitutively express a C-terminally GFP2 -tagged form of human FFA1 (section 3.3.1). These cells also harbour at the Flp-In™ T-REx™ locus a C-terminally mVenus-tagged form of hFFA1. The Flp-In™ T-REx™ locus allows regulated expression of hFFA1-mVenus-HA (which can act as acceptor in FRET pair) upon addition of the inducer doxycycline while levels of hFFA1-GFP2-HA remains constant (section 3.3.1). Moreover, two single stable Flp-In™ T-REx™ 293 cell lines inducibly expressing either hFFA1-mVenus-HA (section 3.1.1) or hFFA1-GFP2-HA (section

3.1.2) were generated and characterised. No visible expression of either construct was observed in the absence of the antibiotic doxycycline. However, sustained addition of doxycycline resulted in expression of each form as revealed by epifluorescence microscopy, immunoblotting and fluorescence measurements (section 3.1.1 and section 3.1.2).

Using the multiple dimensional wavelength acquisition module of MetaMorph, acceptor, FRET, and donor channel images were acquired using the same exposure time (section 2.5.9). Raw FRET images were corrected (cFRET) (Figure 6-1) by using Youvan's fully specified bleed through algorithm (Youvan et al., 1997). All bleed through coefficients were calculated from control cells expressing receptors tagged with mVenus or GFP2 alone. Net corrected FRET values were ratiometrically normalized (section 2.5.10) to generate a final ratiometric value (RFRET). Values greater than 1 reflected the occurrence of FRET and 1.0 considered as absence of energy transfer (Alvarez-Curto et al., 2010). Co-expression of hFFA1-GFP2-HA and hFFA1-mVenus-HA produced RFRET value of 1.42 ± 0.03 indicating homo-oligomerisation of hFFA1 (Figure 6-2). When receptors were expressed separately in single stable cell lines, the calculated RFRET values were 1.00 ± 0.01 for hFFA1-GFP2-HA and 0.99 ± 0.01 for hFFA1-mVenus-HA (Figure 6-2).

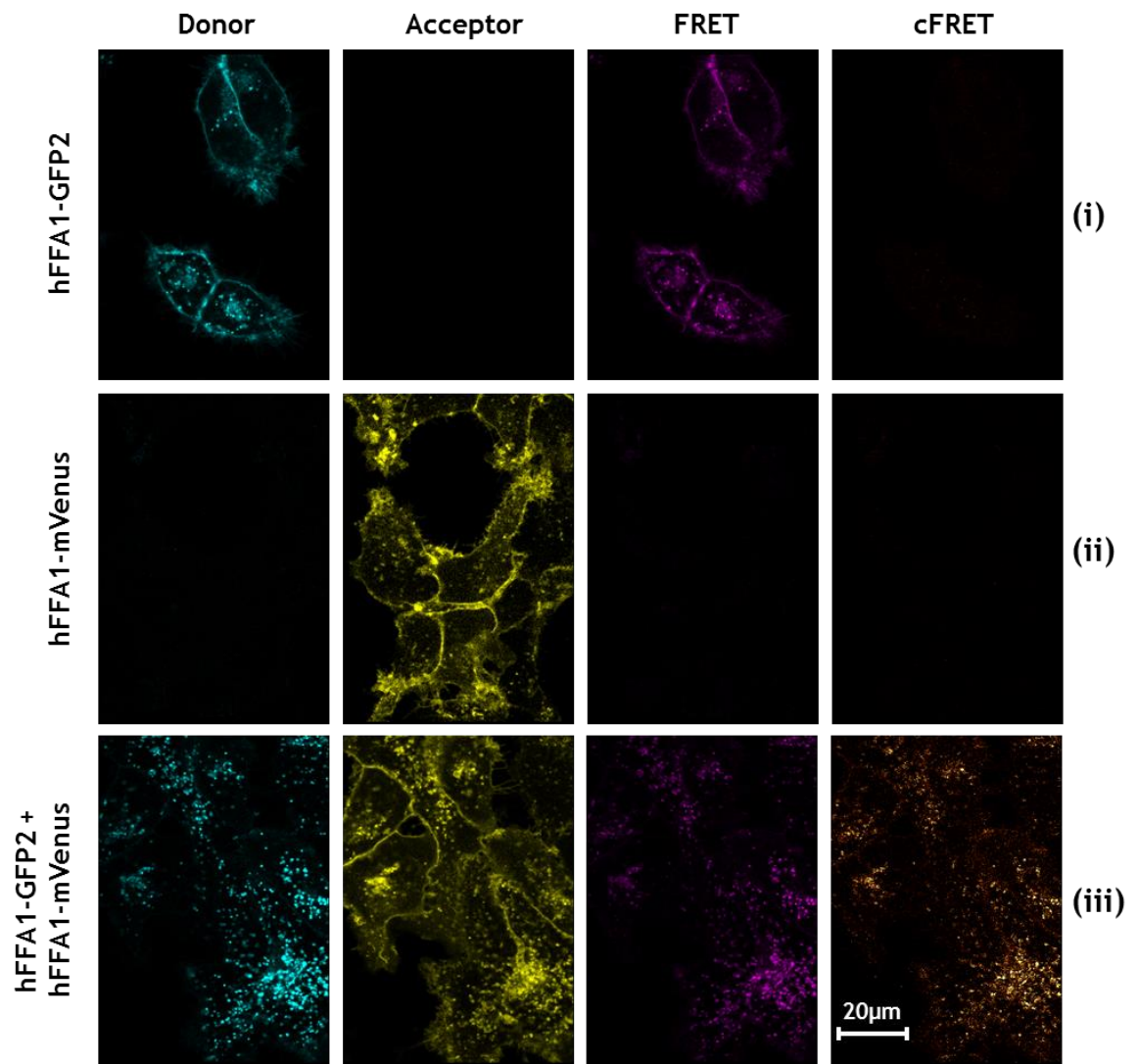


Figure 6-1. FRET analysis of interactions between hFFA1-mVenus-HA and hFFA1-GFP2-HA. Using Flp-In™ T-Rex™ 293 cells with individual expression of hFFA1-GFP2-HA (i) or hFFA1-mVenus-HA (ii) or co-expression of hFFA1-mVenus and hFFA1-GFP2 were performed (iii). Individual cell lines expressing corresponding receptors were imaged. FRET and corrected FRET (cFRET) images obtained from a representative experiment are shown. Images are representative of three independent experiments.

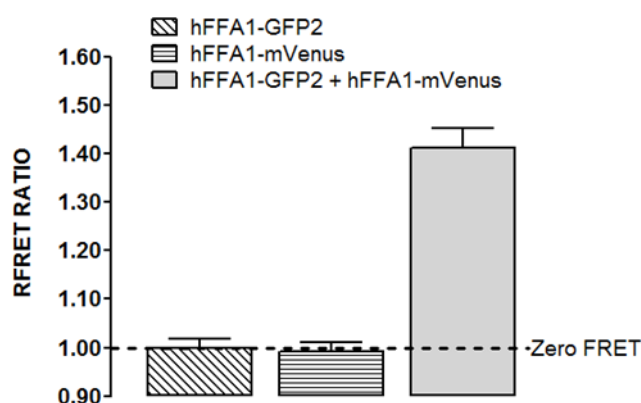


Figure 6-2. RFRET analysis of interactions between hFFA1-mVenus-HA and hFFA1-GFP2-HA. Using Flp-In™ T-REx™ 293 cells with individual expression of hFFA1-GFP2-HA or hFFA1-mVenus-HA or co-expression of hFFA1-mVenus and hFFA1-GFP2 were performed. Individual cell lines expressing corresponding receptors were imaged. FRET and corrected FRET (cFRET) signals from such images (Figure 6-1) were quantified (section 2.5.10). Net corrected FRET values were ratiometrically normalized to the amount of donor and acceptor fluorophore expressed to generate a final ratiometric value (RFRET). The broken line represents a RFRET value of 1.0 which corresponds to lack of FRET when no energy was transferred (zero FRET). RFRET index was expressed as the mean \pm SEM of three independent experiments.

6.1.2 Cell localisation of hFFA1 oligomers

Flp-In™ T-REx™-293 inducibly expressing hFFA1-mVenus-HA and constitutively expressing hFFA1-GFP2-HA were treated with doxycycline and imaged by epifluorescence microscopy (section 2.5.7). Expression of both hFFA1-GFP2-HA (Figure 6-3, A-i) and hFFA1-mVenus-HA (Figure 6-3, A-ii) were observed. Merging of images of hFFA1-GFP2-HA and hFFA1-mVenus-HA indicated almost perfect overlap of expressed receptors preferentially located within punctate intracellular spots (Figure 6-3, A-iii). The localisation of hFFA1 appears predominantly intracellular rather than plasma membrane (Figure 6-3). Pearson's correlation (r) analysis of intracellular regions of interests (ROIs) showed a strong overlap ($r = 0.97$) between GFP2 and mVenus fluorescence (Figure 6-3, B).

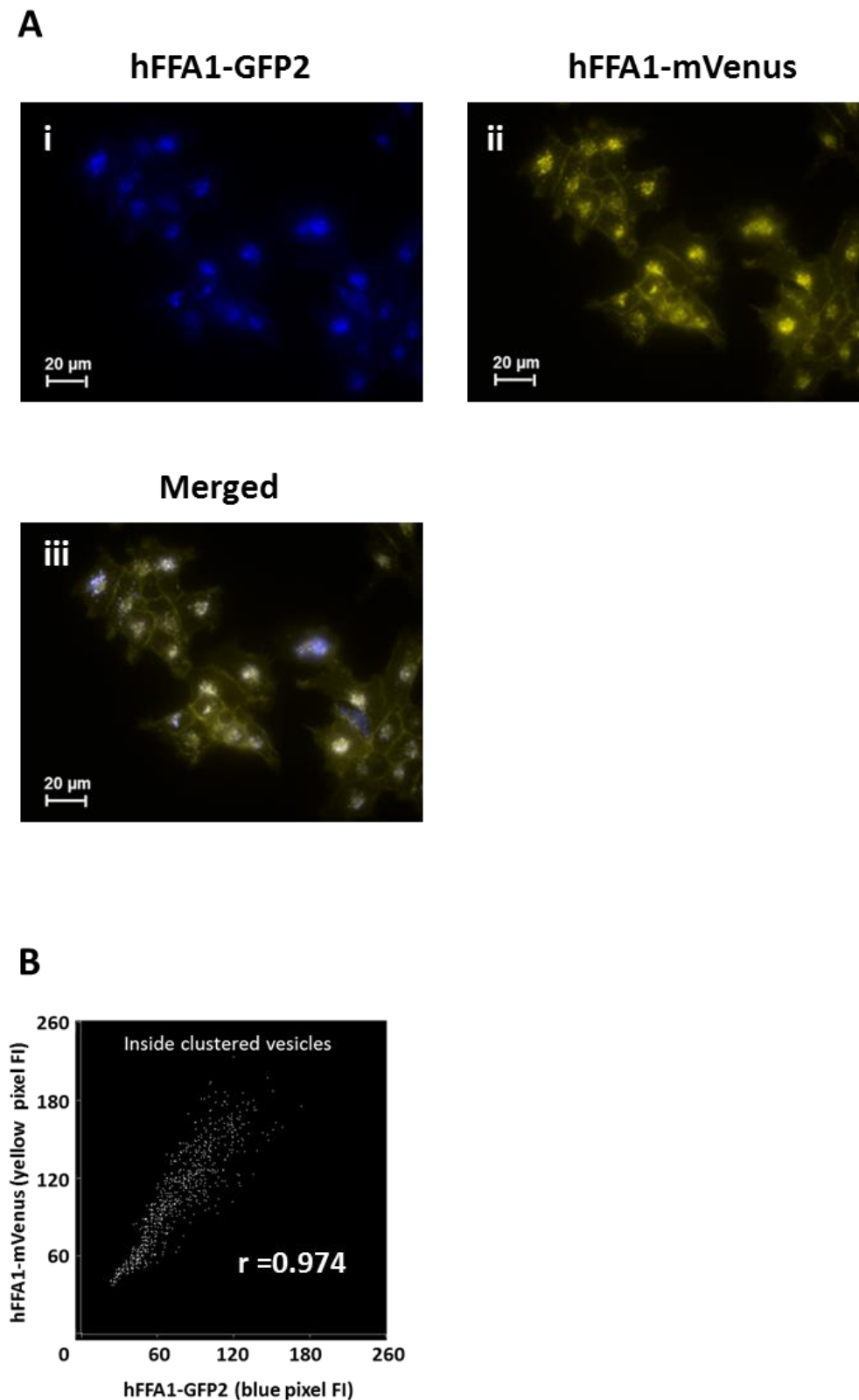


Figure 6-3. Co-localisation of the energy donor and acceptor fluorophores attached to hFFA1. Flp-In™ T-REx™ 293 cells inducibly expressing hFFA1-mVenus-HA and constitutively expressing hFFA1-GFP2-HA were treated with doxycycline (100 ng/ml) for 18-24 hours. **(A)** Images of GFP2-tagged hFFA1 (*blue*), mVenus-tagged hFFA1 (*yellow*), and merging of images (*merged*) from these cells were used to construct correlation analyses of colour overlap (*merged*). **(B)** Correlation analysis of mVenus and GFP2 colour overlap was quantified via Pearson's correlation (*r*).

6.2 Homo-oligomerisation of hFFA4

6.2.1 FRET microscopy reveals homo-oligomerisation of hFFA4

It was previously described that a Flp-InTM T-RExTM 293 double stable cell line was able to express constitutively FLAG-hFFA4-GFP2 whilst treatment with doxycycline was required for turn-on of expression of FLAG-hFFA4-mVenus in these cells (section 3.3.2). This system allowed the study of two forms of hFFA4 in the same cell line with the added benefit of control of expression of the acceptor FRET partner FLAG-hFFA4-mVenus. Moreover, GFP2- and mVenus-tagged forms of hFFA4 were expressed separately in Flp-InTM T-RExTM 293 single stable cell lines (section 3.2.1 and section 3.2.2). Maintained level of receptor expression in each of the cell lines was confirmed by imaging, assessing fluorescence intensity corresponding to the fluorescent protein and immunoblot analysis (section 3.2.1 and section 3.2.2).

To explore potential direct interactions between FLAG-hFFA4-GFP2 and FLAG-hFFA4-mVenus FRET imaging studies were performed (section 2.5.9). Donor, FRET and acceptor channel images were acquired using the same exposure time. Saved donor, acceptor and FRET channel images were background-subtracted (Section 2.5.10) and net-corrected FRET values from raw FRET images were generated (Figure 6-4 A). The RFRET value of 1.88 ± 0.02 indicated potential homo-oligomeric organisation of FLAG-hFFA4-mVenus and FLAG-hFFA4-GFP2 (Figure 6-4, B). In the single stable cell lines expressing either of the fluorophore-tagged forms of hFFA4, the calculated RFRET value was 1.00 ± 0.0 for FLAG-hFFA4-GFP2 and 0.99 ± 0.01 for FLAG-hFFA4-mVenus. These imaging studies offered initial insights into the potential hFFA4 homo-oligomerisation.

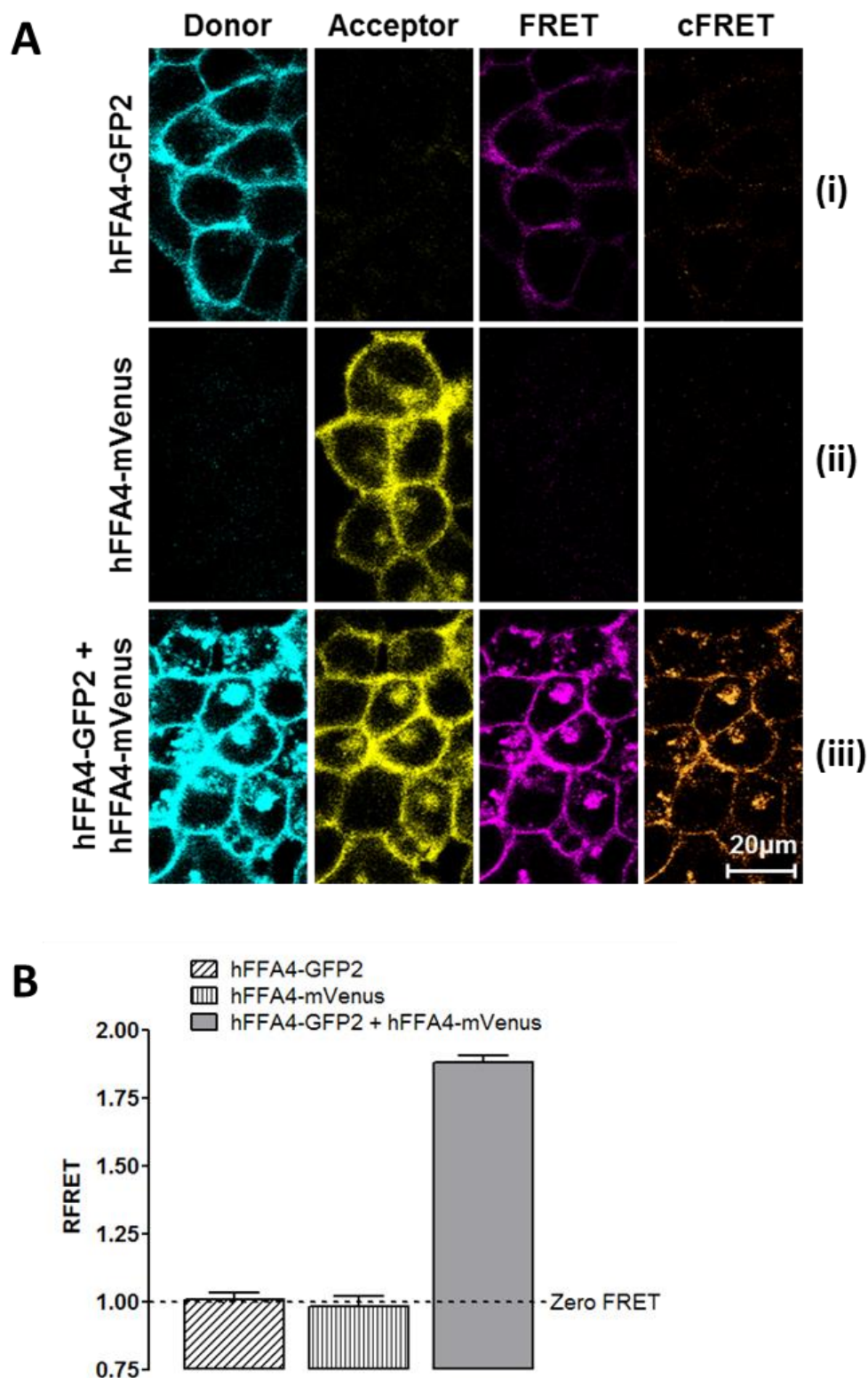


Figure 6-4. FRET analysis of interactions between FLAG-hFFA4-mVenus and FLAG-hFFA4-GFP2. (A) FLAG-hFFA4-GFP2 (i) or FLAG-hFFA4-mVenus (ii) were individually expressed in Flp-In™ T-REx™ 293 single stable inducible cell lines. FLAG-hFFA4-mVenus and FLAG-hFFA4-GFP2 (iii) were co-expressed. Representative FRET and corrected FRET (cFRET) images were generated. (B) FRET and corrected FRET (cFRET) signals from such images were quantified. Net corrected FRET values were ratiometrically normalized to the amount of donor and acceptor fluorophore expressed to generate a final ratiometric value (RFRET). The broken line represents a RFRET value of 1.0 which corresponds to lack of FRET. RFRET index was expressed as the mean \pm SEM of three independent experiments.

6.2.2 Cell localisation of hFFA4 homo-oligomers

Co-expression of FLAG-hFFA4-GFP2 and FLAG-hFFA4-mVenus was accomplished by inducing Flp-In™ T-REx™ 293 double stable cells (section 3.3.2) for 18-24 hours in the presence of doxycycline. Using epifluorescence microscopy (section 2.5.7), expression of both FLAG-hFFA4-GFP2 (Figure 6-5, A-i) and hFFA1-mVenus-HA (Figure 6-5, A-ii) were visualised. Merging of such images showed a strong overlap of GFP2 and mVenus signals. This indicated co-localisation of FLAG-hFFA4-GFP and FLAG-hFFA4-mVenus (Figure 6-5, A-iii). Both intracellular and membrane localisation of hFFA4 was noticed. Pearson's correlation (r) analysis of ROIs of whole cell, cell surface and intracellular regions showed a strong overlap between GFP2 and mVenus expression (Figure 6-5, B).

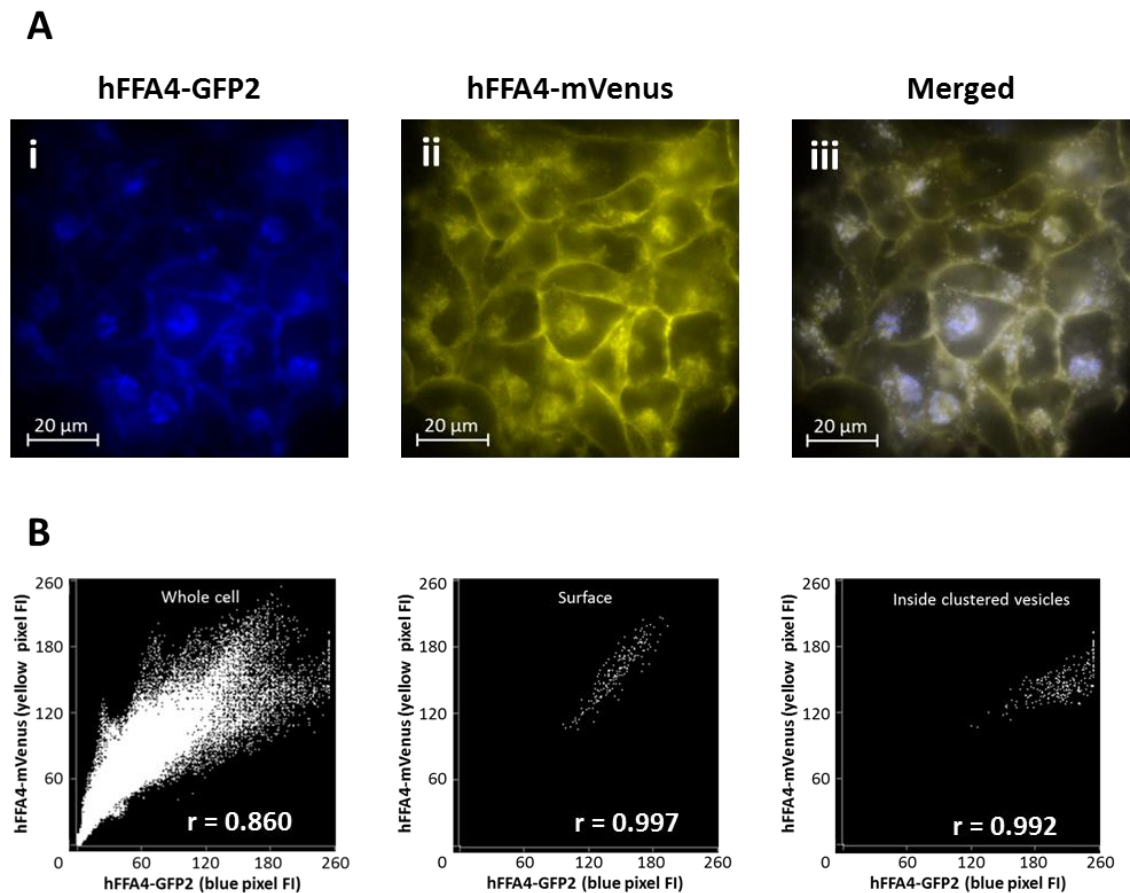


Figure 6-5. Co-localisation of the energy donor and acceptor forms of hFFA4. Flp-In™ T-REx™ 293 cells able to inducibly express FLAG-hFFA4-mVenus and constitutively expressing FLAG-hFFA4-GFP2 were treated with doxycycline (100 ng/ml) for 18-24 hours. (A) Images of GFP2 fluorescent protein (*blue*), mVenus fluorescent protein (*yellow*), and merging of these images (*merged*) from these cells were used to construct correlation analyses of colour overlap (*merged*). (B) Correlation analysis of mVenus and GFP2 colour overlap was quantified via Pearson's correlation (r).

6.2.3 BRET saturation reveals homo-oligomerisation of hFFA4

Conceptually similar to FRET, except that energy is donated to a fluorescent protein energy acceptor by luciferase-mediated oxidation of a substrate, bioluminescence resonance energy transfer (BRET) has become almost as popular an approach as FRET (Ward and Milligan, 2014; Alvarez-Curto et al., 2010; Ayoub and Pflieger, 2010; Milligan and Bouvier, 2005). The FRET imaging studies offered initial insights into the capability of hFFA4 to form homo-oligomeric complexes when two fluorophore-tagged receptors were co-expressed (Figure 6-4).

However, such studies can offer little insight into the relative propensity of pairs of hFFA4 to interact. To assess this, I employed saturation BRET experiments. In these studies I used a new version of the traditional BRET assays using a small (19 kDa) monomeric luciferase derived from a deep-sea shrimp (Nanoluciferase, Nluc) as a donor and the well-characterized monomeric fluorescent protein mVenus as an acceptor (Mo and Fu, 2016). It was hypothesised that mVenus- and Nluc-tagged hFFA4 might allow BRET upon addition of a luciferase-substrate if interactions between the partner proteins bring the luciferase and the mVenus into proximity. By varying the ratio of energy acceptor (the mVenus-tagged hFFA4) and energy donor (the Nluc-tagged hFFA4), BRET saturation curves could be generated in which half-maximal signal provides a measure of the relative affinity of receptor interactions (section 2.5.14). In this context, $BRET_{max}$ values are inversely proportional to the distance between donor and acceptor, whereas $BRET_{50}$ values represent the relative affinity between donor and acceptor (Achour et al., 2011). $BRET_{50}$ also provides an estimate for the relative propensity of the corresponding interaction (Milligan and Bouvier, 2005). The lower the measured- $BRET_{50}$ greater is the possibility of oligomerisation (Busnelli et al., 2013; Achour et al., 2011), while non-specific interactions results in a linear relationship or saturation curve with a high $BRET_{50}$ value (Szalai et al., 2014).

HEK293T cells were transiently transfected with a constant amount of plasmid DNA coding for FLAG-hFFA4-Nluc (BRET-donor fusion protein) in the presence of increasing concentrations of FLAG-hFFA4-mVenus (BRET-acceptor fusion protein). 48 hours after transfection, addition of the substrate coelenterazine *h* to intact cells resulted in BRET signals. The data for each acceptor/donor combination were fit to standard binding curves, from which the maximum BRET

ratio (BRET_{max}) and effective concentration at half BRET_{max} (BRET_{50}) were determined. In these experiments, the BRET signal increased hyperbolically and reached an asymptote with BRET_{max} of 0.28 ± 0.01 and BRET_{50} of 0.14 ± 0.02 (Figure 6-5). As a control, a generic membrane protein CD-86 tagged with mVenus was used, which was predicted to produce no change in BRET ratio or an increase in signal due to non-specific membrane saturation, respectively. Although BRET signals produced from this pairing were low ($\text{BRET}_{\text{max}} = 0.16 \pm 0.01$ and $\text{BRET}_{50} = 0.17 \pm 0.02$), there was not any significant difference with BRET_{50} of hFFA4 homo-oligomer (Figure 6-6).

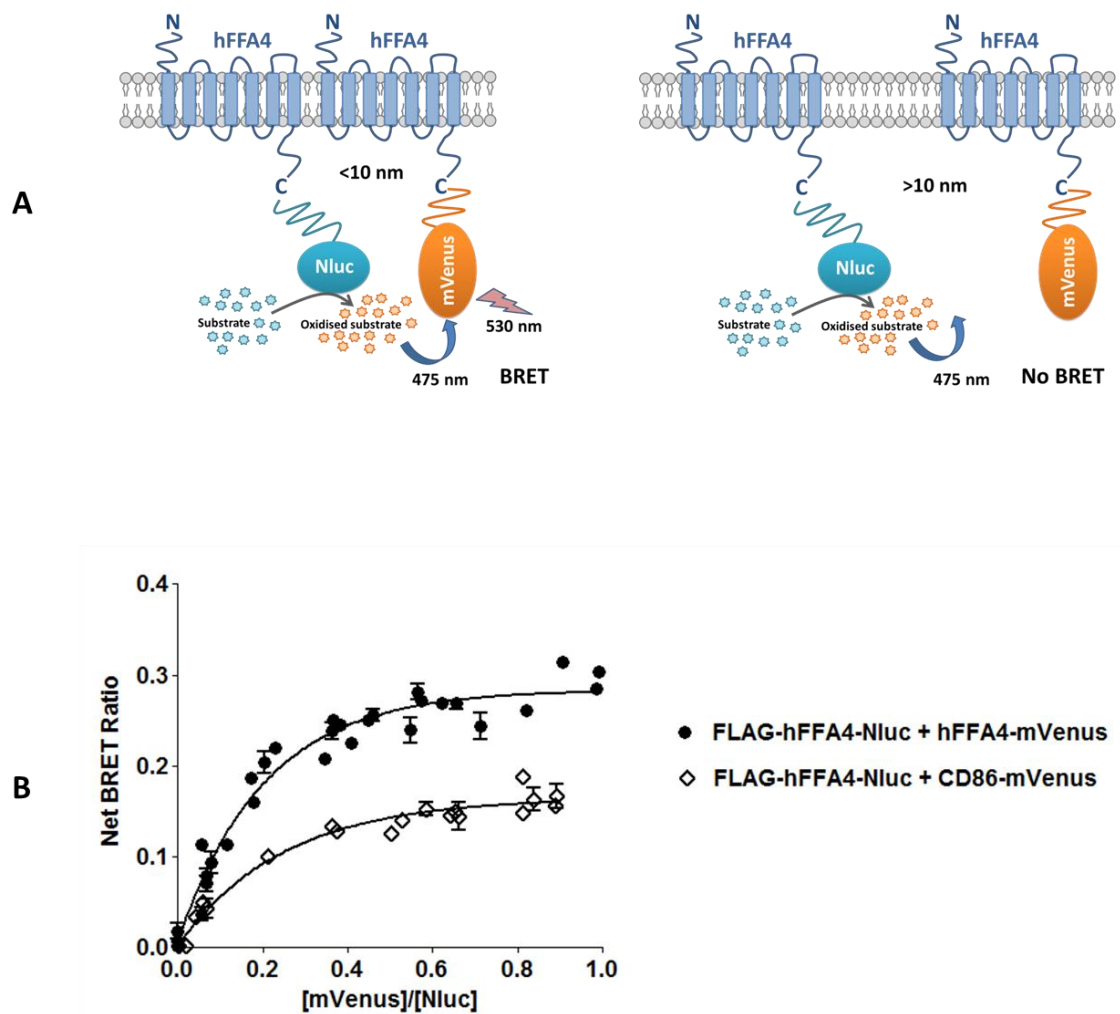


Figure 6-6. Homo-oligomerisation of hFFA4 revealed in BRET saturation studies. (A) The basis of BRET studies. If Nluc- and mVenus-tagged hFFA4 exist within 10 nm distance, oxidation of coelenterazine *h* by Nluc causes emission of 475 nm light which can excite the nearby mVenus with the emission of 535 nm light. If they are not in a complex (>10 nm), no BRET occurs. (B) BRET saturation curves were performed (section 2.5.14) in HEK293T cells co-expressing increasing concentrations of FLAG-hFFA4-mVenus (acceptor) or CD86-mVenus with constant amounts of FLAG-hFFA4-Nluc (donor). Background fluorescence measured in cells not expressing the BRET-acceptor was subtracted from fluorescence values. mVenus/Nluc ratios were plotted using a nonlinear regression equation assuming a single binding site (GraphPad Prism) to estimate BRET_{max} and BRET₅₀ values. Data represent the mean \pm SEM of three independent experiments.

6.3 Hetero-oligomerisation of hFFA1 and hFFA4

6.3.1 FRET microscopy reveals hetero-oligomerisation between hFFA1 and hFFA4

I previously generated a Flp-In™ T-REx™ 293 double stable cell line to constitutively express hFFA1-mVenus-HA and inducibly express FLAG-hFFA4-GFP2 (section 3.3.3). The Flp-In™ T-REx™ locus allowed regulated expression of FLAG-hFFA4-GFP2 (i.e. donor) to be achieved following addition of the inducer doxycycline while levels of hFFA1-mVenus-HA remain constant. Moreover, two single stable Flp-In™ T-REx™ 293 cell lines able to inducibly express either FLAG-hFFA4-GFP2 (section 3.2.2) or hFFA1-mVenus-HA (section 3.1.2) were generated and characterised. In these cells, no visible expression of either construct was observed in the absence of the antibiotic doxycycline. Doxycycline regulated expression of the corresponding receptor was confirmed by epifluorescence microscopy, immunoblotting and fluorescence measurements (section 3.1.1 and section 3.2.2).

Using the multiple dimensional wavelength acquisition module of MetaMorph®, acceptor, FRET, and donor channel images were acquired using the same exposure time (section 2.5.9). All images were background-subtracted and net-corrected FRET values from raw FRET images were corrected (Figure 6-7). Using control cells expressing receptor tagged with either mVenus or GFP2 alone, all bleed through coefficients were calculated and net corrected FRET values were ratiometrically normalized to generate a final RFRET. For single stable cell lines, the calculated RFRET values were 1.00 ± 0.01 for FLAG-hFFA4-GFP2 and 0.99 ± 0.01 for hFFA1-mVenus-HA. However, FRET studies with the co-expression of hFFA1-mVenus and hFFA4-GFP2 resulted a RFRET of 1.42 ± 0.03 in cluster inside of cells and 1.48 ± 0.02 in the cell surface (Figure 6-8 A). This result indicated hetero-oligomerisation between hFFA1 and hFFA4. Mean fluorescence intensities of mVenus of surface ORIs in cells co-expressing hFFA4-GFP2 and hFFA1-mVenus were plotted against surface RFRET ratio. No clear change in RFRET with the change of mVenus expression was noticed (Figure 6-8 B).

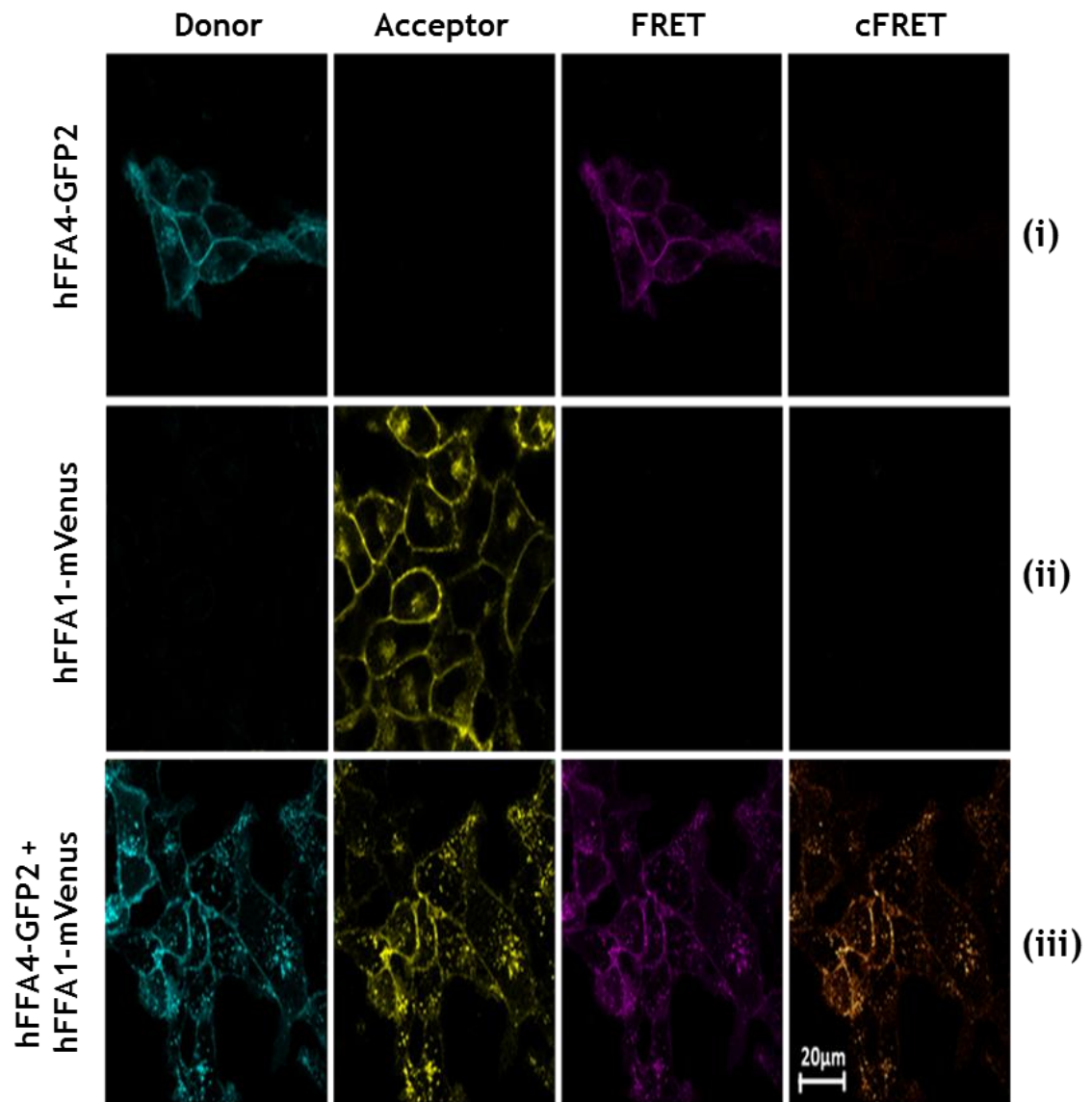


Figure 6-7. FRET analysis of interactions between FLAG-hFFA4-GFP2 and hFFA1-mVenus-HA. FLAG-hFFA4-GFP2 (i) and hFFA1-mVenus-HA (ii) were individually expressed whereas FLAG-hFFA4-GFP2 and hFFA1-mVenus-HA were co-expressed (iii) using Flp-In™ T-REx™ 293 cells. FRET and corrected FRET (cFRET) images were generated. Images are representative of three independent experiments.

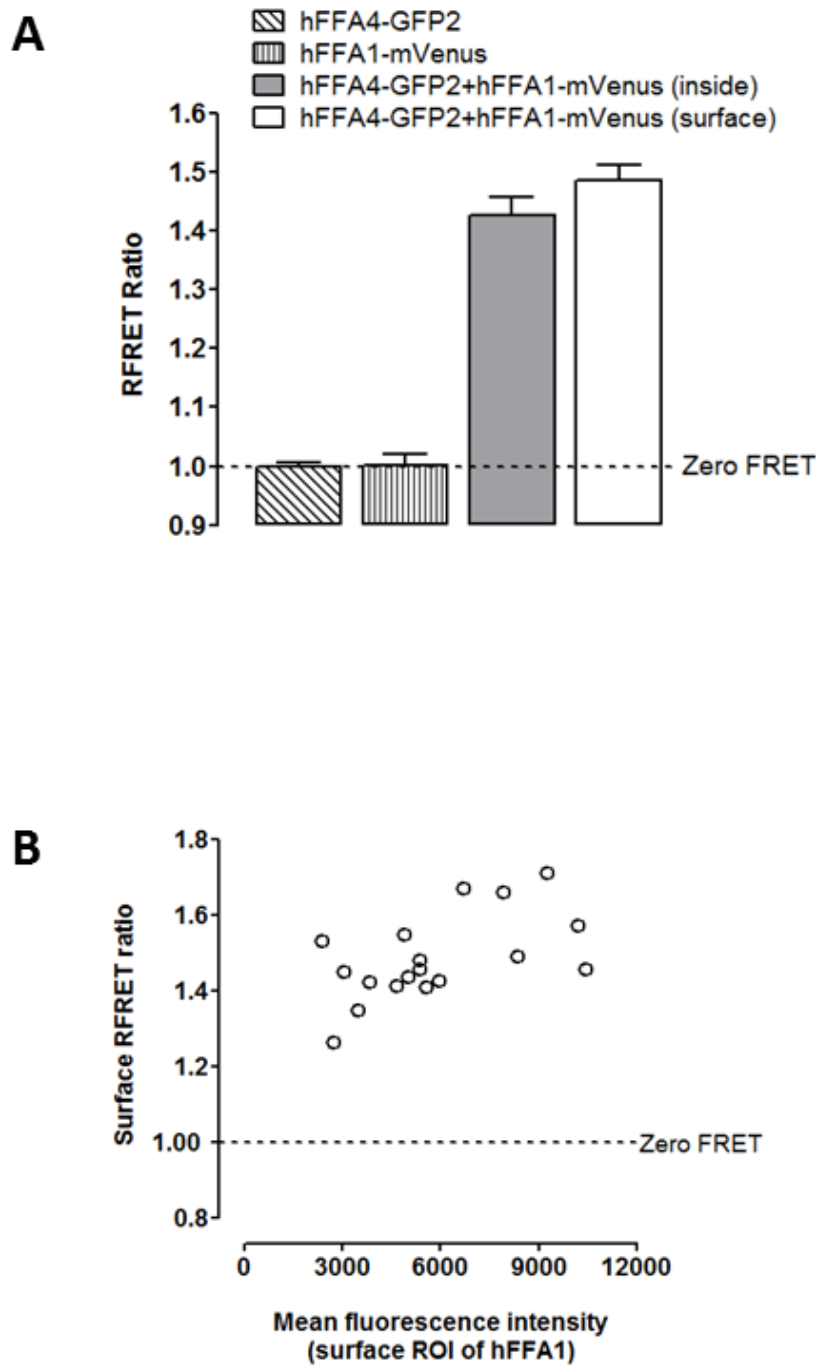


Figure 6-8. RFRET analysis of interactions between FLAG-hFFA4-GFP2 and hFFA1-mVenus-HA . FLAG-hFFA4-GFP2 and hFFA1-mVenus-HA were individually expressed whereas FLAG-hFFA4-GFP2 and hFFA1-mVenus-HA were co-expressed using Flp-In™ T-REx™ 293 cells. FRET and corrected FRET (cFRET) images were generated. FRET and corrected FRET (cFRET) signals from such images were quantified. (A) Net corrected FRET values were ratiometrically normalized to the amount of donor and acceptor fluorophore expressed to generate a RFRET value. The broken line represents a RFRET value of 1.0 which corresponds to a lack of FRET. (B) Surface ORIs mean fluorescence intensity of mVenus was plotted against surface RFRET ratio. RFRET index was expressed as the mean \pm SEM of three independent experiments.

6.3.2 Cell localisation of hFFA1/hFFA4 hetero-oligomers

For co-localisation studies, a Flp-In™ T-REx™ 293 double stable cell line able to inducibly express FLAG-hFFA4-GFP2 and constitutively express hFFA1-mVenus-HA was used (section 3.3.3). Cells were treated with doxycycline for 18-24 hours to induce the expression of FLAG-hFFA4-GFP2. Expression of FLAG-hFFA4-GFP2 (Figure 6-9, A-i) and hFFA1-mVenus-HA (Figure 6-9, A-ii) were then imaged by epifluorescence microscopy (section 2.5.7). Images were background-subtracted and merged. A strong overlap of mVenus and GFP2 signals were noted in these experiments indicating co-localisation of these receptors at the level of light microscopy (Figure 6-9, A-iii). Pearson's correlation (r) analysis of ROIs at the surface and inside of cells showed a strong overlap between GFP2 and mVenus fluorescence (Figure 6-9, B).

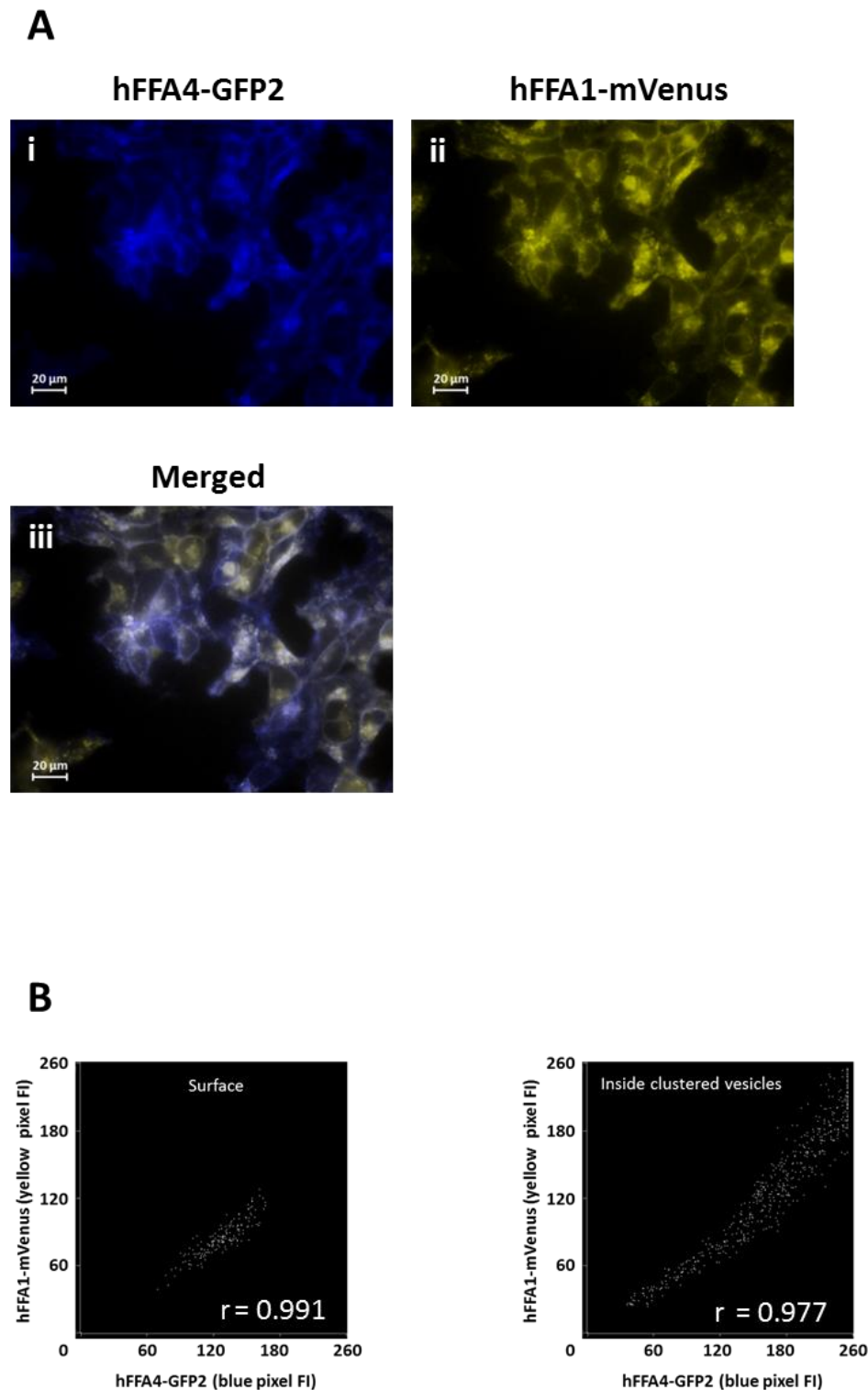


Figure 6-9. Co-localisation of hFFA4 and hFFA1. Flp-In™ T-REx™ 293 cells able to inducibly express FLAG-hFFA4-GFP2 and constitutively expressing hFFA1-mVenus-HA were treated with doxycycline (100 ng/ml) for 18-24 hours. **(A)** Images of FLAG-hFFA4-GFP2 (i), hFFA1-mVenus-HA (ii) were taken by epifluorescence microscopy. Images were background-subtracted and merged (iii). White colour generated from the merge of blue and yellow colour indicated a strong overlap between these two fluorophore-tagged receptors. **(B)** Correlation analysis of mVenus and GFP2 colour-overlap was quantified via Pearson's correlation (r).

6.3.3 Hetero-oligomerisation of hFFA1 and hFFA4 detected by BRET

To perform saturation BRET assays (section 2.5.14), HEK293T cells were transiently transfected with a fixed amount of FLAG-hFFA4-Nluc and increasing amounts of hFFA1-mVenus-HA. 48 hours post transfection, BRET signals were measured upon addition of the substrate coelenterazine *h*. The data for each acceptor/donor combination were fit to standard binding curves, from which the maximum BRET ratio (BRET_{max}) and effective concentration at half BRET_{max} (BRET_{50}) were determined. In this experiment, the BRET signal increased hyperbolically and reached an asymptote with BRET_{max} of 0.33 ± 0.01 and BRET_{50} of 0.08 ± 0.01 (Figure 6-10, B). The control CD86-mVenus generated BRET_{max} value of 0.16 ± 0.01 and BRET_{50} value of 0.17 ± 0.02 when transfected with the donor FFA4-Nluc. Although both FFA1-mVenus and CD86-mVenus showed hyperbolic curve with the association with FFA4-Nluc, relative high BRET_{max} and lower BRET_{50} in hFFA1-hFFA4 interaction indicated hetero-oligomeric interactions in these free fatty acid receptors. Increasing signals with CD86-mVenus levels might reflect physical crowding that was not related to true interactions with FFA4-Nluc.

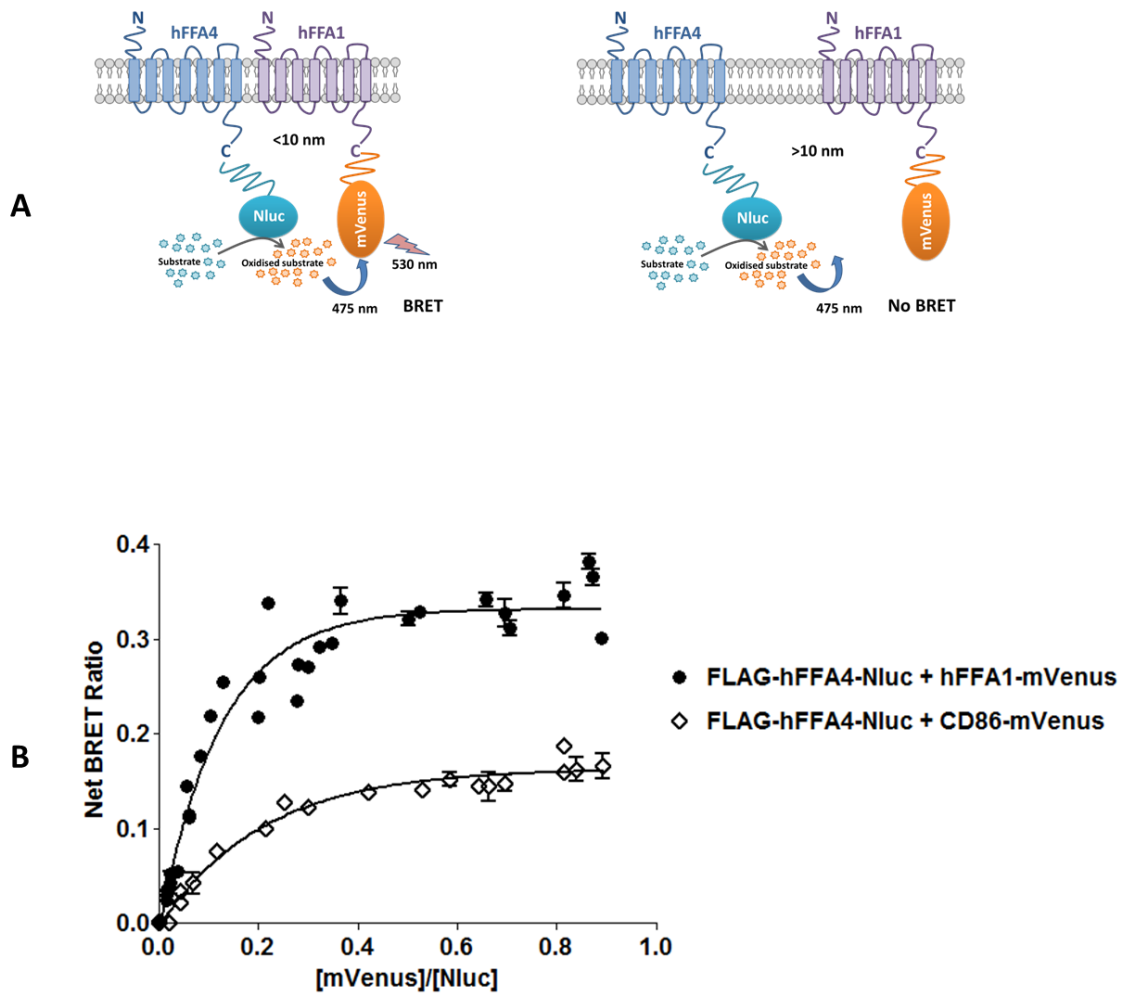


Figure 6-10. Hetero-oligomerisation of hFFA1 and hFFA4 in BRET saturation

studies. (A) The basis of BRET studies. If Nluc-tagged hFFA4 and mVenus-tagged hFFA1 exist within 10 nm distance, addition of the Nluc-substrate coelenterazine h results emission of 475 nm light which can excite the nearby mVenus with emission of 535 nm light. If they are not in close proximity (>10 nm), no BRET happens. (B) BRET saturation curves were performed in HEK293T cells coexpressing increasing concentrations of hFFA1-mVenus (acceptor) or CD86-mVenus with constant amounts of FLAG-hFFA4-Nluc (donor). mVenus /Nluc ratios were plotted against net BRET ratio assuming a single binding site (GraphPad Prism) to estimate BRET_{max} and BRET₅₀ values. Data represent the mean \pm SEM of three independent experiments.

6.4 Discussion

GPCRs have traditionally been considered to exist and function as cell-surface-receptor monomers (Milligan et al., 2015; Kenakin, 2015). However, it is currently assumed that the physiology and pharmacology of GPCRs is much more complex than originally anticipated. A major insight into this complexity has emerged over the last decade, as it became evident that GPCRs are able to oligomerise (Milligan, 2007; Milligan, 2008; Milligan, 2009). Indeed, GPCR oligomers may enhance the diversity and performance by which extracellular signals are transferred to G proteins in the process of receptor transduction (Ferre et al., 2014). Numerous biophysical and biochemical trials have demonstrated the spatial organisation of GPCRs in higher order assemblies, both *in vitro* and *in vivo* (Milligan, 2013). Biological fingerprint experiments have shown that formation of homo- and hetero-oligomers may influence important aspects in GPCR signalling pathways, such as ligand binding affinity, receptor activation or internalisation and interactions with heterotrimeric G-proteins (Milligan, 2013; Milligan, 2006a). Oligomerisation is established in the family C GPCRs including the metabotropic glutamate receptors, the calcium-sensing receptor and the γ -aminobutyric acid receptors. These receptors associate with themselves and function as constitutive dimers. However, rising evidence indicates that class A GPCRs can form oligomers when expressed in heterologous cell systems (Ferre et al., 2014; Milligan, 2013). For example, muscarinic receptors M_2 and M_3 form homo- and hetero-oligomers when expressed in Flp-InTM T-RExTM 293 cells and the oligomerisation is ligand-regulated (Aslanoglou et al., 2015). Selective agonist occupancy of the M_2 receptor favours M_2 - M_2 homo-oligomerisation but decrease the M_2 - M_3 hetero-oligomeric interactions (Aslanoglou et al., 2015). Ward et al. (2015) showed that serotonin 5-hydroxytryptamine 2C (5-HT_{2C}) receptor forms oligomers where use of antagonists favours monomeric and dimeric forms.

Both biochemical and biophysical approaches have been employed to study the basis of GPCRs oligomerisation (Milligan and Bouvier, 2005). Adaptations of resonance energy transfer techniques are invaluable way to explore protein-protein interactions (Ward and Milligan, 2014; Milligan and Bouvier, 2005). For example, attachment of FRET-competent pairs to the receptor or a fluorescent protein and an enzyme able to generate bioluminescence allow investigation of

possible oligomerisation (Milligan and Bouvier, 2005). FRET is based on the sensitisation of an acceptor molecule by the energy transfer from a donor when there is an overlap between the emission spectrum of the donor and the excitation spectrum of the acceptor and close proximity between the two fluorophore species (Marsango et al., 2015). A key feature of the FRET imaging studies is to employ the inducible expression of DNA located at the Flp-InTM locus of Flp-InTM T-RExTM 293 cells (Ward et al., 2013). Herein, I have investigated the presence of oligomeric complexes of hFFA1 or hFFA4 or both receptors in Flp-InTM T-RExTM 293 cells stably expressing mVenus or GFP2 tagged forms of either receptor. This allowed the regulated expression of one form of the receptor in the presence of an unaltered amount of a second form of receptor in the same cell. FRET experiments revealed homo- and hetero-oligomeric interaction in these free fatty acid receptors (Figure 6-1; Figure 6-4). Strong FRET signals (RFRET>1.0) between these receptor forms were observed. Strong co-localisation was also seen in all of the oligomeric interactions (Figure 6-3; Figure 6-5; Figure 6-9). However, such co-localisation studies can only define proximity within a distance of some 300 nm because of the current limits of light microscopy (Alvarez-Curto et al., 2010).

The issue of hFFA1 or hFFA4 oligomerisation was investigated with well-controlled BRET experiments. As a ratiometric measure, BRET signals reflects specific protein/protein interactions which should be independent of absolute expression levels (Milligan and Bouvier, 2005). I have employed saturation BRET assays using Nluc-tagged hFFA4 and mVenus tagged-hFFA1 or hFFA4 to test this model of oligomerisation. The BRET signal increased hyperbolically and reached an asymptote for hFFA4 homo-oligomerisation (Figure 6-6) as well as hFFA1/hFFA4 hetero-oligomerisation (Figure 6-10). A negative control fusion protein was included in this BRET-donor saturation assay to verify the specificity of the generated BRET. Ideally, negative control proteins should have a similar topology as the GPCR of interest (i.e., another GPCR) and should be localized in the same subcellular compartment (Achour et al., 2011). As many GPCRs have a natural tendency to associate, finding a true negative control was challenging. Therefore, membrane protein with different topology (non-interacting type-I membrane protein CD86) was used as negative control protein (James et al., 2006). Here in my experiments, the hydrophobic properties of hFFA4-CD86

complex showed false-positive interactions. In this context, quantitative issues were critical to consider. Although CD86 is a well-characterised monomeric protein, false positive results are not uncommon for this protein (Felce et al., 2014). Increasing signals with CD86-mVenus levels might reflect physical crowding that was not related to true interactions with FFA4-Nluc.

A common question in the context of GPCR homo- and hetero-oligomerisation is the relative propensity of formation of the complex. The $BRET_{max}$ is achieved as a function of distance between the donor and acceptor whereas the $BRET_{50}$ values in BRET-donor saturation assays for each pair of fatty acid receptors provides an estimate for the relative propensity of the corresponding interaction (Milligan and Bouvier, 2005). In my experiments, $BRET_{max}$ and $BRET_{50}$ indicated strong homo-oligomeric (hFFA4-Nluc/hFFA4-mVenus) and hetero-oligomeric (hFFA4-Nluc/hFFA1-mVenus) interactions (Figure 6-6; Figure 6-10). To obtain meaningful results in these experiments, the amount of Nluc fusion protein was kept equivalent for all transfections.

As oligomerisation is not an absolute prerequisite for proper signalling (Milligan, 2013; Milligan, 2008), GPCR oligomerisation and its functional relevance remain controversial topics (Milligan, 2013). However, oligomerisation could have an important role during biosynthesis, ligand-driven transactivation or inhibition (Fuxe et al., 2010). Transient transfection into heterologous cell lines of GPCRs in general and, in particular the modified forms used for resonance energy transfer studies often results in incomplete folding and their retention in the endoplasmic reticulum and Golgi. This is a major issue in efforts to explore oligomerisation in so-called saturation resonance energy transfer studies (Milligan and Bouvier, 2005). Also, reconstitution systems used for BRET analysis might artificially drive the synthesis of the receptors to be studied in the same cell at the same time and the interactions might not be representative of a physiological situation (Milligan, 2013). Although FRET and BRET techniques overcome a number of the issues with the biochemical approaches, they both generally require genetic manipulation of the proteins. Applying these RET methods, I have described here first time some preliminary data on oligomerisation of long chain free fatty acid receptors hFFA1 and hFFA4. Due to time constraint, ligand regulations of these oligomeric interactions were yet to explore. Oligomerisation in hFFA1 and hFFA4 might answer many questions of

regulation and desensitisation of these receptors. Moreover, biosynthesis of these therapeutically important receptors, their transport along the secretory pathway, mechanisms of activation, signal transduction, ligand regulation, transactivation, co-internalisation and cross desensitisation needed to be addressed in future. More structural evidence and studies are needed to explore if there are common underlying mechanisms for this oligomerisation and how such oligomers function in physiological states.

7 Final discussion

Over a decade after deorphanisation, both FFA1 and FFA4 have been reported to be associated with various metabolic disorders, particularly type-2 diabetes, obesity and inflammatory conditions (Milligan et al., 2017; Milligan et al., 2015). Both receptors are coupled to $G_{\alpha q/11}$ and β -arrestin mediated pathways, trigger a number of intracellular events and influence systemic metabolic function in physiological and pathophysiological conditions (Milligan et al., 2017; Moran et al., 2016). Their diversified expression and functions have been linked directly or indirectly to promoting insulin secretion, improved insulin sensitivity, good control of blood glucose levels and energy homeostasis. With this background both of these receptors are being studied as potential therapeutic targets for the control of metabolic diseases. FFA1 has been clinically validated as a target for treatment of type-2 diabetes by a phase 2 clinical study of TAK-875 (Burant et al., 2012) although this compound was later discontinued due to liver toxicity (Mancini and Poitout, 2015b). Genetic and systems biology studies in both humans and mouse models link FFA4 dysfunction to obesity and insulin resistance (Milligan et al., 2015; Ichimura et al., 2012) and also inflammation (Oh et al., 2010). The general consensus now strongly favours agonism as the desired mode of action in targeting both FFA1 and FFA4 receptor (Milligan et al., 2017; Cornall et al., 2014, Hudson et al., 2013c). However, agonist-promoted receptor desensitisation is a common phenomenon in GPCRs (Kohout and Lefkowitz, 2003). Desensitisation provides a means for terminating relevant acute signalling (Shenoy and Lefkowitz, 2011; Drake et al., 2006), regulates receptor trafficking (Zhuo et al., 2014) and in some cases increases signalling diversity (Thomsen et al., 2016). So, it is important to explore the detailed mechanisms of desensitisation of FFA1 and FFA4 which might aid in the development of agonist-based therapies. Moreover, receptor oligomerisation is now-a-days gaining attention in many GPCRs as it has been found to regulate receptor biology, receptor activation, signal transduction and receptor trafficking (Milligan, 2013; Milligan, 2007). After deorphanisation, although the pharmacology of FFA1 and FFA4 has been documented, insights into desensitisation, trafficking and oligomerisation have remained elusive. In this dissertation I have described the regulation, desensitisation and possible oligomerisation of hFFA1 and hFFA4, with greater emphasis on hFFA4.

The choice of the expression system has great influence on the quality and quantity of the produced recombinant protein (Bussow, 2015). The successful study of receptor pharmacology largely depends on using a specific heterologous system able to express the protein of interest in sufficient amount in its functional form (Chakraborty et al., 2015; Andrell and Tate, 2013; Spitzer et al., 2013). There are lots of challenges in this that range from poor expression to cell viability. The Human Embryonic Kidney cell line, HEK293 is an excellent host cell for robust expression of mammalian proteins (Thomas and Smart, 2005). Easy reproduction and maintenance, high efficiency of transfection and protein production and faithful translation and processing of proteins have made this cell line popular for expressing proteins of interest (Thomas and Smart, 2005). FLP-In™ T-REx™ stable cell lines are isogenic and hence protein expression is constant across a population of cells. FLP-In™ T-Rex™ 293 cell lines contains a single integrated FRT site and are able to stably express the tetracycline repressor protein. Addition of tetracycline or doxycycline releases the tetracycline repressor protein and enables the translation of the receptor of interest (Ward et al., 2011a; Koener and Hermans, 2011). This cell line allows expression of receptors to be controlled by the addition of a small molecule inducer to the cell culture medium (Ward et al., 2011a). I successfully generated FLP-In™ T-REx™ 293 inducible single stable cell lines able to express hFFA1-mVenus-HA (section 3.1.1), hFFA1-GFP2-HA (section 3.1.2), FLAG-hFFA4-mVenus (section 3.2.1) and FLAG-hFFA4-GFP2 (section 3.2.2). The doxycycline-inducible expression was demonstrated by epifluorescence microscopy (section 3.1 and section 3.2). The regulated expression of these receptors was confirmed by immunoblotting and measurement of fluorescence intensity. The functional activities e.g. agonist-promoted mobilisation of intracellular calcium was dependent on the amount of doxycycline used to induce receptor expression (section 3.1 and section 3.2). The inducible system allowed scaling up the desired level of receptor expression which is very important in many biochemical and biophysical experiments. Constitutive expression of either hFFA1 (section 3.1) or hFFA4 (section 3.2) was also successfully achieved. However, clonal selection and characterisation were required to identify cells homogeneously expressing the receptor of interest. For potential oligomeric interactions of hFFA1 and hFFA4, double stable cell lines were generated where expression of

one form of a receptor was doxycycline-regulated and expression of the other was constitutive.

Although FFA1 and FFA4 are not closely related, both receptors are activated by the same group of natural free fatty acids. For target validation, development of a selective pharmacological tool compound is a valuable approach. Moreover, development of novel ligands offers great opportunities to further unravel the contributions of these receptors.

Fasiglifam (TAK-875), developed by Negoro et al. (2010), progressed to phase III clinical trials but was withdrawn due to potential liver toxicity (Kaku et al., 2015). Our medicinal chemistry group has developed a series of selective and potent FFA1 receptor agonists, including TUG-905 (Christiansen et al., 2012) and TUG-770 (Christiansen et al., 2013a). In my studies, TUG-770 and TUG-905 showed high potency and efficacy in a number of experiments including BRET-based β -arrestin2 recruitment (Figure 4-12) and mobilisation of intracellular calcium (Figure 4-10). TUG-770 was also found to be highly potent and a 157-fold selective hFFA1-ligand over hFFA4 (Figure 4-11). Christiansen et al. (2012) developed TUG-905 by modification of their previous compound TUG-469 (Christiansen et al., 2010) where these authors incorporate a hydrophilic 3-mesylpropoxy appendage akin to TAK-875. They found that this compound can promote release of insulin from rat β -cell line INS-IE. Using the same cell line, Christiansen et al. (2013a) showed that TUG-770 causes insulin release with excellent physicochemical and pharmacokinetic properties. Elevation of intracellular calcium level via FFA1 activation by these ligands might be related with the improved insulin secretion. Insurmountable antagonism by GW-1100 was seen in both agonist-promoted recruitment of β -arrestin (Figure 4-13) and mobilisation of intracellular calcium (Figure 4-14). The findings validated the nature of antagonism of this antagonist tool compound to study FFA1.

Our medicinal chemistry group developed TUG-891 as a potent FFA4 agonist (Shimpukade et al., 2012; Hudson et al., 2013b), however, showed limited selectivity at mouse FFA4. TUG-891 is commercially available and has become a frequently employed tool compound in both studies at this receptor. Azevedo et al. (2016) recently reported TUG-1197 as highly selective FFA4 agonist promoting improved glucose homeostasis. Both TUG-891 and TUG-1197 showed elevation of

intracellular calcium (Figure 4-1) and recruitment of β -arrestin2 (Figure 4-3). Both of the ligands phosphorylated hFFA4 (Figure 5-5). All of these outcomes were ligand-concentration-dependent. I have extensively characterised the nature of antagonism of TUG-1275 in a number of assays including ligand-promoted receptor phosphorylation (Figure 4-4), β -arrestin2 recruitment (Figure 4-5), receptor internalisation (Figure 4-6), intracellular calcium mobilisation (Figure 4-8) and accumulation of inositol monophosphate (Figure 4-9). The nature of antagonism was non-competitive. Sparks et al. (2014) identified compound 39 (AH 7614) which was later synthesised by our medicinal chemistry group named as TUG-1275. However, Sparks et al. (2014) did not characterise the nature of the antagonism of this compound. Although my data preliminary shows that this compound might be a non-competitive antagonist of FFA4, the mode of binding of TUG-1275 with the receptor yet to be explained. In my experiments, TUG-1275 appeared to be insurmountable antagonist in assays measuring intracellular calcium levels (Figure 4-9), recruitment of β -arrestin2 (Figure 4-5) and FFA4 internalisation (Figure 4-6). TUG-1275 might be a promising pharmacological tool compound to FFA4.

The biological effects associated with FFA1 and FFA4 activation are anticipated to be mediated by $G\alpha_{q/11}$ signalling pathways (Milligan et al., 2017; Ferdaoussi et al., 2012; Hirasawa et al., 2005). Inhibition of this signal by the use of a $G\alpha_q$ inhibitor indicated that the signalling pathways were $G\alpha_{q/11}$ dependent (Hudson et al., 2013b). However, knockout strategies are best suited system to investigate GPCR signalling and desensitisation (Alvarez-Curto et al., 2016b). hFFA1 and hFFA4 expressed in a $G\alpha_q/G\alpha_{11}$ knockout were unable to generate agonist promoted mobilisation of intracellular calcium (Figure 5-22; Figure 5-24). This was also the case for the release of inositol monophosphates (Figure 5-23; Figure 5-25). However, in $G\alpha_{q/11}$ -null cells, agonists were still able to phosphorylate (Figure 5-26) and internalise hFFA4 (Figure 5-27). These findings confirmed that functional signalling particularly agonist-promoted elevation of intracellular calcium levels is mediated through $G\alpha_{q/11}$ signalling for these receptors. Moreover, these findings validate $G\alpha_{q/11}$ -null cell lines as tool cell line to study GPCR signalling.

Repeated exposure of hFFA1 and hFFA4 to appropriate agonists resulted in desensitisation of calcium signalling mediated by these receptors although cells

were functional as they still produced a full calcium signal on ATP treatment (section 5.1.1 and section 5.2.1). These findings suggest that receptor desensitisation might be a significant challenge for agonist-based drug development targeting these therapeutically important receptors.

Phosphorylation is the initial step in receptor desensitisation (Paing et al., 2002). FFA4-agonists TUG-891 and TUG-1197 caused phosphorylation of hFFA4 in a concentration-dependent fashion (Figure 5-5). This homologous phosphorylation was blocked by the use of TUG-1275. $G_{q/11}$ signalling pathways allow activation of second messenger-dependent kinases including PKA and PKC (Reiter and Lefkowitz, 2006; Shenoy and Lefkowitz, 2003). To investigate heterologous pathway in hFFA4-phosphorylation, PKC activator PMA found to phosphorylate hFFA4 in a concentration-dependent manner (Figure 5-6) which was significantly blocked by the PKC inhibitors BIM-I and Go-6979 (Figure 5-6). Agonist-promoted phosphorylation was partially inhibited with the use of PKC inhibitors (Figure 5-7). Moreover, PKC caused robust internalisation of hFFA4 (Figure 5-9). These results suggest the second messenger-mediated pathway is involved in the phosphorylation and internalisation of FFA4.

Phosphorylation of the receptor by GRKs and the recruitment of β -arrestins is critical to both these short- and long-term desensitisation mechanisms (Smith and Rajagopal, 2016; Thomsen et al., 2016). An agonist-concentration dependent recruitment of β -arrestin2 was seen in both hFFA1 (Figure 4-12 and hFFA4 (Figure 4-3). The canonical mechanism is that β -arrestin sterically hinders further coupling to G proteins, and this interruption of signalling generates receptor desensitisation (Reiter and Lefkowitz, 2006; van Koppen and Jakobs, 2004; Kohout and Lefkowitz, 2003). To investigate the contribution of β -arrestin2 in this desensitisation process, I have used CRISPR/Cas9-mediated genome edited HEK293 cells lacking β -arrestin1/2 proteins (Alvarez-Curto et al., 2016b) and stable cell lines were generated expressing hFFA1 (section 3.1.4) or hFFA4 (section 3.2.1). Interestingly, elimination of β -arrestin1 and β -arrestin2 proteins did not show any significant differences in the desensitisation of both receptors on repeated agonist treatment at hFFA1 (Figure 5-15) and hFFA4 (Figure 5-20). A single chronic exposure of TUG-891 however, showed a significant change in total calcium levels (Figure 5-21) which might be due to a minor contribution of β -arrestin in the desensitisation of hFFA4.

Agonist-promoted receptor internalisation sometimes contributes to receptor desensitisation (Ferguson, 2001). TUG-891 caused rapid internalisation of hFFA4 in an agonist-concentration-dependent manner (Figure 5-12) and the internalisation increased with time of agonist exposure (Figure 5-13). However, β -arrestin1/2-null did not show any detectable change of internalisation of hFFA4 (Figure 5-18). These findings indicate that other regulatory proteins might be involved in the internalisation process of hFFA4. In contrast, Alvarez-Curto et al. (2016b) used this CRISPR/Cas9-mediated genome edited HEK293 cell lines lacking β -arrestin1/2 and expressed mouse form of FFA4. These authors found that β -arrestin1/2-null significantly compromise mFFA4 desensitisation and internalisation indicating that there might be species difference in the desensitisation pattern on FFA4. It has become increasingly clear that the canonical mechanism of β -arrestins mediated desensitisation is by no means universal for all GPCRs (Reiter and Lefkowitz, 2006; van Koppen and Jakobs, 2004). β -arrestin-independent internalisation has been reported in many GPCRs (Premont and Gainetdinov, 2007; Mundell et al., 2006; Paing et al., 2002; Kohout et al., 2001; Lee et al., 1998).

Growing evidence has been accumulated over few years that GPCRs can exist as oligomers (Milligan, 2013; Milligan, 2009; Milligan, 2006a) and receptor biology, signalling and trafficking might be modulated by this oligomerisation (Ferre et al., 2014; Milligan, 2013; Milligan, 2010; Milligan, 2007). Development of a number of biochemical and biophysical approaches has enabled to study the potential oligomerisation in GPCRs (Ward and Milligan, 2014; Milligan and Bouvier, 2005). Applying FRET microscopy, I have first time explored that hFFA1 and hFFA4 can form homo-oligomers (Figure 6-1 and Figure 6-3) and hetero-oligomers (Figure 6-6). The result was consistent in BRET saturation experiments (Figure 6-5 and Figure 6-8). Both receptors were strongly co-localised (Figure 6-2; Figure 6-4; Figure 6-7). However, due to time constrain, I was not able to investigate the ligand regulation of this oligomerisation. As receptor biosynthesis, transport along the secretory pathway, mechanisms of receptor activation, signal transduction and regulation are greatly influenced by receptor oligomerisation (Fuxe et al., 2010; Terrillon and Bouvier, 2004), oligomerisation in hFFA1 and hFFA4 might answer many questions of regulation and desensitisation of these receptors. However, GPCR oligomerisation and its

functional relevance remain controversial topics (Milligan, 2013) as this complexation is not an absolute prerequisite for proper signalling (Milligan, 2013; Milligan, 2008). Although promising, oligomerisation using FRET and BRET techniques generally require genetic manipulation of the proteins and the interactions might not be representative of a physiological situation (Milligan, 2013). Further studies are required to establish their oligomeric interactions and functional significance.

As described throughout this thesis, much work remains to be done to unite receptor desensitisation and oligomerisation with the complex signalling phenomena in FFA1 and FFA4. Genetic and systems biology studies in both humans and mouse models have established that both FFA1 and FFA4 receptors are linked to various metabolic diseases, particularly obesity and type-2 diabetes. Exploring pharmacology and desensitisation of these receptors are prerequisite to the development of novel drug discovery based on this therapeutically important receptor family. Using selective tool compounds for FFA1 (TUG-905 and GW-1100) and FFA4 (TUG-1197 and TUG-1275), the pharmacology of these receptors might be adequately explored in future. Selective ligands will also allow further analysis of the physiological responses and to explore the extent of overlaps in the functions between these receptors. Apart from the role of β -arrestins in the desensitisation of these receptors, role of other regulatory proteins, i.e. GRKs and various isoforms of PKCs are needed to be investigated. The findings, herein my project might enable unprecedented insights into the regulation and desensitisation of hFFA1 and hFFA4.

References

- AbdAlla, S., Lothar, H., Quitterer, U. (2000) AT1-receptor heterodimers show enhanced G-protein activation and altered receptor sequestration. *Nature*, 407, 94-98.
- Achour, L., Kamal, M., Jockers, R., Marullo, S. (2011) Using quantitative BRET to assess G protein-coupled receptor homo- and heterodimerization. *Methods Mol Biol*, 756, 183-200.
- Adams, G.L., Velazquez, F., Jayne, C., Shah, U., Miao, S., Ashley, E.R., Madeira, M., Akiyama, T.E., Di Salvo, J., Suzuki, T., Wang, N., Truong, Q., Gilbert, E., Zhou, D., Verras, A., Kirkland, M., Pachanski, M., Powles, M., Yin, W., Ujjainwalla, F., Venkatraman, S., Edmondson, S.D. (2016) Discovery of Chromane Propionic Acid Analogues as Selective Agonists of GPR120 with in Vivo Activity in Rodents. *ACS Med Chem Lett*, 8, 96-101.
- Ahn, S.H., Park, S.Y., Baek, J.E., Lee, S.Y., Baek, W.Y., Lee, S.Y., Lee, Y.S., Yoo, H.J., Kim, H., Lee, S.H., Im, D.S., Lee, S.K., Kim, B.J., Koh, J.M. (2016) Free Fatty Acid Receptor 4 (GPR120) Stimulates Bone Formation and Suppresses Bone Resorption in the Presence of Elevated n-3 Fatty Acid Levels. *Endocrinology*, 157, 2621-2635.
- Alfonzo-Mendez, M.A., Alcantara-Hernandez, R., Garcia-Sainz, J.A. (2016) Novel Structural approaches to study GPCR regulation. *Int J Mol Sci*, 18, E27.
- Alvarez-Curto, E., Milligan, G. (2016a) Metabolism meets immunity: The role of free fatty acid receptors in the immune system. *Biochem Pharmacol*, 114, 3-13.
- Alvarez-Curto, E., Inoue, A., Jenkins, L., Raihan, S.Z., Prihandoko, R., Tobin, A.B., Milligan, G. (2016b) Targeted elimination of G proteins and arrestins defines their specific contributions to both intensity and duration of G protein-coupled receptor signaling. *J Biol Chem*, 291, 27147-27159.

Alvarez-Curto, E., Padiani, J.D., Milligan, G. (2010) Applications of fluorescence and bioluminescence resonance energy transfer to drug discovery at G protein coupled receptors. *Anal Bioanal Chem*, 398, 167-180.

Andrell, J., Tate, C.G. (2013) Overexpression of membrane proteins in mammalian cells for structural studies. *Mol Membr Biol*, 30, 52-63.

Arunlakshana, O., Schild, H.O. (1959) Some quantitative uses of drug antagonists. *Br J Pharmacol Chemother*, 14, 48-58.

Aslanoglou, D., Alvarez-Curto, E., Marsango, S., Milligan, G. (2015) Distinct agonist regulation of muscarinic acetylcholine M2-M3 heteromers and their corresponding homomers. *J Biol Chem*, 290, 14785-14796.

Ayoub, M.A., Pflieger, K.D. (2010) Recent advances in bioluminescence resonance energy transfer technologies to study GPCR heteromerization. *Curr Opin Pharmacol*, 10, 44-52.

Azevedo, C.M., Watterson, K.R., Wargent, E.T., Hansen, S.V., Hudson, B.D., Kepczynska, M.A., Dunlop, J., Shimpukade, B., Christiansen, E., Milligan, G., Stocker, C.J., Ulven, T. (2016) Non-Acidic Free Fatty Acid Receptor 4 Agonists with Antidiabetic Activity. *J Med Chem*, 59, 8868-8878.

Benredjem, B., Dallaire, P., Pineyro, G. (2016) Analyzing biased responses of GPCR ligands. *Curr Opin Pharmacol*, 32, 71-76.

Bjarnadottir, T.K., Gloriam, D.E., Hellstrand, S.H., Kristiansson, H., Fredriksson, R., Schioth, H.B. (2006) Comprehensive repertoire and phylogenetic analysis of the G protein-coupled receptors in human and mouse. *Genomics*, 88, 263-273.

Bjursell, M., Admyre, T., Goransson, M., Marley, A.E., Smith, D.M., Oscarsson, J., Bohlooly, Y. M. (2011) Improved glucose control and reduced body fat mass in free fatty acid receptor 2-deficient mice fed a high-fat diet. *Am J Physiol Endocrinol Metab*, 300, E211-E220.

- Blad, C.C., Tang, C., Offermanns, S. (2012) G protein-coupled receptors for energy metabolites as new therapeutic targets. *Nat Rev Drug Discov*, 11, 603-619.
- Bockaert, J., Pin, J.P. (1999) Molecular tinkering of G protein-coupled receptors: an evolutionary success. *EMBO J*, 18, 1723-1729.
- Bolognini, D., Moss, C.E., Nilsson, K., Petersson, A.U., Donnelly, I., Sergeev, E., Konig, G.M., Kostenis, E., Kurowska-Stolarska, M., Miller, A., Dekker, N., Tobin, A.B., Milligan, G. (2016b) A Novel Allosteric Activator of Free Fatty Acid 2 Receptor Displays Unique Gi-functional Bias. *J Biol Chem*, 291, 18915-18931.
- Bolognini, D., Tobin, A.B., Milligan, G., Moss, C.E. (2016a) The Pharmacology and Function of Receptors for Short-Chain Fatty Acids. *Mol Pharmacol*, 89, 388-398.
- Bolsover, S., Ibrahim, O., O'lunaigh, N., Williams, H., Cockcroft, S. (2001) Use of fluorescent Ca^{2+} dyes with green fluorescent protein and its variants: problems and solutions. *Biochem J*, 356, 345-352.
- Bouvier, M. (2001) Oligomerization of G-protein-coupled transmitter receptors. *Nat Rev Neurosci*, 2, 274-286.
- Bouvier, M., Heveker, N., Jockers, R., Marullo, S., Milligan, G. (2007) BRET analysis of GPCR oligomerization: newer does not mean better. *Nat Methods*, 4, 3-4.
- Briscoe, C.P., Peat, A.J., McKeown, S.C., Corbett, D.F., Goetz, A.S., Littleton, T.R., McCoy, D.C., Kenakin, T.P., Andrews, J.L., Ammala, C., Fornwald, J.A., Ignar, D.M., Jenkinson, S. (2006) Pharmacological regulation of insulin secretion in MIN6 cells through the fatty acid receptor GPR40: identification of agonist and antagonist small molecules. *Br J Pharmacol*, 148, 619-628.
- Briscoe, C.P., Tadayyon, M., Andrews, J.L., Benson, W.G., Chambers, J.K., Eilert, M.M., Ellis, C., Elshourbagy, N.A., Goetz, A.S., Minnick, D.T., Murdock, P.R., Sauls, H.R Jr., Shabon, U., Spinage, L.D., Strum, J.C., Szekeres, P.G., Tan,

K.B., Way, J.M., Ignar, D.M., Wilson, S., Muir, A.I. (2003) The orphan G protein-coupled receptor GPR40 is activated by medium and long chain fatty acids. *J Biol Chem*, 278, 11303-11311.

Brown, A.J., Goldsworthy, S.M., Barnes, A.A., Eilert, M.M., Tcheang, L., Daniels, D., Muir, A.I., Wigglesworth, M.J., Kinghorn, I., Fraser, N.J., Pike, N.B., Strum, J.C., Steplewski, K.M., Murdock, P.R., Holder, J.C., Marshall, F.H., Szekeres, P.G., Wilson, S., Ignar, D.M., Foord, S.M., Wise, A., Dowell, S.J. (2003) The Orphan G protein-coupled receptors GPR41 and GPR43 are activated by propionate and other short chain carboxylic acids. *J Biol Chem*, 278, 11312-11319.

Bulenger, S., Marullo, S., Bouvier, M. (2005) Emerging role of homo- and heterodimerization in G-protein-coupled receptor biosynthesis and maturation. *Trends Pharmacol Sci*, 26, 131-137.

Burant, C.F., Viswanathan, P., Marcinak, J., Cao, C., Vakilynejad, M., Xie, B., Leifke, E. (2012) TAK-875 versus placebo or glimepiride in type 2 diabetes mellitus: a phase 2, randomised, double-blind, placebo-controlled trial. *Lancet*, 379, 1403-1411.

Burns, R.N., Moniri, N.H. (2010) Agonism with the omega-3 fatty acids alpha-linolenic acid and docosahexaenoic acid mediates phosphorylation of both the short and long isoforms of the human GPR120 receptor. *Biochem Biophys Res Commun*, 396, 1030-1035.

Burns, R.N., Singh, M., Senatorov, I.S., Moniri, N.H. (2014) Mechanisms of homologous and heterologous phosphorylation of FFA receptor 4 (GPR120): GRK6 and PKC mediate phosphorylation of Thr³⁴⁷, Ser³⁵⁰, and Ser³⁵⁷ in the C-terminal tail. *Biochem Pharmacol*, 87, 650-659.

Busnelli, M., Mauri, M., Parenti, M., Chini, B. (2013) Analysis of GPCR dimerization using acceptor photobleaching resonance energy transfer techniques. *Methods Enzymol*, 521:311-327.

Bussow, K. (2015) Stable mammalian producer cell lines for structural biology. *Curr Opin Struct Biol*, 32, 81-90.

Butcher, A.J., Bradley, S.J., Prihandoko, R., Brooke, S.M., Mogg, A., Bourgognon, J.M., Macedo-Hatch, T., Edwards, J.M., Bottrill, A.R., Challiss, R.A., Broad, L.M., Felder, C.C., Tobin, A.B. (2016) An Antibody Biosensor Establishes the Activation of the M1 Muscarinic Acetylcholine Receptor during Learning and Memory. *J Biol Chem*, 291, 8862-8875.

Butcher, A.J., Hudson, B.D., Shimpukade, B., Alvarez-Curto, E., Prihandoko, R., Ulven, T., Milligan, G., Tobin, A.B. (2014) Concomitant action of structural elements and receptor phosphorylation determine arrestin-3 interaction with the free fatty acid receptor FFA4. *J. Biol. Chem*, 289, 18451-18465.

Butcher, A.J., Prihandoko, R., Kong, K.C., McWilliams, P., Edwards, J.M., Bottrill, A., Mistry, S., Tobin, A.B. (2011) Differential G-protein-coupled receptor phosphorylation provides evidence for a signaling bar code. *J. Biol. Chem*, 286, 11506-11518.

Caffrey, M. (2011) Crystallizing membrane proteins for structure-function studies using lipidic mesophases. *Biochem Soc Trans*, 39, 725-732.

Calebiro, D., Rieken, F., Wagner, J., Sungkaworn, T., Zabel, U., Borzi, A., Cocucci, E., Zurn, A., Lohse, M.J. (2013) Single-molecule analysis of fluorescently labeled G-protein-coupled receptors reveals complexes with distinct dynamics and organization. *Proc Natl Acad Sci U S A*. 110, 743-748.

Charlton, S.J., Vauquelin, G. (2010) Elusive equilibrium: the challenge of interpreting receptor pharmacology using calcium assays. *Br J Pharmacol*, 161, 1250-1265.

Chakraborty, R., Xu, B., Bhullar, R.P., Chelikani, P. (2015) Expression of G protein-coupled receptors in Mammalian cells. *Methods Enzymol*, 556, 267-281.

Chandrashekar, J., Hoon, M.A., Ryba, N.J., Zuker, C.S. (2006) The receptors and cells for mammalian taste. *Nature*, 444, 288-294.

Chen, C., Li, H., Long, Y.Q. (2016) GPR40 agonists for the treatment of type 2 diabetes mellitus: The biological characteristics and the chemical space. *Bioorg Med Chem Lett*, 26, 5603-5612.

Cherezov, V., Rosenbaum, D.M., Hanson, M.A., Rasmussen, S.G., Thian, F.S., Kobilka, T.S., Choi, H.J., Kuhn, P., Weis, W.I., Kobilka, B.K., Stevens, R.C. (2007) High-resolution crystal structure of an engineered human beta2-adrenergic G protein-coupled receptor. *Science*, 318, 1258-1265.

Christiansen, E., Due-Hansen, M.E., Urban, C., Grundmann, M., Schröder, R., Hudson, B.D., Milligan, G., Cawthorne, M.A., Kostenis, E., Kassack, M.U., Ulven, T. (2012) Free fatty acid receptor 1 (FFA1/GPR40) agonists: mesylpropoxy appendage lowers lipophilicity and improves ADME properties. *J Med Chem*, 55, 6624-6628.

Christiansen, E., Due-Hansen, M.E., Urban, C., Grundmann, M., Schmidt, J., Hansen, S.V., Hudson, B.D., Zaibi, M., Markussen, S.B., Hagesaether, E., Milligan, G., Cawthorne, M.A., Kostenis, E., Kassack, M.U., Ulven, T. (2013b) Discovery of a potent and selective free fatty acid receptor 1 agonist with low lipophilicity and high oral bioavailability. *J Med Chem*, 56, 982-992.

Christiansen, E., Due-Hansen, M.E., Urban, C., Merten, N., Pfeleiderer, M., Karlsen, K.K., Rasmussen, S.S., Steensgaard, M., Hamacher, A., Schmidt, J., Drewke, C., Petersen, R.K., Kristiansen, K., Ullrich, S., Kostenis, E., Kassack, M.U., Ulven, T. (2010) Structure-Activity Study of Dihydrocinnamic Acids and Discovery of the Potent FFA1 (GPR40) Agonist TUG-469. *ACS Med Chem Lett*, 1, 345-349.

Christiansen, E., Hansen, S.V., Urban, C., Hudson, B.D., Wargent, E.T., Grundmann, M., Jenkins, L., Zaibi, M., Stocker, C.J., Ullrich, S., Kostenis, E., Kassack, M.U., Milligan, G., Cawthorne, M.A., Ulven, T. (2013a) Discovery of TUG-770: A Highly Potent Free Fatty Acid Receptor 1 (FFA1/GPR40) Agonist for Treatment of Type 2 Diabetes. *ACS Med Chem Lett*, 4, 441-445.

Christiansen, E., Urban, C., Merten, N., Liebscher, K., Karlsen, K.K., Hamacher, A., Spinrath, A., Bond, A.D., Drewke, C., Ullrich, S., Kassack, M.U., Kostenis, E.,

Ulven, T. (2008) Discovery of potent and selective agonists for the free fatty acid receptor 1 (FFA(1)/GPR40), a potential target for the treatment of type II diabetes. *J Med Chem*, 51, 7061-7064.

Christiansen, E., Watterson, K.R., Stocker, C.J., Sokol, E., Jenkins, L., Simon, K., Grundmann, M., Petersen, R.K., Wargent, E.T., Hudson, B.D., Kostenis, E., Ejsing, C.S., Cawthorne, M.A., Milligan, G., Ulven, T. (2015) Activity of dietary fatty acids on FFA1 and FFA4 and characterisation of pinolenic acid as a dual FFA1/FFA4 agonist with potential effect against metabolic diseases. *Br J Nutr*, 113, 1677-1688.

Civelli, O., Reinscheid, R.K., Zhang, Y., Wang, Z., Fredriksson, R., Schioth, H.B. (2013) G protein-coupled receptor deorphanizations. *Annu Rev Pharmacol Toxicol*, 53, 127-146.

Civelli, O., Saito, Y., Wang, Z., Nothacker, H.P., Reinscheid, R.K. (2006) Orphan GPCRs and their ligands. *Pharmacol Ther*, 110, 525-532.

Conway, B.R., Minor, L.K., Xu, J.Z., Gunnet, J.W., DeBiasio, R., D'Andrea, M.R., Rubin, R., DeBiasio, R., Giuliano, K., DeBiasio, L., Demarest, K.T. (1999) Quantification of G-Protein coupled receptor internalization using G-Protein coupled receptor-green fluorescent protein conjugates with the ArrayScan® High-content screening system. *J Biomol Screen*, 4, 75-86.

Cornall, L.M., Mathai, M.L., Hryciw, D.H., McAinch, A.J. (2014) GPR120 agonism as a countermeasure against metabolic diseases. *Drug Discov Today*, 19, 670-679.

Cox, J.M., Chu, H.D., Chelliah, M.V., Debenham, J.S., Eagen, K., Lan, P., Lombardo, M., London, C., Plotkin, M.A., Shah, U., Sun, Z., Vaccaro, H.M., Venkatraman, S., Suzuki, T., Wang, N., Ashley, E.R., Crespo, A., Madeira, M., Leung, D.H., Alleyne, C., Ogawa, A.M., Souza, S., Thomas-Fowlkes, B., Di Salvo, J., Weinglass, A., Kirkland, M., Pachanski, M., Powles, M.A., Tozzo, E., Akiyama, T.E., Ujjainwalla, F., Tata, J.R., Sinz, C.J. (2016) Design, Synthesis, and Evaluation of Novel and Selective G-protein Coupled Receptor 120 (GPR120) Spirocyclic Agonists. *ACS Med Chem Lett*, 8, 49-54.

Cristovao-Ferreira, S., Navarro, G., Brugarolas, M., Perez-Capote, K., Vaz, S.H., Fattorini, G., Conti, F., Lluís, C., Ribeiro, J.A., McCormick, P.J., Casado, V., Franco, R., Sebastiao, A.M. (2013) A1R-A2AR heteromers coupled to Gs and G i/o proteins modulate GABA transport into astrocytes. *Purinergic Signal*, 9, 433-449.

Dalrymple, M.B., Pflieger, K.D., Eidne, K.A. (2008) G protein-coupled receptor dimers: functional consequences, disease states and drug targets. *Pharmacol Ther*, 118, 359-371.

Davenport, A.P., Alexander, S.P., Sharman, J.L., Pawson, A.J., Benson, H.E., Monaghan, A.E., Liew, W.C., Mpamhanga, C.P., Bonner, T.I., Neubig, R.R., Pin, J.P., Spedding, M., Harmar, A.J. (2013) International Union of Basic and Clinical Pharmacology. LXXXVIII. G protein-coupled receptor list: recommendations for new pairings with cognate ligands. *Pharmacol Rev*, 65, 967-986.

De Vadder, F., Kovatcheva-Datchary, P., Goncalves, D., Vinera, J., Zitoun, C., Duchampt, A., Backhed, F., Mithieux, G. (2014) Microbiota-generated metabolites promote metabolic benefits via gut-brain neural circuits. *Cell*, 156, 84-96.

DeWire, S.M., Ahn, S., Lefkowitz, R.J., Shenoy, S.K. (2007) Beta-arrestins and cell signaling. *Annu Rev Physiol*, 69, 483-510.

Drake, M.T., Shenoy, S.K., Lefkowitz, R.J. (2006) Trafficking of G protein-coupled receptors. *Circ Res*, 99, 570-582.

Dranse, H.J., Kelly, M.E., Hudson, B.D. (2013) Drugs or diet?--Developing novel therapeutic strategies targeting the free fatty acid family of GPCRs. *Br J Pharmacol*, 170, 696-711.

Edfalk, S., Steneberg, P., Edlund, H. (2008) Gpr40 is expressed in enteroendocrine cells and mediates free fatty acid stimulation of incretin secretion. *Diabetes*, 57, 2280-2287.

Egerod, K.L., Engelstoft, M.S., Lund, M.L., Grunddal, K.V., Zhao, M., Barir-Jensen, D., Nygaard, E.B., Petersen, N., Holst, J.J., Schwartz, T.W. (2015)

Transcriptional and Functional Characterization of the G Protein-Coupled Receptor Repertoire of Gastric Somatostatin Cells. *Endocrinology*, 156, 3909-3923.

Elzein, E., Zablocki, J. (2008) A1 adenosine receptor agonists and their potential therapeutic applications. *Expert Opin Investig Drugs*, 17, 1901-1910.

Engelstoft, M.S., Park, W.M., Sakata, I., Kristensen, L.V., Husted, A.S., Osborne-Lawrence, S., Piper, P.K., Walker, A.K., Pedersen, M.H., Nohr, M.K., Pan, J., Sinz, C.J., Carrington, P.E., Akiyama, T.E., Jones, R.M., Tang, C., Ahmed, K., Offermanns, S., Egerod, K.L., Zigman, J.M., Schwartz, T.W. (2013) Seven transmembrane G protein-coupled receptor repertoire of gastric ghrelin cells. *Mol Metab*, 2, 376-392.

Fallahi-Sichani, M., Linderman, J.J. (2009) Lipid raft-mediated regulation of G-protein coupled receptor signaling by ligands which influence receptor dimerization: a computational study. *PLoS One*, e6604.

Fan, G.H., Yang, W., Wang, X.J., Qian, Q., Richmond, A. (2001) Identification of a motif in the carboxyl terminus of CXCR2 that is involved in adaptin 2 binding and receptor internalization. *Biochemistry*, 40, 791-800.

Felce, J.H., Knox, R.G., Davis, S.J. (2014) Type-3 BRET, an improved competition-based bioluminescence resonance energy transfer assay. *Biophys J*, 106, L41-L43.

Ferdaoussi, M., Bergeron, V., Zarrouki, B., Kolic, J., Cantley, J., Fielitz, J., Olson, E.N., Prentki, M., Biden, T., MacDonald, P.E., Poitout, V. (2012) G protein-coupled receptor (GPR) 40-dependent potentiation of insulin secretion in mouse islets is mediated by protein kinase D1. *Diabetologia*, 55, 2682-2692.

Ferguson, S.S. (2001) Evolving concepts in G protein-coupled receptor endocytosis: the role in receptor desensitization and signaling. *Pharmacol Rev*, 53, 1-24.

Ferguson, S.S., Downey, W.E., Colapietro, A.M., Barak, L.S., Ménard, L., Caron, M.G. (1996) Role of beta-arrestin in mediating agonist-promoted G protein-coupled receptor internalization. *Science*, 271, 363-366.

Ferre, S., Casadó, V., Devi, L.A., Filizola, M., Jockers, R., Lohse, M.J., Milligan, G., Pin, J.P., Guitart, X. (2014) G protein-coupled receptor oligomerization revisited: functional and pharmacological perspectives. *Pharmacol Rev*, 66, 413-434.

Feinstein, T.N., Yui, N., Webber, M.J., Wehbi, V.L., Stevenson, H.P., King, J.D. Jr, Hallows, K.R., Brown, D., Bouley, R., Vilardaga, J.P. (2013) Noncanonical control of vasopressin receptor type 2 signaling by retromer and arrestin. *J Biol Chem*, 288, 27849-27860.

Flodgren, E., Olde, B., Meidute-Abaraviciene, S., Winzell, M.S., Ahren, B., Salehi, A. (2007) GPR40 is expressed in glucagon producing cells and affects glucagon secretion. *Biochem Biophys Res Commun*, 354, 240-245.

Fourgeaud, L., Bessis, A.S., Rossignol, F., Pin, J.P., Olivo-Marin, J.C., Hémar, A. (2003) The metabotropic glutamate receptor mGluR5 is endocytosed by a clathrin-independent pathway. *J Biol Chem*, 278, 12222-12230.

Franco, R., Martínez-Pinilla, E., Lanciego, J.L., Navarro, G. (2016) Basic Pharmacological and Structural Evidence for Class A G-Protein-Coupled Receptor Heteromerization. *Front Pharmacol*, 7, 76.

Fredriksson, R., Lagerstrom, M.C., Lundin, L.G., Schioth, H.B. (2003) The G-protein-coupled receptors in the human genome form five main families. Phylogenetic analysis, paralogon groups, and fingerprints. *Mol Pharmacol*, 63, 1256-1272.

Fujiwara, K., Maekawa, F., Yada, T. (2005) Oleic acid interacts with GPR40 to induce Ca²⁺ signaling in rat islet beta-cells: mediation by PLC and L-type Ca²⁺ channel and link to insulin release. *Am J Physiol Endocrinol Metab*, 289, E670-E677.

Fuxe, K., Marcellino, D., Leo, G., Agnati, L.F. (2010) Molecular integration via allosteric interactions in receptor heteromers. A working hypothesis. *Curr Opin Pharmacol*, 10, 14-22.

Gahbauer, S., Bockmann, R.A. (2016) Membrane-Mediated Oligomerization of G Protein Coupled Receptors and Its Implications for GPCR Function. *Front Physiol*, 7, 494.

Gan, S.D., Patel, K.R. (2013) Enzyme immunoassay and enzyme-linked immunosorbent assay. *J Invest Dermatol*, 133, e12.

Gao, B., Han, Y.H., Wang, L., Lin, Y.J., Sun, Z., Lu, W.G., Hu, Y.Q., Li, J.Q., Lin, X.S., Liu, B.H., Jie, Q., Yang, L., Luo, Z.J. (2016) Eicosapentaenoic acid attenuates dexamethasone-induced apoptosis by inducing adaptive autophagy via GPR120 in murine bone marrow-derived mesenchymal stem cells. *Cell Death Dis*, 7, e2235.

Gao, B., Huang, Q., Jie, Q., Lu, W.G., Wang, L., Li, X.J., Sun, Z., Hu, Y.Q., Chen, L., Liu, B.H., Liu, J., Yang, L., Luo, Z.J. (2015) GPR120: A bi-potential mediator to modulate the osteogenic and adipogenic differentiation of BMSCs. *Sci Rep*, 5, 14080.

Gao, Z., Yin, J., Zhang, J., Ward, R.E., Martin, R.J., Lefevre, M., Cefalu, W.T., Ye, J. (2009) Butyrate improves insulin sensitivity and increases energy expenditure in mice. *Diabetes*, 58, 1509-1517.

Gartner, F., Seidel, T., Schulz, U., Gummert, J., Milting, H. (2013) Desensitization and internalization of endothelin receptor A: impact of G protein-coupled receptor kinase 2 (GRK2)-mediated phosphorylation. *J Biol Chem*, 288, 32138-32148.

Gavi, S., Shumay, E., Wang, H.Y., Malbon, C.C. (2006) G-protein-coupled receptors and tyrosine kinases: Crossroads in cell signaling and regulation. *Trends Endocrinol. Metab*, 17, 48-54.

George, S.R., O'Dowd, B.F., Lee, S.P. (2002) G-protein-coupled receptor oligomerization and its potential for drug discovery. *Nat Rev Drug Discov*, 1, 808-820.

Gether, U. (2000) Uncovering molecular mechanisms involved in activation of G protein-coupled receptors. *Endocr Rev*, 21, 90-113.

Giuliano, K.A., DeBiasio, R.L., Dunlay, R.T., Gough, A., Volosky, J.M., Zock, J., Pavlakis, G.N., Taylor, D.L. (1997) High-Content Screening: A New Approach to Easing Key Bottlenecks in the Drug Discovery Process. *J Biomol Screening*, 2, 249-259.

Goddard, A.D., Dijkman, P.M., Adamson, R.J., Watts, A. (2013) Lipid-dependent GPCR dimerization. *Methods Cell Biol*, 117, 341-357.

Gomes, I., Ayoub, M.A., Fujita, W., Jaeger, W.C., Pflieger, K.D., Devi, L.A. (2016) G Protein-Coupled Receptor Heteromers. *Annu Rev Pharmacol Toxicol*, 56, 403-425.

Goodman, OB Jr., Krupnick, J.G., Santini, F., Gurevich, V.V., Penn, R.B., Gagnon, A.W., Keen, J.H., Benovic, J.L. (1996) Beta-arrestin acts as a clathrin adaptor in endocytosis of the beta2-adrenergic receptor. *Nature*, 383, 447-450.

Gotoh, C., Hong, Y.H., Iga, T., Hishikawa, D., Suzuki, Y., Song, S.H., Choi, K.C., Adachi, T., Hirasawa, A., Tsujimoto, G., Sasaki, S., Roh, S.G. (2007) The regulation of adipogenesis through GPR120. *Biochem Biophys Res Commun*, 354, 591-597.

Grynkiewicz, G., Poenie, M., Tsien, R.Y. (1985) A new generation of Ca²⁺ indicators with greatly improved fluorescence properties. *J Biol Chem*, 260, 3440-3450.

Gundry, J., Glenn, R., Alagesan, P., Rajagopal, S. (2017) A Practical Guide to Approaching Biased Agonism at G Protein Coupled Receptors. *Front Neurosci*, 11, 17.

Gurevich, V.V., Gurevich, E.V. (2006) The structural basis of arrestin-mediated regulation of G-protein-coupled receptors. *Pharmacol Ther*, 110, 465-502.

Hamdan, F.F., Audet, M., Garneau, P., Pelletier, J., Bouvier, M. (2005) High-throughput screening of G protein-coupled receptor antagonists using a bioluminescence resonance energy transfer 1-based beta-arrestin2 recruitment assay. *J Biomol Screen*, 10, 463-475.

Hamdouchi, C., Kahl, S.D., Patel, Lewis, A., Cardona, G.R., Zink, R.W., Chen, K., Eessalu, T.E., Ficorilli, J.V., Marcelo, M.C., Otto, K.A., Wilbur, K.L., Lineswala, J.P., Piper, J.L., Coffey, D.S., Sweetana, S.A., Haas, J.V., Brooks, D.A., Pratt, E.J., Belin, R.M., Deeg, M.A., Ma, X., Cannady, E.A., Johnson, J.T., Yumibe, N.P., Chen, Q., Maiti, P., Montrose-Rafizadeh, C., Chen, Y., Reifel Miller, A. (2016) The Discovery, Preclinical, and Early Clinical Development of Potent and Selective GPR40 Agonists for the Treatment of Type 2 Diabetes Mellitus (LY2881835, LY2922083, and LY2922470). *J Med Chem*, 59, 10891-10916.

Hansen, S.V., Christiansen, E., Urban, C., Hudson, B.D., Stocker, C.J., Due-Hansen, M.E., Wargent, E.T., Shimpukade, B., Almeida, R., Ejlsing, C.S., Cawthorne, M.A., Kassack, M.U., Milligan, G., Ulven, T. (2016) Discovery of a Potent Free Fatty Acid 1 Receptor Agonist with Low Lipophilicity, Low Polar Surface Area, and Robust in Vivo Efficacy. *J Med Chem*, 59, 2841-2846.

Hansen, S.V., Ulven, T. (2017) Pharmacological Tool Compounds for the Free Fatty Acid Receptor 4 (FFA4/GPR120). *Handb Exp Pharmacol*, 236, 33-56.

Hanson, M.A., Roth, C.B., Jo, E., Griffith, M.T., Scott, F.L., Reinhart, G., Desale, H., Clemons, B., Cahalan, S.M., Schuerer, S.C., Sanna, M.G., Han, G.W., Kuhn, P., Rosen, H., Stevens, R.C. (2012) Crystal structure of a lipid G protein-coupled receptor. *Science*, 335, 851-855.

Hara, T. (2017) Ligands at Free Fatty Acid Receptor 1 (GPR40). *Handb Exp Pharmacol*, 236, 1-16.

Hara, T., Hirasawa, A., Sun, Q., Sadakane, K., Itsubo, C., Iga, T., Adachi, T., Koshimizu, T.A., Hashimoto, T., Asakawa, Y., Tsujimoto, G. (2009) Novel

selective ligands for free fatty acid receptors GPR120 and GPR40. *Naunyn Schmiedebergs Arch Pharmacol*, 380, 247-255.

Hara, T., Ichimura, A., Hirasawa, A. (2014a) Therapeutic role and ligands of medium- to long-chain Fatty Acid receptors. *Front Endocrinol (Lausanne)*, 5, 83.

Hara, T., Kashiwara, D., Ichimura, A., Kimura, I., Tsujimoto, G., Hirasawa, A. (2014b) Role of free fatty acid receptors in the regulation of energy metabolism. *Biochim Biophys Acta*, 1841, 1292-1300.

Hauge, M., Vestmar, M.A., Husted, A.S., Ekberg, J.P., Wright, M.J., Di Salvo, J., Weinglass, A.B., Engelstoft, M.S., Madsen, A.N., Luckmann, M., Miller, M.W., Trujillo, M.E., Frimurer, T.M., Holst, B., Howard, A.D., Schwartz, T.W. (2014) GPR40 (FFAR1) - Combined Gs and Gq signaling in vitro is associated with robust incretin secretagogue action ex vivo and in vivo. *Mol Metab*, 4, 3-14.

Hirasawa, A., Hara, T., Katsuma, S., Adachi, T., Tsujimoto, G. (2008) Free fatty acid receptors and drug discovery. *Biol Pharm Bull*, 31, 1847-1851.

Hirasawa, A., Tsumaya, K., Awaji, T., Katsuma, S., Adachi, T., Yamada, M., Sugimoto, Y., Miyazaki, S., Tsujimoto, G. (2005) Free fatty acids regulate gut incretin glucagon-like peptide-1 secretion through GPR120. *Nat Med*, 11, 90-94.

Holliday, N.D., Watson, S.J., Brown, A.J. (2012) Drug discovery opportunities and challenges at G protein coupled receptors for long chain free Fatty acids. *Front Endocrinol (Lausanne)*, 2, 112.

Hopkins, M.M., Meier, K.E. (2017) Free Fatty Acid Receptors and Cancer: From Nutrition to Pharmacology. *Handb Exp Pharmacol*, 236, 233-251.

Houthuijzen, J.M. (2016) For Better or Worse: FFAR1 and FFAR4 Signaling in Cancer and Diabetes. *Mol Pharmacol*, 90, 738-743.

Houthuijzen, J.M., Oosterom, I., Hudson, B.D., Hirasawa, A., Daenen, L.G., McLean, C.M., Hansen, S.V., van Jaarsveld, M.T., Peeper, D.S., Jafari Sadatmand, S., Roodhart, J.M., van de Lest, C.H., Ulven, T., Ishihara, K.,

Milligan, G., Voest, E.E. (2017) Fatty acid 16:4(n-3) stimulates a GPR120-induced signaling cascade in splenic macrophages to promote chemotherapy resistance. *FASEB J*, [Epub ahead of print], PMID: 28183801, doi: 10.1096/fj.201601248R.

Hu, H., He, L.Y., Gong, Z., Li, N., Lu, Y.N., Zhai, Q.W., Liu, H., Jiang, H.L., Zhu, W.L., Wang, H.Y. (2009) A novel class of antagonists for the FFAs receptor GPR40. *Biochem Biophys Res Commun*, 390, 557-563.

Hudson, B.D., Christiansen, E., Tikhonova, I.G., Grundmann, M., Kostenis, E., Adams, D.R., Ulven, T., Milligan, G. (2012) Chemically engineering ligand selectivity at the free fatty acid receptor 2 based on pharmacological variation between species orthologs. *FASEB J*, 26, 4951-4965.

Hudson, B.D., Due-Hansen, M.E., Christiansen, E., Hansen, A.M., Mackenzie, A.E., Murdoch, H., Pandey, S.K., Ward, R.J., Marquez, R., Tikhonova, I.G., Ulven, T., Milligan, G. (2013a) Defining the molecular basis for the first potent and selective orthosteric agonists of the FFA2 free fatty acid receptor. *J Biol Chem*, 288, 17296-17312.

Hudson, B.D., Shimpukade, B., Mackenzie, A.E., Butcher, A.J., Pediani, J.D., Christiansen, E., Heathcote, H., Tobin, A.B., Ulven, T., Milligan, G. (2013b) The pharmacology of TUG-891, a potent and selective agonist of the free fatty acid receptor 4 (FFA4/GPR120), demonstrates both potential opportunity and possible challenges to therapeutic agonism. *Mol Pharmacol*, 84, 710-725.

Hudson, B.D., Shimpukade, B., Milligan, G., Ulven, T. (2014) The molecular basis of ligand interaction at free fatty acid receptor 4 (FFA4/GPR120). *J Biol Chem*, 289, 20345-20358.

Hudson, B.D., Smith, N.J., Milligan, G. (2011) Experimental challenges to targeting poorly characterized GPCRs: uncovering the therapeutic potential for free fatty acid receptors. *Adv Pharmacol*, 62, 175-218.

Hudson, B.D., Ulven, T., Milligan, G. (2013c) The therapeutic potential of allosteric ligands for free fatty acid sensitive GPCRs. *Curr Top Med Chem*, 13, 14-25.

Ichimura, A., Hara, T., Hirasawa, A. (2014) Regulation of Energy Homeostasis via GPR120. *Front Endocrinol (Lausanne)*, 5, 111.

Ichimura, A., Hirasawa, A., Poulain-Godefroy, O., Bonnefond, A., Hara, T., Yengo, L., Kimura, I., Leloire, A., Liu, N., Iida, K., Choquet, H., Besnard, P., Lecoeur, C., Vivequin, S., Ayukawa, K., Takeuchi, M., Ozawa, K., Tauber, M., Maffeis, C., Morandi, A., Buzzetti, R., Elliott, P., Pouta, A., Jarvelin, M.R., Korner, A., Kiess, W., Pigeyre, M., Caiazzo, R., Van Hul, W., Van Gaal, L., Horber, F., Balkau, B., Levy-Marchal, C., Rouskas, K., Kouvatsi, A., Hebebrand, J., Hinney, A., Scherag, A., Pattou, F., Meyre, D., Koshimizu, T.A., Wolowczuk, I., Tsujimoto, G., Froguel, P. (2012) Dysfunction of lipid sensor GPR120 leads to obesity in both mouse and human. *Nature*, 483, 350-354.

Imamura, T., Vollenweider, P., Egawa, K., Clodi, M., Ishibashi, K., Nakashima, N., Ugi, S., Adams, J.W., Brown, J.H., Olefsky, J.M. (1999) G alpha-q/11 protein plays a key role in insulin-induced glucose transport in 3T3-L1 adipocytes. *Mol Cell Biol*, 19, 6765-6774.

Irannejad, R., Tomshine, J.C., Tomshine, J.R., Chevalier, M., Mahoney, J.P., Steyaert, J., Rasmussen, S.G., Sunahara, R.K., El-Samad, H., Huang, B., von Zastrow, M. (2013) Conformational biosensors reveal GPCR signalling from endosomes. *Nature*, 495, 534-538.

Itoh, Y., Kawamata, Y., Harada, M., Kobayashi, M., Fujii, R., Fukusumi, S., Ogi, K., Hosoya, M., Tanaka, Y., Uejima, H., Tanaka, H., Maruyama, M., Satoh, R., Okubo, S., Kizawa, H., Komatsu, H., Matsumura, F., Noguchi, Y., Shinohara, T., Hinuma, S., Fujisawa, Y., Fujino, M. (2003) Free fatty acids regulate insulin secretion from pancreatic beta cells through GPR40. *Nature*, 422, 173-176.

Iwasaki, K., Harada, N., Sasaki, K., Yamane, S., Iida, K., Suzuki, K., Hamasaki, A., Nasteska, D., Shibue, K., Joo, E., Harada, T., Hashimoto, T., Asakawa, Y., Hirasawa, A., Inagaki, N. (2015) Free fatty acid receptor GPR120 is highly expressed in enteroendocrine K cells of the upper small intestine and has a critical role in GIP secretion after fat ingestion. *Endocrinology*, 156, 837-846.

James, J.R., Oliveira, M.I., Carmo, A.M., Iaboni, A., Davis, S.J. (2006) A rigorous experimental framework for detecting protein oligomerization using bioluminescence resonance energy transfer. *Nat Methods*, 3, 1001-1006.

Kaji, I., Karaki, S., Kuwahara, A. (2014) Short-chain fatty acid receptor and its contribution to glucagon-like peptide-1 release. *Digestion*, 89, 31-36.

Kaku, K., Enya, K., Nakaya, R., Ohira, T., Matsuno, R. (2015) Efficacy and safety of fasiglifam (TAK-875), a G protein-coupled receptor 40 agonist, in Japanese patients with type 2 diabetes inadequately controlled by diet and exercise: a randomized, double-blind, placebo-controlled, phase III trial. *Diabetes Obes Metab*, 17, 675-681.

Kang, D. S., Kern, R. C., Puthenveedu, M. A., von Zastrow, M., Williams, J. C., and Benovic, J. L. (2009) Structure of an arrestin2-clathrin complex reveals a novel clathrin binding domain that modulates receptor trafficking. *J. Biol. Chem*, 284, 29860-29872.

Kang, D.S., Tian, X., Benovic, J.L. (2014) Role of β -arrestins and arrestin domain-containing proteins in G protein-coupled receptor trafficking. *Curr Opin Cell Biol*, 27, 63-71.

Karlsson, F., Tremaroli, V., Nielsen, J., Backhed, F. (2013) Assessing the human gut microbiota in metabolic diseases. *Diabetes*, 62, 3341-3349.

Katritch, V., Cherezov, V., Stevens, R.C. (2012) Diversity and modularity of G protein-coupled receptor structures. *Trends Pharmacol Sci*, 33, 17-27.

Kebede, M.A., Alquier, T., Latour, M.G., Poitout, V. (2009) Lipid receptors and islet function: therapeutic implications? *Diabetes Obes Metab*, 4, 10-20.

Kelly, E., Bailey, C.P., Henderson, G. (2008) Agonist-selective mechanisms of GPCR desensitization. *Br J Pharmacol*, 1, S379-S388.

Kenakin, T. (1995) Agonist-receptor efficacy II: agonist trafficking of receptor signals. *Trends Pharmacol Sci*, 16, 232-238.

Kenakin, T. (2007) Collateral efficacy in drug discovery: taking advantage of the good (allosteric) nature of 7TM receptors. *Trends Pharmacol Sci*, 28, 407-415.

Kenakin, T. (2015) New Lives for Seven Transmembrane Receptors as Drug Targets. *Trends Pharmacol Sci*, 36, 705-706.

Kennedy, J.E., Marchese, A. (2015) Regulation of GPCR Trafficking by Ubiquitin. *Prog Mol Biol Transl Sci*, 132, 15-38.

Khan, S.M., Sleno, R., Gora, S., Zylbergold, P., Laverdure, J.P., Labbé, J.C., Miller, G.J., Hébert, T.E. (2013) The expanding roles of Gβγ subunits in G protein-coupled receptor signaling and drug action. *Pharmacol Rev*, 65, 545-577.

Kim, H.J., Yoon, H.J., Kim, B.K., Kang, W.Y., Seong, S.J., Lim, M.S., Kim, S.Y., Yoon, Y.R. (2016) G Protein-Coupled Receptor 120 Signaling Negatively Regulates Osteoclast Differentiation, Survival, and Function. *J Cell Physiol*, 231, 844-851.

Kim, H.S., Hwang, Y.C., Koo, S.H., Park, K.S., Lee, M.S., Kim, K.W., Lee, M.K. (2013b) PPAR-γ activation increases insulin secretion through the up-regulation of the free fatty acid receptor GPR40 in pancreatic β-cells. *PLoS One*, 8, e50128.

Kim, M.H., Kang, S.G., Park, J.H., Yanagisawa, M., Kim, C.H. (2013a) Short-chain fatty acids activate GPR41 and GPR43 on intestinal epithelial cells to promote inflammatory responses in mice. *Gastroenterology*, 145, 396-406.

Kimura, I., Inoue, D., Maeda, T., Hara, T., Ichimura, A., Miyauchi, S., Kobayashi, M., Hirasawa, A., Tsujimoto, G. (2011) Short-chain fatty acids and ketones directly regulate sympathetic nervous system via G protein-coupled receptor 41 (GPR41). *Proc Natl Acad Sci USA*, 108, 8030-8035.

Kimura, I., Ozawa, K., Inoue, D., Imamura, T., Kimura, K., Maeda, T., Terasawa, K., Kashihara, D., Hirano, K., Tani, T., Takahashi, T., Miyauchi, S., Shioi, G., Inoue, H., Tsujimoto, G. (2013) The gut microbiota suppresses insulin-mediated fat accumulation via the short-chain fatty acid receptor GPR43. *Nat Commun*, 4, 1829.

- Klabunde, T., Hessler, G. (2002) Drug design strategies for targeting G-protein-coupled receptors. *Chembiochem*, 3, 928-944.
- Kobilka, B.K. (2007) G protein coupled receptor structure and activation. *Biochim Biophys Acta*, 1768, 794-807.
- Koener, B., Hermans, E. (2011) Inducible expression of G protein-coupled receptors in transfected cells. *Methods Mol Biol*, 746, 3-20.
- Koenig, J.A., Edwardson, J.M. (1997) Endocytosis and recycling of G protein-coupled receptors. *Trends Pharmacol Sci*, 18, 276-287.
- Kohout, T.A., Lefkowitz, R.J. (2003) Regulation of G protein-coupled receptor kinases and arrestins during receptor desensitization. *Mol Pharmacol*, 63, 9-18.
- Kohout, T.A., Lin, F.S., Perry, S.J., Conner, D.A., Lefkowitz, R.J. (2001) beta-Arrestin 1 and 2 differentially regulate heptahelical receptor signaling and trafficking. *Proc Natl Acad Sci USA*, 98, 1601-1606.
- Kotarsky, K., Nilsson, N.E., Flodgren, E., Owman, C., Olde, B. (2003) A human cell surface receptor activated by free fatty acids and thiazolidinedione drugs. *Biochem Biophys Res Commun*, 301, 406-410.
- Krasel, C., Bünemann, M., Lorenz, K., and Lohse, M. J. (2005) B-Arrestin binding to the β_2 -adrenergic receptor requires both receptor phosphorylation and receptor activation. *J Biol Chem*, 280, 9528-9535.
- Krilov, L., Nguyen, A., Miyazaki, T., Unson, C.G., Williams, R., Lee, N.H., Ceryak, S., Bouscarel, B. (2011) Dual mode of glucagon receptor internalization: role of PKC α , GRKs and B-arrestins. *Exp Cell Res*, 317, 2981-2994.
- Kristinsson, H., Smith, D.M., Bergsten, P., Sargsyan, E. (2013) FFAR1 is involved in both the acute and chronic effects of palmitate on insulin secretion. *Endocrinology*, 154, 4078-4088.
- Kuszak, A.J., Pitchiaya, S., Anand, J.P., Mosberg, H.I., Walter, N.G., Sunahara, R.K. (2009) Purification and functional reconstitution of monomeric mu-opioid

receptors: allosteric modulation of agonist binding by Gi2. *J Biol Chem*, 284, 26732-26741.

Kuwahara, A. (2014) Contributions of colonic short-chain Fatty Acid receptors in energy homeostasis. *Front Endocrinol (Lausanne)*, 5, 144.

Lagerstrom, M.C., Schioth, H.B. (2008) Structural diversity of G protein-coupled receptors and significance for drug discovery. *Nat Rev Drug Discov*, 7, 339-357.

Latour, M.G., Alquier, T., Oseid, E., Tremblay, C., Jetton, T.L., Luo, J., Lin, D.C., Poitout, V. (2007) GPR40 is necessary but not sufficient for fatty acid stimulation of insulin secretion in vivo. *Diabetes*, 56, 1087-1094.

Lee, K. B., Pals-Rylaarsdam, R., Benovic, J. L., and Hosey, M. M. (1998) Arrestin-independent internalization of the m1, m3, and m4 subtypes of muscarinic cholinergic receptors. *J Biol Chem*, 273, 12967-12972.

Lee, S.U., In, H.J., Kwon, M.S., Park, B.O., Jo, M., Kim, M.O., Cho, S., Lee, S., Lee, H.J., Kwak, Y.S., Kim, S. (2013) β -Arrestin 2 mediates G protein-coupled receptor 43 signals to nuclear factor- κ B. *Biol Pharm Bull*, 36, 1754-1759.

Lefkowitz, R.J, Shenoy, S.K. (2005) Transduction of receptor signals by beta-arrestins. *Science*, 308, 512-517.

Lefkowitz, R.J. (2000) The superfamily of heptahelical receptors. *Nat Cell Biol*, 2, E133-E136.

Lefkowitz, R.J. (2004) Historical review: a brief history and personal retrospective of seven-transmembrane receptors. *Trends Pharmacol Sci*, 25, 413-422.

Lefkowitz, R.J. (2013) Arrestins come of age: a personal historical perspective. *Prog Mol Biol Transl Sci*, 118, 3-18.

Li, G., Shi, Y., Huang, H., Zhang, Y., Wu, K., Luo, J., Sun, Y., Lu, J., Benovic, J.L., Zhou, N. (2010) Internalization of the human nicotinic acid receptor

GPR109A is regulated by G(i), GRK2, and arrestin3. *J Biol Chem*, 285, 22605-22618.

Li, X., Yu, Y., Funk, C.D. (2013) Cyclooxygenase-2 induction in macrophages is modulated by docosahexaenoic acid via interactions with free fatty acid receptor 4 (FFA4). *FASEB J*, 27, 4987-4997.

Li, Z., Qiu, Q., Geng, X., Yang, J., Huang, W., Qian, H. (2016) Free fatty acid receptor agonists for the treatment of type 2 diabetes: drugs in preclinical to phase II clinical development. *Expert Opin Investig Drugs*, 25, 871-890.

Liaw, C.W., Connolly, D.T. (2009) Sequence polymorphisms provide a common consensus sequence for GPR41 and GPR42. *DNA Cell Biol*, 28, 555-560.

Lin, D.C., Zhang, J., Zhuang, R., Li, F., Nguyen, K., Chen, M., Tran, T., Lopez, E., Lu, J.Y., Li, X.N., Tang, L., Tonn, G.R., Swaminath, G., Reagan, J.D., Chen, J.L., Tian, H., Lin, Y.J., Houze, J.B., Luo, J. (2011) AMG 837: a novel GPR40/FFA1 agonist that enhances insulin secretion and lowers glucose levels in rodents. *PLoS One*, 6, e27270.

Liou, A.P., Lu, X., Sei, Y., Zhao, X., Pechhold, S., Carrero, R.J., Raybould, H.E., Wank, S. (2011) The G-protein-coupled receptor GPR40 directly mediates long-chain fatty acid-induced secretion of cholecystokinin. *Gastroenterology*, 140, 903-912.

Liu, J.J., Wang, Y., Ma, Z., Schmitt, M., Zhu, L., Brown, S.P., Dransfield, P.J., Sun, Y., Sharma, R., Guo, Q., Zhuang, R., Zhang, J., Luo, J., Tonn, G.R., Wong, S., Swaminath, G., Medina, J.C., Lin, D.C., Houze, J.B. (2014) Optimization of GPR40 Agonists for Type 2 Diabetes. *ACS Med Chem Lett*, 5, 517-521.

Longo, P.A., Kavran, J.M., Kim, M.S., Leahy, D.J. (2013) Transient mammalian cell transfection with polyethylenimine (PEI). *Methods Enzymol*, 529, 227-240.

Lourenco, E.V., Roque-Barreira, M.C. (2010) Immunoenzymatic quantitative analysis of antigens expressed on the cell surface (cell-ELISA). *Methods Mol Biol*, 588, 301-309.

- Lu, M., Wu, B. (2016) Structural studies of G protein-coupled receptors. *IUBMB Life*, 68, 894-903.
- Lu, X., Zhao, X., Feng, J., Liou, A.P., Anthony, S., Pechhold, S., Sun, Y., Lu, H., Wank, S. (2012) Postprandial inhibition of gastric ghrelin secretion by long-chain fatty acid through GPR120 in isolated gastric ghrelin cells and mice. *Am J Physiol Gastrointest Liver Physiol*, 303, G367-G376.
- Luttrell, L.M., Lefkowitz, R.J. (2002) The role of beta-arrestins in the termination and transduction of G-protein-coupled receptor signals. *J Cell Sci*, 115, 455-465.
- Ma, Z., Lin, D.C., Sharma, R., Liu, J., Zhu, L., Li, A.R., Kohn, T., Wang, Y., Liu, J.J., Bartberger, M.D., Medina, J.C., Zhuang, R., Li, F., Zhang, J., Luo, J., Wong, S., Tonn, G.R., Houze, J.B. (2016) Discovery of the imidazole-derived GPR40 agonist AM-3189. *Bioorg Med Chem Lett*, 26, 15-20.
- Mancini, A.D., Bertrand, G., Vivot, K., Carpentier, É., Tremblay, C., Ghislain, J., Bouvier, M., Poitout, V. (2015a) β -Arrestin Recruitment and Biased Agonism at Free Fatty Acid Receptor 1. *J Biol Chem*, 290, 21131-21140.
- Mancini, A.D., Poitout, V. (2013) The fatty acid receptor FFA1/GPR40 a decade later: how much do we know? *Trends Endocrinol Metab*, 24, 398-407.
- Mancini, A.D., Poitout, V. (2015b) GPR40 agonists for the treatment of type 2 diabetes: life after 'TAKing' a hit. *Diabetes Obes Metab*, 17, 622-629.
- Manosalva, C., Mena, J., Velasquez, Z., Colenso, C.K., Brauchi, S., Burgos, R.A., Hidalgo, M.A. (2015) Cloning, identification and functional characterization of bovine free fatty acid receptor-1 (FFAR1/GPR40) in neutrophils. *PLoS One*, 10, e0119715.
- Marchese, A., Chen, C., Kim, Y.M., Benovic, J.L. (2003) The ins and outs of G protein-coupled receptor trafficking. *Trends Biochem Sci*, 28, 369-376.

- Marsango, S., Varela, M.J., Milligan, G. (2015) Approaches to Characterize and Quantify Oligomerization of GPCRs. *Methods Mol Biol*, 1335, 95-105.
- Masuho, I., Ostrovskaya, O., Kramer, G.M., Jones, C.D., Xie, K., Martemyanov, K.A. (2015) Distinct profiles of functional discrimination among G proteins determine the actions of G protein-coupled receptors. *Sci Signal*, 8, ra123.
- Matsumura, S., Mizushige, T., Yoneda, T., Iwanaga, T., Tsuzuki, S., Inoue, K., Fushiki, T. (2007) GPR expression in the rat taste bud relating to fatty acid sensing. *Biomed Res*, 28, 49-55.
- Micu, I., Ridsdale, A., Zhang, L., Woulfe, J., McClintock, J., Brantner, C.A., Andrews, S.B., Stys, P.K. (2007) Real-time measurement of free Ca²⁺ changes in CNS myelin by two-photon microscopy. *Nat Med*, 13, 874-879.
- Milligan, G. (2002) Strategies to identify ligands for orphan G-protein-coupled receptors. *Biochem Soc Trans*, 30, 789-793.
- Milligan, G. (2004) Applications of bioluminescence- and fluorescence resonance energy transfer to drug discovery at G protein-coupled receptors. *Eur J Pharm Sci*, 21, 397-405.
- Milligan, G. (2006a) G-protein-coupled receptor heterodimers: pharmacology, function and relevance to drug discovery. *Drug Discov Today*, 11, 541-549.
- Milligan, G. (2007) G protein-coupled receptor dimerisation: molecular basis and relevance to function. *Biochim Biophys Acta*, 1768, 825-835.
- Milligan, G. (2008) A day in the life of a G protein-coupled receptor: the contribution to function of G protein-coupled receptor dimerization. *Br J Pharmacol*, 1, S216-S229.
- Milligan, G. (2009) G protein-coupled receptor hetero-dimerization: contribution to pharmacology and function. *Br J Pharmacol*, 158, 5-14.
- Milligan, G. (2010) The role of dimerisation in the cellular trafficking of G-protein-coupled receptors. *Curr Opin Pharmacol*, 10, 23-29.

- Milligan, G. (2013) The prevalence, maintenance, and relevance of G protein-coupled receptor oligomerization. *Mol Pharmacol*, 84, 158-169.
- Milligan, G., Alvarez-Curto, E., Watterson, K.R., Ulven, T., Hudson, B.D. (2015) Characterizing pharmacological ligands to study the long-chain fatty acid receptors GPR40/FFA1 and GPR120/FFA4. *Br J Pharmacol*, 172, 3254-3265.
- Milligan, G., Bouvier, M. (2005) Methods to monitor the quaternary structure of G protein-coupled receptors. *FEBS J*, 272, 2914-2925.
- Milligan, G., Shimpukade, B., Ulven, T., Hudson, B.D. (2017) Complex Pharmacology of Free Fatty Acid Receptors. *Chem Rev*, 117, 67-110.
- Milligan, G., Stoddart, L.A., Brown, A.J. (2006b) G protein-coupled receptors for free fatty acids. *Cell Signal*, 18, 1360-1365.
- Milligan, G., Ulven, T., Murdoch, H., Hudson, B.D. (2014) G-protein-coupled receptors for free fatty acids: nutritional and therapeutic targets. *Br J Nutr*, 116, S3-7.
- Mills, A., Duggan, M.J. (1994) Orphan seven transmembrane domain receptors: reversing pharmacology. *Trends Biotechnol*, 12, 47-49.
- Miyamoto, J., Hasegawa, S., Kasubuchi, M., Ichimura, A., Nakajima, A., Kimura, I. (2016) Nutritional Signaling via Free Fatty Acid Receptors. *Int J Mol Sci*, 17, 450.
- Mo, X.L., Fu, H. (2016) BRET: NanoLuc-Based Bioluminescence Resonance Energy Transfer Platform to Monitor Protein-Protein Interactions in Live Cells. *Methods Mol Biol*, 1439, 263-271.
- Mobarec, J.C., Sanchez, R., Filizola, M. (2009) Modern homology modeling of G-protein coupled receptors: which structural template to use? *J Med Chem*, 52, 5207-5216.
- Mondal, S., Johnston, J.M., Wang, H., Khelashvili, G., Filizola, M., Weinstein, H. (2013) Membrane driven spatial organization of GPCRs. *Sci Rep*, 3, 2909.

- Moniri, N.H. (2016) Free-fatty acid receptor-4 (GPR120): Cellular and molecular function and its role in metabolic disorders. *Biochem Pharmacol*, 110-111, 1-15.
- Montiel, M., Quesada, J., Jiménez, E. (2004) Activation of second messenger-dependent protein kinases induces muscarinic acetylcholine receptor desensitization in rat thyroid epithelial cells. *Mol Cell Endocrinol*, 223, 35-41.
- Moore, C.A., Milano, S.K., Benovic, J.L. (2007) Regulation of receptor trafficking by GRKs and arrestins. *Annu Rev Physiol*, 69, 451-482.
- Moore, K., Zhang, Q., Murgolo, N., Hosted, T., Duffy, R. (2009) Cloning, expression, and pharmacological characterization of the GPR120 free fatty acid receptor from cynomolgus monkey: comparison with human GPR120 splice variants. *Comp Biochem Physiol B Biochem Mol Biol*, 154, 419-426.
- Moran, B.M., Abdel-Wahab, Y.H., Flatt, P.R., McKillop, A.M. (2014) Evaluation of the insulin-releasing and glucose-lowering effects of GPR120 activation in pancreatic β -cells. *Diabetes Obes Metab*, 16, 1128-1139.
- Moran, B.M., Flatt, P.R., McKillop, A.M. (2016) G protein-coupled receptors: signalling and regulation by lipid agonists for improved glucose homeostasis. *Acta Diabetol*, 53, 177-188.
- Mundell, S.J., Luo, J., Benovic, J.L., Conley, P.B., Poole, A.W. (2006) Distinct clathrin-coated pits sort different G protein-coupled receptor cargo. *Traffic*, 7, 1420-1431.
- Munk, C., Isberg, V., Mordalski, S., Harpsøe, K., Rataj, K., Hauser, A.S., Kolb, P., Bojarski, A.J., Vriend, G., Gloriam, D.E. (2016) GPCRdb: the G protein-coupled receptor database - an introduction. *Br J Pharmacol*, 173, 2195-2207.
- Nagasumi, K., Esaki, R., Iwachidow, K., Yasuhara, Y., Ogi, K., Tanaka, H., Nakata, M., Yano, T., Shimakawa, K., Taketomi, S., Takeuchi, K., Odaka, H., Kaisho, Y. (2009) Overexpression of GPR40 in pancreatic beta-cells augments glucose-stimulated insulin secretion and improves glucose tolerance in normal and diabetic mice. *Diabetes*, 58, 1067-1076.

Negoro, N., Sasaki, S., Mikami, S., Ito, M., Suzuki, M., Tsujihata, Y., Ito, R., Harada, A., Takeuchi, K., Suzuki, N., Miyazaki, J., Santou, T., Odani, T., Kanzaki, N., Funami, M., Tanaka, T., Kogame, A., Matsunaga, S., Yasuma, T., Momose, Y. (2010) Discovery of TAK-875: A Potent, Selective, and Orally Bioavailable GPR40 Agonist. *ACS Med Chem Lett*, 1, 290-294.

Negoro, N., Sasaki, S., Mikami, S., Ito, M., Tsujihata, Y., Ito, R., Suzuki, M., Takeuchi, K., Suzuki, N., Miyazaki, J., Santou, T., Odani, T., Kanzaki, N., Funami, M., Morohashi, A., Nonaka, M., Matsunaga, S., Yasuma, T., Momose, Y. (2012) Optimization of (2,3-dihydro-1-benzofuran-3-yl)acetic acids: discovery of a non-free fatty acid-like, highly bioavailable G protein-coupled receptor 40/free fatty acid receptor 1 agonist as a glucose-dependent insulinotropic agent. *J Med Chem*, 55, 3960-3974.

Neubig, R.R., Spedding, M., Kenakin, T., Christopoulos, A. (2003) International Union of Pharmacology Committee on Receptor Nomenclature and Drug Classification. XXXVIII. Update on terms and symbols in quantitative pharmacology. *Pharmacol Rev*, 55, 597-606.

Ngo, T., Kufareva, I., Coleman, J.L., Graham, R.M., Abagyan, R., Smith, N.J. (2016) Identifying ligands at orphan GPCRs: current status using structure-based approaches. *Br J Pharmacol*, 173, 2934-2951.

Nichols, B.J., Lippincott-Schwartz, J. (2001) Endocytosis without clathrin coats. *Trends Cell Biol*, 11, 406-412.

Nilsson, N.E., Kotarsky, K., Owman, C., Olde, B. (2003) Identification of a free fatty acid receptor, FFA2R, expressed on leukocytes and activated by short-chain fatty acids. *Biochem Biophys Res Commun*, 303, 1047-1052.

Nygaard, R., Frimurer, T.M., Holst, B., Rosenkilde, M.M., Schwartz, T.W. (2009) Ligand binding and micro-switches in 7TM receptor structures. *Trends Pharmacol Sci*, 30, 249-259.

Offermanns, S. (2014) Free fatty acid (FFA) and hydroxy carboxylic acid (HCA) receptors. *Annu Rev Pharmacol Toxicol*, 54, 407-434.

Oh, D.Y., Talukdar, S., Bae, E.J., Imamura, T., Morinaga, H., Fan, W., Li, P., Lu, W.J., Watkins, S.M., Olefsky, J.M. (2010) GPR120 is an omega-3 fatty acid receptor mediating potent anti-inflammatory and insulin-sensitizing effects. *Cell*, 142, 687-698.

Oh, D.Y., Walenta, E., Akiyama, T.E., Lagakos, W.S., Lackey, D., Pessentheiner, A.R., Sasik, R., Hah, N., Chi, T.J., Cox, J.M., Powels, M.A., Di Salvo, J., Sinz, C., Watkins, S.M., Armando, A.M., Chung, H., Evans, R.M., Quehenberger, O., McNelis, J., Bogner-Strauss, J.G., Olefsky, J.M. (2014) A Gpr120-selective agonist improves insulin resistance and chronic inflammation in obese mice. *Nat Med*, 20, 942-947.

Paing, M.M., Stutts, A.B., Kohout, T.A., Lefkowitz, R.J., Trejo, J. (2002) beta - Arrestins regulate protease-activated receptor-1 desensitization but not internalization or Down-regulation. *J Biol Chem*, 277, 1292-300.

Palczewski, K. (2010) Oligomeric forms of G protein-coupled receptors (GPCRs). *Trends Biochem Sci*, 35, 595-600.

Palczewski, K., Kumasaka, T., Hori, T., Behnke, C.A., Motoshima, H., Fox, B.A., Le, Trong, I., Teller, D.C., Okada, T., Stenkamp, R.E., Yamamoto, M., Miyano, M. (2000) Crystal structure of rhodopsin: A G protein-coupled receptor. *Science*, 289, 739-745.

Parker, H.E., Habib, A.M., Rogers, G.J., Gribble, F.M., Reimann, F. (2009) Nutrient-dependent secretion of glucose-dependent insulintropic polypeptide from primary murine K cells. *Diabetologia*, 52, 289-298.

Paulsen, S.J., Larsen, L.K., Hansen, G., Chelur, S., Larsen, P.J., Vrang, N. (2014) Expression of the fatty acid receptor GPR120 in the gut of diet-induced-obese rats and its role in GLP-1 secretion. *PLoS One*, 9, e88227.

Pawson, A.J., Sharman, J.L., Benson, H.E., Faccenda, E., Alexander, S.P., Buneman, O.P., Davenport, A.P., McGrath, J.C., Peters, J.A., Southan, C., Spedding, M., Yu, W., Harmar, A.J., NC-IUPHAR. (2014) The IUPHAR/BPS Guide

to PHARMACOLOGY: an expert-driven knowledgebase of drug targets and their ligands. *Nucleic Acids Res*, 42, D1098-1106.

Perreault, M.L., O'Dowd, B.F., George, S.R. (2011) Dopamine receptor homooligomers and heterooligomers in schizophrenia. *CNS Neurosci Ther*, 17, 52-57.

Pin, J.P., Comps-Agrar, L., Maurel, D., Monnier, C., Rives, M.L., Trinquet, E., Kniazeff, J., Rondard, P., Prézeau, L. (2009) G-protein-coupled receptor oligomers: two or more for what? Lessons from mGlu and GABA_B receptors. *J Physiol*, 587, 5337-5344.

Pluznick, J.L., Protzko, R.J., Gevorgyan, H., Peterlin, Z., Sipos, A., Han, J., Brunet, I., Wan, L.X., Rey, F., Wang, T., Firestein, S.J., Yanagisawa, M., Gordon, J.I., Eichmann, A., Peti-Peterdi, J., Caplan, M.J. (2013) Olfactory receptor responding to gut microbiota-derived signals plays a role in renin secretion and blood pressure regulation. *Proc Natl Acad Sci USA*, 110, 4410-4415.

Pou, C., Mannoury, la Cour, C., Stoddart, L.A., Millan, M.J., Milligan, G. (2012) Functional homomers and heteromers of dopamine D2L and D3 receptors co-exist at the cell surface. *J Biol Chem*, 287, 8864-8878.

Premont, R.T., Gainetdinov, R.R. (2007) Physiological roles of G protein-coupled receptor kinases and arrestins. *Annu Rev Physiol*, 69, 511-534.

Prihandoko, R., Alvarez-Curto, E., Hudson, B.D., Butcher, A.J., Ulven, T., Miller A.M., Tobin, A.B., Milligan, G. (2016) Distinct Phosphorylation Clusters Determine the Signaling Outcome of Free Fatty Acid Receptor 4/G Protein-Coupled Receptor 120. *Mol Pharmacol*, 89, 505-520.

Puhl, H.L. 3rd, Won, Y.J., Lu, V.B., Ikeda, S.R. (2015) Human GPR42 is a transcribed multisite variant that exhibits copy number polymorphism and is functional when heterologously expressed. *Sci Rep*, 5, 12880.

Qian, J., Wu, C., Chen, X., Li, X., Ying, G., Jin, L., Ma, Q., Li, G., Shi, Y., Zhang, G., Zhou, N. (2014) Differential requirements of arrestin-3 and clathrin

for ligand-dependent and -independent internalization of human G protein-coupled receptor 40. *Cell Signal*, 26, 2412-2423.

Rajagopal, S., Rajagopal, K., Lefkowitz, R.J. (2010) Teaching old receptors new tricks: biasing seven-transmembrane receptors. *Nat Rev Drug Discov*, 9, 373-386.

Rajagopal, S., Shenoy, S.K. (2017) GPCR desensitization: Acute and prolonged phases. *Cell Signal*, [Epub ahead of print] PMID: 28137506, doi: 10.1016/j.cellsig.2017.01.024.

Ranjan, R., Gupta, P., Shukla, A.K. (2016) GPCR Signaling: B-arrestins Kiss and Remember. *Curr Biol*, 26, R285-R288.

Rashid, A.J., So, C.H., Kong, M.M., Furtak, T., El-Ghundi, M., Cheng, R., O'Dowd, B.F., George, S.R. (2007) D1-D2 dopamine receptor heterooligomers with unique pharmacology are coupled to rapid activation of Gq/11 in the striatum. *Proc Natl Acad Sci USA*, 104, 654-659.

Rask-Andersen, M., Almén, M.S., Schioth, H.B. (2011) Trends in the exploitation of novel drug targets. *Nat Rev Drug Discov*. 10, 579-590.

Reimann, F., Tolhurst, G., Gribble, F.M. (2012) G-protein-coupled receptors in intestinal chemosensation. *Cell Metab*, 15, 421-431.

Reiter, E., Lefkowitz, R.J. (2006) GRKs and beta-arrestins: roles in receptor silencing, trafficking and signaling. *Trends Endocrinol Metab*, 17, 159-165.

Rhee, S.G. (2001) Regulation of phosphoinositide-specific phospholipase C. *Annu Rev Biochem*, 70, 281-312.

Rosenbaum, D.M., Cherezov, V., Hanson, M.A., Rasmussen, S.G., Thian, F.S., Kobilka, T.S., Choi, H.J., Yao, X.J., Weis, W.I., Stevens, R.C., Kobilka, B.K. (2007) GPCR engineering yields high-resolution structural insights into beta2-adrenergic receptor function. *Science*, 318, 1266-1273.

Rosenbaum, D.M., Rasmussen, S.G., Kobilka, B.K. (2009) The structure and function of G-protein-coupled receptors. *Nature*, 459, 356-363.

- Rosethorne, E.M., Bradley, M.E., Kent, T.C., Charlton, S.J. (2015) Functional desensitization of the β_2 adrenoceptor is not dependent on agonist efficacy. *Pharmacol Res Perspect*, 3, e00101.
- Russell, J.T. (2011) Imaging calcium signals in vivo: a powerful tool in physiology and pharmacology. *Br J Pharmacol*, 163, 1605-1625.
- Salahpour, A., Angers, S., Mercier, J.F., Lagacé, M., Marullo, S., Bouvier, M. (2004) Homodimerization of the β_2 -adrenergic receptor as a prerequisite for cell surface targeting. *J Biol Chem*, 279, 33390-33397.
- Salon, J.A., Lodowski, D.T., Palczewski, K. (2011) The significance of G protein-coupled receptor crystallography for drug discovery. *Pharmacol Rev*, 63, 901-937.
- Samama, P., Cotecchia, S., Costa, T., Lefkowitz, R.J. (1993) A mutation-induced activated state of the β_2 -adrenergic receptor. Extending the ternary complex model. *J Biol Chem*, 268, 4625-4636.
- Sánchez-Reyes, O.B., Romero-Ávila, M.T., Castillo-Badillo, J.A., Takei, Y., Hirasawa, A., Tsujimoto, G., Villalobos-Molina, R., García-Sáinz, J.A. (2014) Free fatty acids and protein kinase C activation induce GPR120 (free fatty acid receptor 4) phosphorylation. *Eur J Pharmacol*, 723, 368-374.
- Sawzdargo, M., George, S.R., Nguyen, T., Xu, S., Kolakowski, L.F., O'Dowd, B.F. (1997) A cluster of four novel human G protein-coupled receptor genes occurring in close proximity to CD22 gene on chromosome 19q13.1. *Biochem Biophys Res Commun*, 239, 543-547.
- Scheerer, P., Park, J.H., Hildebrand, P.W., Kim, Y.J., Krauss, N., Choe, H.W., Hofmann, K.P., Ernst, O.P. (2008) Crystal structure of opsin in its G-protein-interacting conformation. *Nature*, 455, 497-502.
- Schindelin, J., Arganda-Carreras, I., Frise, E., Kaynig, V., Longair, M., Pietzsch, T., Preibisch, S., Rueden, C., Saalfeld, S., Schmid, B., Tinevez, J.Y., White,

- D.J., Hartenstein, V., Eliceiri, K., Tomancak, P., Cardona, A. (2012) Fiji: an open-source platform for biological-image analysis. *Nat Methods*, 9, 676-682.
- Schmidt, J., Liebscher, K., Merten, N., Grundmann, M., Mielenz, M., Sauerwein, H., Christiansen, E., Due-Hansen, M.E., Ulven, T., Ullrich, S., Gomeza, J., Drewke, C., Kostenis, E. (2011) Conjugated linoleic acids mediate insulin release through islet G protein-coupled receptor FFA1/GPR40. *J Biol Chem*, 286, 11890-11894.
- Schrage, R., Schmitz, A.L., Gaffal, E., Annala, S., Kehraus, S., Wenzel, D., Büllsach, K.M., Bald, T., Inoue, A., Shinjo, Y., Galandrin, S., Shridhar, N., Hesse, M., Grundmann, M., Merten, N., Charpentier, T.H., Martz, M., Butcher, A.J., Slodczyk, T., Armando, S., Efferm, M., Namkung, Y., Jenkins, L., Horn, V., Stöbel, A., Dargatz, H., Tietze, D., Imhof, D., Galés, C., Drewke, C., Müller, C.E., Hölzel, M., Milligan, G., Tobin, A.B., Gomeza, J., Dohlman, H.G., Sondek, J., Harden, T.K., Bouvier, M., Laporte, S.A., Aoki, J., Fleischmann, B.K., Mohr, K., König, G.M., Tüting, T., Kostenis, E. (2015) The experimental power of FR900359 to study Gq-regulated biological processes. *Nat Commun*, 6, 10156.
- Shenoy, S.K., Lefkowitz, R.J. (2003) Multifaceted roles of beta-arrestins in the regulation of seven-membrane-spanning receptor trafficking and signalling. *Biochem J*, 375: 503-515.
- Shenoy, S.K., Lefkowitz, R.J. (2011) β -Arrestin-mediated receptor trafficking and signal transduction. *Trends Pharmacol Sci*, 32, 521-533.
- Shimpukade, B., Hudson, B.D., Hovgaard, C.K., Milligan, G., Ulven, T. (2012) Discovery of a potent and selective GPR120 agonist. *J Med Chem*, 55, 4511-4515.
- Shukla, A.K., Xiao, K., Lefkowitz, R.J. (2011) Emerging Paradigms of β -Arrestin-Dependent Seven Transmembrane Receptor Signaling. *Trends Biochem Sci*, 36, 457-469.
- Smith, J.S., Rajagopal, S. (2016) The β -Arrestins: Multifunctional Regulators of G Protein-coupled Receptors. *J Biol Chem*, 291, 8969-8977.

Sparks, S.M., Aquino, C., Banker, P., Collins, J.L., Cowan, D., Diaz, C., Dock, S.T., Hertzog, D.L., Liang, X., Swiger, E.D., Yuen, J., Chen, G., Jayawickreme, C., Moncol, D., Nystrom, C., Rash, V., Rimele, T., Roller, S., Ross, S. (2017) Exploration of phenylpropanoic acids as agonists of the free fatty acid receptor 4 (FFA4): Identification of an orally efficacious FFA4 agonist. *Bioorg Med Chem Lett*, 27, 1278-1283.

Sparks, S.M., Chen, G., Collins, J.L., Danger, D., Dock, S.T., Jayawickreme, C., Jenkinson, S., Laudeman, C., Leesnitzer, M.A., Liang, X., Maloney, P., McCoy, D.C., Moncol, D., Rash, V., Rimele, T., Vulimiri, P., Way, J.M., Ross, S. (2014) Identification of diarylsulfonamides as agonists of the free fatty acid receptor 4 (FFA4/GPR120). *Bioorg Med Chem Lett*, 24, 3100-3103.

Spitzer, J., Landthaler, M., Tuschl, T. (2013) Rapid creation of stable mammalian cell lines for regulated expression of proteins using the Gateway® recombination cloning technology and Flp-In T-REx® lines. *Methods Enzymol*, 529, 99-124.

Srivastava, A., Gupta, B., Gupta, C., Shukla, A.K. (2015) Emerging Functional Divergence of β -Arrestin Isoforms in GPCR Function. *Trends Endocrinol Metab*, 26, 628-642.

Srivastava, A., Yano, J., Hirozane, Y., Kefala, G., Gruswitz, F., Snell, G., Lane, W., Ivetac, A., Aertgeerts, K., Nguyen, J., Jennings, A., Okada, K. (2014) High-resolution structure of the human GPR40 receptor bound to allosteric agonist TAK-875. *Nature*, 513, 124-127.

Stinkens, R., Goossens, G.H., Jocken, J.W., Blaak, E.E. (2015) Targeting fatty acid metabolism to improve glucose metabolism. *Obes Rev*, 16, 715-757.

Stockert, J.A., Devi, L.A. (2015) Advancements in therapeutically targeting orphan GPCRs. *Front Pharmacol*, 6, 100.

Stoddart, L.A., Brown, A.J., Milligan, G. (2007) Uncovering the pharmacology of the G protein-coupled receptor GPR40: high apparent constitutive activity in

guanosine 5'-O-(3-[³⁵S]thio)triphosphate binding studies reflects binding of an endogenous agonist. *Mol Pharmacol*, 71, 994-1005.

Stoddart, .L.A., Smith, N.J., Milligan, G. (2008) International Union of Pharmacology. LXXI. Free fatty acid receptors FFA1, -2, and -3: pharmacology and pathophysiological functions. *Pharmacol Rev*, 60, 405-417.

Stoddart, L.A., Johnstone, E.K., Wheal, A.J., Goulding, J., Robers, M.B., Machleidt, T., Wood, K.V., Hill, S.J., Pflieger, K.D. (2015) Application of BRET to monitor ligand binding to GPCRs. *Nat Methods*, 12, 661-663.

Stoddart, L.A., Smith, N.J., Jenkins, L., Brown, A.J., Milligan, G. (2008) Conserved polar residues in transmembrane domains V, VI, and VII of free fatty acid receptor 2 and free fatty acid receptor 3 are required for the binding and function of short chain fatty acids. *J Biol Chem*, 283, 32913-32924.

Stone, V.M., Dhayal, S., Brocklehurst, K.J., Lenaghan, C., Sörhede Winzell, M., Hammar, M., Xu, X., Smith, D.M., Morgan, N.G. (2014) GPR120 (FFAR4) is preferentially expressed in pancreatic delta cells and regulates somatostatin secretion from murine islets of Langerhans. *Diabetologia*, 57, 1182-1191.

Strange, P.G. (2008) Signaling mechanisms of GPCR ligands. *Curr Opin Drug Discov Devel*, 11, 196-202.

Suckow, A.T., Briscoe, C.P. (2017) Key Questions for Translation of FFA Receptors: From Pharmacology to Medicines. *Handb Exp Pharmacol*, 236, 101-131.

Suzuki, T., Igari, S., Hirasawa, A., Hata, M., Ishiguro, M., Fujieda, H., Itoh, Y., Hirano, T., Nakagawa, H., Ogura, M., Makishima, M., Tsujimoto, G., Miyata, N. (2008) Identification of G protein-coupled receptor 120-selective agonists derived from PPARgamma agonists. *J Med Chem*, 51, 7640-7644.

Syrovatkina, V., Alegre, K.O., Dey, R., Huang, X.Y. (2016) Regulation, Signaling, and Physiological Functions of G-Proteins. *J Mol Biol*, 428, 3850-3868.

Szalai, B., Hoffmann, P., Prokop, S., Erdélyi, L., Várnai, P., Hunyady, L. (2014) Improved methodical approach for quantitative BRET analysis of G Protein Coupled Receptor dimerization. *PLoS One*, 9, e109503.

Takahashi, K., Fukushima, K., Onishi, Y., Node, Y., Inui, K., Fukushima, N., Honoki, K., Tsujiuchi, T. (2017) Different effects of G-protein-coupled receptor 120 (GPR120) and GPR40 on cell motile activity of highly migratory osteosarcoma cells. *Biochem Biophys Res Commun*, 484, 675-680.

Takasaki, J., Saito, T., Taniguchi, M., Kawasaki, T., Moritani, Y., Hayashi, K., Kobori, M. (2004) A novel Galphaq/11-selective inhibitor. *J Biol Chem*, 279, 47438-47445.

Talukdar, S., Olefsky, J.M., Osborn, O. (2011) Targeting GPR120 and other fatty acid-sensing GPCRs ameliorates insulin resistance and inflammatory diseases. *Trends Pharmacol Sci*, 32, 543-550.

Tanaka, T., Katsuma, S., Adachi, T., Koshimizu, T.A., Hirasawa, A., Tsujimoto, G. (2008b) Free fatty acids induce cholecystokinin secretion through GPR120. *Naunyn Schmiedebergs Arch Pharmacol*, 377, 523-527.

Tanaka, T., Yano, T., Adachi, T., Koshimizu, T.A., Hirasawa, A., Tsujimoto, G. (2008a) Cloning and characterization of the rat free fatty acid receptor GPR120: in vivo effect of the natural ligand on GLP-1 secretion and proliferation of pancreatic beta cells. *Naunyn Schmiedebergs Arch Pharmacol*, 377, 515-522.

Taneera, J., Lang, S., Sharma, A., Fadista, J., Zhou, Y., Ahlqvist, E., Jonsson, A., Lyssenko, V., Vikman, P., Hansson, O., Parikh, H., Korsgren, O., Soni, A., Krus, U., Zhang, E., Jing, X.J., Esguerra, J.L., Wollheim, C.B., Salehi, A., Rosengren, A., Renström, E., Groop, L. (2012) A systems genetics approach identifies genes and pathways for type 2 diabetes in human islets. *Cell Metab*, 16, 122-134.

Tautermann, C.S. (2014) GPCR structures in drug design, emerging opportunities with new structures. *Bioorg Med Chem Lett*, 24, 4073-4079.

Tazoe, H., Otomo, Y., Karaki, S., Kato, I., Fukami, Y., Terasaki, M., Kuwahara, A. (2009) Expression of short-chain fatty acid receptor GPR41 in the human colon. *Biomed Res*, 30, 149-156.

Terrillon, S., Bouvier, M. (2004) Roles of G-protein-coupled receptor dimerization. *EMBO Rep*, 5, 30-34.

Thomas, P., Smart, T.G. (2005) HEK293 cell line: a vehicle for the expression of recombinant proteins. *J Pharmacol Toxicol Methods*, 51, 187-200.

Thomsen, A.R., Plouffe, B., Cahill, T.J., Shukla, A.K., Tarrasch, J.T., Dosey, A.M., Kahsai, A.W., Strachan, R.T., Pani, B., Mahoney, J.P., Huang, L., Breton, B., Heydenreich, F.M., Sunahara, R.K., Skiniotis, G., Bouvier, M., Lefkowitz, R.J. (2016) GPCR-G Protein- β -Arrestin Super-Complex Mediates Sustained G Protein Signaling. *Cell*, 166, 907-919.

Tian, X., Kang, D.S., Benovic, J.L. (2014) β -arrestins and G protein-coupled receptor trafficking. *Handb Exp Pharmacol*, 219, 173-186.

Tobin, A.B. (2008) G-protein-coupled receptor phosphorylation: Where, when and by whom. *Br. J. Pharmacol*, 153, S167-S176.

Tolhurst, G., Heffron, H., Lam, Y.S., Parker, H.E., Habib, A.M., Diakogiannaki, E., Cameron, J., Grosse, J., Reimann, F., Gribble, F.M. (2012) Short-chain fatty acids stimulate glucagon-like peptide-1 secretion via the G-protein-coupled receptor FFAR2. *Diabetes*, 61, 364-371.

Trinquet, E., Fink, M., Bazin, H., Grillet, F., Maurin, F., Bourrier, E., Ansanay, H., Leroy, C., Michaud, A., Durroux, T., Maurel, D., Malhaire, F., Goudet, C., Pin, J.P., Naval, M., Hernout, O., Chrétien, F., Chapleur, Y., Mathis, G. (2006) D-myo-inositol 1-phosphate as a surrogate of D-myo-inositol 1,4,5-tris phosphate to monitor G protein-coupled receptor activation. *Anal Biochem*, 358, 126-135.

Ulven, T. (2012) Short-chain free fatty acid receptors FFA2/GPR43 and FFA3/GPR41 as new potential therapeutic targets. *Front Endocrinol (Lausanne)*, 3, 111.

- Ulven, T., Christiansen, E. (2015) Dietary Fatty Acids and Their Potential for Controlling Metabolic Diseases Through Activation of FFA4/GPR120. *Annu Rev Nutr*, 35, 239-263.
- Unal, H., Karnik, S.S. (2012) Domain coupling in GPCRs: the engine for induced conformational changes. *Trends Pharmacol Sci*, 33, 79-88.
- van Koppen, C.J., Jakobs, K.H. (2004) Arrestin-independent internalization of G protein-coupled receptors. *Mol Pharmacol*, 66, 365-367.
- Venkatakrisnan, A.J., Deupi, X., Lebon, G., Tate, C.G., Schertler, G.F., Babu, M.M. (2013) Molecular signatures of G-protein-coupled receptors. *Nature*, 494, 185-194.
- Violin, J.D., Crombie, A.L., Soergel, D.G., Lark, M.W. (2014) Biased ligands at G-protein-coupled receptors: promise and progress. *Trends Pharmacol Sci*, 35, 308-316.
- Ward, R.J., Alvarez-Curto, E., Milligan, G. (2011) Using the Flp-In™ T-Rex™ system to regulate GPCR expression. *Methods Mol Biol*, 746, 21-37.
- Ward, R.J., Milligan, G. (2014) Structural and biophysical characterisation of G protein-coupled receptor ligand binding using resonance energy transfer and fluorescent labelling techniques. *Biochim Biophys Acta*, 1838, 3-14.
- Ward, R.J., Pediani, J.D., Godin, A.G., Milligan, G. (2015) Regulation of oligomeric organization of the serotonin 5-hydroxytryptamine 2C (5-HT2C) receptor observed by spatial intensity distribution analysis. *J Biol Chem*, 290, 12844-12857.
- Ward, R.J., Pediani, J.D., Milligan, G. (2011) Heteromultimerization of cannabinoid CB(1) receptor and orexin OX(1) receptor generates a unique complex in which both protomers are regulated by orexin A. *J Biol Chem*, 286, 37414-37428.

- Ward, R.J., Xu, T.R., Milligan, G. (2013) GPCR oligomerization and receptor trafficking. *Methods Enzymol*, 521, 69-90.
- Watson, S.J., Brown, A.J., Holliday, N.D. (2012) Differential signaling by splice variants of the human free fatty acid receptor GPR120. *Mol Pharmacol*, 81, 631-642.
- Watterson, K.R., Hudson, B.D., Ulven, T., Milligan, G. (2014) Treatment of type 2 diabetes by free Fatty Acid receptor agonists. *Front Endocrinol (Lausanne)*, 28, 5:137.
- Watterson, K.R., Hansen, S.V., Hudson, B., Alvarez-Curto, E, Raihan, S.Z., Azevedo, C.M., Martin, G., Dunlop, J., Yarwood, S.J., Ulven, T., Milligan, G. (2017) Probe-dependent negative allosteric modulators of the long-chain free fatty acid receptor FFA4. *Mol Pharmacol*, [Epub ahead of print], doi: 10.1124/mol.116.107821.
- Werry, T.D., Wilkinson, G.F., Willars, G.B. (2003) Mechanisms of cross-talk between G-protein-coupled receptors resulting in enhanced release of intracellular Ca²⁺. *Biochem J*, 374, 281-296.
- Wess, J. (1997) G-protein-coupled receptors: molecular mechanisms involved in receptor activation and selectivity of G-protein recognition. *FASEB J*, 11, 346-354.
- Wettschureck, N., Offermanns, S. (2005) Mammalian G proteins and their cell type specific functions. *Physiol Rev*, 85, 1159-1204.
- Whalen, E.J., Rajagopal, S., Lefkowitz, R.J. (2011) Therapeutic potential of B-arrestin- and G protein-biased agonists. *Trends Mol Med*, 17, 126-139.
- Wheatley, M., Wootten, D., Conner, M.T., Simms, J., Kendrick, R., Logan, R.T., Poyner, D.R., Barwell, J. (2012) Lifting the lid on GPCRs: the role of extracellular loops. *Br J Pharmacol*, 165, 1688-1703.

Whorton, M.R., Bokoch, M.P., Rasmussen, S.G., Huang, B., Zare, R.N., Kobilka, B., Sunahara, R.K. (2007) A monomeric G protein-coupled receptor isolated in a high-density lipoprotein particle efficiently activates its G protein. *Proc Natl Acad Sci USA*, 104, 7682-7687.

Wise, A., Jupe, S.C., Rees, S. (2004) The identification of ligands at orphan G-protein coupled receptors. *Annu Rev Pharmacol Toxicol*, 44:43-66.

Wisler, J.W., Xiao, K., Thomsen, A.R., Lefkowitz, R.J. (2014) Recent developments in biased agonism. *Curr Opin Cell Biol*, 27, 18-24.

Wu, Q., Wang, H., Zhao, X., Shi, Y., Jin, M., Wan, B., Xu, H., Cheng, Y., Ge, H., Zhang, Y. (2013) Identification of G-protein-coupled receptor 120 as a tumor-promoting receptor that induces angiogenesis and migration in human colorectal carcinoma. *Oncogene*, 32, 5541-5550.

Xiong, Y., Miyamoto, N., Shibata, K., Valasek, M.A., Motoike, T., Kedzierski, R.M., Yanagisawa, M. (2004) Short-chain fatty acids stimulate leptin production in adipocytes through the G protein-coupled receptor GPR41. *Proc Natl Acad Sci USA*, 101, 1045-1050.

Xiong, Y., Swaminath, G., Cao, Q., Yang, L., Guo, Q., Salomonis, H., Lu, J., Houze, J.B., Dransfield, P.J., Wang, Y., Liu, J.J., Wong, S., Schwandner, R., Steger, F., Baribault, H., Liu, L., Coberly, S., Miao, L., Zhang, J., Lin, D.C., Schwarz, M. (2013) Activation of FFA1 mediates GLP-1 secretion in mice. Evidence for allosterism at FFA1. *Mol Cell Endocrinol*, 369, 119-129.

Xu, Z.Q., Zhang, X., Scott, L. (2007) Regulation of G protein-coupled receptor trafficking. *Acta Physiol (Oxf)*, 190, 39-45.

Yates, C.M., Calder, P.C., Ed Rainge, r G. (2014) Pharmacology and therapeutics of omega-3 polyunsaturated fatty acids in chronic inflammatory disease. *Pharmacol Ther*, 141, 272-282.

Yonezawa, T., Katoh, K., Obara, Y. (2004) Existence of GPR40 functioning in a human breast cancer cell line, MCF-7. *Biochem Biophys Res Commun*, 314, 805-809.

Youvan, D.C., Silva, C.M., Bylina, E.J., Coleman, W.J., Dilworth, M.R., Yang, M.M. (1997) Calibration of fluorescence resonance energy transfer in microscopy using genetically engineered GFP derivatives on nickel chelating beads. *Biotechnology*, 3, 1-18.

Zhang, D., Zhao, Q., Wu, B. (2015) Structural Studies of G Protein-Coupled Receptors. *Mol Cells*, 38, 836-842.

Zhang, X., Kim, K.M. (2017) Multifactorial Regulation of G Protein-Coupled Receptor Endocytosis. *Biomol Ther (Seoul)*, 25, 26-43.

Zheng, M., Zhang, X., Guo, S., Zhang, X., Min, C., Cheon, S.H., Oak, M.H., Kim, Y.R., Kim, K.M. (2016) Agonist-induced changes in RalA activities allows the prediction of the endocytosis of G protein-coupled receptors. *Biochim Biophys Acta*, 1863, 77-90.

Zhuo, Y., Vishnivetskiy, S.A., Zhan, X., Gurevich, V.V., Klug, C.S. (2014) Identification of receptor binding-induced conformational changes in non-visual arrestins. *J Biol Chem*, 289, 20991-21002.